# FROM FIRES TO OCEANS: DYNAMICS OF FIRE-DERIVED ORGANIC MATTER IN TERRESTRIAL AND AQUATIC ECOSYSTEMS

EDITED BY: Samuel Abiven and Cristina Santín
PUBLISHED IN: Frontiers in Earth Science and Frontiers in Environmental Science

frontiers Research Topics

ISSN 1664-8714
ISBN 978-2-88945-824-0
DOI 10.3389/978-2-88945-824-0

## About Frontiers

Frontiers is more than just an open-access publisher of scholarly articles: it is a pioneering approach to the world of academia, radically improving the way scholarly research is managed. The grand vision of Frontiers is a world where all people have an equal opportunity to seek, share and generate knowledge. Frontiers provides immediate and permanent online open access to all its publications, but this alone is not enough to realize our grand goals.

## Frontiers Journal Series

The Frontiers Journal Series is a multi-tier and interdisciplinary set of open-access, online journals, promising a paradigm shift from the current review, selection and dissemination processes in academic publishing. All Frontiers journals are driven by researchers for researchers; therefore, they constitute a service to the scholarly community. At the same time, the Frontiers Journal Series operates on a revolutionary invention, the tiered publishing system, initially addressing specific communities of scholars, and gradually climbing up to broader public understanding, thus serving the interests of the lay society, too.

## Dedication to Quality

Each Frontiers article is a landmark of the highest quality, thanks to genuinely collaborative interactions between authors and review editors, who include some of the world's best academicians. Research must be certified by peers before entering a stream of knowledge that may eventually reach the public - and shape society; therefore, Frontiers only applies the most rigorous and unbiased reviews.
Frontiers revolutionizes research publishing by freely delivering the most outstanding research, evaluated with no bias from both the academic and social point of view. By applying the most advanced information technologies, Frontiers is catapulting scholarly publishing into a new generation.

## What are Frontiers Research Topics?

Frontiers Research Topics are very popular trademarks of the Frontiers Journals Series: they are collections of at least ten articles, all centered on a particular subject. With their unique mix of varied contributions from Original Research to Review Articles, Frontiers Research Topics unify the most influential researchers, the latest key findings and historical advances in a hot research area! Find out more on how to host your own Frontiers Research Topic or contribute to one as an author by contacting the Frontiers Editorial Office: researchtopics@frontiersin.org

# FROM FIRES TO OCEANS: DYNAMICS OF FIRE-DERIVED ORGANIC MATTER IN TERRESTRIAL AND AQUATIC ECOSYSTEMS

Topic Editors:
**Samuel Abiven,** University of Zurich, Switzerland
**Cristina Santín,** Swansea University, United Kingdom

Image: Prof. Stefan Doerr, Swansea University, United Kingdom; used with permission.

Fire-derived organic matter, also known as pyrogenic carbon (PyC), is ubiquitous on Earth. It can be found in soils, sediments, water and air. In this wide range of environments, fire-derived organic matter, represents a key component of the organic matter pool, and, in many cases, the largest identifiable group of organic compounds. PyC is also one of the most persistent organic matter fractions in the ecosystems, and its study is, therefore, particularly relevant for the global carbon cycle.

From its production during vegetation fires to its transfer into soils, sediments and waters, PyC goes through different transformations, both abiotic and biotic. Contrary to early assumptions, PyC is not inert and interacts strongly with the environment: evidence of microbial decomposition, oxidation patterns and interactions with

minerals have been described in different matrices. PyC travels across these different environments and it is modified chemically and physically, but remains persistent.

This Research Topic explores important questions in our understanding of fire-derived organic matter, from the characterization and quantification of PyC components, to the transformation and mobilization processes taking place on terrestrial and aquatic ecosystems. The studies compiled here provide novel and, often, unexpected results. They all answer some of the questions posed and, more importantly, provide scope for many more.

**Citation:** Abiven, S., Santín, C., eds. (2019). From Fires to Oceans: Dynamics of Fire-Derived Organic Matter in Terrestrial and Aquatic Ecosystems. Lausanne: Frontiers Media. doi: 10.3389/978-2-88945-824-0

# Table of Contents


06 ***Editorial: From Fires to Oceans: Dynamics of Fire-Derived Organic Matter in Terrestrial and Aquatic Ecosystems***
Samuel Abiven and Cristina Santín

## 1. IDENTIFICATION AND CHARACTERIZATION OF PYC

10 ***Trial by Fire: On the Terminology and Methods Used in Pyrogenic Organic Carbon Research***
Andrew R. Zimmerman and Siddhartha Mitra

18 ***What Can Charcoal Reflectance Tell us About Energy Release in Wildfires and the Properties of Pyrogenic Carbon?***
Claire M. Belcher, Stacey L. New, Cristina Santín, Stefan H. Doerr, Rebecca A. Dewhirst, Mark J. Grosvenor and Victoria A. Hudspith

## 2. PYC ON-SITE: PRODUCTION AND STORAGE IN SOILS

31 ***Quantifying Changes in Total and Pyrogenic Carbon Stocks Across Fire Severity Gradients Using Active Wildfire Incidents***
Jessica Miesel, Alicia Reiner, Carol Ewell, Bernardo Maestrini and Matthew Dickinson

52 ***Charcoal in Organic Horizon and Surface Mineral Soil in a Boreal Forest Fire Chronosequence of Western Quebec: Stocks, Depth Distribution, Chemical Properties and a Synthesis of Related Studies***
Caroline M. Preston, Martin Simard, Yves Bergeron, Guy M. Bernard and Roderick E. Wasylishen

72 ***Pyrogenic Carbon Lacks Long-Term Persistence in Temperate Arable Soils***
Suzanne Lutfalla, Samuel Abiven, Pierre Barré, Daniel B. Wiedemeier, Bent T. Christensen, Sabine Houot, Thomas Kätterer, Andy J. Macdonald, Folkert van Oort and Claire Chenu

82 ***Pyrogenic Carbon in Soils: A Literature-Based Inventory and a Global Estimation of its Content in Soil Organic Carbon and Stocks***
Moritz Reisser, Ross S. Purves, Michael W. I. Schmidt and Samuel Abiven

96 ***Function of Wildfire-Deposited Pyrogenic Carbon in Terrestrial Ecosystems***
Melissa R. A. Pingree and Thomas H. DeLuca

## 3. PYC DEGRADATION PROCESSES

103 ***Dynamics of Charcoal Alteration in a Tropical Biome: A Biochar-Based Study***
Philippa L. Ascough, Michael I. Bird, William Meredith, Colin Snape, D. Large, Emma Tilston, David Apperley, Ana Bernabé and Licheng Shen

118 ***Physical Processes Dictate Early Biogeochemical Dynamics of Soil Pyrogenic Organic Matter in a Subtropical Forest Ecosystem***
Jason M. Stuart, Russell Anderson, Patrick Lazzarino, Kevin A. Kuehn and Omar R. Harvey

136 ***Fire as a Removal Mechanism of Pyrogenic Carbon From the Environment: Effects of Fire and Pyrogenic Carbon Characteristics***
Stefan H. Doerr, Cristina Santín, Agustín Merino, Claire M. Belcher and Greg Baxter

149 ***Production and Composition of Pyrogenic Dissolved Organic Matter From a Logical Series of Laboratory-Generated Chars***
Kyle W. Bostick, Andrew R. Zimmerman, Andrew. S. Wozniak, Siddhartha Mitra and Patrick G. Hatcher

## 4. PYC MOBILIZATION: THE IMPORTANCE OF LEACHING AND EROSION

163 ***Impact of a Historical Fire Event on Pyrogenic Carbon Stocks and Dissolved Pyrogenic Carbon in Spodosols in Northern Michigan***
Fernanda Santos, Sasha Wagner, David Rothstein, Rudolf Jaffe and Jessica R. Miesel

172 ***Pyrogenic Carbon Erosion: Implications for Stock and Persistence of Pyrogenic Carbon in Soil***
Rebecca B. Abney and Asmeret Asefaw Berhe

188 ***Post-wildfire Erosion in Mountainous Terrain Leads to Rapid and Major Redistribution of Soil Organic Carbon***
Rebecca B. Abney, Jonathan Sanderman, Dale Johnson, Marilyn L. Fogel and Asmeret Asefaw Berhe

204 ***Preferential Production and Transport of Grass-Derived Pyrogenic Carbon in NE-Australian Savanna Ecosystems***
Gustavo Saiz, Iain Goodrick, Christopher Wurster, Paul N. Nelson, Jonathan Wynn and Michael Bird

## 5. FROM LAND TO THE OCEAN

217 ***A New Perspective on the Apparent Solubility of Dissolved Black Carbon***
Sasha Wagner, Yan Ding and Rudolf Jaffé

233 ***Dissolved Black Carbon in the Headwaters-to-Ocean Continuum of Paraíba Do Sul River, Brazil***
Jomar S. J. Marques, Thorsten Dittmar, Jutta Niggemann, Marcelo G. Almeida, Gonzalo V. Gomez-Saez and Carlos E. Rezende

245 ***Distribution and Sources of Dissolved Black Carbon in Surface Waters of the Chukchi Sea, Bering Sea, and the North Pacific Ocean***
Motohiro Nakane, Taku Ajioka and Youhei Yamashita

frontiers in Earth Science

EDITORIAL
published: 27 February 2019
doi: 10.3389/feart.2019.00031

# Editorial: From Fires to Oceans: Dynamics of Fire-Derived Organic Matter in Terrestrial and Aquatic Ecosystems

*Samuel Abiven*[1]* *and Cristina Santín*[2]

[1] Department of Geography, University of Zurich, Zurich, Switzerland, [2] Geography Department, Swansea University, Swansea, United Kingdom

**Keywords: fire-derived carbon, pyrogenic carbon, methods, decomposition, stocks, terrestrial and aquatic ecosystems**

**Editorial on the Research Topic**

**From Fires to Oceans: Dynamics of Fire-Derived Organic Matter in Terrestrial and Aquatic Ecosystems**

## INTRODUCTION

Fire is a global phenomenon,which has contributed to create the Earth's landscapes for several millions of years. Fire can greatly impact the carbon (C) cycle, and it can act in opposite directions, depending on which timescale one considers. On the one hand, over short timescales, a vast amount of organic C is rapidly oxidized and emitted as gases and aerosols during burning, in a much more intense and faster process than respiration. Depending on the magnitude of the fire, the $CO_2$ released by burning can be very relevant in terms of net ecosystem $CO_2$ exchange with the atmosphere. On the other hand, over longer timescales, fire can actually contribute to $CO_2$ drawdown. Due to the incomplete combustion of the fuel biomass, fire not only releases C to the atmosphere but it also converts a substantial fraction of the vegetation C into pyrogenic organic matter also named charcoal, black carbon, or pyrogenic carbon (PyC). This fire-derived organic matter is more resistant to environmental degradation than unburnt biomass and can act as a long-term C sink. Some remains for centuries to millennia in the environment, not statically but changing form and moving between terrestrial and aquatic pools. The relics of fire, in the form of PyC, are present in all compartments of the Earth: In the air, soils, marine and fresh water sediments, rivers, and the oceans...

Despite its global importance, our understanding of the dynamics of fire-derived organic matter is limited. Simple questions like "how much," "how fast," or "how old" remain only partially answered. There are diverse reasons for these gaps in our knowledge. To start with, not all fire-derived organic matter is born equal. PyC is not a single, chemically well-defined organic compound, but a large continuum of different materials, from slightly charred plant material to soot. It is therefore difficult to estimate its initial production and to quantify and characterize this type of organic matter in environment matrices. Another reason is the spatial heterogeneity of the fire phenomenon and the myriad ways and forms fire-derived organic matter can be produced, deposited, and stored in the environment. The processes leading to mobilization of fire-derived organic matter within land, from land to rivers, and from rivers to the ocean also need to be further clarified.

OPEN ACCESS

***Edited by:***
*Alexandra V. Turchyn, University of Cambridge, United Kingdom*

***Reviewed by:***
*Robert Hilton, Durham University, United Kingdom*

***Correspondence:**
*Samuel Abiven*
*samuel.abiven@geo.uzh.ch*

***Specialty section:***
*This article was submitted to Biogeoscience, a section of the journal Frontiers in Earth Science*

***Received:*** *07 December 2018*
***Accepted:*** *08 February 2019*
***Published:*** *27 February 2019*

***Citation:***
*Abiven S and Santín C (2019) Editorial: From Fires to Oceans: Dynamics of Fire-Derived Organic Matter in Terrestrial and Aquatic Ecosystems. Front. Earth Sci. 7:31. doi: 10.3389/feart.2019.00031*

This research topic explores these different questions in our understanding of fire-derived organic matter, from the characterization and quantification of PyC components, to the transformation and mobilization processes taking place on land and in rivers and oceans. The studies compiled here provide novel and, often, unexpected results. They all answer some of the questions posed and, more importantly, provide scope for many more.

## IDENTIFICATION AND CHARACTERIZATION OF PYC

Fire-derived organic matter differs physically and chemically from all other types of organic matter. Identifying it specificities is a major part of ongoing research. The first step is usually to detect it in the environment, in different forms and associated with different matrixes. Zimmerman and Mitra describe the current methodological hurdles we are facing. They note that many of the terms and methods used to quantify and characterize PyC do not match. They recommend linking the reported values to the method applied and propose implementation of a new "ring trial" study that cross-compares the most recently developed methods and examines a wider set of samples, including biochar. They also pose the interesting question of why quantities of PyC and total organic C in waters and soils are, in many cases, directly correlated.

While complex laboratory methods are useful to understand in detail the characteristics of PyC, quick and inexpensive methods are also fundamental in order to explore the inherent high variability of PyC materials. In their study, Belcher et al. propose charcoal reflectance as an indicator of how different fire behavior may lead to PyC with different physical and chemical properties. They found that the total heat released during combustion positively correlates with charcoal reflectance and with its resistance to degradation. This method can be a useful tool to reconstruct fire history and to predict PyC residence in the long term.

## PYC ON-SITE: PRODUCTION AND STORAGE IN SOILS

Our knowledge about PyC production and its relationships with different ecosystem properties such as vegetation cover or fire type or behavior is still very limited. Using an adventurous field approach, Miesel et al. quantify immediate impacts on PyC and total ecosystem C stocks of wildfires of various severities in a Californian mixed-conifer forest. Fire resulted in a net ecosystem gain in PyC of around 1t PyC $ha^{-1}$, but they did not find any difference of PyC production with fire severity.

Information about immediate fire effects is indeed important, but knowledge of the residence of PyC in the longer term is essential in its role as a durable carbon sink. Preston et al. quantify the PyC (>2 mm charcoal) stocks and characteristics in boreal forest soils using a fire chronosequence (24–2,355 years since fire). They find that charcoal stocks are highly variable (50–5,527 kg $ha^{-1}$) but, generally, they decrease with time since fire. Importantly, old charcoal is more aromatic and, therefore, more relevant in terms of long-term C storage. From this C sequestration perspective, both PyC stocks and their residence times need to be quantified. Based on a unique set of soils from five European long-term bare fallows, Lutfalla et al. provide the first direct comparison between the persistence of PyC and total soil organic C in temperate arable soils. They find that soil PyC content decreased more rapidly than expected, with the mean residence time of PyC being just 1.6 times longer than that of total soil organic C.

At the global level, Reisser et al. compile all published data on soil PyC. They find that PyC represent on average 13.7% of the global soil organic C pool, making it one of the largest groups of identifiable soil compounds. They estimate global PyC stock at 200 Pg for the uppermost 2 m of soil. For this global database, soil properties (clay and pH) are better predictors of PyC content than climate or frequency of fire.

PyC is not only important from a C cycle perspective, but it also affects ecosystem properties. Pingree and DeLuca review our current knowledge about the functions of wildfire-produced PyC in terrestrial ecosystems. They discuss the implications of its C-rich, N-poor nature, and its high surface area. They particularly review our knowledge about the "charosphere," the soil near PyC, with its enhanced microbial activity and implications for soil functioning.

## PYC DEGRADATION PROCESSES

While initially PyC was considered inert, it is now well-established that part of it can suffer degradation in the short term. Ascough et al. carried out a 1-year litterbag field experiment in the tropical rainforests of northeast Australia. Their results show that all types of PyC studied partially degraded. Depositional environment characteristics, in particular oxygen availability and protection from sunlight and rainwater, were the main drivers. Along the same lines, Stuart et al. investigate the environmental parameters influencing early-stage PyC dynamics in a subtropical forest. Their study points not to biological decomposition but to losses by volatilization and leaching as the main drivers in the first months of PyC degradation.

One obvious ecosystem process modifying the PyC pools is actually fire burning the charcoal produced in previous events. Doerr et al. observe that, in the boreal forest, fire can be indeed a significant removal mechanism for the PyC that remains on the ground. In their study, higher wildfire maximum temperatures result in higher PyC losses. Such losses also depend on the characteristics of the material, with wildfire charcoal being more readily consumed than slash-and-burn charcoal (which has a higher recalcitrance). Interestingly, fire also increased the recalcitrance of the remaining "twice-heated" PyC making it, therefore, more resistant to subsequent fires.

It is important to note that PyC degradation does not always imply PyC mineralization (and therefore net loss). A good example of this is PyC leaching. In this process, some of the solid PyC retains its pyrogenic nature but becomes soluble in water (but see Wagner et al. for more details about PyC solubility).

Bostick et al. assess the solubility of PyC by characterizing "new" and "old" leachates from laboratory charcoals. They observed than up to 7% of the PyC can be lost in the dissolved forms in about a year, with the chemical characteristics of the leached PyC differing from those of the original solid PyC material.

## PYC MOBILIZATION: THE IMPORTANCE OF LEACHING AND EROSION

The two main mechanisms described in the literature for PyC mobilization are leaching and erosion. In this research topic, Santos et al. quantify losses by leaching, as dissolved PyC, from two spodosols: one in a site burnt 100 years ago and one with no evidence of burning for the past 250 years. While soil PyC stocks are larger in the burnt site, they do not detect any differences in the dissolved PyC concentrations between the two sites (∼3% total organic C pool). This result may indicate that the release of dissolved PyC is a continuous, long-term process, or alternatively, that there are other PyC sources, such as atmospheric deposition, that should also be considered.

In addition to leaching, erosion is a key but still poorly understood mechanism in PyC fluxes. Abney and Berhe present a synthesis of available data to compare the magnitude of the water-driven erosional PyC flux with other important pathways of PyC loss from soil, including leaching and decomposition. Depending on the topograpy, timescale, and initial concentrations of PyC in soil, ignoring the role of erosion in distributing PyC across a landscape can lead to discrepancies of several 100 g PyC $m^{-2}$. In a more specific study, Abney et al. assess the amount and types of soil organic C in different landform positions before and after a wildfire in California. Even if they observed an accumulation of PyC and soil organic C in the post-fire depositional positions 1 year after the fire, both of these C pools decreased 10 years after fire, indicating further erosion or decomposition.

Another way of assessing PyC erosion is to study the sediment transported off-site. Saiz et al. quantify and characterize PyC using $\delta^{13}C$ HyPy in recent sediment (from farm dams) and burnt and unburnt soils in savanna ecosystems with different grass/tree covers. They observe that grass-derived PyC, compared with tree-derived PyC, is both preferentially produced and preferentially eroded. This higher mobility is probably related to its smaller particle size, which is also important to take into account for accurately reconstructing savanna fire regimes using PyC particles.

## FROM LAND TO THE OCEAN

As explained earlier, a key characteristic in terms of PyC mobilization is its solubility in water, especially when considering long distance mobilization and transfer from terrestrial to aquatic environments. Wagner et al. investigate the apparent solubility of different dissolved PyC-type molecules by calculating octanol-water partition coefficients. Their approach reveals that only a minor proportion of the PyC molecules are truly soluble in water (those that are small aromatic structures with hydrophilic moieties), whereas large condensed structures, which are present in large quantities, are not. The authors suggest that other dissolved organic molecules can mediate in PyC solubilisation, but their experimental approach is not able to confirm this hypothesis.

Marques et al. study the main processes behind the release and turnover of dissolved PyC (DBC) in the Paraíba do Sul River catchment (Brazil). Their results show a clear relationship between hydrology and river DBC concentrations. DBC is mainly mobilized from the upper soil horizons during heavy rainfall (wet season) and most of it is derived not from the sugar cane plantations that are the main vegetation cover today, but from relic charcoal produced decades ago during the slash burning of the Atlantic rain forest. They also found that a substantial (23–40%) part of this DBC is photo-oxidized in the river, but, interestingly, not in the estuary.

And, moving further into the ocean, Nakane et al. characterize the dissolved PyC (DBC) in surface waters of the North Pacific. They found that whereas the main input of DBC in coastal waters was fluvial, atmospheric deposition was the main source of DBC in open waters. Their results point to photodegradation and adsorption on to sinking particles as the main removal processes.

## MOVING FORWARD: RESEARCH NEEDS AND CHALLENGES

This research topic provides new insights about the PyC dynamics in ecosystems, but also highlights the upcoming research needs and challenges. While progress is tangible regarding the nomenclature, characterization of PyC in different matrices still remains a frontier to our general understanding. New systematic ring trials, more specifications about the techniques and, maybe, new and more integrative methodsare still needed in order to unify existing knowledge. This research topic indicates two main directions to be followed: methods that can characterize and quantify precisely PyC, so we understand better the mechanisms and processes of transformation within terrestrial and aquatic systems, and screening methods, cheaper and faster than the previous ones, in order to explore the PyC spatial heterogeneity.

Understanding the variability of PyC stocks and fluxes in the ecosystems is another important challenge to address. Our understanding of PyC residence time and quantities remains scare. In particular, we still need to identify the drivers that lead to larger and older stocks of PyC. New methodological developments combining radiocarbon dating on PyC specific compounds, and quantitative estimations of PyC stocks in soils, sediments and dissolved organic carbon should help us to address this issue. Also, the spatial variability within the landscape is still largely unknown, like, for example, the identification of accumulation or preferential losses zones. This would help to identify intermediate pools and better connect the different processes leading from the fire to the oceans. This understanding is a pre-requisite for a third

challenge we identified here, which is the need to include PyC in models.

Up to now, modeling efforts have been very limited, and PyC has been often considered as a passive pool adjusted to explain model mismatches in the long term. As PyC emerges as a substantial contributor to total organic carbon, both in soils and waters, and a much more dynamic one that previously thought, it is now urgent to integrate it into mechanistic models, in order to test the validity of the processes, but also in earth system models, in order to constrain better soil, water and sediment carbon fluxes and budgets.

## AUTHOR CONTRIBUTIONS

SA and CS contributed to the writing and editing of the publication.

## ACKNOWLEDGMENTS

We thank all authors for their contributions and the reviewers for their valuable feedback. They all have made possible this Research Topic. We also thank Satish Myneni, Moritz F. Lehmann, and Francien Peterse for their editorial roles for some of the articles. Special thanks to Rob Bryant for proof-reading this manuscript.

**Conflict of Interest Statement:** The authors declare that the research was conducted in the absence of any commercial or financial relationships that could be construed as a potential conflict of interest.

frontiers in Earth Science

PERSPECTIVE
published: 17 November 2017
doi: 10.3389/feart.2017.00095

# Trial by Fire: On the Terminology and Methods Used in Pyrogenic Organic Carbon Research

*Andrew R. Zimmerman*[1]* *and Siddhartha Mitra*[2]

[1] Department of Geological Sciences, University of Florida, Gainesville, FL, United States, [2] Department of Geological Sciences, East Carolina University, Greenville, NC, United States

Our understanding of the cycling of fire-derived, i.e., pyrogenic organic matter (pyOM), as well as the goals of the community of researchers who study it, may be inhibited by the many terms and methods currently used in its quantification and characterization. Terms currently used for pyOM have evolved by convention, but are often poorly defined. Further, each of the different methods now used to quantify solid and dissolved pyrogenic carbon (pyC) comes with its own biases and artifacts. That is, each detects only a fraction of the total pyrogenic products produced by fire, while, at the same time, include some fraction of non-pyrogenic OM. This may be evident in the commonly observed correlations between pyC and total organic C reported for both soils and dissolved OM in many different systems. We suggest that our research area can be placed on a stronger footing by: (1) agreement upon a common set of terms tied to the method used for detection (e.g., of the form $pyC_{method}$), (2) implementation of another "ring trial" study with a wider set of natural soil and water samples that cross-compare more recently developed methods, and (3) further investigation of the processes which preserve/degrade/transport pyOM in the environment.

**Keywords: pyrogenic carbon, black carbon, quantification, artifacts, biochar, ring trial**

OPEN ACCESS

***Edited by:***
*Cristina Santin,*
*Swansea University, United Kingdom*

***Reviewed by:***
*Michael W. I. Schmidt,*
*University of Zurich, Switzerland*
*Philippa Louise Ascough,*
*Scottish Universities Environmental Research Centre, United Kingdom*
*Michael Ian Bird,*
*James Cook University Cairns, Australia*

***Correspondence:**
*Andrew R. Zimmerman*
*azimmer@ufl.edu*

***Specialty section:***
*This article was submitted to Biogeoscience, a section of the journal Frontiers in Earth Science*

***Received:*** *10 August 2017*
***Accepted:*** *06 November 2017*
***Published:*** *17 November 2017*

***Citation:***
*Zimmerman AR and Mitra S (2017) Trial by Fire: On the Terminology and Methods Used in Pyrogenic Organic Carbon Research. Front. Earth Sci. 5:95. doi: 10.3389/feart.2017.00095*

## INTRODUCTION

The understanding that fire and pyrogenic organic matter (pyOM) have contributed to shaping Earth's biosphere is one that has evolved within a number of disparate fields including geology, ecology, atmosphere science, agriculture/soil science, and anthropology. In each field, this realization, along with associated terminology and methodology, has tended to evolve separately, with limited cross-disciplinary communication. Humans have been using pyOM in industry (charcoal used in the smelting of copper as early as 5,000 BCE) and medicine for thousands of years (Scott and Damblon, 2010). However, formal research into charcoal's properties began as early the beginning of the twentieth century (e.g., Hedin, 1907; Sweetser, 1908; Homfray, 1910). Charcoal was noted in soils even earlier (e.g., Heer, 1866; Fliche, 1907; Godwin and Tansley, 1941), but was not treated quantitatively and used as an indicator of past vegetation and human settlement by paleoecologists and archeologists, respectively, until much later (Western, 1963; Camps, 1971). Detection and quantification of charcoal in marine and lake sediments led to the first use of pyOM as a proxy for past fire-frequency and climate in the 1970's (Smith et al., 1973; Herring, 1976; Swain, 1978), though there was some debate at this time as to its pyrogenic origin (Schopf, 1975).

Consideration of the pyrogenic component of aerosols and the development of the first instrument to measure aerosol soot concentrations (Thomas, 1952) was sparked by the "London fog" of December 1952 which killed at least 4,000 (Wilkins, 1954). The dark color of the filters used to collect the "soot" derived from coal-burning led to use of the term "black carbon" (BC) within the field of atmospheric chemistry (e.g., Novakov, 1981, 1984; Gundel et al., 1984). Novakov (1981, 1984) defined BC as "combustion-produced black particulate carbon having a graphitic microstructure" and soon, the term "BC" was applied more broadly to pyOM in both its atmospheric and geological forms (Goldberg, 1985). However, the term "elemental carbon," reflecting its C-rich character, was and is still also widely used by the atmospheric community, which has largely been concerned with its light absorption and associated direct radiative forcing of Earth's climate (Bond et al., 2004). Although there have been quite a few inter-laboratory comparisons of methods used to quantify aerosol BC (e.g., Countess, 1990; Birch, 1998; Hitzenberger et al., 1999, 2006; Schmid et al., 2001; ten Brink et al., 2004), there is still no universally accepted method for isolating aerosol pyOM (discussed further in next section).

Awareness of elevated atmosphere $CO_2$ and other atmosphere greenhouse gas concentrations in the 1970's led to consideration of the role of fire in the global C cycle. The first estimate of global biomass burning and charcoal production, 500–700 Tg $yr^{-1}$ (Seiler and Crutzen, 1980) was an attempt to balance the poor match between C inputs to the atmosphere with known removal mechanisms. This estimate was since revised downward and is now generally agreed to be in the range of 50–300 Tg $yr^{-1}$ (Kuhlbusch and Crutzen, 1996; Forbes et al., 2006; Bird et al., 2015; Santin et al., 2016). Another turning point in geochemists' understanding of pyOM was the "BC combustion continuum" first proposed by Hedges et al. (2000) and Schmidt and Noack (2000) and later elaborated upon by others (Masiello, 2004; Elmquist et al., 2006; Preston and Schmidt, 2006). It maintained that pyOM is composed of a wide range of materials from slightly charred biomass to highly condensed graphite and soot. With this "continuum perspective" came the wider recognition that pyOM cannot be wholly refractory, but is degraded to different extents through a variety of abiotic and microbially-enhanced processes.

A call to compare methods used to quantify pyrogenic carbon (pyC) in soils and sediments, which requires the use of techniques different from those used in atmospheric sciences due to the presence of interfering matrices, came at much the same time. The first method comparison efforts examined a limited range of sample types (Currie et al., 2002) or resulted in widely ranging values for individual samples (Schmidt et al., 2001). Thus, a "Steering Committee for Black Carbon Reference Materials" was established and recommended a larger set of pyrogenic and non-pyrogenic test materials (Schmidt et al., 2003). The resulting comprehensive evaluation of pyC quantification methods (Hammes et al., 2007), the so called "BC ring trial," made it clear that each analytical method is selective for a different part of the pyOM continuum.

At the same time that soil scientists and agronomists were realizing the potential of soil amendments of pyC to enhance soil fertility and mitigate climate change through C sequestration (Lehmann et al., 2002; Lehmann, 2007a,b), environmental scientists identified substantial amounts of pyC in an ever-widening range of settings including river water (Ding et al., 2013; Jaffe et al., 2013), marshes (Dittmar et al., 2012b) and the ocean (Dittmar, 2008; Stubbins et al., 2010; Ziolkowski and Druffel, 2010). However, all of these pursuits require the ability to accurately quantify pyC and to track the chemical evolution and transport of pyOM in the environment.

## PYROGENIC SUBSTANCES QUANTIFICATION METHODS

The methods used to quantify pyC vary widely in their cost, ease of application, and unfortunately, in the pyOM fraction that they target. These methods can be categorized as those that rely on pyOM detection of: (1) morphology, (2) light absorption, (3) thermal or chemical stability, and (4) chemical composition. Archeologists and some geoscientists commonly use light microscopy and particle morphology to count the number and size of charcoal particles (e.g., Smith et al., 1975; Figueiral and Mosbrugger, 2000; Scott and Damblon, 2010). However, these methods cannot quantify pyC and are biased toward detection of particles of larger sizes (Masiello, 2004; Crawford and Belcher, 2016). Atmospheric scientists quantify pyC using optical techniques (Rosen and Novakov, 1977), thermal heating combined with optical methods, or laser-induced incandescence (Watson et al., 2005; for a historical perspective, see Novakov and Rosen, 2013). While many of these methods are subject to interferences introduced during mixing of combustion-derived aerosols with non-pyrogenic OM (Bond et al., 2013), quantification of pyC in soil or sedimentary matrices is even more difficult due to the even greater presence of minerals and complex non-pyrogenic geopolymers. To cope with this, many approaches assume pyOM to be the most refractory OM fraction. Thus, different thermal and/or chemical oxidation techniques (e.g., CTO-375, dichromate oxidation, UV oxidation, catalytic hydrogen pyrolysis (hy-py) have been used to remove more labile OM and assume the residual to be pyOM (e.g., Lim and Cachier, 1996; Gustafsson et al., 1997, 2001; Thevenon et al., 2010).

A final group of methods identify pyOM using some aspect of its chemical structure. The abundance of both levoglucosan, an anhydrous sugar formed during cellulose combustion (Elias et al., 2001; Kuo et al., 2008), and benzenepolycarboxylic acids (BPCAs) which are formed via nitric acid oxidation (Glaser et al., 1998; Brodowski et al., 2005; Dittmar, 2008) have been used as chemical markers for lower temperature charred OM and condensed aromatic C, respectively. Another technique infers the pyC content of a sample using the sorptive characteristics of pyrene onto the sample (Flores-Cervantes et al., 2009a,b). Spectroscopic tools such as $^{13}$C-nuclear magnetic resonance (NMR) and mid-infrared (MIR) spectroscopy provide information on the structure and chemical bonds of OM present in a material. In the case of NMR, it is generally aromatic C that is quantified and associated with pyC (Simpson and Hatcher, 2004; Nelson and Baldock, 2005), though specialized techniques have been

developed to estimate the condensed aromatic fraction (Knicker et al., 2005; McBeath et al., 2011). Though MIR also examines a sample's spectral characteristics, it requires calibration using one of the other pyC methods in order to be quantitative (Janik et al., 2007; Bornemann et al., 2008; Cotrufo et al., 2016). More detailed reviews of methods used to quantify pyC can be found elsewhere (Meredith et al., 2012; Bird et al., 2015).

## PROBLEMS AND PERPLEXITIES

While the methods used to study pyOM production and cycling have advanced greatly in the last decade, we believe that there are still terminology, methodology/conceptual impediments to further progress that urgently need to be addressed. This inhibits both research funding opportunities and implementation of the fire-science community findings and recommendations, be they in settings of agriculture, policy, or climate/geochemical model incorporation.

### Terminology Issues

From the discussion above, it should be clear that different fire research sub-communities have adopted various terms for pyOM or pyOM fractions, often for historical reasons only. Confusion arises because these terms are often not associated with specific definitions, or because terms have been adopted across research community boundaries without regard for their original narrow definitions. For example, the atmospheric community refers to BC as combustion-generated aerosols that absorb visible light, are insoluble in water, and exist as aggregates of carbon spherules (Novakov, 1984; Bond et al., 2013). On the other hand, BC has come to be used by many as shorthand for pyrogenic C of all forms. The term "dissolved black carbon" conflicts with the atmospheric community's definition that BC should not be soluble in water. Organic compounds detected in the aqueous fraction of combustion-derived aerosols are typically referred to by the atmospheric community as water soluble organic carbon (Decesari et al., 2000; Mayol-Bracero et al., 2002). In the past, soot was defined as the total carbonaceous material produced by combustion (Novakov, 1984). However, for others, soot is the condensate of combustion gases and has graphitic structure (Hammes et al., 2007). The materials referred to as charcoal, biochar, and agrichar may all be the same, or somewhat different (Lehmann and Joseph, 2015). While it is understood that different analytical methods target different pyC fractions, there is as yet no consistent method or property-based terminology applied across different research communities. This lack of consistency may inhibit cross-disciplinary communication and fertilization of new concepts.

### Methodology/Conceptual Issues

Several methodological issues and recent observations should cause us to question our ability to quantify the amount of pyOM (or pyC) in natural samples. The first issue is that many of these methods require a "*conversion factor*" of some type to transform measured parameters such as a post-treatment residue weight or compound abundance to an amount of pyOM or pyC present in a sample. For example, a conversion factor has been calculated based on theoretical BPCA yields of organic structures of marine DOM observed via ultrahigh-resolution mass spectrometry (about 3, Dittmar, 2008; Stubbins et al., 2012) or from the BPCA yields of various aromatic substances including activated C (2.27, Glaser et al., 1998) PAHs, soot and C nanotubes (about 4, Ziolkowski et al., 2011). However, application of any single BPCA conversion factor to a variety of pyOM types has been called into question (Brodowski et al., 2005). For the dichromate oxidation procedure, a correction factor derived from the residual yield of plant char oxidation was used to account for pyC losses during the chemical treatment (Knicker et al., 2008). A degree of uncertainty has been generated in the fire science community because of the variety and range of conversion and correction factors used, even within specific analytical methods.

The second issue is that pyC can be falsely identified as non-pyC and vice versa. Underestimates in pyC quantification certainly occur because not all pyC is recalcitrant or purely condensed aromatic, as assumed by most analytical methods (e.g., Bostick et al., this issue, Nguyen and Lehmann, 2009; Zimmerman, 2010; Singh et al., 2012). Some portion of pyC is likely destroyed in the harsh thermal and chemical oxidation steps used. Overestimates can occur in a number of ways. Not all non-pyC is removed by thermal/chemical oxidation steps (e.g., Knicker et al., 2007). Oxidative treatments can even generate apparently "pyrogenic" OM (e.g., Derenne and Largeau, 2001; Hammes et al., 2007; Novakov and Rosen, 2013). This has been shown to occur, for example, during the oxidation required to form BPCA compounds (Brodowski et al., 2005; Kappenberg et al., 2016) as well as in steps used to remove non-pyrogenic aromatic C prior to NMR analysis (Simpson and Hatcher, 2004). Other NMR quantification approaches use spectral editing or molecular mixing models to separate condensed aromatic from non-condensed aromatic biomolecules, both of which require assumptions or corrections that have not been fully validated (Cusack et al., 2012; Paetsch et al., 2017). Light absorption-based methods used mainly by atmosphere chemists suffer from uncertainties related to non-linearities in the light attenuation coefficient which vary with filter loading and particle type, as well as to interferences from non-pyrogenic OM (reviewed in Kirchstetter and Novakov, 2007).

Light absorption, BPCA and some NMR quantification techniques use the assumption that only pyOM, takes the form of condensed aromatics structures. But increasingly, this has been shown not to be the case. For instance, melanoidins, several plants, fungi and pigments yielded quantities of BPCAs (even highly-carboxylated BPCAs which are indicative of very condensed aromatic OM) like that of charred plant material (Brodowski et al., 2005; Glaser and Knorr, 2008). These may be derived from lignin or tannin, which include a wide variety of polycondensed aromatics (Hernes and Hedges, 2000; Waggoner et al., 2015). Other non-pyrogenic OM sources of condensed aromatic OM are abundant in the geosphere, including woody peat, coal, kerogen, and oil (Yoshioka and Ishiwatari, 2005; Hammes et al., 2007; Wang et al., 2012; Hartman et al., 2015; Li et al., 2017). Still other studies have found that non-pyrogenic OM can be readily transformed to condensed aromatic OM, which would appear to be pyrogenic, through photolytic,

microbial, or chemical degradative processes (Glaser and Knorr, 2008; Chen et al., 2014; Waggoner et al., 2015; DiDonato et al., 2016).

Given that we are finding ever more ways in which pyOM can cross the analytical window into non-pyOM and vice versa, it is perhaps not surprising that many have observed correlations between pyC and total C concentrations in soils regionally (Glaser and Amelung, 2003; Jauss et al., 2015; Ahmed et al., 2017; Qi et al., 2017) and globally (Reisser et al., 2016), and dissolved in natural waters regionally (Dittmar et al., 2012a; Ding et al., 2013, 2014, 2015; Guerena et al., 2015) and globally (Jaffe et al., 2013; Wagner et al., 2015) and even in aqueous leachates of marine aerosols (Bao et al., 2017). These correlations indicate, as do other more detailed statistical examinations (in the same studies), a lack of dependence of pyC concentrations on fire history or climate. A plot of data compiled by a recent literature review (Reisser et al., 2016) shows a significant relationship between pyC and total C in global soils across all quantification methods and within each method (except CTO-375, **Figure 1**). The strongest correlations are found for data derived from BPCA and NMR, suggesting that these methods may have the greatest likelihood for artifacts that misidentify pyC. Alternatively, the finding of correlation between pyC and total C regardless of the analytical method used, might suggest the relationship is present in nature. That is, production, degradation/preservation or mobilization processes may act on pyC and non-pyC in ways that cause them to co-vary. For example, regions of higher productivity, thus higher soil C, also have more biomass to burn and are therefore likely to have greater pyC in soils and drainage waters (Alexis et al., 2007; van Leeuwen et al., 2014). Soils with greater amounts of clay or metal oxide mineral or even charcoals, are likely to sorb and therefore protect both pyOM and non-pyOM from microbial mineralization through sorptive protection (Kasozi et al., 2010; Zimmerman et al., 2011) or aggregate stabilization (Wang et al., 2017). And soil translocation, erosion, leaching, and other hydrologic/climatic-related processes of a region are likely to act to mobilize both pyOM and non-pyOM in similar ways (Hilscher and Knicker, 2011; Jien and Wang, 2013), though not necessarily to equal extents (Rumpel et al., 2009). Finally, it has been suggested that pyC mobilization may occur via association with other OM in dissolved (Jaffe et al., 2013) or perhaps colloidal (Zand and Grathwohl, 2016; Kumari et al., 2017) form, but the controlling mechanisms are still unknown (Wagner et al., 2017).

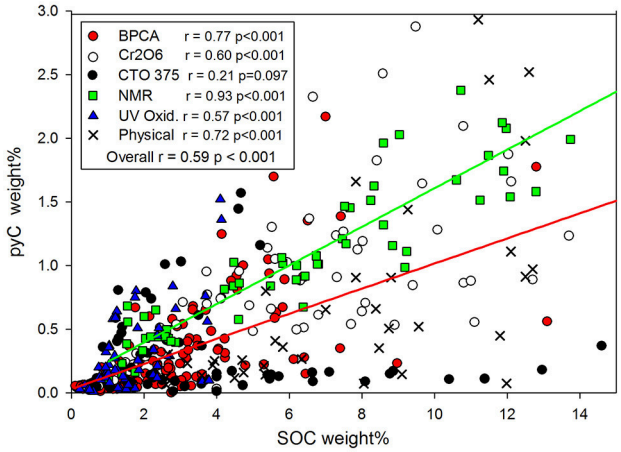


**FIGURE 1 |** Relationships between total soil organic carbon (SOC) and pyrogenic carbon (pyC) as determined by different methods. Pearson linear correlation coefficients (*r*) and levels of significance (*p*) are given in the legend. Data are taken from Reisser et al. (2016), a compilation of results of global soil data from 55 studies.

## RECOMMENDATIONS

Despite, or possibly even because of the many issues facing the pyC cycling research community, we may be on the brink of making great advances in this field, but only if these issues are acknowledged and dealt with. First, we suggest more stringent use of terminology. The terms "pyOM" or "pyC" should be used when referring to the totality of fire-derived carbonaceous substances. These terms represent the broadest short forms for the total substance of pyrogenic origin and the carbon in these substances, respectively. When reporting analytical results, we suggest that terms tied to the method or properties used for detection should be used. For greatest clarity, we these terms could take the form "$pyC_{method}$" (**Figure 2**). For example, substances quantified via light microscopy might be referred to as $pyC_{mic}$. Substances isolated based on their chemical or thermal resistance could be designated $pyC_{CTR}$. The term "$pyC_{LE}$" should be used for substances detected based upon their near complete light extinction properties, but failing to convince the mainly atmospheric community of this, we suggest that terrestrial and aquatic scientists leave the term "black carbon" to them. Use of these terms will serve as continuous reminder that a quantity of C refers only to a portion of the substances produced by fires and may even contain a non-pyrogenic portion.

Regarding the potential for analytical artifacts that plague pyC cycling research, we recommend, first, that another "ring trial" study be conducted so that techniques that have been developed since the last ring trial (such as MIR spectroscopy and catalytic hydrogen pyrolysis and improvements in NMR and BPCA analytical methods) can be compared and their relative strengths and weaknesses re-evaluated. This ring study should include not just geochemists, but also those that study pyOM from the anthropology, atmosphere and agriculture communities. Moreover, the new ring trial should also make use of modern analytical techniques that can deconvolve composition of pyOM at unprecedented levels (e.g., aerosol mass spectrometer, Fourier transform ion cyclotron resonance mass spectrometer). In addition to the set of pyrogenic and "potentially interfering" materials included in the first ring trial (Hammes et al., 2007), this new ring trial should include a biochar thermal series, which would be expected to have a regularly increasing degree of aromatic condensation (Cao et al., 2012). Furthermore, we recommend a broader set of atmosphere-derived samples such as the diesel soot standard (NIST

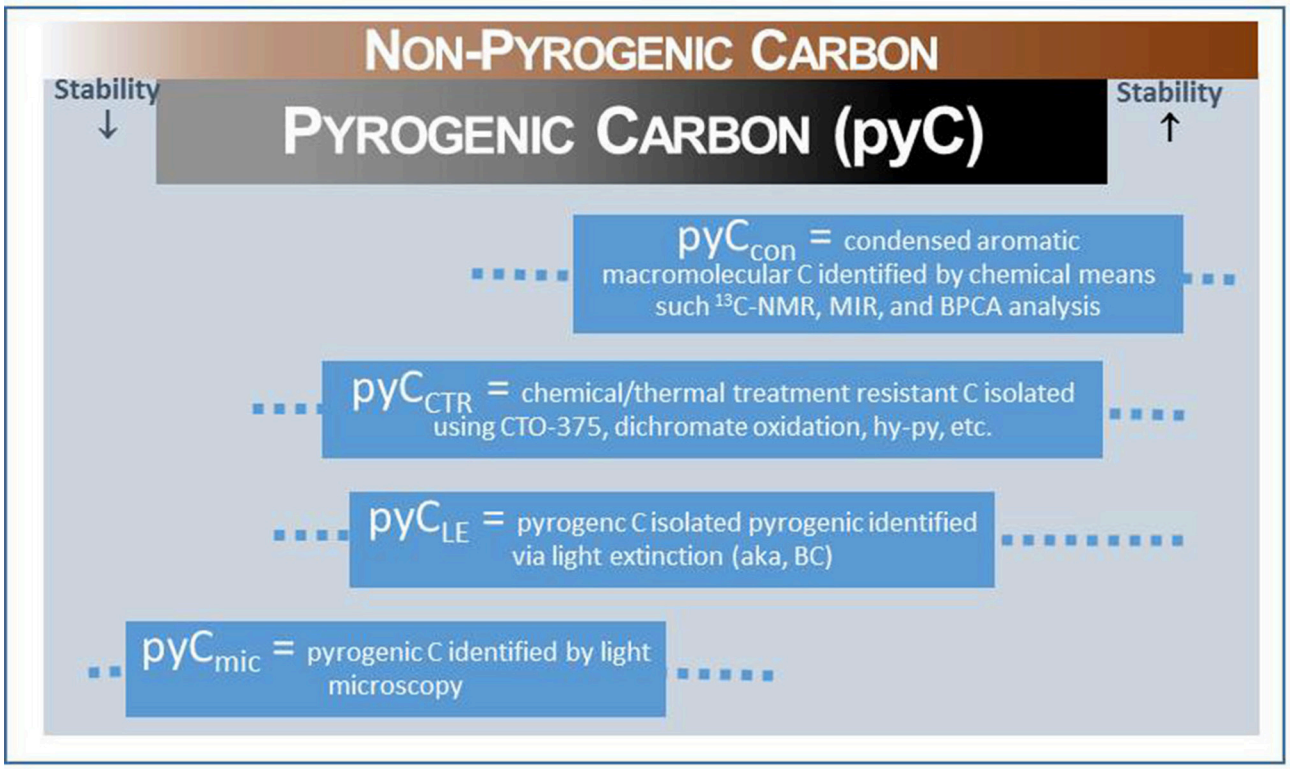


**FIGURE 2 |** Proposed pyrogenic carbon terminology based upon methods used for identification/quantification and estimated placement of these materials on the "combustion/stability continuum." Dotted lines represent estimated uncertainly range.

SRM 2975) and aqueous samples (preferably not freeze-dried) isolated from river and ocean water. Additional non-pyrogenic materials such as wood biomass, leachate from this biomass, and photodegraded biomass leachate should also be considered for analyses. To evaluate matrix effects associated with each method, a standard addition experiment should be added to the method intercomparison, whereby different amounts of a pyOM, such as wood char, are added to a soil-like mixture containing no pyOM. This ring trial should be followed up not only with a report of results, but with a best-practices paper that includes consensus recommendations for use of terminology.

Until now, the focus of many fire science studies has been to establish properties of pyrogenic substances and their inventories in different systems. Given the major question of the cause of the often-observed pyC/TOC correlation, a greater focus should be placed on studies that compare transformation and movement of pyrogenic relative to different types of non-pyrogenic substances. Mechanistic pyOM investigations are needed to understand both preservation processes such as adsorption, metal-complexation and aggregate formation, and transformation processes such as solubilization, volatilization, and microbial, chemical and photo-degradation. In addition, pyC mobilization studies should focus not just on particle movement in soil via translocation and erosion, but transport in aerosol, colloid, and dissolved forms via atmosphere and aqueous processes. We hope this comment stimulates greater dialog between research communities that study various aspects of pyrogenic substances. The desired result would be not only a more complete understanding of the production and cycling of pyC, but also a greater application of these insights in such areas as agriculture and climate modeling.

## AUTHOR CONTRIBUTIONS

All authors listed have made a substantial, direct and intellectual contribution to the work, and approved it for publication.

## FUNDING

This work was funded by the U.S. National Science Foundation—Geobiology and Low-Temperature Geochemistry Program (EAR-1451367).

## ACKNOWLEDGMENTS

This work was substantially improved through helpful conversations with Drs. Gerard Cornelissen and Michael Bird.

## REFERENCES


Ahmed, Z. U., Woodbury, P. B., Sanderman, J., Hawke, B., Jauss, V., Solomon, D., et al. (2017). Assessing soil carbon vulnerability in the Western USA by geospatial modeling of pyrogenic and particulate carbon stocks. *J. Geophys. Res. Biogeosci.* 122, 354–369. doi: 10.1002/2016JG003488

Alexis, M. A., Rasse, D. P., Rumpel, C., Bardoux, G., Pechot, N., Schmalzer, P., et al. (2007). Fire impact on C and N losses and charcoal production in a scrub oak ecosystem. *Biogeochemistry* 82, 201–216. doi: 10.1007/s10533-006-9063-1

Bao, H. Y., Niggemann, J., Luo, L., Dittmar, T., and Kao, S. J. (2017). Aerosols as a source of dissolved black carbon to the ocean. *Nat. Commun.* 8, 1–7. doi: 10.1038/s41467-017-00437-3

Birch, M. E. (1998). Analysis of carbonaceous aerosols: interlaboratory comparison. *Analyst* 123, 851–857. doi: 10.1039/a800028j

Bird, M. I., Wynn, J. G., Saiz, G., Wurster, C. M., and McBeath, A. (2015). The Pyrogenic Carbon Cycle. *Annu. Rev. Earth Planet. Sci.* 43, 273–298. doi: 10.1146/annurev-earth-060614-105038

Bond, T. C., Doherty, S. J., Fahey, D. W., Forster, P. M., Berntsen, T., DeAngelo, B. J., et al. (2013). Bounding the role of black carbon in the climate system: a scientific assessment. *J. Geophys. Res. Atmospheres* 118, 5380–5552. doi: 10.1002/jgrd.50171

Bond, T. C., Streets, D. G., Yarber, K. F., Nelson, S. M., Woo, J. H., and Klimont, Z. (2004). A technology-based global inventory of black and organic carbon emissions from combustion. *J. Geophys. Res.* 109:D14203. doi: 10.1029/2003JD003697

Bornemann, L., Welp, G., Brodowski, S., Rodionov, A., and Amelung, W. (2008). Rapid assessment of black carbon in soil organic matter using mid-infrared spectroscopy. *Org. Geochem.* 39, 1537–1544. doi: 10.1016/j.orggeochem.2008.07.012

Brodowski, S., Rodionov, A., Haumaier, L., Glaser, B., and Amelung, W. (2005). Revised black carbon assessment using benzene polycarboxylic acids. *Org. Geochem.* 36, 1299–1310. doi: 10.1016/j.orggeochem.2005.03.011

Camps, G. (1971). Study of prehistoric charcoal – preparation of thin sections and structural analysis – French - Couvert, M. *Anthropologie* 75, 282–283.

Cao, X., Pignatello, J. J., Li, Y., Lattao, C., Chappell, M. A., Chen, N., et al. (2012). Characterization of wood chars produced at different temperatures using advanced solid-state 13C NMR spectroscopic techniques. *Energy Fuels* 26, 5983–5991. doi: 10.1021/ef300947s

Chen, H. M., Abdulla, H. A. N., Sanders, R. L., Myneni, S. C. B., Mopper, K., and Hatcher, P. G. (2014). Production of black carbon-like and aliphatic molecules from terrestrial dissolved organic matter in the presence of sunlight and iron. *Environ. Sci. Technol. Lett.* 1, 399–404. doi: 10.1021/ez5002598

Cotrufo, M. F., Boot, C., Abiven, S., Foster, E. J., Haddix, M., Reisser, M., et al. (2016). Quantification of pyrogenic carbon in the environment: an integration of analytical approaches. *Org. Geochem.* 100, 42–50. doi: 10.1016/j.orggeochem.2016.07.007

Countess, R. J. (1990). Interlaboratory analysis of carbonaceous aerosol samples. *Aerosol Sci. Technol.* 12, 114–121. doi: 10.1080/02786829008959331

Crawford, A. J., and Belcher, C. M. (2016). Area-volume relationships for fossil charcoal and their relevance for fire history reconstruction. *Holocene* 26, 822–826. doi: 10.1177/0959683615618264

Currie, L. A., Benner, B. A. Jr., Kessler, J. D., Klinedinst, D. B., Klouda, G. A., Marolf, J. V. et al. (2002). A critical evaluation of interlaboratory data on total, elemental, and isotopic carbon in the carbonaceous particle reference material, NIST SRM 1649a. *J. Natl. Inst. Stand. Technol.* 107, 279–298. doi: 10.6028/jres.107.022

Cusack, D. F., Chadwick, O. A., Hockaday, W. C., and Vitousek, P. M. (2012). Mineralogical controls on soil black carbon preservation. *Glob. Biogeochem. Cycle* 26:GB2019. doi: 10.1029/2011GB004109

Decesari, S., Facchini, M. C., Fuzzi, S., and Tagliavini, E. (2000). Characterization of water-soluble organic compounds in atmospheric aerosol: a new approach. *J. Geophys. Res. Atmos.* 105, 1481–1489. doi: 10.1029/1999JD900950

Derenne, S., and Largeau, C. (2001). A review of some important families of refractory macromolecules: composition, origin, and fate in soils and sediments. *Soil Sci.* 166, 833–847. doi: 10.1097/00010694-200111000-00008

DiDonato, N., Chen, H. M., Waggoner, D., and Hatcher, P. G. (2016). Potential origin and formation for molecular components of humic acids in soils. *Geochim. Cosmochim. Acta* 178, 210–222. doi: 10.1016/j.gca.2016.01.013

Ding, Y., Cawley, K. M., da Cunha, C. N., and Jaffe, R. (2014). Environmental dynamics of dissolved black carbon in wetlands. *Biogeochemistry* 119, 259–273. doi: 10.1007/s10533-014-9964-3

Ding, Y., Yamashita, Y., Dodds, W. K., and Jaffe, R. (2013). Dissolved black carbon in grassland streams: is there an effect of recent fire history? *Chemosphere* 90, 2557–2562. doi: 10.1016/j.chemosphere.2012.10.098

Ding, Y., Yamashita, Y., Jones, J., and Jaffe, R. (2015). Dissolved black carbon in boreal forest and glacial rivers of central Alaska: assessment of biomass burning versus anthropogenic sources. *Biogeochemistry* 123, 15–25. doi: 10.1007/s10533-014-0050-7

Dittmar, T. (2008). The molecular level determination of black carbon in marine dissolved organic matter. *Org. Geochem.* 39, 396–407. doi: 10.1016/j.orggeochem.2008.01.015

Dittmar, T., de Rezende, C. E., Manecki, M., Niggemann, J., Ovalle, A. R. C., Stubbins, A., et al. (2012a). Continuous flux of dissolved black carbon from a vanished tropical forest biome. *Nat. Geosci.* 5, 618–622. doi: 10.1038/ngeo1541

Dittmar, T., Paeng, J., Gihring, T. M., Suryaputra, I., and Huettel, M. (2012b). Discharge of dissolved black carbon from a fire-affected intertidal system. *Limnol. Oceanogr.* 57, 1171–1181. doi: 10.4319/lo.2012.57.4.1171

Elias, V. O., Simoneit, B. R. T., Cordeiro, R. C., and Turcq, B. (2001). Evaluating levoglucosan as an indicator of biomass burning in Carajas, Amazonia: a comparison to the charcoal record. *Geochim. Cosmochim. Acta* 65, 267–272. doi: 10.1016/S0016-7037(00)00522-6

Elmquist, M., Cornelissen, G., Kukulska, Z., and Gustafsson, Ö. (2006). Distinct oxidative stabilities of char versus soot black carbon: implications for quantification and environmental recalcitrance. *Glob. Biogeochem. Cycle* 20:GB2009. doi: 10.1029/2005GB002629

Figueiral, I., and Mosbrugger, V. (2000). A review of charcoal analysis as a tool for assessing quaternary and tertiary environments: achievements and limits. *Palaeogeogr. Palaeoclimatol. Palaeoecol.* 164, 397–407. doi: 10.1016/S0031-0182(00)00195-4

Fliche, P. (1907). Note sur un charbon quaternaire de Chataignier. *Bull. Soc. Bot. Fr.* 54, 132–136. doi: 10.1080/00378941.1907.10831239

Flores-Cervantes, D. X., Plata, D. L., MacFarlane, J. K., Reddy, C. M., and Gschwend, P. M. (2009a). Black carbon in marine particulate organic carbon: inputs and cycling of highly recalcitrant organic carbon in the Gulf of Maine. *Mar. Chem.* 113, 172–181. doi: 10.1016/j.marchem.2009.01.012

Flores-Cervantes, D. X., Reddy, C. M., and Gschwend, P. M. (2009b). Inferring black carbon concentrations in particulate organic matter by observing pyrene fluorescence losses. *Environ. Sci. Technol.* 43, 4864–4870. doi: 10.1021/es900043c

Forbes, M. S., Raison, R. J., and Skjemstad, J. O. (2006). Formation, transformation and transport of black carbon (charcoal) in terrestrial and aquatic ecosystems. *Sci. Total Environ.* 370, 190–206. doi: 10.1016/j.scitotenv.2006.06.007

Glaser, B., and Amelung, W. (2003). Pyrogenic carbon in native grassland soils along a climosequence in North America. *Glob. Biogeochem. Cycle* 17, 1064. doi: 10.1029/2002GB002019

Glaser, B., Haumaier, L., Guggenberger, G., and Zech, W. (1998). Black carbon in soils: the use of benzenecarboxylic acid as specific markers. *Org. Geochem.* 29, 811–819. doi: 10.1016/S0146-6380(98)00194-6

Glaser, B., and Knorr, K. H. (2008). Isotopic evidence for condensed aromatics from non-pyrogenic sources in soils - implications for current methods for quantifying soil black carbon. *Rapid Commun. Mass Spectrom.* 22, 935–942. doi: 10.1002/rcm.3448

Godwin, H., and Tansley, A. G. (1941). Prehistoric charcoals as evidence of former vegetation, soil and climate. *J. Ecol.* 29, 117–126. doi: 10.2307/2256222

Goldberg, E. (1985). *Black Carbon in the Environment: Properties and Distribution*. New York, NY: John Wiley and Sons.

Guerena, D. T., Lehmann, J., Walter, T., Enders, A., Neufeldt, H., Odiwour, H., et al. (2015). Terrestrial pyrogenic carbon export to fluvial ecosystems: lessons learned from the White Nile watershed of East Africa. *Glob. Biogeochem. Cycle* 29, 1911–1928. doi: 10.1002/2015GB005095

Gundel, L. A., Dod, R. L., Rosen, H., and Novakov, T. (1984). The relationship between optical attenuation and black carbon concentration for ambient and source particles. *Sci. Total Environ.* 36, 197–202. doi: 10.1016/0048-9697(84)90266-3

Gustafsson, O., Bucheli, T. D., Kululska, M., Andersson, C., Largeau, C., Rouzard, J. N., et al. (2001). Evaluation of a protocol for the quantification of black carbon

in sediments, soils, and aquatic sediments. *Glob. Biogeochem. Cycle* 15, 881–890. doi: 10.1029/2000GB001380

Gustafsson, O., Haghseta, F., Chan, C., MacFarlane, J., and Gschwend, P. M. (1997). Quantification of the dilute sedimentary soot phase: implications for PAH speciation and bioavailability. *Environ. Sci. Technol.* 31, 203–209. doi: 10.1021/es960317s

Hammes, K., Schmidt, M. W. I., Smernik, R. J., Currie, L. A., Ball, W. P., Nguyen, T. H., et al. (2007). Comparison of quantification methods to measure fire-derived (black/elemental) carbon in soils and sediments using reference materials from soil, water, sediment and the atmosphere. *Glob. Biogeochem. Cycle* 21:GB3016. doi: 10.1029/2006GB002914

Hartman, B. E., Chen, H. M., and Hatcher, P. G. (2015). A non-thermogenic source of black carbon in peat and coal. *Int. J. Coal Geol.* 144, 15–22. doi: 10.1016/j.coal.2015.03.011

Hedges, J. I., Eglinton, G., Hatcher, P. G., Kirchman, D. L., Arnosti, C., Derenne, S., et al. (2000). The molecularly-uncharacterized component of nonliving organci matter in natural environments. *Org. Geochem.* 31, 945–958. doi: 10.1016/S0146-6380(00)00096-6

Hedin, S. G. (1907). On extraction by casein of trypsin, adsorbed by charcoal. *Biochem. J.* 2, 81–88. doi: 10.1042/bj0020081

Heer, O. (1866). "Die Pflanzen der Pfahlbauten," in *Neujahrsblatt, Herausgegeben von der Naturforschende Gesellschaft Zürich,* 1–54.

Hernes, P. J., and Hedges, J. I. (2000). Determination of condensed tannin monomers in environmental samples by capillary gas chromatography of acid depolymerization extracts. *Anal. Chem.* 72, 5115–5124. doi: 10.1021/ac991301y

Herring, J. R. (1976). Cenozoic charcoal flux increase to North Pacific sediments. *Trans. Am. Geophys. Union* 57, 259–259.

Hilscher, A., and Knicker, H. (2011). Degradation of grass-derived pyrogenic organic material, transport of the residues within a soil column and distribution in soil organic matter fractions during a 28 month microcosm experiment. *Org. Geochem.* 42, 42–54. doi: 10.1016/j.orggeochem.2010.10.005

Hitzenberger, R., Jennings, S. G., Larson, S. M., Dillner, A., Cachier, H., Galambos, Z., et al. (1999). Intercomparison of measurement methods for black carbon aerosols. *Atmos. Environ.* 33, 2823–2833. doi: 10.1016/S1352-2310(98)00360-4

Hitzenberger, R., Petzold, A., Bauer, H., Ctyroky, P., Pouresmaeil, P., Laskus, L., et al. (2006). Intercomparison of thermal and optical measurement methods for elemental carbon and black carbon at an urban location. *Environ. Sci. Technol.* 40, 6377–6383. doi: 10.1021/es051228v

Homfray, I. F. (1910). On the absorption of gases by charcoal. *Proc. Royal Soc. Lond. Ser. A Contain. Pap. Math. Phys. Character* 84, 99–106. doi: 10.1098/rspa.1910.0060

Jaffe, R., Ding, Y., Niggemann, J., Vahatalo, A. V., Stubbins, A., Spencer, R. G. M., et al. (2013). Global charcoal mobilization from soils via dissolution and riverine transport to the oceans. *Science* 340, 345–347. doi: 10.1126/science.1231476

Janik, L. J., Skjemstad, J. O., Shepherd, K. D., and Spouncer, L. R. (2007). The prediction of soil carbon fractions using mid-infrared-partial least square analysis. *Aust. J. Soil Res.* 45, 73–81. doi: 10.1071/SR06083

Jauss, V., Johnson, M., Krull, E., Daub, M., and Lehmann, J. (2015). Pyrogenic carbon controls across a soil catena in the Pacific Northwest. *Catena* 124, 53–59. doi: 10.1016/j.catena.2014.09.001

Jien, S.-H., and Wang, C.-S. (2013). Effects of biochar on soil properties and erosion potential in a highly weathered soil. *Catena* 110, 225–233. doi: 10.1016/j.catena.2013.06.021

Kappenberg, A., Blaesing, M., Lehndorff, E., and Amelung, W. (2016). Black carbon assessment using benzene polycarboxylic acids: limitations for organic-rich matrices. *Org. Geochem.* 94, 47–51. doi: 10.1016/j.orggeochem.2016.01.009

Kasozi, G. N., Zimmerman, A. R., Nkedi-Kizza, P., and Gao, B. (2010). Catechol and humic acid sorption onto a range of laboratory-produced black carbons (biochars). *Environ. Sci. Technol.* 44, 6189–6195. doi: 10.1021/es1014423

Kirchstetter, T. W., and Novakov, T. (2007). Controlled generation of black carbon particles from a diffusion flame and applications in evaluating black carbon measurement methods. *Atmos. Environ.* 41, 1874–1888. doi: 10.1016/j.atmosenv.2006.10.067

Knicker, H., Hilscher, A., Gonzalez-Vila, F. J., and Almendros, G. (2008). A new conceptual model for the structural properties of char produced during vegetation fires. *Org. Geochem.* 39, 935–939. doi: 10.1016/j.orggeochem.2008.03.021

Knicker, H., Muffler, P., and Hilscher, A. (2007). How useful is chemical oxidation with dichromate for the determination of "black carbon" in fire-affected soils? *Geoderma* 142, 178–196. doi: 10.1016/j.geoderma.2007.08.010

Knicker, H., Totsche, K. U., Almendros, G., and Gonzalez-Vila, F. J. (2005). Condensation degree of burnt peat and plant residues and the reliability of solid-state VACP MAS C-13 NMR spectra obtained from pyrogenic humic material. *Org. Geochem.* 36, 1359–1377. doi: 10.1016/j.orggeochem.2005.06.006

Kuhlbusch, T., and Crutzen, P. (1996). "Black carbon, the global carbon cycle, and atmospheric carbon dioxide," in *Biomass Burning and Global Change,* ed J. Levine (Cambridge, MA: The MIT Press), Chapter 16, 160–169.

Kumari, K., Moldrup, P., Paradelo, M., Elsgaard, L., and de Jonge, L. W. (2017). Effects of biochar on dispersibility of colloids in agricultural soils. *J. Environ. Qual.* 46, 143–152. doi: 10.2134/jeq2016.08.0290

Kuo, L. J., Herbert, B. E., and Louchouarn, P. (2008). Can levoglucosan be used to characterize and quantify char/charcoal black carbon in environmental media? *Org. Geochem.* 39, 1466–1478. doi: 10.1016/j.orggeochem.2008.04.026

Lehmann, J. (2007a). Bio-energy in the black. *Front. Ecol. Environ.* 5, 381–387. doi: 10.1890/1540-9295(2007)5[381:BITB]2.0.CO;2

Lehmann, J. (2007b). A handful of carbon. *Nature* 447, 143–144. doi: 10.1038/447143a

Lehmann, J., and Joseph, S. (2015). "Biochar for environmental management: an introduction," in *Environmental Management: Science, Technology and Implementation,* eds J. Lehmann, and S. Joseph (London: Earthscan), 235.

Lehmann, J., da Silva, J. P. Jr., Rondon, M., Cravo, M., Greenwood, J., Hehls, B. et al. (2002). "Slash and char: a feasible alternative for soil fertility management in the central amazon?" in *17th World Conference of Soil Science*, ed S. T1UoS (Bangkok: International Union of Soil Sciences), 449, 1–12.

Li, W. B., Hou, Y. C., Yang, F., and Wu, W. Z. (2017). Production of benzene carboxylic acids and small-molecule fatty acids from lignite by two-stage alkali-oxygen. *Ind. Eng. Chem. Res.* 56, 1971–1978. doi: 10.1021/acs.iecr.6b04562

Lim, B., and Cachier, H. (1996). Determination of black carbon by chemical oxidation and thermal treatment in recent marine and lake sediments and cretaceous-tertiary clays. *Chem. Geol.* 131, 143–154. doi: 10.1016/0009-2541(96)00031-9

Masiello, C. A. (2004). New directions in black carbon organic geochemistry. *Mar. Chem.* 92, 201–213. doi: 10.1016/j.marchem.2004.06.043

Mayol-Bracero, O. L., Gabriel, R., Andreae, M. O., Kirchstetter, T. W., Novakov, T., Ogren, J., et al. (2002). Carbonaceous aerosols over the Indian ocean during the Indian ocean experiment (INDOEX): chemical characterization, optical properties, and probable sources. *J. Geophys. Res.* 107, 8030. doi: 10.1029/2000JD000039

McBeath, A. V., Smernik, R. J., Schneider, M. P. W., Schmidt, M. W. I., and Plant, E. L. (2011). Determination of the aromaticity and the degree of aromatic condensation of a thermosequence of wood charcoal using NMR. *Org. Geochem.* 42, 1194–1202. doi: 10.1016/j.orggeochem.2011.08.008

Meredith, W., Ascough, P. L., Bird, M. I., Large, D. J., Snape, C. E., Sun, Y., et al. (2012). Assessment of hydropyrolysis as a method for the quantification of black carbon using standard reference materials. *Geochim. Cosmochim. Acta* 97, 131–147. doi: 10.1016/j.gca.2012.08.037

Nelson, P. N., and Baldock, J. A. (2005). Estimating the molecular composition of a diverse range of natural organic materials from solid-state $^{13}$C NMR and elemental analyses. *Biogeochemistry* 72, 1–34. doi: 10.1007/s10533-004-0076-3

Nguyen, B. T., and Lehmann, J. (2009). Black carbon decomposition under varying water regimes. *Org. Geochem.* 40, 846–853. doi: 10.1016/j.orggeochem.2009.05.004

Novakov, T. (1981). "Microchemical characterization of aerosols," in *Proceedings of the 8th International Microchemical Symposium,* eds H. Malissa, M. Grasserbauer, and R. Belcher (Graz: Springer), 141–165.

Novakov, T. (1984). The role of soot and primary oxidants in atmospheric chemistry. *Sci. Total Environ.* 36, 1–10. doi: 10.1016/0048-9697(84)90241-9

Novakov, T., and Rosen, H. (2013). The black carbon story: early history and new perspectives. *Ambio* 42, 840–851. doi: 10.1007/s13280-013-0392-8

Paetsch, L., Mueller, C. W., Rumpel, C., Angst, Š., Wiesheu, A. C., Girardin, C., et al. (2017). A multi-technique approach to assess the fate of biochar in soil and to quantify its effect on soil organic matter composition. *Organ. Geochem.* 112, 177–186. doi: 10.1016/j.orggeochem.2017.06.012

Preston, C. M., and Schmidt, M. W. I. (2006). Black (pyrogenic) carbon: a synthesis of current knowledge and uncertainties with special

consideration of boreal regions. *Biogeosciences* 3, 397–420. doi: 10.5194/bg-3-397-2006

Qi, F. J., Naidu, R., Bolan, N. S., Dong, Z. M., Yan, Y. B., Lamb, D., et al. (2017). Pyrogenic carbon in Australian soils. *Sci. Total Environ.* 586, 849–857. doi: 10.1016/j.scitotenv.2017.02.064

Reisser, M., Purves, R. S., Schmidt, M. W. I., and Abiven, S. (2016). Pyrogenic carbon in soils: a literature-based inventory and a global estimation of its content in soil organic carbon and stocks. *Front. Earth Sci.* 4:80. doi: 10.3389/feart.2016.00080

Rosen, H., and Novakov, T. (1977). Raman scattering and the characterisation of atmospheric aerosol particles. *Nature* 266, 708–710. doi: 10.1038/266708a0

Rumpel, C., Ba, A., Darboux, F., Chaplot, V., and Planchon, O. (2009). Erosion budget and process selectivity of black carbon at meter scale. *Geoderma* 154, 131–137. doi: 10.1016/j.geoderma.2009.10.006

Santin, C., Doerr, S. H., Kane, E. S., Masiello, C. A., Ohlson, M., de la Rosa, J. M., et al. (2016). Towards a global assessment of pyrogenic carbon from vegetation fires. *Glob. Chang. Biol.* 22, 76–91. doi: 10.1111/gcb.12985

Schmid, H., Laskus, L., Abraham, H. J., Baltensperger, U., Lavanchy, V., Bizjak, M., et al. (2001). Results of the "carbon conference" international aerosol carbon round robin test stage I. *Atmos. Environ.* 35, 2111–2121. doi: 10.1016/S1352-2310(00)00493-3

Schmidt, M. W. I., Masiello, C. A., and Skjemstad, J. O. (2003). Final recommendations for reference materials in black carbon analysis. *Eos Trans. AGU* 84, 582–583. doi: 10.1029/2003EO520006

Schmidt, M. W. I., and Noack, A. G. (2000). Black carbon in soils and sediments: analysis, distribution, implications, and current challenges. *Glob. Biogeochem. Cycle* 14, 777–793. doi: 10.1029/1999GB001208

Schmidt, M. W. I., Skjemstad, J. O., Czimczik, C. I., Glaser, B., Prentice, K. M., Gelinas, Y., et al. (2001). Comparative analysis of black carbon in soils. *Glob. Biogeochem. Cycle* 15, 163–167. doi: 10.1029/2000GB001284

Schopf, J. M. (1975). Modes of fossil preservation. *Rev. Palaeobot. Palynol.* 20, 27–53. doi: 10.1016/0034-6667(75)90005-6

Scott, A. C., and Damblon, F. (2010). Charcoal: taphonomy and significance in geology, botany and archaeology. *Palaeogeogr. Palaeoclimatol. Palaeoecol.* 291, 1–10. doi: 10.1016/j.palaeo.2010.03.044

Seiler, W., and Crutzen, P. J. (1980). Estimates of gross and net fluxes of carbon between the biosphere and the atmosphere from biomass burning. *Clim. Change* 2, 207–247. doi: 10.1007/BF00137988

Simpson, M. J., and Hatcher, P. G. (2004). Determination of black carbon in natural organic matter by chemical oxidation and solid-state $^{13}C$ nuclear magnetic resonance spectroscopy. *Org. Geochem.* 35, 923–935. doi: 10.1016/j.orggeochem.2004.04.004

Singh, N., Abiven, S., Torn, M. S., and Schmidt, M. W. I. (2012). Fire-derived organic carbon in soil turns over on a centennial scale. *Biogeosciences* 9, 2847–2857. doi: 10.5194/bg-9-2847-2012

Smith, D. M., Griffin, J. J., and Goldberg, E. D. (1973). Elemental carbon in marine sediments - baseline for burning. *Nature* 241, 268–270. doi: 10.1038/241268a0

Smith, D. M., Griffin, J. J., and Goldberg, E. D. (1975). Spectrometric method for the quantitative determination of elemental carbon. *Anal. Chem.* 47, 233–238. doi: 10.1021/ac60352a032

Stubbins, A., Hood, E., Raymond, P. A., Aiken, G. R., Sleighter, R. L., Hernes, P. J., et al. (2012). Anthropogenic aerosols as a source of ancient dissolved organic matter in glaciers. *Nat. Geosci.* 5, 198–201. doi: 10.1038/ngeo1403

Stubbins, A., Spencer, R. G. M., Chen, H. M., Hatcher, P. G., Mopper, K., Hernes, P. J., et al. (2010). Illuminated darkness: molecular signatures of Congo river dissolved organic matter and its photochemical alteration as revealed by ultrahigh precision mass spectrometry. *Limnol. Oceanogr.* 55, 1467–1477. doi: 10.4319/lo.2010.55.4.1467

Swain, A. M. (1978). Environmental changes during the past 2000 years in north-central Wisconsin: analysis of pollen, charcoal, and seeds from varved lake sediments. *Quat. Res.* 10, 55–68. doi: 10.1016/0033-5894(78)90013-3

Sweetser, R. H. (1908). Charcoal and coke as blast-furnace fuels. *Trans. Am. Inst. Min. Metall. Eng.* 39, 228–235.

ten Brink, H., Maenhaut, W., Hitzenberger, R., Gnauk, T., Spindler, G., Even, A., et al. (2004). INTERCOMP2000: the comparability of methods in use in Europe for measuring the carbon content of aerosol. *Atmos. Environ.* 38, 6507–6519. doi: 10.1016/j.atmosenv.2004.08.027

Thevenon, F., Williamson, D., Bard, E., Anselmetti, F. S., Beaufort, L., and Cachier, H. (2010). Combining charcoal and elemental black carbon analysis in sedimentary archives: implications for past fire regimes, the pyrogenic carbon cycle, and the human-climate interactions. *Glob. Planet. Change* 72, 381–389. doi: 10.1016/j.gloplacha.2010.01.014

Thomas, M. D. (1952). The present status of the development of instrumentation from the study of air pollution. *Proc. Natl. Air Pollut. Sympos.* 2, 16–23.

van Leeuwen, T. T., van der Werf, G. R., Hoffmann, A. A., Detmers, R. G., Rucker, G., French, N. H. F., et al. (2014). Biomass burning fuel consumption rates: a field measurement database. *Biogeosciences* 11, 7305–7329. doi: 10.5194/bg-11-7305-2014

Waggoner, D. C., Chen, H. M., Willoughby, A. S., and Hatcher, P. G. (2015). Formation of black carbon-like and alicyclic aliphatic compounds by hydroxyl radical initiated degradation of lignin. *Org. Geochem.* 82, 69–76. doi: 10.1016/j.orggeochem.2015.02.007

Wagner, S., Ding, Y., and Jaffé, R. (2017). A new perspective on the apparent solubility of dissolved black carbon. *Front. Earth Sci.* 5:75. doi: 10.3389/feart.2017.00075

Wagner, S., Riedel, T., Niggemann, J., Vähätalo, A. V., Dittmar, T., and Jaffé, R. (2015). Linking the molecular signature of heteroatomic dissolved organic matter to watershed characteristics in world rivers. *Environ. Sci. Technol.* 49, 13798–13806. doi: 10.1021/acs.est.5b00525

Wang, D. Y., Fonte, S. J., Parikh, S. J., Six, J., and Scow, K. M. (2017). Biochar additions can enhance soil structure and the physical stabilization of C in aggregates. *Geoderma* 303, 110–117. doi: 10.1016/j.geoderma.2017.05.027

Wang, W. H., Hou, Y. C., Wu, W. Z., Niu, M. G., and Liu, W. N. (2012). Production of benzene polycarboxylic acids from lignite by alkali-oxygen oxidation. *Ind. Eng. Chem. Res.* 51, 14994–15003. doi: 10.1021/ie3021297

Watson, J. G., Chow, J. C., and Chen, L. W. A. (2005). Summary of organic and elemental carbon/black carbon analysis methods and intercomparisons. *Aerosol Air Qual. Res.* 5, 65–102. doi: 10.4209/aaqr.2005.06.0006

Western, A. C. (1963). "Wood and charcoal in archaeology," in *Science in Archaeology: A Comprehensive Survey of Progress and Research*, eds D. Brothwell and E. Higgs (London: Thames and Hudson), 150–158.

Wilkins, E. T. (1954). Air pollution aspects of the London fog of december 1952-discussion. *Q. J. Royal Meteorol. Soc.* 80, 267–271. doi: 10.1002/qj.49708034420

Yoshioka, H., and Ishiwatari, R. (2005). An improved ruthenium tetroxide oxidation of marine and lacustrine kerogens: possible origin of low molecular weight acids and benzenecarboxylic acids. *Org. Geochem.* 36, 83–94. doi: 10.1016/j.orggeochem.2004.07.002

Zand, A. D., and Grathwohl, P. (2016). Enhanced immobilization of polycyclic aromatic hydrocarbons in contaminated soil using forest wood-derived biochar and activated carbon under saturated conditions, and the importance of biochar particle size. *Pol. J. Environ. Stud.* 25, 427–441. doi: 10.15244/pjoes/60160

Zimmerman, A. (2010). Abiotic and microbial oxidation of laboratory-produced black carbon (biochar). *Environ. Sci. Technol.* 44, 1295–1301. doi: 10.1021/es903140c

Zimmerman, A. R., Gao, B., and Ahn, M.-Y. (2011). Positive and negative carbon mineralization priming effects among a variety of biochar-amended soils. *Soil Biol. Biochem.* 43, 1169–1179. doi: 10.1016/j.soilbio.2011.02.005

Ziolkowski, L. A., Chamberlin, A. R., Greaves, J., and Druffel, E. R. M. (2011). Quantification of black carbon in marine systems using the benzene polycarboxylic acid method: a mechanistic and yield study. *Limnol. Oceanogr. Methods* 9, 140–149. doi: 10.4319/lom.2011.9.140

Ziolkowski, L. A., and Druffel, E. R. M. (2010). Aged black carbon identified in marine dissolved organic carbon. *Geophys. Res. Lett.* 37:L16601. doi: 10.1029/2010GL043963

**Conflict of Interest Statement:** The authors declare that the research was conducted in the absence of any commercial or financial relationships that could be construed as a potential conflict of interest.

frontiers in Earth Science

ORIGINAL RESEARCH
published: 25 October 2018
doi: 10.3389/feart.2018.00169

# What Can Charcoal Reflectance Tell Us About Energy Release in Wildfires and the Properties of Pyrogenic Carbon?

*Claire M. Belcher[1]*, Stacey L. New[1], Cristina Santín[2], Stefan H. Doerr[2], Rebecca A. Dewhirst[1], Mark J. Grosvenor[1] and Victoria A. Hudspith[1]*

*[1] wildFIRE Lab, University of Exeter, Exeter, United Kingdom, [2] Geography Department, Swansea University, Swansea, United Kingdom*

Here, we explore how charcoal formation under different heating regimes and circumstances leads to chars of different physical properties. In order to do this, we have undertaken (1) carefully controlled laboratory experiments that replicate the different heating regimes that might be experienced during a wildfire and (2) two experimental wildfires where heat variations were monitored across the burn from which resulting charcoal has been studied. The charcoal properties were assessed using charcoal reflectance that measures the light reflected back from the charcoals structure and which links to changes in its structural properties. We find that increased total heat released during combustion positively correlates with increased charcoal reflectance and that this is evidenced from both our laboratory experiments and experimental wildfires. Charcoals that related to lower total heat release were found to have more lignin remaining than those subjected to greater heating indicating that charcoals formed in lower energy regimes are likely to be more susceptible to post-fire degradation. We conclude that charcoal reflectance may make a useful metric with which to determine the distribution of energy delivery across a burned area and that this may be utilized to inform both variations in fire severity and enable the prediction of long-term C budgeting for different types of wildfire.

**Keywords: charcoal reflectance, fire-behavior, charcoal degradation, fire-severity, pyrolysis**

OPEN ACCESS

***Edited by:***
*Francien Peterse, Utrecht University, Netherlands*

***Reviewed by:***
*Gustavo Saiz, Imperial College London, United Kingdom*
*William Patrick Gilhooly III, Indiana University–Purdue University Indianapolis, United States*

****Correspondence:***
*Claire M. Belcher*
*c.belcher@exeter.ac.uk*

***Specialty section:***
*This article was submitted to Biogeoscience, a section of the journal Frontiers in Earth Science*

***Received:*** *25 April 2018*
***Accepted:*** *28 September 2018*
***Published:*** *25 October 2018*

***Citation:***
*Belcher CM, New SL, Santín C, Doerr SH, Dewhirst RA, Grosvenor MJ and Hudspith VA (2018) What Can Charcoal Reflectance Tell Us About Energy Release in Wildfires and the Properties of Pyrogenic Carbon? Front. Earth Sci. 6:169. doi: 10.3389/feart.2018.00169*

## INTRODUCTION

Charcoals are a key component of the continuum of products that comprise the fire-derived organic matter pool, known as pyrogenic carbon (PyC) (Bird et al., 2015; Santín et al., 2016). The properties of charcoals relate not only to the nature of the fuel from which they are formed, but also to the characteristics of the fire that generated them (Ascough et al., 2008; McBeath et al., 2013; Michelotti and Miesel, 2015; Belcher and Hudspith, 2016; Hudspith et al., 2017b). These properties should also determine how different charcoals are then subsequently modified chemically and physically in the post fire environment (Harvey et al., 2012; Santín et al., 2017). However, because fire is a complex chemical reaction that also relates to the physical state of the fuel it has been difficult to disentangle how the nature of fire might impact the production of different charcoals and therefore

to what extent individual fire and fuel characteristics might lead to charcoals with varying levels of resistance to biological and physical degradation or to combustion in subsequent fires (e.g., Doerr et al., 2018).

Building this understanding is important because most wildfires are considered 'net zero carbon emission events', where the carbon released to the atmosphere is balanced by the re-uptake of C from the atmosphere by regrowth of the ecosystem. Notwithstanding this, PyC products that remain following a fire can indeed act as a carbon sink (Santín et al., 2015), but they are not yet fully considered or included in carbon fluxes and budgeting models (Santín et al., 2016). The charcoal fraction of PyC is known to have the potential to add to geologically long carbon stores as indicated by the presence of fossil charcoals found in deposits as old as 410 Ma (Belcher et al., 2013). This long-term presence of charcoals makes it tempting to assume that charcoal must be rather resistant to biotic and abiotic degradation over the long term. However, charcoal is not pure carbon and contains a variety of compounds that have been shown to have lower or greater reactivity (Ascough et al., 2010) and therefore ought to determine the likelihood of a charcoal's long-term preservation and carbon burial potential (Bird et al., 2015). In order to further understand the contribution of charcoals in carbon budgeting we need to explore how differences in fuel type and fire behavior influence the production and properties of charcoals.

To address this, methodologies need to be developed and applied that link the nature of the fuel and the dynamics of combustion to charcoal formation. Measurement of the reflective properties of charcoals has been an area of study for decades (e.g., Jones et al., 1991). This is achieved by embedding charcoal in resin, polishing the sample and studying the charcoal under oil in reflected light with a photometric measurement taken of the fraction of incident light radiation reflected from the samples surface (e.g., Belcher and Hudspith, 2016; Hudspith et al., 2017a). More highly reflecting chars (**Figure 1A**) are thought to contain more stable, well organized graphite-like domains while lower reflecting chars (**Figure 1B**) are characterized by a more complex disorganized phase containing a greater proportion of less stable aliphatic phases (Cohen-Ofri et al., 2006; Ascough et al., 2008).

Previous research using oven formed charcoals has linked the formation of varying reflectance with the temperature of their formation (McParland et al., 2009; Ascough et al., 2010). However, more recently Belcher and Hudspith (2016) argued that charcoals produced in ovens relate to a single heat flux/temperature while charcoals formed in wildfires are the product of varying heat fluxes and energy exchanges that cannot be described by a single temperature. They found that charcoal surface reflectance increased between char extracted at peak heat release rate (pHRR; peak fire intensity) and at the end of flaming combustion, leading to the conclusion that charcoal reflectance must continually evolve throughout the combustion process. Oven based charring fails to capture the transitions in energy release that occurs during a wildfire and therefore the progressive development of reflectance as combustion proceeds (Belcher and Hudspith, 2016). Along these same lines, Santín et al. (2017) have proven that wildfire and man-made PyC sequestration potential and physio-chemical properties differ, even when produced from the same original materials. Recently, changes in the cellular level structural properties in charcoals have been observed to relate to energy transfer, where the energy transfer through a char layer leads firstly to the fusion of cell walls in the plant material and as heating continues refracturing along the middle lamella of the cell walls causing fragmentation (Hudspith and Belcher, 2017). This is also in contrast to charcoals produced in ovens that appear to reach only the cell wall fusion stage (Hudspith and Belcher, 2017). This evidence supports the idea that charcoal reflectance should change throughout the phases of combustion that allow for pyrolysis, however, to date no research has been able to provide satisfactory understanding about the relationship between how fuel and fire properties relate to the formation of charcoal reflectance.

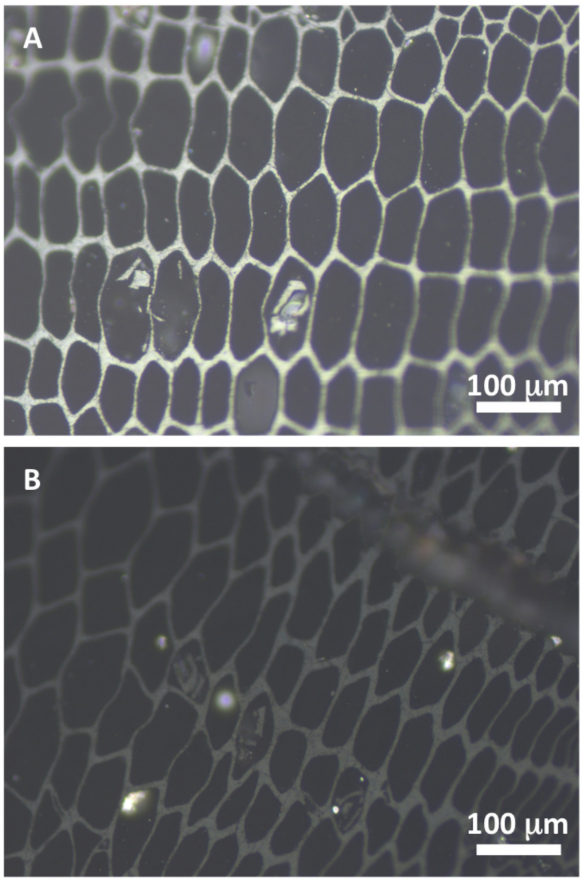


**FIGURE 1 |** Shows charred western red cedar as studied in reflected light. **(A)** Shows higher reflecting cell walls (bright gray) and **(B)** shows lower reflecting cell walls (darker gray).

Despite the lack of knowledge on the formation of different charcoal reflectance in wildfires as opposed to ovens, there has been previous research that compares their conditions of formation, reflectance and recalcitrance. Large differences have been shown between oxidation experiments of charcoals generated at 300°C compared to those generated at 400°C

or greater (oven formed), leading to the conclusion that oxidative resistance is positively correlated with production temperature (Ascough et al., 2011). While, we disagree that single temperatures are representative of wildfires, these results indicate that charcoal generated at higher temperatures appear to lose aliphatics, oxygenated functional groups of cellulose and lignin, and become dominated by aromatic carbon=carbon bonds (Keiluweit et al., 2010; Ascough et al., 2011; Santín et al., 2017). Preliminary work linking charcoal reflectance and reactive/oxidative properties of chars indicates that low reflecting chars (formed at 300°C) appear less recalcitrant than more highly reflecting chars (generated at 400°C or greater) (Ascough et al., 2010).

Here, we explore the relationship between a range of measurable fuel (wood bulk-density) and fire properties both in the lab [heat release rate (HRR), total heat release (THR)] and in field scale experimental fires (variations in temperature over time) to begin to develop a better understanding of charcoal reflectance. We then explore the possibility of whether charcoal reflectance also relates to the degradative/oxidative properties of the remaining charcoal. The aim being that with further development, it might be possible to link fire behavior, charcoal reflectance and the recalcitrance of the charcoals produced to better estimate the contribution of PyC to long term carbon pools for different wildfire types.

# MATERIALS AND METHODS

## Laboratory Fire Experiments

There have been many analyses linking charcoal reflectance with oven temperature during oven-based pyrolysis experiments (Jones et al., 1991; McParland et al., 2009; Ascough et al., 2010). In order to improve upon these experiments and find linkages between the properties of wildfires, such as fire intensity and total energy release we have used an iCone Calorimeter (Fire Testing Technology, East Grinstead, United Kingdom), that better replicates the combustion processes that occur in the natural environment compared to oven heating. The iCone allows for charring to occur in ambient pressure and oxygen conditions in which the samples (described below) were exposed to a heat flux of 50 kW.m$^2$ in the iCone calorimeter, following ISO 5660–1/ASTM E1354 (International Organization for Standardization (ISO) 2015/(ASTM International, 2016). This mimicked the heat flux from an approaching fire front and began to decompose the wood samples, generating pyrolysis gases (pyrolysate) as the surface began to char (pyrolyse). Once the volume of pyrolysate released was sufficient, a spark igniter ignited the pyrolysate, leading to flaming ignition. During combustion, the iCone calorimeter measured the time taken for each sample to ignite (time to ignition, TTI), the rate of heat release throughout the burn, enabling it to quantifying HRR, pHRR, and THR during the flaming phase of the fire.

To investigate variations in charcoal reflectance we undertook two sets of experiments: the first examined one fuel type, western red cedar (WRC) wood (*Thuja plicata*) and subjected it to four different flaming durations; the second considered different bulk density woods [four species; Oak (*Quercus robur*), Beech (*Fagus sylvatica*), Eucalyptus (*Eucalyptus* sp.) and Balsa (*Ochroma pyramidale*) for two flaming durations. In all cases samples were dried at 45°C until fully dry (until no further mass loss was observed) and left in a drying oven until ready for testing.

### WRC Experiments

9.5 cm × 9.5 cm × 3 cm blocks of WRC were placed in the standard iCone calorimeter holder of same length and width dimensions, the sample was then raised up flush to the surface of the holder using ceramic wool beneath the wood. The samples were tested using an incident heat flux of 50 kW.m$^{-2}$ and ignited after a mean time of 24 s. Samples were then allowed to flame for 5, 10, 15, and 20 min, with duplicates of each flaming duration run. The TTI, HRR, and THR were measured throughout the duration of flaming combustion. Following the allotted time, the sample was taken away from the heat, wrapped tightly in foil and buried in sand to exclude oxygen and cease the combustion process. This allowed the collection of a suite of charcoal samples that were representative of the different flaming durations.

### Bulk Density Experiments

A similar protocol was followed using different bulk density woods. Eucalyptus, Oak, Beech, and Balsa wood were tested, representing densities of 0.8, 0.74, 0.7, and 0.16 × 10$^3$ kg.m$^3$, respectively. The samples were subject to an incident heat flux of 40 kW.m$^{-2}$ and one set heated for 4 min and a second set heated until flaming ceased naturally on each sample. In both cases, duplicates of each sample were run. As before TTI, HRR and THR were measured. The samples were removed and oxygen excluded in the same way.

## Experimental Field Scale Fires

Two fires in the boreal forest (Northwest Territories, Canada) were studied: (A) a high-intensity crown fire and (B) a low-intensity surface fire.

The high-intensity crown fire (Triangle plot) was an experimental fire conducted on 15/6/2015 as part of the Canadian Boreal Community FireSmart Project (61°34′55″ N; 117°10′13″ W) and aimed at simulating wildfire conditions. The experimental site was a mature stand of black spruce (*Picea mariana*) and jack pine (*Pinus banksiana*). The understory was very sparse, the forest floor composed of litter, mosses and lichens (<10 cm depth), with some downed wood present (see Santín et al., 2015 for details). The fire was fast moving with a total burn time of <5 min and flame lengths >5 m above canopy height. Fireline intensity was estimated as ∼8,000–12,000 kW.m$^{-1}$, which is within the range typical of high-intensity boreal crown fires in Canada (de Groot et al., 2009). The fire resulted in the complete consumption of the canopy, small branches and the understory.

The low-intensity surface fire (Pine Point) was a slow-moving, backing surface wildfire (Fire 28, Hay River 60°49′38″ N; 114°24′28″ W). It affected a mixed black spruce and jack pine stand of comparable stand characteristics to the high intensity fire, but with an organic soil layer of up 50 cm depth. This lightning-caused wildfire burnt across the site on 29/6/2017

during calm atmospheric conditions advancing at <5 $m.h^{-1}$. This allowed sufficient time to place samples, thermocouples and data loggers ahead of the advancing fire. This surface fire led to the patchy smoldering combustion of the forest floor to a depth of up to 30 cm and the "torching" of a few individual trees.

The same WRC wood used in the laboratory experiments, but in blocks of 3 cm × 3 cm × 3 cm, and pieces of wood of the native Jack Pine (JP) (*Pinus banksiana*) (small twigs of 2–3 cm diameter and 2–4 cm length) were exposed to these two contrasting fire conditions. 15 samples of each type were placed onto the forest floor < 24 h prior to each fire. In the Triangle plot, the wood pieces were placed randomly within an area of 15 m × 15 m. In Pine Point, the wood pieces were placed 2 m apart along a transect parallel to the fire front. Within <12 h after the fires, samples were relocated (unless completely consumed) and placed in sealed containers for subsequent laboratory analysis.

In order to remove consideration of variations of moisture content in our experiments the WRC and JP were dried in an oven at 40°C until no further mass loss was observed, and stored in sealed bags until deposited in the burn ahead of the fires. By standardizing the fuel moisture of the samples our approach was to be able to look at how fire behavior directly influenced the char properties by limiting any variations in fuel moisture of the items that will be collected for analysis.

To provide a temperature-duration record for each individual wood sample, K-type thermocouples were attached directly to the surface of the wood pieces, connected to data loggers (Lascar, Easylog) that were buried in the adjacent soil. Due to the patchy nature of the low-intensity fire in Pine Point, not all samples were exposed to burning and, in some cases, the combustion of the organic soil led to the destruction and associated data loss of some of the loggers. For more details on the characteristics of the fires, sites, and experimental settings, see Doerr et al. (2018). Following the fires, the integrated area under each thermocouple curve was calculated for the duration each sample spent at >300°C. This served as a guide to the total heating experienced by the sample throughout the duration of the fire.

## Preparation of Charcoal Samples and Measurement of Charcoal Reflectance

The laboratory generated charcoal blocks were cut into sections approximately 2 cm wide and 3 cm deep and embedded in resin with the surface exposed to flaming facing the upper surface of the resin block, and this surface polished ready for analysis in reflected light (c.f. Belcher and Hudspith, 2016). The samples subject to 20 min flaming duration were additionally embedded on their side and the side/depth profile polished, allowing measurements with depth from the surface to the base of the char layer to be observed and the reflective properties measured. The field charcoal samples varied in their remains if the samples were <1 $cm^3$ the entire sample was embedded in resin with the most charred side polished for analysis. If larger samples were available approximately half the sample was embedded in resin and again the most charred side polished for analysis.

Both the polished laboratory and wildfire charcoals were then analyzed under oil of refractive index 1.514 (at 23°C), using a Zeiss Axio-Scope A1 optical microscope, with a TIDAS-MSP 200 microspectrometer, at the wildFIRE Lab at the University of Exeter. Samples were studied using a ×50 objective (with ×32 eyepiece magnification), and reflectance measurements were obtained manually using MSP200 v 3.47 software. The system was calibrated with three synthetic reflectance standards, where reflectance is denoted as Ro) Strontium Titanite (5.41% Ro), Gadolinium Gallium Garnet (GGG) (1.719% Ro) and spinel (0.42% Ro). Manual reflectance measurements were taken at cell wall junctions across the polished surface of the charcoal. Thirty measurements were taken of each charcoal sample. Representative color micrographs were taken using an AxioCam 105 color 5-megapixel eyepiece camera attached to the reflectance microscope, and Zeiss Zen software (e.g., **Figure 1**)

## Exploration of Laboratory Produced Charcoal Reactivity and Thermal Recalcitrance

Any lignin remaining in the WRC charcoals subject to flaming for 5 and 20 min was analyzed using the acetyl bromide method (Moreira-Vilar et al., 2014). Char was carefully scraped from the upper surface of the charcoals, so as to capture the same surface that had been analyzed for charcoal reflectance; two samples were collected from each flaming duration. 2 mg of each char sample was incubated in acetyl bromide (0.5 ml, 25% v/v in acetic acid) at 50°C for 2 h. After incubation, sodium hydroxide (0.9 ml, 2 M) and hydroxylamine hydrochloride (0.1 ml, 1 M) were added, along with acetic acid (5 ml). The lignin content of the extracts was then quantified by measuring the absorbance at 280 nm using a UV-1600PC Spectrophotometer (VWR, Leicestershire, United Kingdom) (three replicates of each sample).

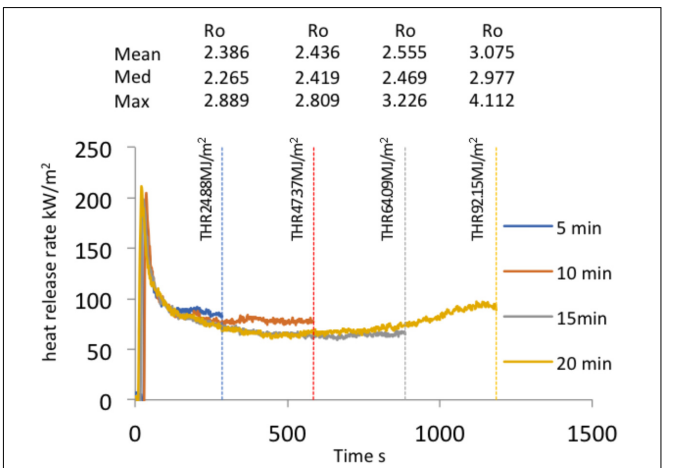


**FIGURE 2 |** Summary overview of heat release rate profiles, total heat release and the range of surface Ro% generated during flaming combustion tests of WRC. Blue line flaming for 5 min, orange line 10 min, gray line 15 min, and yellow line 20 min.

The reactivity of the chars was considered using a Federal Aviation Administration (United States, FAA) Microcalorimeter (Fire Testing Technology, East Grinstead, United Kingdom) that was developed to allow direct measurements of HRR in respect to material properties and chemical composition of materials (Lyon and Walters, 2002). The FAA microcalorimeter is a pyrolysis combustion flow calorimeter and was used to reproduce the solid-state and gas phase processes of flaming combustion by reheating the char in an inert gas stream (Nitrogen gas) where upon the remaining volatile gases are driven off and oxidized at high-temperature in excess oxygen. The microcalorimeter then measures the rate of heat release based on the oxygen consumption history of the fuel (Lyon and Walters, 2002). Approximately 3 mg was scraped from the charred surface of the WRC samples that had been exposed to flaming combustion for 5, 10, 15, and 20 min and tested in the microcalorimeter. The samples were re-heated using a heating program that ramped up to 750°C at a rate of 3°C per second. The volatile gases released during heating were combusted to estimate the remaining reactivity of the char. Each sample was analyzed in triplicate. The microcalorimeter in this case was utilized to consider the reactivity of the charred samples, where the nature of the compounds in the char determines the temperature at which the maximum decomposition rate of the solid fuel occurs and the time taken for each sample to reach pHRR. We anticipated that (a) those samples containing a more reactive fraction would reach their maximum rate of decomposition more rapidly and at a lower temperature, as lignocellulosic structures should be easier to break down than large polyaromatic compounds (Drysdale, 2011) and (b) that samples containing a higher abundance of lignocellulosic compounds would have a lower pHRR than those containing abundance polyaromatics (Drysdale, 2011).

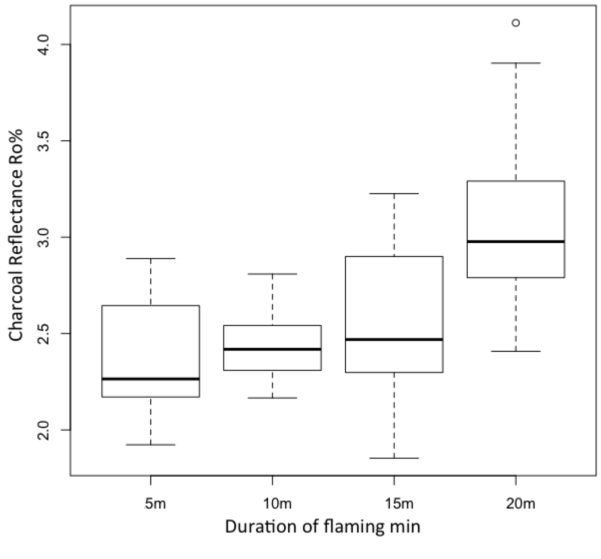


**FIGURE 3 |** Box plot of the range of measured charcoal reflectance values from WRC subject to 5, 10, 15, and 20 min flaming combustion where $n = 90$ for each box.

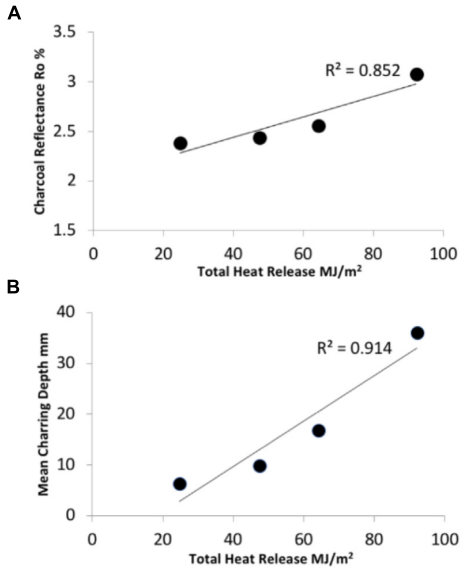


**FIGURE 4 |** Graphs indicating strong positive correlations between the total heat released during flaming combustion of WRC in respect to **(A)** charcoal reflectance and **(B)** mean charring depth attained. The mean of 90 measurements is represented by each data point on both graphs.

# RESULTS

## Formation of and Variations in Charcoal Reflectance

The HRR and THR were measured during all laboratory experiments. **Figure 2** provides a summary overview of HRR profiles, THR and the range of surface Ro% generated during flaming combustion tests of WRC. **Figure 3** reports the changes in reflectance that resulted from the range of flame durations tested in the lab and shows that surface Ro% increases throughout flaming combustion and markedly following 20 min of flaming. The mean surface Ro% was found to be positively correlated to THR during flaming combustion ($r^2 = 0.852$, **Figure 4A**). THR was also shown to correlate with mean char depth ($r^2 = 0.914$; **Figure 4B**). When charcoal reflectance was measured at depth intervals throughout the char layer, the reflectance could be seen to decrease with depth through the char profile (**Figure 5**).

When woods of different bulk densities were considered over two flaming durations both the duration of flaming and the bulk density of the wood influenced mean surface Ro% (**Figure 6A**). As in the WRC experiments the mean surface Ro% from each species was positively correlated with THR ($r^2 = 0.836$, **Figure 6B**).

## Field Scale Experimental Fires

As explained in the methodology, WRC and *Pinus banksiana* samples were also exposed to two different fire behaviors in the two experimental fires. At the Triangle plot site, which experienced a high intensity fast-moving crown fire, the mean maximum temperature recorded from the thermocouples

attached to the wood pieces was 842°C (range of max temperatures recorded from the loggers was 661–1,002°C, the upper limit may have been higher as this is typically the upper point up to which type K thermocouples read). Mean integrated area under the thermocouple curves >300°C) was 50,306°C s (range 21,406–122,798°C s).

At the Pine Point site, which was subject to a low intensity, slow burning surface fire, the mean maximum temperature recorded from the thermocouples was 482°C (range of maximum temperatures recorded was 40–791.5°C). Mean energy release (area integrated under the thermocouple curves >300°C) was 22,090°C s (range 0–99,327°C s).

Correspondingly, the resulting surface Ro% for both species (WRC and *Pinus banksiana*) was significantly different from the two fires ($p$ = 0.00291). The high intensity crown fire at the Triangle site produced more highly reflecting chars than the slower moving surface fire at Pine Point (**Figures 7A,B**). *Pinus banksiana* generated slightly lower surface Ro% than WRC (**Figure 7C**). The integrated area under the thermocouple temperature profile curves produce an estimate of the energy release that was >300°C, during the field scale fires and serve as a comparator to our measurements of THR taken in the laboratory. The difference in surface Ro% appears to relate to the different total energy release from the fires (Kruskall–Wallis $p$ = 0.01287).

## Preliminary Exploration of Variations in Charcoal Recalcitrance

We used two approaches to preliminarily assess the recalcitrance/reactivity of the charcoals formed in our laboratory experiments. On re-heating in the FAA microcalorimeter the WRC char samples that had been subject to flaming combustion for 5 min had a mean maximum temperature of decomposition around half that of the other chars (**Figure 8A**). They also reached pHRR twice as rapidly as those previously subject to flaming for 10, 15, or 20 min (**Figure 8B**). However, pHRR revealed a positive correlation with their original duration of heating ($r^2$ = 0.888, **Figure 8C**). When the remaining lignin content of the chars was examined the samples subject to flaming for 5 min were found to contain up to three times the amount of lignin than the chars analyzed after 20 min of flaming (**Figure 9**, $p$ = 0.004).

# DISCUSSION

## The Formation of Charcoal Reflectance

The formation of charcoal in wildfires is affected by the properties of the fuel, which in turn, together with terrain and atmospheric conditions, influence the combustion dynamics. Charcoal yields

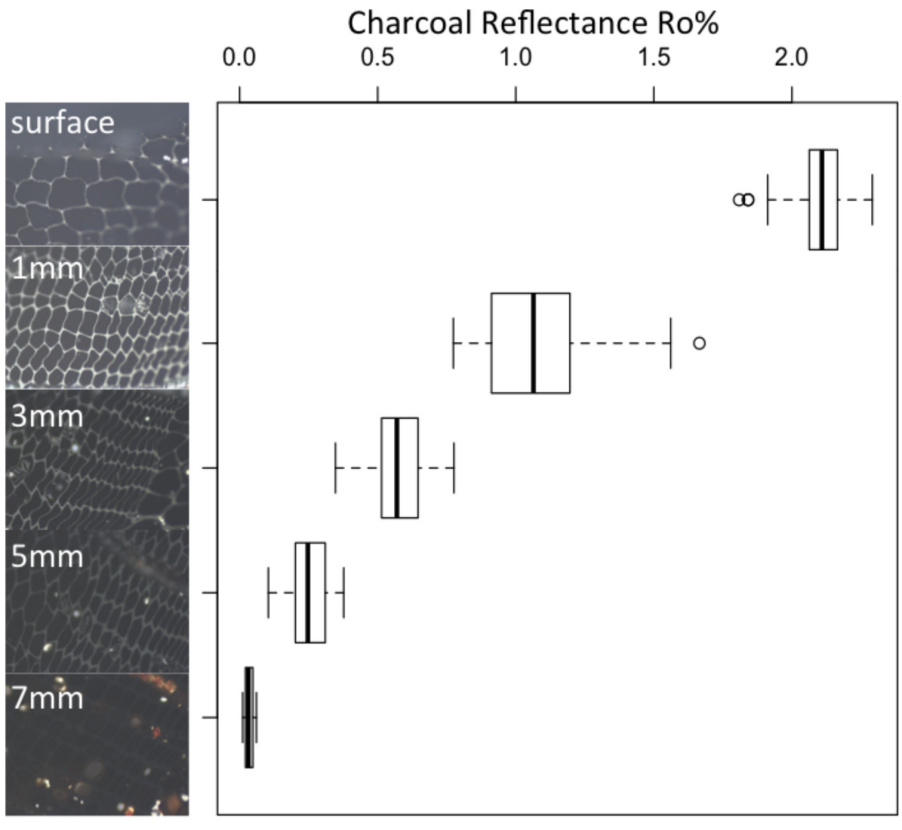


**FIGURE 5 |** Reflectance images and box plots ($n$ = 90 for each box) showing the variations in charcoal reflectance with depth in a charred block of WRC. Indicating that charcoal reflectance decreases away from the heated sample surface and into the char layer.

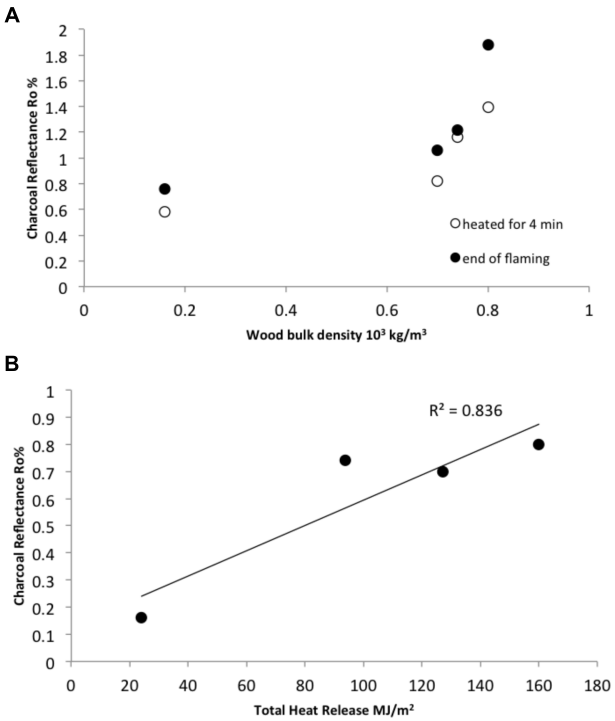


**FIGURE 6 |** The influence of wood bulk density on charcoal reflectance. **(A)** Indicates bulk density and charcoal reflectance for samples subject to 4 min of flaming combustion and sampled at the end of flaming combustion. **(B)** The mean total heat released measured at the end of flaming combustion four different bulk density woods and the corresponding mean charcoal reflectance attained for each bulk density set. The mean of 90 measurements is represented by each data point on both graphs.

are known to depend on the rate and amount of heating that relates to the imposed heat flux and the supply of oxygen at the fuel surface (Kashiwagi et al., 1987). These interact to alter the rate and volume of volatile gas release, which are required to initiate flaming combustion. In the case of wildfires, the imposed heat flux would be the approaching and passing fireline. **Figure 10A** provides a schematic of a fire and highlights the exchanges of energy that occur during the formation of charcoal reflectance during flaming combustion. The iCone calorimeter used in our laboratory experiments measures the HRR per unit area as a function of the external radiant heat flux (the cone heater, used to decompose the virgin and generate pyrolysate). It then calculates the THR from ignition to the point at which we removed samples, and therefore charring must relate to the rate of heat release and duration of heat supplied by the flame. The formation of charcoal reflectance must directly relate to the net heat transfer through the fuels surface and must be equal to the absorbed external radiant flux (the cone heater), plus the heat transfer from the flame (see **Figure 10A**). Our laboratory experiments indicate that these properties influence charcoal reflectance, where THR (heat release over time) and fuel density (which itself influences THR), both showed strong correlations with surface charcoal reflectance and the depth of charring (e.g., **Figures 4–6**). A substantial volume of previous research has linked increasing charcoal reflectance with increasing oven temperatures during the formation of the char (e.g., Scott and Glasspool, 2007; McParland et al., 2009; Ascough et al., 2010) leading to the suggestion that Ro% can be used to estimate wildfire temperature. The energy field around a burning solid fuel is illustrated in **Figure 10A** and described above; and indicates why most oven-based charcoal forming experiments (that often include the formation of charcoal in sealed metal tubes (McParland et al., 2009), do not capture the mechanism of char formation during flaming combustion in wildfires. **Table 1** compares the typical charcoal reflectance generated at similar temperatures in an oven and in the iCone and contrasts these to the mean Ro% resulting from the wildfires studied. Here, we monitored the surface temperature of the fuel during combustion in the iCone and found the mean surface temperature to be ∼586°C which we compare to oven produced chars formed at 600°C. Scott and Glasspool (2007) produced chars in an oven at 600°C for 1,200 s (the minimum duration they explored), the iCone charcoal reflectances were found to be 22% lower than those generated in an oven over the same duration (**Table 1**).

Higher reflectance should be expected in oven formed chars because oven based experiments are designed to generate perfect char. The oven setting minimizes heat losses and oxygen is excluded by either placing the samples in metal tubes (Scott and Glasspool, 2007) or burying samples in sand (Crawford and Belcher, 2016). This prevents oxidation of the volatile gases released (i.e., no flaming combustion) and oxidation of the solid fuel (char consumption). As such this poorly replicates char formation in a wildfire. A similar conclusion was reached by Santín et al. (2017) when comparing wildfire charcoals and slow-pyrolysis biochars, the latter produced in pyrolytic ovens. The heating regime is also significantly different. Wood placed in an oven takes ∼15 min to match the temperature of the oven (Scott and Glasspool, 2007) and does not ignite (because oxygen is excluded). In contrast the WRC tested in the iCone takes a mean of 30 s to ignite using a radiant heat flux of 50 $kW.m^{-2}$. A small amount of charring occurs during the period of pre-heating ahead of ignition, which is also characteristic of pre-heating from an approaching fire-front during wildfires. Once flaming combustion is established (e.g., after ∼30 s of pre-heating) this then leads to the main charring phase in the iCone calorimeter.

However, we note that the mean reflectance for all durations of heating in our laboratory experiments using WRC, yielded higher Ro% than were observed in either of the wildfires studied (compare **Figure 3** to **Figure 7A** and see **Table 1**). The mean from the charcoals formed by 5 min (300 s) flaming combustion in the laboratory experiments was 2.39 Ro% (range 1.92–2.89) while for 20 min (1,200 s) it was 3.07 Ro% (range 2.41–4.11) (**Figure 3** and **Table 1**). This indicates that the surface reflectance of our laboratory char is on average higher than that observed in either of the wildfires (**Figure 7A**). This appears to relate to the fact that the duration of heating in the both the wildfires studied, as determined from the thermocouple readings taken from the WRC blocks in the field (**Table 1**) was ∼100 s shorter (e.g., between total heating of 209 and 236 s) than our shortest laboratory experiments (e.g., 300 s). The higher mean reflectance

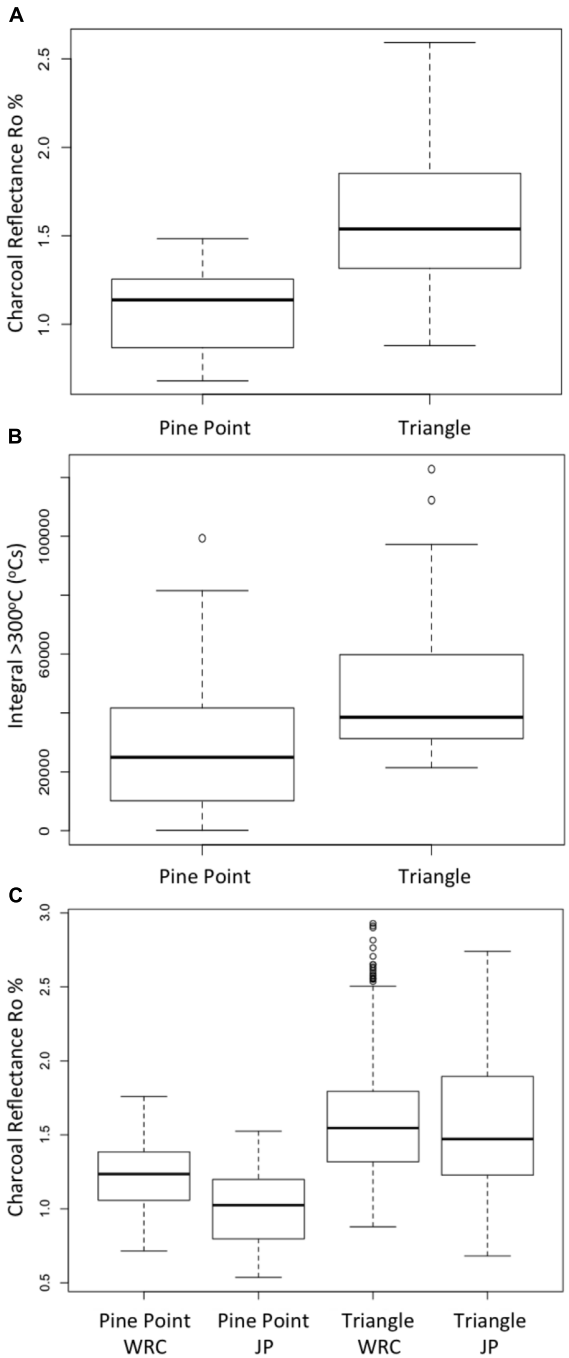


**FIGURE 7 |** Box plots ($n$ = 30 for each boxes) exploring the distribution of charcoal reflectance and the integral >300°C for the fires at the Pine Point and Triangle sites, Canada **(A)** shows the range of reflectance values from WRC samples for the two sites. **(B)** Indicates the integrated area under the thermal couple curve >300°C (as an estimate of energy flux to the fuel). **(C)** Shows charcoal reflectance variations between WRC and Jack Pine (JP) (*Pinus banksiana*) for both sites.

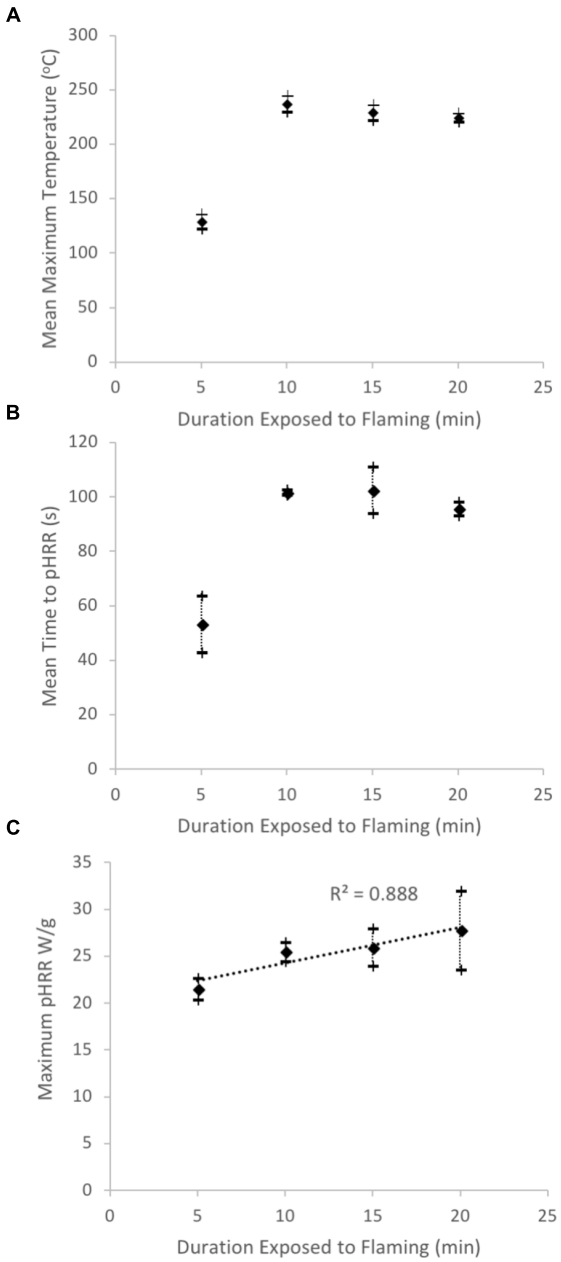


**FIGURE 8 |** Thermal reactivity of chars as measured in the microcalorimeter showing results from the analysis of four sets of charcoal formed during flaming combustion in the iCone calorimeter for 5, 10, 15, and 20 min. **(A)** The mean temperature at which the charcoals reached their maximum rate of decomposition during re-heating in the microcalorimeter. **(B)** The mean time taken for the charcoals to reach peak heat release rate (pHRR) in the microcalorimeter and **(C)** shows a strong positive relationship between the duration of heating over which the samples were originally formed in the iCone calorimeter and the maximum pHRR attained on re-heating in the microcalorimeter.

of charcoals formed by the Triangle site fire experienced a shorter duration of heating but double the amount of 'energy' as represented by the integrated area under the thermocouples curves when compared to the fire at Pine Point (**Table 1**). This highlights that Ro% not only relates to the duration of heating but also the flux of heat, hence charcoal reflectance must relate to

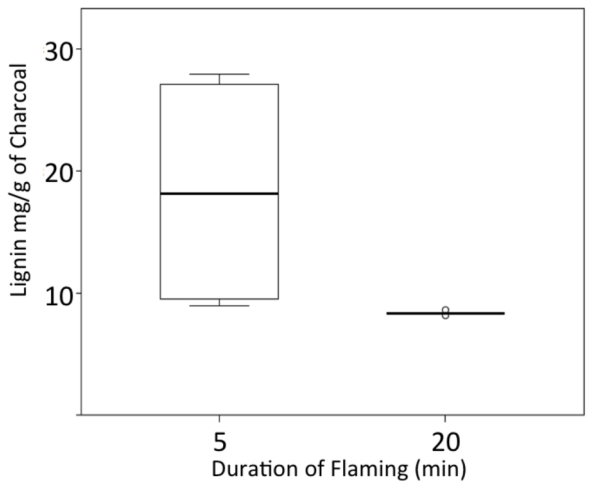


**FIGURE 9 |** Amount of lignin remaining in chars formed over two different flame durations ($n$ = 6 per box).

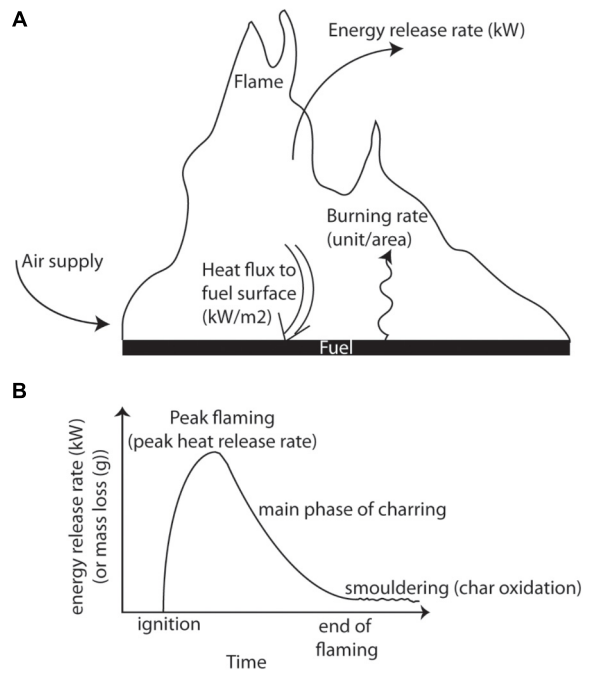


**FIGURE 10 | (A)** Schematic of the directions of energy release and energy fluxes associated with flaming combustion of a solid fuel. **(B)** Schematic heat release rate profile highlighting key transitions during combustion.

the balance of energy released over time and the total energy it receives.

The importance of quantifying energy as opposed to a single temperature can be illustrated by considering a single candle; this candle burns producing a given temperature and the energy release of a single candle. However, if 10 candles are lit, they will still produce the same measurable temperature, but they will release 10 times the amount of energy that the single candle did. Hence the single temperature and typically relatively long duration of heating utilized in oven charring is not appropriate for considering the development of charcoal reflectance in wildfires. A passing fireline delivers a transient energy flux to the fuel present in a wildfire. The fuel is pre-heated, ignites rapidly leading to peak energy release which then declines and eventually decays over time (related to the fuel load available) (see **Figure 2**). In the case of our laboratory experiments each WRC block experiences approximately the same TTI (mean 30 s) and a similar pHRR ($\sim$ 200 kW.m$^{-2}$) (**Figure 2**). The differences in Ro% then relate to a combination of duration of burning (e.g., 5 –20 min) and the amount of energy delivered over this period, which relates well to THR. Char forming fuels rapidly reach a peak burning flux and the maximum point of energy release from flaming, then their energy release rate decays over time (**Figures 2**, **10B**). Therefore, the mean HRR decreases while the surface charcoal Ro% increases over time. This decay is due to the insulative properties of the forming char layer that protects the virgin fuel beneath from the heat flux to the surface of the fuel (Moghtaderi et al., 2006) and slows volatile release (until it eventually ceases). This process is captured in the Ro% measurements taken through the depth of the char layer (e.g., **Figures 4B**, **5**). While the entire char layer appears blackened to the naked eye, Ro% declines significantly throughout the profile of the char layer. Here, the time taken for the heat to penetrate through the forming char layer will vary with HRR, the duration over which the heat is applied as well as the insulative properties of the char layer being formed.

Because mean HRR decreases as combustion proceeds (e.g., **Figure 2**), the rate of increase in Ro% also decreases with the duration of heating. By standardizing Ro% as a function of time (Ro%.s) it can be seen that samples of the same fuel under the same conditions, but heated for longer will have a lower mean HRR and Ro%.s (**Figure 11**). **Figure 11** shows that the mean rate of Ro% increase is strongly positively correlated with mean HRR ($r^2$ = 0.919). These data are taken from the experiments that allowed WRC to burn for 5, 10, 15, and 20 min; the rate of Ro% increase for both Canadian wildfires are also indicated on **Figure 11** and reveals that, despite our laboratory experiments allowing heating for longer durations that the Ro%.s for the Canadian fires falls within a similar HRR-Ro% rate space. Our results indicate the rate of increase in Ro% decreases with time despite Ro% increasing with increased burn duration. Therefore, the final Ro% and the rate of change in Ro% between different fires is a balance between the HRR kW/m$^{-2}$ and the duration that materials are exposed to flaming; the end product of which (%Ro) is best related to THR. Future work should seek to undertake laboratory experiments under the shorter durations to those observed in wildfires to improve upon this relationship and gain a better understanding of the relationship between duration, THR and surface Ro%. Despite this, our results presented here indicate that, in respect to wildfires, THR is a better correlate with Ro% than temperature because THR is a more meaningful description of the energy release from a wildfire. We note, however, that because different wood densities were found to show clear differences in their

**TABLE 1 |** Comparison of charcoal reflectance and heating regimes for oven char (taken from Scott and Glasspool, 2007), and those generated in the laboratory and the field in this research.

| Charring process and material | Temperature°C and/or total heat release kW.m$^{-2}$ | Mean Ro% | Heating duration(s) |
|---|---|---|---|
| Oven char *Sequoia sempervirens* | 600°C (constant temperature) | 3.9 | 1,200 s |
| iCone *Thuja plicata* | ~586°C (mean surface temperature) 92 MJ/m$^{-2}$ total heat release | 3.07 | 1,200 s |
| iCone *Thuja plicata* | ~586°C (mean surface temperature) 24 MJ/m$^{-2}$ total heat release | 2.39 | 300 s (at >300°C) |
| Surface fire Pine Point *Thuja plicata* | 482°C (mean max surface temperature) 22,090°C s (integrated area under the thermocouple curve) | 1.2 | 236 s (at >300°C) |
| Crown fire Triangle Site *Thuja plicata* | 842°C (mean maximum surface temperature) 50,306°C s (integrated area under the thermocouple curve) | 1.6 | 209 s (at >300°C) |

*Charcoals formed at either similar temperatures and/or similar durations of heatings are compared.*

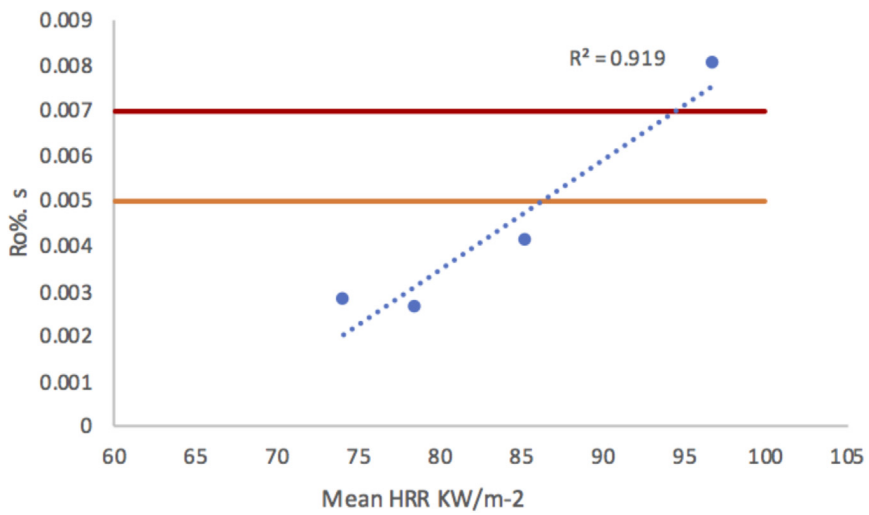


**FIGURE 11 |** Graph of mean heat release and standardized charcoal reflectance as a function of time (Ro%.s) indicating a strong positive correlation.

reflective properties, that variations in the Ro% and THR relationship should be considered within species and not between species.

## Charcoal Reactivity and Likely Resistance to Future Degradation

Wood charcoal is the most common form of PyC found after wildfires because wood contains a complex mixture of polymers of high molecular weight, including cellulose, hemicellulose and lignin. As a passing fireline heats the plant materials, hemicellulose and cellulose decompose more rapidly than lignin. Cellulose is suggested to leave just 5% charcoal, highlighting why leaf material typically leaves much less charcoal and more ash, while fuels with higher lignin contents (such as wood) leave greater volumes of charred material (15–25% of the original material; Drysdale, 2011). In oven formed charcoals, those produced at or above 400°C have been suggested to appear homogeneous, largely aromatic and recalcitrant when compared to those formed at 300°C (Ascough et al., 2011). It has been indicated that the size of polyaromatic units in lower temperature charcoals is smaller and retain incompletely

converted lignocellulosic structures (Knicker et al., 2010; Ascough et al., 2011). Our laboratory results are consistent with these observations where the samples that were subject to flaming for 5 min contained three times the amount of lignin (greater reactivity) than those subject to heating for 20 min (lower reactivity) (**Figure 9**). Our microcalorimetry results support the notion that smaller aromatic molecules remain in the chars formed during 5 min, where these were observed to require a shorter period of re-heating in the microcalorimeter before pHRR was reached and that this was observed to occur at lower temperatures (**Figure 8**) (e.g., lower thermal recalcitrance). Interestingly the chars subject to flaming for 10, 15, and 20 min reveal little difference in their reaction time to reheating in the microcalorimeter, suggesting that there is a critical threshold in changes in the chemical structure of charcoals formed between 5 and 10 min flame durations, or in the case of WRC (in these experiments) between ∼25 $kW.m^{-2}$ and ∼47 $kW.m^{-2}$ THR. However, their pHRR did increase with previous heating duration, where we anticipate that more highly aromatic molecules are capable of delivering higher heat release than shorter chained aliphatic fractions.

Our laboratory results indicate that charcoals formed over short periods of heating and leading to low THR will be more susceptible to post fire oxidative processes owing to the presence of incompletely degraded lignin fragments and the predominance of shorted chained aromatic molecules. While, those formed above a critical threshold of energy transfer, contain little reactive lignocellulosic substances and a large fraction of polyaromatic compounds. The rise in median Ro% between the WRC samples subject to flaming for 5 min (25 $kW.m^{-2}$ THR) as compared to 10 min (47 $kW.m^{-2}$ THR) (**Figure 3**) indicates that Ro% may show some relevance toward estimating the long-term resistance of charcoals produced by wildfires. However, although reflectance continued to evolve between 10 and 20 min heating at 47–92 $kW.m^{-2}$ THR, likely increasing the ordering of polyaromatic microcrystalline domains, we did not observe a decrease in reactivity during subsequent heating in the microcalorimeter (**Figure 8**). However, there was an observable increase in the charcoals pHRR, implying that the those previously subject to longer duration heating (and THR) can be related to increased surface Ro% (**Figure 8**). Where increasing Ro% must relate to increased amounts of larger aromatic molecules, leading to more recalcitrant polyaromatic charcoals.

Our comparison of charcoal reflectance between two different wildfires at Triangle (high-intensity) and Pine Point (low-intensity) has revealed promising results. The crown fire at the Triangle site produced a mean reflectance of 1.58 Ro% (both wood species) while, the surface fire at Pine Point produced a mean reflectance of 1.11 Ro%. This seems to make intuitive sense because crown fires typically burn more intensely than surface and ground fires in this region. This is evidenced by the double mean integrated area under the thermocouple curve, measured at the surface by the fire at the Triangle site, 50,306 compared to 22,327°C s at Pine Point. The WRC samples placed at the two sites came from the same tree as were used in the laboratory experiments and were all of equal moisture content when deployed into the fires, allowing direct comparison between the behavior of these samples in the lab and in the wildfires. WRC surface Ro% measured at the Triangle site ranged 1.07–2.59, while at Pine Point it ranged 0.87–1.48 (**Figure 7A**). In terms of charcoal reactivity/recalcitrance, our laboratory experiments suggest that the Pine Point fire would have produced charcoal that remained more reactive (due to the lower Ro%), while those from the Triangle fire are likely to be more recalcitrant owing to their higher Ro%. This is in agreement with the results of Doerr et al. (2018), where Ro% has been proven to be positively related to several indicators of chemical recalcitrance and the properties of these same fires. For example, the temperature at which 50% of the total energy was released showed positive correlations with Ro% ($r^2 = 0.77$) where the percentage of carbon in the charred remains was also found to increase with Ro% (Doerr et al., 2018). Doerr et al. (2018) also report that previously generated charcoals exposed to a second fire (the two fires in this study) increased their thermal recalcitrance particularly in the high-intensity fire at the Triangle site. Therefore, charcoals with higher reflectances will not only be more chemically resistance to post-fire degradative processes but can become increasingly resistant if subject to subsequent high intensity fires.

In summary, our results that link THR and Ro% are intriguing because they imply that charcoal reflectance may have utility in determining the distribution of energy delivery across a burned area. This could provide useful links to fire severity that describes the immediate impacts of heat pulses above ground and below ground, including, for example, tree mortality and soil and duff consumption (Keeley, 2009). With further development, Ro% measurements might have the potential to enable estimation of what fraction of the charcoals produced by a fire that might be considered reactive versus recalcitrant and therefore which will be more resistant to degradation over the long-term in the post fire environment. Future research should additionally consider involving methods that are better placed to identify the compounds/molecular groups (such as FTIR, e.g., see Ascough et al., 2011) that form in higher energy regimes and closely link these to observed transitions in surface Ro%. Such approaches may be suitable for considering fire characteristics and the contribution of char to C-cycling over the longer-term, including utility in both historic, pre-historic, and paleontological analyses (e.g., Hudspith et al., 2015). In all cases, however, it is critical that further research is conducted using charcoals generated by flaming combustion and/or instrumented field-scale fires if we are to move forward our understanding of charcoal reactivity and resistance to degradation in respect to fire dynamics and charcoal reflectance.

## AUTHOR CONTRIBUTIONS

CB, SD, CS, and SN conceived the work. SD and CS carried out the field experimentation. CB, VH, SN, and MG conducted the various charring experiments. CB, VH, and SN carried out the reflectance

analyses and RD the lignin analyses. All authors contributed to the interpretation of the data and to drafting the manuscript.

## FUNDING

Fieldwork and sample analysis was supported a Leverhulme Trust Grant to SD (RPG-2014-095) and a European Research Council Starter Grant ERC-2013-StG-335891-ECOFLAM to CB. SN received funding from the Natural Environment Research Council (NE/L002434/1) as part of the GW4+ Doctoral Training Partnership and CS by a Sêr Cymru Fellowship co-funded by European Union's Horizon 2020 research and innovation programme (Marie Skłodowska-Curie Grant Agreement No. 663830).

## ACKNOWLEDGMENTS

Special thanks go to Westly Steed and his Department of Environment and Natural Resources, Government of the North-West Territories, Canada and also the staff of FPInnovations, Alberta Environment and Sustainable Resource Development for supporting the fieldwork.

## REFERENCES

Ascough, P., Bird, M. I., Wormald, P., Snape, C. E., and Apperley, D. (2008). Influence of pyrolysis variables and starting material on charcoal stable isotopic and molecular characteristics. *Geochim. Cosmochim. Acta* 72, 6090–6102. doi: 10.1016/j.gca.2008.10.009

Ascough, P. L., Bird, M. I., Scott, A. C., Collinson, M. E., Cohen-Ofri, I., Snape, C. E., et al. (2010). Charcoal reflectance measurements: implications for structural characterization and assessment of diagenetic alteration. *J. Archaeol. Sci.* 37, 1590–1599. doi: 10.1016/j.jas.2010.01.020

Ascough, P. L., Bird, M. I., Francis, S. M., Thornton, B., Midwood, A. J., Scott, A. C., et al. (2011). Variability in oxidative degradation of charcoal: influence of production conditions and environmental exposure. *Geochim. Cosmochim. Acta* 75, 2361–2378. doi: 10.1016/j.gca.2011.02.002

ASTM International (2016). *E1354: Standard Test Method for heat and Visible Smoke Release Rates for Materials and Products Using an Oxygen Consumption Calorimeter*. West Conshohocken, PA: ASTM International.

Belcher, C. M., and Hudspith, V. A. (2016). The formation of charcoal reflectance and its potential use in post-fire assessments. *Int. J. Wildl. Fire* 25, 775–779. doi: 10.1071/WF15185

Belcher, C. M., Collinson, M. E., and Scott, A. C. (2013). "A 450-million-year history of fire," in *Fire Phenomena and the Earth System an Interdisciplinary Guide to Fire Science*, ed. C. M. Belcher (Hoboken, NJ: Wiley), 229–249. doi: 10.1002/9781118529539.ch12

Bird, M. I., Wynn, J. G., Saiz, G., Wurster, C. M., and McBeath, A. (2015). The pyrogenic carbon cycle. *Annu. Rev. Earth Planet. Sci.* 43, 273–298. doi: 10.1146/annurev-earth-060614-105038

Cohen-Ofri, I., Weiner, L., Boaretto, E., Mintz, G., and Weiner, S. (2006). Modern and fossil charcoal: aspects of structure and diagenesis. *J. Archaeol. Sci.* 33, 428–439. doi: 10.1016/J.JAS.2005.08.008

Crawford, A. J., and Belcher, C. M. (2016). Area-volume relationships for fossil charcoal and their relevance for fire history reconstruction. *Holocene* 26, 822–826. doi: 10.1177/0959683615618264

de Groot, W. J., Pritchard, J. M., and Lynham, T. J. (2009). Forest floor fuel consumption and carbon emissions in Canadian boreal forest fires. *Can. J. For. Res.* 39, 367–382. doi: 10.1139/X08-192

Drysdale, D. (2011). *An Introduction to Fire Dynamics*, 3rd Edn. Hoboken, NJ: Wiley. doi: 10.1002/9781119975465

Doerr, S. H., Santin, C., Merino, A. G., Belcher, C. M., and Baxter, G. (2018). Fire as a removal mechanism of pyrogenic carbon from the environment: effects of fire and pyrogenic carbon characteristics. *Front. Earth Sci.* 6:127. doi: 10.3389/feart.2018.00127

Harvey, O. R., Kuo, L. J., Zimmerman, A. R., Louchouarn, P., Amonette, J. E., and Herbert, B. E. (2012). An index-based approach to assessing recalcitrance and soil carbon sequestration potential of engineered black carbons (biochars). *Environ. Sci. Technol.* 46, 1415–1421. doi: 10.1021/es2040398

Hudspith, V. A., and Belcher, C. M. (2017). Observations of the structural changes that occur during charcoalification: implications for identifying charcoal in the fossil record. *Palaeontology* 60, 503–510. doi: 10.1111/pala.12304

Hudspith, V. A., Belcher, C. M., Kelly, R., and Hu, F. S. (2015). Charcoal reflectance reveals early Holocene boreal deciduous forests burned at high intensities. *PLoS One* 10:e0120835. doi: 10.1371/JOURNAL.PONE.0120835

Hudspith, V. A., Belcher, C. M., Barnes, J., Dash, C. B., Kelly, R., and Hu, F. S. (2017a). Charcoal reflectance suggests heating duration and fuel moisture affected burn severity in four Alaskan tundra wildfires. *Int. J. Wildl. Fire* 26, 306–316. doi: 10.1071/WF16177

Hudspith, V. A., Hadden, R. M., Bartlett, A. I., and Belcher, C. M. (2017b). Does fuel type influence the amount of charcoal produced in wildfires? Implications for the fossil record. *Palaeontology* 61, 159–171. doi: 10.1111/pala.12341

Jones, T., Scott, A. C., and Cope, M. (1991). Reflectance measurements against temperature of formation for modern charcoals and their implications for the study of fusain. *Bulletin Soc. Ge'ol. France* 162, 193–200.

Kashiwagi, T., Ohlemiller, T. J., and Werner, K. (1987). Effects of external radiant heat flux and ambient oxygen concentration on non-flaming gasification rates and evolved products in white pine. *Combust. Flame* 69, 331–345. doi: 10.1016/0010-2180(87)90125-8

Keeley, J. E. (2009). Fire intensity, fire severity and burn severity: a brief review and suggested usage. *Int. J. Wildl. Fire* 18, 116–126. doi: 10.1071/WF07049

Keiluweit, M., Nico, P. S., Johnson, M., and Kleber, M. (2010). Dynamic molecular structure of plant biomass-derived black carbon (biochar). *Environ. Sci. Technol.* 44, 1247–1253. doi: 10.1021/es9031419

Knicker, H., Muller, P., and Hilscher, A. (2010). How useful is chemical oxidation with dichromate for the determination of "Black Carbon" in fire-affected soils? *Geoderma* 142, 178–196. doi: 10.1016/j.geoderma.2007.08.010

Lyon, R. E., and Walters, R. (2002). "A microscale combustion calorimeter," in *Federal Aviation Administration William J. Hughes Technical Centre. Report No. DOT/FAA/AR-01/117*. Washington, DC: US Department of Transport.

McBeath, A. V., Smernik, R. J., and Krull, E. S. (2013). A demonstration of the high variability of chars produced from wood in bushfires. *Org. Geochem.* 55, 38–44. doi: 10.1016/j.orggeochem.2012.11.006

McParland, L. C., Collinson, M. E., Scott, A. C., and Campbell, G. (2009). The use of reflectance values for the interpretation of natural and anthropogenic charcoal assemblages. *Archaeol. Anthropol. Sci.* 1, 249–261. doi: 10.1007/S12520-009-0018-Z

Michelotti, L., and Miesel, J. (2015). Source material and concentration of wildfire-produced pyrogenic carbon influence post-fire soil nutrient dynamics. *Forests* 6, 1325–1342. doi: 10.3390/f6041325

Moghtaderi, B., Novozhilov, V., Flectcher, D. F., and Kent, J. H. (2006). A new correlation for bench-scale piloted ignition of wood. *Fire Saf. J.* 29, 41–59. doi: 10.1016/S0379-7112(97)00004-0

Moreira-Vilar, F. C., Ferro, A. P., and Finger-Teixeira, A. (2014). The acetyl bromide method is faster, simpler and presents best recovery of lignin in different herbaceous tissues than klason and thioglycolic acid methods. *PLoS One* 9:e110000. doi: 10.1371/journal.pone.0110000

Santín, C., Doerr, S. H., Preston, C. M., and González-Rodríguez, G. (2015). Pyrogenic organic matter production from wildfires: a missing sink in the global carbon cycle. *Glob. Chang. Biol.* 21, 1621–1633. doi: 10.1111/gcb.12800

Santín, C., Doerr, S. H., Kane, E. S., Masiello, C. A., Ohlson, M., de la Rosa, J. M., et al. (2016). Towards a global assessment of pyrogenic carbon from vegetation fires. *Glob. Chang. Biol.* 22, 76–91. doi: 10.1111/gcb.12985

Santín, C., Doerr, S. H., Merino, A., Bucheli, T. D., Bryant, R., Ascough, P., et al. (2017). Carbon sequestration potential and physicochemical properties differ between wildfire charcoals and slow-pyrolysis biochars. *Sci. Rep.* 7:11233. doi: 10.1038/s41598-017-10455-2

Scott, A. C., and Glasspool, I. J. (2007). Observations and experiments on the origin and formation of inertinite group macerals. *Int. J. Coal. Geol.* 70, 53–66. doi: 10.1016/j.coal.2006.02.009

**Conflict of Interest Statement:** The authors declare that the research was conducted in the absence of any commercial or financial relationships that could be construed as a potential conflict of interest.

frontiers in Earth Science

ORIGINAL RESEARCH
published: 14 May 2018
doi: 10.3389/feart.2018.00041

# Quantifying Changes in Total and Pyrogenic Carbon Stocks Across Fire Severity Gradients Using Active Wildfire Incidents

*Jessica Miesel[1*†], Alicia Reiner[2], Carol Ewell[3], Bernardo Maestrini[1] and Matthew Dickinson[4]*

[1] Department of Forestry, Michigan State University, East Lansing, MI, United States, [2] Enterprise Program, USDA Forest Service, Brevard, NC, United States, [3] Region 5, USDA Forest Service, Sonora, CA, United States, [4] Northern Research Station, USDA Forest Service, Delaware, OH, United States

OPEN ACCESS

**Edited by:**
*Cristina Santin, Swansea University, United Kingdom*

**Reviewed by:**
*Matthew William Jones, University of Exeter, United Kingdom*
*Gustavo Saiz, Imperial College London, United Kingdom*

***Correspondence:**
*Jessica Miesel*
*mieselje@msu.edu*

**†Present Address:**
*Jessica Miesel, Department of Plant, Soil and Microbial Sciences, Michigan State University, East Lansing, MI, United States*

**Specialty section:**
*This article was submitted to Biogeoscience, a section of the journal Frontiers in Earth Science*

**Received:** *09 October 2017*
**Accepted:** *06 April 2018*
**Published:** *14 May 2018*

**Citation:**
*Miesel J, Reiner A, Ewell C, Maestrini B and Dickinson M (2018) Quantifying Changes in Total and Pyrogenic Carbon Stocks Across Fire Severity Gradients Using Active Wildfire Incidents. Front. Earth Sci. 6:41. doi: 10.3389/feart.2018.00041*

Positive feedbacks between wildfire emissions and climate are expected to increase in strength in the future; however, fires not only release carbon (C) from terrestrial to atmospheric pools, they also produce pyrogenic C (PyC) which contributes to longer-term C stability. Our objective was to quantify wildfire impacts on total C and PyC stocks in California mixed-conifer forest, and to investigate patterns in C and PyC stocks and changes across gradients of fire severity, using metrics derived from remote sensing and field observations. Our unique study accessed active wildfires to establish and measure plots within days before and after fire, prior to substantial erosion. We measured pre- and post-fire aboveground forest structure and woody fuels to calculate aboveground biomass, C and PyC, and collected forest floor and 0–5 cm mineral soil samples. Immediate tree mortality increased with severity, but overstory C loss was minimal and limited primarily to foliage. Fire released 85% of understory and herbaceous C (comprising <1.0% of total ecosystem C). The greatest C losses occurred from downed wood and forest floor pools (19.3 ± 5.1 Mg ha$^{-1}$ and 25.9 ± 3.2 Mg ha$^{-1}$, respectively). Tree bark and downed wood contributed the greatest PyC gains (1.5 ± 0.3 Mg ha$^{-1}$ and 1.9 ± 0.8 Mg ha$^{-1}$, respectively), and PyC in tree bark showed non-significant positive trends with increasing severity. Overall PyC losses of 1.9 ± 0.3 Mg ha$^{-1}$ and 0.5 ± 0.1 Mg ha$^{-1}$ occurred from forest floor and 0–5 cm mineral soil, with no clear patterns across severity. Fire resulted in a net ecosystem PyC gain (1.0 ± 1.0 Mg ha$^{-1}$) across aboveground and belowground components of these forests, and there were no differences among severity levels. Carbon emissions represented only 21.6% of total forest C; however, extensive conversion of C from live to dead pools will contribute to large downed wood C pools susceptible to release in a subsequent fire, indicating that there may be a delayed relationship between fire severity and C emissions. This research advances understanding of forest C loss and stabilization as PyC in wildfires; however, poor relationships between C and PyC gains or losses and fire severity highlight the complexity of fire impacts on forest C.

**Keywords: California, fire behavior assessment team, charcoal, pyrogenic organic matter, black carbon, fire effects, burn severity**

## INTRODUCTION

Wildfires play a major role in controlling forest carbon (C) storage and cycling in fire-suppressed forests in the western United States (US) (Earles et al., 2014), and are expected to increase in frequency and size in future climate conditions (Westerling et al., 2011; Moritz et al., 2012). Increased tree density and fuel accumulation in low- to middle-elevation mixed-conifer forests of the western US since the early 1900s have contributed to the present-day occurrence of fires that are larger and burn at greater intensity relative to historic conditions (Covington and Moore, 1994; Schoennagel et al., 2004). Increased fire activity in these forests has also been influenced by warming temperatures in recent decades (Westerling et al., 2006). For example, warming temperatures are associated with earlier and warmer growing seasons, as well as increased fire season length, and, in combination with drought, also increase tree mortality rates, fuel load accumulation, and flammability of live and dead fuels (Breshears et al., 2005; Westerling et al., 2006; Van Mantgem et al., 2009; Littell et al., 2016). Projections of future wildfire area burned in the state of California range from increases of 36–74% by the year 2085, and >100% for forests in northern California (Westerling et al., 2011). These changes are expected to lead to positive feedbacks among climate, fire and fire-mediated C cycling that threaten to exacerbate climate warming (Liu et al., 2014; Barbero et al., 2015; Millar and Stephenson, 2015), which in turn increases drought stress in trees, and, consequently, increased fire severity (Van Mantgem et al., 2013).

The severity of a fire describes the magnitude of impact to an ecosystem, and is represented by a wide variety of definitions and metrics (Keeley, 2009; Jain et al., 2012; Morgan et al., 2014). Keeley (2009) provided a standardized definition of fire severity as "aboveground and belowground organic matter consumption from fire" and he includes fire-caused plant mortality as a type of organic matter consumption. Consequently, accumulated fuels and their increased flammability due to low moisture content during drought conditions are likely to contribute to increased wildfire combustion and, therefore, severity of immediate effects.

Increases in fire severity and patch size of high-severity areas in many conifer forests in California have been reported over recent decades, with above-average increases in low- to middle-elevation forests such as the widespread mixed-conifer forest type (Miller et al., 2009b). The proportion of area burned in conifer forests is also greater in areas dominated by smaller-diameter trees than areas dominated by larger-diameter trees (Miller et al., 2012), suggesting that fire-suppressed forests as well as regenerating forests are susceptible to—and contribute to—increased fire size and severity.

Efforts to develop and apply standard indices for characterizing fire severity are relatively recent and include remote sensing approaches (Key and Benson, 2006; Miller and Thode, 2007; Robichaud et al., 2007) as well as field classification of composite [e.g., Composite Burn Index (CBI), (Key and Benson, 2006)] and stratrum-specific impacts (NPS, 2003; Keeley, 2009; Jain et al., 2012). Field indices classify fire severity based on the extent of organic matter loss or decomposition (i.e., using metrics such as tree crown scorch, tree mortality, woody fuel consumption, loss of soil organic horizons, etc.), and although vegetation composition, structure, and environmental factors also influence organic matter loss, fire severity indices generally reflect fireline intensity (Keeley, 2009; Morgan et al., 2014). Because of variability in characteristics in vegetation and soil within and across ecosystems (e.g., extent of mineral soil exposure, soil color, vegetation structure and stem density), fire severity is best evaluated based on knowledge of pre-fire ecosystem characteristics (Keeley, 2009), but these data often may not exist in areas that experience unplanned fires.

Understanding how fire severity influences C flux to the atmosphere is crucial, not only for predicting climate impacts, but also for developing mitigation strategies that support forest resilience, especially in a time of shifting disturbance regimes and poorly understood impacts on forest ecosystem services. Over a full post-fire successional sequence and at landscape scales in fire-adapted systems with constant fire return intervals, the net impact of fire on C emissions is zero, because tree growth will offset the C emission due to combustion and dead biomass decomposition (Harmon, 2001; Hurteau and Brooks, 2011; Loehman et al., 2014). However, this theory may not hold if one of its assumptions—full post-fire successional sequence, landscape scale, constant fire return interval, no fire-induced structural change—is not met. Future scenarios of changes in the climate and the socio-economic context in Californian mixed conifer forests are now challenging the applicability of the net-zero emission principle in the future. For example, an increase in fire severity in Sierra Nevada forests, as suggested by Miller and Safford (2012), has potential to impact forest structure by favoring chaparral over mixed conifer forests (Lauvaux et al., 2016). Under a scenario where the net zero emission principle is applicable, the timescale for complete recovery of emitted C is largely dependent on the pre-fire conditions and fire severity. For example, a study conducted 4–5 years after fire in an Oregon mixed-conifer forest showed that low-severity areas were a net sink of C even though they had only partially recovered the lost C, whereas high-severity areas were still a C source because of dead wood decomposition (Meigs et al., 2009). Weichman et al. (2015) found that 50% of emitted C was recovered 10 years after a prescribed burn in a California mixed-conifer forest, whereas Eskelson et al. (2016) reported significant losses of live wood C in low- and moderate-severity areas, but no change in high-severity areas, over 6 years post-fire for 130 Forest Inventory and Analysis plots in the same state. Therefore, in fire-prone forests, increases in fire severity have potential to increase short-term C losses via fire emissions (including emissions from otherwise longer-lived C pools such as dead wood and mineral soil C) as well as decrease longer-term C storage by slowing the rate of post-fire forest recovery (Pan et al., 2011). For example, a shift from historically low- to mixed-severity fire in western mixed-conifer forests to fires that are larger and result in a greater extent of high-severity areas has potential to disrupt successional trajectories and result in ecosystem replacement, with major impacts on post-fire C sequestration (Folke et al., 2004; Bond-Lamberty et al., 2007).

However, the relationship between fire severity and forest C budgets are complex, because wildfires not only release C from

terrestrial to atmospheric pools, they also produce pyrogenic C (PyC) that contributes to C sequestration over longer (i.e., decadal to millennial) time-scales when present in soils (Bird et al., 2015; Santín et al., 2015b). Pyrogenic C defines a class of organic compounds altered by heat under anoxic conditions (pyrolysis). The chemistry of these molecules is heterogenous and can be represented as a "continuum" of compounds ranging from slightly charred biomass to highly condensed aromatic materials (Masiello, 2004; Bird et al., 2015), all of which are characterized by an increase in C concentration relative to their non-pyrolyzed precursors (Bird et al., 2015). Although part of the PyC pool is labile, PyC ages of 100s−1000s of years, and even up to 10,000 years have been reported in the top 1 m of soil, indicating that PyC can be one of the longest-lived C pools in terrestrial ecosystems (Schmidt et al., 2002, 2011; Eckmeier et al., 2009). Therefore, conversion of biomass and soil C into long-lived PyC during fires may help mitigate a proportion of fire-induced C losses.

Seiler and Crutzen (1980) produced the first global estimate of PyC production using a simple model based on burned area, biomass stock and burning efficiency. Since then, charcoal research has reached important milestones in determining the fate of PyC once it become embedded in the soil matrix; however, the production rate of PyC during wildfire in natural conditions still represents a poorly addressed research gap (Santín et al., 2015a). Biomass type and formation conditions (i.e., temperature, oxygen availability) influence PyC stocks and characteristics (Baldock and Smernik, 2002; Hammes et al., 2006; McBeath et al., 2011; Hatton et al., 2016), and natural PyC is known to exhibit a range of physical and chemical characteristics depending on fire characteristics (McBeath and Smernik, 2009; McBeath et al., 2013; Michelotti and Miesel, 2015; Uhelski and Miesel, 2017). Conversion rates for C to PyC in boreal forests for the forest floor layer range between 0.7% using the benzene polycarboxylic acid (BPCA) method (Czimczik et al., 2003) and 24.5% using elemental analysis on visually blackened material (Santín et al., 2015b). Conversion rates also vary across forest components, as low as 7.3% for conifer needles to 67.1% for bark in a boreal jack pine fores (Santín et al., 2015b). Saiz et al. (2015) estimated a 16% conversion rate for surface fuels across contrasting tropical savannas using visual, gravimetric and total C identification. Differences among ecosystems and among quantification methodologies contribute to the variability of these results. Many studies, in fact, report only a partial estimate of charcoal formation, e.g., accounting only for the charcoal present on the ground after fire (Fearnside et al., 2001) or in the bark of standing trees (Makoto et al., 2011). PyC formation rates have also been investigated in laboratory studies, and although the influence of individual factors on PyC formation rate has been well characterized—e.g., temperature (Keiluweit et al., 2010), moisture (Brewer et al., 2013), or fuel type (Hammes et al., 2006)—their interaction in the field remains largely unpredictable (Santín et al., 2017). Therefore, there is a pressing need to produce data that will help predict PyC formation rate from data on biomass and fire characteristics that are increasingly available at relatively high spatial and temporal resolution, e.g., data derived from remote sensing.

Remote sensing as well as field observations can be used to assess fire severity after a fire, which, in general, represents combined effects of fire intensity and residence time (Eidenshink et al., 2007; Keeley, 2009). Fire behavior drives the magnitude and duration of heating of biomass, which in turn influences PyC characteristics. However, current understanding of the influences of fire severity and pre-fire forest fuel loads on PyC formation during forest fires is limited (González-Pérez et al., 2004; DeLuca and Aplet, 2008). Previous efforts to quantify PyC across gradients of fire severity have focused primarily on PyC stocks or concentrations in soil (Pingree et al., 2012; Boot et al., 2015; Miesel et al., 2015), although a recent investigation of post-erosion PyC pools in California mixed-conifer forest quantified PyC in the aboveground and belowground pools (Maestrini et al., 2017). Santín et al. (2015b) provided the first estimation of pre- and post-fire PyC stocks in a boreal jack pine forest by measuring changes in C concentration in visually blackened material; however, their study site represented high-severity fire only (i.e., as defined by mortality to forest overstory) in which impacts to mineral soil were negligible due to high moisture content. A critical next step is to obtain the information necessary for understanding the direct impacts of wildfire and fire severity level on forest PyC stocks, especially in forests vulnerable to ecosystem type conversion via fire activity that falls outside the range of historic variability.

Our overarching objectives were to quantify wildfire impacts on aboveground and belowground total C and PyC stocks in California mixed-conifer forests, and to investigate relationships between net changes in C or PyC and fire severity level, using three fire severity classification systems. We used nearly immediate pre- and postfire (i.e., typically within less than a week before and after fire) measurements of the forest overstory, understory, herbaceous layer, downed wood, and soil (organic horizon and 0–5 cm mineral soil) to quantify fire-induced changes to ecosystem-level C and PyC stocks, across fire severity levels derived from remote sensing imagery, as well as from vegetation and substrate severity indicators classified in the field.

# METHODS

## Study Area

Our study sites included five active wildfire incidents that occurred in 2014 and 2015 in mixed-conifer forest in California, USA (**Figure 1**, **Table 1**). Both years of the study were part of a record-setting drought that began in 2012, and all fires occurred during the hottest months of the year. These forests are characterized by a mixture of conifer species including ponderosa, Jeffrey and sugar pines (*P. ponderosa, P. jeffreyi,* and *P. lambertiana*), white fir (*Abies concolor*), Douglas-fir (*Pseudotsuga menziesii*), and incense cedar (*Calocedrus decurrens*). This is a widespread forest type on US Forest Service (FS) and National Park Service (NPS) land in the Sierra Nevada ecoregion of California, with a history of low-severity fires occurring at 11–16 year intervals prior to Euro-American settlement, documented by tree ring studies and fire records dating to the early 1900s (Van de Water and Safford, 2011). Soils at these sites are coarse-textured and characterized

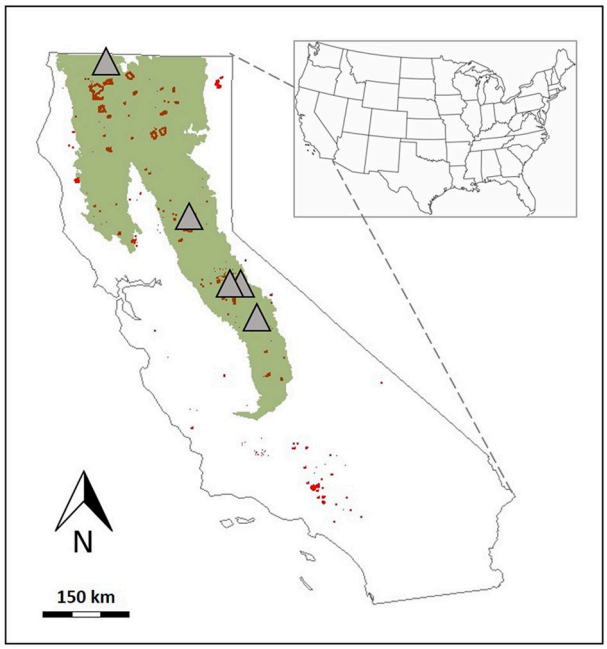


**FIGURE 1 |** Map of California, USA showing Sierra Nevada mixed-conifer vegetation type (green polygon), fires occurring between 2014 and 2015 (red polygons), and locations of the five wildfires from which data were collected for this study (gray triangles). Inset map shows the location of California in the continental United States.

as well-drained to somewhat excessively drained Alfisols and Inceptisols, with the soil derived from material weathered from granitic bedrock; one site supported Andisols formed in material weathered from andesitic breccia or andesitic mudflows, characterized as well- to somewhat excessively drained (NRCS, 2018). Mean annual precipitation ranges between 76.2 and 139.7 cm and occurs primarily as winter snowpack; mean annual temperature ranges between 8.9 and 12.8°C.

## Field Methods

The USDA Forest Service Fire Behavior Assessment Team (FBAT) installed fire behavior instrumentation and conducted pre-fire measurements and sampling at all sites before fire, and duplicated the set of measurements and sampling after the fire passed through a given plot, when it was determined safe to re-enter. During a wildfire incident, the incident management team or other official can request the FBAT team to measure and/or monitor fuels and fire behavior to support fire management decisions. A.R and C.E. led the coordination and training, logistics and resources of the team. The five wildfire sites we used in this study provided 29 plots with pre- and post-fire measurements: 76% of these plots were measured within 5 days post-fire, and another 17% were measured ≤10 days post-fire; only two plots (7% of total) were measured 12 and 14 days post-fire (**Table 1**). Plots were established in areas expected to burn; however, in some cases the path of the fire did not coincide with plot location; we excluded unburned plots from this study. Therefore, the number of plots used for this study were distributed unevenly across the five fires.

Each plot was installed within a relatively homogenous area (in terms of forest structure and environmental characteristics) to avoid the potential for plots to overlap two different fire severity classes derived from the 30-m Landsat pixel scale. We took plot photographs (**Figure 2**) and recorded GPS location, slope, aspect, elevation and topographic position. Because of the need to rapidly measure plots to determine forest structure and composition, we used a Relaskop (using basal area factors of 5, 10, 20 depending on stand density) to record basal area in a variable-radius plot approach, following standard rapid-assessment forest mensuration methods. We then recorded tree species, diameter at breast height (DBH; stem diameter at 1.37 m above ground), total height, height to live crown, and live/dead status for tree (>15.0 cm DBH) and pole (2.5–15.0 cm DBH) size classes for all stems determined to be "in" via the Relaskop approach (NPS, 2003; Jain and Graham, 2007). Dead tree (snag) decay class was also recorded (NPS, 2003; Domke et al., 2011). We measured char height (minimum and maximum) on tree boles, percentage of tree crown scorched (i.e., present but killed) by fire, and percentage of tree crown consumed by fire.

We used the line intercept method to measure dead and down woody debris (hereafter: downed wood) and litter ($O_i$ horizon) and duff ($O_e$+$O_a$ horizons) depths along three 15.24 m transects radiating from plot center (Van Wagner, 1968; Brown, 1974). We also visually estimated the percent cover for each NPS vegetation and substrate burn severity class (NPS, 2003) for the area inside a 15 m radius circular plot overlain on plot center, and then calculated the weighted average of the classes to obtain a plot-level estimate for vegetation burn severity and, separately, for substrate burn severity. The substrate and understory severity classification followed protocol developed by the NPS (2003) presented in Supplementary Material (Table S1), hereafter referred to as "NPS substrate" and "NPS vegetation severity," respectively. We also measured total forest floor (litter and duff) depth and collected volumetric soil samples from the organic horizon (i.e., forest floor) and 0–5 cm mineral soil (Miesel et al., 2015) at an additional three locations per plot for a subset of the plots (i.e., for plots at which soil sample collection was possible based on time and safety considerations). Only six of the plots sampled for soils were affected by fire (producing 18 paired pre- and post-fire samples). Each severity metric was assessed at the plot scale; severity was not assessed separately at the soil sample locations. Post-fire samples of the residual forest floor layer included the ash; therefore the ash mass and C content was quantified as part of the post-fire (i.e., fire-altered) forest floor. The distribution of data for forest floor depths measured for whole-plot estimates and at the soil sample locations are shown in Figure S1.

Our original goal was to collect pre- and post-fire forest floor and mineral soil samples near a soil thermocouple to relate changes in C and PyC to the magnitude or duration of heating (i.e., rather than collecting and pooling a larger number of samples from the plot); however, we were unable to obtain enough satisfactory data from the thermocouples near soil sample locations to confidently include in this analysis. In

**FIGURE 2 |** Paired photos taken during pre-fire and post-fire measurements showing examples of fire impacts on forest vegetation and substrate at four plot locations used in this study. For each pair of photos, pre-fire conditions are shown on the left and post-fire conditions are shown on the right. Photo credit: Reiner and Ewell.

**TABLE 1 |** Fire and location information[a] for the five wildfires used in this study.

| Fire name | Ignition date | Ignition cause | Fire location (lat, long; °) | Area burned (ha) | Number of Plots burned | Elevation (m) | Slope (%) | Aspect (°) | Pre-fire measurement date | Post-fire measurement date |
|---|---|---|---|---|---|---|---|---|---|---|
| French | 28 Jul 2014 | Human | 37.275, −119.337 | 5,600 | 2 | 1,524–1,597 | 25–33 | 130–140 | 31 Jul | 03 Aug |
| Beaver | 30 Jul 2014 | Lightning | 41.930, −122.869 | 13,151 | 7 | 711–1,398 | 25–60 | 80–340 | 06–09 Aug | 12–13 Aug |
| King | 13 Sep 2014 | Human | 38.782, −120.604 | 39,545 | 3 | 1,514–1,669 | 4–20 | 270–0 | 17–19 Sep | 21–23 Sep |
| Rough | 31 Jul 2015 | Lightning | 36.874, −118.905 | 6,1360 | 13 | 1,851–2,476 | 5–45 | 60–360 | 17 Aug−12 Sep | 01–14 Sep |
| Willow | 25 Jul 2015 | Human | 37.282, −119.502 | 2,307 | 4 | 1,320–1,719 | 25–45 | 210–320 | 29–31 Jul | 02 Aug |

*Information on elevation, slope, aspect, and measurement dates are given for only those plots used in this study, rather than for the overall area burned in each fire.* [a]*Fire location, area and cause information available from https://inciweb.nwcg.gov.*

addition to classifying the NPS vegetation and substrate severities described above, we also identified plot-level fire severity level from geospatial layers available from the Monitoring Trends in Burn Severity (MTBS) program, which provided severity classifications derived from Landsat Thematic Mapper imagery via the dNBR approach (Eidenshink et al., 2007) and calibrated to the CBI (Miller et al., 2009a; Miller and Quayle, 2015), hereafter referred to as remote sensing (RS) severity.

## Laboratory Methods

Soil samples were shipped to the laboratory and air-dried to constant mass. Pre- and post-fire forest floor samples were ground to pass a 1 mm screen, and 0–5 cm mineral soil samples were sieved to 2 mm to remove stones and roots. We then pulverized a subsample of each forest floor and mineral soil sample to fine powder and dried to remove all moisture (60°C for forest floor samples; 105°C for mineral soil samples) before elemental analysis for total C and N (Costech, Italy; 1,000°C combustion temperature). We also determined pyrogenic C in forest floor and mineral soil samples as oxidation-resistant C using a weak nitric acid-peroxide method following Kurth et al. (2006) for mineral soil samples and Maestrini and Miesel (2017) for forest floor samples. The modification of Kurth et al. (2006) presented by Maestrini and Miesel (2017) for use in organic matrices requires pre-digestion dilution of organic sample in a carbon-free pulverized quartz matrix to ensure full digestion

of non-resistant C while ensuring sufficient post-digestion solid mass to collect for elemental analysis. Briefly, we digested 0.5 g of sample in a solution of 10 mL 1N nitric acid combined with 20 mL of 30% hydrogen peroxide at 100°C for 16 h in a block digester (BD50, Seal Analytical, USA). Digestion tubes were capped with teardrop stoppers to minimize evaporation, and were periodically agitated during the first 4 h to disperse foam that forms during the digestion. Tubes were removed from the block digester at the end of 16 h and allowed to cool to room temperature before agitating to suspend the solid digestion residue into the solution, and then vacuum filtering (Whatman, Grade 2 filters). We dried the solid residue on each filter at 70°C for 24 h before weighing, and then measured C concentration as described above. All PyC results we present represent estimates derived from this chemical oxidation approach ($PyC_{CTR}$) which, like all PyC quantification methods, cannot fully represent the complete PyC spectrum (Hammes et al., 2007). For brevity we use "PyC" in our Results section where only our data are presented, whereas in the Discussion we will use "$PyC_{CTR}$" to differentiate our oxidation-based estimates of PyC from the broader concept of PyC regardless of method (Zimmerman and Mitra, 2017).

## Calculations and Statistical Approach

We used genus-specific allometric equations to calculate tree and pole biomass for pre- and post-fire measurements, adjusting for foliage and branch loss (Jenkins et al., 2004). Biomass estimates for dead trees (snags) pre- and post-fire were adjusted for snag decay class following Domke et al. (2011). Data for live basal area and quadratic mean diameter are shown in Figure S2; biomass data for all aboveground forest components are shown in Figure S3. We used a biomass fraction of 0.50 to calculate tree and pole C mass, following standard convention. To quantify pyrogenic C in the tree layer, we assimilated tree volume to a cone, and used the measured char height from this study and overall mean char depth from other study sites in mixed-conifer forest the same region (Maestrini et al., 2017) to calculate char volume. Char volume was calculated as the difference between the volume of a frustrum of the tree from base to mean char height, and the volume of the uncharred core of the same frustrum. We then calculated char mass as the product of char volume and the mean bulk density of charred bark, and PyC mass as the mass fraction of PyC in charred bark samples. Bulk density and PyC mass fraction of charred bark from mixed-conifer forests follow values presented by Maestrini et al. (2017). Pre-fire char was noted if present on trees but was determined to be not quantitatively significant; therefore, it is possible that the calculations in this study provide a slight over-estimate of tree char produced by the single fires.

We used field measurements of understory vegetation height and percent cover to categorize understory species by density class and species type (e.g., based on stem thickness), and then calculated understory fuel biomass (for tree seedling and shrubs, and for herbaceous species including grasses) using bulk density coefficients extracted from the BEHAVE Fuel Subsystem (Scott, 2018, Personal communication), where fuel load is the product of bulk density, depth and percent cover (Burgan and Rothermel, 1984). We calculated C mass in the understory and herbaceous layer following C mass fraction for mixed-conifer forest given in Campbell et al. (2009). Because this layer experienced major loss of biomass during fire, we assumed that PyC formed by the fire in the understory and herbaceous layers was transferred to the forest floor. We calculated fuel loadings (biomass) for pre- and post-fire woody fuels and the forest floor following the methods of Van Wagtendonk et al. (1998), and converted to C mass using published values for this region (Harmon et al., 1987). We did not collect field measurements of charring on downed wood; therefore, based on our previous work in other mixed-conifer sites, we assumed negligible pre-fire charring on this component. For post-fire downed wood, we assumed an overall mean of 0.23 PyC/C mass fraction for pieces <8.0 cm diameter, and 0.39 PyC/C mass fraction for pieces >8.0 cm diameter at the point of intersection with the survey line, which represents the mean value for each downed wood size category across severity levels (severity determined via remote sensing data) in burned areas in the same mixed-conifer ecosystem type presented by Maestrini et al. (2017). Maestrini et al. (2017) measured PyC 2–3 years post-fire, so using their values probably underestimates downed wood PyC in our study. Forest floor horizon depth and biomass are presented in Figure S4.

Forest floor C stock was calculated using pre- and post-fire values of mass per unit area determined from the sum of the litter and duff fuel loads (described above, as determined along the fuels transects, Figure S1) multiplied by C concentration measured in the physical samples collected. We used the actual measured plot mean C concentration when possible, and we used the grand mean within NPS substrate severity level for the C concentration for plots for which no physical samples were collected. For mineral soil we calculated C stock by multiplying the fine fraction (<2 mm) soil mass per unit area for the 0–5 cm depth increment from other nearby study sites in mixed-conifer forests by the C concentration measured in the soil samples collected in this study (with "missing values" replaced by the grand mean within severity as described above for forest floor). We used a value of 2.40 g $cm^{-2}$ at one fire site (determined during a follow-up visit 1 year post-fire), whereas we used 3.10 g $cm^{-2}$ for the other four sites based on measurements by Maestrini et al. (2017); both values represent the total mass of fine fraction soil in the 0–5 cm depth increment. Similarly, we used PyC mass fraction as determined by nitric acid digestion described above to calculate PyC stocks for the forest floor and for 0–5 cm mineral soil. Pre- and post-fire total C and PyC stocks for the physical samples of forest floor and mineral soil are shown in Figure S5. For the purposes of this study, we took a conservative approach and calculated within-plot means for forest floor and mineral soil C and PyC stocks. All statistical analyses were performed using the plot as the unit of replication.

We calculated change in C and PyC by subtracting post-fire C and PyC stocks from pre-fire C and PyC stocks within plot, for each individual forest component and also for the sum of all forest components (hereafter, "total ecosystem" C or PyC). We interpreted a loss of total ecosystem C as C emissions, following North et al. (2009), whereas negative changes in C stock in individual forest components could indicate either a conversion to PyC in (and/or a transfer to) another component and/or

emitted C; therefore, changes in individual component C stocks are not assumed to be emitted C. We calculated the C affected by fire as the sum of C lost and C converted to PyC, and the conversion rate of C to PyC as the ratio of PyC to C affected (i.e., sum of C loss and conversion to PyC; hereafter PyC/CA), following Santín et al. (2015b). We used general linear models (GLMs) to investigate differences in C or PyC stocks between pre- and post-fire measurements within severity classes, for each forest component (SAS 9.4, SAS Institute, Inc., Cary, NC), using elevation as a covariate to control for variability in plot characteristics due to elevation. We also used GLMs to investigate differences in the magnitude of C or PyC change between pre- and post-fire measurements, among severity classes, using elevation and pre-fire forest biomass measurements from each forest stratum as covariates to control for variation in pre-fire plot characteristics. Quantification of the specific effects of covariates on the response variables was not the focus of the study and they are not discussed further. We log-transformed data where necessary to meet model assumptions, and we ranked data before analysis when standard transformations failed to meet model assumptions. We used Tukey-adjusted pairwise comparisons to identify difference between pre- vs. post-fire C and PyC stocks within severity level, and for comparisons among severity level within pre-fire measurements and within post-fire measurements. Although we present results for all forest components, we recognize that the hypothesis test of no difference between total pre- and postfire C stocks is somewhat paradoxical because combustion of biomass during wildfire by definition releases C from the ecosystem. We determined statistical significance at $p < 0.05$ unless indicated otherwise. Descriptive statistics for all figures and tables presented in this manuscript are also provided in tabular form in supplementary information (Table S2).

**TABLE 2 |** Severity classification matrix showing distribution of plots (count) assessed for fire severity level using remote sensing (RS), and National Park Service (NPS) vegetation and substrate severity metrics assessed in the field post-fire.

| Remote sensing | Unburned | Scorched | Lightly burned | Moderately burned | Heavily burned |
|---|---|---|---|---|---|
| **NPS SUBSTRATE** | | | | | |
| Unchanged | 0 | 0 | 0 | 1 | 0 |
| Low | 0 | 0 | 3 | 5 | 0 |
| Moderate | 0 | 0 | 6 | 5 | 0 |
| High | 0 | 0 | 1 | 8 | 0 |
| **NPS VEGETATION** | | | | | |
| Unchanged | 0 | 0 | 0 | 0 | 1 |
| Low | 1 | 2 | 2 | 0 | 3 |
| Moderate | 0 | 4 | 2 | 2 | 3 |
| High | 0 | 0 | 2 | 1 | 6 |
| **NPS vegetation** | **Unburned** | **Scorched** | **Lightly burned** | **Moderately burned** | **Heavily burned** |
| **NPS SUBSTRATE** | | | | | |
| Unburned | 0 | 0 | 1 | 0 | 0 |
| Scorched | 0 | 0 | 4 | 2 | 0 |
| Lightly | 0 | 0 | 1 | 5 | 0 |
| Moderately | 0 | 0 | 3 | 0 | 0 |
| Heavily | 0 | 0 | 1 | 12 | 0 |

# RESULTS

## Agreement Between Severity Level Measurement Method and Tree Mortality

All plots used in this study were affected by fire, and together represented the full range of severity classes derived from remotely sensed imagery (RS) and the full range of the NPS vegetation severity classes, whereas there was a much more narrow range of severity classes determined by NPS substrate metrics (**Table 2**). In general, we observed relatively low agreement in severity classification, among the three systems applied. For example, although this study omitted plots that were unburned by fire, one burned plot was classified as unchanged by remote sensing metrics, and a different plot was classified as unburned by the NPS vegetation severity metrics (**Table 2**). The plot classified as unchanged by remote sensing metrics demonstrated moderately severe burn when using NPS substrate metrics, and heavily burned conditions when using NPS vegetation metrics. The low RS severity class included plots classified as unburned to moderately burned when using NPS vegetation severity metrics. The majority of plots classified as high RS severity were classified as moderately burned by NPS substrate severity metrics, and as heavily burned using vegetation severity indices. The strongest agreement occurred between the vegetation and substrate severity indices, with 41% of plots classified as heavily burned by vegetation metrics also classified as moderately burned by substrate metrics (**Table 2**).

Across all severity levels, fire caused 74% mortality of live tree stems present before fire, and the difference in stem density between pre-fire and post-fire live trees was significant ($p = 0.0002$) (**Figure 3**). However, when considered by severity level, the loss of live tree stems was significant only for the high RS severity (100% mortality; $p < 0.0001$) and moderate NPS substrate severity (81% mortality; $p = 0.005$) categories (**Figure 3**). There were no differences in pre-fire stem density among any of the post-fire severity classifications, and the only difference among post-fire severity classes occurred between the high and low RS classes (marginal significance; $p = 0.079$). When using RS metrics, tree mortality was 14-fold greater in high severity areas than in low-severity areas ($p = 0.022$), whereas only approximately four times greater than mortality in moderate RS severity areas ($p = 0.066$); there was no tree mortality observed in the RS unchanged class (**Figure 3**). The two NPS severity systems showed trends toward greater tree mortality with severity level, but there were no significant differences among severity levels (**Figure 3**). Elevation explained a significant amount of the variation in tree mortality overall, and for all three of the severity classification systems, but plots that experienced no mortality as well as plots that experienced total mortality

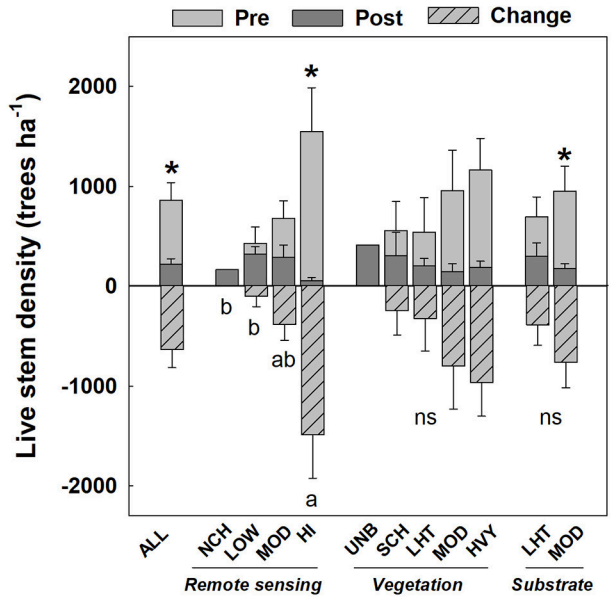


**FIGURE 3 |** Mean (±s.e.) number of live trees ha$^{-1}$ measured pre-fire and post-fire in burned plots, shown for overall severity levels (ALL) and for plots classified by three burn severity classification systems. Fire severity classifications determined from remote sensing includes unchanged (NCH), low (LOW), moderate (MOD), and high (HI) severity. Vegetation and substrate severity follows National Park Service classification scheme, including unburned (UNB), scorched (SCH), lightly burned (LHT), moderately burned (MOD), and heavily burned (HVY). Difference bars below the zero line indicate the number of tree stems killed by the fires used in this study. Asterisks (*) indicate significant differences between pre- and post-fire measurements, within severity level. Lowercase letters below the zero line indicate significant differences in the change between pre- and post-fire measurements (hatched bars) among severity levels within classification system; ns indicates no significant differences ($p < 0.05$). Differences among severity levels for pre-fire and for post-fire measurements are described in the text. All plots used in this study were burned by wildfire, including those classified into the unchanged or unburned severity classes.

occurred across the full range of elevation (711–2,476 and 1,079–2,088 m, respectively).

## Total Fire-Affected Ecosystem C and PyC Stocks

Our results indicated that fire released 54.8 ± 6.6 Mg ha$^{-1}$ C as emissions, and that there was a net ecosystem PyC gain of 1.0 ± 1.0 Mg ha$^{-1}$ (**Figures 4A,B**). However, overall post-fire total ecosystem (forest overstory to 5 cm mineral soil depth) C and PyC (i.e., PyC$_{CTR}$) stocks were 198.2 ± 27.1 Mg ha$^{-1}$ C and 5.3 ± 1.0 Mg ha$^{-1}$ PyC, which was only 21.6% less and 22.5% greater than pre-fire stocks of 253.0 ± 28.4 Mg ha$^{-1}$ C and 4.3 ± 0.3 Mg ha$^{-1}$ PyC, respectively (**Figures 4A,B**). There were no statistically significant differences between pre- and post-fire total ecosystem C or PyC stocks for the grand mean across all severity levels, or for any severity system (**Figures 4A,B**; but see earlier comment about paradoxical hypothesis tests). Total ecosystem C stocks showed greater variability in the RS low-severity class compared to the moderate- and high-severity class for pre-fire as well as post-fire values; however, there were no significant differences among RS severity classes. Neither the total ecosystem C mass loss nor net PyC change between pre- and post-fire measurements differed among severity levels, for any of the three severity classification systems (**Figures 4A,B**).

## Total C and PyC Stocks in Vegetation and Downed Wood

The forest overstory contributed the majority of ecosystem C (71.6%) before fire, whereas downed wood, the forest floor and 0–5 cm mineral soil contributed much lower amounts (9.6, 11.4, and 6.6%, respectively). The understory and herbaceous layers each contributed <1% of total ecosystem C stock. There were no differences in forest overstory (tree layer) C stocks between pre- and post-fire measurements for any of the severity classes (**Figure 4C**). The magnitude of overstory C loss was 4.8 ± 1.9 Mg ha$^{-1}$ overall, and did not differ among RS severity levels (**Figure 4C**). Tree foliage contributed the greatest source of C mass loss from the forest overstory; however, foliage contributed only 3.4% of total overstory C (data not shown). Conversely, overstory PyC mass gain due to fire was greater for high RS severity areas relative to unchanged or low severity areas ($p = 0.014$ and $p = 0.008$, respectively), with a gain of 1.5 ± 0.0 Mg ha$^{-1}$ across all severity levels. Changes in overstory C or PyC stocks due to fire did not differ among severity classes for either the NPS vegetation or substrate indices; however, PyC in tree bark showed non-significant positive trends that followed the severity gradient (**Figures 4C,D**).

We observed an overall loss of 86% of seedling and shrub C stocks due to fire ($p = 0.0163$; **Figure 4E**). However, pairwise comparisons of pre- and post-fire C stocks within severity level showed that the only significant loss occurred in the high RS severity class ($p = 0.001$) and heavily burned NPS vegetation severity systems ($p = 0.033$), both of which showed a 99% loss of C (**Figure 4E**). Similarly, the moderate NPS substrate severity class indicated a 95% loss of C ($p = 0.003$; **Figure 4E**). Areas classified as moderate or high severity by RS metrics supported less overstory C and greater understory C, relative to unchanged and low severity classes (**Figures 4C,E**). No pre-fire differences in seedling and shrub C existed among severity classes for any of the three classification systems, whereas post-fire measurements indicated 97% less C in RS high severity areas relative to moderate severity areas ($p = 0.045$). Although we observed a trend toward increasing C mass loss from the scorched to moderately burned classes in the NPS vegetation system, the pattern was disrupted by the small loss from the heavily burned class; therefore, the magnitude of loss appears to mirror the pre-fire C stocks rather than the severity gradient. Differences in the magnitude of understory C mass loss among severity levels were not statistically significant for any of the three severity classification systems (**Figure 4C**). Similar to our results for understory C, fire caused an overall loss of 93% of herbaceous layer C ($p < 0.0001$; **Figure 4F**). Significant losses also occurred from the moderate ($p = 0.015$) and high ($p = 0.005$) RS severity classes, from moderately ($p = 0.015$) and heavily burned ($p = 0.001$) areas using NPS vegetation metrics, and from areas classified as lightly ($p = 0.042$) and moderately burned ($p <$

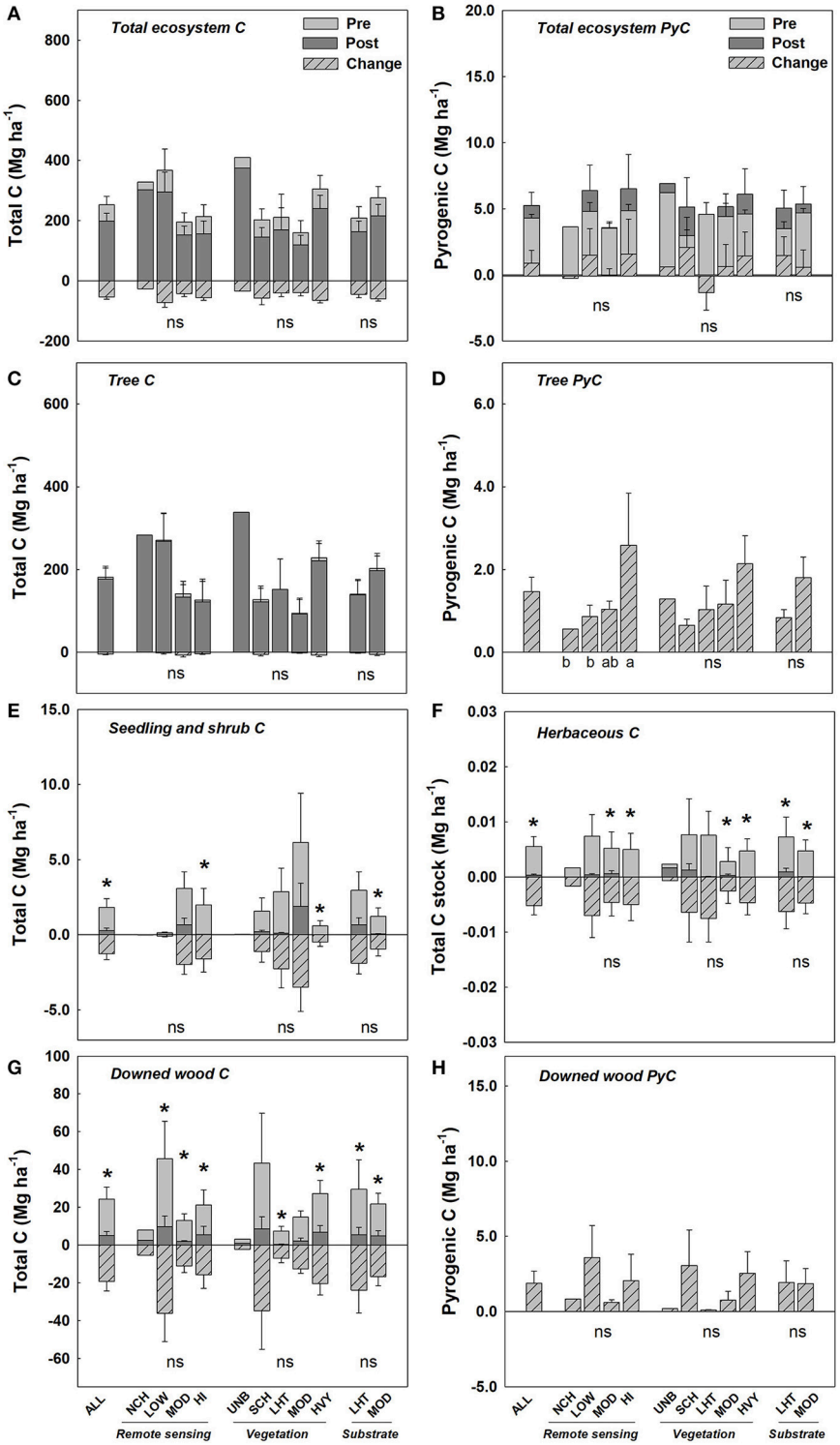


**FIGURE 4 |** Mean (±s.e.) total C and PyC stocks (Mg ha$^{-1}$, estimated as $PyC_{CTR}$ via chemical oxidation) for total ecosystem carbon **(A,B)**, for the forest overstory (i.e., tree layer; **C,D)**; seedling and shrub layer (C only; **E)**, herbaceous and grass layer (C only; **F)**, and downed wood **(G,H)** for pre-fire and post-fire conditions and calculated differences between pre- and post-fire measurements, shown for overall severity levels (ALL) and for plots classified by three fire severity classification systems. Because pre-fire PyC in bark and downed wood was assumed to be negligible, the post-fire PyC stocks in panels **D** and **H** are equivalent to the change (increase) in PyC for these forest components. Severity abbreviations follow those given in **Figure 3**. Asterisks (*) indicate significant differences between pre- and post-fire measurements, within severity level. Lowercase letters below the zero line indicate significant differences in the change between pre- and post-fire measurements (hatched bars) among severity levels within classification system; ns indicates no significant differences ($p < 0.05$). Differences among severity levels for pre-fire and for post-fire measurements are described in the text.

0.0001) using NPS substrate severity metrics (**Figure 4F**).There were no differences in pre-fire herbaceous layer C across severity classes, for any of the three types of severity metrics, and no differences in post-fire C stocks among the RS or NPS vegetation severity indices. In contrast, post-fire C stocks were 100% lower in moderately burned than in lightly burned areas, using the NPS substrate severity classification ($p = 0.034$; **Figure 4F**). There were no differences in the total mass of C lost from the herbaceous layer due to fire among severity levels for any of the severity classification systems (**Figure 4F**).

Fire caused an overall loss of 19.3 ± 5.1 Mg ha$^{-1}$ C from the downed wood pool across all severity levels ($p < 0.0001$ for pre-fire vs. post-fire comparison), as well as for low ($p = 0.047$), moderate ($p = 0.008$), and high ($p = 0.004$) RS severity classes (**Figure 4G**). When using NPS vegetation severity metrics, the only statistically significant changes between pre- and post-fire C stocks occurred for the lightly burned ($p = 0.030$) and heavily burned ($p = 0.001$) areas, whereas for the NPS substrate severity classes, we observed significant losses from both lightly burned ($p = 0.002$) and moderately burned ($p < 0.0001$) areas. There were no differences in downed wood C stocks among severity levels for either pre-fire or post-fire measurements for any of the severity classification systems. The gain in PyC in the downed wood component was 1.9 ± 0.8 Mg ha$^{-1}$ across all severity levels; however, there were no differences in the magnitude of downed wood C mass loss or PyC gain due to fire among severity levels, for any of the severity classification systems (**Figures 4G,H**).

## Total C and PyC Stocks in the Organic Horizon and Upper Mineral Soil

There was an overall effect of fire on forest floor C stocks, across all severity classes (loss of 25.9 ± 3.2 Mg ha$^{-1}$; $p < 0.0001$), and for nearly every severity level in the three severity classification systems ($p \leq 0.001$ for all RS classes; $p = 0.051$, $p < 0.0001$, $p = 0.092$, and $p < 0.0001$ for NPS vegetation scorched, lightly-, moderately-, and heavily burned severity classes; $p = 0.002$ and $p < 0.0001$ for lightly- and moderately burned NPS substrate classes; **Figure 5A**). The only difference in pre-fire forest floor C stock among severity levels was between the moderately and lightly burned substrate severity classes ($p = 0.018$; **Figure 5A**). There were no differences in post-fire forest floor C stocks among severity levels for the RS or substrate severity classification systems, whereas post-fire C stocks were 87% lower in lightly burned areas relative to areas classified as unburned using NPS vegetation indices (marginally significant at $p = 0.094$; **Figure 5A**).

Forest floor PyC stocks (in samples of post-fire forest floor which included the ash and all other fire-altered forest floor material) decreased by 77% (1.9 ± 0.3 Mg ha$^{-1}$) due to fire across all severity levels ($p < 0.0001$), and also showed significant losses for the low, moderate and high RS severity classes (respectively $p = 0.012$, $p = 0.006$, and $p < 0.001$; **Figure 5B**). Only the lightly ($p < 0.001$) and heavily burned ($p < 0.0001$) NPS vegetation severity levels showed significant losses due to fire (**Figure 5B**). The substrate severity metrics indicated losses of 45% (0.7 ± 0.3 Mg ha$^{-1}$; marginally significant at $p = 0.081$) and 86% (2.5 ± 0.4 Mg ha$^{-1}$; $p < 0.0001$) in the lightly and moderately burned severity classes. The only differences in PyC stocks evident among severity levels for either the pre-fire or post-fire values for the three severity classification systems occurred for post-fire PyC stocks between the unburned and lightly burned NPS vegetation severity classes ($p = 0.030$; **Figure 5B**). The magnitude of forest floor total C and PyC loss due to fire showed non-significant increases across the NPS vegetation classes from scorched < moderately burned < heavily burned; the greatest variability in C and PyC losses occurred in the lightly burned class which did not differ significantly from unburned areas (**Figure 5A**). The magnitude of loss also increased with NPS substrate severity, with 18.1 Mg ha$^{-1}$ greater C, and 1.8 Mg ha$^{-1}$ greater PyC, lost from moderately burned areas compared to lightly burned areas, and these differences between severity classes were marginally significant (**Figures 5A,B**).

We found that fire caused an overall C loss of 20% (3.3 ± 0.5 Mg ha$^{-1}$) from the upper mineral soil (**Figure 5C**); with statistically significant differences between pre- and post-fire measurements evident for RS low ($p = 0.017$), moderate ($p = 0.043$), and high ($p = 0.035$) severity classes, the heavily burned NPS vegetation severity class ($p < 0.0001$), and the moderately burned NPS substrate severity classes ($p < 0.0001$; **Figure 5C**). No differences in mineral soil C stocks among severity levels existed before fire. Although post-fire C stocks differed by only 2.34 Mg ha$^{-1}$ between NPS substrate lightly and moderately burned severity classes, this difference was statistically significant ($p = 0.04$).

Fire decreased mineral soil PyC stocks by 23% (0.4 ± 0.1 Mg ha$^{-1}$) relative to pre-fire stocks across all severity classes ($p = 0.003$; **Figure 5D**). Significant losses within individual severity levels were evident for the RS low ($p = 0.003$) and moderate ($p = 0.008$) severity classes, for the NPS vegetation heavily burned class (0.008), and for both of the NPS substrate severity classes ($p < 0.0001$ and $p = 0.0014$ for lightly and moderately burned areas, respectively; **Figure 5D**). There were no differences in pre-fire or post-fire mineral soil PyC stocks among severity levels, for any of the three severity classification systems. Similarly, our calculated mineral soil C and PyC stocks showed that moderately burned areas lost 38% (1.0 Mg ha$^{-1}$) more total C than lightly burned areas ($p = 0.038$), whereas lightly burned areas lost 57% (0.2 Mg ha$^{-1}$) more PyC than moderately burned areas ($p = 0.003$) for the NPS substrate severity classification system. In contrast, the RS and NPS vegetation severity systems failed to indicate statistically significant differences in the magnitude of mineral soil C or PyC between pre- and post-fire measurements.

## Contributions of PyC to Fire-Affected C by Forest Compartment and Across Fire Severity Levels

The PyC proportion of post-fire C (PyC/postfire C) was greatest in the downed wood, forest floor and mineral soil layers for all severity classification systems and overall (**Tables 3–5**). The total mass of C affected by fire (i.e., the sum of pre-fire C emitted to the atmosphere or transformed to PyC), was greatest in the downed wood and forest floor pools for all severity

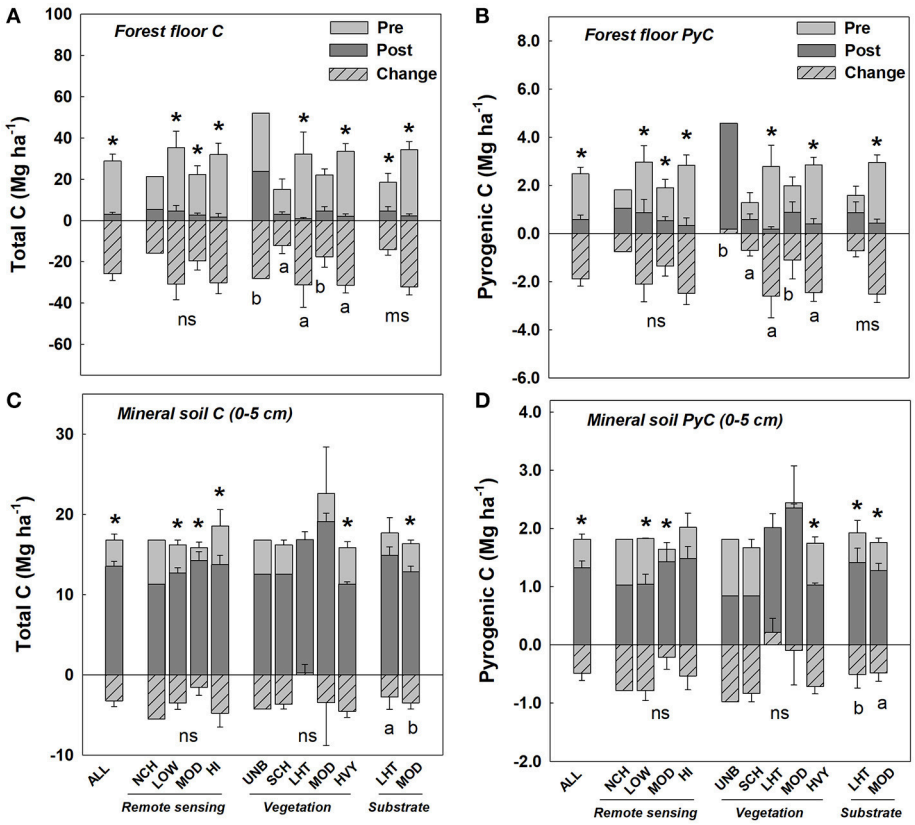


**FIGURE 5 |** Mean (±s.e.) total C and PyC stocks (Mg ha$^{-1}$, estimated as $PyC_{CTR}$ via chemical oxidation) for forest floor **(A,B)** and mineral soil **(C,D)**, for pre-fire and post-fire measurements, and calculated differences between pre- and post-fire measurements, shown for overall severity levels (ALL) and for plots classified by three fire severity classification systems. Severity abbreviations follow those given in **Figure 3**. Asterisks (*) indicate significant differences between pre- and post-fire measurements, within severity level. Lowercase letters below the zero line indicate significant differences in the change between pre- and post-fire measurements (hatched bars) among severity levels within classification system; *ns* indicates no significant differences ($p < 0.05$) and *ms* indicates marginal significance ($p = 0.08$ for forest floor C, and $p = 0.07$ for forest floor PyC). Differences among severity levels for pre-fire and for post-fire measurements are described in the text.

classification, although differences among severity levels were evident only for the forest floor layer in the NPS substrate severity system (**Table 4**). The NPS substrate severity classification system indicated that the mass of C affected in the forest floor increased with severity, and was more than two-fold greater in moderately burned areas relative to lightly burned areas (**Table 5**). Our calculations showed that C affected was only 0.93 Mg ha$^{-1}$ greater in moderately burned areas than lightly burned areas, but this difference was statistically significant (**Table 5**).

Across all severity classes, the proportion of fire-affected C transformed to PyC (PyC/CA) was greatest in the overstory (65% of C affected), and 0–5 cm mineral soil (34% of C affected), relative to the other three forest layers (**Table 3**). The overall mean contribution of PyC to fire-affected C for the total ecosystem was only 10% (**Table 3**). There were no statistically significant differences in PyC/CA among severity levels for individual forest components for the RS and NPS vegetation severity methods (**Tables 3**, **4**). For the NPS substrate severity metrics, our calculations indicated that mineral soil PyC/CA was 32% greater in lightly burned areas relative to moderately burned areas (**Table 5**). The contribution of PyC to total post-fire ecosystem C was quite small, ranging from 0 to 2.6% across the different individual forest components (**Tables 3**–**5**). For the total ecosystem, PyC accounted for between only 1.3 and 5.5% of total ecosystem C across the three severity methods (**Tables 3**–**5**). The mineral soil PyC proportion of total ecosystem C showed a trend of increasing with RS severity; however, the only statistically significant among-severity differences we observed within an individual forest component occurred for the forest overstory when using RS metrics. This showed greater PyC contribution to total ecosystem C in areas of high severity relative to all other severity levels (although the pairwise contrast between high and moderate severity classes was only marginally significant at $p = 0.073$; **Table 3**), and also for the forest overstory when using NPS substrate metrics, with nearly 2-fold greater PyC contribution in moderately burned than in lightly burned areas (**Table 5**).

## Distribution of C and PyC in Burned Mixed-Conifer Forest

When evaluating the distribution of post-fire forest C and PyC materials that are likely susceptible to subsequent fires, we found that 72–93% of total ecosystem C (as determined up to 5 cm

**TABLE 3 |** Post-fire PyC (estimated as $PyC_{CTR}$ via chemical oxidation) proportions of post-fire C, C affected, and post-fire total ecosystem C for plots measured before and after fire in mixed-conifer forest type.

| | | Fire severity (remote sensing) | | | |
|---|---|---|---|---|---|
| **Stratum** | **Overall ($n$ = 29)** | **Unchanged ($n$ = 1)** | **Low ($n$ = 8)** | **Moderate ($n$ = 11)** | **High ($n$ = 9)** |
| **PyC/postfire C (%)** | | | | | |
| Overstory | 1.24 (0.22) | 0.19 (–) | 0.61 (0.27)$^{b}$ | 1.16 (0.40)$^{ab}$ | 2.02 (0.33)$^{a}$ |
| Understory and herb | 0.00 (0.00) | 0.00 (–) | 0.00 (0.00) | 0.00 (0.00) | 0.00 (0.00) |
| Downed wood | 31.51 (1.35) | 27.86 (–) | 31.97 (2.70) | 32.16 (1.88) | 30.09 (3.69) |
| Forest floor | 19.34 (0.19) | 19.18 (–) | 19.19 (0.01) | 19.60 (0.42) | 18.94 (0.24) |
| Mineral soil 0–5 cm | 10.34 (0.25) | 11.10 (–) | 9.93 (0.65) | 9.87 (0.33) | 11.18 (0.30) |
| Total ecosystem | 3.85 (0.57) | 1.26 (–) | 3.90 (1.59) | 3.39 (0.85) | 4.66 (0.67) |
| **C affected (Mg ha$^{-1}$)** | | | | | |
| Overstory | 6.25 (1.98) | 0.55 (–) | 3.20 (2.29) | 8.95 (4.58) | 6.30 (2.32) |
| Understory and herb | 1.57 (0.47) | 0.01 (–) | 0.11 (0.06) | 2.44 (0.79) | 1.98 (1.09) |
| Downed wood | 20.63 (5.35) | 6.25 (–) | 38.48 (16.13) | 11.70 (3.45) | 17.26 (7.10) |
| Forest floor | 26.44 (3.17) | 16.94 (–) | 31.71 (7.58) | 20.09 (4.38) | 30.58 (5.16) |
| Mineral soil 0–5 cm | 5.00 (0.53) | 5.54 (–) | 4.42 (0.61) | 3.94 (0.42) | 6.74 (1.44) |
| Total ecosystem | 60.15 (6.94) | 29.45 (–) | 79.16 (17.04) | 46.85 (9.91) | 62.93 (9.25) |
| **PyC/CA (%)** | | | | | |
| Overstory | 64.88 (7.23) | 100.00 (–) | 86.30 (12.11) | 65.09 (13.67) | 41.70 (8.13) |
| Understory and herb | 0.00 (0.00) | 0.00 (–) | 0.00 (0.00) | 0.00 (0.00) | 0.00 (0.00) |
| Downed wood | 8.60 (2.58) | 10.89 (–) | 5.26 (1.91) | 7.67 (1.95) | 12.34 (7.67) |
| Forest floor | 2.72 (0.72) | 6.14 (–) | 3.12 (1.64) | 3.64 (1.22) | 0.97 (0.94) |
| Mineral soil 0–5 cm | 34.30 (3.11) | 25.38 (–) | 35.04 (6.03) | 37.67 (4.69) | 30.89 (6.44) |
| Total ecosystem | 10.43 (1.42) | 13.01 (–) | 8.89 (1.86) | 9.92 (1.78) | 12.08 (3.71) |
| **PyC/Tot Eco C (%)** | | | | | |
| Overstory | 0.88 (0.14) | 0.18 (–) | 0.40 (0.12)$^{b}$ | 0.72 (0.12)$^{ab}$ | 1.57 (0.31)$^{a}$ |
| Understory and herb | 0.00 (0.00) | 0.00 (–) | 0.00 (0.00) | 0.00 (0.00) | 0.00 (0.00) |
| Downed wood | 0.75 (0.29) | 0.22 (–) | 1.33 (0.98) | 0.62 (0.25) | 0.45 (0.26) |
| Forest floor | 0.40 (0.13) | 0.34 (–) | 0.39 (0.17) | 0.47 (0.20) | 0.34 (0.34) |
| Mineral soil 0–5 cm | 1.57 (0.33) | 0.46 (–) | 1.16 (0.66) | 1.51 (0.47) | 2.12 (0.70) |
| Total ecosystem | 3.85 (0.57) | 1.26 (–) | 3.90 (1.59) | 3.39 (0.85) | 4.66 (0.67) |

*Data presented are means (±s.e.) for measurements within forest component, and for total ecosystem (canopy to 5 cm mineral soil depth), shown by fire severity level classified using remote sensing (dNBR). Lowercase letters indicate statistically significant ($p < 0.05$) differences among fire severity levels within rows.*

mineral soil depth) occurs in the forest overstory, and up to 24% occurs in the 0–5 cm mineral soil layer (**Figure 6A**). In contrast, <3% of post-fire ecosystem C occurred in either the understory, downed wood, or forest floor (including ash layer) pools, when considering the grand mean across all severity classes (**Figure 6A**). The 0–5 cm mineral soil layer accounted for the greatest proportion of PyC out of total post-fire ecosystem PyC stocks, contributing 40% of total ecosystem PyC across all severity levels (**Figure 6B**). The overstory contributed 29% of total ecosystem PyC, whereas only 18 and 12% of ecosystem PyC occurred in the downed wood and forest floor, respectively (**Figure 6B**). The contribution of forest floor PyC to total measured PyC stocks decreased with increasing severity levels for all systems, whereas there was no clear pattern of change across NPS vegetation severity levels.

Between pre-fire and post-fire samples, our results indicated a loss of C and net loss of PyC from the forest floor (post-fire samples included the ash layer as part of the post-fire forest floor). Contrary to our expectations, the mass fraction of PyC in forest floor mass did not show an increase between pre-fire (30 g kg$^{-1}$) and post-fire (25 g kg$^{-1}$) samples, whereas the contribution of PyC to forest floor C increased from 8.46 to 19.6% between pre-fire and post-fire sampling events. The overall mass fraction of PyC in mineral soil was 6 g kg$^{-1}$ pre-fire and 5 g kg$^{-1}$ post-fire, contributing only 15 and 13% of mineral soil C pre- and post-fire, respectively (data not shown).

## DISCUSSION

Our study provides data on three primary ways that fire affects forest C: C emissions; PyC formation, and C transfer from live to dead biomass pools. The lack of available data for PyC from a full range of fire-prone forest types has been a challenge identified in the literature, especially in regards to data needed for modeling fire and carbon dynamics (North et al., 2009; Liu et al., 2011). Important advancements in providing this much-needed data (Bird et al., 2015; Santín et al., 2015a; Reisser et al., 2016) led to a recent modeling study of global PyC

**TABLE 4 |** Post-fire PyC (estimated as $PyC_{CTR}$ via chemical oxidation) proportions of post-fire C, C affected, and post-fire total ecosystem C for plots measured before and after fire in mixed-conifer forest type.

| | Fire severity (NPS vegetation metrics) | | | | |
|---|---|---|---|---|---|
| **Stratum** | **Unburned ($n = 1$)** | **Scorched ($n = 6$)** | **Lightly burned ($n = 6$)** | **Moderately burned ($n = 3$)** | **Heavily burned ($n = 13$)** |
| **PyC/postfire C (%)** | | | | | |
| Overstory | 0.38 (–) | 1.24 (0.74) | 1.16 (0.33) | 0.93 (0.47) | 1.42 (0.33) |
| Understory and herb | 0.00 (–) | 0.00 (0.00) | 0.00 (0.00) | 0.00 (0.00) | 0.00 (0.00) |
| Downed wood | 39.00 (–) | 32.03 (2.98) | 36.29 (2.71) | 28.99 (5.99) | 28.84 (1.79) |
| Forest floor | 19.18 (–)[a] | 19.74 (0.56)[ab] | 19.18 (0.00)[ab] | 19.18 (0.00)[ab] | 19.12 (0.09)[b] |
| Mineral soil 0-5 cm | 8.94 (–) | 9.66 (0.45) | 11.04 (0.51) | 9.97 (1.02) | 10.51 (0.39) |
| Total ecosystem | 1.96 (–) | 5.48 (2.15) | 3.74 (1.20) | 4.28 (0.87) | 3.20 (0.59) |
| **C affected (Mg ha$^{-1}$)** | | | | | |
| Overstory | 1.29 (–) | 6.22 (3.54) | 1.15 (0.54) | 3.06 (2.07) | 9.74 (3.92) |
| Understory and herb | 0.002 (–)[b] | 1.37 (0.88)[ab] | 2.77 (1.55)[a] | 4.27 (1.99)[a] | 0.60 (0.34)[a] |
| Downed wood | 2.69 (–) | 37.07 (21.81) | 7.21 (2.39) | 13.26 (2.47) | 22.32 (5.96) |
| Forest floor | 32.73 (–) | 12.76 (4.07) | 31.41 (10.75) | 18.45 (4.70) | 31.82 (3.74) |
| Mineral soil 0-5 cm | 3.34 (–) | 4.04 (0.48) | 4.88 (0.42) | 7.70 (4.37) | 4.99 (0.69) |
| Total ecosystem | 39.91 (–) | 61.70 (24.07) | 46.86 (11.82) | 46.96 (9.65) | 70.18 (9.34) |
| **PyC/CA (%)** | | | | | |
| Overstory | 100.00 (–) | 62.01 (19.22) | 83.68 (13.55) | 50.43 (24.11) | 57.05 (10.50) |
| Understory and herb | 0.00 (–) | 0.00 (0.00) | 0.00 (0.00) | 0.00 (0.00) | 0.00 (0.00) |
| Downed wood | 12.51 (–) | 8.40 (2.76) | 2.36 (0.91) | 3.19 (3.19) | 12.10 (5.24) |
| Forest floor | 14.00 (–) | 4.67 (1.22) | 0.86 (0.50) | 5.11 (5.11) | 1.44 (0.76) |
| Mineral soil 0-5 cm | 39.62 (–) | 35.34 (3.18) | 33.25 (5.53) | 27.17 (12.45) | 34.99 (6.01) |
| Total ecosystem | 18.51 (–) | 11.57 (2.27) | 9.71 (4.22) | 10.48 (3.94) | 9.61 (2.15) |
| **PyC/Tot Eco C (%)** | | | | | |
| Overstory | 0.34 (–) | 0.53 (0.13) | 0.75 (0.20) | 0.78 (0.39) | 1.16 (0.27) |
| Understory and herb | 0.00 (–) | 0.00 (0.00) | 0.00 (0.00) | 0.00 (0.00) | 0.00 (0.00) |
| Downed wood | 0.09 (–) | 2.11 (1.28) | 0.25 (0.11) | 0.63 (0.32) | 0.42 (0.18) |
| **PyC/postfire C (%)** | | | | | |
| Forest floor | 1.21 (–) | 0.38 (0.13) | 0.20 (0.12) | 1.11 (0.66) | 0.28 (0.23) |
| Mineral soil 0-5 cm | 0.35 (–) | 1.68 (0.84) | 2.62 (1.06) | 1.66 (0.45) | 1.10 (0.38) |
| Total ecosystem | 1.96 (–) | 5.48 (2.15) | 3.74 (1.20) | 4.28 (0.87) | 3.20 (0.59) |

*Data presented are means (±s.e.) for measurements within forest component, and for total ecosystem (canopy to 5 cm mineral soil depth), shown by fire severity level classified in the field post-fire using NPS vegetation metrics. Lowercase letters indicate statistically significant differences among severity levels, within row.*

cycling in contrasting climate scenarios, although the authors still emphasize that the relatively limited existing data cause uncertainties in their estimates (Landry and Matthews, 2017). Our study contributes to advancements in data availability by providing measurements of direct effects of fire on forest C and $PyC_{CTR}$ for each forest component susceptible to fire impacts, in a widespread forest type in the western US that historically experienced frequent fires of primarily low- to moderate-severity (Van de Water and Safford, 2011). This dataset is unique because it provides pre- and post-fire measurements for plots across five active wildfire incidents, and allows comparison of fire impact across severity levels using three contrasting systems for classifying the magnitude of fire's impacts in forested ecosystems. To our knowledge, this is the first study using measurements collected very close to the timing of actual burning in active wildfire incidents (i.e., in contrast to prescribed fire studies and to wildfire studies relying only on post-fire measurements) to determine direct impacts of fire on forest C and PyC.

## Wildfire Impacts on Aboveground Forest C and PyC

Much concern exists about the increasing scale of high-severity fires in this and similar forest types of the western US as well as globally (Attiwill and Binkley, 2013; Stephens et al., 2013; Millar and Stephenson, 2015), but limited information exists about how increases in wildfire severity will affect forest C emissions during fire, or potential for C stabilization as PyC. The majority of forest C in our study (overstory to 5 cm mineral soil depth) occurred in the forest overstory; however, the contribution of the overstory to C emissions during fire was relatively low compared to C lost from the downed wood and forest floor components, which contributed the most to total C affected by fire. The more frequent occurrence of statistically

**TABLE 5 |** Post-fire PyC (estimated as $PyC_{CTR}$ via chemical oxidation) proportions of post-fire C, C affected, and post-fire total ecosystem C for plots measured before and after fire in mixed-conifer forest type.

| Stratum | Fire severity (NPS substrate metrics) | |
|---|---|---|
| | Lightly burned ($n = 10$) | Moderately burned ($n = 19$) |
| **PyC/postfire C (%)** | | |
| Overstory | 1.06 (0.45)*b* | 1.34 (0.24)*a* |
| Understory and herb | 0.00 (0.00) | 0.00 (0.00) |
| Downed wood | 32.32 (2.29) | 31.06 (1.72) |
| Forest floor | 19.61 (0.42) | 19.13 (0.05) |
| Mineral soil 0–5 cm | 8.96 (0.44)b | 11.06 (0.13)a |
| Total ecosystem | 4.56 (1.36) | 3.48 (0.52) |
| **C affected (Mg ha$^{-1}$)** | | |
| Overstory | 2.88 (1.55) | 8.03 (2.86) |
| Understory and herb | 2.32 (0.88) | 1.17 (0.55) |
| Downed wood | 25.51 (12.83) | 18.06 (4.86) |
| Forest floor | 14.90 (2.95)*b* | 32.51 (3.95)*a* |
| Mineral soil 0–5 cm | 4.39 (1.36)b | 5.32 (0.42)a |
| Total ecosystem | 50.14 (12.67) | 65.43 (8.21) |
| **PyC/CA (%)** | | |
| Overstory | 74.53 (12.01) | 60.30 (9.03) |
| Understory and herb | 0.00 (0.00) | 0.00 (0.00) |
| Downed wood | 7.50 (2.17) | 9.12 (3.69) |
| Forest floor | 4.86 (1.72) | 1.71 (0.60) |
| Mineral soil 0–5 cm | 41.00 (5.00)a | 31.12 (3.79)b |
| Total ecosystem | 11.34 (2.03) | 10.00 (1.89) |
| **PyC/Tot Eco C (%)** | | |
| Overstory | 0.58 (0.13)*b* | 1.03 (0.20)*a* |
| Understory and herb | 0.00 (0.00) | 0.00 (0.00) |
| Downed wood | 1.41 (0.80) | 0.40 (0.13) |
| Forest floor | 0.55 (0.24) | 0.33 (0.16) |
| Mineral soil 0–5 cm | 1.56 (0.52) | 1.57 (0.43) |
| Total ecosystem | 4.56 (1.36) | 3.48 (0.52) |

*Data presented are means (±s.e.) for measurements within forest component, and for total ecosystem (canopy to 5 cm mineral soil depth), shown by fire severity level classified in the field post-fire using NPS substrate (forest floor and mineral soil) metrics. Lowercase letters in plain font indicate differences significant at p<0.05, whereas letters in italicized font indicate marginal significance ($p < 0.10$).*

significant effects of fire on C in forest components closer to the ground (i.e., progressing from forest overstory to the understory, herbaceous vegetation, downed wood, and forest floor layers) indicates greater magnitude of relative change in C stocks in lower forest components. Our results indicated that although these fires caused an overall loss of 54.8 ± 6.6 Mg ha$^{-1}$ C to the atmosphere, there was no clear pattern of increased C loss with fire severity. Even though more than half of the different forest C pools we measured showed significant differences in C stocks between pre- and post-fire measurements, the lack of overall difference in total ecosystem C stocks was caused by the relatively minimal loss of C from the overstory, which was by far the largest C pool before and after fire. The overstory is mostly unaffected by fire because the main component of mass (and C) is the standing live tree stems. Because the majority of trees in our study areas were alive at the time of fire, PyC in the overstory was formed primarily as charred bark. Although these fires killed 74% of trees overall, charring of stemwood occurs only when the stemwood tissue is dead and exposed (i.e., exposed dead wood present on a live tree), or when trees are dead prior to fire (personal observation). Therefore, the effects of fire on overstory C are typically limited to the foliage and fine branches, which comprise a relatively small proportion of overstory C.

Similar to our results, Meigs et al. (2009) reported overall C emissions of 22% of forest C across severity levels in mixed-conifer and ponderosa pine (*P. ponderosa)* forests in Oregon, USA and no differences in post-fire total ecosystem C among severity levels, using the same approach we used for RS severity. However, their measurements were taken 4–5 years post-fire and they attributed the lack of change in total ecosystem C to increased vegetation production post-fire, whereas our measurements taken nearly immediately post-fire capture direct effects of fire. Although their study did not address erosion, they observed no evidence of severe erosion between burned and unburned sites. In contrast to our results, the modeling approach used by Meigs et al. (2009) indicated that C emissions increased with fire severity.

In general, post-fire overstory $PyC_{CTR}$ stocks exhibited the strongest trend toward increased stocks across fire severity gradients. Maestrini et al. (2017) also observed greater $PyC_{CTR}$ stocks in areas classified as high severity relative to low-to-moderate severity using remote sensing metrics, in another mixed-conifer forest 3 years after fire. These patterns result from greater charring on tree stems (i.e., indicating greater flame height) in higher severity areas relative to lower-severity areas, but fire effects and severity are influenced more by total heat output, maximum temperature, and/or duration of heating than by fire intensity, especially for soils (Hartford and Frandsen, 1992; Keeley, 2009). Although the greatest losses of $PyC_{CTR}$ in our study occurred from the two largest pre-fire PyC pools (i.e., forest floor and mineral soil), there was a net gain of total ecosystem $PyC_{CTR}$, overall and for most of the individual fire severity levels, as a result of gains in the overstory and downed wood components.

## Wildfire Impacts on Organic Horizon and Mineral Soil C and PyC

The gains observed in the forest overstory and downed wood components, compared to the $PyC_{CTR}$ losses observed from the forest floor and 0–5 cm mineral soil support previous observations that although fires have created PyC for millennia, PyC can also be consumed during fire (Santin et al., 2013; Saiz et al., 2014). Our results on the magnitude of PyC loss during fire are much greater than loss estimates presented by Santin et al. (2013), who used two size classes of macroparticle jack pine (*P. banksiana*) wood charred during a pile burn to determine loss in subsequent fire by exposing particles to a prescribed burn, and others to laboratory heating in a muffle furnace. In contrast, the pre-fire forest floor PyC in our study system likely represents a greater diversity of natural PyC types and particle sizes, which contribute to a total PyC pool formed incrementally over multiple (presumably low- to moderate-severity) fires prior

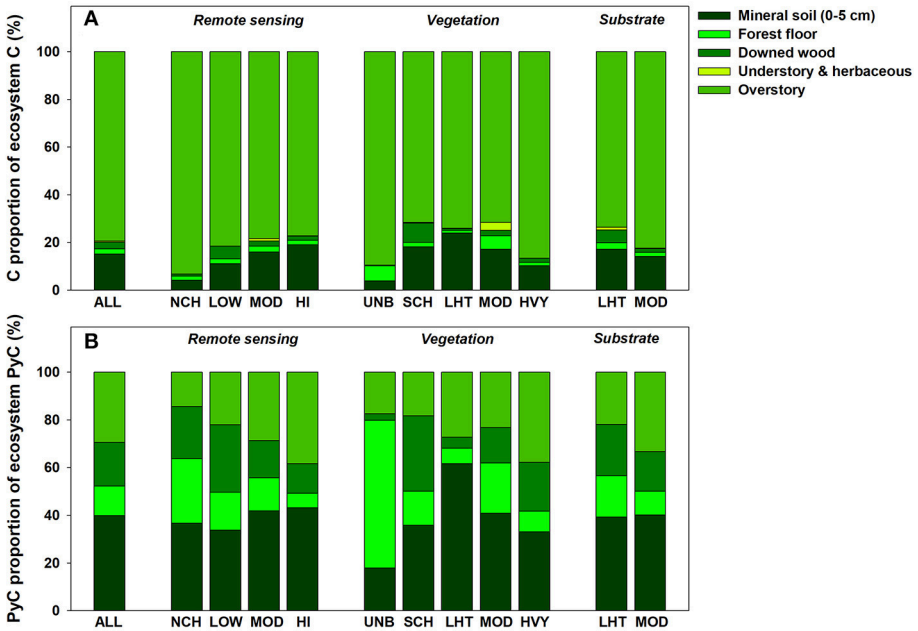


**FIGURE 6 | (A)** Proportions of total measured ecosystem C stocks contributed by C stocks in each forest component; **(B)** proportions of total measured ecosystem PyC stocks contributed by PyC stocks in each forest component (for PyC estimated as $PyC_{CTR}$ via chemical oxidation), in post-fire mixed-conifer forest, shown by fire severity levels classified using remote sensing and field observation (vegetation, substrate) approaches. Total ecosystem PyC and C stocks included the 0–5 cm mineral soil depth increment to the tree layer, to represent the pool of C most directly exposed to fire or heating during fire. Severity abbreviations follow those given in **Figure 3**.

to the time that US fire suppression policy began. Small or microscopic PyC in our study would be present inside the forest floor, and likely would have experienced greater combustion and loss, especially given that this region was in a prolonged drought when the fires occurred. It is also possible that the chemical oxidation method we used may overestimate PyC in pre-fire samples; for example, Maestrini and Miesel (2017) determined that 5.4% of C in unpyrolyzed pine needle material may be erroneously indicated as PyC using this method. Assuming that 100% of the pre-fire forest floor material was derived from pine needle litter, this would translate to an over-estimation of 1.6 $\pm$ 0.2 Mg ha$^{-1}$ PyC in the pre-fire forest floor, and an over-estimation of PyC loss of 0.4 Mg ha$^{-1}$ between pre- and post-fire measurement events.

Because our study measured forest floor C and $PyC_{CTR}$ stocks before rainfall occurred, our results overestimate the pool of PyC that will persist in the ecosystem and/or become incorporated into mineral soil. However, even the PyC produced during these fires and eroded and deposited elsewhere in the landscape—or ultimately in aquatic and marine sediments—still represents a C pool with increased chemical stability relative to the original biomass materials. PyC fluxes between sites do not represent PyC losses at larger scales (Santín et al., 2016). In efforts to quantify the role of fires and PyC in global C cycles it will be important to avoid double accounting issues that may arise if estimates of direct formation during fire (such as we present here) are coupled with PyC stock estimates obtained in older fire sites that have already experienced PyC loss via erosion. The lack of change in $PyC_{CTR}$ mass fraction of forest floor material in our study was likely caused by the presence of mineral ash present in the post-fire residual forest floor material, much of which erodes downslope and/or downstream during post-fire rainfall events (Bodí et al., 2014). Some proportion of the lightweight/transient mineral ash component likely would have been omitted if we had collected the post-fire forest floor samples at a later time after fire, and especially after rainfall and/or significant erosion events. For example, results from Maestrini et al. (2017) indicate increased $PyC_{CTR}$ concentration in post-fire forest floor mass collected 3 years post-fire, relative to unburned areas. Although forest soil is a major C pool, the depth of heat penetration into mineral soil (and consequently the impact on soil properties) depends on the amount of heat produced as well as its duration, which are influenced by aboveground fuel load (Massman et al., 2010; Bento-Gonçalves et al., 2012; Massman, 2012). Significant heating at depths greater than a few centimeters is unlikely during fire, except in localized areas of heavy fuel load (Neary et al., 2008; Bento-Gonçalves et al., 2012), or where duff is consumed (Hartford and Frandsen, 1992). Our study limited estimates of total ecosystem C to the upper 5 cm of mineral soil to best represent the forest ecosystem components that typically experience direct impact from fire, rather than sampling to greater depth where the effects of fire may be diluted. The statistically significant 23% overall loss of total C and $PyC_{CTR}$ from the 0 to 5 cm mineral soil layer suggest that total C and $PyC_{CTR}$ in the uppermost mineral soil were either consumed by fire, or lost via convection of

fine mineral particles (Bormann et al., 2008; Homann et al., 2011).

Our measurements indicating loss of C and PyC from the upper mineral soil agree with those of Bormann et al. (2008), Homann et al. (2011), and Pingree et al. (2012) from similar mixed-conifer forests, and contrast with the general assumption that fire has minimal impacts on mineral soil C (for example, see reviews from Certini (2005) and González-Pérez et al. (2004). The apparent discrepancy can be explained by differences in sampling depth, as most studies have investigated mineral soil C to >5 cm sampling depth. For example, Buma et al. (2014) sampled mineral soil to 10 cm in a mixed forest 9 years after wildfire in subalpine mixed conifer forest in Colorado, USA and found no effect of fire on C stock, and Miesel et al. (2015) found no effect of fire on 0–10 cm mineral soil C in southern boreal forest. In contrast, Homann et al. (2011) reported a loss of 10–50% (depending on the pre-fire forest management) of mineral soil C stock in the upper 6 cm after wildfire in an Oregon Douglas-fir (*P. menziesii)* forest, and estimates from Campbell et al. (2007) indicate 2–8% loss of C in the top 10 cm mineral soil in an Oregon mixed conifer forest, where surface temperatures of >700°C were recorded during fire. They remarked that "*. . . it is also reasonable to believe that soil carbon could have completely combusted to depths of up to 5 cm or that complete combustion never exceeded 2 cm.*" (Campbell et al., 2007). Therefore, although there are multiple literature reports that fire does not decrease mineral soil C stock, an actual decrease in C stock may be observed if the analysis is limited to the first few centimeters of the mineral soil, where SOM is more likely to be directly impacted during the fire.

Losses of this magnitude from the mineral soil seem surprising because the substrate severity at all plots was classified either as only lightly burned or moderately burned, even while the physical post-fire forest floor samples consisted primarily of mineral ash, with few to no recognizable plant-derived structures. The explanation for the apparent disparity in our results is likely based on the much broader scale of substrate severity classification in the plots relative to the location of forest floor and mineral soil samples. Because soil sampling was time-consuming during potentially hazardous pre-fire sampling, only a few physical samples per plot could be collected and it would be challenging to substantially increase the pre-fire soil sampling intensity. It is also possible that the substrate severity classification system has low accuracy for characterizing impacts on C and PyC pools. Because our fuels data were collected for the plot scale, we do not have spatially explicit relationships between downed wood biomass and C or $PyC_{CTR}$ loss from soil at the scale of soil sample locations. However, Weichman et al. (2015) found no correlation between PyC stock and distance (up to 60 cm) from charred logs 12 years after a prescribed fire in mixed conifer forest. They suggest that charcoal shed from large-diameter downed wood either takes more than a decade to slough off the bark, or is rapidly redistributed away from the logs. Therefore, we recommend that future studies assess post-fire substrate severity level and woody fuel load at the precise soil sampling locations, immediately before collecting the physical samples, to maximize agreement between changes in C and $PyC_{CTR}$ concentrations and observed substrate severity. Finally, it is also possible that a systematic bias may have also influenced our mineral soil C results, i.e., if the combustion of the duff ($O_e$+$O_a$) layer reduced subjectivity in identifying the boundary between the organic layer and mineral soil, relative to pre-fire conditions, leading to post-fire samples being collected from a slightly lower depth than pre-fire samples. However, the same team of individuals collected both sets of samples within fires.

Our results indicate that mineral soil provides a large proportion of total ecosystem $PyC_{CTR}$ even after fire. This agrees with Buma et al. (2014), who used the same $PyC_{CTR}$ method we did to investigate total C and PyC stocks in high-severity burn areas. Their results contrast with our in that they found significantly less PyC in the 0–10 cm mineral soil in unburned reference areas compared to burned areas. Previous estimates have shown that PyC contributes between <1 and 60% of total soil organic C in mineral soils of conifer forests (Preston and Schmidt, 2006; DeLuca and Aplet, 2008; Reisser et al., 2016). PyC formed in aboveground components of forests and in the forest floor during fire provides a source of input into mineral soil, where it has potential to become further stabilized via physical protection and influence soil physical, chemical and biological properties (DeLuca et al., 2006; MacKenzie et al., 2008; Ball et al., 2010; Bird et al., 2015), and, ultimately, post-fire forest recovery (MacKenzie et al., 2008; Makoto et al., 2011).

This and previous studies suggest that fire and fire severity influences the distribution of PyC in forests, although PyC stocks in mineral soil likely reflect inputs from past fires occurring over long time periods rather than recent single fire events (DeLuca and Aplet, 2008; Miesel et al., 2015; Reisser et al., 2016). Over time, PyC can be added to the newly re-developing forest floor layer as charred bark separates from fire-killed tree stems and falls to the ground surface. We expect that PyC from charred downed wood will also become incorporated into the re-developing forest floor layer and possibly the mineral soil, depending on the rate of physical fragmentation of charred downed wood. The downed wood pool of forest C will also increase over time as fire-killed trees fall to the ground, providing woody fuel for subsequent fires. Thus, the pattern of increased tree mortality across fire severity gradients we observed in this study may contribute to greater C release during a subsequent fire. Although we would assume that greater downed wood biomass would also result in greater impacts to forest floor and mineral soil C, pre-fire downed wood biomass was not a significant covariate in our analyses of C affected in forest floor or mineral soil, for any of the severity classification systems (although it was marginally significant at $p < 0.10$ in the analysis using NPS substrate severity metrics).

## Evaluation of Contrasting Fire Severity Metrics

Efforts to define and classify fire severity are relatively recent, and the diverse existing metrics each have strengths and weaknesses when evaluating the type and magnitude of fire effects within specific ecosystem components, and for the total ecosystem. Keeley (2009) emphasizes that remote sensing has limited ability to predict ecosystem response, and recommends using field

studies to better interpret ecosystem response across remote sensing-derived severity levels. Our results showed that neither post-fire total ecosystem stocks, nor the magnitude of stock change due to fire, corresponded well with remotely sensed estimates of fire severity, for either total C or $PyC_{CTR}$. The presence of pre-existing (pre-fire) differences in C stocks among areas classified with contrasting fire severity levels indicates that knowledge of pre-fire forest conditions is important for interpreting fire impacts. Our study shows that using post-fire severity estimates does not give a complete picture of fire effects on forest C; for example, areas classified as high severity using RS imagery were not necessarily associated with greater C losses, or greater $PyC_{CTR}$ gains or losses. Low agreement between field-estimated severities and RS severities can result from mis-alignment due to the registration accuracy of satellite images, the location of field plots relative to mapped severity polygons, variability in fire effects within the 30 m pixel scale of Landsat-derived images, and the proportion of ground covered by ash (Miller and Quayle, 2015).

The high tree stem density yet low tree biomass and C, combined with high pre-fire seedling and shrub C stocks, in areas classified as moderate and high RS severity are an example of the limitations of this approach that challenge efforts to extrapolate fire severity to C release across broader scales. In particular, relatively low agreement among the three types of severity classification indicates that fire severity determined from RS metrics may not be a good indication of impacts to the organic and mineral horizons of soil, where the majority of $PyC_{CTR}$ occurred. In contrast, Kolka et al. (2017) reported that forest floor C loss increased with soil burn severity after a wildfire in southern boreal forest in Minnesota, USA, and combined remote sensing with field observations of burn severity to scale up plot-level measurements to whole-fire C emissions. Although Meigs et al. (2009, 2011) extrapolated C emissions across severity levels in a similar forest type to our mixed-conifer sites, our results highlight some of the challenges likely to arise in efforts to predict C loss at large scales, given the variability at smaller scales (among plots within severity level, and among individual ecosystem components) and poor differentiation among severity levels.

The RS severity classifications we used represent composite impacts of fire across forest components including soil and surface char, but are heavily weighted to vegetation. Greater uncertainty in the low- and moderate-severity classes (relative to high-severity) results from fire effects on surface vegetation and substrate being obscured by live canopy cover (Miller and Thode, 2007; Meigs et al., 2009, 2011; Miller et al., 2009a), and this uncertainty may contribute to difficulty resolving differences in C stocks and losses among severity classes. Landsat-based indices of fire effects correlate well with forest overstory characteristics, and can show relatively good relationships with understory vegetation and soil severity when canopy severity is also high; however, the correlations with surface severity weaken when there is high post-fire live vegetation cover (Hudak et al., 2007; Robichaud et al., 2007).

Our results showing that C emissions from forest floor combustion can be high even in areas of relatively low severity and low change in component C stocks or overstory mortality agree with studies in similar forest types (Campbell et al., 2007; Meigs et al., 2011), and illustrate that fire also creates vertical heterogeneity in terms of effects on forest C. Our observations of large differences in pre-fire overstory and understory C stocks between plots burned at low RS severity vs. those burned at moderate or high RS severity also illustrate that loss of shrub or seedling cover, not just tree cover, can also contribute to classification as high severity (Miller et al., 2009a). A relatively high number of smaller trees contributed to the high pre-fire live tree stem density in these areas.

In general, the NPS vegetation severity metrics corresponded with patterns of C loss in the understory (seedling and shrub), and for the downed wood components, whereas NPS substrate severity metrics corresponded with the magnitude of forest floor C and $PyC_{CTR}$ loss, and with tree mortality. Together, our results show that the influence of severity level on the magnitude of change in C or $PyC_{CTR}$ in a burned forest depends on the ecosystem component(s) being evaluated. Our study shows that any one of these published methods does not show strong informative potential for evaluating whole-ecosystem impacts of fire, at least for forest C and $PyC_{CTR}$ and for our sites representing single fire events.

## Additional Data Needs

Continued efforts to improve accuracy in ecosystem and global C accounting, especially in the context of changes in historic disturbance regimes, depends on the availability of information on PyC stocks and distribution in burned forests (Lehmann et al., 2008; Stockmann et al., 2013; Santín et al., 2015b). Additional data are needed to advance the research community's ability to quantify fire's impact on forest C and PyC. For example, knowing how to best characterize fire severity within and across ecosystem components and scales will be important for relating fire impacts to forest C pools, and to short- and longer-term C flux to the atmosphere. Although significant advancements in standardizing severity assessments have been made in recent years, data on ecosystem response (i.e., process rates) remains much more limited and will be essential for understanding how shifts in fire regimes are likely to affect the pattern and timeframe of forest recovery.

Greater resolution in charring depth and extent in downed wood across standard woody fuel size classes would improve estimates of PyC stocks. Standard methods have been developed but can be time-consuming (Lutes et al., 2006; Donato et al., 2009) and are therefore not suitable for use in active fire situations such as our study used. Standardization of methods for quantifying PyC in environmental samples remains challenging (see Zimmerman and Mitra, 2017): we presented $PyC_{CTR}$ estimates based on a chemical oxidation method for all forest components, whereas visual quantification of post-fire charred bark or forest floor samples would have indicated near-total quantification of mass as charred material or "black ash" (Bodí et al., 2014). However, our chemical analyses showed that the C and PyC mass fractions were much lower than expected. Weather conditions during a fire may also influence where particulate matter—including PyC particles—become deposited,

and longer-term conditions such as drought can influence fuel moisture content and, therefore, the amount of C emitted vs. converted to PyC. Finally, information on the rate of PyC transfer across forest components over time after fire—especially in areas of contrasting fire severity using any severity classification system—remains limited, and represents an important area of research need in ongoing efforts to understand the full life cycle of C and PyC in fire-affected ecosystems. Additional whole-ecosystem investigations of PyC stocks will improve our understanding of PyC production in vegetation fires, and its role in the global C and PyC budgets. These data will become increasingly important given the ecologically important role of fires historically in this ecosystem type, and the expected increases in warming temperatures and record-setting droughts in the future (Belmecheri et al., 2016). These factors will likely contribute to increased burn severity and PyC formation conditions that differ from historical fires in ways that influence the physical and chemical persistence of PyC, and its role in ecosystem processes.

## CONCLUSIONS

Our study evaluated fire effects on forest C and $PyC_{CTR}$ using pre- and post-fire measurements and samples from plots across five wildfire incidents in California mixed-conifer forest that occurred during drought years. This study is unique in that we were able to install and re-measure study plots within days before and after fire, by working within the US wildfire incident management system to access active wildfire incidents. Our results indicated that even severe fire effects to an ecosystem during drought years may not directly relate to major forest C loss during a given fire, because the ecosystem components consumed during fire represent a small proportion of forest C. Stabilization of C as PyC was also relatively minor. However, tree mortality converted the largest pool of forest C from the live to dead tree pool. Extensive tree mortality raises concern about a delayed relationship between fire severity and C emissions because overstory C in fire-killed trees, when transferred to the downed wood pool, will be available for major release in a subsequent fire. Thus, C emissions may be influenced more by the severity of past fire events than the severity of a current fire. Extensive mortality caused by increasingly large and high-severity fire raises concern about the potential for altered successional trajectories and ecosystem type conversion (Hurteau and Brooks, 2011; Loudermilk et al., 2013), with consequences for the rate of C uptake and, ultimately, C sequestration by a potentially novel ecosystem (Millar and Stephenson, 2015; Trumbore et al., 2015). Therefore, managers and policymakers should pursue the use of prescribed burns and managed wildfires as part of a strategy to manage forest ecosystems to promote long-term resilience to fire (i.e., supporting survival of the forest overstory through multiple fires) as the optimal approach to avoiding wildfire emissions, and potential ecosystem conversion, in subsequent fires. Forest management actions taken now—even those that produce minor C emissions—will be essential for enabling mature tree survival, and avoiding major C emissions in the next wildfire. Forest recovery is the fundamental process necessary to uphold the assumption that wildfires are (or will continue to be) net zero emissions events. Continued improvements in methods for relating fire severity to specific ecosystem properties such as forest C stocks will be important to support scaling-up of fire impacts to landscapes and regions, and for anticipating C and PyC dynamics over the longer term.

## AUTHOR CONTRIBUTIONS

JM: conceived the study in consultation with AR, oversaw sample analysis, conducted the data analysis, and wrote the manuscript; AR and CE: conducted and led field measurement and sampling activities, and contributed to the manuscript; BM: calculated overstory PyC stocks and contributed to the manuscript. MD: contributed to planning and conducting field measurement and sampling activities.

## ACKNOWLEDGMENTS

We thank Eleanor Domer, Merissa Strawsine, and Dominic Uhelski for laboratory assistance, and FBAT personnel for field assistance. We thank Joe Scott (Pyrologix) for development of the spreadsheet used to calculate understory and herbaceous biomass. Jaron Adkins and two reviewers provided helpful comments that improved the quality of the manuscript. This study was supported by funding from Michigan State University (MSU), MSU AgBioResearch, and the USDA Forest Service Northern Research Station.

## SUPPLEMENTARY MATERIAL

The Supplementary Material for this article can be found online at: https://www.frontiersin.org/articles/10.3389/feart.2018.00041/full#supplementary-material

## REFERENCES

Attiwill, P., and Binkley, D. (2013). Exploring the mega-fire reality: a 'Forest Ecology and Management' conference. *For. Ecol. Manage.* 294, 1–3. doi: 10.1016/j.foreco.2012.12.025

Baldock, J. A., and Smernik, R. J. (2002). Chemical composition and bioavailability of thermally-altered *Pinus resinosa* (Red Pine) wood. *Org. Geochem.* 33, 1093–1109. doi: 10.1016/S0146-6380(02)00062-1

Ball, P. N., MacKenzie, M. D., DeLuca, T. H., and Holben, W. E. (2010). Wildfire and charcoal enhance nitrification and ammonium-oxidizing bacterial abundance in dry montane forest soils. *J. Environ. Qual.* 39, 1243–1253. doi: 10.2134/jeq2009.0082

Barbero, R., Abatzoglou, J. T., Larkin, N. K., Kolden, C. A., and Stocks, B. (2015). Climate change presents increased potential for very large fires in the contiguous United States. *Int. J. Wildland Fire* 24, 892–899. doi: 10.1071/WF15083

Belmecheri, S., Babst, F., Wahl, E. R., Stahle, D. W., and Trouet, V. (2016). Multi-century evaluation of Sierra Nevada snowpack. *Nat. Clim. Change* 6, 2–3. doi: 10.1038/nclimate2809

Bento-Gonçalves, A., Vieira, A., Úbeda, X., and Martin, D. (2012). Fire and soils: key concepts and recent advances. *Geoderma* 191, 3–13. doi: 10.1016/j.geoderma.2012.01.004

Bird, M. I., Wynn, J. G., Saiz, G., Wurster, C. M., and McBeath, A. (2015). The pyrogenic carbon cycle. *Annu. Rev. Earth Planet. Sci.* 43, 273–278. doi: 10.1146/annurev-earth-060614-105038

Bodí, M. B., Martin, D. A., Balfour, V. N., Santín, C., Doerr, S. H., Pereira, P., et al. (2014). Wildland fire ash: production, composition and eco-hydro-geomorphic effects. *Earth Sci. Rev.* 130, 103–127. doi: 10.1016/j.earscirev.2013.12.007

Bond-Lamberty, B., Peckham, S. D., Ahl, D. E., and Gower, S. T. (2007). Fire as the dominant driver of central Canadian boreal forest carbon balance. *Nature* 450, 89–92. doi: 10.1038/nature06272

Boot, C. M., Haddix, M., Paustian, K., and Cotrufo, M. F. (2015). Distribution of black carbon in *ponderosa* pine forest floor and soils following the High Park wildfire. *Biogeosciences* 12, 3029–3039. doi: 10.5194/bg-12-3029-2015

Bormann, B. T., Homann, P. S., Darbyshire, R. L., and Morrissette, B. A. (2008). Intense forest wildfire sharply reduces mineral soil C and N: the first direct evidence. *Can. J. For. Res.* 38, 2771–2783. doi: 10.1139/X08-136

Breshears, D. D., Cobb, N. S., Rich, P. M., Price, K. P., Allen, C. D., Balice, R. G., et al. (2005). Regional vegetation die-off in response to global-change-type drought. *Proc. Natl. Acad. Sci. U.S.A.* 102, 15144–15148. doi: 10.1073/pnas.0505734102

Brewer, N. W., Smith, A. M. S., Hatten, J. A., Higuera, P. E., Hudak, A. T., Ottmar, R. D., et al. (2013). Fuel moisture influences on fire-altered carbon in masticated fuels: an experimental study. *J. Geophysic. Res. Biogeosci.* 118, 30–40. doi: 10.1029/2012JG002079

Brown, J. K. (1974). *Handbook for inventorying downed woody material. GTR-INT-16.* Ogden, UT: USDA Forest Service, Intermountain Forest and Range Experiment Station.

Buma, B., Poore, R. E., and Wessman, C. A. (2014). Disturbances, their interactions, and cumulative effects on carbon and charcoal stocks in a forested ecosystem. *Ecosystems* 17, 947–959. doi: 10.1007/s10021-014-9770-8

Burgan, R. E., and Rothermel, R. C. (1984). "BEHAVE: fire behavior prediction and fuel modeling system - FUEL subsystem," in *USDA Forest Service Gen. Tech. Rep. INT-167* (Ogden, UT: USDA Forest Service, Intermountain Forest and Range Experiment Station).

Campbell, J., Alberti, G., Martin, J., and Law, B. E. (2009). Carbon dynamics of a *ponderosa* pine plantation following a thinning treatment in the northern Sierra Nevada. *For. Ecol. Manage.* 257, 453–463. doi: 10.1016/j.foreco.2008.09.021

Campbell, J., Donato, D. C., Azuma, D., and Law, B. (2007). Pyrogenic carbon emission from a large wildfire in Oregon, United States. *J. Geophys. Res. Biogeosci.* 112:G04014. doi: 10.1029/2007JG000451

Certini, G. (2005). Effects of fire on properties of forest soils: a review. *Oecologia* 143, 1–10. doi: 10.1007/s00442-004-1788-8

Covington, W. W., and Moore, M. M. (1994). Southwestern ponderosa forest structure: changes since Euro-American settlement. *J. For.* 92, 39–47.

Czimczik, C. I., Preston, C. M., Schmidt, M. W. I., and Schulze, E. D. (2003). How surface fire in Siberian Scots pine forests affects soil organic carbon in the forest floor: stocks, molecular structure, and conversion to black carbon (charcoal). *Glob. Biogeochem. Cycles* 17:1020. doi: 10.1029/2002GB001956

DeLuca, T. H., and Aplet, G. H. (2008). Charcoal and carbon storage in forest soils of the Rocky Mountain West. *Front. Ecol. Environ.* 6, 18–24. doi: 10.1890/070070

DeLuca, T. H., MacKenzie, M. D., Gundale, M. J., and Holben, W. E. (2006). Wildfire-produced charcoal directly influences nitrogen cycling in ponderosa pine forests. *Soil Sci. Soc. Am. J.* 70, 448–453. doi: 10.2136/sssaj2005.0096

Domke, G. M., Woodall, C. W., and Smith, J. E. (2011). Accounting for density reduction and structural loss in standing dead trees: implications for forest biomass and carbon stock estimates in the United States. *Carbon Balance Manag.* 6:14. doi: 10.1186/1750-0680-6-14

Donato, D. C., Campbell, J. L., Fontaine, J. B., and Law, B. E. (2009). Quantifying char in postfire woody detritus inventories. *Fire Ecol.* 5, 104–115. doi: 10.4996/fireecology.0502104

Earles, J. M., North, M. P., and Hurteau, M. D. (2014). Wildfire and drought dynamics destabilize carbon stores of fire-suppressed forests. *Ecol. Appl.* 24, 732–740. doi: 10.1890/13-1860.1

Eckmeier, E., van der Borg, K., Tegtmeier, U., Schmidt, M. W. I., and Gerlach, R. (2009). Dating charred soil organic matter: comparison of radiocarbon ages from macrocharcoals and chemically separated charcoal carbon. *Radiocarbon* 51, 437–443. doi: 10.1017/S0033822200055831

Eidenshink, J., Schwind, B., Brewer, K., Zhu, Z.-L., Quayle, B., and Howard, S. (2007). A project for monitoring trends in burn severity. *Fire Ecol.* 3, 3–21. doi: 10.4996/fireecology.0301003

Eskelson, B. N. I., Monleon, V. J., and Fried, J. S. (2016). A 6 year longitudinal study of post-fire woody carbon dynamics in California's forests. *Can. J. For. Res.* 46, 610–620. doi: 10.1139/cjfr-2015-0375

Fearnside, P. M., Graca, P., and Rodrigues, F. J. A. (2001). Burning of Amazonian rainforests: burning efficiency and charcoal formation in forest cleared for cattle pasture near Manaus, Brazil. *For. Ecol. Manage.* 146, 115–128. doi: 10.1016/S0378-1127(00)00450-3

Folke, C., Carpenter, S., Walker, B., Scheffer, M., Elmqvist, T., Gunderson, L., et al. (2004). Regime shifts, resilience, and biodiversity in ecosystem management. *Annu. Rev. Ecol. Evol. Syst.* 35, 557–581. doi: 10.1146/annurev.ecolsys.35.021103.105711

González-Pérez, J. A., González-Vila, F. J., Almendros, G., and Knicker, H. (2004). The effect of fire on soil organic matter - a review. *Environ. Int.* 30, 855–870. doi: 10.1016/j.envint.2004.02.003

Hammes, K., Schmidt, M. W. I., Smernik, R. J., Currie, L. A., Ball, W. P., Nguyen, T. H., et al. (2007). Comparison of quantification methods to measure fire-derived (black/elemental) carbon in soils and sediments using reference materials from soil, water, sediment and the atmosphere. *Glob. Biogeochem. Cycles* 21:GB3016. doi: 10.1029/2006GB002914

Hammes, K., Smernik, R. J., Skjemstad, J. O., Herzog, A., Vogt, U. F., and Schmidt, M. W. I. (2006). Synthesis and characterisation of laboratory-charred grass straw (*Oryza saliva*) and chestnut wood (*Castanea sativa*) as reference materials for black carbon quantification. *Org. Geochem.* 37, 1629–1633. doi: 10.1016/j.orggeochem.2006.07.003

Harmon, M. E. (2001). Carbon sequestration in forests - addressing the scale question. *J. For.* 99, 24–29. doi: 10.1093/jof/99.4.24

Harmon, M. E., Kromack, K. Jr., and Smith, B.G. (1987). Coarse woody debris in mixed-conifer forests, Sequioa National Park, California. *Can. J. For. Res.* 17, 1265–1272. doi: 10.1139/x87-196

Hartford, R., and Frandsen, W. (1992). When it's hot, it's hot... or maybe it's not! (surface flaming may not portend extensive soil heating). *Int. J. Wildland Fire* 2, 139–144. doi: 10.1071/WF9920139

Hatton, P.-J., Chatterjee, S., Filley, T. R., Dastmalchi, K., Plante, A. F., Abiven, S., et al. (2016). Tree taxa and pyrolysis temperature interact to control the efficacy of pyrogenic organic matter formation. *Biogeochemistry* 130, 103–116. doi: 10.1007/s10533-016-0245-1

Homann, P. S., Bormann, B. T., Darbyshire, R. L., and Morrissette, B. A. (2011). Forest soil carbon and nitrogen losses associated with wildfire and prescribed fire. *Soil Sci. Soc. Am. J.* 75, 1926–1934. doi: 10.2136/sssaj2010-0429

Hudak, A. T., Morgan, P., Bobbitt, M. J., Smith, A. M. S., Lewis, S. T., Lentile, L. B., et al. (2007). The relationship of multispectral satellite imagery to immediate fire effects. *Fire Ecol.* 3, 64–90. doi: 10.4996/fireecology.0301064

Hurteau, M. D., and Brooks, M. L. (2011). Short- and long-term effects of fire on carbon in US dry temperate forest systems. *Bioscience* 61, 139–146. doi: 10.1525/bio.2011.61.2.9

Jain, T. B., and Graham, R. T. (2007). "The relation between tree burn severity and forest structure in the Rocky Mountains," in *Restoring Fire-Adapted Ecosystems: Proceedings of the 2005 National Silviculture Sorkshop. Gen. Tech. Rep. PSW-GTR-203,* ed R. F. Powers (Albany, CA: USDA Forest Service, Pacific Southwest Research Station), 213–250.

Jain, T. B., Pilliod, D. S., Graham, R. T., Lentile, L. B., and Sandquist, J. E. (2012). Index for characterizing post-fire soil environments in temperate coniferous forests. *Forests* 3, 445–466. doi: 10.3390/f3030445

Jenkins, J. C., Chojnacky, D. C., Heath, L. S., and Birdsey, R. A. (2004). Comprehensive database of diameter-based biomass regressions for North American tree species," in *Gen. Tech. Rep. NE-319* (Newton Square, PA: U.S. Department of Agriculture, Forest Service, Northeastern Research Station.

Keeley, J. E. (2009). Fire intensity, fire severity and burn severity: a brief review and suggested usage. *Int. J. Wildland Fire* 18, 116–126. doi: 10.1071/WF07049

Keiluweit, M., Nico, P. S., Johnson, M. G., and Kleber, M. (2010). Dynamic molecular structure of plant biomass-derived black carbon (Biochar). *Environ. Sci. Technol.* 44, 1247–1253. doi: 10.1021/es9031419

Key, C. H., and Benson, N. C. (2006). "Landscape Assessment (LA) sampling and analysis methods," in *FIREMON: Fire Effects Monitoring And Inventory System, Gen. Tech. Rep. RMRS-GTR-164-CD,* eds D. C. Lutes, R. E. Keane, J. F. Caratti, C. H. Key, N. C. Benson, S. Sutherland, and L. J. Gangi (Fort Collins, CO: U.S. Department of Agriculture, Forest Service, Rocky Mountain Research Station), LA1–LA55.

Kolka, R. K., Sturtevant, B. R., Miesel, J. R., Singh, A., Wolter, P. T., Fraver, S., et al. (2017). Emissions of forest floor and mineral soil carbon, nitrogen and mercury pools and relationships with fire severity for the pagami creek fire in the boreal forest of northern Minnesota. *Int. J. Wildland Fire* 26, 296–305. doi: 10.1071/WF16128

Kurth, V. J., MacKenzie, M. D., and DeLuca, T. H. (2006). Estimating charcoal content in forest mineral soils. *Geoderma* 137, 135–139. doi: 10.1016/j.geoderma.2006.08.003

Landry, J. S., and Matthews, H. D. (2017). The global pyrogenic carbon cycle and its impact on the level of atmospheric $CO_2$ over past and future centuries. *Glob. Chang. Biol.* 23, 3205–3218. doi: 10.1111/gcb.13603

Lauvaux, C. A., Skinner, C. N., and Taylor, A. H. (2016). High severity fire and mixed conifer forest-chaparral dynamics in the southern Cascade Range, USA. *For. Ecol. Manage.* 363, 74–85. doi: 10.1016/j.foreco.2015.12.016

Lehmann, J., Skjemstad, J., Sohi, S., Carter, J., Barson, M., Falloon, P., et al. (2008). Australian climate-carbon cycle feedback reduced by soil black carbon. *Nat. Geosci.* 1, 832–835. doi: 10.1038/ngeo358

Littell, J. S., Peterson, D. L., Riley, K. L., Liu, Y., and Luce, C. H. (2016). A review of the relationships between drought and forest fire in the United States. *Glob. Chang. Biol.* 22, 2353–2369. doi: 10.1111/gcb.13275

Liu, S. G., Bond-Lamberty, B., Hicke, J. A., Vargas, R., Zhao, S. Q., Chen, J., et al. (2011). Simulating the impacts of disturbances on forest carbon cycling in North America: processes, data, models, and challenges. *J. Geophysic. Res. Biogeosci.* 116:G00K08. doi: 10.1029/2010JG001585

Liu, Y. Q., Goodrick, S., and Heilman, W. (2014). Wildland fire emissions, carbon, and climate: wildfire-climate interactions. *For. Ecol. Manage.* 317, 80–96. doi: 10.1016/j.foreco.2013.02.020

Loehman, R. A., Reinhardt, E., and Riley, K. L. (2014). Wildland fire emissions, carbon, and climate: seeing the forest and the trees - a cross-scale assessment of wildfire and carbon dynamics in fire-prone, forested ecosystems. *For. Ecol. Manage.* 317, 9–19. doi: 10.1016/j.foreco.2013.04.014

Loudermilk, E. L., Scheller, R. M., Weisberg, P. J., Yang, J., Dilts, T. E., Karam, S. L., et al. (2013). Carbon dynamics in the future forest: the importance of long-term successional legacy and climate-fire interactions. *Glob. Chang. Biol.* 19, 3502–3515. doi: 10.1111/gcb.12310

Lutes, D. C., Keane, R. E., Caratti, J. F., Key, C. H., Benson, N. C., Sutherland, S., et al. (2006). *FIREMON: Fire Effects Monitoring And Inventory System, Gen. Tech. Rep. RMRS-GTR-164-CD.* Fort Collins, CO: U.S. Department of Agriculture, Forest Service, Rocky Mountain Research Station.

MacKenzie, M. D., McIntire, E. J. B., Quideau, S. A., and Graham, R. C. (2008). Charcoal distribution affects carbon and nitrogen contents in forest soils of California. *Soil Sci. Soc. Am. J.* 72, 1774–1785. doi: 10.2136/sssaj2007.0363

Maestrini, B., Alvey, E. C., Hurteau, M., Safford, H., and Miesel, J. (2017). Fire severity alters the distribution of pyrogenic carbon stocks across ecosystem pools in a Californian mixed-conifer forest. *J. Geophysic. Res. Biogeosci.* 122, 2338-2355. doi: 10.1002/2017JG003832

Maestrini, B., and Miesel, J. R. (2017). Modification of the weak nitric acid digestion method for the quantification of black carbon in organic matrices. *Org. Geochem.* 103, 136–139. doi: 10.1016/j.orggeochem.2016.10.010

Makoto, K., Hirobe, M., DeLuca, T. H., Bryanin, S. V., Procopchuk, V. F., and Koike, T. (2011). Effects of fire-derived charcoal on soil properties and seedling regeneration in a recently burned *Larix gmelinii/Pinus sylvestris* forest. *J. Soils Sediments* 11, 1317–1322. doi: 10.1007/s11368-011-0424-6

Masiello, C. A. (2004). New directions in black carbon organic geochemistry. *Mar. Chem.* 92, 201–213. doi: 10.1016/j.marchem.2004.06.043

Massman, W. J. (2012). Modeling soil heating and moisture transport under extreme conditions: forest fires and slash pile burns. *Water Resour. Res.* 48:W10548. doi: 10.1029/2011WR011710

Massman, W. J., Frank, J. M., and Mooney, S. J. (2010). Advancing investigation and physical modeling of first-order fire effects on soils. *Fire Ecol.* 6, 36–54. doi: 10.4996/fireecology.0601036

McBeath, A. V., and Smernik, R. J. (2009). Variation in the degree of aromatic condensation of chars. *Org. Geochem.* 40, 1161–1168. doi: 10.1016/j.orggeochem.2009.09.006

McBeath, A. V., Smernik, R. J., and Krull, E. S. (2013). A demonstration of the high variability of chars produced from wood in bushfires. *Org. Geochem.* 55, 38–44. doi: 10.1016/j.orggeochem.2012.11.006

McBeath, A. V., Smernik, R. J., Schneider, M. P. W., Schmidt, M. W. I., and Plant, E. L. (2011). Determination of the aromaticity and the degree of aromatic condensation of a thermosequence of wood charcoal using NMR. *Org. Geochem.* 42, 1194–1202. doi: 10.1016/j.orggeochem.2011.08.008

Meigs, G. W., Donato, D. C., Campbell, J. L., Martin, J. G., and Law, B. E. (2009). Forest fire impacts on carbon uptake, storage, and emission: the role of burn severity in the eastern cascades, oregon. *Ecosystems* 12, 1246–1267. doi: 10.1007/s10021-009-9285-x

Meigs, G. W., Turner, D. P., Ritts, W. D., Yang, Z., and Law, B. E. (2011). Landscape-scale simulation on heterogeneous fire effects on pyrogenic carbon emissions, tree mortality, and net ecosystem production. *Ecosystems* 14, 758–775. doi: 10.1007/s10021-011-9444-8

Michelotti, L. A., and Miesel, J. R. (2015). Source material and concentration of wildfire-produced pyrogenic carbon influence post-fire nutrient dynamics. *Forests* 6, 1325–1342. doi: 10.3390/f6041325

Miesel, J. R., Hockaday, W. C., Kolka, R. K., and Townsend, P. A. (2015). Soil organic matter composition and quality across fire severity gradients in coniferous and deciduous forests of the southern boreal region. *J. Geophysic. Res. Biogeosci.* 120, 1124–1141. doi: 10.1002/2015JG002959

Millar, C. I., and Stephenson, N. L. (2015). Temperate forest health in an era of emerging megadisturbance. *Science* 349, 823–826. doi: 10.1126/science.aaa9933

Miller, J. D., Knapp, E. E., Key, C. H., Skinner, C. N., Isbell, C. J., Creasy, R. M., et al. (2009a). Calibration and validation of the relative differenced Normalized Burn Ratio (RdNBR) to three measures of fire severity in the Sierra Nevada and Klamath Mountains, California, USA. *Remote Sens. Environ.* 113, 645–656. doi: 10.1016/j.rse.2008.11.009

Miller, J. D., and Safford, H. (2012). Trends in wildfire severity: 1984 to 2010 in the Sierra Nevada, Modoc Plateau, and southern Cascades, California, USA. *Fire Ecol.* 8, 41–57. doi: 10.4996/fireecology.0803041

Miller, J. D., Safford, H. D., Crimmins, M., and Thode, A. E. (2009b). Quantitative evidence for increasing forest fire severity in the Sierra Nevada and southern Cascade mountains, California and Nevada, USA. *Ecosystems* 12, 16–32. doi: 10.1007/s10021-008-9201-9

Miller, J. D., and Thode, A. E. (2007). Quantifying burn severity in a heterogeneous landscape with a relative version of the delta Normalized Burn Ratio (dNBR). *Remote Sens. Environ.* 109, 66–80. doi: 10.1016/j.rse.2006.12.006

Miller, J., and Quayle, B. (2015). Calibration and validation of immediate post-fire satellite-derived data to three severity metrics. *Fire Ecol.* 11, 12–30. doi: 10.4996/fireecology.1102012

Miller, J. D., Skinner, C. N., Safford, H. D., Knapp, E. E., and Ramirez, C. M. (2012). Trends and causes of severity, size, and number of fires in northwestern California, USA. *Ecol. Appl.* 22, 184–203. doi: 10.1890/10-2108.1

Morgan, P., Keane, R. E., Dillon, G. K., Jain, T. B., Hudak, A. T., Karau, E. C., et al. (2014). Challenges of assessing fire and burn severity using field measures, remote sensing and modelling. *Int. J. Wildland Fire* 23, 1045–1060. doi: 10.1071/WF13058

Moritz, M. A., Parisien, M., Batllori, E., Krawchuk, M. A., Van Dorn, J., Ganz, D. J., et al. (2012). Climate change and disruptions to global fire activity. *Ecosphere* 3:49. doi: 10.1890/ES11-00345.1

Neary, D. G., Ryan, K. C., and DeBano, L. F. (2008). "Wildland fire in ecosystems: effects of fire on soils and water," in *General Technical Report RMRS-GTR-42-Vol. 4,* Ogden, UT: USDA Forest Service, Rocky Mountain Research Station.

North, M., Hurteau, M., and Innes, J. (2009). Fire suppression and fuels treatment effects on mixed-conifer carbon stocks and emissions. *Ecol. Appl.* 19, 1385–1396. doi: 10.1890/08-1173.1

NPS (2003). *Fire Monitoring Handbook*. Boise, ID: USDI National Park Service, Fire Management Program Center, National Interagency Fire Center.

NRCS (2018). *Web Soil Survey*. Soil Survey Staff, Natural Resources Conservation Service, United States Department of Agriculture. Available online at http://websoilsurvey.nrcs.usda.gov/ (Accessed January 18, 2018).

Pan, Y., Birdsey, R. A., Fang, J. Y., Houghton, R., Kauppi, P. E., Kurz, W. A., et al. (2011). A large and persistent carbon sink in the world's forests. *Science* 333, 988–993. doi: 10.1126/science.1201609

Pingree, M. R. A., Homann, P. S., Morrissette, B., and Darbyshire, R. (2012). Long and short-term effects of fire on soil charcoal of a conifer forest in southwest Oregon. *Forests* 3, 353–369. doi: 10.3390/f3020353

Preston, C. M., and Schmidt, M. W. I. (2006). Black (pyrogenic) carbon: a synthesis of current knowledge and uncertainties with special consideration of boreal regions. *Biogeosciences* 3, 397–420. doi: 10.5194/bg-3-397-2006

Reisser, M., Purves, R. S., Schmidt, M. W. I., and Abiven, S. (2016). Pyrogenic carbon in soils: a literature-based inventory and a global estimation of its content in soil organic carbon and stocks. *Front. Earth Sci.* 4:80. doi: 10.3389/feart.2016.00080

Robichaud, P. R., Lewis, S. A., Laes, D. Y. M., Hudak, A. T., Kokaly, R. F., and Zamudio, J. A. (2007). Postfire soil burn severity mapping with hyperspectral image unmixing. *Remote Sens. Environ.* 108, 467–480. doi: 10.1016/j.rse.2006.11.027

Saiz, G., Goodrick, L., Wurster, C. M., Zimmermann, M., Nelson, P. N., and Bird, M. I. (2014). Charcoal re-combustion efficiency in tropical savannas. *Geoderma* 219, 40–45. doi: 10.1016/j.geoderma.2013.12.019

Saiz, G., Wynn, J. G., Wurster, C. M., Goodrick, I., Nelson, P. N., and Bird, M. I. (2015). Pyrogenic carbon from tropical savanna burning: production and stable isotope composition. *Biogeosciences* 12, 1849–1863. doi: 10.5194/bg-12-1849-2015

Santín, C., Doerr, S. H., Kane, E. S., Masiello, C. A., Ohlson, M., de la Rosa, J. M., et al. (2015a). Towards a global assessment of pyrogenic carbon from vegetation fires. *Glob. Chang. Biol.* 22, 76–91. doi: 10.1111/gcb.12985

Santín, C., Doerr, S. H., Merino, A., Bryant, R., and Loader, N. J. (2016). Forest floor chemical transformations in a boreal forest fire and their correlations with temperature and heating duration. *Geoderma* 264, 71–80. doi: 10.1016/j.geoderma.2015.09.021

Santín, C., Doerr, S. H., Merino, A., Bucheli, T. D., Bryant, R., Ascough, P., et al. (2017). Carbon sequestration potential and physicochemical properties differ between wildfire charcoals and slow-pyrolysis biochars. *Sci. Rep.* 7:11233. doi: 10.1038/s41598-017-10455-2

Santin, C., Doerr, S. H., Preston, C., and Bryant, R. (2013). Consumption of residual pyrogenic carbon by wildfire. *Int. J. Wildland Fire* 22, 1072–1077. doi: 10.1071/WF12190

Santín, C., Doerr, S. H., Preston, C. M., and González-Rodríguez, G. (2015b). Pyrogenic organic matter production from wildfires: a missing sink in the global carbon cycle. *Glob. Chang. Biol.* 21, 1621–1633. doi: 10.1111/gcb.12800

Schmidt, M. W. I., Skjemstad, J. O., and Jager, C. (2002). Carbon isotope geochemistry and nanomorphology of soil black carbon: black chernozemic soils in central Europe originate from ancient biomass burning. *Global Biogeochem. Cycles* 16, 70.1–70.8. doi: 10.1029/2002GB001939

Schmidt, M. W. I., Torn, M. S., Abiven, S., Dittmar, T., Guggenberger, G., Janssens, I. A., et al. (2011). Persistence of soil organic matter as an ecosystem property. *Nature* 478, 49–56. doi: 10.1038/nature10386

Schoennagel, T., Veblen, T. T., and Romme, W. H. (2004). The interaction of fire, fuels, and climate across rocky mountain forests. *Bioscience* 54, 661–676. doi: 10.1641/0006-3568(2004)054[0661:TIOFFA]2.0.CO;2

Scott, J. (2018). Personal communication, January 18, 2018. Founder and Principal Consultant, Pyrologix LLC (http://www.pyrologix.com), Missoula, MT, USA.

Seiler, W., and Crutzen, P. J. (1980). Estimates of gross and net fluxes of carbon between the biosphere and the atmosphere from biomass burning. *Clim. Change* 2, 207–247. doi: 10.1007/BF00137988

Stephens, S. L., Agee, J. K., Fulé, P., North, M., Romme, W. H., Swetnam, T. W., et al. (2013). Managing forests and fire in changing climates. *Science* 342, 41–42. doi: 10.1126/science.1240294

Stockmann, U., Adams, M. A., Crawford, J. W., Field, D. J., Henakaarchchi, N., Jenkins, M., et al. (2013). The knowns, known unknowns and unknowns of sequestration of soil organic carbon. *Agric. Ecosystems Environ.* 164, 80–99. doi: 10.1016/j.agee.2012.10.001

Trumbore, S., Brando, P., and Hartmann, H. (2015). Forest health and global change. *Science* 349, 814–818. doi: 10.1126/science.aac6759

Uhelski, D., and Miesel, J. R. (2017). Physical location in the tree during forest fire influences element concentrations of bark-derived pyrogenic carbon from charred jack pines (*Pinus banksiana* Lamb.). *Org. Geochem.* 110, 87–91. doi: 10.1016/j.orggeochem.2017.04.014

Van de Water, K. M., and Safford, H. D. (2011). A summary of fire frequency estimates for California vegetation before Euro-American settlement. *Fire Ecol.* 7, 26–58. doi: 10.4996/fireecology.0703026

Van Mantgem, P. J., Nesmith, J. C. B., Keifer, M., Knapp, E. E., Flint, A., and Flint, L. (2013). Climatic stress increases forest fire severity across the western United States. *Ecol. Lett.* 16, 1151–1156. doi: 10.1111/ele.12151

Van Mantgem, P. J., Stephenson, N. L., Byrne, J. C., Daniels, L. D., Franklin, J. F., Fulé, P. Z., et al. (2009). Widespread increase of tree mortality rates in the western United States. *Science* 323, 521–524. doi: 10.1126/science.1165000

Van Wagner, C. E. (1968). The line intersect method in forest fuel sampling. *For. Sci.* 14, 20–26.

Van Wagtendonk, J. W., Benedict, J. M., and Sydoriak, W. M. (1998). Fuel bed characteristics of Sierra Nevada conifers. *West. J. Appl. For.* 13, 73–84.

Weichman, M. L., Hurteau, M. D., Kaye, J. P., and Miesel, J. R. (2015). Macro-particle charcoal C content following prescribed burning in a mixed-conifer forest, Sierra Nevada, California. *PLoS ONE* 10:e0135014. doi: 10.1371/journal.pone.0135014

Westerling, A. L., Bryant, B. P., Preisler, H. K., Holmes, T. P., Hidalgo, H. G., Das, T., et al. (2011). Climate change and growth scenarios for California wildfire. *Clim. Change* 109, 445–463. doi: 10.1007/s10584-011-0329-9

Westerling, A. L., Hidalgo, H. G., Cayan, D. R., and Swetnam, T. W. (2006). Warming and earlier spring increase western US forest wildfire activity. *Science* 313, 940–943. doi: 10.1126/science.1128834

Zimmerman, A. R., and Mitra, S. (2017). Trial by fire: on the terminology and methods used in pyrogenic organic carbon research. *Front. Earth Sci.* 5:95. doi: 10.3389/feart.2017.00095

**Conflict of Interest Statement:** The authors declare that the research was conducted in the absence of any commercial or financial relationships that could be construed as a potential conflict of interest.

frontiers in Earth Science

ORIGINAL RESEARCH
published: 29 November 2017
doi: 10.3389/feart.2017.00098

# Charcoal in Organic Horizon and Surface Mineral Soil in a Boreal Forest Fire Chronosequence of Western Quebec: Stocks, Depth Distribution, Chemical Properties and a Synthesis of Related Studies

*Caroline M. Preston[1]*, Martin Simard[2], Yves Bergeron[3], Guy M. Bernard[4] and Roderick E. Wasylishen[4]*

*[1] Pacific Forestry Centre, Natural Resources Canada, Victoria, BC, Canada, [2] Department of Geography, Centre for Forest Research and Centre for Northern Studies, Laval University, Québec, QC, Canada, [3] Centre for Forest Research, Institut de Recherche sur les Forêts and Chaire Industrielle CRSNG-UQAT-UQAM en Aménagement Forestier Durable, Université du Québec en Abitibi-Témiscamingue, Rouyn-Noranda, QC, Canada, [4] Department of Chemistry, University of Alberta, Edmonton, AB, Canada*

OPEN ACCESS

***Edited by:***
*Samuel Abiven, University of Zurich, Switzerland*

***Reviewed by:***
*Philippa Louise Ascough, Scottish Universities Environmental Research Centre, United Kingdom*
*Caitlin E. Hicks Pries, Dartmouth College, United States*

****Correspondence:***
*Caroline M. Preston*
*caroline.preston@canada.ca*

***Specialty section:***
*This article was submitted to Biogeoscience, a section of the journal Frontiers in Earth Science*

***Received:*** *31 July 2017*
***Accepted:*** *10 November 2017*
***Published:*** *29 November 2017*

***Citation:***
*Preston CM, Simard M, Bergeron Y, Bernard GM and Wasylishen RE (2017) Charcoal in Organic Horizon and Surface Mineral Soil in a Boreal Forest Fire Chronosequence of Western Quebec: Stocks, Depth Distribution, Chemical Properties and a Synthesis of Related Studies. Front. Earth Sci. 5:98. doi: 10.3389/feart.2017.00098*

Wildfires are a major driver of carbon stocks and ecosystem development in Canadian boreal forests, but there is little information on amounts and properties of the charcoal produced. Using data and samples available from a previous study, we determined amounts, depth distribution and chemical properties of visually-determined charcoal (>2 mm) in a boreal chronosequence in the Abitibi region of Quebec, Canada. Sites ranged from 24 to 2,355 years since fire (ysf) and originated from low- and high-severity soil burns (>5 or <5 cm organic horizon unburned, respectively). Two or three pits were sampled at 1-cm depth intervals from 20 jack pine (*Pinus banksiana*) sites (one low severity and 19 high severity) and 31 black spruce (*Picea mariana*) sites (12 low severity and 19 high severity). Site-level charcoal stocks ranged from 50 to 5,527 kg ha$^{-1}$ with high within-site variability and lower stocks for the oldest sites. Depth distributions typically peaked around the organic-mineral interface, but some low-severity sites also had charcoal layers within the organic horizon. Means from 30 charcoal samples were 569 mg g$^{-1}$ total C, 4.1 mg g$^{-1}$ total N and 140 C/N (molar), with total C and C/N showing a trend of decline with time since fire, and total N showing an increase. Solid-state $^{13}$C CPMAS NMR spectra of nine samples showed high variability among the younger samples, but a trend to higher aromaticity for the older ones. A literature survey focusing on boreal forests similarly showed highly variable stocks and chemical properties of charcoal in organic horizon and upper mineral soil, with reduction of variance and lower stocks after several hundred years. This initial variation was also consistent with reports of highly variable temperatures and duration of charring in wildfires. Adding reports available for char production, and considering that most studies of char stocks and production are limited to the organic horizon (forest floor), suggests that initial production of charred material from boreal wildfires might be around 5–10 tons ha$^{-1}$.

**Keywords: pyrogenic carbon, charcoal, boreal forest, wildfire, postfire chronosequence, NMR**

## INTRODUCTION

Fire is the major disturbance in boreal forests and thus a major driver of C cycling and ecosystem function (de Groot et al., 2013; Boulanger et al., 2014). In the Canadian north, for example, in the absence of fire, stands of black spruce [*Picea mariana* (Mill.) BSP] on poorly drained sites undergo gradual paludification, with increasing thickness of organic horizons and dominance of sphagnum moss and ericaceous shrubs (Lecomte et al., 2005, 2006; Simard et al., 2007). From a C cycling perspective, pyrogenic C (PyC) is expected to have a longer lifetime than other pools of soil organic matter, and thus contribute to long-term C sequestration by partially offsetting C losses due to fire (Bird et al., 2015; Santín et al., 2015, 2016a; Reisser et al., 2016), although this scenario has been challenged (Landry and Matthews, 2017). Recent studies have investigated stocks and properties of PyC in boreal forests of Canada (Bélanger et al., 2004; Hart and Luckai, 2014; Soucémarianadin et al., 2014, 2015a,b) and Alaska (Kane et al., 2010), but there is still insufficient information to develop an integrated picture of the production, stocks, longevity, chemical properties and ecological role of boreal PyC.

PyC is a general term for materials with a wide range of chemical properties and resistance to decomposition, due to variation in the degree of thermal transformation of living biomass or organic matter. This range is often described as the "black carbon (BC) continuum" (Preston and Schmidt, 2006; Bird et al., 2015). The defining characteristic of PyC is the presence of fused aromatic rings (polycyclic aromatic hydrocarbons, PAHs), culminating in graphene sheets and spherical soot structures almost entirely composed of C. Enhanced chemical resistance to decomposition is associated with PAH clusters greater than seven (Bird et al., 2015; McBeath et al., 2015), but much PyC has a smaller average cluster size and considerable substitution by N and O functional groups (Knicker, 2011).

A further complexity arises from the variety of methods used to quantify PyC (Reisser et al., 2016). In general, BC is often used to define the yield of C-containing fractions resistant to various chemical/thermal/photochemical oxidation procedures, or from their yield of benzene polycarboxylic acids (BPCAs) (Preston and Schmidt, 2006; Hammes et al., 2007), as well as from molecular modeling of $^{13}C$ nuclear magnetic resonance (NMR) spectra (Kane et al., 2010; Soucémarianadin et al., 2015a). On the other hand, the term "charcoal" typically defines PyC identified visually and often picked out by hand, especially in paleoecology. Results from a milder oxidation procedure specifically developed to capture PyC in forest soil and organic horizon (Kurth et al., 2006; Soucémarianadin et al., 2014; Maestrini and Miesel, 2017) have been variously reported as charcoal or BC. Methods comparison has been undertaken for BC (Hammes et al., 2007), but in general there is little interaction between research groups using chemical vs. visual methods. The chemical methods are more commonly associated with geochemistry or soil science, and the visual with forest ecology and paleobotany.

The charred material visually apparent after wildfire comprises a continuum of structures and inherent recalcitrance, likely skewed toward lower transformation (Knicker, 2011). To build a complete understanding of the role of PyC in boreal forests requires a wide array of information, including inputs and stocks of different forms of PyC in above- and below-ground pools. Linking initial production, stocks and chemical properties of charcoal, which have often been determined in the organic horizon, and those of BC mostly determined in mineral soil, is essential in closing the gaps in our understanding of the PyC cycle for boreal forests. With a dearth of information available from targeted studies designed to quantify, characterize and link these pools, much relevant information may be gleaned from studies designed for other purposes, mainly paleoecology and forest fire history. Our study utilizes an opportunity that emerged from extensive studies of fire history in the Abitibi region of Quebec, Canada. As reported in Lecomte et al. (2005, 2006), charcoal fragments (>2 mm) were picked out and weighed by 1-cm increments in the organic horizon and upper mineral soil in 51 black spruce and jack pine (*Pinus banksiana* Lamb) chronosequence plots [24–2,355 years-since-fire (ysf)], but area-based results were not included in the original papers focusing on fire frequency. Our first objective was to use these data to examine in more detail the amounts, depth distribution and spatial variability of charcoal in these plots, and to determine chemical characteristics of selected samples. The second objective was to place these results in a broader review of published data on charcoal stocks and properties in boreal forests.

## MATERIALS AND METHODS

### Site Selection

Detailed information has been published previously (Lecomte et al., 2005, 2006; Simard et al., 2007), including descriptions of the forest region, understory vegetation dynamics since fire, plot selection and classification, determination of ysf by dendrochronology or by radiocarbon dating of charcoal (when post-fire stand age was greater than maximum tree longevity), soil sampling separation of charcoal, and determination of fire severity. Briefly, the fire chronosequence study area (49°-51°20′N; 78°30′–79°50′W) is located in the Clay Belt of northeastern Ontario and northwestern Quebec, within the *Picea mariana*-feathermoss bioclimatic domain, with mean annual temperature around 0°C and mean annual precipitation around 900 mm. Most of the area is covered by forests dominated by black spruce or jack pine, with fire as the main disturbance. Due to complex interactions of climate variability, human influence and forest composition, fire cycle length has increased from 101 y before 1850 to 398 y since 1920, with a mean stand age of 148 y at present (Bergeron et al., 2004).

We used a stand initiation map developed for the study area by Bergeron et al. (2004) to select black spruce- and jack pine-dominated stands of different post-fire age (ysf). The stand initiation map was created by mapping recent (approximately <100 years ago) fires using aerial photos and archives, and then

**Abbreviations:** BC, black carbon; CP, cross polarization; DP, direct polarization; HI, site originating from a high-severity soil burn; LO, site originating from a low-severity soil burn; ICP, inductively coupled plasma; MAS, magic-angle spinning; NMR, nuclear magnetic resonance; PyC, pyrogenic carbon; Ysf, years since fire.

assigning a fire date using archives and dendroecological data (fire scars and dating of post-fire cohorts). To date older fires, whose extent could not be delimited using archives and aerial photographs, the study area was divided into a grid of 100-km$^2$ sections where at least one site would be visited and sampled for dendroecological analyses. When the post-fire cohort could not be identified (at least five trees of pioneer species having a germination date within 10 years of each other), a minimum stand age was given, corresponding to the age of the oldest tree (Bergeron et al., 2004). In sites that were selected for the chronosequence but that were assigned a minimum stand age, charcoal fragments collected at the mineral-organic soil interface were radiocarbon-dated to obtain postfire stand age (Simard et al., 2007).

Each black spruce or jack pine stand selected for study had to be on fine-textured mineral deposits, on a slight incline, and free of any sign of anthropogenic disturbance. The thickness of the organic horizon not consumed by the last fire (residual organic layer) was used to distinguish sites originating from high- or low-severity soil burns (defined as $<5$ or $>5$ cm organic horizon remaining, respectively), abbreviated HI or LO. Ideally, soil burn severity is quantified as the amount of organic horizon consumed. Nonetheless, as it is impossible to know organic layer depth of the pre-fire stand, fire severity was defined as the depth of the organic layer not consumed by the fire (Lecomte et al., 2005, 2006; Simard et al., 2007). From an ecological perspective, residual organic layer thickness is also more meaningful than organic layer burned because it influences seed germination and tree growth and therefore post-fire succession and stand structure. Seed germination is hindered when the residual organic layer is thicker than 5 cm (Johnstone and Chapin, 2006), which is the threshold that we used to separate low and high-severity soil burns. Residual organic layer thickness was determined by two methods: by meticulous laboratory examination of the monoliths sampled from each site (see next paragraph), and by *in situ* observation of charcoal layers within numerous pits and trenches dug into the organic horizon. The residual organic layer is easy to identify because it is located between the mineral soil and the uppermost charcoal layer within the organic layer. Above that charcoal layer is the organic soil that accumulated after the fire, which is also much less decomposed than the residual organic layer. The 51 plots (**Table 1**) include 1 LO and 19 HI jack pine sites, and 12 LO and 19 HI black spruce sites. Forty-eight of these plots correspond to those listed in Appendix 1 of Lecomte et al. (2005, 2006); the three additional plots included in this study are a LO jack pine site of 24 ysf, a LO black spruce site of 24 ysf, and a HI black spruce site of 88 ysf.

## Soil Sampling

At each site, two to four 10 cm × 10 cm monoliths of the organic layer, in most cases extending some cm into the mineral soil, were collected. The monoliths were frozen and sliced into 1-cm sections. Subsamples (50 cm$^3$) from the organic and mineral horizons were defloculated with a solution of 2% NaOH or KOH for 24 h at 60°C. They were neutralized with 10–20% HCl during which the supernatant turned pale, then passed through sieves (2, 1, and 0.250 mm) for paleobotanical analysis. The mineral soil/organic matter interface was established where the mineral soil represented <25% of the particles retained in the 2 mm mesh. Charcoal fragments were only recovered from the >2 mm material. If no charcoal was seen in the >2 mm material, but it was seen in the >1 mm material, the amount of charcoal was set at 0.0001 g. The recovered charcoal fragments were dried at 70°C.

The experimental design to recover charcoal from the >2 mm material was based on the original objectives of the ecological studies (Lecomte et al., 2005, 2006; Simard et al., 2007) for which the recovered fragments were identified as to plant component and species. Similarly, the original study's plan was to sample the organic horizon only, but in most cases, this extended some variable distance into the mineral soil. Unusual for such retrospective paleobotanical studies, the decision to quantify the mass of charcoal on an area basis and to save the samples enabled us to carry out the study reported here. More recent studies have shown the common occurrence of charcoal/PyC at the interface of the organic and mineral layers in these boreal forests (Cyr et al., 2005; Ohlson et al., 2009; Hart and Luckai, 2014; Soucémarianadin et al., 2015a), consistent with the authors' field experience. Thus with a few exceptions, our sampling depths would have captured most of the charcoal in the organic horizon (sometimes also referred to as "forest floor" or "organic layer") and upper mineral soil. Investigation of charcoal or other forms of PyC in deeper mineral horizons was beyond the scope of our study.

Inspection of the depth profiles showed that for some monoliths, sampling was probably not deep enough to capture the charcoal peak at the organic/mineral interface (e.g., JP-HI-76B and JP-HI-135B). To quantify how likely charcoal abundance was underestimated, we identified (star-shaped symbols in **Figure 2**) all monoliths whose deepest 1-cm horizon contained a significant proportion (>10%) of the total charcoal mass and that also had a significant amount of charcoal: >10 g m$^{-2}$: 1 star; >15 g m$^{-2}$: 2 stars; >20 g m$^{-2}$: 3 stars; >25 g m$^{-2}$: 4 stars. Monoliths that most likely under-sampled the charcoal (4 stars) are identified as open bars in **Figure 1**.

## Chemical Analysis

From a large number of mostly very small samples, 30 samples for chemical analysis were obtained by selecting the largest samples and also by making composites. Examination of the depth distribution showed that most charcoal, especially from high-severity fires, was concentrated in one layer at or near the organic-mineral interface. In most cases, composites were made of 2–4 samples representing the peak of charcoal content for a single monolith. In a few cases where sample amount was very limited, composites were assembled from two monoliths of the same site but from similar points in the charcoal vs. depth profile. In all cases, samples used for composites were similar in color and morphology. Samples were then ground by hand using a mortar and pestle, and dried at 70°C. Because of the need for a reasonable amount of sample for chemical analysis, samples largely represent monoliths with >800 kg ha$^{-1}$ charcoal, although some very small samples were taken to capture older sites and layers from low-severity fires.

**TABLE 1 |** Characteristics of the chronosequence stands.

| Plot ID | Soil burn Severity | YSF | N | Charcoal mass (g $m^{-2}$) | | |
|---|---|---|---|---|---|---|
| | | | | Org + Min | Org only | Fraction in org |
| **JACK PINE** | | | | | | |
| JP-LO-24 | LO | 24 | 2 | 256.9 | 150.7 | 0.59 |
| JP-HI-45 | HI | 45 | 2 | 319.6 | 219.0 | 0.69 |
| JP-HI-51 | HI | 51 | 2 | 73.6 | 8.5 | 0.12 |
| JP-HI-52 | HI | 52 | 2 | 115.6 | 36.3 | 0.31 |
| JP-HI-76 | HI | 76 | 2 | 108.4 | 54.2 | 0.50 |
| JP-HI-84 | HI | 84 | 2 | 61.7 | 14.1 | 0.23 |
| JP-HI-86 | HI | 86 | 2 | 72.5 | 3.6 | 0.05 |
| JP-HI-88 | HI | 88 | 2 | 7.6 | 0.2 | 0.02 |
| JP-HI-135 | HI | 135 | 2 | 303.1 | 259.2 | 0.86 |
| JP-HI-149a | HI | 149 | 2 | 149.6 | 8.3 | 0.06 |
| JP-HI-149b | HI | 149 | 2 | 67.2 | 13.1 | 0.20 |
| JP-HI-150 | HI | 150 | 2 | 79.3 | 44.0 | 0.56 |
| JP-HI-151 | HI | 151 | 2 | 246.5 | 71.0 | 0.29 |
| JP-HI-155 | HI | 155 | 2 | 41.3 | 22.5 | 0.54 |
| JP-HI-176 | HI | 176 | 2 | 111.2 | 40.4 | 0.36 |
| JP-HI-177 | HI | 177 | 2 | 121.0 | 1.7 | 0.01 |
| JP-HI-179 | HI | 179 | 2 | 69.4 | 7.0 | 0.10 |
| JP-HI-204 | HI | 204 | 2 | 40.2 | 4.6 | 0.12 |
| JP-HI-222 | HI | 222 | 2 | 127.2 | 65.4 | 0.51 |
| JP-HI-229 | HI | 229 | 2 | 138.7 | 27.6 | 0.20 |
| JP HI | | | 19 | 118.6 ± 85.3 [108] | 47.4 ± 71.3 [22.5] | 0.30 ± 0.25 [0.23] |
| JP all | | | 20 | 125.5 ± 88.6 [109.8] | 52.6 ± 73.1 [25.1] | 0.32 ± 0.25 [0.26] |
| **BLACK SPRUCE** | | | | | | |
| BS-LO-24 | LO | 24 | 2 | 73.6 | 47.9 | 0.65 |
| BS-LO-38 | LO | 38 | 2 | 257.2 | 145.3 | 0.57 |
| BS-LO-52 | LO | 52 | 3 | 200.2 | 45.3 | 0.23 |
| BS-LO-53 | LO | 53 | 2 | 261.4 | 149.1 | 0.57 |
| BS-LO-62 | LO | 62 | 2 | 61.2 | 44.2 | 0.72 |
| BS-LO-75 | LO | 75 | 2 | 32.8 | 8.5 | 0.26 |
| BS-LO-85 | LO | 85 | 2 | 168.5 | 47.5 | 0.28 |
| BS-LO-94 | LO | 94 | 3 | 62.8 | 43.5 | 0.69 |
| BS-LO-143 | LO | 143 | 3 | 94.6 | 51.2 | 0.54 |
| BS-LO-149 | LO | 149 | 2 | 170.7 | 60.5 | 0.35 |
| BS-LO-151 | LO | 151 | 2 | 168.6 | 152.6 | 0.91 |
| BS-LO-169 | LO | 169 | 3 | 137.0 | 103.5 | 0.76 |
| BS-HI-52 | HI | 52 | 3 | 75.7 | 33.4 | 0.44 |
| BS-HI-53 | HI | 53 | 2 | 46.1 | 37.3 | 0.81 |
| BS-HI-72 | HI | 72 | 2 | 120.2 | 11.4 | 0.09 |
| BS-HI-76 | HI | 76 | 3 | 67.9 | 1.6 | 0.02 |
| BS-HI-85 | HI | 85 | 2 | 254.3 | 50.6 | 0.20 |
| BS-HI-86 | HI | 86 | 2 | 552.7 | 344.6 | 0.62 |
| BS-HI-88 | HI | 88 | 2 | 267.8 | 121.2 | 0.45 |
| BS-HI-94 | HI | 94 | 2 | 192.6 | 163.1 | 0.85 |
| BS-HI-95 | HI | 95 | 3 | 97.5 | 6.4 | 0.07 |
| BS-HI-126 | HI | 126 | 3 | 103.5 | 32.3 | 0.31 |
| BS-HI-128 | HI | 128 | 2 | 331.6 | 280.3 | 0.85 |
| BS-HI-174 | HI | 174 | 2 | 69.2 | 5.2 | 0.08 |
| BS-HI-184 | HI | 184 | 2 | 68.8 | 4.0 | 0.06 |

*(Continued)*

**TABLE 1** | Continued

| Plot ID | Soil burn Severity | YSF | N | Charcoal mass (g $m^{-2}$) | | |
|---|---|---|---|---|---|---|
| | | | | Org + Min | Org only | Fraction in org |
| BS-HI-365 | HI | 365 | 2 | 64.7 | 0.1 | 0.00 |
| BS-HI-710 | HI | 710 | 3 | 252.7 | 58.9 | 0.23 |
| BS-HI-790 | HI | 790 | 2 | 5.8 | 0.0 | 0.00 |
| BS-HI-1225 | HI | 1225 | 3 | 16.4 | 1.6 | 0.10 |
| BS-HI-1585 | HI | 1585 | 2 | 5.0 | 0.5 | 0.10 |
| BS-HI-2355 | HI | 2355 | 2 | 82.2 | 2.1 | 0.03 |
| BS LO | | | 12 | 140.7 ± 76.7 [152.7] | 74.9 ± 49.3 [49.5] | 0.54 ± 0.22 [0.57] |
| BS HI | | | 19 | 140.8 ± 138.3 [82.2] | 60.8 ± 99.5 [11.4] | 0.28 ± 0.30 [0.10] |
| BS all | | | 31 | 140.8 ± 116.7 [97.5] | 66.3 ± 83.0 [44.2] | 0.38 ± 0.30 [0.31] |
| All sites | | | 51 | 134.8 ± 105.9 [103.5] | 60.9 ± 78.8 [37.3] | 0.36 ± 0.28 [0.29] |

*Plot identification (Plot ID) includes stand type (BS, black spruce; JP, jack pine), soil burn severity (HI, high; LO, low), and years since fire (YSF). N is the number of monoliths sampled per plot. Charcoal mass (mean ± standard deviation [median]) is given for the organic layer only (Org only) and for the whole profile, which includes the organic and mineral horizons (Org + Min). The fraction of charcoal in the organic layer is also given.*

Total C and N were determined on a Fisons NA1500 (Thermo Fisher Scientific Inc., Waltham MA) combustion analyzer using Costech EAS32 software (Costech Analytical Technologies Inc., Valencia, CA) for data collection and processing. Typically, 10–15 mg of finely ground sample was sealed into tin cups containing 3–4 mg of ACS grade vanadium pentoxide as combustion accelerant. The methods were validated by using NIST certified reference materials, which for plant tissue and high organic soils are NIST 1515 (Apple), 1575 (Pine), 1547 (Peach) and 1567a (Wheat Flour). Ash was determined by heating at 600°C in a muffle furnace for 18 h.

For analysis by ICP (inductively coupled plasma) spectrometry, samples were digested in 10 mL concentrated nitric acid spiked with Y and/or Sc internal standards using the SCP Science (Baie D'Urfé, Quebec, Canada) NovaWave closed-vessel microwave system with quartz tubes sealed with teflon caps. Samples were then finished with the addition of 4 mL concentrated hydrochloric acid and deionized water to approximately 50 mL. This procedure was developed with minor modifications from previous studies showing that the nitric acid digestion without $H_2O_2$ captures most macro and micro nutrients in plants, soils and related materials (Wu et al., 1997; Araújo et al., 2002; Sandroni and Smith, 2002). A 100% complete digestion is not possible, mainly due to the inability for the acid mixture to digest silicates, so that elements such as Al and Fe may not be fully released without inclusion of HF. Good agreement was found for two plant reference materials, and in an inter-laboratory proficiency testing program, results were close to the median ($n = 27$) for all reported elements. The ICP analysis was carried out on a Thermo Duo 6500 ICP equipped with CETAC autosampler and controlled by Thermo iTEVA instrument control and data acquisition software (Thermo Fisher Scientific Inc., Waltham MA). Instrument calibration was performed and verified by independent mixed NIST-traceable ICP standards prior to every analytical run using analyte/internal standard intensity ratios.

## C-13 NMR

Solid-state carbon-13 NMR spectra were obtained for samples selected to represent different stand types, ysf and fire severity, the choices being limited by the large amount of time required to run samples, and also by the need for sufficient sample quantity. Spectra were acquired with variable-amplitude cross-polarization (VACP, Peerson et al., 1993) and magic-angle spinning (MAS) on a 4.7 T Chemagnetics CMX Infinity 200 NMR spectrometer (Agilent, Loveland CO, formerly Varian, Ft. Collins CO) at 50.3 MHz with MAS at 14 kHz in a rotor of 4.0 mm outside diameter. The spectra were acquired with two-pulse phase modulation (TPPM) decoupling (Preston et al., 2014a), a $^1$H 90° pulse of 2.5 μs, 1 ms contact time, 34 ms acquisition time, 3 s recycle delay, and acquisition of 27,000 to 32,000 transients. After background correction, spectra were processed with 100 Hz line-broadening and baseline correction (Preston et al., 2014a).

Spectra were divided into the following chemical-shift areas: 0–47 ppm, alkyl C; 47–110 ppm, O, N-alkyl and di-O-alkyl C; 110–165 ppm, aryl C comprising aromatic and phenolic C; 165–210 ppm, carboxyl, amide and ester C. The di-O-alkyl signal typical of C-1 of carbohydrates was not separated from the broad aryl C peak, and was sometimes only a broad residual shoulder. Thus, rather than using a vertical boundary, a baseline for the di-O-alkyl region was sketched in to allow a more accurate estimate of this region. Relative areas were determined by copying the spectra, and cutting and weighing the spectral regions, an old technique that is still useful for spectra with low signal-to-noise ratios (Preston, 2014; Preston et al., 2014a). Aromaticity was calculated as the ratio of intensities 110–165 ppm/0–165 ppm. Relative areas and aromaticity were treated qualitatively to show trends, as CP efficiency varies for different C structures and environments. The VACP technique helps to overcome this, but compared to quantitative direct-polarization (DP) spectra, CP spectra underestimate aromatic C without attached hydrogens although as samples become almost completely aromatic the effect is diminished (Preston, 2014).

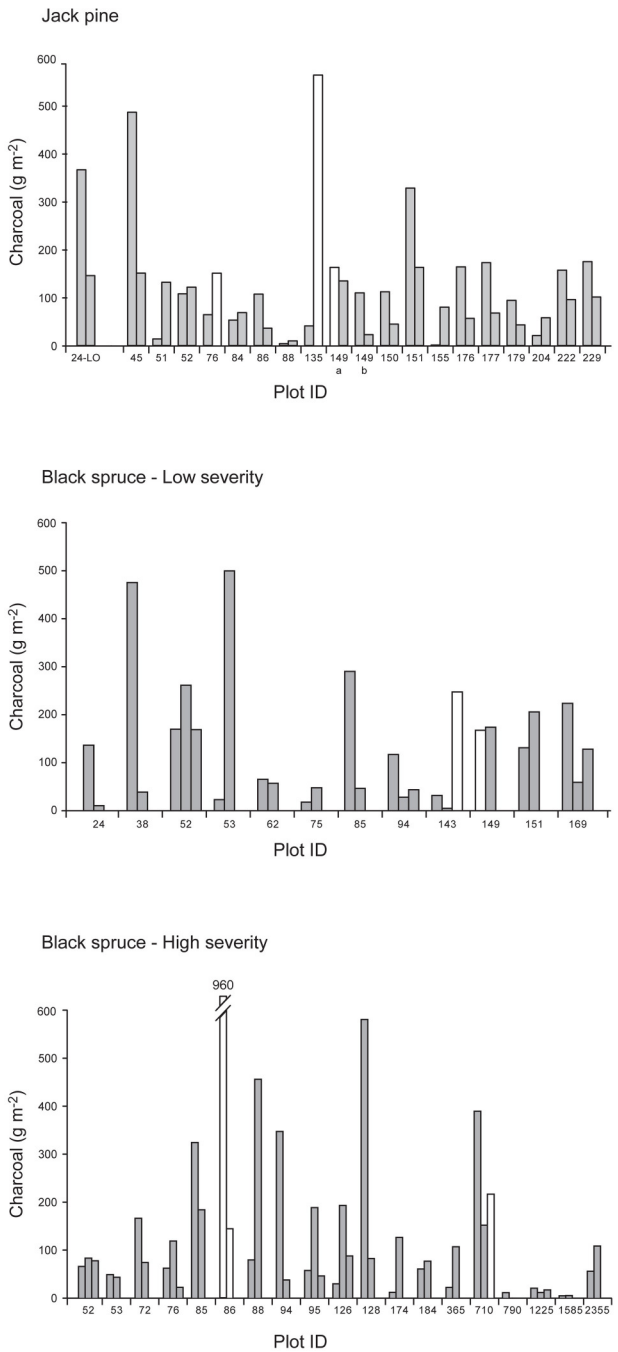


**FIGURE 1 |** Charcoal content for the two or three individual monoliths sampled at each site. Open bars indicate monoliths where the charcoal content was likely underestimated (indicated with 4 stars in **Figure 2**). Refer to **Table 1** for explanation of plot identification (Plot ID).

# RESULTS

## Amounts and Depth Distribution

Charcoal content ranged over 100-fold, from 5 to 553 g $m^{-2}$ for the whole profiles and 0.01 to 345 g $m^{-2}$ for the organic layer only (site means; **Table 1**). The older sites generally had lower charcoal stocks, but only a few sites were older than 400 ysf. There was also very high variability in charcoal content between monoliths within each plot (**Figure 1**).The depth profiles for individual pits showed a peak in charcoal concentration close to the organic-mineral interface, typically around −2 to 2 cm (**Figure 2**) but a few profiles showed a deeper peak (e.g., plot BS-HI-52A at −5 cm). In addition to the charcoal peak at the organic-mineral interface, LO black spruce sites also had charcoal layers in the residual organic layer (**Figure 2C**). Because the soils were sampled with the original intent of reconstructing fire history and not charcoal stocks and depth distribution, the maximum sampling depth in the mineral soil was variable. As a result, some charcoal peaks may have been missed in some sites (indicated by stars in **Figure 2**), leading to an underestimation of charcoal stocks in those sites (indicated by open bars in **Figure 1**).

## Chemical Properties

In charcoal samples taken in organic and mineral horizons, total C ranged from 429 to 700 mg $g^{-1}$ (mean = 569), total N from 1.0 to 8.4 mg $g^{-1}$ (mean = 4.1) and the C/N ratio (molar) from 71 to 646 (mean = 140; **Table 2**). Due to the small amounts of sample available, ash was not determined on the four oldest samples, but for the others ($n$ = 26) ranged from 46 to 311 mg $g^{-1}$. On an ash-free basis, means were 676 mg $g^{-1}$ for total C and 4.5 mg $g^{-1}$ for total N. Our field data indicated weak trends for decreases in charcoal C ($P = 0.1021$), and increases in charcoal N ($P = 0.0084$) and ash (not shown), as well as a more distinct decline of the C/N ratio ($P = 0.0150$) with ysf (**Figure 3**).

Concentrations of other elements in charcoal, except for the four oldest samples, are shown in **Table 3**. Highest values were generally found for potassium, calcium, aluminum and iron and lowest for zinc, copper and boron. There appeared to be little variation in concentration with ysf, although iron and aluminum tended to increase with ysf.

## C-13 NMR

Interpretation of the NMR spectra is based on previous studies of wood, organic matter and effects of charring (Baldock and Smernik, 2002; Czimczik et al., 2002; McBeath et al., 2011; Merino et al., 2015; Santín et al., 2016b). All of the $^{13}C$ CPMAS spectra have broad peaks for aromatic C at approximately 127 ppm and at 31–34 ppm for alkyl C (**Figure 4**). There is considerable variation in the O/N- and di-O-alkyl regions, with some samples retaining sharp peaks characteristic of cellulose. These are most distinct for sample JP-HI-45, at 63 and 66 ppm for C6, 75 ppm for C2, C3, and C5, 84 and 89 ppm for C4, and 106 ppm for C1. Samples BS-HI-128 and BS-HI-88 also retain sharp features at 75, 88, and 106 ppm, but lack the splitting due to more crystalline and more disordered cellulose. Other samples show less intensity due to cellulose or carbohydrate, especially the two oldest samples (BS-HI-710 and BS-HI-2355). The phenolic region mostly appears as a weak shoulder of the aromatic signal around 150 ppm but even this cannot be seen for the oldest sample BS-HI-2355. Carboxyl signals are generally broad and weak, with samples BS-LO-151 and BS-HI-2355 having the most distinct peaks at 176 ppm.

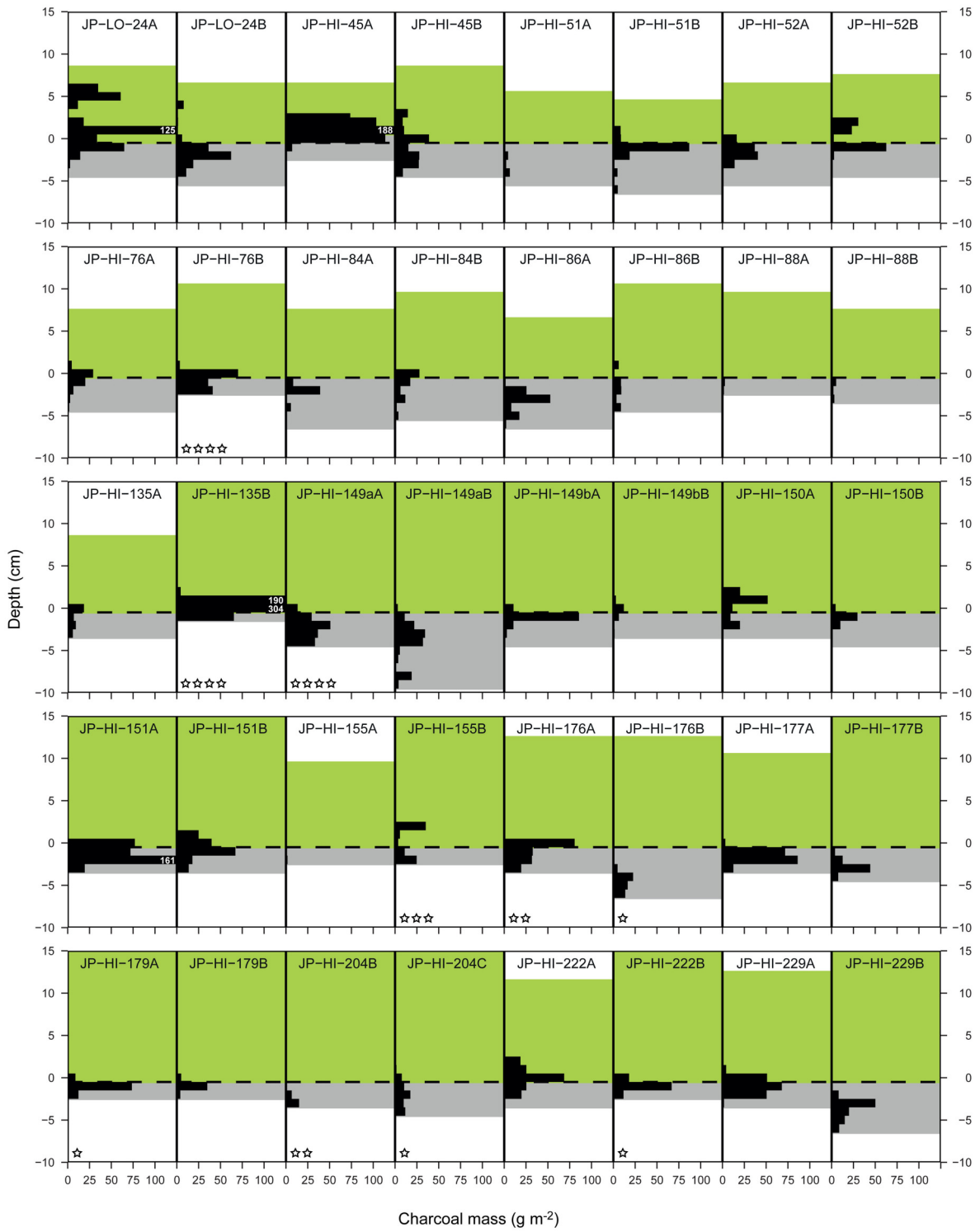


**FIGURE 2 |** Continued

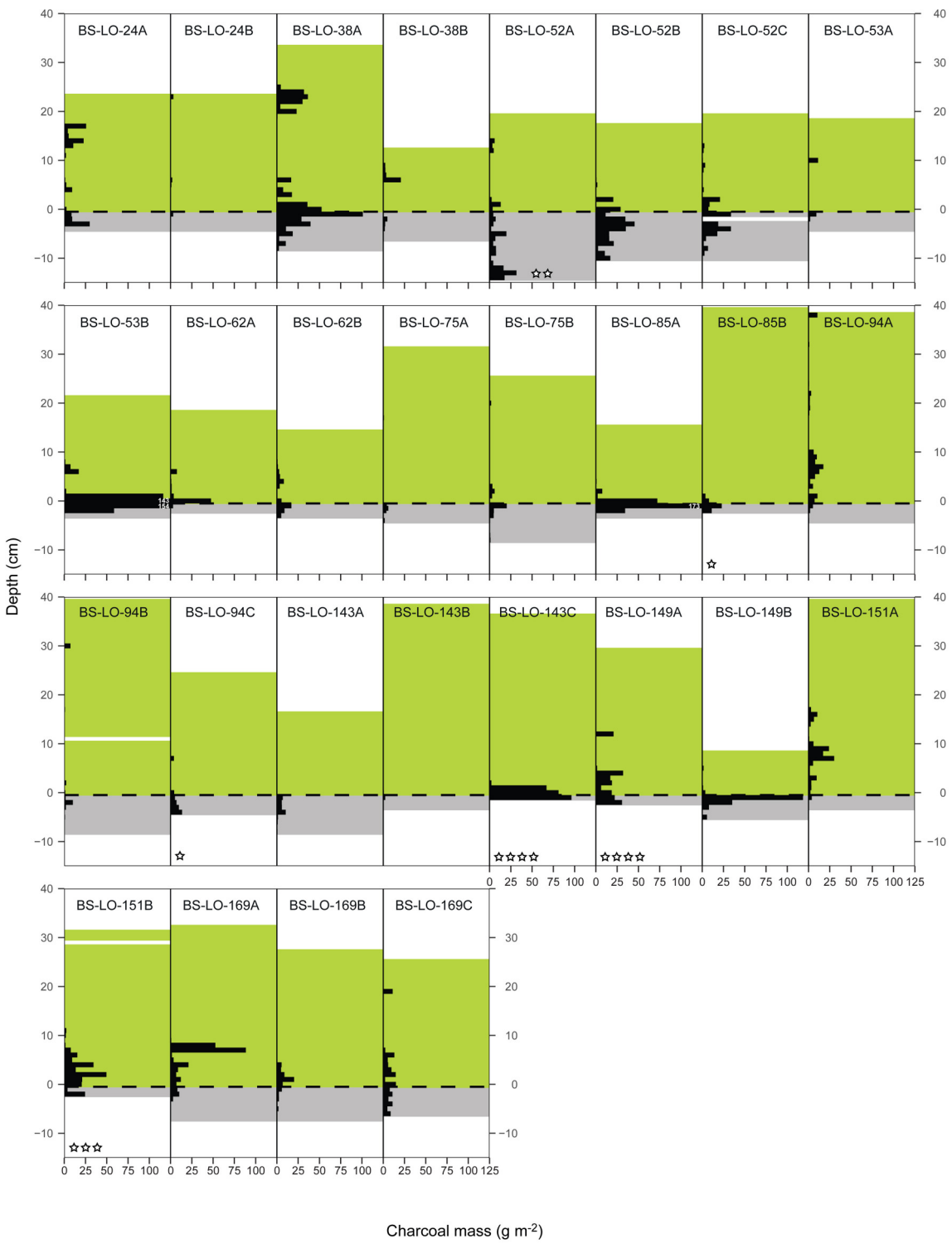


**FIGURE 2 |** Continued

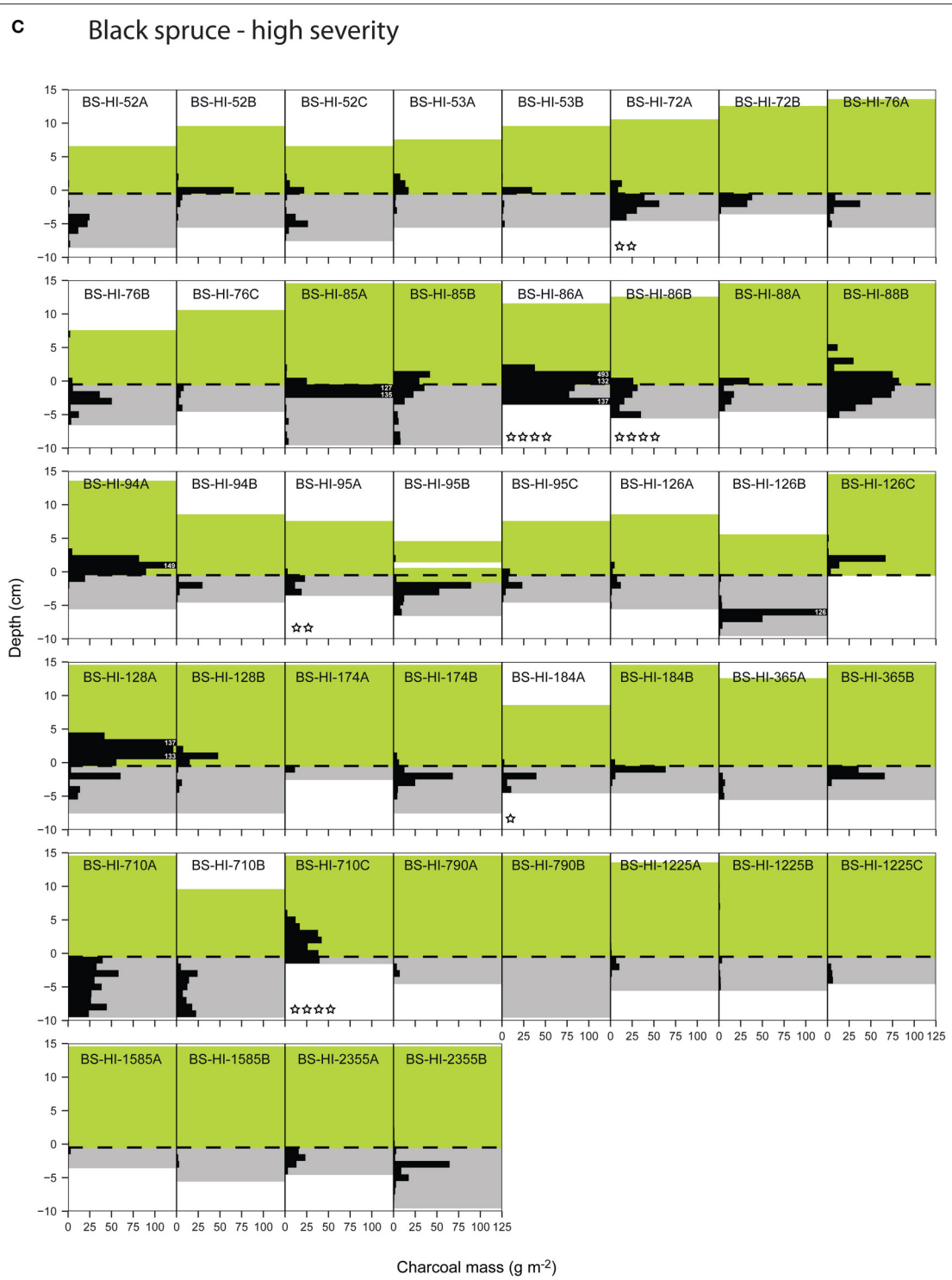


**FIGURE 2 |** Depth distributions of charcoal by 1-cm increments for each monolith in **(A)** jack pine, **(B)** low-severity black spruce, and **(C)** high-severity black spruce sites. The black horizontal bars represent charcoal mass up to a value of 125 g $m^{-2}$; when charcoal mass exceeds this value, the exact value is indicated in small white characters. The green area above the organic-mineral interface (dashed line at depth = 0) represents the organic layer, and the gray area below the interface represents the mineral soil that was sampled. For some monoliths, sampling was probably not deep enough to capture the charcoal peak (e.g., JP-HI-76B and JP-HI-135B). To quantify how likely charcoal abundance was underestimated, we identified (star-shaped symbols) all monoliths whose deepest 1-cm horizon contained a significant proportion (>10%) of the total charcoal mass and that also had a significant amount of charcoal: >10 g $m^{-2}$: 1 star; >15 g $m^{-2}$: 2 stars; >20 g $m^{-2}$: 3 stars; >25 g $m^{-2}$: 4 stars. Monoliths that most likely under-sampled the charcoal (4 stars) are identified as open bars in **Figure 1**.

**TABLE 2 |** Chemical composition of charcoal samples >2 mm extracted from organic (Org) or mineral (Min) horizons.

| Plot ID | Horizon | Monolith (sample depth) | C (mg $g^{-1}$) | N (mg $g^{-1}$) | C/N (molar) | Ash (mg $g^{-1}$) | C ash-free (mg $g^{-1}$) | N ash-free (mg $g^{-1}$) |
|---|---|---|---|---|---|---|---|---|
| **JACK PINE** | | | | | | | | |
| JP-LO-24 | Org | A (−6, −5) | 621 | 2.9 | 247 | 92 | 684 | 3.2 |
| JP-LO-24 | Org | A (−1) | 700 | 2.4 | 342 | 153 | 826 | 2.8 |
| JP-HI-45 | Org + Min | A (−1, 0, 1) | 560 | 1.4 | 484 | 120 | 636 | 1.5 |
| JP-HI-51 | Min | B (1) | 488 | 2.1 | 267 | 106 | 546 | 2.4 |
| JP-HI-135 | Org | B (−1, 0) | 576 | 1.0 | 646 | 166 | 691 | 1.2 |
| JP-HI-149 | Min | A (1) | 546 | 4.3 | 150 | 211 | 693 | 5.4 |
| JP-HI-151 | Min | A (3) | 567 | 2.2 | 308 | 193 | 702 | 2.7 |
| JP-HI-176 | Org | A (0) | 570 | 4.7 | 142 | 137 | 661 | 5.4 |
| JP-HI-177 | Min | A (1, 2) | 586 | 4.9 | 140 | 135 | 678 | 5.7 |
| JP-HI-229 | Min | A (1, 2, 3); B (3) | 512 | 3.2 | 189 | 219 | 655 | 4.0 |
| **BLACK SPRUCE** | | | | | | | | |
| BS-LO-38 | Org | A (−24, −23, −22, −20) | 630 | 2.8 | 263 | 98 | 698 | 3.1 |
| BS-LO-38 | Min | A (1) | 543 | 5.1 | 124 | 132 | 626 | 5.9 |
| BS-LO-53 | Org + Min | B (−1, 0, 1) | 577 | 1.7 | 408 | 195 | 717 | 2.1 |
| BS-LO-85 | Min | A (1) | 557 | 3.1 | 207 | 201 | 697 | 3.9 |
| BS-LO-143 | Org + Min | C (0, −1) | 444 | 3.1 | 167 | 311 | 643 | 4.5 |
| BS-LO-149 | Min | B (1) | 636 | 4.9 | 150 | 83 | 693 | 5.4 |
| BS-LO-151 | Org | A (−9, −7); B (−4, −2) | 548 | 6.2 | 103 | 137 | 635 | 7.2 |
| BS-LO-169 | Org | A (−7) | 659 | 5.4 | 142 | 79 | 716 | 5.9 |
| BS-HI-85 | Min | A (1, 2) | 592 | 5.7 | 122 | 115 | 670 | 6.4 |
| BS-HI-86 | Org | A (−1) | 661 | 2.9 | 267 | 98 | 733 | 3.2 |
| BS-HI-86 | Org + Min | A (0, 1, 2, 3) | 571 | 2.2 | 304 | 113 | 643 | 2.5 |
| BS-HI-88 | Org + Min | B (−1, 0, 1, 2) | 529 | 4.2 | 147 | 187 | 650 | 5.1 |
| BS-HI-94 | Org | A (−2, −1, 0) | 582 | 5.2 | 131 | 164 | 697 | 6.2 |
| BS-HI-95 | Min | B (1) | 512 | 8.4 | 71 | 179 | 624 | 10.2 |
| BS-HI-126 | Min | B (6) | 602 | 5.8 | 122 | 134 | 696 | 6.7 |
| BS-HI-128 | Org | A (−3, −2, −1) | 644 | 3.7 | 206 | 46 | 675 | 3.8 |
| BS-HI-365 | Min | A (2, 3, 4, 5) | 537 | 6.8 | 92 | | | |
| BS-HI-710 | Org + Min | B (39); C (−3, −2, 0, 1) | 429 | 6.7 | 75 | | | |
| BS-HI-1225 | Min | A (4, 5) | 505 | 5.2 | 113 | | | |
| BS-HI-2355 | Min | B (3) | 593 | 4.5 | 154 | | | |
| Mean | | | 569 | 4.1 | 140 | 146 | 676 | 4.5 |
| Median | | | 570 | 4.2 | 152 | 136 | 681 | 4.3 |

The younger samples (38–229 ysf) show a wide range in intensity distribution (**Table 4**), whereas the two oldest samples (710 and 2,355 ysf) are higher in aromatic C, with a loss of other structures. The oldest sample (2,355 ysf) has the highest proportion of aryl C (71%) and aromaticity (0.79). The CP spectra underestimate aromatic C without attached hydrogens; this effect is more important for samples high in O and di-O-alkyl C including carbohydrate but becomes less important as the proportion of aromatic C increases (Baldock and Smernik, 2002; Czimczik et al., 2002; Ascough et al., 2008; McBeath et al., 2011; Preston, 2014; Preston et al., 2014a,b). Our spectra indicate a trend to higher aromaticity with increasing ysf (not shown), but obviously, the low sample size, especially at higher ysf and the qualitative aspect of the NMR areas does not allow us to establish statistical inference.

# DISCUSSION

## C and N in Field Charcoal Samples

Our values for total C concentrations in charcoal are in keeping with those compiled from the literature (Table S1) for field samples from temperate and boreal regions. A survey of sites sampled from immediately after fire to >500 ysf gave a mean value of 584 mg $g^{-1}$ for C, with a lower mean of 534 mg $g^{-1}$ for field sites ≥28 ysf. Some of the highest values, around 800 mg $g^{-1}$, come from wood and bark burned outside to provide a

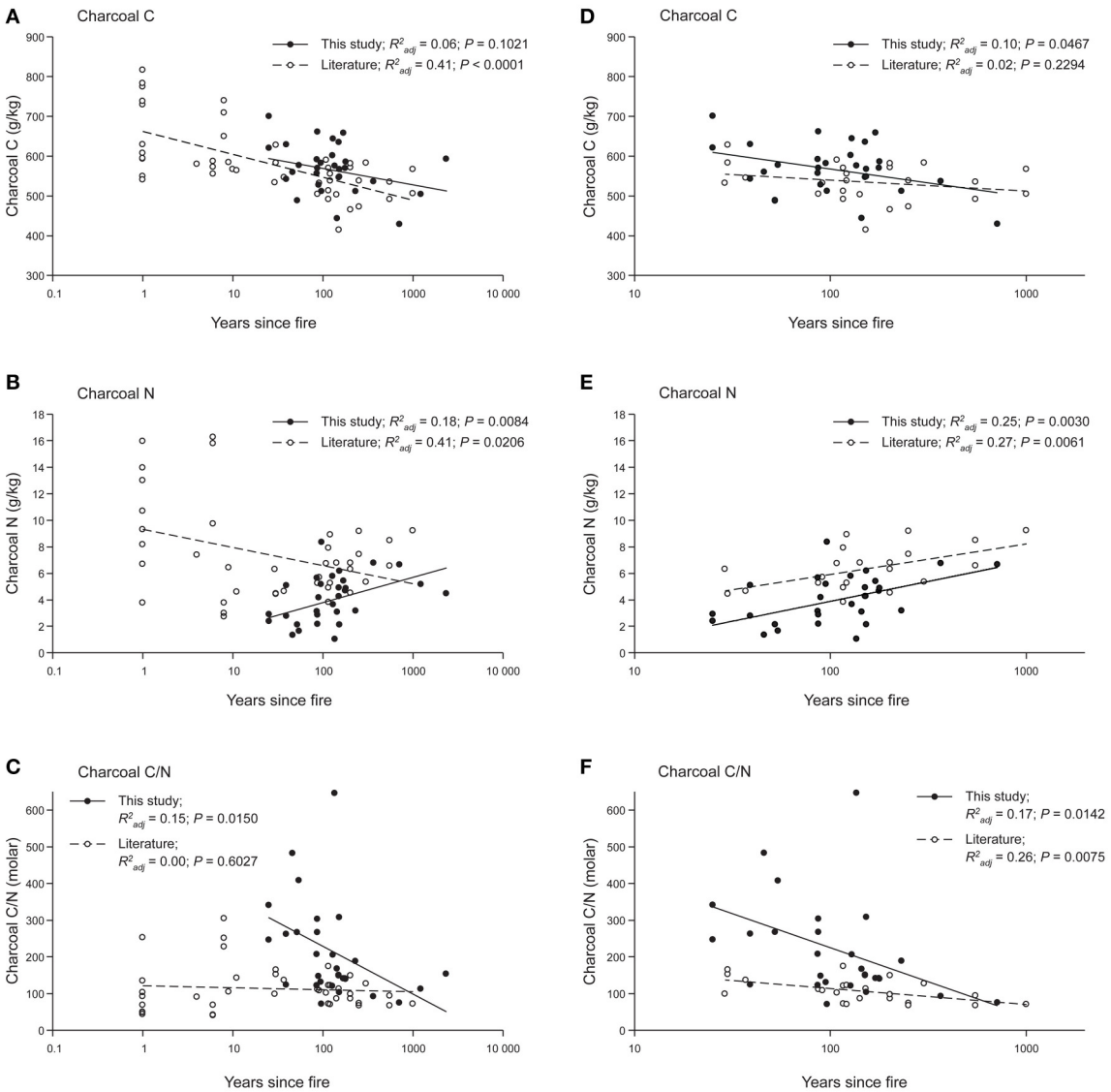


**FIGURE 3 |** Trends in charcoal C, N, and C/N ratio (molar) with ysf for this study (solid symbols) and for field data taken from the literature (open symbols). Linear regression on log-transformed ysf+1 is shown for all data **(A–C)** and for the time period (20–1,000 ysf) common to both datasets **(D–F)**. Data from Schiffman and Johnson (1989), Eckmeier et al. (2007), Ohlson et al. (2009) plus pers comm., Alexis et al. (2010), Clay and Worrall (2011), Briggs et al. (2012), Finkral et al. (2012), Buma et al. (2014), Hart and Luckai (2014), Santín et al. (2015, 2016b) plus pers comm., Soucémarianadin et al. (2015b).

baseline sample (Ohlson et al., 2009) and from burning of slash piles (Finkral et al., 2012), both of which are likely to generate more extensive transformation than in most wildfires. Total N values in this study (mean 4.1 mg $g^{-1}$) were at the lower end of those reported in the literature, which are on average 7.4 mg $g^{-1}$ for all years (0 to >500 ysf) and 6.2 mg $g^{-1}$ for sites 28 years and older (Table S1). Charcoal C, N, and C/N values from the literature are very variable immediately and soon after fire, but converge with increasing ysf (**Figures 3A–C**). Trends in N with ysf in the literature appear to be opposite of the trend found in this study (**Figure 3B**); however, both datasets showed the same trend when only their common ysf period (20–1,000) was considered (**Figure 3E**). Trends of increasing N concentration and decreasing C/N ratio are similar to those seen in decomposition of foliar litter (Moore et al., 2011) and wood over both short time scales of *ca*. 20 years (Preston et al., 2012) and centuries (Preston et al., 1998) corresponding to the timescales in this study.

## C and N Comparison with Laboratory Char Studies

To gain some insight into factors influencing field samples, we compiled total C and N values for a range of laboratory charring experiments of coniferous substrates (Table S2). Despite the wide range of substrates (mostly clean wood, sometimes including bark), and the resulting differences in ash content, as

**TABLE 3 |** Elemental composition of charcoal samples >2 mm determined by ICP **(A)** for this study and **(B)** in the literature.

| Plot ID | Ca ($g\ kg^{-1}$) | Mg ($g\ kg^{-1}$) | K ($g\ kg^{-1}$) | Na ($g\ kg^{-1}$) | Fe ($g\ kg^{-1}$) | Al ($g\ kg^{-1}$) | P ($mg\ kg^{-1}$) | Mn ($mg\ kg^{-1}$) | Zn ($mg\ kg^{-1}$) | Cu ($mg\ kg^{-1}$) | B ($mg\ kg^{-1}$) | S ($mg\ kg^{-1}$) |
|---|---|---|---|---|---|---|---|---|---|---|---|---|
| **(A) THIS STUDY** | | | | | | | | | | | | |
| **Jack pine** | | | | | | | | | | | | |
| JP-LO-24a | 4.69 | 0.48 | 52.7 | 1.01 | 0.28 | 0.39 | 102 | 195 | 39 | 84 | 47 | 446 |
| JP-LO-24b | 10.7 | 0.53 | 66.8 | 0.88 | 0.32 | 0.52 | 60 | 47 | 59 | 10 | 1.1 | 205 |
| JP-HI-45 | 2.58 | 0.40 | 59.9 | 0.38 | 1.09 | 1.34 | 142 | 44 | 30 | 35 | 1.0 | 244 |
| JP-HI-51 | 2.79 | 0.33 | 57.0 | 0.48 | 1.29 | 2.70 | 132 | 133 | 33 | 26 | 3.9 | 314 |
| JP-HI-135 | 4.99 | 0.49 | 82.7 | 0.38 | 0.96 | 0.93 | 158 | 136 | 37 | 9.8 | <0.4 | 285 |
| JP-HI-149 | 1.89 | 0.39 | 87.3 | 0.50 | 4.78 | 2.16 | 160 | 12 | 42 | 7.8 | 4.9 | 195 |
| JP-HI-151 | 2.84 | 0.46 | 85.4 | 0.43 | 2.60 | 6.22 | 212 | 16 | 19 | 7.9 | <0.4 | 302 |
| JP-HI-176 | 4.27 | 0.61 | 45.8 | 0.15 | 5.06 | 3.81 | 271 | 73 | 35 | 11 | 3.6 | 291 |
| JP-HI-177 | 2.31 | 0.55 | 48.3 | 0.32 | 5.53 | 3.79 | 292 | 25 | 31 | 25 | 10 | 382 |
| JP-HI-229 | 3.65 | 1.22 | 53.8 | 0.39 | 11.1 | 5.38 | 147 | 58 | 34 | 75 | 3.9 | 246 |
| **Black spruce** | | | | | | | | | | | | |
| BS-LO-38a | 4.90 | 0.44 | 54.9 | 0.19 | 0.47 | 1.14 | 194 | 85 | 33 | 6.0 | 1.4 | 368 |
| BS-LO-38b | 25.8 | 1.65 | 32.8 | 0.12 | 12.5 | 5.38 | 408 | 182 | 37 | 6.3 | 7.0 | 787 |
| BS-LO-53 | 3.70 | 0.30 | 88.7 | 0.34 | 2.37 | 1.26 | 107 | 14 | 23 | 8.9 | <0.4 | 182 |
| BS-LO-85 | 2.16 | 0.53 | 82.6 | 0.47 | 5.19 | 3.57 | 189 | 39 | 23 | 14 | <0.4 | 296 |
| BS-LO-143 | 5.45 | 2.83 | 57.3 | 0.48 | 21.1 | 16.3 | 335 | 66 | 40 | 61 | 1.8 | 313 |
| BS-LO-149 | 1.88 | 0.35 | 37.4 | 0.30 | 1.34 | 1.54 | 586 | 325 | 26 | 14 | 2.4 | 360 |
| BS-LO-151 | 32.6 | 1.78 | 20.1 | 15.5 | 2.62 | 4.08 | 172 | 223 | 6.9 | 186 | 1.2 | 353 |
| BS-LO-169 | 15.1 | 1.24 | 28.4 | 0.11 | 5.16 | 0.64 | 147 | 61 | 28 | 9.8 | 9.5 | 303 |
| BS-HI-85 | 6.91 | 1.26 | 23.7 | 0.19 | 10.4 | 5.58 | 266 | 43 | 16 | 10 | 6.8 | 498 |
| BS-HI-86a | 2.10 | 0.24 | 52.4 | 0.30 | 0.15 | 0.63 | 131 | 149 | 77 | 22 | 1.8 | 235 |
| BS-HI-86b | 2.43 | 0.43 | 56.9 | 0.38 | 2.43 | 2.43 | 152 | 86 | 39 | 18 | 1.4 | 243 |
| BS-HI-88 | 23.2 | 2.12 | 46.1 | 0.30 | 8.20 | 5.36 | 258 | 1192 | 42 | 14 | 1.2 | 407 |
| BS-HI-94 | 1.91 | 0.39 | 79.9 | 0.29 | 3.60 | 2.12 | 230 | 86 | 19 | 14 | 0.5 | 245 |
| BS-HI-95 | 1.44 | 0.61 | 0.53 | 62.2 | 3.77 | 3.24 | 347 | 55 | 41 | 13 | 3.4 | 281 |
| BS-HI-126 | 2.13 | 0.58 | 0.55 | 13.1 | 2.54 | 1.66 | 110 | 95 | 47 | 20 | 2.6 | 243 |
| BS-HI-128 | 2.13 | 0.41 | 0.66 | 7.52 | 0.22 | 0.36 | 71 | 98 | 31 | 18 | 1.9 | 230 |
| Mean | 6.72 | 0.79 | 50.1 | 4.11 | 4.43 | 3.17 | 207 | 136 | 34 | 28 | 4.7 | 317 |
| Median | 3.24 | 0.51 | 53.2 | 0.38 | 2.61 | 2.29 | 166 | 79 | 34 | 14 | 1.9 | 293 |
| **(B) PUBLISHED STUDIES** | | | | | | | | | | | | |
| [a]Biochar, maple/spruce sawdust, 773 g $kg^{-1}$ C | 2.42 | 0.29 | 1.24 | | | | 75 | | | | | 200 |
| [b]Biochar, lodgepole pine chips, 802 g $kg^{-1}$ C | 10.9 | 1.79 | 6.72 | | | | 525 | | | | | 230 |
| [c]Fresh char, *Larix decidua* wood, 760 g $kg^{-1}$ C | 5.91 | 1.52 | 2.91 | 0.21 | | | 308 | | | | | |
| [d]Fresh wood and bark (unspecified) | 1.78 | 0.21 | 0.71 | 0.02 | 0.085 | 0.083 | 87 | 298 | 21 | 2.1 | | |
| [e]Black spruce stemwood | 1.41 | 0.19 | 0.43 | | | | 70 | | | | | |
| [e]Black spruce branch | 0.75 | 0.40 | 1.34 | | | | 400 | | | | | |
| [e]Black spruce bark | 1.39 | 0.42 | 1.54 | | | | 470 | | | | | |
| [e]Jack pine stemwood | 0.68 | 0.13 | 0.45 | | | | 50 | | | | | |
| [e]Jack pine branch | 2.16 | 0.40 | 1.55 | | | | 290 | | | | | |
| [e]Jack pine bark | 4.61 | 0.42 | 1.15 | | | | 260 | | | | | |

*Location (horizon: organic vs. mineral) and depth of samples are the same as in **Table 2**.*
*[a]Sackett et al. (2015); [b]Robertson et al. (2012); [c]Criscuoli et al. (2017); [d]Baernthaler et al. (2006); [e]Paré et al. (2013).*

well as variation in substrate size, charring apparatus, duration and oxygen exposure, resulting total C values follow a fairly consistent trend (**Figure 5A**). Trends in total N (not shown) and C/N (**Figure 5B**) were more difficult to discern, partly due to fewer reports of total N in studies, as well as large variations in N concentrations in starting materials. Two of the series (Baldock

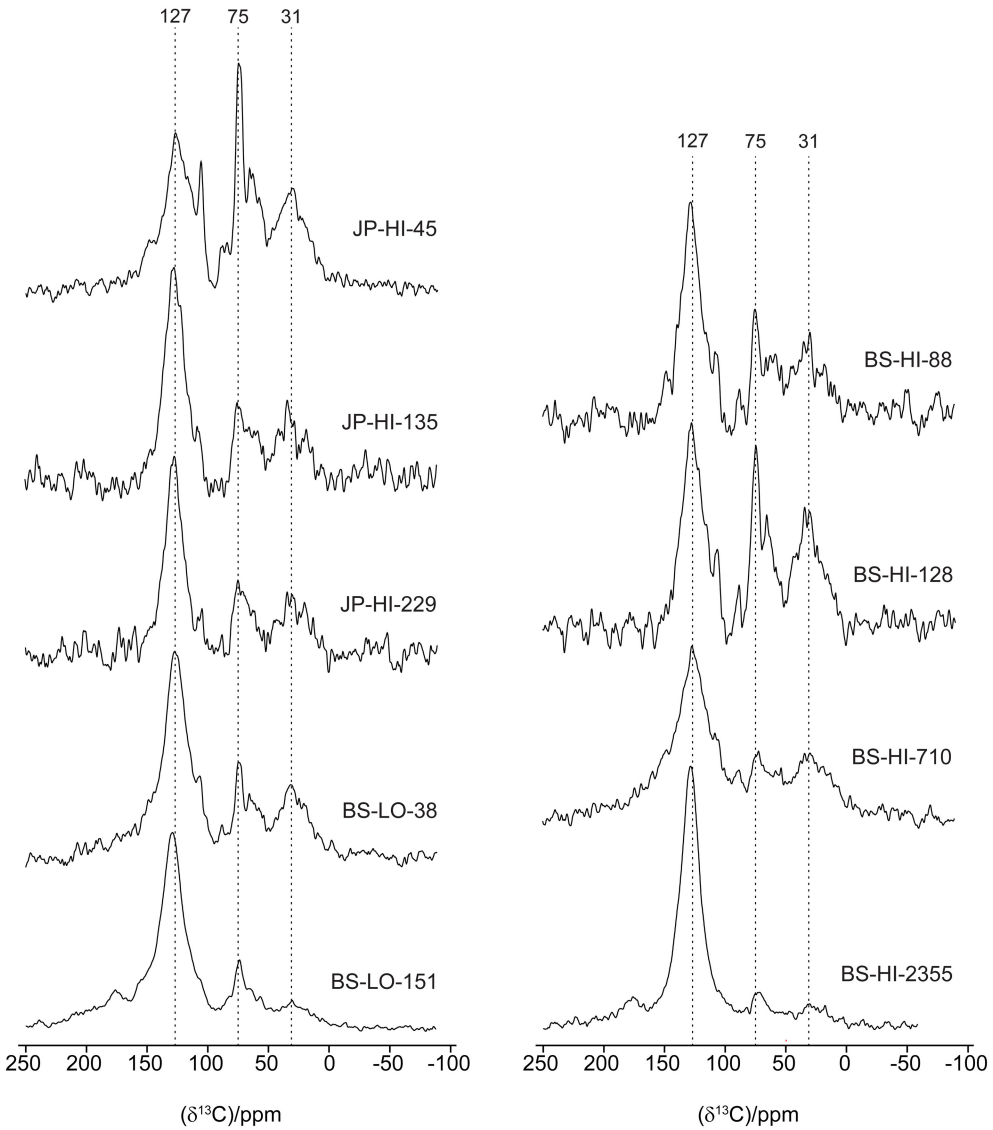


**FIGURE 4 |** Solid-state $^{13}C$ CPMAS NMR spectra of representative samples.

and Smernik, 2002; Hart and Luckai, 2014) show similar values and a trend of decreasing C/N with increasing temperature, whereas data from other studies (Soucémarianadin et al., 2013; Wolf et al., 2013; Hatton et al., 2016; Pingree et al., 2016) show little change as the initial C/N values were much lower. The value from Briggs et al. (2012) is unusually high but with only a single point in their study, we do not know how C/N evolved with charring. The laboratory charring data are thus consistent with field observations which show wide variation in C/N for younger samples, likely resulting from both variations in substrate composition and heating exposure. The few values for older field samples suggest convergence to lower C/N values; this could result from a multiplicity of factors, including lower C/N values in the initial fuel, longer survival of fuel charred under hotter temperatures or absorption of N during field exposure.

Overlaying our total C concentrations onto **Figure 5A** shows that most of the values fall between 490 and 660 g $kg^{-1}$, corresponding to laboratory chars produced at <300°C. Most of the laboratory chars were lower in ash, and the bulk of our ash-free C values fall in with those produced around 350–450°C (**Figure 5A**). These are within the temperature ranges suggested from attempts to develop a "molecular thermometer" based on the ratio of BPCA products with 5 vs. 6 carboxyl groups (B5CA/B6CA; Wolf et al., 2013). Wolf et al. (2013) classified three typical fire temperature regimes: grass and forest groundfires at 285 ± 143°C, shrubland fires at 503 ± 211°C, and domestic fires at 797 ± 165°C. However, other field observations, especially for crown fires, show that substrates may experience much higher temperatures, albeit briefly. In an experimental crown fire near Fort Providence NWT, Canada, dataloggers showed a pattern of

**TABLE 4 |** Relative intensity of chemical-shift regions of solid-state $^{13}C$ CPMAS NMR spectra of char samples.

| Plot ID | Chemical shift region (ppm) % of total area | | | | Aromaticity[a] |
|---|---|---|---|---|---|
| | 0–47 | 47–110 | 110–165 | 165–210 | |
| JP-HI-45 | 24 | 35 | 38 | 3 | 0.39 |
| JP-HI-135 | 22 | 22 | 51 | 4 | 0.54 |
| JP-HI-229 | 21 | 20 | 50 | 8 | 0.55 |
| BS-LO-38 | 18 | 20 | 54 | 8 | 0.58 |
| BS-LO-151 | 8 | 17 | 62 | 13 | 0.72 |
| BS-HI-88 | 21 | 24 | 48 | 6 | 0.52 |
| BS-HI-128 | 27 | 30 | 40 | 4 | 0.42 |
| BS-HI-710 | 19 | 19 | 56 | 7 | 0.60 |
| BS-HI-2355 | 8 | 11 | 71 | 10 | 0.79 |

[a]*Ratio of intensities in ppm regions: 110–165/0–165.*

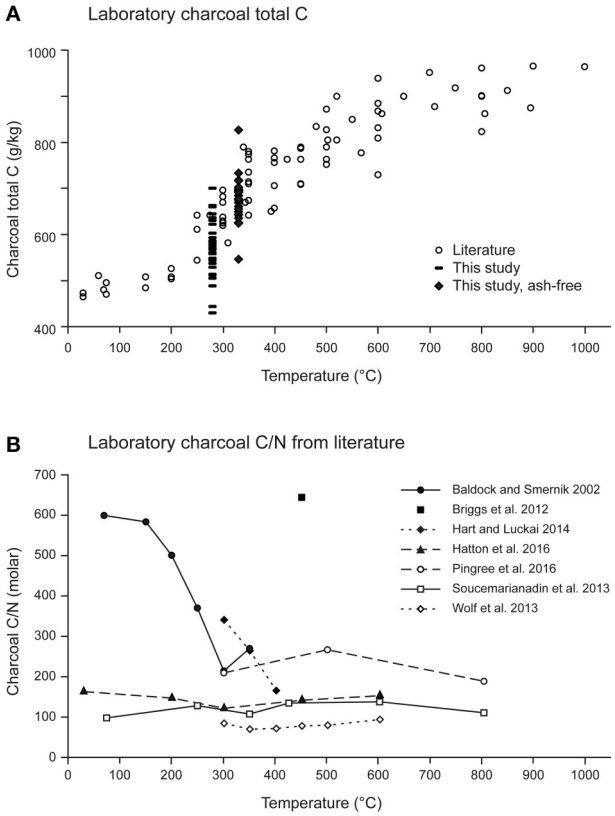


**FIGURE 5 |** Chemical properties reported from laboratory charring experiments for coniferous substrates: **(A)** charcoal total C and **(B)** C/N ratio (molar). Data in **(A)** from Baldock and Smernik (2002), Czimczik et al. (2002), Gundale and DeLuca (2006), Ascough et al. (2008), Briggs et al. (2012), Bergeron et al. (2013), Kasin and Ohlson (2013), Soucémarianadin et al. (2013), Wolf et al. (2013), Hart and Luckai (2014), McBeath et al. (2015) plus pers comm., Hatton et al. (2016), and Pingree et al. (2016). Our data for charcoal total C (whole sample and ash-free basis) are overlaid to give a general indication of how they might correspond to those of char samples produced under laboratory conditions.

a very steep initial temperature rise followed by a slower rate of cooling, which was very difficult to reproduce in a subsequent laboratory charring experiment (Santín et al., 2013). Maximum temperatures in the organic horizon ranged from 550 to 976°C, with average durations of 150, 100, and 60 s above 370, 470, and 570°C, respectively. Similar results were found in experimental burns of open savanna woodland in northern Australia (Saiz et al., 2014). Physical and chemical properties of charred pitch pine (*Pinus rigida*) wood collected after a prescribed burn in New Jersey were also consistent with charring conditions of a quick rise (650°C $h^{-1}$) to a final temperature of 500–600°C (Brown et al., 2006). Thermosensitive paints recorded temperatures from 371 to 760°C with a mean of 493°C during prescribed burning of a Florida scrub-oak site (Alexis et al., 2007). Righi et al. (2009) noted that many aluminum plates used for tagging stems melted during their slash-and-burn fire, indicating that the temperatures must have exceeded 660°C. Thus, even though total C concentrations of our charcoal samples are consistent with fairly low formation temperatures in the laboratory, it is likely that at least some fuel may have been exposed to much higher temperatures, (see further discussion of NMR).

## Chemistry—Other Elements

No comparable multi-element compositional data were located for wildfire char. Many studies of wood and/or bark ash are available (e.g., Ingerslev et al., 2011; Omil et al., 2013; Brais et al., 2015; Hansen et al., 2016) but these show highly variable properties, and are lower in total C than our samples. They also tend to be higher in elements such as Ca, Fe, Al and heavy metals, due to factors such as soil contamination of logging waste, mixing of sand or soil in fluidized bed combustion and presumably contact with heated metal surfaces. Three biochar preparations (primarily from softwood; Robertson et al., 2012; Sackett et al., 2015; Criscuoli et al., 2017) had Ca, Mg, P, and S concentrations comparable to our median values, but our K concentrations were much higher (**Table 3B**). Additional expectation of the composition of wildfire chars may be found by comparison of fresh biomass, and of element recoveries in ash of heating plants. A study of "ash-forming elements" in an unspecified wood/bark mixture showed that the highest concentrations were for Ca, K, Mn, and Mg (Baernthaler et al., 2006, **Table 3B**), and reasonably similar values were reported for Ca, Mg, and P in stemwood, branches and bark of black spruce and jack pine (Paré et al., 2013, **Table 3B**). Recovery of nutrients in bottom and fly ash of a heating plant was quite high (Ingerslev et al., 2011), with >75% for P, Ca, Mg, Mn, and Cu, > 50% for K, Al, and Fe, and >30% for S and Na. Thus, compositions of our samples, especially of the younger chars, are in line with reasonable trajectories of formation and change with time. Our K concentrations (median 53.2 g $kg^{-1}$) are much higher than might be expected from these studies, although some similarly high K values are reported elsewhere for ash (Ingerslev et al., 2011; Hansen et al., 2016). Char samples from our sites could be a source of major and minor nutrient elements.

## NMR

Similar to C and N values determined on a larger sample set, the nine NMR spectra obtained show a wide variation in appearance and intensity distribution for the younger samples, whereas the oldest samples generally have higher aromaticity and simpler features, with greater dominance of the aryl C signal around 130 ppm. These structural variations are consistent with observations of increasing aromaticity with temperature in laboratory charring studies (Baldock and Smernik, 2002; Czimczik et al., 2002; Ascough et al., 2008; Soucémarianadin et al., 2013; Hart and Luckai, 2014). Organic horizon/biomass char produced in field settings (wildfire or prescribed fire) also shows a range of intensity distributions depending on fire severity, from little alteration to high aromaticity (Nocentini et al., 2010; Miesel et al., 2015; Soucémarianadin et al., 2015b). Similar to laboratory charring, samples referenced to actual temperatures documented in the field show increasing aromaticity with temperature (Alexis et al., 2010; Santín et al., 2016b), and illustrate the variability in formation conditions.

There is little information on NMR characteristics of boreal forest char with varying ysf. Most similar to our study is a series of five $^{13}$C CPMAS NMR spectra (Hart and Luckai, 2014), which also shows considerable variation in the younger samples (14, 28, and 90 ysf), whereas the two oldest samples (140 and 208 ysf) have the highest proportions of aromatic C (we do not compare relative areas or aromaticity directly due to the different conditions used to acquire spectra which influence the relative areas, especially for CP spectra). Soucémarianadin et al. (2015a) also found that aromatic C was higher in the highly humified H (American Oa) horizon and where it could be separated, in "historical" PyC which sometimes formed a distinct layer at the interface with the mineral soil. Similarly, charcoal fragments picked out from the black spruce organic horizon in northern Manitoba were much more aromatic than the bulk material, especially when characterized by quantitative DP rather than CP NMR (Preston et al., 2014b). In addition to complexities in direct comparison of NMR data, perusal of the various studies of laboratory and field charring indicate that increase in aromaticity and loss of other spectra features may occur at lower temperatures for clean wood compared to the more complex substrates such as organic horizon or bark-wood mixtures (Baldock and Smernik, 2002; Czimczik et al., 2002; McBeath et al., 2011; Merino et al., 2015; Santín et al., 2016b). Also, laboratory chars are often produced by pyrolysis in an inert atmosphere and with long duration, compared to the short exposure, oxygen availability and rapid temperature change more characteristic of a fast-moving field event (Santín et al., 2013; Saiz et al., 2014). For example, samples subjected to maxima of 683°C and even 950°C during an experimental crown fire still had considerable intensity in other NMR regions (Santín et al., 2016b), whereas laboratory chars produced at 600°C were completely aromatic. They concluded that structural changes in field fire situations may have required higher temperatures than corresponding changes induced during laboratory charring.

These issues aside, data on charcoal total C, N, and organic C composition for a range of field and laboratory studies indicate wide variation in the initial properties of charred material, due to both initial material type and to heating conditions. With time, however, properties become more consistent, including a trend to higher aromaticity. This could be due to longer survival of more highly transformed components, or possibly to loss of more labile structures with time, leaving the more aromatic and polycondensed components. All of these questions should be fodder for further investigation.

## Comparison of Amounts

Our results for amounts of charcoal are underestimates as they included only fragments <2 mm and sampling of mineral soil was inconsistent. However, our data are unique in the large number of sites, the length of the chronosequence, and the fine resolution by depth. Comparison with other studies is challenging, as sampling protocols varied, including the range of charcoal size extracted, the exact definition of "charcoal" used in each study, and whether the sampling included upper mineral soil, or only organic horizon. These studies were similarly focused on fire and vegetation history, so that experimental design would not have been optimized to quantify charcoal stocks. However, in the absence of completely comparable studies, much insight can be gained from this imperfect exercise. Data were located for five studies (Table S3), four of which were located in boreal and predominantly coniferous forests in Norway and Sweden (Zackrisson et al., 1996; Ohlson et al., 2009; Kasin et al., 2013) and northern Ontario (Hart and Luckai, 2014). Another study of temperate and deciduous forests was included because it is close to the transition to the boreal in Quebec (Bélanger et al., 2004). In each study, charcoal or charred biomass were determined by visual criteria and picked out from organic horizon only (Zackrisson et al., 1996; Bélanger et al., 2004), in organic horizon plus some upper mineral soil (Ohlson et al., 2009; Kasin et al., 2013; Hart and Luckai, 2014), and in our study, sometimes from organic horizon only, but usually penetrating a short distance into the mineral soil. As shown in **Figure 6A**, our results for charcoal stocks vs. ysf are quite similar to those from five disparate studies. Also in line with the data in **Figure 6A**, a more recent study of Norway spruce (Ohlson et al., 2017), also of charcoal from organic horizon and upper mineral soil, showed an average stock of 930 kg ha$^{-1}$ in 10 plots, with charcoal having an average radiocarbon age of 570 ± 102 y. **Figure 6A** shows widely variable charcoal stocks (0–5,000 kg ha$^{-1}$) in the first centuries after fire followed by lower values (0–2,000 kg ha$^{-1}$) afterwards. This sharp decline in maximum stock values in the first centuries after fire could be due in part to the decomposition of the less-transformed and thus most labile components of the visually-determined charcoal; the remaining, more recalcitrant components, would form a relatively stable charcoal stock in the following centuries.

Similar to our results, high spatial variability has been observed elsewhere (Ohlson et al., 2006, 2009, 2017; Kasin et al., 2017), as well as the common occurrence of charcoal/PyC at the interface of the organic and mineral layers (Cyr et al., 2005; Ohlson et al., 2009; Hart and Luckai, 2014; Soucémarianadin et al., 2015a). Our depth profiles also show charcoal layers within the organic horizon of some LO plots. These widespread trends

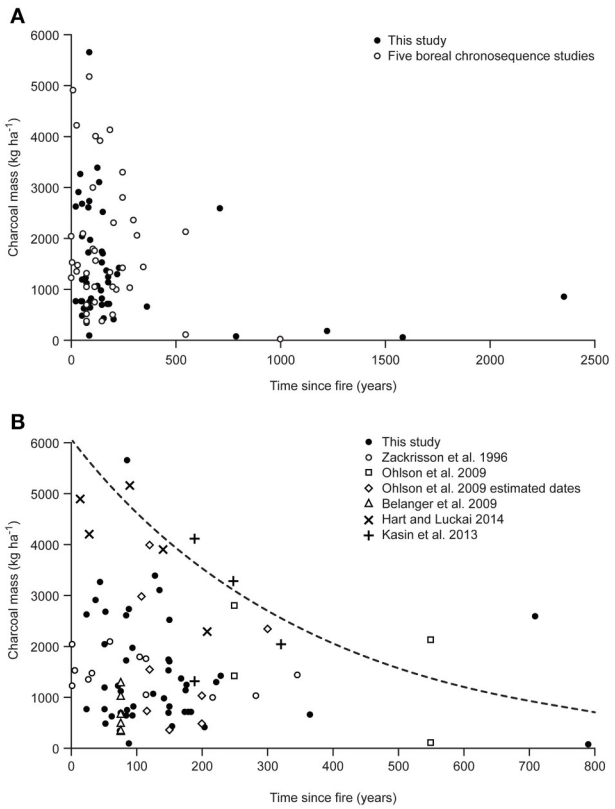


**FIGURE 6 |** Charcoal stocks (kg ha$^{-1}$) for this study compared with data from five studies of mainly boreal, coniferous forest sites **(A)**. The expansion **(B)** shows data from individual studies up to 800 ysf. The outer envelope of the data cloud (dashed line) was defined by selecting the 5% highest charcoal mass values for each 100-yr classes (up to 399 ysf: 0–99, 100–199, 200–299, and 300–399 ysf), and passing a logarithmic regression curve through these data points ($R^2$: 0.80). Sources for **(A)** as shown in **(B)** plus pers. comm. from Stephen Hart.

can inform design of sampling strategies to optimize charcoal capture in boreal forests.

The more detailed comparison of stocks up to 790 ysf (**Figure 6B**) gives a better insight into the effects of sampling protocols. The lowest values are from Bélanger et al. (2004), which were for charcoal >2 mm in organic horizon only. Overlapping but somewhat higher values were found for organic horizon only, but without size exclusion on charcoal extraction (Zackrisson et al., 1996). The other three published studies included some mineral soil, with the higher values found for Kasin et al. (2013) and Hart and Luckai (2014). Data from Ohlson et al. (2009) included mineral soil of variable depth, with rigorous extraction of charcoal particles >125 μm; results span a wide range. Our data are for charcoal >2 mm, and mineral soil was not always sampled; they tend to fall among the lower values. Data from these disparate studies show that stocks can be highly variable, and that higher values are found when charcoal is not restricted to larger sizes, and also when upper mineral soil is included.

Our data are thus in reasonable agreement with published results; our stocks would have been higher if smaller size classes of charcoal had been extracted, and if all cores had been consistently sampled into the mineral soil. Like many studies, our results are only for charcoal on the ground, but fire also produces charred biomass on woody debris and standing stems (see below). With the passage of time, some of this char is transferred to the organic horizon as snags fall, or charred bark falls off (Boulanger and Sirois, 2006; Aakala et al., 2008; Angers et al., 2010, 2012; Boulanger et al., 2011) the process can cover several decades. Similarly to the dynamics of CWD production from snags and branches, sampling at longer ysf would include higher proportions of char originally produced above-ground.

## Linking Estimates of Production

Can this assemblage of charcoal stocks be related to estimates of production? For **Figure 6B**, a logarithmic regression curve drawn through the 5% highest values defines an outer envelope that intersects the y-axis around 6,000 kg ha$^{-1}$. This range is not out of line with studies of charcoal production (Table S4). Studies on aerial deposition from experimental crown fires (Clark et al., 1998; Ohlson and Tryterud, 2000; Lynch et al., 2004) report low charcoal values (top of Table S4); however, these values do not represent production of charcoal from experimental crown fires, although they have often been cited as such. Rather, they represent the mass of charcoal particles captured in trays that were mainly outside the burned block, resulting in relatively low values. The objective of these studies was to understand transfer processes of airborne charcoal from a wildfire to nearby sediments.

Five studies from the Amazon region (Fearnside et al., 1993, 1999, 2001; Gráça et al., 1999; Righi et al., 2009) present a very different scenario; in keeping with local practice of slash-and-burn cultivation, most trees were felled, left to dry for some months and then burned. While this may seem remote from boreal wildfires, the comparison is not completely unreasonable, as wildfires also burn much down wood and stems close to the ground. The Brazilian studies were also thoroughly documented, with measurements of biomass before the fires, and a complete accounting of charcoal produced on the ground and on woody stems. The slash-and-burn study by Eckmeier et al. (2007) was quite different, as it aimed to emulate Neolithic practices, so that stems >10 cm in diameter were removed before burning, and the plot was raked during the burn to encourage fuel consumption. The two prescribed fires were quite different, with Schiffman and Johnson (1989) representing operational conditions after harvest of loblolly pine (*Pinus taeda*), whereas Alexis et al. (2007) describe burning of an oak shrubland in Florida (stems 2–3 m high) to reduce the danger of wildfire. The only experimental crown fire study, carried out near Fort Providence (NWT, Canada) in 2012 (Santín et al., 2015), reported a value of 7900 kg ha$^{-1}$ of charcoal and, like the Brazilian slash-and-burn studies, was a complete accounting of charred biomass in organic horizon (including ash), down wood, burned bark on stems, and charred canopy needles. Lastly, two studies exclusively determined char produced on down wood, the higher value (6,400 kg ha$^{-1}$) being

**TABLE 5 |** Reported distribution of charcoal produced in fires conducted for research purposes.

| Source* | Location | Type of fire** | Total (kg ha$^{-1}$) | Percent of total | | | | | | | |
|---|---|---|---|---|---|---|---|---|---|---|---|
| | | | | On ground | Stems, total | Stems, >10 cm | Stems, <10 cm | Stems, <5 cm | Stems, 5–10 cm | Downed wood | Canopy needles |
| 1 | Amazonia (Brazil) | S&B | 2,200 | | | 68.2 | | | | | |
| 2 | Amazonia (Brazil) | S&B | 4,300 | 27.9 | 72.1 | 51.2 | 20.9 | | | | |
| 3 | Amazonia (Brazil) | S&B | 6,400 | | | 48.4 | | | | | |
| 4 | Amazonia (Brazil) | S&B | 8,670 | 37.4 | 62.6 | 54.3 | 8.3 | 1.9 | 6.5 | | |
| 5 | Florida (USA) | PB | 2,369 | 57.5 | 42.9 | 42.9 | | | | | |
| 6 | NWT (Canada) | ECF | 7,900 | 41.9 | 29.1 | | | | | 22.1 | 7.0 |

*1, Fearnside et al. (1999); 2, Fearnside et al. (2001); 3, Gráça et al. (1999); 4, Righi et al. (2009); 5, Alexis et al. (2007); 6, Santín et al. (2015).*

***S&B, slash and burn; PB, prescribed burn; ECF, experimental crown fire.*

from a wildfire in Yellowstone National Park (Tinker and Knight, 2000), and the two lower values from lodgepole pine sites that had burned once (394 kg ha$^{-1}$) and twice (865 kg ha$^{-1}$) in Oregon (Donato et al., 2009).

Results from the above studies of total char production (all of the slash-and-burn, the shrubland prescribed fire, and the experimental crown fire) show a wide variation, from approximately 2,000–9,000 kg ha$^{-1}$. The two studies of down wood show a similar, but somewhat lower range (approximately 400–6,400 kg ha$^{-1}$), and the organic horizon charcoal from the operational postharvest prescribed fire (Schiffman and Johnson, 1989) is 7,400 kg ha$^{-1}$. Clearly, char production will depend on the amount and nature of both the fuels and the fire, but these rather disparate studies nonetheless suggest that a complete accounting of surface and aboveground char from boreal wildfires might reasonably lie around the range of 5,000–10,000 kg ha$^{-1}$. Of the few studies partitioning distribution of char from a single event, the four Brazilian studies reported 48–68% on wood >10 cm diameter, similar to the 43% reported by Alexis et al. (2007) on standing stems from his prescribed burn study (**Table 5**). Santín et al. (2015) reported 42% on the ground, 22% on down wood, 29% on burned stems (bark) and 7% as charred canopy needles, and the more detailed breakdown of data from Righi et al. (2009) shows a similar proportion of 38% of char produced on the ground and the rest distributed among three size classes of wood.

Thus, it could be reasonably suggested that in boreal wildfires, around half to two-thirds of char production might initially be found on the organic horizon or forest floor and down wood, and most of the remainder on standing stems. Whereas charred needles presumably will fall within a short time and become part of the organic horizon or exposed mineral soil, charred wood and bark on standing trees may take several years to fall to the ground. This could explain in part the temporal patterns of charcoal stocks in organic horizon and surface mineral soil found in our postfire chronosequence, which show high variability and no distinct trend with time in the first 200 years or so (**Figure 6**). In the first few years after a fire, much of the char may still remain on snags or downed coarse wood and is thus not captured in organic horizon surveys, especially those designed to study fire and vegetation history. As time goes on, bark flakes off, snags fall to the ground, and various sizes of down wood collapse and thus these pools are transferred to the organic horizon. On the other hand, charcoal and all forms of PyC are subject to losses by various mechanisms, including microbial decomposition, chemical and photo-oxidation, and transport downward or away from the site (Preston and Schmidt, 2006; Bird et al., 2015; Santín et al., 2016a). Surveys of organic horizon charcoal taken several decades or centuries after fire would thus capture varying amounts of the char originally present on the ground, on coarse down wood or on standing stems, minus whatever has been lost to microbial or chemical degradation, erosion, or downward transport. The high variability in charcoal stocks in the first 200 years could thus result in part from the variable timing of char transfer from the aboveground pool to the ground surface pool, which is itself influenced by a series of abiotic and biotic factors such as stand structure, weather, and topography. Char is of course not BC, and likely only a small proportion of charred biomass will have the polycondensed structure to resist decomposition (Preston and Schmidt, 2006; McBeath et al., 2011; Bird et al., 2015; Santín et al., 2016a; Maestrini and Miesel, 2017). However, charred biomass is the starting pyrogenic input, and we can hardly start to model BC as a component of the forest C cycle without this basic input.

## CONCLUSIONS

We investigated amounts, depth distribution and chemical properties of visually determined charcoal (>2 mm) in the organic horizon and upper mineral soil in a boreal forest fire chronosequence in Quebec, and combined our results with those from a general survey of reported data. The latter also were visually reported charcoal, although studies varied in their sampling protocols, including organic layer only or inclusion of upper mineral soil, and some instructive cases were included from warmer regions. We found very wide variation in charcoal production by wildfires, and also in charcoal stocks up to around 200 years. Charcoal stocks showed high spatial variability and tended to be concentrated near the organic/mineral soil interface. Chemical properties of wildfire charcoal also show

considerable variation for younger samples, and with some caveats, can be sensibly connected with results from laboratory studies. With increasing time since fire (several hundred years), both stocks and properties tend to converge, with much lower stocks reported in older plots. We speculate that the general trends of increasing aromaticity, decreasing C/N ratio, and decreasing maximum stocks in the first centuries after fire may result from the decomposition of the more labile forms of the visually-determined charcoal, leaving the more recalcitrant forms of charcoal as a relatively stable stock. This statement should be taken with caution however because our study was not designed to test this hypothesis and because very few sites older than 500 ysf were analyzed. While reports of charcoal production are even scarcer than of charcoal stocks, our initial survey indicates a rough match, suggesting that initial charcoal production on stems, downed coarse wood and forest floor might reasonably be supposed to fall around 5,000–10,000 kg $ha^{-1}$. In order to develop models of PyC for boreal forests, clearly more studies are required, including total initial production, more data on sites at least several hundred ysf, and consideration of all components of PyC production, including the fate of PyC formed on standing stems and downed coarse wood. There is also need for more interdisciplinary studies to allow conversion of visually determined charcoal to the proportion of more resistant BC likely to contribute to more persistent soil C stocks.

## AUTHOR CONTRIBUTIONS

CP designed the study and acquired the chemical data. Field data and char samples were provided by MS and YB. MS especially contributed to data analysis. GB acquired the NMR data. All authors contributed to writing the manuscript.

## FUNDING

RW and YB thank NSERC for financial support.

## ACKNOWLEDGMENTS

We thank David Dunn for careful laboratory analysis and ICP method development, plus colleagues who generously shared their raw data: Stephen A. Hart, Lakehead University, Thunder Bay, ON, Canada; Mikael Ohlson, Norwegian University of Life Sciences, Ås, Norway; Anna V. McBeath, James Cook University, Cairns Australia; Cristina Santín, Swansea University, Swansea UK. RW and YB thank NSERC for financial support.

## SUPPLEMENTARY MATERIAL

The Supplementary Material for this article can be found online at: https://www.frontiersin.org/articles/10.3389/feart.2017.00098/full#supplementary-material

## REFERENCES

Aakala, T., Kuuluvainen, T., Gauthier, S., and De Grandpré, L. (2008). Standing dead trees and their decay-class dynamics in the northeastern boreal old-growth forests of Quebec. *For. Ecol. Manage.* 255, 410–420. doi: 10.1016/j.foreco.2007.09.008

Alexis, M. A., Rasse, D. P., Rumpel, C., Bardoux, G., Péchot, N., Schmalzer, P., et al. (2007). Fire impact on C and N losses and charcoal production in a scrub oak ecosystem. *Biogeochemistry* 82, 201–216. doi: 10.1007/s10533-006-9063-1

Alexis, M. A., Rumpel, C., Knicker, H., Leifeld, J., Rasse, D., Péchot, N., et al. (2010). Thermal alteration of organic matter during a shrubland fire: a field study. *Org. Geochem.* 41, 690–697. doi: 10.1016/j.orggeochem.2010.03.003

Angers, V. A., Bergeron, Y., and Deapeau, P. (2012). Morphological attributes and snag classification of four North American boreal tree species: relationships with time since death and wood density. *For. Ecol. Manage.* 263, 138–147. doi: 10.1016/j.foreco.2011.09.004

Angers, V. A., Drapeau, P., and Bergeron, Y. (2010). Snag degradation pathways of four North American boreal tree species. *For. Ecol. Manage.* 259, 246–256. doi: 10.1016/j.foreco.2009.09.026

Araújo, G. C. L., Gonzalez, M. H., Ferreira, A. G., Nogueira, A. R. A., and Nóbrega, J. A. (2002). Effect of acid concentration on closed-vessel microwave-assisted digestion of plant materials. *Spectrochim. Acta Part B* 57, 2121–2132. doi: 10.1016/S0584-8547(02)00164-7

Ascough, P. L., Bird, M. J., Wormald, P., Snape, C. E., and Apperley, D. (2008). Influence of production, variables and starting material on charcoal stable isotopes and molecular characteristics. *Geochim. Cosmochim. Acta* 72, 6090–6102. doi: 10.1016/j.gca.2008.10.009

Baernthaler, G., Zischka, M., Haraldsson, C., and Obernberger, I. (2006). Determination of major and minor ash-forming elements in solid biofuels. *Biomass Bioenergy* 30, 983–997. doi: 10.1016/j.biombioe.2006.06.007

Baldock, J. A., and Smernik, R. J. (2002). Chemical composition and bioavailability of thermally altered *Pinus resinosa* (Red pine) wood. *Org. Geochem.* 33, 1093–1109. doi: 10.1016/S0146-6380(02)00062-1

Bélanger, N., Côté, B., Fyles, J. W., Courchesne, F., and Hendershot, W. H. (2004). Forest regrowth as the controlling factor of soil nutrient availability 75 years after fire in a deciduous forest of Southern Quebec. *Plant Soil* 262, 363–372. doi: 10.1023/B:PLSO.0000037054.21561.85

Bergeron, S. P., Bradley, R. L., Munson, A., and Parsons, W. (2013). Physico-chemical and functional characteristics of soil charcoal produced at five different temperatures. *Soil Biol. Biochem.* 58, 140–146. doi: 10.1016/j.soilbio.2012.11.017

Bergeron, S. P., Gauthier, S., Flannigan, M., and Kafka, V. (2004). Fire regimes at the transition between mixedwood and coniferous boreal forest in northwestern Quebec. *Ecology* 85, 1916–1932. doi: 10.1890/02-0716

Bird, M. I., Wynn, J. G., Saiz, G., Wurster, C. M., and McBeath, A. (2015). The pyrogenic carbon cycle. *Ann. Rev. Earth Planet. Sci.* 43, 273–298. doi: 10.1146/annurev-earth-060614-105038

Boulanger, Y., Gauthier, S., and Burton, P. (2014). A refinement of models projecting future Canadian fire regimes using homogeneous fire regime zones. *Can. J. For. Res.* 44, 365–376. doi: 10.1139/cjfr-2013-0372

Boulanger, Y., and Sirois, L. (2006). Postfire dynamics of black spruce coarse woody debris in northern boreal forest of Quebec. *Can. J. For. Res.* 36:1770–1780. doi: 10.1139/x06-070

Boulanger, Y., Sirois, L., and Hébert, C. (2011). Fire severity as a determinant factor of the decomposition rate of fire-killed black spruce in the northern boreal forest. *Can. J. For. Res.* 41, 370–379. doi: 10.1139/X10-218

Brais, S., Bélanger, N., and Guillemette, T. (2015). Wood ash and N fertilization in the Canadian boreal forest: Soil properties and response of jack pine and black spruce. *For Ecol. Manage.* 348, 1–14. doi: 10.1016/j.foreco.2015.03.021

Briggs, C., Breiner, J. M., and Graham, R. C. (2012). Physical and chemical properties of *Pinus ponderosa* charcoal: implications for soil modification. *Soil Sci.* 177, 263–268. doi: 10.1097/SS.0b013e3182482784

Brown, R. A., Kercher, A. K., Nguyen, T. H., Nagle, D. C., and Ball, W. P. (2006). Production and characterization of synthetic wood chars for use as surrogates for natural sorbents. *Org. Geochem.* 37, 321–333. doi: 10.1016/j.orggeochem.2005.10.008

Buma, B., Poore, R. E., and Wessman, C. A. (2014). Disturbances, their interactions, and cumulative effects on carbon and charcoal stocks in a forested ecosystem. *Ecosystems* 17, 947–959. doi: 10.1007/s10021-014-9770-8

Clark, J. S., Lynch, J., Stocks, B. J., and Goldammer, J. G. (1998). Relationships between charcoal particles in air and sediments in west-central Siberia. *Holocene* 8, 19–29. doi: 10.1191/095968398672501165

Clay, G. D., and Worrall, F. (2011). Charcoal production in a UK moorland wildfire – How important is it? *J. Environ. Manage.* 92, 676–682. doi: 10.1016/j.jenvman.2010.10.006

Criscuoli, I., Baronti, S., Alberti, G., Rumpel, C., Giordan, M., Camin, F., et al. (2017). Anthropogenic charcoal-rich soils of the XIX century reveal that biochar leads to enhanced fertility and fodder quality of alpine grasslands. *Plant Soil* 411, 499–516. doi: 10.1007/s11104-016-3046-3

Cyr, D., Bergeron, Y., Gauthier, S., and Larouche, A. C. (2005). Are the old-growth forests of the Clay Belt part of a fire-regulated mosaic? *Can. J. For. Res.* 35, 65–73. doi: 10.1139/x04-204

Czimczik, C. I., Preston, C. M., Schmidt, M. W. I., Werner, R. A., and Schulze, E.-D. (2002). Effects of charring on mass, organic carbon, and stable carbon isotope composition of wood. *Org. Geochem.* 33, 1207–1223. doi: 10.1016/S0146-6380(02)00137-7

de Groot, W. J., Flannigan, M. D., and Cantin, A. S. (2013). Climate change impacts on future fire regimes. *For. Ecol. Manage.* 294, 35–44. doi: 10.1016/j.foreco.2012.09.027

Donato, D. C., Campbell, J. L., Fontaine, J. B., and Law, B. E. (2009). Quantifying char in postfire woody detritus inventories. *Fire Ecol.* 5, 104–115. doi: 10.4996/fireecology.0502104

Eckmeier, E., Rösch, M., Ehrmann, O., Schmidt, M. W. I., Schier, W., and Gerlach, R. (2007). Conversion of biomass to charcoal and the carbon mass balance from a slash-and-burn experiment in a temperate deciduous forest. *Holocene* 17, 539–542. doi: 10.1177/0959683607077041

Fearnside, P. M., Gráça, P. M. L. A., Filho, N. L., Rodrigues, F. J. A., and Robinson, J. M. (1999). Tropical forest burning in Brazilian Amazonia: measurement of biomass loading, burning efficiency and charcoal formation at Altamira, Pará. *For. Ecol. Manage.* 123, 65–79. doi: 10.1016/S0378-1127(99)00016-X

Fearnside, P. M., Gráça, P. M. L. A., and Rodrigues, F. J. A. (2001). Burning of Amazonian rainforests: burning efficiency and charcoal formation in forest cleared for cattle pasture near Manaus, Brazil. *For. Ecol. Manage.* 146, 115–128. doi: 10.1016/S0378-1127(00)00450-3

Fearnside, P. M., Leal, N., and Fernandes, F. M. (1993). Rain-forest burning and the global carbon budget – Biomass, combustion efficiency, and charcoal formation in the Brazilian Amazon. *J. Geophys. Res. Atmospheres* 98, 16733–16743. doi: 10.1029/93JD01140

Finkral, A. J., Evans, A. M., and Sorensen, C. D., and Affleck, D. L. R. (2012). Estimating consumption and remaining carbon in burned slash piles. *Can. J. For. Res.* 42, 1744–1749. doi: 10.1139/x2012-112

Gráça, P. M. L. A., Fearnside, P. M., and Cerri, C. C. (1999). Burning of Amazonian forest in Ariquemes, Rondonia, Brazil: biomass, charcoal formation and burning efficiency. *For. Ecol. Manage.* 120, 179–191. doi: 10.1016/S0378-1127(98)00547-7

Gundale, M. J., and DeLuca, T. H. (2006). Temperature and source material influence ecological attributes of ponderosa pine and Douglas-fir charcoal. *For. Ecol. Manage.* 231, 86–93. doi: 10.1016/j.foreco.2006.05.004

Hammes, K., Schmidt, M. W. I., Smernik, R. J., Currie, L. A., Ball, W. P., Nguyen, T. H., et al. (2007). Comparison of quantification methods to measure fire-derived (black/elemental) carbon in soils and sediments using reference materials from soil, water, sediment and the atmosphere. *Glob. Biogeochem. Cycles* 21:GB3016. doi: 10.1029/2006GB002914

Hansen, M., Saarsalmi, A., and Peltre, C. (2016). Changes in SOM composition and stability to microbial degradation over time in response to wood chip ash fertilization. *Soil Biol. Biochem.* 99, 179–186. doi: 10.1016/j.soilbio.2016.05.012

Hart, S. A., and Luckai, N. J. (2014). Charcoal carbon pool in North American boreal forests. *Ecosphere* 5:99. doi: 10.1890/ES13-00086.1

Hatton, P.-J., Chatterjee, S., Filley, T. R., Dastmalchi, K., Plante, A. F., Abiven, S., et al. (2016). Tree taxa and pyrolysis temperature interact to control the efficacy of pyrogenic organic matter formation. *Biogeochemistry* 130, 103–116. doi: 10.1007/s10533-016-0245-1

Ingerslev, M., Skov, S., Sevel, L., and Pedersen, L. B. (2011). Element budgets of forest biomass combustion and ash fertilization – a Danish case study. *Biomass Bioenergy* 35, 2697–2704. doi: 10.1016/j.biombioe.2011.03.018

Johnstone, J. F., and Chapin, I. I. I., F.S. (2006). Effects of soil burn severity on post-fire tree recruitment in boreal forest. *Ecosystems* 9, 14–31. doi: 10.1007/s10021-004-0042-x

Kane, E. S., Hockaday, W. C., Turetsky, M. R., Masiello, C. A., Valentine, D. W., Finney, B. P., et al. (2010). Topographic controls on black carbon accumulation in Alaskan black spruce forest soils: implications for organic matter dynamics. *Biogeochemistry* 100, 39–56. doi: 10.1007/s10533-009-9403-z

Kasin, I., Blanck, Y-li., Storaunit, K. O., and Rolstad, J. (2013). The charcoal record in peat and mineral soil across a boreal landscape and possible linkages to climate change and recent fire history. *Holocene* 23, 1052–1065. doi: 10.1177/0959683613479678

Kasin, I., Ellingsen, V. M., Asplund, J., and Ohlson, M. (2017). Spatial and temporal dynamics of the soil charcoal pool in relation to fire history in a boreal forest landscape. *Can. J. For. Res.* 47, 28–35. doi: 10.1139/cjfr-2016-0233

Kasin, I., and Ohlson, M. (2013). An experimental study of charcoal degradation in a boreal forest. *Soil Biol. Biochem.* 65, 39–49. doi: 10.1016/j.soilbio.2013.05.005

Knicker, H. (2011). Pyrogenic organic matter in soil: its origin and occurrence, its chemistry and survival in soil environments. *Quatern. Int.* 243, 251–263. doi: 10.1016/j.quaint.2011.02.037

Kurth, V. J., MacKenzie, M. D., and DeLuca, T. H., (2006). Estimating charcoal content in forest mineral soils. *Geoderma* 137, 135–139. doi: 10.1016/j.geoderma.2006.08.003

Landry, J.-S., and Matthews, H. D. (2017). The global pyrogenic carbon cycle and its impact on the level of atmospheric $CO_2$ over past and future centuries. *Glob. Change Biol.* 23, 3205–3218. doi: 10.1111/gcb.13603

Lecomte, N., Simard, M., Bergeron, Y., Larouche, A., Asnong, H., and Richard, P. J. H. (2005). Effects of fire severity and initial tree composition on understorey vegetation dynamics in a boreal landscape inferred from chronosequence and paleoecological data. *J. Veg. Sci.* 16, 665–674. doi: 10.1111/j.1654-1103.2005.tb02409.x

Lecomte, N., Simard, M., Fenton, N., and Bergeron, Y. (2006). Fire severity and long-term ecosystem biomass dynamics in coniferous boreal forests of eastern Canada. *Ecosystems* 9, 1215–1230. doi: 10.1007/s10021-004-0168-x

Lynch, J. A., Clark, J. S., and Stocks, B. J. (2004). Charcoal production, dispersal, and deposition from the Fort Providence experimental fire: interpreting fire regimes from charcoal records in boreal forests. *Can. J. For. Res.* 34, 1642–1656. doi: 10.1139/x04-071

Maestrini, B., and Miesel, J. R. (2017). Modification of the weak nitric acid digestion method for the quantification of black carbon in organic matrices. *Soil Biol. Biochem.* 103, 136–139. doi: 10.1016/j.orggeochem.2016.10.010

McBeath, A. V., Smernik, R. J., Schneider, M. P. W., Schmidt, M. W. I., and Plant, E. L. (2011). Determination of the aromaticity and the degree of aromatic condensation of a thermosequence of wood charcoal using NMR. *Org. Geochem.* 42, 1194–1202. doi: 10.1016/j.orggeochem.2011.08.008

McBeath, A. V., Wurster, C. M., and Bird, M. I. (2015). Influence of feedstock properties and pyrolysis conditions on biochar carbon stability as determined by hydrogen pyrolysis. *Biomass Bioenergy* 73, 155–173. doi: 10.1016/j.biombioe.2014.12.022

Merino, A., Chávez-Vergara, B., Salgado, J., Fonturbel, M. T., García-Oliva, F., and Vega, J. A. (2015). Variability in the composition of charred litter generated by wildfire in different ecosystems. *Catena* 133, 52–63. doi: 10.1016/j.catena.2015.04.016

Miesel, J. R., Hockaday, W. C., Kolka, R. K., and Townsend, P. A. (2015). Soil organic matter composition and quality across fire severity gradients in coniferous and deciduous forests of the southern boreal region. *J. Geophys. Res. Biogeosci.* 120, 1124–1141. doi: 10.1002/2015JG002959

Moore, T. R., Trofymow, J. A., Prescott, C. E., Titus, B. D., and C. I. D. E.T., Working Group (2011). Nature and nurture in the dynamics of C, N and P during litter decomposition in Canadian forests. *Plant Soil* 339, 163–175. doi: 10.1007/s11104-010-0563-3

Nocentini, C., Certini, G., Knicker, H., Francisco, O., and Rumpel, C. (2010). Nature and reactivity of charcoal produced and added to soil during wildfire are particle-size dependent. *Org. Geochem.* 41, 682–689. doi: 10.1016/j.orggeochem.2010.03.010

Ohlson, M., Dahlberg, B., Økland, T., Brown, K. J., and Halvorsen, R. (2009). The charcoal carbon pool in boreal forest soils. *Nat. Geosci.* 2, 692–695. doi: 10.1038/ngeo617

Ohlson, M., Ellingsten, V. M., del Olmo, M. V., Lie, M. H., Nybakken, L., and Asplund, J. (2017). Late-Holocene fire history as revealed by size, age and composition of the soil charcoal pool in neighbouring beech and spruce forest landscapes in SE Norway. *Holocene* 27, 397–403. doi: 10.1177/0959683616660174

Ohlson, M., Korbøl, A., and Økland, R. H. (2006). The macroscopic charcoal record in forested boreal peatlands in southeast Norway. *Holocene* 16, 731–741. doi: 10.1191/0959683606hl955rp

Ohlson, M., and Tryterud, E. (2000). Interpretation of the charcoal record in forest soils: forest fires and their production and deposition of macroscopic charcoal. *Holocene* 10, 519–525. doi: 10.1191/095968300667442551

Omil, B., Piñeiro, V., and Merino, A. (2013). Soil and tree response to the application of wood ash containing charcoal in two soils with contrasting properties. *For. Ecol. Manage.* 295, 199–212. doi: 10.1016/j.foreco.2013.01.024

Paré, D., Bernier, P., Lafleur, B., Titus, B. D., Thiffault, E., Maynard, D. G., et al. (2013). Estimating stand-scale biomass, nutrient contents and associated uncertainties for tree species of Canadian forests. *Can. J. For. Res.* 43, 599–608. doi: 10.1139/cjfr-2012-0454

Peerson, O. B., Wu, X., Kustanovich, I., and Smith, S. O. (1993). Variable-amplitude cross-polarization MAS NMR. *J. Magn. Reson. A* 104, 334–339. doi: 10.1006/jmra.1993.1231

Pingree, M. R. A., DeLuca, E. E., Schwartz, D. T., and DeLuca, T. H. (2016). Adsorption capacity of wildfire-produced charcoal from Pacific Northwest forests. *Geoderma* 283, 68–77. doi: 10.1016/j.geoderma.2016.07.016

Preston, C. M. (2014). Environmental NMR: solid-state Methods. Encyclopedia of Magnetic Resonance. *eMagRes* 3, 29–42. doi: 10.1002/9780470034590.emrstm1338

Preston, C. M., Bhatti, J. S., and Norris, C. E. (2014b). Chemical quality of aboveground litter inputs for jack pine and black spruce stands along the Canadian Boreal Forest Transect Case Study. *Écoscience* 21, 202–216. doi: 10.2980/21-(3-4)-3690

Preston, C. M., Norris, C. E., Bernard, G. M., Beilman, D. W., Quideau, S. A., and Wasylishen, R. E. (2014a). Carbon and nitrogen in the silt-size fraction and its HCl-hydroysis residues from coarse-textured Canadian boreal forest soils. *Can. J. Soil Sci.* 94, 157–168. doi: 10.4141/cjss2013-082

Preston, C. M., and Schmidt, M. W. I. (2006). Black (pyrogenic) carbon: a synthesis of current knowledge and uncertainties with special consideration of boreal regions. *Biogeosciences* 3, 397–420. doi: 10.5194/bg-3-397-2006

Preston, C. M., Trofymow, J. A., and Nault, J. (2012). Decomposition and change in N and organic composition of small-diameter Douglas-fir woody debris over 23 years. *Can. J. For. Res.* 42, 1153–1167. doi: 10.1139/x2012-076

Preston, C. M., Trofymow, J. A., Niu, J., and Fyfe, C. A. (1998). CPMAS $^{13}$C NMR spectroscopy and chemical analysis of coarse woody debris in coastal forests of Vancouver Island. *For. Ecol. Manage.* 111, 51–68. doi: 10.1016/S0378-1127(98)00307-7

Reisser, M., Purves, R. S., Schmidt, M. W. I., and Abiven, S. (2016). Pyrogenic carbon in soils: a literature-based inventory and a global estimation of its content in soil organic carbon and stocks. *Front. Earth Sci.* 4:80. doi: 10.3389/feart.2016.00080

Righi, C. A., Gráça, P. M. L. A., Cerri, C. C., Feigl, B. J., and Fearnside, P. M. (2009). Biomass burning in Brazil's Amazonian "arc of deforestation": burning efficiency and charcoal formation in a fire after mechanized clearing at Feliz Natal, Mato Grosso. *For. Ecol. Manage.* 258, 2535–2546. doi: 10.1016/j.foreco.2009.09.010

Robertson, S. J., Rutherford, P. M., López-Gutiérrez, J. C., and Massicotte, H. B. (2012). Biochar enhances seedling growth and alters root symbioses and properties of sub-boreal forest soils. *Can. J. Soil Sci.* 92:329340. doi: 10.4141/cjss2011-066

Sackett, T. E., Basiliko, N., Noyce, G. L., Winsborough, C., Schurman, J., Ikeda, C., et al. (2015). Soil and greenhouse gas response to biochar additions in a temperate hardwood forest. *Glob. Change Biol. Bioenergy* 7, 1062–1074. doi: 10.1111/gcbb.12211

Saiz, G., Goodrick, I., Wurster, C., Zimmermann, M. P. N., and Bird, M. I. (2014). Charcoal recombustion efficiency in tropical savannas. *Geoderma* 219, 40–45. doi: 10.1016/j.geoderma.2013.12.019

Santín, C., Doerr, S. H., Kane, E. S., Masiello, C. A., Ohlson, M., de la Rosa, J. M., et al. (2016a). Towards a global assessment of pyrogenic carbon from vegetation fires. *Glob. Change Biol.* 22, 76–91. doi: 10.1111/gcb.12985

Santín, C., Doerr, S. H., Merino, A., and Loader, N. J. (2016b). Forest floor chemical transformations in a boreal forest fire and their correlations with temperature and heating duration. *Geoderma* 264, 71–80. doi: 10.1016/j.geoderma.2015.09.021

Santín, C., Doerr, S. H., Preston, C., and Bryant, R. (2013). Consumption of residual pyrogenic carbon by wildfire. *Int. J. Wildl. Fire* 22, 1072–1077. doi: 10.1071/WF12190

Santín, C., Doerr, S. H., Preston, C. M., and González-Rodríguez, G. (2015). Pyrogenic organic matter production from wildfires: a missing sink in the global carbon cycle. *Glob. Change Biol.* 21, 1621–1633. doi: 10.1111/gcb.12800

Schiffman, P. M., and Johnson, W. C. (1989). Phytomass and detrital carbon storage during forest regrowth in the southeastern United States Piedmont. *Can. J. For. Res.* 19, 69–78. doi: 10.1139/x89-010

Simard, M., Lecomte, N., Bergeron, Y., Bernier, P. Y., and Par,é, D. (2007). Forest productivity decline caused by successional paludification of boreal soils. *Ecol. Appl.* 17, 1619–1637. doi: 10.1890/06-1795.1

Soucémarianadin, L. N., Quideau, S. A., and MacKenzie, M. D. (2014). Pyrogenic carbon stocks and storage mechanisms in podzolic soils of fire-affected Quebec black spruce forests. *Geoderma* 217–218, 118–128. doi: 10.1016/j.geoderma.2013.11.010

Soucémarianadin, L. N., Quideau, S. A., MacKenzie, M. D., Bernard, G. M., and Wasylishen, R. E. (2013). Laboratory charring conditions affect black carbon properties: a case study from Quebec black spruce forests. *Org. Geochem.* 62, 45–55. doi: 10.1016/j.orggeochem.2013.07.005

Soucémarianadin, L. N., Quideau, S. A., MacKenzie, M. D., Munson, A. D., Boiffin, J., Bernard, G. M., et al. (2015a). Total and pyrogenic carbon stocks in black spruce forest floors from eastern Canada. *Org. Geochem.* 82, 1–11. doi: 10.1016/j.orggeochem.2015.02.004

Soucémarianadin, L. N., Quideau, S. A., Wasylishen, R. E., and Munson, A. D. (2015b). Early-season fires in boreal black spruce forests produce pyrogenic carbon with low intrinsic recalcitrance. *Ecology* 96, 1575–1585. doi: 10.1890/14-1196.1

Tinker, D. B., and Knight, D. H. (2000). Coarse woody debris following fire and logging in Wyoming lodgepole pine forests. *Ecosystems* 3, 472–483. doi: 10.1007/s100210000041

Sandroni, V., and Smith, C. M. M. (2002). Microwave digestion of sludge, soil and sediment samples for metal analysis by inductively coupled plasma-atomic emission spectrometry. *Anal. Chim. Acta* 468, 335–344. doi: 10.1016/S0003-2670(02)00655-4

Wolf, M., Lehndorff, E., Wiesenberg, G. L. B., Stockhausen, M., Schwark, L., and Amelung, W. (2013). Towards reconstruction of past fire regimes from geochemical analysis of charcoal. *Org. Geochem.* 55, 11–21. doi: 10.1016/j.orggeochem.2012.11.002

Wu, S., Feng, X., and Wittmeier, A. (1997). Microwave digestion of plant and grain reference materials in nitric acid or a mixture of nitric acid and hydrogen peroxide for the determination of multi-elements by inductively coupled plasma mass spectrometry. *J. Anal. Atom. Spectr.* 12, 797–806. doi: 10.1039/a607217h

Zackrisson, O., Nilsson, M.-C., and Wardle, D. A. (1996). Key ecological function of charcoal from wildfire in the boreal forest. *Oikos* 77, 10–19. doi: 10.2307/3545580

**Conflict of Interest Statement:** The authors declare that the research was conducted in the absence of any commercial or financial relationships that could be construed as a potential conflict of interest.

frontiers in Earth Science

ORIGINAL RESEARCH
published: 23 November 2017
doi: 10.3389/feart.2017.00096

# Pyrogenic Carbon Lacks Long-Term Persistence in Temperate Arable Soils

*Suzanne Lutfalla[1,2], Samuel Abiven[3], Pierre Barré[2]*, Daniel B. Wiedemeier[3], Bent T. Christensen[4], Sabine Houot[1], Thomas Kätterer[5], Andy J. Macdonald[6], Folkert van Oort[1] and Claire Chenu[1]**

[1] AgroParisTech, Institut National de la Recherche Agronomique, UMR 1402 ECOSYS, Thiverval Grignon, France, [2] Laboratoire de Géologie de l'ENS-PSL Research University–Centre National de la Recherche Scientifique UMR8538, Paris, France, [3] Department of Geography, University of Zurich, Zurich, Switzerland, [4] Department of Agroecology, Aarhus University, Aarhus, Denmark, [5] Department of Ecology, Swedish University of Agricultural Sciences, Uppsala, Sweden, [6] Department of Sustainable Soils and Grassland Systems, Rothamsted Research, Harpenden, United Kingdom

Pyrogenic organic carbon (PyOC) derived from incomplete burning of biomass is considered the most persistent fraction of soil organic carbon (SOC), being expected to remain in soil for centuries. However, PyOC persistence has seldom been evaluated under field conditions. Based on a unique set of soils from five European long-term bare fallows (LTBF), i.e., vegetation-free field experiments, we provide the first direct comparison between PyOC and SOC persistence in temperate arable soils. We found that soil PyOC contents decreased more rapidly than expected from current concepts, the mean residence time (MRT) of native PyOC being just 1.6 times longer than that of SOC. At the oldest experimental site, 55% of the initial PyOC remained after 80 years of bare fallow. Our results suggest that while the potential for long-term C storage exists, the persistence of PyOC in soil may currently be overestimated.

**Keywords: soil organic matter persistence, soil carbon sequestration, carbon cycle, pyrogenic carbon, climate change mitigation, long term bare fallows**

OPEN ACCESS

***Edited by:***
*Moritz Felix Lehmann, University of Basel, Switzerland*

***Reviewed by:***
*Carlos A. Sierra, Max Planck Institute for Biogeochemistry (MPG), Germany*
*Caitlin E. Hicks Pries, Dartmouth College, United States*

***Correspondence:**
*Pierre Barré*
*barre@geologie.ens.fr*
*Claire Chenu*
*claire.chenu@agroparistech.fr*

***Specialty section:***
*This article was submitted to Biogeoscience, a section of the journal Frontiers in Earth Science*

***Received:*** *31 July 2017*
***Accepted:*** *09 November 2017*
***Published:*** *23 November 2017*

***Citation:***
*Lutfalla S, Abiven S, Barré P, Wiedemeier DB, Christensen BT, Houot S, Kätterer T, Macdonald AJ, van Oort F and Chenu C (2017) Pyrogenic Carbon Lacks Long-Term Persistence in Temperate Arable Soils. Front. Earth Sci. 5:96. doi: 10.3389/feart.2017.00096*

## INTRODUCTION

Pyrogenic Organic Carbon (PyOC) is a charred residue derived from the incomplete burning of biomass and is a native component of most soils. PyOC represents on average about 14% of the soil organic carbon (SOC) and ranges between 0 and 60% depending on the conditions of fire, soils and climate (Reisser et al., 2016). This corresponds to a stock of about 200 Pg of C (Reisser et al., 2016), within the same order of magnitude as the global vegetation C stocks. Since PyOC inputs are mostly coming from fires, their occurrence and amount should be low as compared to uncharred organic material (i.e., litter). One reason for these high stocks can be related to the specific persistence of PyOC in terrestrial ecosystems.

Recent reviews suggest that the persistence of PyOC in soil may range from a few years to millennia (Singh et al., 2012a; Lehmann et al., 2015). These differences can be explained by the heterogeneity of PyOC material, but also by the different methods used to assess its presence in soils. While being a limited tool to assess the persistence of SOC (Sierra et al., 2017), mean residence time (MRT) is widely used to compare the different turnovers of organic materials. Assessing the MRT of PyOC is complex, because of the large time span that should be considered. Lehmann et al. (2015) described the existing approaches and their current limitations, among which: laboratory soil incubations, field setups, and space for time approaches.

Laboratory soil incubations can be well constrained, however they are limited by their duration and their lack of litter inputs, plants, macro-fauna, micro-organisms variations and water, and temperature dynamics. They address mainly the first phase of PyOC mineralization and are mainly useful to compare PyOC to an uncharred material (Zimmerman, 2010; Singh et al., 2012b).

Field studies are more realistic but also suffer from different hurdles. Purposeful additions of PyOC in field setups share the advantages of controlled conditions with incubations and allow C budget, particularly in the case of isotopically labeled material, but only address few years of mineralization at maximum (Whitman et al., 2014). Calculating the PyOC balance of natural char dynamics is a way to address longer time scales (Lehmann et al., 2008; Lehndorff et al., 2014). It requires a well-known input of chars over time, estimated for a period that well exceeds MRT, and PyOC exports from other processes than mineralization must be small (Lehmann et al., 2015). These conditions are difficult to fulfill, and the MRT thus estimated is very dependent on the assumptions considered for PyOC inputs.

PyOC MRT can also be estimated via a space for time approach, also named chronosequence (Lehmann et al., 2015). It consists in sampling soils where PyOC entered the soil at different times in the past (Nguyen et al., 2009; Vasilyeva et al., 2011; Alexis et al., 2012), as a substitute for archived samples of the same site at different times. The advantage of this approach is that the MRT can be calculated over long periods, provided one can find samples from comparable environmental conditions, receiving a similar amount of PyOC at several year or decade intervals. These conditions are very difficult to find, and the pre-required hypothesis nearly impossible to validate.

As described above, field studies are more realistic than laboratory incubations to estimate the PyOC MRT, but the requirements regarding the inputs and the site are difficult to match. Long-term bare fallow (LTBF) is another field approach that has been successfully applied to different fractions of SOC (Barré et al., 2010; Paradelo et al., 2013). It consists in following over time (with archived samples) the degradation of organic material while the soil does not receive any new organic inputs (Rühlmann, 1999). This approach solves part of the shortcomings described above: there is no input considered in this setup, so no hypothesis about their amount and characteristics. Also, there is no need to speculate about the difference between sites as in the space for time approach since all samples originate from the same location. Compared to laboratory incubations, LTBF which have no litter inputs by design have the advantage of representing *in situ* environmental, climatic and biological conditions and preventing soils from being physically disturbed.

Our study is based on archived soils sampled in five European LTBF experiments that allowed us to study the corresponding decay rates of PyOC and SOC over several decades and under different temperate pedo-climatic settings (Barré et al., 2010; **Table 1**). In these experiments, soils do not receive any organic inputs and are kept free of vegetation by weeding (manual weeding and/or chemical weeding on a yearly basis) for up to 80 years. As the largest C inputs to soils are derived from plants, the total C inputs during the bare fallow period are negligible, thanks to the absence of plants. The vegetation-free setup of the LTBF experiments represents a unique opportunity for studying *in situ* the long-term turnover of PyOC and SOC in agricultural soils. Indeed, they provide information on initial stocks and subsequent decadal-scale changes without interference from fresh C inputs.

# MATERIALS AND METHODS

## European Network of Long Term Bare Fallows (LTBF)

Soil samples were taken from the archives of a European network of LTBF experiments located in five different sites (see **Table 1**). The experiments were originally initiated for agronomic studies on arable soil fertility. The characteristics of the five sites involved in this study have been described in Barré et al. (2010). For each LTBF experiment, we selected two adjacent field plot replicates (four replicates at Versailles). For analyses, we used archived soils sampled at the start of the bare fallow treatment and after different fallow periods (samples are air-dried and kept in the dark). Except at Rothamsted, there are no significant changes

**TABLE 1 |** Selected characteristics of the five LTBF sites.

| | Askov (DK) | Grignon (FR) | Rothamsted (UK) | Ultuna (SW) | Versailles (FR) |
|---|---|---|---|---|---|
| Coordinates | 55°28N 9°07E | 48°51N 55°E | 51°82N 0°35E | 59°49N 17°38E | 48°48N 2°08E |
| First year of bare fallow | 1956 | 1959 | 1959 | 1956 | 1928 |
| Last sampling for this study | 1983 | 2007 | 2008 | 2009 | 2008 |
| Duration (years) | 27 | 48 | 49 | 53 | 79 |
| Previous land use | arable | grassland | grassland | arable | grassland |
| Mean annual temperature (°C) | 7.8 | 10.7 | 9.5 | 5.5 | 10.7 |
| Annual precipitation (mm) | 862 | 649 | 712 | 533 | 628 |
| Soil texture and type IUSS Working Group WRB, 2006 | Coarse sandy loam Orthic Luvisol | Silty loam Luvisol | Flinty silty clay loam Chromic Luvisol | Clay loam Eutric Cambisol | Silty loam Luvisol |
| Sampling depth (cm) | 20 | 25 | 23 | 20 | 25 |
| Initial SOC (g $kg^{-1}$) | 16.8 | 13.6 | 29.5 | 14.5 | 17.9 |
| Final SOC (g $kg^{-1}$) | 11.0 | 8.6 | 10.0 | 8.9 | 6.0 |

in the bulk density of the soils. The fire history at those sites is not known in detail but the PyOC measured in this study most probably comes from the burning of herbaceous, scrubs and other low woodland vegetation during the century before the fallow treatment (based on the history of the sites and the distribution of the different BPCA molecular markers). The soils at Askov and Ultuna are known to have been under arable management for centuries before the start of the bare-fallow experiments in 1956.

## PyOC Assessment

Revealing the dynamics of PyOC requires a reliable method for its determination in soil. Several methods have been proposed (Hammes et al., 2007). The Benzene Polycarboxylic Acid (BPCA) molecular marker method (Glaser et al., 1998; Wiedemeier et al., 2013) has the advantage of only targeting pyrogenic derived molecular markers, thus yielding conservative but quantitative estimates of PyOC as well as information about its quality (Wiedemeier et al., 2015). The BPCA method is, to date, the most widely used approach to measure PyOC contents in soils (Reisser et al., 2016).

PyOC contents were assessed with the BPCA method following the previously described state-of-the-art molecular marker approach for PyOC analysis in environmental samples (Wiedemeier et al., 2013). Samples were analyzed in duplicate and analytical error was always <10%. For

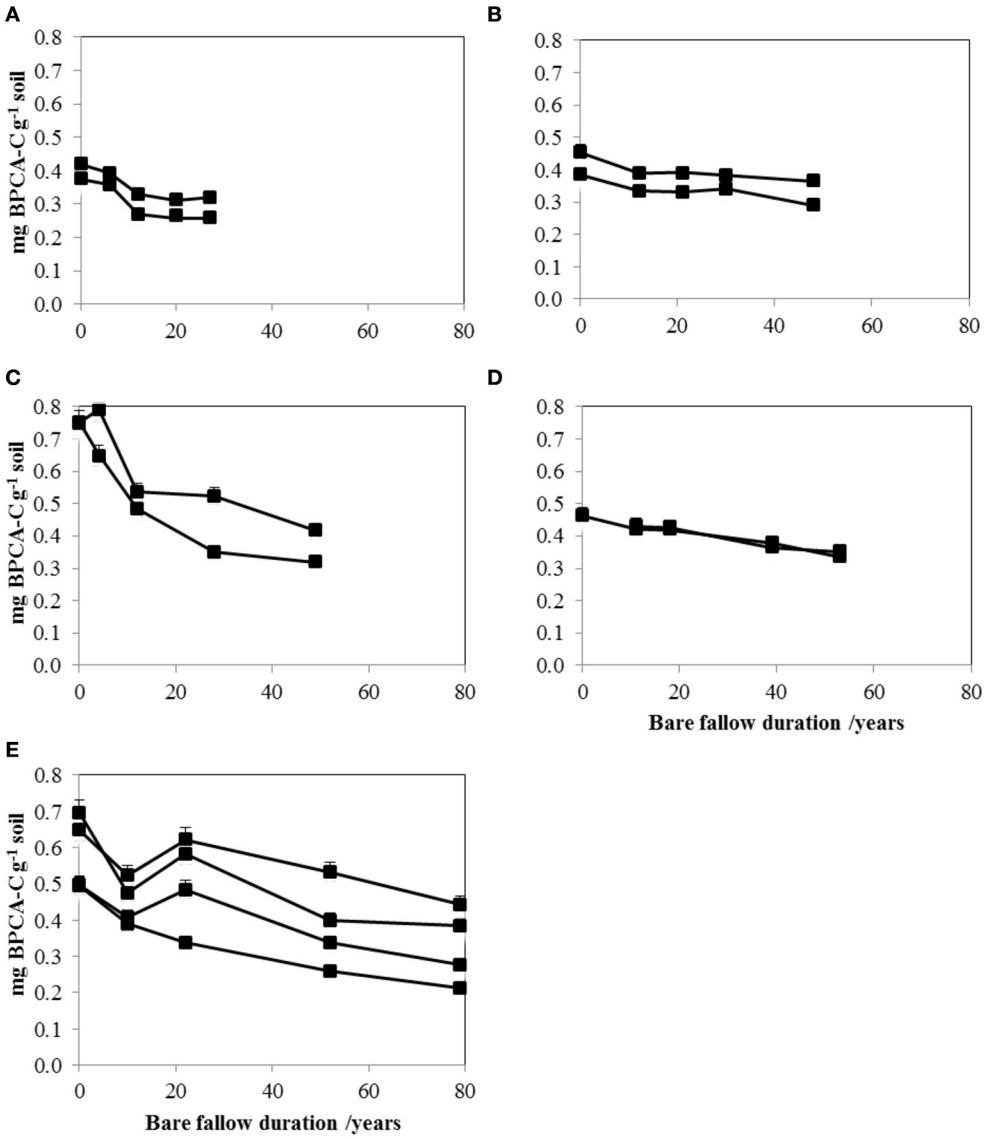


**FIGURE 1 |** Contents of native pyrogenic organic carbon (PyOC) in soil decrease with time at all LTBF sites and for all field replicates (mg BPCA-C $g^{-1}$ soil, time in years): Askov **(A)**, Grignon **(B)**, Rothamsted **(C)**, Ultuna **(D)**, and Versailles **(E)**. Each line corresponds to an experimental plot. Error bars represent PyOC variability within analytical replicates (always <10%).

each analytical batch of soils, a laboratory reference soil (Chernozem) was included to ensure the quality of the analytical procedures. The BPCA method is consistent but probably underestimates the absolute amount of PyOC (Glaser et al., 1998), and a conversion factor of 2.27 has been proposed to convert "BPCA-PyOC" to "total-PyOC." We refrained from this and present unconverted PyOC-values because only relative changes in the PyOC content were of interest.

## SOC Assessment

The content of SOC in the samples was measured by dry combustion employing a CHN Autoanalyser (Carlo Erba NA 1500). Except for Grignon, the soils contained no carbonates, therefore total C is equivalent to organic C contents. The Grignon soils were treated with HCl to remove soil carbonates (Harris et al., 2001).

## Statistical Analysis

The statistical analyses were conducted using the free software environment for statistical computing R (http://www.r-project.org).

## One Pool Model

In a first step we unsuccessfully tried to fit a two pool model on the experimental data. Indeed, because of the small number of date points for each experimental plot, five dates per plot, we were unable to constrain the model parameters (see Supplementary Table 1). We therefore decided to use a simpler model to estimate and compare the MRT of both PyOC and SOC.

Although simplistic, single pool models have been used to describe SOC dynamics (Parton et al., 1988) and allow a direct and transparent comparison between PyOC and SOC dynamics and between our dataset and previously published data. This model assumes that the loss of PyOC can be described by first

**TABLE 2 |** PyOC contents (mg PyOC-C $g^{-1}$ soil) measured by the BPCA method and coefficient of variation CV (%) for all samples and all sites.

| **Time under bare fallow (years)** | | **0** | **6** | **12** | **20** | **27** |
|---|---|---|---|---|---|---|
| Askov1 | PyOC content (mg PyOC-C $g^{-1}$ soil) | 0.38 | 0.36 | 0.27 | 0.27 | 0.26 |
| | Coefficient of variation (CV, %) | 2.17 | 4.58 | 1.35 | 1.62 | 10.00 |
| Askov2 | PyOC content | 0.42 | 0.39 | 0.33 | 0.31 | 0.32 |
| | CV | 0.34 | 3.10 | 3.77 | 3.73 | 2.64 |
| **Time under bare fallow (years)** | | **0** | **12** | **21** | **30** | **48** |
| Grignon1 | PyOC content | 0.38 | 0.34 | 0.33 | 0.34 | 0.29 |
| | CV | 0.43 | 6.85 | 3.50 | 1.07 | 2.04 |
| Grignon2 | PyOC content | 0.46 | 0.39 | 0.39 | 0.38 | 0.37 |
| | CV | 2.64 | 1.03 | 0.84 | 6.96 | 7.19 |
| **Time under bare fallow (years)** | | **0** | **4** | **12** | **28** | **49** |
| Rothamsted1 | PyOC content | 0.75 | 0.65 | 0.48 | 0.35 | 0.32 |
| | CV | 4.26 | 7.51 | 2.93 | 1.72 | 2.07 |
| Rothamsted2 | PyOC content | 0.75 | 0.79 | 0.54 | 0.52 | 0.42 |
| | CV | 2.92 | 2.07 | 0.75 | 6.63 | 10.00 |
| **Time under bare fallow (years)** | | **0** | **11** | **18** | **39** | **53** |
| Ultuna1 | PyOC content | 0.46 | 0.42 | 0.42 | 0.38 | 0.34 |
| | CV | 8.80 | 0.77 | 3.23 | 2.73 | 3.61 |
| Ultuna2 | PyOC content | | 0.43 | 0.43 | 0.37 | 0.35 |
| | CV | | 0.76 | 1.99 | 1.67 | 8.72 |
| **Time under bare fallow (years)** | | **0** | **10** | **22** | **52** | **79** |
| Versailles1 | PyOC content | 0.65 | 0.52 | 0.62 | 0.53 | 0.44 |
| | CV | 6.98 | 1.86 | 1.26 | 0.53 | 2.65 |
| Versailles2 | PyOC content | 0.70 | 0.47 | 0.58 | 0.40 | 0.39 |
| | CV | 2.81 | 0.48 | 7.51 | 0.40 | 0.39 |
| Versailles3 | PyOC content | 0.49 | 0.39 | 0.34 | 0.26 | 0.21 |
| | CV | 4.79 | 6.49 | 7.91 | 0.74 | 6.66 |
| Versailles4 | PyOC content | 0.50 | 0.41 | 0.48 | 0.34 | 0.28 |
| | CV | 0.17 | 5.37 | 4.92 | 3.02 | 7.12 |

order kinetics:

$$C(t) = C(0)^* \exp(-t/MRT)$$

Where C(t) is concentration of PyOC (mg PyOC-C $g^{-1}$ soil) at time t (years after the bare fallow start), C(0) is the initial PyOC concentration (mg PyOC-C $g^{-1}$ soil), and MRT is the Mean Residence Time of PyOC (years). The same model was used to assess the MRT of SOC. The Least Square method was used to estimate model parameters.

# RESULTS

## PyOC Contents Decrease Rapidly

We found contents of soil PyOC detected by the BPCA method to decrease surprisingly fast at all LTBF sites (**Figure 1** and **Table 2**). Initial concentrations varied between 0.38 mg PyOC-C $g^{-1}$ soil (plots Grignon1 and Askov1) and 0.75 mg PyOC-C $g^{-1}$ soil (Rothamsted1 and 2) corresponding to 2 and 4% of the total organic carbon (TOC) contents (TOC = PyOC + SOC). This is consistent with results from other studies using similar methods (Glaser et al., 1998; Schneider et al., 2011). For all LTBF sites, the final PyOC concentrations were significantly lower than the initial concentrations ($p < 0.001$). The loss of PyOC between the first and the last soil sampling ranged from 19.8 to 57.3% of the initial PyOC content but was not related to the length of the bare fallow period. At Versailles and Rothamsted, PyOC contents showed steep initial declines, with 20–35% of the initial PyOC being lost during the first decade, corresponding to average annual losses of 1.35% at Versailles and 2% at Rothamsted. The PyOC increased between year 10 and year 22 in soils from the Versailles bare fallow, probably due to the impact of nearby bombings during the Second World War (WW2). In the longest running field experiment (Versailles), 55% ($SD = 10\%$) of the initial PyOC remained after 80 years of bare fallow.

## PyOC Becomes Enriched in Condensed Material

The evolution of the quantities of the different BPCA molecular markers showed a consistent decrease of the ratio B5CA:B6CA with time for all sites and all replicates (**Figure 2**). This translates into a relative increase in the quantity of B6CAs, which are the most condensed BPCA molecular markers.

## PyOC and SOC Loss Differs Little

As previously reported (Barré et al., 2010), TOC contents decreased at all LTBF sites due to the absence of C inputs and the on-going decomposition of organic matter formed during the pre-bare fallow period. At the last sampling, between 34 and 72% of the initial SOC was lost (**Table 1** and **Figure 3**).

The PyOC and SOC pools showed similar dynamics (**Figure 4**) and the PyOC loss patterns were consistent across the range of pedo-climatic settings. Loss rates of PyOC were significantly smaller than those observed for SOC ($p < 0.001$). The difference between PyOC and SOC loss rates was reflected in a relative PyOC enrichment at all LTBF sites; the initial PyOC content ranged from 2 to 4% of the SOC while final PyOC contents ranged from 2 to 6% of the SOC. At Rothamsted, one sample taken 4 years after the beginning of the bare fallow contained more PyOC than the initial amount at the beginning of the bare fallow (**Table 2**). This outlier, ascribed to spatial heterogeneity, is thus located above the 100% line of PyOC in **Figure 4**, but remains within the 10% variation.

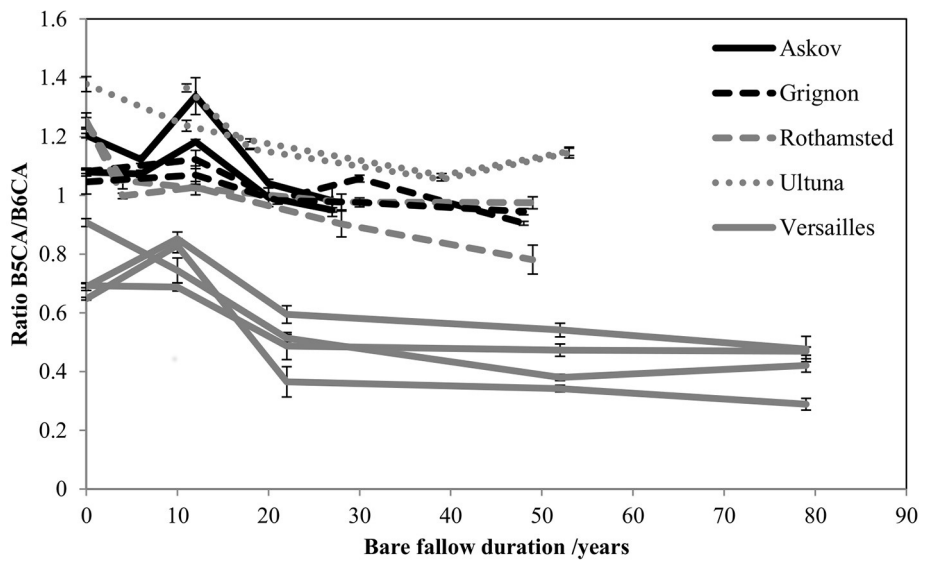


**FIGURE 2 |** Consistent qualitative evolution of PyOC at all LTBF sites. Evolution of the ratio between the quantities (mg PyOC-C $g^{-1}$ soil) of two molecular markers (B5CA and B6CA) out of the four molecular markers analyzed with the BPCA method. Error bars represent the variability observed between technical replicates.

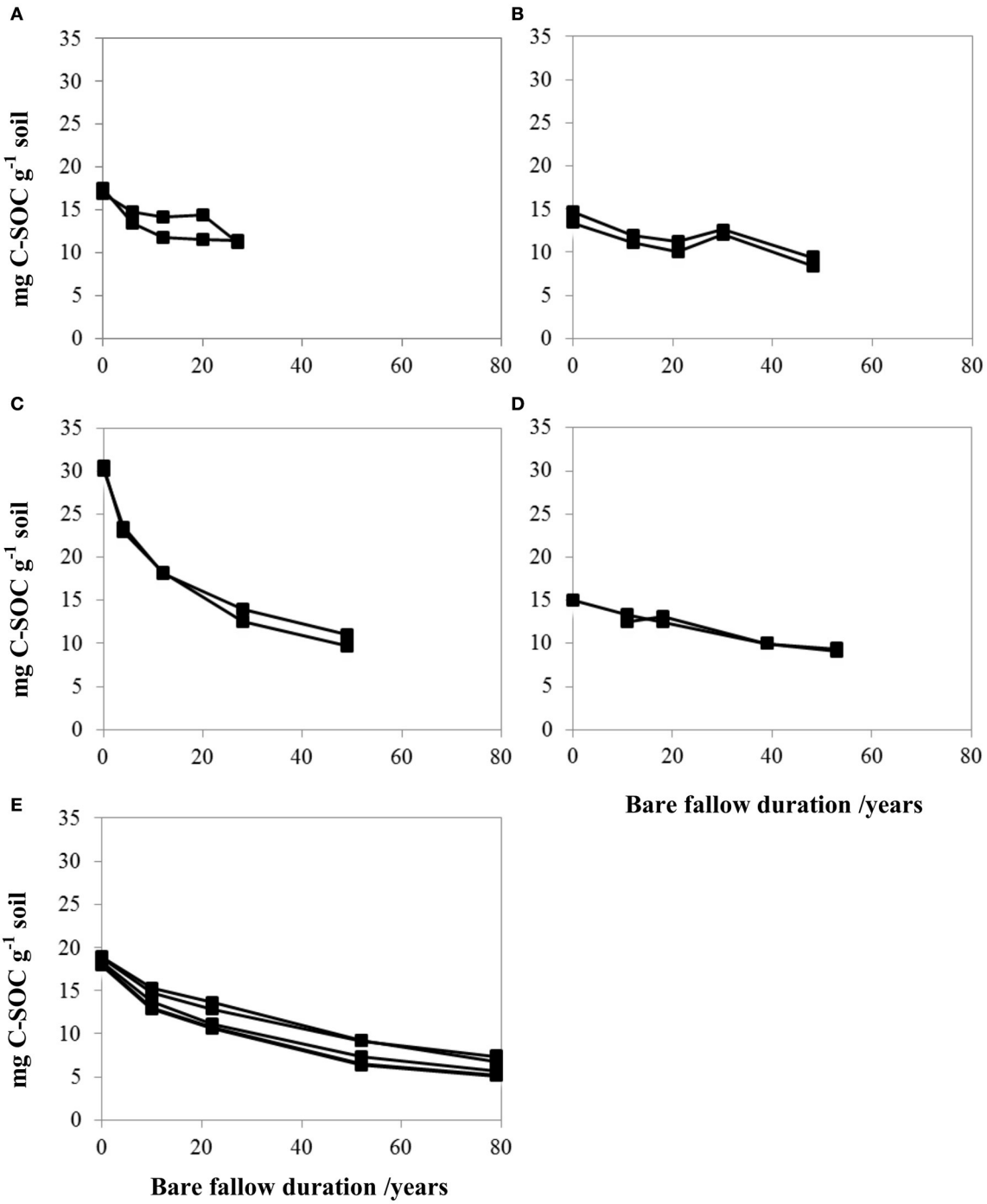


**FIGURE 3 |** SOC degradation dynamics with time at all sites (mg C.g$^{-1}$ soil) for all field replicates: Askov **(A)**, Grignon **(B)**, Rothamsted **(C)**, Ultuna **(D)**, and Versailles **(E)**. SOC represents the portion of total organic carbon which is not pyrogenic, SOC contents are calculated as the difference between TOC contents determined by elemental analysis and PyOC contents determined by BPCA analysis.

## PyOC Residence Time Ranges from 42 to 183 Years

The MRT for PyOC and SOC was estimated using first order kinetics in order to compare the relative persistence of PyOC and SOC (**Table 3**). After unsuccessfully trying to model our data using a two pool model, we applied single pool models with mono-exponential decay assuming PyOC and SOC to be homogeneous pools.

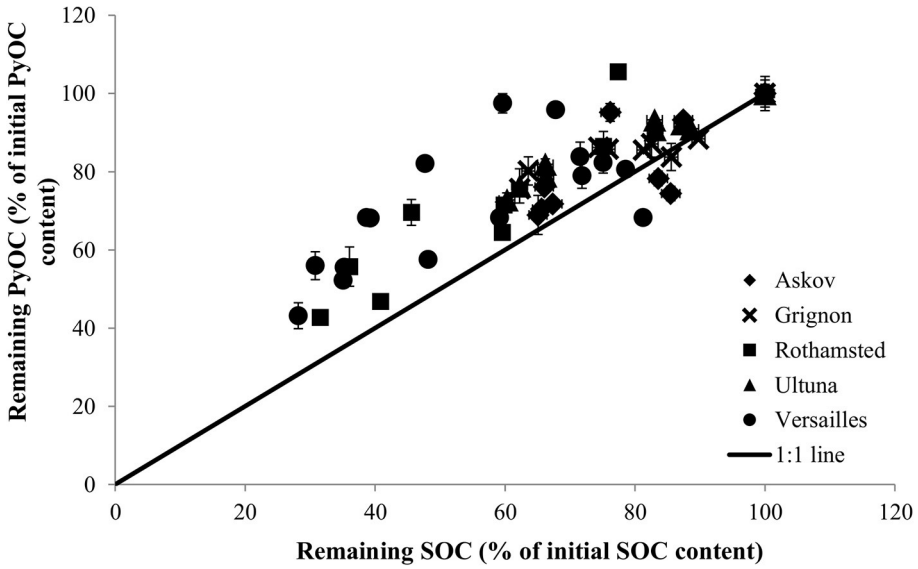


**FIGURE 4 |** PyOC losses occur more slowly than SOC losses (1:1 line), far from the concept of PyOC being inert (0:1 line). Values are expressed as % of initial SOC and PyOC contents. Time series start at the 100% values for both PyOC and SOC, vertical error bars represent PyOC variability within analytical replicates (<10%), horizontal error bars represent analytical errors on SOC measurements (<3%). The average annual loss of SOC ranged from 0.7% at Ultuna to 1.4% at Rothamsted while losses of PyOC varied from 0.4% at Versailles to 1.2% at Rothamsted.

The MRT obtained (**Table 3**) represent the average time an atom of C in PyOC or in SOC remains in the PyOC or SOC reservoirs. For instance in Rothamsted, modeling results show that PyOC has a MRT of 42 years ($SD = 7$ years) and 76 years ($SD = 15$ years) in the two plots studied (**Table 3**). This means that part of the PyOC material is expected to persist for time periods well exceeding the calculated MRT. Details of the calculations of the age distribution of material with a one pool model can be found in Manzoni et al. (2009). Given the results of the model, even though MRT of PyOC is 80 years for the Versailles3 plot, after 240 years of LTBF there would still be 5% of the initial PyOC remaining (Supplementary Figure 1).

Excluding data from the three Versailles plots distorted by bombing impacts, the MRT of PyOC ranged from 42 to 183 years, with an average of 116 years across all sites (the standard deviation is 15 years). The average MRT for PyOC (116 years) is 1.6 times longer than the MRT estimated for SOC (73 years). This difference is significant ($p < 0.001$) and falls in the low end of estimates (decades to centuries) reported by the Intergovernmental Panel on Climate Change (IPCC) (Ciais et al., 2013).

The ratio between MRT of PyOC and SOC differed among LTBF sites. For the Askov2 plot, the MRT of PyOC and SOC are the same, evidencing no specific PyOC persistence, while for the Versailles1 plot the MRT of PyOC was three times larger than that of SOC. Despite large differences in the pedo-climatic setting among the LTBF sites, no relationship could be established between PyOC loss and general site characteristics, such as soil type and climate. However, sites with a pre-fallow history of permanent grasslands (Rothamsted and Versailles) showed a steeper initial decline in PyOC than sites with a long pre-fallow history of arable land use (Askov and Ultuna).

## DISCUSSION

The small difference in PyOC and SOC persistence contrasts with current concepts on this topic. The MRT of SOC in the LTBF plots are similar to those estimated from alternative approaches, such as C3-C4 vegetation conversion experiments under similar pedo-climatic conditions (Dignac et al., 2005; Rasse et al., 2006) and also to those estimated from similar approaches using more complex models (Barré et al., 2010; Cardinael et al., 2015). Barré et al. (2010) have extensively studied the dynamics of TOC in six long term bare fallows including the five sites of the present study. They present numerical results of turnover times, equivalent to MRT in this study, using a two pool model (mono exponential + constant). They found turnover times ranging from 24 years at Versailles to 66 years at Ultuna with an average of 47 years, for what they refer to as the intermediate pool of their two pool model. In our study, the MRT of SOC are within the same order of magnitude but tend to be bigger, ranging from 31 years in Rothamsted to 111 years in Grignon and averaging at 73 years. Therefore, by using a one pool model we overestimated the MRT of SOC. In the same way, if similar models had been fitted to PyOC dynamics, they probably would have led to smaller MRT for PyOC compared to the results presented in this study.

The MRT for PyOC in the soils from these five North European sites are three to ten times shorter than MRT values for PyOC often reported in the literature for long-term field studies (Singh et al., 2012a; Lehmann et al., 2015), except for Bird et al. (1999) and Nguyen et al. (2009) which found comparable MRT of 130 and 141 years, respectively for a chronosequence in tropical contexts. Litter inputs, which do not occur in LTBF soils, might have had an impact, either positive or negative on PyOC dynamics: priming effect could have resulted in a quicker decline

**TABLE 3 |** Mean residence time (in years) for PyOC and SOC calculated from the whole data set and estimates from previous studies.

| | MRT PyOC (years) | | MRT SOC (years) | | Ratio MRT PyOC/SOC |
|---|---|---|---|---|---|
| | mean | *SD* | mean | *SD* | |
| Askov1 | 59 | 9 | 46 | 8 | 1.3 |
| Askov2 | 76 | 10 | 77 | 11 | 1.0 |
| Grignon1 | 183 | 22 | 111 | 25 | 1.6 |
| Grignon2 | 169 | 31 | 109 | 19 | 1.5 |
| Rothamsted1 | 42 | 7 | 31 | 5 | 1.3 |
| Rothamsted2 | 76 | 15 | 35 | 6 | 2.2 |
| Ultuna1 | 183 | 11 | 99 | 3 | 1.8 |
| Ultuna2 | 179 | 18 | 95 | 13 | 1.9 |
| Versailles1 | 214* | 53 | 70* | 8 | 3.1* |
| Versailles2 | 106* | 27 | 71* | 4 | 1.5* |
| Versailles3 | 80 | 9 | 49 | 6 | 1.6 |
| Versailles4 | 141* | 25 | 54* | 6 | 2.6* |
| Average | 116 (126**) | 15 (20**) | 73 (72**) | 10 (10**) | 1.58 (1.8**) |
| Singh et al., 2012a | 291 (353***) | | – | | |
| Lehmann et al., 2015 | 300–6,000 | | – | | |
| Forbes et al., 2006 | >1,000 | | – | | |

*The significance of the model is shown in the standard deviation (SD) of each MRT estimates (in years).*
**Data impacted by WW2 bombing event at Versailles.*
***Including hampered data.*
****For field studies.*

of PyOC (Kuzyakov, 2010) whereas preferential biodegradation of fresh litter could have slowed down the degradation of PyOC. However, published evidence suggests that priming effect is not a significant factor for explaining long term soil organic carbon dynamics (Cardinael et al., 2015). Additionnally, Vasilyeva et al. (2011) compared the PyOC contents of bare fallow soils (after 55 years of bare fallow) to the PyOC contents of soils from an adjacent native grass steppe. They found that the absence of vegetation did not interact with the persistence of PyOC in soil as the observed changes in PyOC contents were similar for fallowed and vegetated soils. For all these reasons, our results, i.e., relatively short MRT for PyOC, are likely not due to the fact that the considered soils were kept bare.

Losses of PyOC are ascribed to biotic (microbial degradation) and abiotic mechanisms (photo-oxidation, erosion, and leaching). We consider that the consistent loss of PyOC observed across the contrasted pedo-climatic settings is mainly due to biotic processes. Except for Rothamsted, no significant soil bulk density changes were observed in the different LTBF sites, the same soil layers were therefore consistently sampled over the duration of the experiments (see Materials and Methods). Photo-oxidation impacts charred materials situated at the soil surface, but can only be of minor importance in our study since soil samples were extracted from the Ap-horizon (0–20 or 0–30 cm soil depth depending on the site). Furthermore, the experimental setup of the LTBF experiments ensured that losses of PyOC and SOC by horizontal transport (e.g., erosion) were insignificant during the fallow period. Although migration of PyOC may occur, previous studies of potential loss mechanisms found that migration of soluble PyOC in the soil profile plays an insignificant role compared to biological degradation (Major et al., 2010; Abiven et al., 2011; Maestrini et al., 2014). Moreover, similar changes in PyOC molecular characteristics were observed across sites (**Figure 2**), supporting the idea that biological decay was the dominating mechanism for the observed loss of PyOC.

In their recommendations for future estimations of PyOC MRT, Lehmann et al. (2015) recommended considering at least a two pool model, to take into account the heterogeneity of the PyOC material. Despite our large dataset, it was not possible to fit any multiple pool models to the five data chronicles, which might lead one to question the accuracy of this recommendation. Since our dataset is particularly large, in particular along time thanks to the archived samples, it is very unlikely to find better time-framed setups to estimate MRT. Instead of increasing the complexity of the model with poorly constrained parameters, it would be more useful to always compare the PyOC MRT to the SOC MRT of the same site as a way to normalize the persistence of the organic materials. Even though our results might represent minimum estimates of MRT since one pool models do not consider long term pools, our study is to our knowledge the first direct comparison between PyOC and SOC persistence in temperate arable soils. It conveys new and essential experimental evidence on the stability of native PyOC and expands current concepts of PyOC persistence in soil. We found PyOC to be more persistent than SOC and as such, our results align with the current notion of PyOC being the most persistent fraction of TOC (Schmidt et al., 2002; Amelung et al., 2008). While our results may be consistent with this notion, the relatively short MRT observed for PyOC in LTBF soils suggest that PyOC persistence might have been overestimated in previous reports.

## AUTHOR CONTRIBUTIONS

SL, CC, PB, and SA: designed the study and wrote the paper; SL: carried out analyses; DW developed the improved BPCA method and provided technical advice; FvO, AM, TK, SH, and BC: provided the LTBF soil samples. All authors subsequently reviewed and amended the manuscript.

## ACKNOWLEDGMENTS

We gratefully acknowledge the colleagues and the institutions who initiated and maintained the LTBF experiments and who thereby made it possible for us to undertake this study. We thank ABIES doctoral school and the European Climate KIC mobility program for funding the missions of SL to the University of Zurich. We thank Rothamsted Research and the Lawes Agricultural Trust for access to archived soil samples from their long-term experiments. The Rothamsted Long-term Experiments National Capability is supported by the UK Biotechnology and Biological Sciences Research Council and

the Lawes Agricultural Trust. The Danish contribution was financially supported by the EU FP7 project SmartSOIL (Grant agreement 289694). The Swiss contribution was supported by the Zurich University Research Priority Program "Global Change and Biodiversity."

## SUPPLEMENTARY MATERIAL

The Supplementary Material for this article can be found online at: https://www.frontiersin.org/articles/10.3389/feart.2017.00096/full#supplementary-material

## REFERENCES


Abiven, S., Hengartner, P., Schneider, M. P. W., Singh, N., and Schmidt, M. W. I. (2011). Pyrogenic carbon soluble fraction is larger and more aromatic in aged charcoal than in fresh charcoal. *Soil Biol. Biochem.* 43, 1615–1617. doi: 10.1016/j.soilbio.2011.03.027

Alexis, M. A., Rasse, D. P., Knicker, H., Anquetil, C., and Rumpel, C. (2012). Evolution of soil organic matter after prescribed fire: a 20-year chronosequence. *Geoderma* 189, 98–107. doi: 10.1016/j.geoderma.2012.05.003

Amelung, W., Brodowski, S., Sandhage-Hofmann, A., and Bol, R. (2008). Chapter 6: Combining biomarker with stable isotope analyses for assessing the transformation and turnover of soil organic matter. *Adv. Agron.* 100, 155–250. doi: 10.1016/S0065-2113(08)00606-8

Barré, P., Eglin, T., Christensen, B. T., Ciais, P., Houot, S., Kätterer, T., et al. (2010). Quantifying and isolating stable soil organic carbon using long-term bare fallow experiments. *Biogeosciences* 7, 3839–3850. doi: 10.5194/bg-7-3839-2010

Bird, M. I., Moyo, C., Veenendaal, E. M., Lloyd, J., and Frost, P. (1999). Stability of elemental carbon in a savanna soil. *Glob. Biogeochem. Cycles* 13, 923–932. doi: 10.1029/1999GB900067

Cardinael, R., Eglin, T., Guenet, B., Neill, C., Houot, S., and Chenu, C. (2015). Is priming effect a significant process for long-term SOC dynamics? Analysis of a 52-years old experiment. *Biogeochemistry* 123, 203–219. doi: 10.1007/s10533-014-0063-2

Ciais, P., Sabine, C., Bala, G., Bopp, L., Brovkin, V., Canadell, J., et al. (2013). "Carbon and other biogeochemical cycles," in *Climate Change 2013: The Physical Science Basis, Contribution of Working Group I to the Fifth Assessment Report of the Intergovernmental Panel on Climate Change*, eds T. F. Stocker, D. Qin, G. K. Plattner, M. Tignor, S. K. Allen, J. Boschung, A. Nauels, Y. Xia, V. Bex, and P. M. Midgley (Cambridge; New York, NY: Cambridge University Press).

Dignac, M.-F., Bahri, H., Rumpel, C., Rasse, D. P., Bardoux, G., Balesdent, J., et al. (2005). Carbon-13 natural abundance as a tool to study the dynamics of lignin monomers in soil: an appraisal at the Closeaux experimental field (France). *Geoderma* 128, 3–17. doi: 10.1016/j.geoderma.2004.12.022

Forbes, M. S., Raison, R. J., and Skjemstad, J. O. (2006). Formation, transformation and transport of black carbon (charcoal) in terrestrial and aquatic ecosystems. *Sci. Total Environ.* 370, 190–206. doi: 10.1016/j.scitotenv.2006.06.007

Glaser, B., Haumaier, L., Guggenberger, G., and Zech, W. (1998). Black carbon in soils: the use of benzenecarboxylic acids as specific markers. *Org. Geochem.* 29, 811–819. doi: 10.1016/S0146-6380(98)00194-6

Hammes, K., Schmidt, M. W. I., Smernik, R. J., Currie, L. A., Ball, W. P., Nguyen, T. H., et al. (2007). Comparison of quantification methods to measure fire-derived (black/elemental) carbon in soils and sediments using reference materials from soil, water, sediment and the atmosphere. *Glob. Biogeochem. Cycles* 21:GB3016. doi: 10.1029/2006GB002914

Harris, D., Horwáth, W. R., and van Kessel, C. (2001). Acid fumigation of soils to remove carbonates prior to total organic carbon or CARBON-13 isotopic analysis. *Soil Sci. Soc. Am. J.* 65:1853. doi: 10.2136/sssaj.2001.1853

IUSS Working Group WRB (2006). *World Reference Base for Soil Resources*. Rome: FAO.

Kuzyakov, Y. (2010). Priming effects: interactions between living and dead organic matter. *Soil Biol. Biochem.* 42, 1363–1371 doi: 10.1016/j.soilbio.2010.04.003

Lehmann, J., Abiven, S., Kleber, M., Genxing, P., Singh, B., Sohi, S., et al. (2015). "Persistence of biochar in soil," in *Biochar for Environmental Management*, eds J. Lehmann and S. Joseph (London; New York, NY: Routledge).

Lehmann, J., Skjemstad, J., Sohi, S., Carter, J., Barson, M., Falloon, P., et al. (2008). Australian climate–carbon cycle feedback reduced by soil black carbon. *Nat. Geosci.* 1, 832–835. doi: 10.1038/ngeo358

Lehndorff, E., Roth, P. J., Cao, Z. H., and Amelung, W. (2014). Black carbon accrual during 2000 years of paddy-rice and non-paddy cropping in the Yangtze River Delta, China. *Glob. Change Biol.* 20, 1968–1978. doi: 10.1111/gcb.12468

Maestrini, B., Abiven, S., Singh, N., Bird, J., Torn, M. S., and Schmidt, M. W. I. (2014). Carbon losses from pyrolysed and original wood in a forest soil under natural and increased N deposition. *Biogeosciences* 11, 5199–5213. doi: 10.5194/bg-11-5199-2014

Major, J., Lehmann, J., Rondon, M., and Goodale, C. (2010). Fate of soil-applied black carbon: downward migration, leaching and soil respiration. *Glob. Change Biol.* 16, 1366–1379. doi: 10.1111/j.1365-2486.2009.02044.x

Manzoni, S., Katul, G. G., and Porporato, A. (2009). Analysis of soil carbon transit times and age distributions using network theories, *J. Geophys. Res.* 114:G04025. doi: 10.1029/2009JG001070

Nguyen, B. T., Lehmann, J., Kinyangi, J., Smernik, R., Riha, S. J., and Engelhard, M. H. (2009). Long-term black carbon dynamics in cultivated soil. *Biogeochemistry* 92, 163–176. doi: 10.1007/s10533-008-9248-x

Paradelo, R., van Oort, F., and Chenu, C. (2013). Water-dispersible clay in bare fallow soils after 80 years of continuous fertilizer addition. *Geoderma* 200–201, 40–44. doi: 10.1016/j.geoderma.2013.01.014

Parton, W. J., Stewart, J. W. B., and Cole, C. V. (1988). 357 Dynamics of C, N, P and S in grassland soils: a model. *Biogeochemistry* 5, 109–131. doi: 10.1007/BF02180320

Rasse, D. P., Mulder, J., Moni, C., and Chenu, C. (2006). Carbon turnover kinetics with depth in a french loamy soil. *Soil Sci. Soc. Am. J.* 70:2097. doi: 10.2136/sssaj2006.0056

Reisser, M., Purves, R. S., Schmidt, M. W. I., and Abiven, S. (2016). Pyrogenic carbon in soils: a literature-based inventory and a global estimation of its content in soil organic carbon and stocks. *Front. Earth Sci.* 4:80. doi: 10.3389/feart.2016.00080

Rühlmann, J. (1999). A new approach to estimating the pool of stable organic matter in soil using data from long-term field experiments. *Plant Soil* 213, 149–160. doi: 10.1023/A:1004552016182

Schmidt, M. W. I., Skjemstad, J. O., and Jäger, C. (2002). Carbon isotope geochemistry and nanomorphology of soil black carbon: black chernozemic soils in central Europe originate from ancient biomass burning. *Glob. Biogeochem. Cycles* 16:1123. doi: 10.1029/2002GB001939

Schneider, M. P. W., Smittenberg, R. H., Dittmar, T., and Schmidt, M. W. I. (2011). Comparison of gas with liquid chromatography for the determination of benzenepolycarboxylic acids as molecular tracers of black carbon. *Org. Geochem.* 42, 275–282. doi: 10.1016/j.orggeochem.2011.01.003

Sierra, C. A., Müller, M., Metzler, H., Manzoni, S., and Trumbore, S. E. (2017). The muddle of ages, turnover, transit, and residence times in the carbon cycle. *Glob. Change Biol.* 23, 1763–1773. doi: 10.1111/gcb.13556

Singh, N., Abiven, S., Torn, M. S., and Schmidt, M. W. I. (2012a). Fire-derived organic carbon in soil turns over on a centennial scale. *Biogeosciences* 9, 2847–2857. doi: 10.5194/bg-9-2847-2012

Singh, B. P., Cowie, A. L., and Smernik, R. J. (2012b). Biochar carbon stability in a clayey soil as a function of feedstock and pyrolysis temperature. *Environ. Sci. Technol.* 46, 11770–11778. doi: 10.1021/es302545b

Vasilyeva, N. A., Abiven, S., Milanovskiy, E. Y., Hilf, M., Rizhkov, O. V., and Schmidt, M. W. I. (2011). Pyrogenic carbon quantity and quality unchanged after 55 years of organic matter depletion in a Chernozem. *Soil Biol. Biochem.* 43, 1985–1988. doi: 10.1016/j.soilbio.2011.05.015

Whitman, T., Enders, A., and Lehmann, J. (2014). Pyrogenic carbon additions to soil counteract positive priming of soil carbon mineralization by plants. *Soil Biol. Biochem.* 73, 33–41. doi: 10.1016/j.soilbio.2014.02.009

Wiedemeier, D. B., Abiven, S., Hockaday, W. C., Keiluweit, M., Kleber, M., Masiello, C. A., et al. (2015). Aromaticity and degree of aromatic condensation of char. *Org. Geochem.* 78, 135–143. doi: 10.1016/j.orggeochem.2014.10.002

Wiedemeier, D. B., Hilf, M. D., Smittenberg, R. H., Haberle, S. G., and Schmidt, M. W. I. (2013). Improved assessment of pyrogenic carbon quantity and quality in environmental samples by high-performance liquid chromatography. *J. Chromatogr. A* 1304, 246–250. doi: 10.1016/j.chroma.2013.06.012

Zimmerman, A. R. (2010). Abiotic and microbial oxidation of laboratory-produced black carbon (Biochar). *Environ. Sci. Technol.* 44, 1295–1301. doi: 10.1021/es903140c

**Conflict of Interest Statement:** The authors declare that the research was conducted in the absence of any commercial or financial relationships that could be construed as a potential conflict of interest.

frontiers in Earth Science

ORIGINAL RESEARCH
published: 31 August 2016
doi: 10.3389/feart.2016.00080

# Pyrogenic Carbon in Soils: A Literature-Based Inventory and a Global Estimation of Its Content in Soil Organic Carbon and Stocks

*Moritz Reisser, Ross S. Purves, Michael W. I. Schmidt and Samuel Abiven **

*Department of Geography, University of Zurich, Zurich, Switzerland*

Pyrogenic carbon (PyC) is considered one of the most stable components in soil and can represent more than 30% of total soil organic carbon (SOC). However, few estimates of global PyC stock or distribution exist and thus PyC is not included in any global carbon cycle models, despite its potential major relevance for the soil pool. To obtain a global picture, we reviewed the literature for published PyC content in SOC data. We generated the first PyC database including more than 560 measurements from 55 studies. Despite limitations due to heterogeneous distribution of the studied locations and gaps in the database, we were able to produce a worldwide PyC inventory. We found that global PyC represent on average 13.7% of the SOC and can be even up to 60%, making it one of the largest groups of identifiable compounds in soil, together with polysaccharides. We observed a consistent range of PyC content in SOC, despite the diverse methods of quantification. We tested the PyC content against different environmental explanatory variables: fire and land use (fire characteristics, land use, net primary productivity), climate (temperature, precipitation, climatic zones, altitude), and pedogenic properties (clay content, pH, SOC content). Surprisingly, soil properties explain PyC content the most. Soils with clay content higher than 50% contain significantly more PyC (>30% of the SOC) than with clay content lower than 5% (<6% of the SOC). Alkaline soils contain at least 50% more PyC than acidic soils. Furthermore, climatic conditions, represented by climatic zone or mean temperature or precipitation, correlate significantly with the PyC content. By contrast, fire characteristics could only explain PyC content, if site-specific information was available. Datasets derived from remote sensing did not explain the PyC content. To show the potential of this database, we used it in combination with other global datasets to create a global worldwide PyC content and a stock estimation, which resulted in around 200 Pg PyC for the uppermost 2 m. These modeled estimates indicated a clear mismatch between the location of the current PyC studies and the geographical zones where we expect high PyC stocks.

**Keywords: fire derived organic matter, pyrogenic carbon, soil organic matter stabilization processes, database, global distribution, soil organic carbon, global carbon cycle**

OPEN ACCESS

***Edited by:***
*Francien Peterse,*
*Utrecht University, Netherlands*

***Reviewed by:***
*Philippa Louise Ascough,*
*Scottish Universities Environmental Research Centre, UK*
*Stefan Doerr,*
*Swansea University, UK*

****Correspondence:***
*Samuel Abiven*
*samuel.abiven@geo.uzh.ch*

***Specialty section:***
*This article was submitted to Biogeoscience, a section of the journal Frontiers in Earth Science*

***Received:*** *30 May 2016*
***Accepted:*** *08 August 2016*
***Published:*** *31 August 2016*

***Citation:***
*Reisser M, Purves RS, Schmidt MWI and Abiven S (2016) Pyrogenic Carbon in Soils: A Literature-Based Inventory and a Global Estimation of Its Content in Soil Organic Carbon and Stocks. Front. Earth Sci. 4:80. doi: 10.3389/feart.2016.00080*

## INTRODUCTION

Fires affect about 4.64 million $km^2$ of biomass per year, corresponding to about 4% of the earth's vegetated surface (Randerson et al., 2012). A major part of the carbon involved in these vegetation fires is emitted as $CO_2$ into the atmosphere, yet recent studies suggest up to 15% of fire affected biomass (Santín et al., 2015) is converted into pyrogenic organic carbon (PyC; also known as fire-derived organic matter, charcoal or black carbon, Hammes and Abiven, 2013). This PyC has particular features: high relative carbon content, high chemical aromaticity, a comparably long mean residence time in the soil ranging from decades to millennia (Singh et al., 2012) and, under certain circumstances, it may have a variety of positive effects on soil properties e.g., increasing pH, water retention capacity, or nutrient availability and the retention of pollutants (Biederman and Harpole, 2013; Crane-Droesch et al., 2013). Due to these positive effects, PyC has been intentionally produced and deployed as a soil amendment, better known as biochar.

PyC is found ubiquitously in the environment (Preston and Schmidt, 2006) and soils play a key role in the PyC cycle since PyC is first deposited at the soil surface. From there, it may either physically erode, get transported by wind or water and leave the soil system or fragment into smaller pieces (Pignatello et al., 2015) and move down the soil profile where it can age, react and alter chemically and physically before being transferred to other potential pools including rivers, oceans, or sediments (Bird et al., 2015; Santín et al., 2016).

PyC content in the SOC has been approximated to represent between 0 and 35% of the total soil organic carbon (SOC; Forbes et al., 2006), but up to now, there have been few attempts to estimate complete global PyC stocks in soil. Bird et al. (2015) calculated a pool of 54–109 Pg of PyC in soil (0–100 cm depth), based on a series of assumptions regarding the PyC content in the total SOC depending on ecosystem. Santín et al. (2016) calculated a pool of 71–212 Pg of C, based on the assumption that PyC represents 5–15% of the SOC, multiplied by global SOC stocks. In both cases, the calculated amount of PyC is very sensitive to the percentage of PyC to SOC. This proportion is however unknown, and may vary as a function of not only ecosystem type (Bird et al., 2015), but also soil properties, fire characteristics, type of biomass, or climatic conditions. To date PyC distribution across ecosystems or types of soil remains unknown and furthermore we have limited knowledge as to the main parameters controlling the content of PyC in SOC.

Nonetheless, it is possible to distinguish three main groups of parameters likely to influence the PyC content in a given soil: (i) **fire and land use**: the inputs to the soil, which may vary, based on the amount and type of burning biomass, or the frequency, return interval and intensity of fires—this might further depend on the climatic zones and available feedstock but also on the land use; (ii) **climatic**: the climatic conditions, such as average temperature and moisture, which may influence decomposition or preservation patterns of PyC; (iii) **pedogenic**: the inherent physical and chemical soil parameters, including clay content and pH, play a role on the decomposition and the stabilization processes of PyC as well as the topography, which has impact on erosion rates or accumulation of PyC.

In this study, we reviewed the literature reporting content of PyC in SOC and analyzed these values as functions of these three drivers (fire and land use, climatic, and pedogenic). Our aims were: (1) to calculate the PyC stocks in soils based on published data, (2) to investigate which of the three main drivers has the largest influence on the PyC content in SOC, and (3) to show a possible application of our database, by using it in combination with other global datasets to create a global estimation of PyC contents and stocks.

## MATERIALS AND METHODS

### Data Collection

The database was extracted from articles selected using the keywords "black carbon," "charcoal," "pyrogenic organic matter," "fire-derived carbon" associated to "soil" in Google scholar and Web of Science (last search June 2015). Since our focus was on natural fire-derived organic matter, we excluded obvious cases where PyOM was added as a soil amendment (e.g., biochar) or was found as archaeological residue (e.g., hearths). We also discarded datasets where the sampling procedure was not described, the raw data not given or PyC only qualitatively described but not quantitatively. Using these criteria, we were able to collect 569 individual values, from 55 articles.

Values of PyC were reported as PyC mass % of the total SOC. When the stocks were reported, we calculated the concentration from the SOC and bulk density data. We chose to report the PyC content in SOC instead of stocks, because only 31% of the studies we collected reported PyC stock data or the bulk density values, which would be needed for stock estimations (**Table 1**).

In addition to the PyC content, we collected information corresponding to the three main drivers (fire and land use, climatic, and pedogenic). These drivers-related data were extracted directly from the articles or, if not reported, derived

**TABLE 1 | Literature extracted database description.**

| Parameter | Data reported [%] | 1st quartile | Median | Mean | 3rd quartile |
|---|---|---|---|---|---|
| Pyrome | 92.2 | – | – | – | – |
| Vegetation | 91.7 | – | – | – | – |
| SOC [wt%] | 88.1 | 1.14 | 2.46 | 4.19 | 5.63 |
| Precipitation [mm $m^{-2}$ $yr^{-1}$] | 86.6 | 510 | 843 | 1068 | 1618 |
| Temperature [°C] | 80.2 | 7 | 10 | 10.8 | 14.8 |
| pH | 52.1 | 4.8 | 5.7 | 5.9 | 6.8 |
| BDD [g $dm^{-3}$] | 31.1 | 0.67 | 0.94 | 0.96 | 1.25 |
| Clay [wt%] | 23.1 | 8 | 19.25 | 22.2 | 30 |
| Fire frequency [$yr^{-1}$] or qualitative | 12.1 | – | – | – | – |

*For each parameter, we report the number of data reported as percent of the global database (n = 569), the first and third quartile, as well as the median and the mean values.*

from other sources. **Table 2** summarizes datasets, references, and assumptions used to complete the database.

We included the altitude using the World Elevation Service of ESRI© (ESRI, 2016), which is derived from the GMTED2010 data set (Danielson and Gesch, 2011). Remote sensing data were used to associate Köppen-Geiger climate zone (KG; Rubel and Kottek, 2010), net primary productivity (from the NASA NPP dataset) and the fire regime, based on the concept of pyromes, as proposed by Archibald et al. (2013), including also the raw fire return interval (FRI) and fire-frequency data to our dataset. According to this pyrome concept, the terrestrial ecosystems are divided into five different zones characterized by fire intensity and return interval: frequent intense large (FIL), frequent cool small (FCS), rare intense large (RIL), rare cool small (RCS), and intermediate cool small (ICS). Frequent occurrence corresponds to annual fires, while rare occurrence corresponds to a return period of more than 50 years. The intensity is based on the fire radiative power. Small fires correspond to areas smaller than 25 $km^2$, while large fires correspond to areas larger than 100 $km^2$. When existing in the article, we also added the on-site fire frequency, but fire history was not consistently reported in the literature. In some cases, only qualitative information was given (e.g., "high" or "low"). All data were transformed to these nominal categories as follow: less than every 10 years = high; 10–100 years = medium; less fires than every 1000 years = low.

We also included the land use (forest, grassland, agriculture, peatland, urban, shrubland) from the NASA MODIS land cover product, the mean annual precipitation (MAP) and mean annual air temperature (MAT), soil type, bulk density, sampling depth, SOC the clay content, and soil pH. All these parameters were extracted directly from the articles, or from reference datasets (**Table 2**).

Soil depth was distinguished into top- and subsoil, where topsoil was defined as the uppermost 10 cm and subsoil as soil horizon below this limit. There was no significant difference (95% confidence interval) between these two soil depths so the data set was analyzed considering the whole soil profile. In order to compare continuous and discrete variables, parameters were categorized into 5–7 groups according their initial distribution.

## Representativeness of the Dataset

The percentage of data available in the database as well as the median, average and the quartile values for continuous data are given for each parameter in **Table 1**. The vegetation related parameters are well represented in the database, while soil parameters were present in <50% of the studies. Local fire history was indicated in only 12% of studies. Interpretation of patterns can be strongly limited, depending on this availability of local data.

**TABLE 2 | Datasets used to fill missing values or add additional investigated variables.**

| Variable | Extraction method | Data source | Limitations | References | Usage (inventory = *; PyC evaluation = §) |
|---|---|---|---|---|---|
| Mean Annual Precipitation (MAP) | Join attributes by coordinates | Precipitation map | Only mean, no variability included | New et al., 2002 | *§ |
| Mean Annual Temperature (MAT) | Join attributes by coordinates | Temperature map | Only mean, no variability included | | *§ |
| Köppen-Geiger Zone (KG) | Join attributes by coordinates | Köppen-Geiger map | Strongly generalized | Kottek et al., 2006 | * |
| Altitude | World Elevation Service of ESRI | USGS GTOPO 30 and SRTM 90 m | No information on relief and interpolated | ESRI, 2016 | * |
| Clay content | Join attributes by coordinates | HWSD | Interpolated and modeled data | FAO/IIASA/ISRIC/ISSCAS/JRC, 2012 | § |
| pH | Join attributes by coordinates | HWSD | Interpolated and modeled data | | § |
| Soil Organic Carbon content (SOC) | Join attributes by coordinates | HWSD | Interpolated and modeled data | | § |
| Bulk Dry Density (BDD) | Join attributes by coordinates | HWSD | Interpolated and modeled data | | § |
| Pyrome | Join attributes by coordinates | Pyrome dataset | Only a concept | Archibald et al., 2013 | *§ |
| Fire frequency | Join attributes by coordinates | Pyrome dataset | Data since two decades | | * |
| Fire intensity | Join attributes by coordinates | Pyrome dataset | Data since two decades; resolution of acquisition and fires do not match at all. | | * |
| Net primary productivity | Join attributes by coordinates | NASA npp dataset | Modeled data, derived from proxies | Zhao et al., 2005 | * |
| Land use | Join attributes by coordinates | NASA land cover dataset | Derived from proxies | Friedl et al., 2010 | *§ |

*HWSD is the harmonized world soil database.*

The distribution of each parameter in the dataset was compared to its worldwide distribution extracted from a reference database [i.e., soil parameters like pH, clay content, and SOC content from the harmonized world soil database (FAO/IIASA/ISRIC/ISSCAS/JRC, 2012) and the pyromes from Archibald et al. (2013)]. The distribution histograms are present in **Figures 5**, **6**.

## Quantification of PyC

A wide variety of methods exist to quantify the PyC in soil. It has been shown in the past that these methods do not always yield the same results for a given sample (Schmidt et al., 2001; Hammes et al., 2007). In this work, we considered six major different methods:

(i) Physical method: simple visual assessment (charcoal pieces counting), generally done with the naked eye or under microscope und mostly preceded by a physical separation step (for example flotation);
(ii) Chemo-thermal oxidation method (CTO 375; Gustafsson et al., 1997, 2001): the soil sample is exposed to strong oxidants, mainly trifluoroacetic acid and HCl and heated up to 375°C in an oven. This method includes a decarbonization step, which can be conducted after (Gustafsson et al., 1997) or before (Gustafsson et al., 2001; Bucheli et al., 2004) the thermal treatment. Both versions of the methods were accepted in this work. Quantification of the PyC residual is usually done by elemental analysis.
(iii) Dichromate oxidation method: the soil is treated with $K_2Cr_20_7$, a very strong oxidant, which is supposed to oxidize all labile organic carbon and the residual is considered oxidation resistant elemental carbon (OREC; Bird et al., 1999). These OREC values are also quantified with an elemental analyser and are multiplied by 2.36, using the factor proposed by Knicker et al. (2008);
(iv) Benzenepolycarboxylic acid (BPCA) molecular marker method, initially developed by Glaser et al. (1998). In this method, PyC is broken down with help of $HNO_3$ into specific BPCAs, which can be quantified with either gas or liquid chromatography (Schneider et al., 2011; Wiedemeier et al., 2013) using a standard. The conversion factor of 2.27 (Glaser et al., 1998) was used to calculate the actual PyC;
(v) UV oxidation: PyC is considered as the organic residues after a strong UV irradiation treatment. Quantification is achieved by comparison of the material before and after treatment, using solid-state $^{13}C$ nuclear magnetic resonance (NMR) spectroscopy (Skjemstad et al., 1996).
(vi) NMR method: the PyC content in SOC is estimated directly from the NMR spectrum, using a mixing model (Nelson and Baldock, 2005), without any chemical or physical separation step.

Any other reported methods were grouped under the label "others."

## Statistical Analysis

All continuous variables, except MAP and MAT, were grouped into five to seven groups, in order to allow the comparison of the database with to global distributions. Grouping was done according to relevant physical thresholds for each parameter and aiming for a balanced grouping, i.e., roughly the same number of points in each group. Data were log transformed to conform them to normality. These variables were tested with a One-Way ANOVA using R statistics (R Core Team, 2015) against the PyC concentration as a percentage of SOC. We conducted Student-Newman-Keuls *post-hoc* tests in order to compare groups with each other (difference tested for $p < 0.05$). MAT and MAP were tested with Spearman's rank correlation ρ.

## Case Study: Global Evaluation of the PyC Content and Stocks

In order to show the potential of our database, we created a linear model in combination with other existing global datasets for a global evaluation of PyC content in SOC and stocks. First, we filled the missing values in the dataset with values from the global datasets by joining the attributes in QGIS© (QGIS Development Team, 2015): clay, pH, and SOC with the harmonized world soil database (FAO/IIASA/ISRIC/ISSCAS/JRC, 2012), a temperature and precipitation dataset (New et al., 2002), the land cover dataset from NASA (Friedl et al., 2010), and the fire-frequency dataset of Archibald et al. (2013). Dataset description and related assumptions are compiled in **Table 2**.

A linear model was then fitted on this extended database using R. After simplification, the model corresponded to the Equation (1):

$$\log(\text{PyC}) = \text{clay} + \text{pH} + \text{MAP} + \text{MAT} + \text{land use} + \varepsilon \quad (1)$$

Where PyC is the PyC content as % of SOC, clay the % of clay in soils, pH the pH of the soil, MAP the mean annual precipitation from the database, extracted as described above, MAT the mean annual temperature from the database, extracted as described above, land use the different categories of land use in the database and ε the error term, which accounts for the variability which can't be explained by the considered variables.

Together, the variables explained 33% of the total variance in the dataset (more detailed statistics are shown in **Table 3**). We then applied this model to predict the PyC content in SOC at a resolution of 20 km to produce a global map. PyC stocks were calculated by multiplying the values with the bulk dry density (BDD) and SOC content. As the maximum depth of the used soil parameters was 200 cm, the model does not predict anything deeper than these 200 cm.

# RESULTS

## PyC Content in the SOC

**Figure 1** presents the PyC content distribution histogram from our literature database. Values range between 0 and 50% with one outlier above 60% (Caria et al., 2011): first quartile at 5.2%, median 12.3%, third quartile 18.6%, and the arithmetic mean at 13.7%.

**TABLE 3 | Summary of the model statistics used for the global evaluation.**

| Residuals | | | | | |
|---|---|---|---|---|---|
| **Min** | **1st Quartile** | **Median** | **3rd Quartile** | **Max** | |
| −4.8932 | −0.4427 | 0.0455 | 0.5346 | 2.4265 | |
| **Coefficients** | | | | | |
| | **Estimate** | **Std. Error** | ***t*-value** | **Pr(>\|t\|)** | **Lvl of signif.** |
| (Intercept) | 2.34 | 0.56 | 4.17 | 3.70E-05 | *** |
| clay 0–5% | −1.00 | 0.42 | −2.40 | 0.017 | * |
| clay 5–10% | −1.04 | 0.39 | −2.71 | 0.007 | ** |
| clay 10–25% | −0.87 | 0.36 | −2.41 | 0.016 | * |
| clay 25–50% | −0.61 | 0.36 | −1.67 | 0.095 | · |
| pH 4–5% | 0.16 | 0.28 | 0.57 | 0.568 | |
| pH 5–6% | 0.48 | 0.26 | 1.84 | 0.067 | · |
| pH 6–7% | 0.45 | 0.28 | 1.59 | 0.113 | |
| pH >7% | 0.77 | 0.28 | 2.80 | 0.005 | ** |
| MAP 0–600 | −0.38 | 0.19 | −1.96 | 0.051 | · |
| MAP 601–1200 | −0.55 | 0.18 | −3.09 | 0.002 | ** |
| MAP 1201–1800 | −0.76 | 0.19 | −3.90 | 0.000 | *** |
| MAP 1801–2400 | 0.44 | 0.21 | 2.06 | 0.040 | * |
| MAT 0–7.5° | 0.89 | 0.25 | 3.51 | 0.000 | *** |
| MAT 15–22.5° | 0.77 | 0.28 | 2.75 | 0.006 | ** |
| MAT 7.5–15° | 0.91 | 0.24 | 3.74 | 0.000 | *** |
| MAT > 22.5° | 0.87 | 0.30 | 2.94 | 0.003 | ** |
| Forest | −0.40 | 0.14 | −2.95 | 0.003 | ** |
| Grass | −0.28 | 0.10 | −2.65 | 0.008 | ** |
| Peat | 0.07 | 0.33 | 0.22 | 0.825 | |
| Shrub land | −0.77 | 0.23 | −3.26 | 0.001 | ** |
| Urban | −1.00 | 0.22 | −4.60 | 5.47E-06 | *** |

*Signif. codes: 0 < "***" < 0.001 < "**" < 0.01 < "*" < 0.05 < "." < 0.1 < " " < 1.*
*Residual standard error: 0.844 on 467 degrees of freedom.*
*Multiple R-squared: 0.3587; Adjusted R-squared: 0.3298.*
*F-statistic: 12.44 on 21 and 467 DF. p < 2.2e-16.*

## Method Comparison and Data Representativeness

As described above, the diversity of quantification methods existing in the literature may induce bias in the collected data on PyC content in SOC. **Figure 2** presents the PyC values according to the analytical method used to determine the PyC content in the soil samples. The $K_2Cr_2O_7$ oxidation, the NMR, and the UV oxidation methods present significantly higher values (16.9, 17.6, and 17.6% in average, respectively; $p < 0.001$) than the BPCA (11.3%), CTO 375 (12.5%), and the physical approaches (10.1%). These differences are in line with the literature focussing on method comparisons (Hammes et al., 2007; Bird, 2014), with however, much smaller variations in than in these systematic comparison. In these previous studies, content of PyC in SOC varied by several factors of magnitude depending on the type of sample analyzed. Here the differences, observed for different samples, are on average only of few per cent. For all the methods except NMR, the range of PyC measured is large, from about 0 to more than 30% in all cases, meaning that all the methods are able to detect very low and very high levels of PyC. So, despite small variations, we consider that the choice of the quantifying method does not play a major role in the database analysis.

Another issue concerns the spatial representativity of the database. **Figure 3** presents the world wide geographical distribution of the sites from which the literature data were collected. Africa, central Russia, high latitudes, and southwest Asia are almost absent of the database, while Europe and North America are heavily represented. The PyC content does not seem to be related to large-scale spatial patterns: for example within Europe a very large range of PyC values can be observed (data not shown). This heterogeneity is a clear weakness of this database and more generally of the literature related to PyC in soils.

## PyC Content in the SOC As a Function of Fire Characteristics

**Figure 4** presents the content of PyC in SOC as a function of the fire intensity and -frequency, defined by the pyrome concept (a), the global FRI dataset (b), or the local fire frequency, for a subset of samples where this information was available ($n = 64$, less than 12% of the whole dataset) (c).

Surprisingly, almost no difference was observed between pyromes. Despite clear fire characteristic differences in terms of fire return period and intensity, the resulting PyC contents in SOC were very similar between the different pyromes. The only difference was observed for the zone with frequent, large and intense fires (FIL), where lower PyC contents were observed (4.8%).

The PyC content in SOC is also not related to the global FRI. Values range from 12.1% in regions with very long FRIs to 14.3% in regions with very frequent fires. This may be due to the resolution (1 km) of the FRI dataset, which may not capture local fire properties.

When the site has a clear reported fire history, the fire frequency has a significant effect ($p < 0.001\%$) on the PyC content (**Figure 4C**). Sites with high frequency contain about twice the PyC, 24.4%, compared to values of 9.2 and 4.5% respectively for medium and low fire frequencies.

## PyC Content in the SOC As a Function of Land Use

The highest content of PyC in SOC was found in soils used for agriculture (16.0%; **Figure 5**). The corresponding samples were not only collected on sites where traditional slash and burn-like techniques are still in use, but also in Europe and North America, where this specific technique has not been widely used as an agricultural practice for at least a century (Peters and Neuenschwander, 1988; Wiedner and Glaser, 2015). The PyC content is lower in grasslands and forests than in agricultural land, with forests presenting the lowest content of PyC in SOC of all the land use types (9.7%). Grassland PyC content was slightly higher with a mean of 12.1%. Peatland and urban land uses had values of 12.3 and 10.8% respectively.

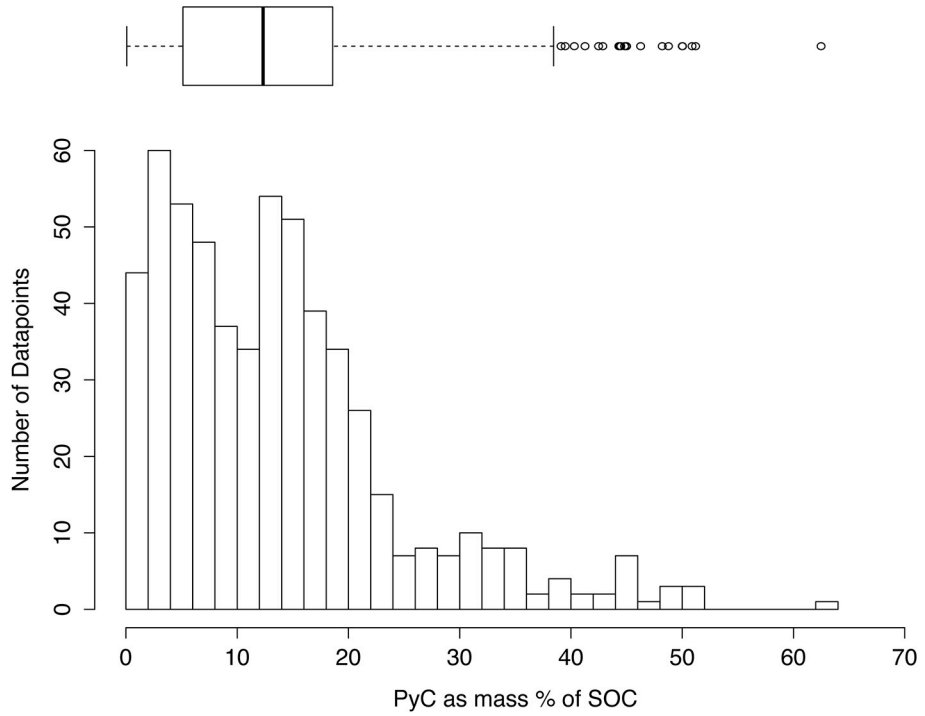


**FIGURE 1 | Frequency histogram of PyC content as mass % of the total SOC for the entire database ($n = 569$).** Each column represents an increment of 2% of the PyC content.

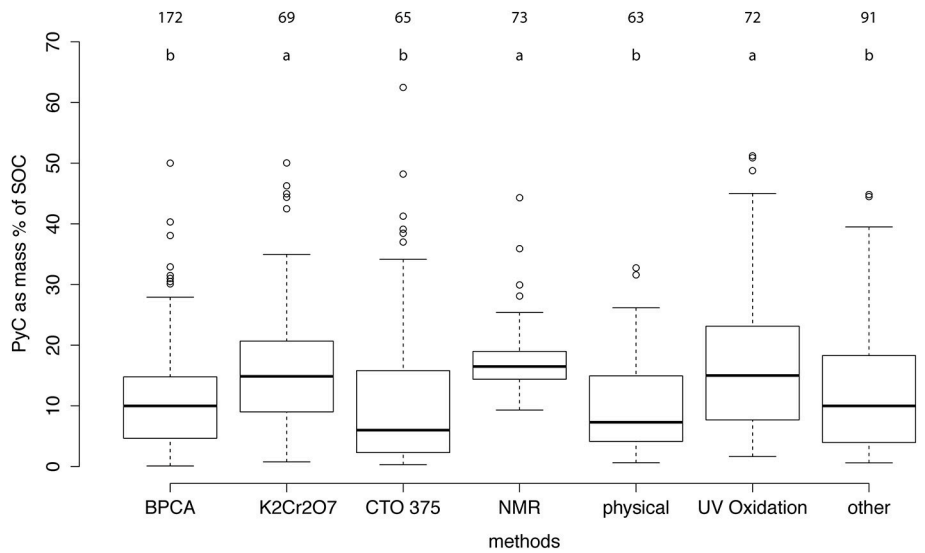


**FIGURE 2 | PyC content as mass % of the total SOC as a function of the methods used in the literature database and their respective PyC content distribution as mass % of total SOC.** One-Way-ANOVA for the methods results in a $p < 0.001$. The different letters on the top indicate significant differences ($p < 0.05$ TukeyHSD test) between the methods.

## PyC Content in the SOC As a Function of the Climatic Conditions

Content of PyC in SOC does not follow a consistent trend when compared to the annual precipitation (**Figure 6A**). Dry and wet sites show similar PyC content in the SOC. Spearman's correlation coefficient was very low ($\rho = -0.02$). We observe a clearer trend for mean annual temperatures (**Figure 6B**). Colder sites (especially below 0°C) present lower PyC content


**FIGURE 3 | Spatial distribution of the PyC values which were published and taken into account in our database.**

than warmer sites with a maximum around 10°C, even slightly decreasing toward warmer temperatures. Here, a clear correlation could be found ($\rho = 0.33$; $p < 0.0001$). This positive temperature effect can be related to different factors: biomass productivity promoted by higher temperature, higher probability of fires starting under warmer conditions or/and higher decomposition rate of PyC in the soil in warmer climate zones, compared to colder zones.

**Figure 7** shows the content of PyC in SOC as a function of the KG climate zone. The highest PyC content is found in the equatorial (16.8%) temperate (15.5%) and desertic zones (12.7%). These three systems are significantly richer in PyC ($p < 0.001\%$) than the continental (8.9%) and the polar zones (4.4%), respectively and mirror the trends observed in the temperature data, above all for the polar sites, where low PyC content coincides with very little fire, slow decomposition and possible break down, due to freeze-thawing. The database has generally a representative distribution in the KG zones, except for the temperate zone (over-represented) and the polar zone (under-represented).

## PyC Content in the SOC As a Function of the Soil Characteristics

The content of PyC in SOC seems to be more directly related to the soil properties. First, PyC content in the SOC is significantly related ($p < 0.001\%$) to the clay content (**Figure 8A**). When the clay content is higher than 50%, the PyC content was on average more than twice that of lower clay contents (32.7% compared to 12–14%). When the clay content of the soil was between 0 and 5%, then the PyC content was much lower (5.7%). Our database represents relatively well the clay content distribution worldwide (as described by the harmonized world soil database), with the notable exception of an underrepresentation of low clay content soils.

Soil pH also has a statistically significant ($p < 0.001\%$) and large effect on the PyC content in SOC (**Figure 8B**): a pH above 7 translates into larger PyC content than between 6 and 7 (21 vs. 14.9%), and acid soils (below 5) contained much less PyC (8.6–11.7%).

The overall SOC content seems to have also an influence on its relative PyC proportion (**Figure 8C**). Soils with low SOC content (0–0.1% and to a lesser extent 0.1–0.5%) have a significantly ($p < 0.01\%$) higher PyC content in its SOC than SOC-rich soils. However, the distribution of our database favors high SOC content and the number of samples with low SOC content is relatively low compared to the global distribution.

# DISCUSSION

## PyC Content in the SOC

Our large collection of data is globally in line with previous estimations of the content of PyC in the SOC. We observed a mean of 13.7% of the SOC, ranging from 0 to 60%, while previous estimations ranged from 0 to 35% (Forbes et al., 2006; Bird et al., 2015; Santín et al., 2016).

Compared to other specific identified compounds in soils, PyC seems to be a major contributor to the SOC: lignin content ranges only between 0 and 6%, with an average around 1.5% of the SOC (review of 27 studies by Thevenot et al., 2010); soil lipids rarely exceed 2% of the SOC (Dinel et al., 1990); carbohydrates have a comparable distribution (5–20%; Lowe, 1978), however very few recent estimates exist for the latter two groups of compounds.

In comparison to the above mentioned compounds, fire-derived organic matter enters the soil usually only sporadically and in relative small quantities (the biomass transformation rate

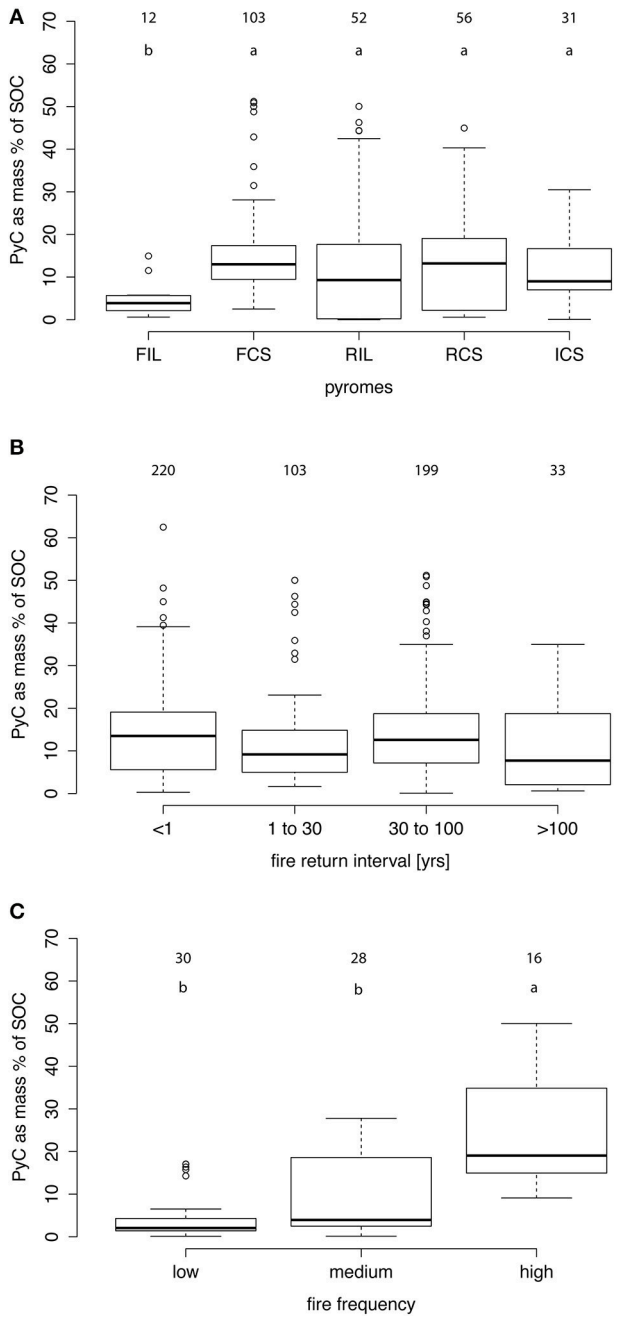


**FIGURE 4 | PyC content as mass % of the total SOC described by fire parameters: the pyromes of Archibald et al. (2013) (A); global fire return interval (B); on-site fire-frequency information (C).** One-Way-ANOVA results in $p < 0.001$, <0.001, and 0.19 for the pyromes, the global fire return interval, and on-site fire frequency, respectively. The different letters on the top indicate significant differences ($p < 0.05$) within the datasets.

to PyC is estimated to be around 1–26% during a fire; Czimczik et al., 2003; Forbes et al., 2006; Eckmeier et al., 2007; Santín et al., 2015), compared to lignin which represents a continuous or seasonal input of >20% of the litter (Thevenot et al., 2010) to the SOC.

## Drivers Explaining PyC Content in the SOC

Our analysis of the content of PyC in SOC drivers leads to an unexpected new picture on PyC distribution in soils. Fire characteristics as reported here do not seem to play a major role in the constitution of a PyC stock. Neither pyromes nor the FRI can explain the PyC content patterns. The only significant factor corresponds to very intense fires at a local scale, indicating, that fire impacts can be seen only very locally. Land use also gives an interesting picture: higher contents of PyC in the SOC in agricultural soils than in grassland and forests, respectively. On the other hand, the PyC content variations correlated very well with soil properties, i.e., higher clay and pH lead to high PyC%.

Soil properties clearly define conditions for stabilization of PyC. Higher clay content might lead to more organo-mineral interactions (Sørensen, 1972; Merckx et al., 1985; Hassink, 1997; Six et al., 2002) and higher pH to less decomposition of PyC in general. Archaeologists usually use the pH as a parameter to identify sites where charcoal remains may be found (Braadbaart et al., 2009), well in accordance with our observations. Fresh organic matter decomposes slower at low (5.0) and high (8.0) pH (DeLaune et al., 1981). However, soil respiration tends to be higher at high pH than at low pH (Kemmitt et al., 2006; Aciego Pietri and Brookes, 2008), indicating that alkaline conditions do not always imply a lower microbial activity. In a manipulative experiment, Braadbaart et al. (2009) observed an increase in the charcoal fragmentation in alkaline solutions, probably because of the cation ($Ca^{2+}$ and $K^{+}$) transfer inside the graphitic structure of the charcoal pieces. These smaller particles may be easier to stabilize on the long term, since they can bind more directly to minerals in finer fractions of the soil (Nocentini et al., 2010).

However, the three types of drivers we identified earlier cannot be exactly compared. Both spatial and temporal scales are problematic for information related to land use, fire characteristics, or even climate. These parameters may vary greatly over the time, particularly at the time scale we are considering here. Several authors reviewed the literature related to PyC turnover in soil and the estimates vary between 100 and 1000 years (Preston and Schmidt, 2006; Lehmann et al., 2008; Liang et al., 2008; Singh et al., 2012). At this time scale, information on fire frequency and intensity, land use or climate may vary greatly, while PyC in the soils remains relatively unchanged over long timescales. This all indicates, that we may see a temporal mismatch between our measured PyC and its predictors with which we try to explain it. For example, the higher content of PyC in the SOC in agricultural land might not be explained by the recent land use, but could be linked to stubble burning in the last century, or even much older agricultural practices from the Middle Ages or earlier, which may have included much more common use of fire. Another explanation might be the relative preservation of PyC due to increased SOC turnover by tillage and generally agricultural practices. Yet, one might also speculate that PyC-rich soils, being more fertile, have been turned into agricultural land more often than other lands, and thus that we would observe a feedback between PyC stocks and land-use over long time scales.

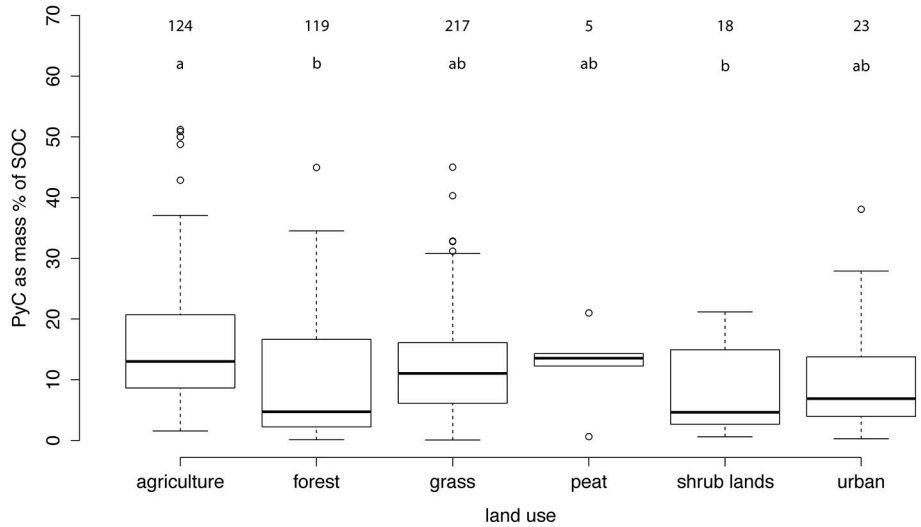


**FIGURE 5 | PyC content in % as mass of the total SOC described by different land use types.** One-Way-ANOVA results in $p < 0.001$. The different letters on the top indicate the significant differences ($p < 0.05$) between the different land uses.

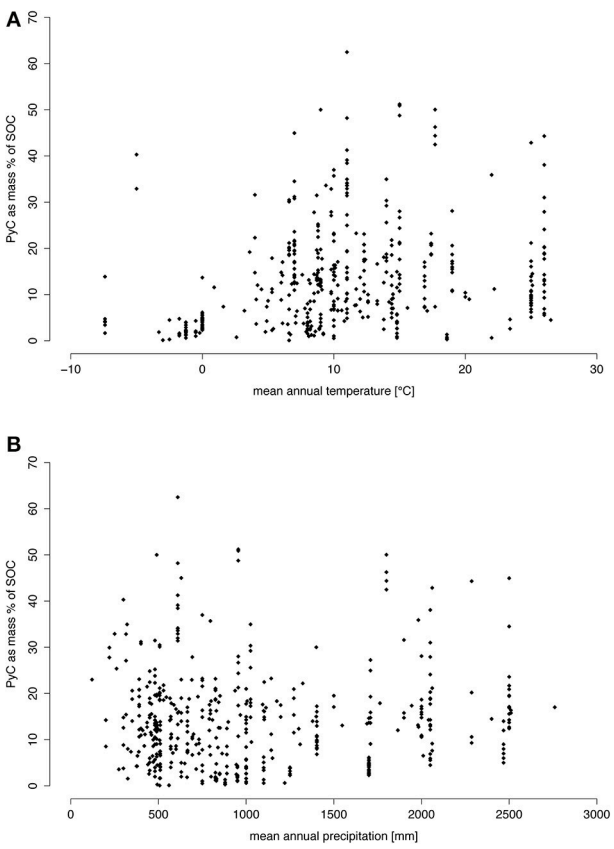


**FIGURE 6 | PyC content as mass % of the total SOC plotted against climatic variables: mean annual precipitation (A) and mean annual temperature (B).** Spearman's rank correlation yielded a $p$-value of 0.66 and a rho of −0.02 for the precipitation and a $p < 0.001$ with a rho of 0.33 for the temperature.

Fire frequency derived from remotely sensed satellite data cannot cover more than the last two decades, due to the availability of data (Dwyer et al., 2000; Archibald et al., 2013; Bowman et al., 2014). Furthermore, the spatial resolution of the data does most often not mirror the natural heterogeneity of fires very well. Even if only parts of a pixel burn, it is stated that this specific pixel burnt. However, one might still find places in this pixel, which were not affected by fire at all.

When the history of fire is known for a given place, the fire frequency is more relevant.

Compared to fire characteristics, land use or even climate, soil properties are relatively constant and are more integrative of the time where PyC effectively spent in the soil. It may be a reason why soil parameters appear particularly relevant for the PyC content.

## CASE STUDY: GLOBAL EVALUATION OF THE PYC CONTENTS IN THE SOC AND STOCKS

### Observations

Modeled PyC values are slightly lower than the literature dataset (**Figure 1**). The mean is 8.7%, the median is 7.5% with the first quartile at 5.8% and the third quartile at 10.5%. This is unexpected, since the five parameters in the model are relatively well distributed in the initial database, so we expected modeled values closer to the literature. One consequence might be that either the model underestimates the total content of PyC in the SOC or the database rather overestimates it.

**Figure 9** shows the maps for the global PyC content in total SOC and **Figure 10** for the stocks. Highest PyC contents are found mostly in the large steppe regions of between around 23° and 50° north, as well as in Patagonia and in

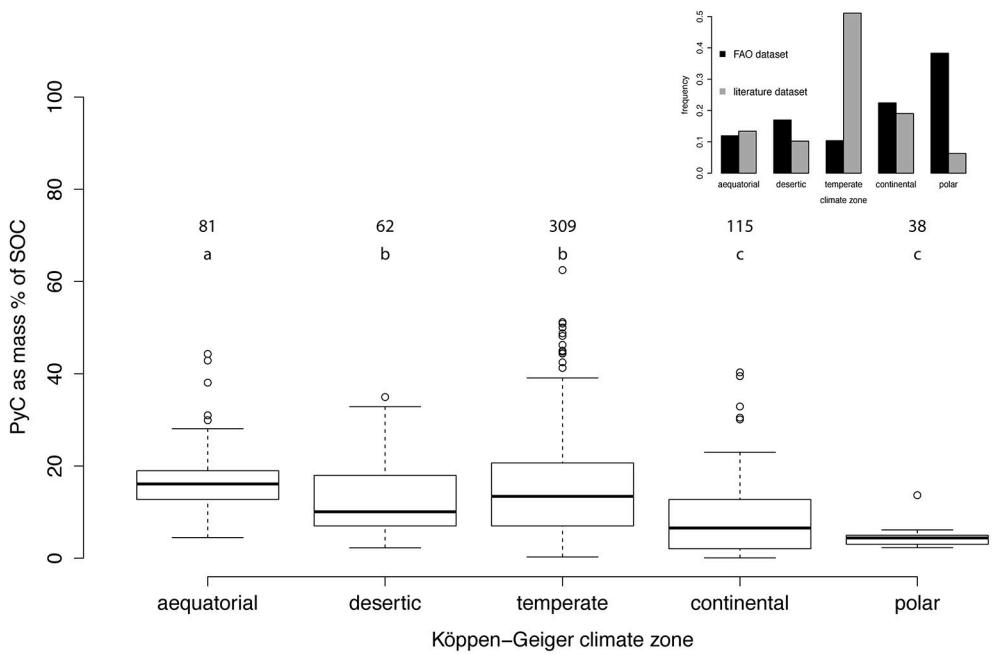


**FIGURE 7 | PyC content as mass % of the total SOC as a function of the climatic zone.** Only the five KG supergroups were used. Equatorial relates to all groups starting with a A in the KG classification, desertic with a B, temperate with a C, continental with a D and polar with a E. The One-Way-ANOVA resulted in a $p < 0.001$. The different letters on the top indicate the significant differences ($p < 0.05$) between the different KG zones.

tropical rainforests. These high values could be explained for a large part by the pH and clay content of the soils, two of the five parameters of the model. Lowest concentrations are above all situated in boreal regions on the northern hemisphere.

The picture changes radically in most regions when it comes to stocks. Very high PyC stocks are found in the boreal zones. PyC contents in the SOC are low in boreal areas but SOC stocks are very important, while in some other regions PyC contents are high, for example in Australia, Africa, and the Indian subcontinent, but the SOC stocks are much lower and thus the PyC stocks are also low. In tropical regions, both the content of PyC in the SOC as well as the SOC stocks are high. Global PyC stock is estimated, based on the integration of all values to be roughly around 200 Pg.

## Limitations and Perspectives

Based on a large data collection from the literature, we propose here the first global estimation of PyC content as a function of SOC in soils. Based on this estimation, we are able to identify hotspots of PyC presence. Some of these locations are not surprising, for example where chernozems or mollisols can be found. More unexpected are locations such as tropical forests, which seem to yield high contents of PyC in SOC as well. The high clay and low SOC contents would explain these patterns. It does not seem that one simple rule can explain high levels of PyC in soils, but rather a conjunction of soil properties (pH or clay, both parameters do not need to be met) and ecosystem properties (large biomass in tropical forests, frequent fires on easy fragmentable grass material in central Asia). This would also indicate that the qualitative properties related to this PyC (chemical functions, physical structure) might also vary greatly with the region. On the other hand, we can identify zones where in absolute numbers only very little PyC can be found, despite frequent fires or apparent other favorable conditions for high PyC content. This is the case for large parts of Australia, where stocks are largely limited through the small overall SOC stocks, or boreal forests. Both regions were used frequently in previous studies. As for the hotspots, it is difficult to identify a unified explanation for these low values. There is a need to selectively identify the main missing drivers at a regional scale. The example of boreal forests is particularly interesting. This ecosystem is prone to fire, and decomposition rate should be highly reduced by low temperature and high moisture content. From this point of view, it is comparable to high latitude soils. However, the literature dataset and the global evaluation indicate rather low PyC contents in the SOC, compared to other climatic zones. This can only be explained by parameters we did not take into account in our analysis, such as lateral transport in the landscape, the combustion of the PyC by successive fires (although estimated to have only small influence; Santín et al., 2013; Saiz et al., 2014; Tinkham et al., 2016) or higher degradability of PyC which is produced at lower temperature (Schneider et al., 2010; Ascough et al., 2011; McBeath et al., 2015).

Since the variation range of SOC is much larger than the PyC one (in particular, our estimation tends to reduce this range), the largest projected PyC stocks appear in zones that are not directly related to fire or PyC stabilization parameters. The largest stocks are in high latitude soils where it is probable that

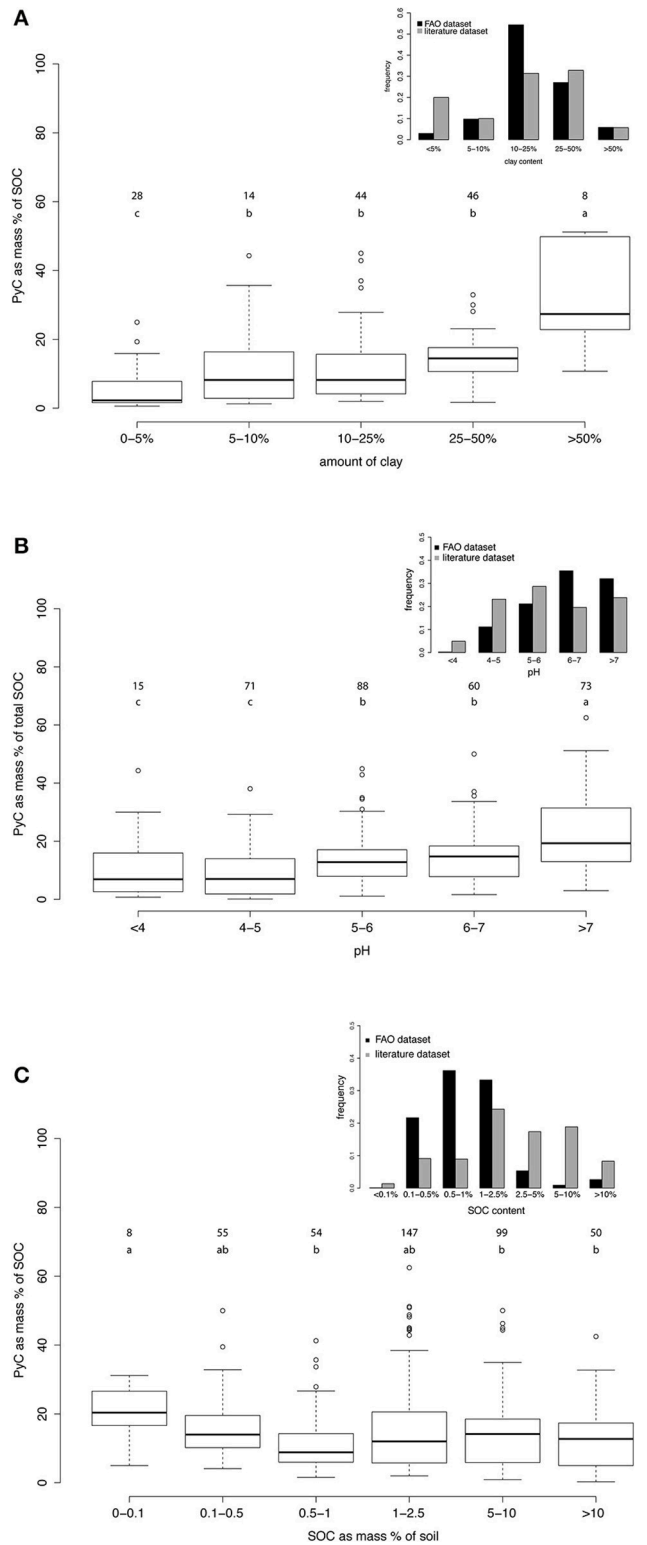


**FIGURE 8 | PyC content as mass % of the total SOC described by different soil parameters: The clay content (A); pH (B); total SOC content (C).** The One-Way-ANOVA resulted in $p < 0.001$ for the clay content, <0.001 for the pH, and <0.01 for the SOC content. The different letters on the top indicate the significant differences ($p < 0.05$) within each dataset.

little PyC content is present per unit of SOC, but where large stocks of SOC are stored. Tropical forests would be the location where both content and stocks are within the highest on the planet.

Our model has also a series of limitations. First, it explains only 33% of the total variance. This rather low power can be explained by different reasons: the time and space scale mismatch between the parameters and the PyC content dynamics (see above), the location of the sampling places or the method multiplicity. There are important differences in the location of the original sites from the literature and the global evaluation of PyC by our model. Most of our data come from Europe, East Australia and Northern America, while larger contents in the SOC are expected in boreal forest and central Asian steppes and larger stocks in high latitude soils. A direct consequence of this bias is that our evaluation rather tends to underestimate the content of PyC in SOC overall. Some zones are not explored at all, including for example most of Africa, southern Asia or central Russia, locations where high PyC contents in the SOC would be expected.

The diversity of methodological approaches may also be an issue. Hammes et al. (2007) and more recently Bird (2014) showed that a large range of PyC contents could be measured on a given sample depending on the method used. In this study, we considered seven methods, surprisingly giving consistent and comparable results. If we consider that there is no potential systematic bias that would associate a method to samples with intrinsic lower or higher PyC samples, this relative comparability around the same average value rather contradicts the existing literature. One explanation would be that when studies compare different methods to detect PyC, they use mainly PyC rich material (chernozem, pure charcoals, soot samples, etc.) and so artificially increase the range of values detected. In our case, since all types of soils are included, the differences between the values produced are not that important anymore. As a conclusion, we expect the different methods to have only a minor impact on the complete picture.

## CONCLUSION AND PERSPECTIVES

Based on a large literature database, we assessed the content of PyC in SOC, investigated a variety of drivers related to PyC production and ecosystem properties to explain these contents. Then we used these in combination with several other datasets to model the distribution of PyC on a global scale. Our key achievements and findings are as follows:

- We have produced the first unified database of published PyC measurements;
- PyC represents on average around 14% of the SOC, corresponding to one of the largest identified groups of chemical compounds in soil;
- High soil pH and clay content are the most significant parameters explaining a high PyC content in the SOC;
- PyC production parameters, such as fire or land use, do not well explain PyC content patterns.

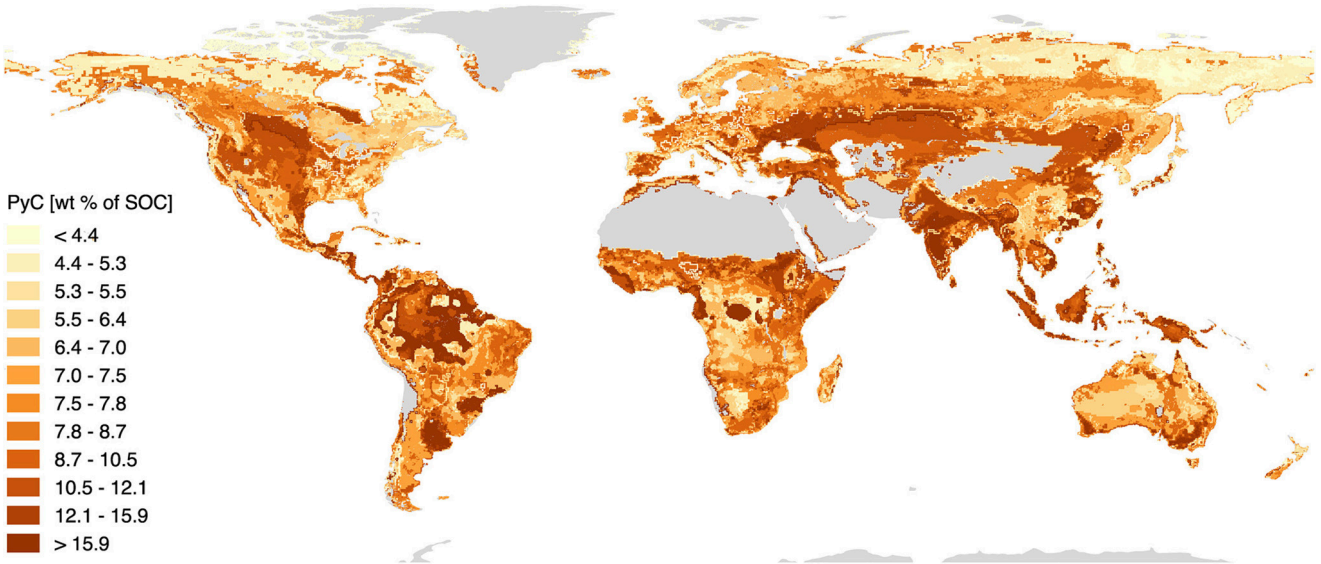


**FIGURE 9 | Global predicted PyC content as mass % of the total SOC.** Explained variance by the used linear model is 33%. Variables used were clay content, pH, mean annual precipitation, mean annual temperature, and land use. Land mass is colored in gray.

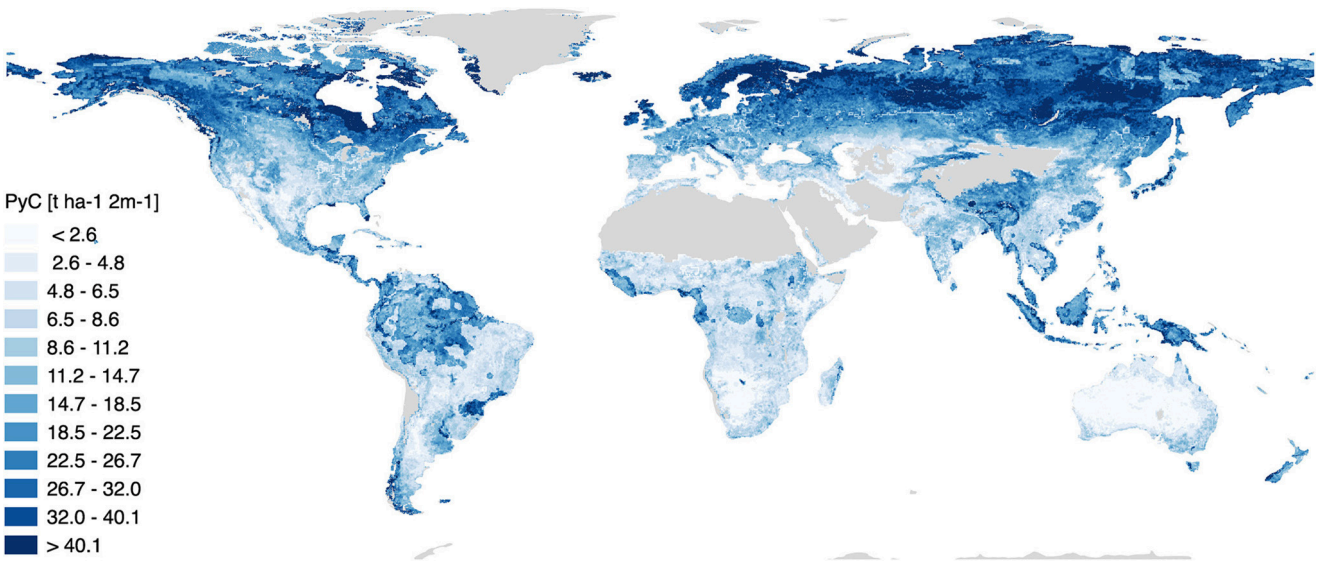


**FIGURE 10 | Global predicted PyC stocks as t ha$^{-1}$ for the first 2 m soil depth.** Explained variance by the used linear model is 33%. BDD and total SOC content from the global dataset were used to calculate the stocks from the PyC content in SOC data. Land mass is colored in gray.

- There is a temporal mismatch between the time scales over which PyC is expected to vary and the time scales over which it (and its related variables) are observed.
- There is a spatial mismatch between the regions with expected high PyC stocks and those, which are actually studied.
- There are still many limitations to overcome, if we want to improve our global picture of PyC, for example data scarcity in remote locations, resolution and derivation of global datasets or quantification method comparability.

The database is available in the Supplementary Material and can be used for other studies. We want to encourage scientists to improve the database, expand it with other variables or find new ways of filling the gaps and missing values.

## AUTHOR CONTRIBUTIONS

MR and SA conceived the paper structure. MR collected the database. MR, SA, and RP contributed to the data analysis. MR

and SA wrote the manuscript and all authors contributed to the writing of the manuscript.

## ACKNOWLEDGMENTS

We thank S. Archibald for providing the fire dataset. We also thank the reviewers for their valuable comments. This research is supported by the University of Zurich, through the URPP GCB (University Research Priority Program Global Change and Biodiversity).

## SUPPLEMENTARY MATERIAL

The Supplementary Material for this article can be found online at: http://journal.frontiersin.org/article/10.3389/feart.2016.00080

## REFERENCES

Aciego Pietri, J. C., and Brookes, P. C. (2008). Relationships between soil pH and microbial properties in a UK arable soil. *Soil Biol. Biochem.* 40, 1856–1861. doi: 10.1016/j.soilbio.2008.03.020

Archibald, S., Lehmann, C. E. R., Gómez-Dans, J. L., and Bradstock, R. A. (2013). Defining pyromes and global syndromes of fire regimes. *Proc. Natl. Acad. Sci. U.S.A.* 110, 6442–6447. doi: 10.1073/pnas.1211466110

Ascough, P. L., Bird, M. I., Francis, S. M., Thornton, B., Midwood, A. J., Scott, A. C., et al. (2011). Variability in oxidative degradation of charcoal: influence of production conditions and environmental exposure. *Geochim. Cosmochim. Acta* 75, 2361–2378. doi: 10.1016/j.gca.2011.02.002

Biederman, L. A., and Harpole, W. S. (2013). Biochar and its effects on plant productivity and nutrient cycling: a meta-analysis. *GCB Bioenergy* 5, 202–214. doi: 10.1111/gcbb.12037

Bird, M. (2014). "Test procedures for biochar analysis in soils," in *Biochar for Environmental Management - Science, Technology and Implementation*, eds J. Lehmann and S. Joseph (London: Routledge), 677–714.

Bird, M. I., Moyo, C., Veenendaal, E. M., Lloyd, J., and Frost, P. (1999). Stability of elemental carbon in a savanna soil. *Geoderma* 13, 923–932. doi: 10.1029/1999gb900067

Bird, M. I., Wynn, J. G., Saiz, G., Wurster, C. M., and McBeath, A. (2015). The pyrogenic carbon cycle. *Annu. Rev. Earth Planet. Sci.* 43, 273–298. doi: 10.1146/annurev-earth-060614-105038

Bowman, D. M. J. S., Murphy, B. P., Williamson, G. J., and Cochrane, M. A. (2014). Pyrogeographic models, feedbacks and the future of global fire regimes. *Glob. Ecol. Biogeogr.* 23, 821–824. doi: 10.1111/geb.12180

Braadbaart, F., Poole, I., and van Brussel, A. A. (2009). Preservation potential of charcoal in alkaline environments: an experimental approach and implications for the archaeological record. *J. Archaeol. Sci.* 36, 1672–1679. doi: 10.1016/j.jas.2009.03.006

Bucheli, T. D., Blum, F., Desaules, A., and Gustafsson, O. (2004). Polycyclic aromatic hydrocarbons, black carbon, and molecular markers in soils of Switzerland. *Chemosphere* 56, 1061–1076. doi: 10.1016/j.chemosphere.2004.06.002

Caria, G., Arrouays, D., Dubromel, E., Jolivet, C., Ratié, C., Bernoux, M., et al. (2011). Black carbon estimation in French calcareous soils using chemo-thermal oxidation method. *Soil Use Manag.* 27, 333–339. doi: 10.1111/j.1475-2743.2011.00349.x

Crane-Droesch, A., Abiven, S., Jeffery, S., and Torn, M. S. (2013). Heterogeneous global crop yield response to biochar: a meta-regression analysis. *Environ. Res. Lett.* 8:044049. doi: 10.1088/1748-9326/8/4/044049

Czimczik, C. I., Preston, C. M., Schmidt, M. W. I., and Schulze, E.-D. (2003). How surface fire in Siberian Scots pine forests affects soil organic carbon in the forest floor: stocks, molecular structure, and conversion to black carbon (charcoal). *Global Biogeochem. Cycles* 17, 1–14. doi: 10.1029/2002GB001956

Danielson, J. J., and Gesch, D. B. (2011). *Global Multi-Resolution Terrain Elevation Data 2010 (GMTED2010)*. U.S. Geological Survey Open-File Report 2011–1073, 26. Available online at: http://pubs.usgs.gov/of/2011/1073

DeLaune, R. D., Patrick, J. W. H., and Casselman, M. E. (1981). Effect of sediment pH and redox conditions on degradation of benzo(a)pyrene. *Mar. Pollut. Bull.* 12, 251–253. doi: 10.1016/0025-326X(81)90366-0

Dinel, H., Schnitzer, M., and Meyhuys, G. R. (1990). "Soil lipids: origin, nature, content, decomposition, and effect on soil physical properties," in *Soil Biochemistry*, 6th Edn., eds J. M. Bollag and G. Stotzky (New York, NY: Marcel Dekker Inc.), 397–429.

Dwyer, E., Pinnock, S., Gregoire, J.-M., and Pereira, J. M. C. (2000). Global spatial and temporal distribution of vegetation fire as determined from satellite observations. *Int. J. Remote Sens.* 21, 1289–1302. doi: 10.1080/014311600210182

Eckmeier, E., Rosch, M., Ehrmann, O., Schmidt, M. W. I., Schier, W., and Gerlach, R. (2007). Conversion of biomass to charcoal and the carbon mass balance from a slash-and-burn experiment in a temperate deciduous forest. *Holocene* 17, 539–542. doi: 10.1177/0959683607077041

ESRI (2016). *ArcGIS Online*. Available online at: www.arcgis.com

FAO/IIASA/ISRIC/ISSCAS/JRC (2012). *Harmonized World Soil Database (Version 1.2)*. Rome; Laxenburg: FAO; IIASA.

Forbes, M. S., Raison, R. J., and Skjemstad, J. O. (2006). Formation, transformation and transport of black carbon (charcoal) in terrestrial and aquatic ecosystems. *Sci. Total Environ.* 370, 190–206. doi: 10.1016/j.scitotenv.2006.06.007

Friedl, M. A., Sulla-Menashe, D., Tan, B., Schneider, A., Ramankutty, N., Sibley, A., et al. (2010). MODIS Collection 5 global land cover: algorithm refinements and characterization of new datasets. *Remote Sens. Environ.* 114, 168–182. doi: 10.1016/j.rse.2009.08.016

Glaser, B., Haumaier, L., Guggenberger, G., and Zech, W. (1998). Black carbon in soils : the use of benzenecarboxylic acids as specific markers. *Org. Geochem.* 29, 811–819. doi: 10.1016/S0146-6380(98)00194-6

Gustafsson, O., Bucheli, D., Kukulska, Z., Andersson, M., Largeau, C., Rouzaud, J.-N., et al. (2001). Evaluation of a protocol for the quantification of black carbon in sediments. *Global Biogeochem. Cycles* 15, 881–890. doi: 10.1029/2000GB001380

Gustafsson, O., Haghseta, F., Chan, C., Macfarlane, J., and Gschwend, P. M. (1997). Quantification of the dilute sedimentary soot phase: implications for PAH speciation and bioavailability. *Environ. Sci. Technol.* 31, 203–209. doi: 10.1021/es960317s

Hammes, K., and Abiven, S. (2013). "Identification of black carbon in the earth system," in *Fire Phenomena and the Earth System*, ed C. M. Belcher (Chichester, UK: John Wiley & Sons), 157–176.

Hammes, K., Schmidt, M. W. I., Smernik, R. J., Currie, L. A., Ball, W. P., Nguyen, T. H., et al. (2007). Comparison of quantification methods to measure fire-derived (black/elemental) carbon in soils and sediments using reference materials from soil, water, sediment and the atmosphere. *Global Biogeochem. Cycles* 21, 1–18. doi: 10.1029/2006GB002914

Hassink, J. (1997). The capacity of soils to preserve organic C and N by their association with clay and silt particles. *Plant Soil* 191, 77–87. doi: 10.1023/A:1004213929699

Kemmitt, S. J., Wright, D., Goulding, K. W. T., and Jones, D. L. (2006). pH regulation of carbon and nitrogen dynamics in two agricultural soils. *Soil Biol. Biochem.* 38, 898–911. doi: 10.1016/j.soilbio.2005.08.006

Knicker, H., Wiesmeier, M., and Dick, D. P. (2008). A simplified method for the quantification of pyrogenic organic matter in grassland soils via chemical oxidation. *Geoderma* 147, 69–74. doi: 10.1016/j.geoderma.2008.07.008

Kottek, M., Grieser, J., Beck, C., Rudolf, B., and Rubel, F. (2006). World map of the Köppen-Geiger climate classification updated. *Meteorol. Zeitschrift* 15, 259–263. doi: 10.1127/0941-2948/2006/0130

Lehmann, J., Skjemstad, J., Sohi, S., Carter, J., Barson, M., Falloon, P., et al. (2008). Australian climate–carbon cycle feedback reduced by soil black carbon. *Nat. Geosci.* 1, 832–835. doi: 10.1038/ngeo358

Liang, B., Lehmann, J., Solomon, D., Sohi, S., Thies, J. E., Skjemstad, J. O., et al. (2008). Stability of biomass-derived black carbon in soils. *Geochim. Cosmochim. Acta* 72, 6069–6078. doi: 10.1016/j.gca.2008.09.028

Lowe, L. E. (1978). "Carbohydrates distribution in soil," in *Soil Organic Matter*, eds M. Schnitzer and S. U. Khan (Amsterdam: Elsevier), 67–74.

McBeath, A. V., Wurster, C. M., and Bird, M. I. (2015). Influence of feedstock properties and pyrolysis conditions on biochar carbon stability as determined by hydrogen pyrolysis. *Biomass Bioenergy* 73, 155–173. doi: 10.1016/j.biombioe.2014.12.022

Merckx, R., den Hartog, A., and van Veen, J. A. (1985). Turnover of root-derived material and related microbial biomass formation in soils of different texture. *Soil Biol. Biochem.* 17, 565–569. doi: 10.1016/0038-0717(85)90026-4

Nelson, P. N., and Baldock, J. A. (2005). Estimating the molecular composition of a diverse range of natural organic materials from solid-state 13C NMR and elemental analyses. *Biogeochemistry* 72, 1–34. doi: 10.1007/s10533-004-0076-3

New, M., Lister, D., Hulme, M., and Makin, I. (2002). A high-resolution data set of surface climate over global land areas. *Clim. Res.* 21, 1–25. doi: 10.3354/cr021001

Nocentini, C., Certini, G., Knicker, H., Francioso, O., and Rumpel, C. (2010). Nature and reactivity of charcoal produced and added to soil during wildfire are particle-size dependent. *Org. Geochem.* 41, 682–689. doi: 10.1016/j.orggeochem.2010.03.010

Peters, W. J., and Neuenschwander, L. F. (1988). *Slash and Burn. Farming in the* Third *World Forest*. Moscow, ID: University of Idaho Press.

Pignatello, J. J., Uchimiya, M., Abiven, S., and Schmidt, M. W. I. (2015). "Evolution of biochar properties in soil," in *Biochar for Environmental Management - Science, Technology and Implementation*, eds J. Lehmann and S. Joseph (London: Routledge), 195–233.

Preston, C. M., and Schmidt, M. W. I. (2006). Black (pyrogenic) carbon: a synthesis of current knowledge and uncertainties with special consideration of boreal regions. *Biogeosciences* 3, 397–420. doi: 10.5194/bg,-3-397-2006

QGIS Development Team (2015). *QGIS Geographic Information System*. Available online at: http://qgis.osgeo.org

Randerson, J. T., Chen, Y., van der Werf, G. R., Rogers, B. M., and Morton, D. C. (2012). Global burned area and biomass burning emissions from small fires. *J. Geophys. Res.* 117, G04012. doi: 10.1029/2012JG002128

R Core Team (2015). *R: A Language and Environment for Statistical Computing*. Available online at: https://www.r-project.org

Rubel, F., and Kottek, M. (2010). Observed and projected climate shifts 1901-2100 depicted by world maps of the Köppen-Geiger climate classification. *Meteorol. Zeitschrift* 19, 135–141. doi: 10.1127/0941-2948/2010/0430

Saiz, G., Goodrick, I., Wurster, C. M., Zimmermann, M., Nelson, P. N., and Bird, M. I. (2014). Charcoal re-combustion efficiency in tropical savannas. *Geoderma* 219–220, 40–45. doi: 10.1016/j.geoderma.2013.12.019

Santín, C., Doerr, S. H., Kane, E. S., Masiello, C. A., Ohlson, M., de la Rosa, J. M., et al. (2016). Towards a global assessment of pyrogenic carbon from vegetation fires. *Glob. Chang. Biol.* 22, 76–91. doi: 10.1111/gcb.12985

Santín, C., Doerr, S. H., Preston, C., and Bryant, R. (2013). Consumption of residual pyrogenic carbon by wildfire. *Int. J. Wildl. Fire* 22, 1072–1077. doi: 10.1071/WF12190

Santín, C., Doerr, S. H., Preston, C. M., and González-Rodríguez, G. (2015). Pyrogenic organic matter production from wildfires: a missing sink in the global carbon cycle. *Glob. Chang. Biol.* 21, 1621–1633. doi: 10.1111/gcb.12800

Schmidt, M. W. I., Skjemstad, J. O., Czimczik, C. I., Glaser, B., Prentice, K. M., Gelinas, Y., et al. (2001). Comparative analysis of black carbon in soils. *Global Biogeochem. Cycles* 15, 163–167. doi: 10.1029/2000GB001284

Schneider, M. P. W., Hilf, M., Vogt, U. F., and Schmidt, M. W. I. (2010). The benzene polycarboxylic acid (BPCA) pattern of wood pyrolyzed between 200°C and 1000°C. *Org. Geochem.* 41, 1082–1088. doi: 10.1016/j.orggeochem.2010.07.001

Schneider, M. P. W., Smittenberg, R. H., Dittmar, T., and Schmidt, M. W. I. (2011). Comparison of gas with liquid chromatography for the determination of benzenepolycarboxylic acids as molecular tracers of black carbon. *Org. Geochem.* 42, 275–282. doi: 10.1016/j.orggeochem.2011.01.003

Singh, N., Abiven, S., Torn, M. S., and Schmidt, M. W. I. (2012). Fire-derived organic carbon in soil turns over on a centennial scale. *Biogeosciences* 9, 2847–2857. doi: 10.5194/bg-9-2847-2012

Six, J., Conant, R. T., Paul, E. A., and Paustian, K. (2002). Stabilization mechanisms of soil organic matter: implications for C-saturatin of soils. *Plant Soil* 241, 155–176. doi: 10.1023/A:1016125726789

Skjemstad, J. O., Clarke, P., Taylor, J. A., Oades, J. M., and McClure, S. G. (1996). The chemistry and nature of protected carbon in soil. *Aust. J. Soil Res.* 34, 251–271. doi: 10.1071/SR9960251

Sørensen, L. H. (1972). Stabilization of newly formed amino acid metabolites in soil by clay minerals. *Soil Sci.* 114, 5–11. doi: 10.1097/00010694-197207000-00002

Thevenot, M., Dignac, M. F., and Rumpel, C. (2010). Fate of lignins in soils: a review. *Soil Biol. Biochem.* 42, 1200–1211. doi: 10.1016/j.soilbio.2010.03.017

Tinkham, W. T., Smith, A. M. S., Higuera, P. E., Hatten, J. A., Brewer, N. W., and Doerr, S. H. (2016). Replacing time with space: using laboratory fires to explore the effects of repeated burning on black carbon degradation. *Int. J. Wildl. Fire* 25, 242–248. doi: 10.1071/WF15131

Wiedemeier, D. B., Hilf, M. D., Smittenberg, R. H., Haberle, S. G., and Schmidt, M. W. I. (2013). Improved assessment of pyrogenic carbon quantity and quality in environmental samples by high-performance liquid chromatography. *J. Chromatogr. A* 1304, 246–250. doi: 10.1016/j.chroma.2013.06.012

Wiedner, K., and Glaser, B. (2015). "Traditional use of biochar," in *BIochar for Environmental Management - Science and Technology*, eds J. Lehmann and S. Joseph (London: Routledge), 15–37.

Zhao, M., Heinsch, F. A., Nemani, R. R., and Running, S. W. (2005). Improvements of the MODIS terrestrial gross and net primary production global data set. *Remote Sens. Environ.* 95, 164–176. doi: 10.1016/j.rse.2004.12.011

**Conflict of Interest Statement:** The authors declare that the research was conducted in the absence of any commercial or financial relationships that could be construed as a potential conflict of interest.

frontiers in Environmental Science

MINI REVIEW
published: 30 August 2017
doi: 10.3389/fenvs.2017.00053

# Function of Wildfire-Deposited Pyrogenic Carbon in Terrestrial Ecosystems

*Melissa R. A. Pingree*[1]* *and Thomas H. DeLuca*[2]

[1] Department of Natural Resources and Society, College of Natural Resources, University of Idaho, Moscow, ID, United States, [2] W.A. Franke College of Forestry and Conservation, University of Montana, Missoula, MT, United States

Fire is an important driver of change in most forest, savannah, and prairie ecosystems and fire-altered organic matter, or pyrogenic carbon (PyC), conveys numerous functions in soils of fire-maintained terrestrial ecosystems. Although an exceptional number of recent review articles and books have addressed agricultural soil application of charcoal or biochar, few reviews have addressed the functional role of naturally formed PyC in fire-maintained ecosystems. Recent advances in molecular spectroscopic techniques have helped strengthen our understanding of PyC as a ubiquitous, complex material that is capable of altering soil chemical, physical, and biological properties and processes. The uniquely recalcitrant nature of PyC in soils is partly a result of its stable C = C double-bonded, graphene-like structure and C-rich, N-poor composition. This attribute allows it to persist in soils for hundreds to thousands of years and represent net ecosystem C sequestration in fire-maintained ecosystems. The rapid formation of PyC during wildfire or anthropogenic fire events short-circuits the normally tortuous pathway of recalcitrant soil C formation. Existing literature also suggests that PyC provides an essential role in the cycling of certain nutrients, greatly extending the timeframe by which fires influence soil processes and facilitating recovery in ecosystems where organic matter inputs are low and post-fire surface soil bacterial and fungal activity is reduced. The high surface area of PyC allows for the adsorption a broad spectrum of organic compounds that directly or indirectly influence microbial processes after fire events. Adsorption capacity and microsite conditions created by PyC yields a "charosphere" effect in soil with heightened microbial activity in the vicinity of PyC. In this mini-review, we explore the function of PyC in natural and semi-natural settings, provide a mechanistic approach to understanding these functions, and examine examples of such mechanisms in published literature.

**Keywords: black carbon, charcoal, carbon sequestration, surface adsorption, sorption, nutrient cycling, soil organic matter, bioactive zones**

OPEN ACCESS

***Edited by:***
*Samuel Abiven,*
*University of Zurich, Switzerland*

***Reviewed by:***
*Michael Ian Bird,*
*James Cook University Cairns, Australia*
*Xavier Domene,*
*Universitat Autònoma de Barcelona, Spain*

***Correspondence:**
*Melissa R. A. Pingree*
*mpingree@uidaho.edu*

***Specialty section:***
*This article was submitted to Soil Processes, a section of the journal Frontiers in Environmental Science*

***Received:*** *01 June 2017*
***Accepted:*** *08 August 2017*
***Published:*** *30 August 2017*

***Citation:***
*Pingree MRA and DeLuca TH (2017) Function of Wildfire-Deposited Pyrogenic Carbon in Terrestrial Ecosystems. Front. Environ. Sci. 5:53. doi: 10.3389/fenvs.2017.00053*

## INTRODUCTION

In recent years, naturally occurring and anthropogenic pyrogenic carbon (PyC) in the environment have become a prominent area of research across scientific disciplines (Zhu et al., 2005; Hammes et al., 2007; Ding et al., 2014; Lehmann and Joseph, 2015; Alam et al., 2016), and yet, to date, there has been little effort to provide a broad ranging synthesis of this unique material that transcends individual disciplines and ecosystems (Sohi et al., 2010; Hart and Luckai, 2013). An increased

emphasis on the importance of PyC in the global carbon (C) cycle and as an amendment for agricultural soils has resulted in a rapid increase in the number of studies across managed, semi-natural, and natural environmental conditions affording a multi-disciplinary framework for improving our mechanistic understanding of PyC (Barrow, 2012; Santín et al., 2015; Dietrich et al., 2017). Applications of molecular spectroscopic analyses to PyC studies in natural environments complement the absolute quantification of PyC and any known information on molecular changes associated with wood pyrolysis (Nishimiya et al., 1998), transport and oxidation of PyC particles (Hockaday et al., 2006; Cheng et al., 2008; Inoue et al., 2017), change in soil organic matter quality due to wildfires (Miesel et al., 2015), and interactions of PyC surfaces with the surrounding soil environment (Archanjo et al., 2017). In this review, we describe these potential functions and explore the mechanisms underlying PyC functionality in natural and semi-natural environments for the advancement of multi-disciplinary research endeavors (see **Figure 1**).

## BELOWGROUND SEQUESTRATION OF RECALCITRANT CARBON

Pyrogenic C is a high-C and low-nitrogen (N) byproduct of organic matter pyrolysis or incomplete combustion. The residual material consists of aromatic C rings, aliphatic C chains, and a variety of surface pores and cracks (Preston and Schmidt, 2006). Generally, the PyC material found in nature is less graphitic and more amorphous constituent of the black C continuum model (Hedges et al., 2000) which lends physical and chemical properties that convey unique functions in the soil environment.

The production of PyC by wildfires and anthropogenic fires directly adds highly recalcitrant C into soils, sediments, and aquatic systems in contrast to the tortuous pathway for formation of soil humic materials (**Figure 1**). Estimates of PyC persistence in soils and sediments range from hundreds to thousands of years (Meyer et al., 1995; Gavin et al., 2003; Laird et al., 2008; Liang et al., 2008), which provides evidence of wildfires in fossilized PyC from pre-Quaternary periods in the Earth's history (Scott, 2000). Accounting for PyC after fire events is an important aspect of quantifying the impact of fire on the global C cycle in contrasting C storage as PyC versus C loss as $CO_2$, CO, and $CH_4$ during combustion events (Ciais et al., 2013). Empirical measurements of PyC in the surface and sub-surface soils reported in over 500 studies suggest that PyC ranges from 0 to 60% of soil organic matter across forests, agriculture soils, grasslands, peat, and urban soils (Reisser et al., 2016) and yet no standard method exists to quantify PyC in soils. There are numerous PyC quantification methods commonly utilized in soils and sediments that rely on physical separation, chemical and

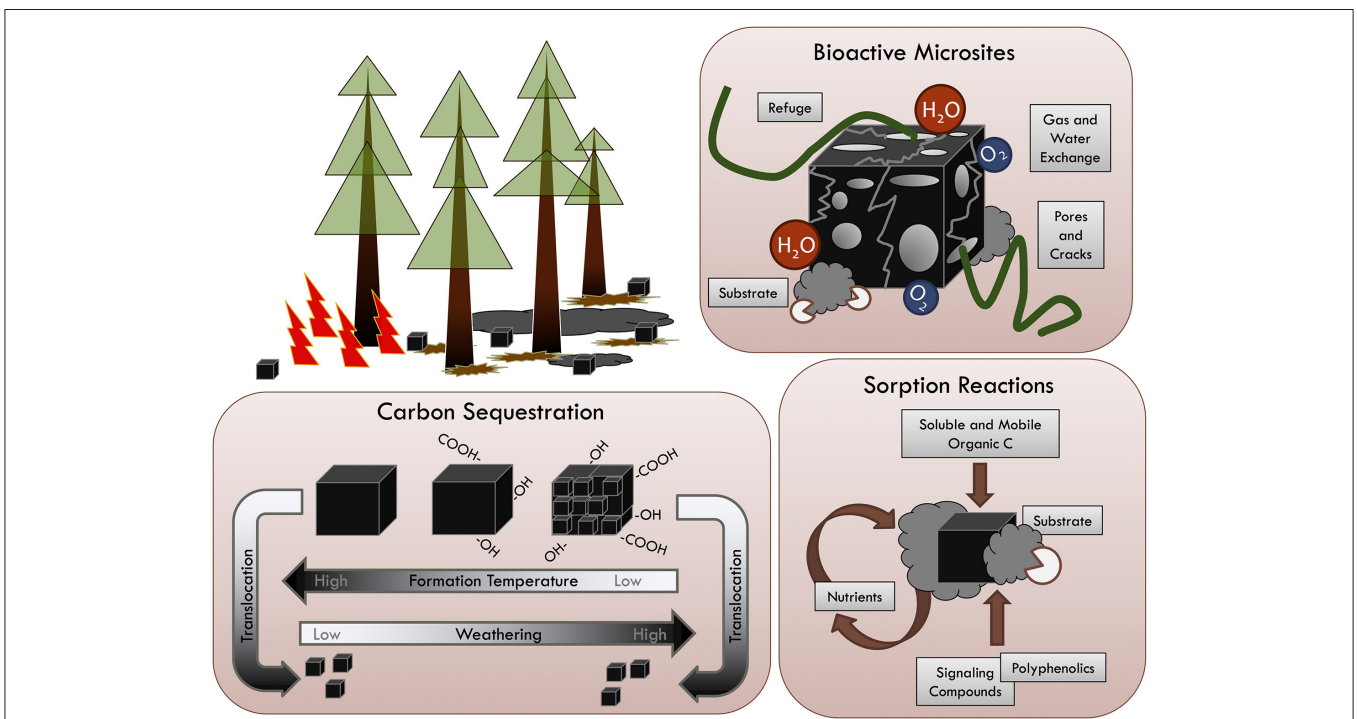


**FIGURE 1 |** Pyrogenic carbon (PyC) provides three primary mechanistic functions in forest soils after organic carbon (C) from aboveground vegetation is redistributed as highly recalcitrant, belowground Pyrogenic C via fire-driven pyrolysis and combustion. The sequestration of C, in the form of PyC is largely driven by formation temperature and subsequent weathering (mean annual temperature and precipitation) as PyC particles oxidize, increase in oxygen and hydrogen functional groups, and are physically disintegrated and translocated over time. As a component of mineral soils, PyC can act as a sorbent of soluble and mobile organic C, nutrients, polyphenolics, plant signaling compounds, and provide substrate for microorganisms. Lastly, PyC in soils may provide bioactive zones with various pores, cracks, and physical refuge for organisms, as well as facilitate gas, water, and nutrient exchange with surrounding mineral soil.

thermal oxidation, spectroscopy, and molecular identification (Mikutta et al., 2005; Rovira and Ramón Vallejo, 2007; Koide et al., 2011; Bird, 2015). While some methods use molecular identification of the unique PyC structure to separate PyC from humic compounds, others rely on comparisons between burned and unburned soils and are limited to a broader definition of PyC (Hedges et al., 2000).

Studies using the weak nitric acid-peroxide digestion method (Kurth et al., 2006), which quantifies chemically recalcitrant C in mineral soils, have reported PyC accounting for 3–25% (with an average of 13%) of soil C (Kurth et al., 2006; Bélanger and Pinno, 2008; MacKenzie et al., 2008; Licata and Sanford, 2012; Pingree et al., 2012; Buma et al., 2014; Soucémarianadin et al., 2014). Where unburned or pre-wildfire sites were measured in concurrence with wildfire-burned sites, PyC fractions accounted for 8% of total ecosystem C in a low fire frequency, high fire intensity subalpine forest (Buma et al., 2014), and 25% of total ecosystem C in a moderate fire frequency, moderate fire intensity temperate forest (Pingree et al., 2012). The PyC on standing boles represents an additional long-term input of PyC into soil as charred bark sloughs onto the forest floor and standing snags fall to the ground (Makoto et al., 2012; Buma et al., 2014). Wildfire-burned standing snags in the Alaskan boreal, USA, accounted for 65–248 kg charcoal $ha^{-1}$ (if charcoal C is assumed 50% C, 33–124 kg C $ha^{-1}$) in a beetle-killed *Picea glauca* forest (Makoto et al., 2012). Most wildfire events are likely to increase PyC storage and PyC as a component of total ecosystem C; however, wildfires may consume PyC remaining on the forest floor from prior wildfire events (Zackrisson et al., 1996; Tinkham et al., 2016).

The resistance of PyC to chemical and biological oxidation can largely be attributed to its stacked aromatic C structure (Pierson, 1993; Cohen-Ofri et al., 2006; Ascough et al., 2011). Short and strong sigma (σ) bonds create one plane of hexagonal C while the fourth valence electron (orthogonal to the σ bonds) forms longer and weaker van der Waals bonds (π) with other hybridized electrons above and below the hexagonal plane (Pierson, 1993; Kleber et al., 2015). The result is a layered, alternating hexagonal structure unique to C.

Oxidation of PyC has been attributed to both the intrinsic structure of PyC material and environmental gradients. Temperature-dependent recalcitrance has been indirectly suggested by several laboratory incubation studies that showed reduced C mineralization in the presence of PyC produced at high temperatures (Baldock and Smernik, 2002; Bruun et al., 2008; Zimmerman, 2010; Hanan et al., 2016). These studies were unable to distinguish the effects of inherent recalcitrance from adsorption to PyC surfaces, which may concurrently reduce available C by adsorption (see next section). Long-term storage of PyC in soils and PyC elemental composition was shown to be influenced by climate variables (precipitation and temperature), which had a greater influence compared to soil characteristics (soil texture, cation exchange capacity, pH), with mean annual temperature being the best predictor of PyC oxidation (Glaser and Amelung, 2003; Cheng et al., 2008). Aged PyC particles showed slightly lower aromaticity and released larger and more aromatic clusters into solution or as colloids, which suggests oxidation over a 10-year study period (Schneider et al., 2010). Similarly, many studies showed aged PyC particles decrease in C concentration and an increase in functional groups relative to fresh PyC (Hockaday et al., 2007; Cheng et al., 2008; Nguyen et al., 2008; Ascough et al., 2011; Singh et al., 2012), which possibly resulted from environmental weathering, microbial decomposition (Hockaday et al., 2006, 2007), or faunal bioturbation (Domene, 2016). PyC particles have been shown to decrease in specific surface area over time (Hockaday et al., 2007), although the physical fragmentation of larger particles may ultimately increase total surface areas in soil. Preferential mobilization of PyC particles has received little attention, but a recent study suggests that more highly condensed PyC may be more readily physically degraded in soils due to its physically less stable structure, leaving behind a more biologically available PyC (Inoue et al., 2017).

## SORPTION INTERACTIONS

The ability for PyC particles to adsorb non-polar organic compounds lends to its function as a surface adsorption foci in soils, sediments, and solutions (**Figure 1**). This mechanism has wide ranging implications for how PyC influences myriad soil processes (Cornelissen and Gustafsson, 2004; Keech et al., 2005; Bornemann et al., 2007; Pingree et al., 2016). First, and perhaps the most obvious, is that most all soluble and mobile organic compounds in soil represent an energy source for microbes. Surface adsorption to PyC particles would concentrate organic compounds around PyC particles, thereby creating a microsite for enhanced microbial activity (Lehmann et al., 2011). Increased decomposition of C adsorbed to PyC may partially account for observations including priming effects (Hamer et al., 2004; Jones et al., 2011), an increase in the nutrient release from mineral precipitates and cation exchange sites, or increased immobilization of inorganic nutrients near PyC particles. Contrasting findings of N mineralization and N immobilization rates (see DeLuca et al., 2015) are likely related to the capacity of PyC to adsorb nutrients and organic compounds. Finally, adsorption of polyphenolic signaling compounds within the rhizosphere could influence plant pathogenic or symbiotic interactions, but to date there has been limited effort to evaluate this in natural ecosystems (Hassan and Mathesius, 2012; Hall et al., 2014; Kolton et al., 2017).

Adsorption capacity is predominantly driven by the specific surface area and pore-size distribution of PyC particles, which are determined by pyrolysis temperature and the innate chemical nature of the feedstock. As formation temperature increases and pyrolysis or combustion takes place, adsorption capacity typically increases exponentially (Zhu et al., 2005; Brimmer, 2006; Bornemann et al., 2007; Pingree et al., 2016), while pore sizes become dominated by micropores (<2 nm) (Braida et al., 2003; Bornemann et al., 2007). Wood-based PyC contains extensive porosity partly due to the partial pyrolysis of tracheid cells associated with xylem, which contributes further to the natural porosity of PyC made from wood (Keech et al., 2005). Sorption behavior as a function of formation temperature is well-documented in the laboratory (Bornemann et al., 2007),

but is likely altered by exposure to environmental influences. Direct measurements of adsorption capacity in soils show a more complicated and less predictable relationship between PyC as an adsorbent and naturally-occurring adsorbate compounds (Cornelissen and Gustafsson, 2004; Pingree et al., 2016). Terrestrial and aquatic ecosystems provide complex matrices for sorption interactions that merit a better understanding of sorption interactions in relation to surface properties of PyC.

The adsorption capacity of PyC as charcoal particles may have a significant effect on N cycling in post-fire forest soils. Previous studies of temperate and boreal forest soils have shown an increase net mineralization of N and in net nitrification with the addition of charcoal through the production of nitrate ($NO_3^-$-N), which otherwise show minimal net nitrification (DeLuca et al., 2002, 2006; MacKenzie and DeLuca, 2006; Ball et al., 2010; Kurth et al., 2014; Michelotti and Miesel, 2015). There are multiple mechanisms that may be responsible for this observed increase in $NO_3^-$-N after the addition of charcoal to soil. The presence of PyC may release nitrifier activity by adsorption of allelopathic C compounds which results in a total reduction of nitrification potential (Paavolainen et al., 1998; MacKenzie and DeLuca, 2006; Uusitalo et al., 2008). The presence of heterocyclic C compounds may provide a source of organic C that results in net immobilization of $NH_4^+$ (Bremner and McCarty, 1988). In addition, the presence of charcoal may reduce the complexation of high molecular weight compounds and indirectly alter the N and C cycles of soils via complexation of $NH_4^+$ and amines by polyphenolics that may eliminate $NH_4^+$ availability for nitrification (Hättenschwiler and Vitousek, 2000). In wildfire-burned chaparral forest soils, the addition of PyC had no significant effect on N dynamics after an incubation study, but instead may have promoted N immobilization by enhancing microbial biomass (Hanan et al., 2016). Alternatively, the surface adsorption of $NH_4^+$ by PyC could also reduce availability for autotrophic oxidation by nitrifying bacteria—a mechanism yet to be evaluated in PyC and soil N dynamics.

The release and reception of molecular signaling compounds is known to directly influence both symbiotic and pathogenic relationships in soils. Both mycorrhizal infection of host plants and nodule establishment in legumes is thought to be dependent upon the release and reception of signaling compounds, which are generally flavonoids or related polyphenolic compounds (Hassan and Mathesius, 2012). It is well-understood that PyC has the capacity to adsorb such compounds (Zackrisson et al., 1996; DeLuca et al., 2002; Keech et al., 2005), but the direct connection between PyC and signaling effectiveness has, to date, been largely ignored. Biochar-induced ethylene production, a plant hormone and soil microbial inhibitor, has been found in some PyC materials although most notably from non-woody sources (Spokas et al., 2010). Legume nodulation has been observed to both increase and decrease in the presence of biochar applications to surface soils, but more often wood charcoal has increased nodulation or $N_2$ fixation in legumes (see DeLuca et al., 2015). Further, numerous studies have demonstrated an increase in mycorrhizal infection rates in the presence of wood char (Thies et al., 2015). However, there has been no strenuous effort to date to evaluate the influence of PyC on signaling-mediated processes in natural forest or prairie ecosystems.

## MICROSITE EFFECTS

The presence of PyC in soils may also serve an important function by creating bioactive zones through the addition of a heterogeneous environment facilitated by the particulate and porous nature of PyC particles, which provides nutrients, organic matter, water availability, and refuge for some organisms (**Figure 1**). Pyrogenic C particles have been cited as creating a novel substrate for microbial growth and as physical habitat for microbes (Pietikäinen et al., 2000; Quilliam et al., 2013; Thies et al., 2015), which may aid in the recovery of surface soils exposed to wildfires or intense prescribed fires. PyC microsites are likely to elicit diverse interactions with surrounding biotic and abiotic constituents in soils as they are most likely to affect plant-microbe-soil interactions in the "charosphere," the soil immediately surrounding a PyC particle (Quilliam et al., 2013).

Surface heterogeneity in naturally-produced PyC particles can further increase soil microorganism activity and abundance via adsorption of compounds utilized as substrate and physical microsites for the exchange of water and gas that may influence redox conditions. While these mechanisms have been evaluated in biochar studies wherein strict pyrolysis conditions and a narrow selection of feedstock were applied to agriculture soils, they have rarely been investigated in natural soils (Briones, 2012; Joseph et al., 2013). Evidence of microbial substrate utilization of adsorbed compounds on PyC surfaces is limited outside of biochar applications, but suggests that surface sorption may play an important role in providing microorganisms with nutrients and C compounds for metabolic oxidation as well as altering the microbial community (Zackrisson et al., 1996; Singh et al., 2014; Kolton et al., 2017). Negative C mineralization priming in high-temperature-produced biochar treatments may be related to the adsorption of C substrate (Zimmerman et al., 2011). Additionally, the similarity of dissolved organic matter released by aged PyC particles to products of polycyclic aromatic hydrocarbon biological decomposition suggests microbial oxidation of PyC (Hockaday et al., 2006, 2007). Enzymatic oxidation of aromatic C structures in lignin, humic acids, and coal are documented and utilized in the bioenergy industry (see review by Fakoussa and Hofrichter, 1999), but have yet to be explored in microbial decomposition of naturally-produced PyC in soils where regular fire events are likely to sustain the activity of microbial populations responsible for such processes. Studies of $^{14}C$ labeled biochar mineralization clearly show that PyC is not resistant to microbial decomposition, however, the interactions between adsorbed substrate utilization and enzymatic oxidation of PyC remain poorly understood (Hamer et al., 2004; Bruun et al., 2008; Kuzyakov et al., 2009; Jones et al., 2011; Quilliam et al., 2013; Maestrini et al., 2014).

There are numerous examples of microbial hyphae habitation of internal and external PyC surfaces via pore infiltration. Wildfire-produced PyC exposed to weathering in forest soils over many decades is often physically inhabited by fine roots, filamentous microorganisms, and coated by minerals compared to recently formed PyC (Zackrisson et al., 1996; Hockaday et al., 2007). Internal and external pores on PyC particles

have often been cited as providing the potential for microbial habitation as refuge from predators, increasing water holding capacity, providing gas exchange, and increasing redox potential (Lehmann et al., 2011; Thies et al., 2015). However, no quantitative efforts have been undertaken to directly connect microbial abundance, activity, or composition with pore size and distribution of wildfire-deposited PyC particles. Further, PyC and its pore distribution is not a static entity, but an attribute that changes with the numerous physical disturbances presented in terrestrial environment. Subsequent wildfires may further pyrolyze PyC and physical processes of freezing and thawing, wetting and drying, wind abrasion, or bioturbation all may lead to partial disintegration of PyC thereby exposing internal surfaces or degrading small pores (Gao et al., 2017). Additionally, the incorporation of PyC bark from tree boles can provide a delayed input of PyC onto soil surfaces that may exhibit larger pore sizes after prolonged physical weathering (Makoto et al., 2012; Gao et al., 2017).

## FUTURE RESEARCH DIRECTIONS

The historical occurrence of wildfires and anthropogenic fires has yielded a rich *ex post facto* experimental design of varied length that allows us to evaluate both the recalcitrance of PyC as well as the functional properties of PyC in terrestrial ecosystems. Knowledge gained from these studies can be used to help elucidate the long-term fate and function of biochar in agricultural soils, which is otherwise limited to "long-term" studies of 10 years or less. Interest in PyC for its role in C storage has also created a foundation for C accounting in isolated studies; however, studies lack the use of systematic, consistent approaches to PyC quantification in post-fire surveys that could provide vital information in a thorough understanding the global C cycle (Parson et al., 2010; Santín et al., 2015). Combining fire ecology, fire science, and PyC research has the potential to directly link wildfire and prescribed fire conditions (such as temperature, duration, fuel load, etc.) to PyC production and characteristics to achieve a better understanding of how fires alter C dynamics and plant-soil-microbe relationships through the deposition of PyC. Studies of PyC occupy a unique place in science as a focal point in paleobotany, paleoecology, archeology, agriculture, and ecological research for decades, which collectively lend to a multi-disciplinary research potential that may lead to a broadened understanding of fire ecology and the role of PyC in ecosystem diversity and function.

## AUTHOR CONTRIBUTIONS

All authors listed have made a substantial, direct and intellectual contribution to the work, and approved it for publication.

## REFERENCES


Alam, M. S., Cossio, M., Robinson, L., Wang, X., Kenney, J. P. L., Konhauser, K. O., et al. (2016). Removal of organic acids from water using biochar and petroleum coke. *Environ. Technol. Innov.* 6, 141–151. doi: 10.1016/j.eti.2016.08.005

Archanjo, B. S., Mendoza, M. E., Albu, M., Mitchell, D. R. G., Hagemann, N., Mayrhofer, C., et al. (2017). Nanoscale analyses of the surface structure and composition of biochars extracted from field trials or after co-composting using advanced analytical electron microscopy. *Geoderma* 294, 70–79. doi: 10.1016/j.geoderma.2017.01.037

Ascough, P. L., Bird, M. I., Francis, S. M., Thornton, B., Midwood, A. J., Scott, A. C., et al. (2011). Variability in oxidative degradation of charcoal: Influence of production conditions and environmental exposure. *Geochim. Cosmochim. Acta* 75, 2361–2378. doi: 10.1016/j.gca.2011.02.002

Baldock, J. A., and Smernik, R. J. (2002). Chemical composition and bioavailability of thermally altered *Pinus resinosa* (Red pine) wood. *Org. Geochem.* 33, 1093–1109. doi: 10.1016/S0146-6380(02)00062-1

Ball, P. N., MacKenzie, M. D., DeLuca, T. H., and Montana, W. E. H. (2010). Wildfire and charcoal enhance nitrification and ammonium-oxidizing bacterial abundance in dry montane forest soils. *J. Environ. Qual.* 39, 1243–1253. doi: 10.2134/jeq2009.0082

Barrow, C. J. (2012). Biochar: potential for countering land degradation and for improving agriculture. *Appl. Geogr.* 34, 21–28. doi: 10.1016/j.apgeog.2011.09.008

Bélanger, N., and Pinno, B. D. (2008). Carbon sequestration, vegetation dynamics and soil development in the Boreal Transition ecoregion of Saskatchewan during the Holocene. *CATENA* 74, 65–72. doi: 10.1016/j.catena.2008.03.005

Bird, M. (2015). "Test procedures for biochar analysis in soils," in *Biochar for Environmental Management: Science, Technology and Implementation, 2nd Edn.,* eds J. Lehmann and S. Joseph (New York, NY: Routledge), 679–716.

Bornemann, L. C., Kookana, R. S., and Welp, G. (2007). Differential sorption behaviour of aromatic hydrocarbons on charcoals prepared at different temperatures from grass and wood. *Chemosphere* 67, 1033–1042. doi: 10.1016/j.chemosphere.2006.10.052

Braida, W. J., Pignatello, J. J., Lu, Y., Ravikovitch, P. I., Neimark, A. V., and Xing, B. (2003). Sorption hysteresis of benzene in charcoal particles. *Environ. Sci. Technol.* 37, 409–417. doi: 10.1021/es020660z

Bremner, J. M., and McCarty, G. W. (1988). Effects of terpenoids on nitrification in soil. *Soil Sci. Soc. Am. J.* 52, 1630–1633. doi: 10.2136/sssaj1988.03615995005200060023x

Brimmer, R. J. (2006). *Sorption Potential of Naturally Occurring Charcoal in Ponderosa Pine Forests of Western Montana.* MS thesis, Missoula, MT: University of Montana.

Briones, A. (2012). The secrets of El Dorado viewed through a microbial perspective. *Front. Microbiol.* 3:239. doi: 10.3389/fmicb.2012.00239

Bruun, S., Jensen, E. S., and Jensen, L. S. (2008). Microbial mineralization and assimilation of black carbon: Dependency on degree of thermal alteration. *Org. Geochem.* 39, 839–845. doi: 10.1016/j.orggeochem.2008.04.020

Buma, B., Poore, R. E., and Wessman, C. A. (2014). Disturbances, their interactions, and cumulative effects on carbon and charcoal stocks in a forested ecosystem. *Ecosystems* 17, 947–959. doi: 10.1007/s10021-014-9770-8

Cheng, C.-H., Lehmann, J., and Engelhard, M. H. (2008). Natural oxidation of black carbon in soils: changes in molecular form and surface charge along a climosequence. *Geochim. Cosmochim. Acta* 72, 1598–1610. doi: 10.1016/j.gca.2008.01.010

Ciais, P., Sabine, C., Bala, G., Bopp, L., Brovkin, V., Canadell, J., et al. (2013). "Carbon and other biogeochemical cycles," in *Climate Change 2013: The Physical Science Basis. Contribution of Working Group I to the Fifth Assessment Report of the Intergovernmental Panel on Climate Change,* eds T. F. Stocker, D. Qin, G.-K. Plattner, M. Tignor, S. K. Allen, J. Boschung, A. Nauels, Y. Xia, V. Bex, and P. M. Midgley (Cambridge, New York, NY: Cambridge University Press), 465–570.

Cohen-Ofri, I., Weiner, L., Boaretto, E., Mintz, G., and Weiner, S. (2006). Modern and fossil charcoal: aspects of structure and diagenesis. *J. Archaeol. Sci.* 33, 428–439. doi: 10.1016/j.jas.2005.08.008

Cornelissen, G., and Gustafsson, Ö. (2004). Sorption of phenanthrene to environmental black carbon in sediment with and without organic matter and native sorbates. *Environ. Sci. Technol.* 38, 148–155. doi: 10.1021/es034776m

DeLuca, T. H., Gundale, M. J., MacKenzie, M. D., and Jones, D. L. (2015). "Biochar effects on soil nutrient transformations," in *Biochar for Environmental Management: Science, Technology and Implementation,* eds J. Lehmann and S. Joseph (New York, NY: Routledge), 421–454.

DeLuca, T. H., MacKenzie, M. D., Gundale, M. J., and Holben, W. E. (2006). Wildfire-produced charcoal directly influences nitrogen cycling in ponderosa pine forests. *Soil Sci. Soc. Am. J.* 70, 448. doi: 10.2136/sssaj2005.0096

DeLuca, T. H., Nilsson, M., and Zackrisson, O. (2002). Nitrogen mineralization and phenol accumulation along a fire chronosequence in northern Sweden. *Oecologia* 133, 206–214. doi: 10.1007/s00442-002-1025-2

Dietrich, S. T., MacKenzie, M. D., Battigelli, J. P., and Enterina, J. R. (2017). Building a better soil for upland surface mine reclamation in northern Alberta: admixing peat, subsoil, and peat biochar in a greenhouse study with aspen. *Can. J. Soil Sci.* doi: 10.1139/CJSS-2017-0021. [Epub ahead of print].

Ding, Y., Cawley, K. M., da Cunha, C. N., and Jaffé, R. (2014). Environmental dynamics of dissolved black carbon in wetlands. *Biogeochemistry* 119, 259–273. doi: 10.1007/s10533-014-9964-3

Domene, X. (2016). "A critical analysis of meso- and macrofauna effects following biochar supplementation," in *Biochar Application: Essential Soil Microbial Ecology,* eds T. K. Ralebitso-Senior and C. H. Orr (San Diego, CA: Elsevier), 268–292.

Fakoussa, R. M., and Hofrichter, M. (1999). Biotechnology and microbiology of coal degradation. *Appl. Microbiol. Biotechnol.* 52, 25–40. doi: 10.1007/s002530051483

Gao, X., Driver, L. E., Kasin, I., Masiello, C. A., Pyle, L. A., Dugan, B., et al. (2017). Effect of environmental exposure on charcoal density and porosity in a boreal forest. *Sci. Total Environ*. 592, 316–325. doi: 10.1016/j.scitotenv.2017.03.073

Gavin, D. G., Brubaker, L. B., and Lertzman, K. P. (2003). Holocene fire history of a costal temperate rain forest based on soil charcoal radiocarbon dates. *Ecology* 84, 186–201. doi: 10.1890/0012-9658(2003)084[0186:HFHOAC2.0.CO;2]

Glaser, B., and Amelung, W. (2003). Pyrogenic carbon in native grassland soils along a climosequence in North America. *Glob. Biogeochem. Cycles* 17:1064. doi: 10.1029/2002GB002019

Hall, K. E., Calderon, M. J., Spokas, K. A., Cox, L., Koskinen, W. C., Novak, J., et al. (2014). Phenolic acid sorption to biochars from mixtures of feedstock materials. *Water Air Soil Pollut.* 225:2031. doi: 10.1007/s11270-014-2031-9

Hamer, U., Marschner, B., Brodowski, S., and Amelung, W. (2004). Interactive priming of black carbon and glucose mineralisation. *Org. Geochem.* 35, 823–830. doi: 10.1016/j.orggeochem.2004.03.003

Hammes, K., Schmidt, M. W. I., Smernik, R. J., Currie, L. A., Ball, W. P., Nguyen, T. H., et al. (2007). Comparison of quantification methods to measure fire-derived (black/elemental) carbon in soils and sediments using reference materials from soil, water, sediment and the atmosphere. *Glob. Biogeochem. Cycles* 21:GB3016. doi: 10.1029/2006GB002914

Hanan, E. J., Schimel, J. P., Dowdy, K., and D'Antonio, C. M. (2016). Effects of substrate supply, pH, and char on net nitrogen mineralization and nitrification along a wildfire-structured age gradient in chaparral. *Soil Biol. Biochem*. 95, 87–99. doi: 10.1016/j.soilbio.2015.12.017

Hart, S., and Luckai, N. (2013). REVIEW: Charcoal function and management in boreal ecosystems. *J. Appl. Ecol*. 50, 1197–1206. doi: 10.1111/1365-2664.12136

Hassan, S., and Mathesius, U. (2012). The role of flavonoids in root–rhizosphere signalling: opportunities and challenges for improving plant–microbe interactions. *J. Exp. Bot*. 63, 3429–3444. doi: 10.1093/jxb/err430

Hättenschwiler, S., and Vitousek, P. M. (2000). The role of polyphenols in terrestrial ecosystem nutrient cycling. *Trends Ecol. Evol*. 15, 238–243. doi: 10.1016/S0169-5347(00)01861-9

Hedges, J. I., Eglinton, G., Hatcher, P. G., Kirchman, D. L., Arnosti, C., Derenne, S., et al. (2000). The molecularly-uncharacterized component of nonliving organic matter in natural environments. *Org. Geochem.* 31, 945–958. doi: 10.1016/S0146-6380(00)00096-6

Hockaday, W. C., Grannas, A. M., Kim, S., and Hatcher, P. G. (2006). Direct molecular evidence for the degradation and mobility of black carbon in soils from ultrahigh-resolution mass spectral analysis of dissolved organic matter from a fire-impacted forest soil. *Org. Geochem.* 37, 501–510. doi: 10.1016/j.orggeochem.2005.11.003

Hockaday, W. C., Grannas, A. M., Kim, S., and Hatcher, P. G. (2007). The transformation and mobility of charcoal in a fire-impacted watershed. *Geochim. Cosmochim. Acta* 71, 3432–3445. doi: 10.1016/j.gca.2007.02.023

Inoue, J., Yoshie, A., Tanaka, T., Onji, T., and Inoue, Y. (2017). Disappearance and alteration process of charcoal fragments in cumulative soils studied using Raman spectroscopy. *Geoderma* 285, 164–172. doi: 10.1016/j.geoderma.2016.09.032

Jones, D. L., Murphy, D. V., Khalid, M., Ahmad, W., Edwards-Jones, G., and DeLuca, T. H. (2011). Short-term biochar-induced increase in soil CO2 release is both biotically and abiotically mediated. *Soil Biol. Biochem*. 43, 1723–1731. doi: 10.1016/j.soilbio.2011.04.018

Joseph, S., Graber, E. R., Chia, C., Munroe, P., Donne, S., Thomas, T., et al. (2013). Shifting paradigms: development of high-efficiency biochar fertilizers based on nano-structures and soluble components. *Carbon Manage.* 4, 323–343. doi: 10.4155/cmt.13.23

Keech, O., Carcaillet, C., and Nilsson, M.-C. (2005). Adsorption of allelopathic compounds by wood-derived charcoal: the role of wood porosity. *Plant Soil* 272, 291–300. doi: 10.1007/s11104-004-5485-5

Kleber, M., Hockaday, W. C., and Nico, P. S. (2015). "Characteristics of biochar: macro-molecular properties," in *Biochar for Environmental Management: Science, Technology and Implementation, 2nd Edn.,* eds J. Lehmann and S. Joseph (New York, NY: Routledge), 111–137.

Koide, R. T., Petprakob, K., and Peoples, M. (2011). Quantitative analysis of biochar in field soil. *Soil Biol. Biochem*. 43, 1563–1568. doi: 10.1016/j.soilbio.2011.04.006

Kolton, M., Graber, E. R., Tsehansky, L., Elad, Y., and Cytryn, E. (2017). Biochar-stimulated plant performance is strongly linked to microbial diversity and metabolic potential in the rhizosphere. *New Phytol.* 213, 1393–1404. doi: 10.1111/nph.14253

Kurth, V. J., Hart, S. C., Ross, C. S., Kaye, J. P., and Fulé, P. Z. (2014). Stand-replacing wildfires increase nitrification for decades in southwestern ponderosa pine forests. *Oecologia* 175, 395–407. doi: 10.1007/s00442-014-2906-x

Kurth, V. J., MacKenzie, M. D., and DeLuca, T. H. (2006). Estimating charcoal content in forest mineral soils. *Geoderma* 137, 135–139. doi: 10.1016/j.geoderma.2006.08.003

Kuzyakov, Y., Subbotina, I., Chen, H., Bogomolova, I., and Xu, X. (2009). Black carbon decomposition and incorporation into soil microbial biomass estimated by 14C labeling. *Soil Biol. Biochem.* 41, 210–219. doi: 10.1016/j.soilbio.2008.10.016

Laird, D. A., Chappell, M. A., Martens, D. A., Wershaw, R. L., and Thompson, M. (2008). Distinguishing black carbon from biogenic humic substances in soil clay fractions. *Geoderma* 143, 115–122. doi: 10.1016/j.geoderma.2007.10.025

Lehmann, J., and Joseph, S. (2015). *Biochar for Environmental Management: Science, Technology and Implementation*. New York, NY: Routledge.

Lehmann, J., Rillig, M. C., Thies, J., Masiello, C. A., Hockaday, W. C., and Crowley, D. (2011). Biochar effects on soil biota—a review. *Soil Biol. Biochem.* 43, 1812–1836. doi: 10.1016/j.soilbio.2011.04.022

Liang, B., Lehmann, J., Solomon, D., Sohi, S., Thies, J. E., Skjemstad, J. O., et al. (2008). Stability of biomass-derived black carbon in soils. *Geochim. Cosmochim. Acta* 72, 6069–6078. doi: 10.1016/j.gca.2008.09.028

Licata, C., and Sanford, R. (2012). Charcoal and total carbon in soils from foothills shrublands to subalpine forests in the Colorado front range. *Forests* 3:944. doi: 10.3390/f3040944

MacKenzie, M. D., and DeLuca, T. H. (2006). Charcoal and shrubs modify soil processes in ponderosa pine forests of western Montana. *Plant Soil* 287, 257–266. doi: 10.1007/s11104-006-9074-7

MacKenzie, M. D., McIntire, E. J. B., Quideau, S. A., and Graham, R. C. (2008). Charcoal distribution affects carbon and nitrogen contents in forest soils of California. *Soil Sci. Soc. Am. J.* 72, 1774–1785. doi: 10.2136/sssaj2007.0363

Maestrini, B., Herrmann, A. M., Nannipieri, P., Schmidt, M. W. I., and Abiven, S. (2014). Ryegrass-derived pyrogenic organic matter changes organic carbon and nitrogen mineralization in a temperate forest soil. *Soil Biol. Biochem.* 69, 291–301. doi: 10.1016/j.soilbio.2013.11.013

Makoto, K., Kamata, N., Kamibayashi, N., Koike, T., and Tani, H. (2012). Bark-beetle-attacked trees produced more charcoal than unattacked trees during a forest fire on the Kenai Peninsula, Southern Alaska. *Scand. J. For. Res.* 27, 30–35. doi: 10.1080/02827581.2011.619566

Meyer, G. A., Wells, S. G., and Jull, A. T. (1995). Fire and alluvial chronology in Yellowstone National Park: climatic and intrinsic controls on Holocene geomorphic processes. *Geol. Soc. Am. Bull.* 107, 1211–1230. doi: 10.1130/0016-7606(1995)107andlt;1211:FAACIYandgt;2.3.CO;2

Michelotti, L., and Miesel, J. (2015). Source material and concentration of wildfire-produced pyrogenic carbon influence post-fire soil nutrient dynamics. *Forests* 6:1325. doi: 10.3390/f6041325

Miesel, J. R., Hockaday, W. C., Kolka, R. K., and Townsend, P. A. (2015). Soil organic matter composition and quality across fire severity gradients in coniferous and deciduous forests of the southern boreal region. *J. Geophys. Res. Biogeosci.* 120, 1124–1141. doi: 10.1002/2015JG002959

Mikutta, R., Kleber, M., Kaiser, K., and Jahn, R. (2005). Review: organic matter removal from soils using hydrogen peroxide, sodium hypochlorite, and disodium peroxodisulfate. *Soil Sci. Soc. Am. J.* 69, 120–135. doi: 10.2136/sssaj2005.0120

Nguyen, B. T., Lehmann, J., Kinyangi, J., Smernik, R., Riha, S. J., and Engelhard, M. H. (2008). Long-term black carbon dynamics in cultivated soil. *Biogeochemistry* 92, 163–176. doi: 10.1007/s10533-008-9248-x

Nishimiya, K., Hata, T., Imamura, Y., and Ishihara, S. (1998). Analysis of chemical structure of wood charcoal by X-ray photoelectron spectroscopy. *J. Wood Sci.* 44, 56–61. doi: 10.1007/BF00521875

Paavolainen, L., Kitunen, V., and Smolander, A. (1998). Inhibition of nitrification in forest soil by monoterpenes. *Plant Soil* 205, 147–154. doi: 10.1023/A:1004335419358

Parson, A., Robichaud, P. R., Lewis, S. A., Napper, C., and Clark, J. T. (2010). *Guide for Mapping Post-Fire Soil Burn Severity*. USFS Rocky Mountain Research Station, Fort Collins, CO.

Pierson, H. O. (1993). *Handbook of Carbon, Graphite, Diamonds and fullerenes: Processing, Properties and Applications.* Park Ridge, NJ: Noyes Publications.

Pietikäinen, J., Kiikkilä, O., and Fritze, H. (2000). Charcoal as a habitat for microbes and its effect on the microbial community of the underlying humus. *Oikos* 89, 231–242. doi: 10.1034/j.1600-0706.2000.890203.x

Pingree, M. R. A., DeLuca, E. E., Schwartz, D. T., and DeLuca, T. H. (2016). Adsorption capacity of wildfire-produced charcoal from Pacific Northwest forests. *Geoderma* 283, 68–77. doi: 10.1016/j.geoderma.2016.07.016

Pingree, M. R. A., Homann, P. S., Morrissette, B., and Darbyshire, R. (2012). Long and short-term effects of fire on soil charcoal of a conifer forest in southwest Oregon. *Forests* 3, 353–369. doi: 10.3390/f3020353

Preston, C. M., and Schmidt, M. W. I. (2006). Black (pyrogenic) carbon: a synthesis of current knowledge and uncertainties with special consideration of boreal regions. *Biogeosciences* 3, 397–420. doi: 10.5194/bg-3-397-2006

Quilliam, R. S., Glanville, H. C., Wade, S. C., and Jones, D. L. (2013). Life in the 'charosphere'—does biochar in agricultural soil provide a significant habitat for microorganisms? *Soil Biol. Biochem.* 65, 287–293. doi: 10.1016/j.soilbio.2013.06.004

Reisser, M., Purves, R. S., Schmidt, M. W. I., and Abiven, S. (2016). Pyrogenic carbon in soils: a literature-based inventory and a global estimation of its content in soil organic carbon and stocks. *Front. Earth Sci.* 4:80. doi: 10.3389/feart.2016.00080

Rovira, P., and Ramón Vallejo, V. (2007). Labile, recalcitrant, and inert organic matter in Mediterranean forest soils. *Soil Biol. Biochem.* 39, 202–215. doi: 10.1016/j.soilbio.2006.07.021

Santín, C., Doerr, S. H., Preston, C. M., and González-Rodríguez, G. (2015). Pyrogenic organic matter production from wildfires: a missing sink in the global carbon cycle. *Glob. Chang. Biol.* 21, 1621–1633. doi: 10.1111/gcb.12800

Schneider, M. P. W., Hilf, M., Vogt, U. F., and Schmidt, M. W. I. (2010). The benzene polycarboxylic acid (BPCA) pattern of wood pyrolyzed between 200°C and 1000°C. *Org. Geochem.* 41, 1082–1088. doi: 10.1016/j.orggeochem.2010.07.001

Scott, A. C. (2000). The Pre-Quaternary history of fire. *Palaeogeography* 164, 281–329. doi: 10.1016/S0031-0182(00)00192-9

Singh, B. P., Cowie, A. L., and Smernik, R. J. (2012). Biochar carbon stability in a clayey soil as a function of feedstock and pyrolysis temperature. *Environ. Sci. Technol.* 46, 11770–11778. doi: 10.1021/es302545b

Singh, N., Abiven, S., Maestrini, B., Bird, J. A., Torn, M. S., and Schmidt, M. W. I. (2014). Transformation and stabilization of pyrogenic organic matter in a temperate forest field experiment. *Glob. Chang. Biol.* 20, 1629–1642. doi: 10.1111/gcb.12459

Sohi, S. P., Krull, E., Lopez-Capel, E., and Bol, R. (2010). "Chapter 2—a review of biochar and its use and function in soil," in *Advances in Agronomy*, ed D. E. Sparks (San Diego, CA: Academic Press), 47–82.

Soucémarianadin, L. N., Quideau, S. A., and MacKenzie, M. D. (2014). Pyrogenic carbon stocks and storage mechanisms in podzolic soils of fire-affected Quebec black spruce forests. *Geoderma* 217–218, 118–128. doi: 10.1016/j.geoderma.2013.11.010

Spokas, K. A., Baker, J. M., and Reicosky, D. C. (2010). Ethylene: potential key for biochar amendment impacts. *Plant Soil* 333, 443–452. doi: 10.1007/s11104-010-0359-5

Thies, J. E., Rillig, M. C., and Graber, E. R. (2015). "Biochar effects on the abundance, activity and diversity of the soil biota," in *Biochar for Environmental Management: Science, Technology and Implementation,* eds J. Lehmann and S. Joseph (New York, NY: Routledge), 327–390.

Tinkham, W. T., Smith, A. M. S., Higuera, P. E., Hatten, J. A., Brewer, N. W., and Doerr, S. H. (2016). Replacing time with space: using laboratory fires to explore the effects of repeated burning on black carbon degradation. *Int. J. Wildland Fire* 25, 242–248. doi: 10.1071/WF15131

Uusitalo, M., Kitunen, V., and Smolander, A. (2008). Response of C and N transformations in birch soil to coniferous resin volatiles. *Soil Biol. Biochem.* 40, 2643–2649. doi: 10.1016/j.soilbio.2008.07.009

Zackrisson, O., Nilsson, M.-C., and Wardle, D. A. (1996). Key ecological function of charcoal from wildfire in the Boreal forest. *Oikos* 77, 10–19. doi: 10.2307/3545580

Zhu, D., Kwon, S., and Pignatello, J. J. (2005). Adsorption of single-ring organic compounds to wood charcoals prepared under different thermochemical conditions. *Environ. Sci. Technol.* 39, 3990–3998. doi: 10.1021/es0 50129e

Zimmerman, A. R. (2010). Abiotic and microbial oxidation of laboratory-produced black carbon (biochar). *Environ. Sci. Technol.* 44, 1295–1301. doi: 10.1021/es903140c

Zimmerman, A. R., Gao, B., and Ahn, M.-Y. (2011). Positive and negative carbon mineralization priming effects among a variety of biochar-amended soils. *Soil Biol. Biochem.* 43, 1169–1179. doi: 10.1016/j.soilbio.2011. 02.005

**Conflict of Interest Statement:** The authors declare that the research was conducted in the absence of any commercial or financial relationships that could be construed as a potential conflict of interest.

frontiers in Earth Science

ORIGINAL RESEARCH
published: 04 June 2018
doi: 10.3389/feart.2018.00061

# Dynamics of Charcoal Alteration in a Tropical Biome: A Biochar-Based Study

*Philippa L. Ascough[1]*, Michael I. Bird[2], William Meredith[3], Colin Snape[3], D. Large[3], Emma Tilston[1,4], David Apperley[5], Ana Bernabé[3,6] and Licheng Shen[3,7]*

*[1] NERC Radiocarbon Facility, Scottish Universities Environmental Research Center, East Kilbride, United Kingdom, [2] College of Science and Engineering, Centre for Tropical Environmental and Sustainability, ARC Centre of Excellence for Australian Biodiversity and Heritage, James Cook University, Cairns, QLD, Australia, [3] Department of Chemical and Environmental Engineering, Faculty of Engineering, University of Nottingham, Nottingham, United Kingdom, [4] NIAB EMR, Kent, United Kingdom, [5] EPSRC Solid-State NMR Service, Department of Chemistry, Durham University, Durham, United Kingdom, [6] Department of Environmental Engineering, Federal University of Espírito Santo, Vitória, Brazil, [7] Laboratory of Sustainable Water Engineering, Department of Engineering Science, University of Oxford, Oxford, United Kingdom*

Pyrogenic carbon (PyC) is a polyaromatic residue of the incomplete combustion of biomass or fossil fuels. There is a growing recognition that PyC forms an important part of carbon budgets, due to production rates of 116–385 Tg C yr, and the size and ubiquity of PyC stocks in global carbon reservoirs. At least a proportion of PyC exists in a highly recalcitrant chemical form, raising the prospect of long-term carbon sequestration through soil amendment with "biochar," which is generally produced with the aim of making a particularly recalcitrant form of PyC. However, there is growing evidence that some PyC, including biochar, can be both physically and chemically altered and degraded upon exposure to the environment over annual timescales, yet there is a lack of information concerning the mechanisms and determining factors of degradation. Here, we investigate three main factors; production temperature, feedstock composition, and the characteristics of the environment to which the material is exposed (e.g., pH, organic matter composition, oxygen availability) by analysis of biochar samples in a litterbag experiment before and after a year-long field study in the tropical rainforests of northeast Australia. We find that non-lignocellulosic feedstock has lower aromaticity, plus lower O/C and H/C ratios for a given temperature, and consequently lower carbon sequestration potential. The rate at which samples are altered is production temperature-dependant; however even in the highest temperature samples loss of the semi-labile aromatic carbon component is observed over 1 year. The results of $^{13}$C-MAS-NMR measurements suggest that direct oxygenation of aromatic structures may be even more important than carboxylation in environmental alteration of biochar (as a subset of PyC). There is a clear effect of depositional environment on biochar alteration even after the relatively short timescale of this study, as changes are most extensive in the most oxygenated material that was exposed on the soil surface. This is most likely the result of mineral ingress and colonization by soil microbiota. Consequently, oxygen availability and physical or chemical protection from sunlight and/or rainwater is vital in determining the alteration trajectory of this material.

**Keywords: pyrogenic carbon, black carbon, PAHs, charcoal, biochar**

OPEN ACCESS

***Edited by:***
*Samuel Abiven,*
*Universität Zürich, Switzerland*

***Reviewed by:***
*Bernardo Maestrini,*
*Michigan State University, United States*
*Christophe Naisse,*
*RITTMO Agroenvironnement, France*

****Correspondence:***
*Philippa L. Ascough*
*philippa.ascough@glasgow.ac.uk*

***Specialty section:***
*This article was submitted to Biogeoscience, a section of the journal Frontiers in Earth Science*

***Received:*** *09 August 2017*
***Accepted:*** *07 May 2018*
***Published:*** *04 June 2018*

***Citation:***
*Ascough PL, Bird MI, Meredith W, Snape C, Large D, Tilston E, Apperley D, Bernabé A and Shen L (2018) Dynamics of Charcoal Alteration in a Tropical Biome: A Biochar-Based Study. Front. Earth Sci. 6:61. doi: 10.3389/feart.2018.00061*

## INTRODUCTION

Pyrogenic carbon (PyC) is the product of incomplete biomass and fossil fuel combustion, forming a continuum from partially charred organic material to soot (Schmidt and Noack, 2000; Bird and Ascough, 2012). PyC is now known to comprise a fraction of every carbon reservoir on Earth (Kuhlbusch, 1998), yet we are only now beginning to understand its role in carbon cycling and carbon budgets (DeLuca and Aplet, 2008; Donato et al., 2009; Santín et al., 2016). The most recent estimate of global PyC production is 116–385 Tg C yr (Santín et al., 2016), equivalent to ∼0.2–0.6% of the terrestrial annual net primary production (Huston and Wolverton, 2009). This emphasizes the importance of PyC in the global carbon cycle, yet raises the question of what happens to PyC after it enters a carbon reservoir. Of particular interest is how PyC is altered by environmental exposure, and what determines the trajectory of this alteration.

We have moved away from understanding PyC as chemically homogeneous and inert in the environment. Some PyC does, however, remain undegraded over millennia, making it one of the most recalcitrant forms of organic carbon, with half-lives on the order of several thousand years (Preston and Schmidt, 2006). This raises the prospect that PyC forms an as yet unquantified long-term carbon sink. These features have generated great interest in the prospect of artificially sequestering carbon in soils over extended timescales in the form of engineered charcoal (or "biochar") (Lehmann et al., 2006).

Biochar is consistent with other forms of PyC in containing a highly polyaromatic fraction, termed stable polyaromatic carbon (SPAC: McBeath et al., 2015), as defined by quantitative methods that work on a chemical basis, e.g., hydropyrolysis (Meredith et al., 2012) where the highly stable fraction is defined as containing 7 or more aromatic rings. This leads to long-term stability in the environment, for example, in a meta-analysis, Wang et al. (2016) found a mean residence time of 556 years for the recalcitrant biochar C pool, and Spokas (2010) predicted a half-life of >1000 years for biochars with an O:C ratio <0.2. On the other hand, although Santín et al. (2017) have shown that biochar (i.e., anthropogenically engineered) differs from "naturally" produced PyC in having higher carbon sequestration potential for a given production temperature, Bird et al. (2017) have shown biotic, and potentially abiotic degradation of a woody biochar after 3 years exposure to a tropical biome. It is clear, therefore, that at least a proportion of Biochar is subject to environmental alteration over shorter timescales of <1 year (Zimmermann et al., 2012; Bird et al., 2015; Wang et al., 2016), with examples of mineralization on timescales of 1 month (Hilscher et al., 2009). This has major implications for the use of biochar as a tool for carbon sequestration for periods on the order of >100 years, if a proportion of biochar carbon is not "locked up" over these timescales, but is mineralized to $CO_2$. Along with chemical degradation, physical processes such as freeze-thaw, and water-mediated erosion, may impact the structure of PyC in soils through physical breakdown and subsequent translocation (Carcaillet, 2001; Lehmann et al., 2003; Hammes and Schmidt, 2009; Major et al., 2010).

Three main factors are thought to control the alteration of PyC, and hence also biochar: the production temperature, feedstock composition, and the depositional environment (Cheng et al., 2008a; Ascough et al., 2011). Production temperature is positively related to aromatization (Ascough et al., 2008), theoretically making high-temperature biochar/PyC less susceptible to biotic and abiotic alteration (Bruun et al., 2008; Ascough et al., 2010c). Regarding feedstock as a factor, biochar from non-woody biomass has been reported to be more "degradable" than that made from wood (Hilscher et al., 2009). Finally, alteration of biochar/PyC has been observed to occur more rapidly in highly alkaline environments (Braadbaart et al., 2009) and in warmer, wetter biomes (Cheng et al., 2008b). Oxidative processes have been proposed as the dominant pathway for alteration, and hence oxygen availability is also thought to be important (Bird et al., 2017).

Our knowledge of alteration/stability according to the factors above is far from complete, including the actual mechanics of any alteration that occurs, i.e., how this process progresses from a molecular standpoint. This study aims to fill this knowledge gap by assessing the effect of (i) production temperature, (ii) starting material, and (iii) depositional environment on the chemical composition of different types of biochar. Here, we focus on the labile and semi-labile components of biochar (*sensu* Bird et al., 2015), with the highly stable polyaromatic carbon (SPAC) component considered in detail in a separate paper. In particular we seek to establish the effect of these variables on the chemical alteration of different forms of biochar. This is achieved by analysis of biochar (i.e., lab-produced charcoal) from four different starting materials and production conditions before and after exposure to the environment in a litterbag experiment at a field site in the tropical Daintree Rainforest, northeast Australia. Samples from one of these starting materials (biochar prepared from wood of Southern Beech (*Nothofagus* spp.), have previously been analyzed after a 3 year period of exposure, revealing indigenous carbon loss and ingrowth of exogenous carbon over this time (Bird et al., 2017). However, the chemical changes underlying these changes are unknown, along with the factors that drive observed differences between the dynamics of different biochar types in the environment. Here, we seek to address both these issues, studying material exposed to environmental conditions over a timeframe of 1 year, using major sources of biochar that are either proposed for use, or in commercial production.

Given the information available concerning factors influencing biochar alteration in the environment (outlined above), we hypothesize that for all starting materials, biochar produced at higher temperatures will be less affected by alteration during environmental exposure, and that this will be visible in the chemical characterizations we perform. Also that, for a given temperature, alteration will progress in the order of: commercial biochar < woody biomass < non-woody biomass. Finally, that samples exposed to more alkaline conditions will be more altered than that exposed to lower pH.

# METHODOLOGY

## Samples and Field Site

*Nothofagus* spp. wood (Southern Beech), chemically consistent with modern angiosperm wood in its lignocellulosic structure (Bird et al., 2014), was obtained from the Yallourn coal seam, as described in Tilston et al. (2016). Sugarcane (*Saccharum officinarum)* bagasse (fibrous matter remaining after crushing of sugarcane) was obtained from Mossman Sugar Mill, Australia, representing a cellulose-rich material. Macroalgae (*Cladophora vagabunda)* was collected at the Townsville Barramundi Fish Farm in Kelso, Townsville Australia. This sample represents a non-woody material with lower carbon concentration and surface area than wood or bagasse, but high in nitrogen and inorganic nutrients (Bird et al., 2011; McBeath et al., 2015). All three materials are important potential sources of biochar for carbon sequestration and/ or agricultural amendment. Finally, a commercial wood waste biochar, prepared at 550°C, was obtained from BEST Energies Ltd., Australia.

The *Nothofagus* spp. wood, *S. officinarum* bagasse and *C. vagabunda* algae were dried at 105°C, chipped and sieved, with the >2 mm fraction retained for pyrolysis, and converted to PyC under a 3.5 L $min^{-1}$ nitrogen flow for 1 h. Three temperatures of 305°C, 414°C, and 512°C were used, as in Bird et al. (2011). This is the temperature range over which the most significant changes in PyC chemistry are observed (Ascough et al., 2008). Following pyrolysis, samples were lightly crushed and sieved to 0.5–2 mm. Together with the BEST biochar, this yielded 10 sample types for field exposure.

Samples were exposed to local environmental conditions using a litterbag approach (see below) for 1 year at the Daintree Rainforest Observatory, Queensland, Australia. The field location is in a UNESCO World Heritage Site at Cape Tribulation, 140 km north of Cairns (16.103°S; 145.447°E; 70 m asl; **Figure 1**). Mean monthly temperature is 22–28°C (annual mean 25°C), and annual rainfall is 3,500 mm, with a pronounced December to March wet season. This site was chosen to maximize the rate of PyC-environment interactions, plus no historical burning is recorded, meaning natural PyC abundance in the soil is very low.

Vegetation is an evergreen mesophyll to notophyll "tall forest" (Torello-Raventos et al., 2013) producing broadleaf litter to 5–10 cm depth in the dry season, which rapidly decays in the wet season. Soils are developed on colluvium from metamorphic and granitic mountains, forming Acidic, Dystrophic, Brown Dermosols (Deckers et al., 1998; Isbell, 2002) or Haplic Cambisols (Hyperdystic, Alumic, Skeletic; Deckers et al., 1998), with a dark grayish brown silty loam to silty clay loam upper A-horizon. The profile contains 20–50% cobbles and stones, and the organic-rich (3.7% C, 0.3% N) soil is mildly acid (pH 5.5–6.5) with the <2 mm faction (0–10 cm) comprising 28% clay, 54% silt and 19% sand.

For each aliquot c.5 g of dry sample was placed within a 125 μm aperture nylon mesh bag, sealed and pegged to the soil surface, which had been cleared of leaf litter. The litterbag approach is well-established in the soil science literature, although potential drawbacks must also be considered, for example partial inaccessibility of litter to decomposers (St John, 1980). Four manipulations (soil chemical environments) were used and samples were duplicated for each of these (i.e., 20 samples per manipulation). The bags were covered with polyester shade cloth and enclosed in a wire mesh cage to exclude foraging wildlife. The treatments comprised:

(i) NL—Samples laid directly on the soil surface without any litter cover;
(ii) L—as for NL but samples covered with a ∼5 cm layer of local leaf litter;
(iii) NL-LM—as for NL but samples covered with a ∼5 cm thick layer of limestone chips (sieved at 2–10 mm) in order to raise the local pH;
(iv) L-LM—as for NL-LM but the layer of limestone chips was mixed with an equal volume of local leaf litter.

The exact pH at the sample site was not determined, but surface soil and leachate water after 1 year of environmental exposure shows that treatments L and NL had a local pH of 5.6–6.5, and treatments L-LM and NL-LM had a local pH of 6.6–8.0. After recovery samples were gently washed free of loosely adhering soil particles, dried at 105°C and weighed. Both freshly prepared samples and exposed material were analyzed as described below.

## Elemental Abundance, Isotopic Analysis and Ash Concentration

Carbon (%C) and nitrogen (%N) concentration was measured using a Costech elemental analyser (EA) (Milan, Italy) fitted with a zero-blank auto-sampler. External reproducibility for %C and %N was better than 0.5%. The stable carbon isotope ratio (expressed as $\delta^{13}C$) of the samples was measured using a ThermoFinnigan Delta$^{plus}$ XL isotope ratio mass spectrometer (Thermo Finnigan GmbH, Bremen, FRG), linked to the EA via a ConFlo III. Analytical precision was ±0.2‰ for $\delta^{13}C$ and ±0.3‰ for $\delta^{15}N$. Oxygen (%O) and hydrogen (%H) concentration was measured using a Thermo Finnigan high temperature conversion elemental analyser (TC/EA) (Thermo Finnigan GmbH, Bremen, FRG). External reproducibility for %O and %H was better than 0.7%. The ash concentration of the samples was determined by loss-on-ignition of 1 g at 900°C in ceramic crucibles in a muffle furnace where reproducibility was better than 1.0%.

## PAH Concentration by Hydrogen Pyrolysis and GC-MS

Hydrogen pyrolysis (HyPy; Ascough et al., 2009, 2010b; Meredith et al., 2012) was used to release the <7 ring polycyclic aromatic hydrocarbons (PAHs, the non-stable PyC fraction), from all samples. Briefly, samples were loaded with an aqueous/methanol solution of ammonium dioxydithiomolybdate $[(NH_4)_2MoO_2S_2]$, and pyrolysed by resistive heating to a final temperature of 550°C, all under a hydrogen pressure of 15 MPa and a sweep gas flow of 5 L $min^{-1}$ (Meredith et al., 2012).

HyPy products were trapped on cooled silica, and desorbed with 10 ml aliquots of n-hexane and dichloromethane (DCM). Eluents were combined and GC–MS analyses in full scan mode (m/z 50–450) were performed on a Varian CP-3800 gas chromatograph equipped with a VF-1MS fused silica capillary column (50 m × 0.25 mm i.d., 0.25 mm thickness) with helium as the carrier gas, interfaced to a Varian 1200 mass spectrometer (EI mode, 70 eV). The abundances of individual PAHs were

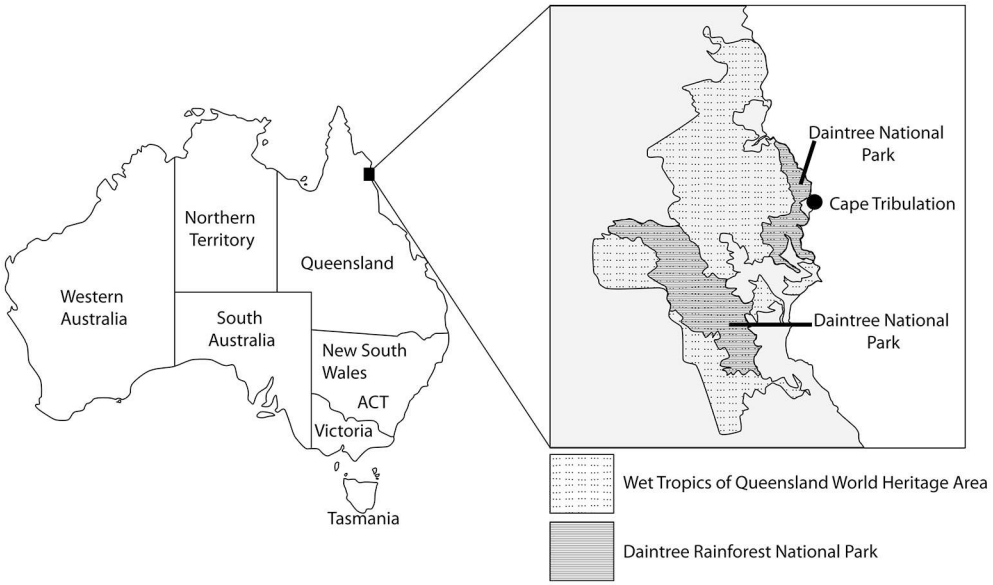


**FIGURE 1 |** Field site location: Daintree Rainforest National Park at Cape Tribulation, Queensland, Australia.

quantified using the mass chromatograms of the molecular ion of each compound, following the addition of squalane (Aldrich) and 1-1 binapthyl (Acros Organics) as internal standards, assuming a response factor for each compound of 1 (Meredith et al., 2013). The PAHs comprise those that are solvent extractable ("free") and those covalently bonded to the biochar released by HyPy.

## $^{13}$C-CPMAS NMR Spectroscopy

Solid-state $^{13}$C Nuclear Magnetic Resonance Spectroscopy, using cross-polarization magic angle spinning ($^{13}$C-CPMAS NMR) was used to identify polyaromatic vs. aliphatic and O-alkyl carbons. A 400 MHz Varian VNMRS instrument was used, operating at 100.56 MHz for $^{13}$C using a 4 mm magic-angle spinning probe with a zirconium oxide rotor and Teflon end caps. Spectra were referenced to external, neat tetramethylsilane, and for cross polarization, typical acquisition conditions were a 1 s recycle delay, 1 ms contact time and a sample spin-rate of 12 kHz. A variable amplitude 1H spin-lock pulse was used for the cross polarization step. The pulse sequence incorporated a spin-echo to suppress background signal from the Vespel spinner housing; this has resulted in a small amount of signal in some spectra at ∼111 ppm.

## Change in Carbon Concentration and Sample Mass

Weights of samples and their carbon concentration were accurately determined before and after exposure in the field, making it possible to quantify changes in sample mass and carbon concentration during exposure of the samples to the environment. The proportional mass difference in samples before ($M_{T0}$) and after exposure ($M_{T1}$) is obtained by:

$$\%\text{mass change} = \left[\frac{(M_{T1} - M_{T0})}{M_{T0}}\right] \times 100$$

The proportional change in carbon concentration (mg C), ash concentration, oxygen, hydrogen, and nitrogen are obtained by substituting values before ($X_{T0}$) and after exposure ($X_{T1}$) into Equation (1).

The potential for significant differences between mass and C/O/H/N for samples was assessed after data was scrutinized for normality using a D'Agostino-Pearson normality test. Subsequently, samples were compared using a Two-way ANOVA followed by Tukey's multiple comparisons test, performed using GraphPad Prism version 7.02 for Windows, GraphPad Software, La Jolla California USA, www.graphpad.com. A $p$-value of $<0.05$ indicated a significant difference.

# RESULTS

## Variations in Sample Mass and Ash Concentration

Full results of measurements for all samples are presented in Supplementary Table S1, and summary data is presented in **Table 1**. The mass and ash concentration changes following field exposure for *Nothofagus* spp. wood biochar samples are presented in Bird et al. (2017) (**Table 1**), but are discussed here in comparison to other samples. *Nothofagus* wood spp., *S. officinarum* bagasse, and BEST biochar contained little ash, with most samples below the limit of detection before and after environmental exposure (**Table 1**). The exception is *C. vagabunda* algae biochar, which contained 28–38% ash by

**TABLE 1 |** Measured ash content, elemental abundance (%C, %O, %H, %N), and stable isotope ratios ($\delta^{13}C$ and $\delta^{15}N$) before and after environmental exposure.

| Sample | Ash% | %C | %O | %H | %N | $\delta^{13}C$ | $\delta^{15}N$ |
|---|---|---|---|---|---|---|---|
| **BEFORE ENVIRONMENTAL EXPOSURE** | | | | | | | |
| *Nothofagus* wood | LD* | 55.7 ± 0.1 | 31.4** | 5.9** | LD* | −21.1 ± 0.1 | LD* |
| *Nothofagus* wood 300°C | LD* | 63.7 ± 0.2 | 26.1** | 5.3** | LD* | −21.1 ± 0.0 | LD* |
| *Nothofagus* wood 400°C | LD* | 71.2 ± 0.3 | 18.8** | 3.3** | LD* | −21.4 ± 0.0 | LD* |
| *Nothofagus* wood 500°C | LD* | 76.9 ± 0.7 | 13.6** | 2.8** | LD* | −21.5 ± 0.0 | LD* |
| *C. vagabunda* algae | 28 ± 0.4 | 40.9 ± 1.6 | 28.9** | 5.7** | 6.3 ± 0.3 | −19.1 ± 0.8 | 8.5 ± 0.1 |
| *C. vagabunda* algae 300°C | 26 ± 2.4 | 53.0 ± 1.8 | 15.2** | 5.0** | 8.6 ± 0.3 | −19.2 ± 0.0 | 10.8 ± 0.2 |
| *C. vagabunda* algae 400°C | 35 ± 1.2 | 54.9 ± 1.6 | 13.7** | 3.2** | 8.5 ± 0.2 | −17.9 ± 0.1 | 10.8 ± 0.2 |
| *C. vagabunda* algae 500°C | 38 ± 1.7 | 54.0 ± 1.7 | 15.7** | 2.3** | 7.8 ± 0.2 | −17.7 ± 0.1 | 10.6 ± 0.4 |
| *S. officinarum* | 2 ± 0.7 | 46.1 ± 0.0 | 40.9** | 6.2** | LD* | −13.0 ± 0.3 | LD* |
| *S. officinarum* 300°C | LD* | 55.6 ± 0.3 | 33.2** | 5.6** | LD* | −13.6 ± 0.1 | LD* |
| *S. officinarum* 400°C | LD* | 69.5 ± 0.5 | 18.3** | 3.6** | LD* | −14.0 ± 0.1 | LD* |
| *S. officinarum* 500°C | LD* | 74.3 ± 0.2 | 12.8** | 2.9** | LD* | −14.3 ± 0.0 | LD* |
| BEST biochar 550°C | 1 ± 1.3 | 84.8 ± 1.1 | 8.1** | 2.5** | LD* | −27.7 ± 0.0 | LD* |
| **AFTER ENVIRONMENTAL EXPOSURE** | | | | | | | |
| *Nothofagus* wood 300°C NL | 2** | 60.9 ± 1.6 | 26.6** | 5.3** | LD* | −21.4 ± 0.0 | LD* |
| *Nothofagus* wood 300°C L | LD* | 65.5 ± 1.8 | 26.0** | 5.4** | LD* | −21.2 ± 0.0 | LD* |
| *Nothofagus* wood 300°C NL-LM | LD* | 65.8 ± 4.6 | 26.6** | 5.5** | LD* | −21.2 ± 0.1 | LD* |
| *Nothofagus* wood 300°C L-LM | LD* | 64.0 ± 2.2 | 27.1** | 5.5** | LD* | −21.2 ± 0.1 | LD* |
| *Nothofagus* wood 400°C NL | 1 ± 2 | 69.6 ± 0.9 | 19.3** | 3.2** | LD* | −21.6 ± 0.0 | LD* |
| *Nothofagus* wood 400°C L | LD* | 71.2 ± 3.0 | 19.5** | 3.2** | LD* | −21.5 ± 0.0 | LD* |
| *Nothofagus* wood 400°C NL-LM | LD* | 72.5 ± 2.7 | 18.9** | 3.2** | LD* | −21.5 ± 0.1 | LD* |
| *Nothofagus* wood 400°C L-LM | LD* | 71.6 ± 2.3 | 18.8** | 3.3** | LD* | −21.5 ± 0.0 | LD* |
| *Nothofagus* wood 500°C NL | 3 ± 3 | 74.5 ± 1.5 | 14.0** | 2.7** | LD* | −21.6 ± 0.0 | LD* |
| *Nothofagus* wood 500°C L | LD* | 77.9 ± 2.0 | 12.9** | 2.7** | LD* | −21.5 ± 0.1 | LD* |
| *Nothofagus* wood 500°C NL-LM | LD* | 78.8 ± 3.2 | 13.6** | 2.9** | LD* | −21.7 ± 0.3 | LD* |
| *Nothofagus* wood 500°C L-LM | LD* | 78.7 ± 2.0 | 13.1** | 2.7** | LD* | −21.6 ± 0.0 | LD* |
| *C. vagabunda* algae 300°C NL | 15 ± 2 | 47.1 ± 1.7 | 15.7** | 4.8** | 7.5 ± 0.7 | −19.4 ± 0.3 | 10.8 ± 0.2 |
| *C. vagabunda* algae 300°C L | 12 ± 1 | 53.0 ± 6.4 | 17.3** | 5.0** | 8.5 ± 1.5 | −19.4 ± 0.1 | 10.9 ± 0.2 |
| *C. vagabunda* algae 300°C NL-LM | 9 ± 1 | 55.5 ± 3.5 | 17.6** | 5.3** | 9.1 ± 0.8 | −19.2 ± 0.2 | 11.0 ± 0.2 |
| *C. vagabunda* algae 300°C L-LM | 10 ± 1 | 54.7 ± 1.9 | 18.5** | 5.2** | 9.0 ± 0.5 | −19.1 ± 0.1 | 11.0 ± 0.2 |
| *C. vagabunda* algae 400°C NL | 16 ± 5 | 52.8 ± 7.9 | 16.7** | 3.9** | 8.2 ± 1.4 | −18.6 ± 0.2 | 11.0 ± 0.0 |
| *C. vagabunda* algae 400°C L | 12 ± 5 | 55.9 ± 6.2 | 15.9** | 3.9** | 8.7 ± 1.2 | −18.1 ± 0.1 | 10.9 ± 0.1 |
| *C. vagabunda* algae 400°C NL-LM | 13 ± 7 | 58.0 ± 5.2 | 15.5** | 3.9** | 9.0 ± 1.2 | −18.0 ± 0.3 | 11.0 ± 0.1 |
| *C. vagabunda* algae 400°C L-LM | 15 ± 7 | 56.2 ± 8.6 | 15.7** | 4.0** | 8.6 ± 1.8 | −18.3 ± 0.2 | 10.8 ± 0.3 |
| *C. vagabunda* algae 500°C NL | 19 ± 1 | 54.4 ± 5.6 | 17.6** | 2.6** | 8.0 ± 1.1 | −18.8 ± 0.2 | 10.7 ± 0.3 |
| *C. vagabunda* algae 500°C L | 22 ± 5 | 56.0 ± 4.2 | 16.9** | 2.5** | 8.3 ± 0.9 | −18.3 ± 0.0 | 11.1 ± 0.3 |
| *C. vagabunda* algae 500°C NL-LM | 18 ± 0 | 56.1 ± 3.5 | 17.0** | 2.5** | 8.2 ± 0.8 | −18.1 ± 0.0 | 11.0 ± 0.0 |
| *C. vagabunda* algae 500°C L-LM | 19 ± 2 | 57.2 ± 3.5 | 17.5** | 2.5** | 8.5 ± 0.7 | −18.0 ± 0.2 | 11.0 ± 0.3 |
| *S. officinarum* 300°C NL | 4** | 52.8 ± 2.5 | 34.1** | 5.3** | LD* | −13.6 ± 0.3 | LD* |
| *S. officinarum* 300°C L | LD* | 54.6 ± 2.3 | 34.4** | 5.6** | LD* | −13.6 ± 0.0 | LD* |
| *S. officinarum* 300°C NL-LM | 3** | 55.2 ± 2.4 | 35.5** | 5.8** | LD* | −13.5 ± 0.1 | LD* |
| *S. officinarum* 300°C L-LM | 3** | 55.9 ± 2.9 | 35.2** | 5.7** | LD* | −13.6 ± 0.2 | LD* |
| *S. officinarum* 400°C NL | 9** | 65.1 ± 3.0 | 20.3** | 3.6** | LD* | −14.4 ± 0.3 | LD* |
| *S. officinarum* 400°C L | 5** | 70.0 ± 1.9 | 19.5** | 3.7** | LD* | −14.0 ± 0.1 | LD* |
| *S. officinarum* 400°C NL-LM | 5** | 67.0 ± 1.5 | 20.5** | 3.7** | LD* | −14.2 ± 0.0 | LD* |
| *S. officinarum* 400°C L-LM | 4** | 67.6 ± 0.3 | 18.6** | 3.6** | LD* | −14.2 ± 0.0 | LD* |
| *S. officinarum* 500°C NL | 10** | 66.8 ± 0.7 | 16.4** | 3.0** | LD* | −14.7 ± 0.1 | LD* |
| *S. officinarum* 500°C L | 5** | 72.7 ± 0.9 | 13.3** | 2.8** | LD* | −14.3 ± 0.1 | LD* |
| *S. officinarum* 500°C NL-LM | 8** | 71.6 ± 0.9 | 14.3** | 2.9** | LD* | −14.6 ± 0.1 | LD* |
| *S. officinarum* 500°C L–LM | 4** | 73.5 ± 0.7 | 13.0** | 2.9** | LD* | −14.3 ± 0.0 | LD* |
| BEST biochar 550°C NL | 3** | 80.0 ± 1.7 | 9.3** | 2.5** | LD* | −27.6 ± 0.1 | LD* |
| BEST biochar 550°C L | LD* | 82.3 ± 1.7 | 8.5** | 2.5** | LD* | −27.7 ± 0.1 | LD* |
| BEST biochar 550°C NL-LM | LD* | 81.0 ± 2.1 | 9.1** | 2.5** | LD* | −27.7 ± 0.0 | LD* |
| BEST biochar 550°C L-LM | 2** | 82.7 ± 3.5 | 8.8** | 2.5** | LD* | −27.6 ± 0.1 | LD* |

*NB: values are the average of two replicates with the standard deviation presented as ± the average. LD*, At or below the limit of detection. **Not replicated.*

weight, increasing with production temperature. A large amount (65–83%) of this ash was lost during exposure (**Table 2**).

The mass of BEST biochar changed little with environmental exposure, and (excluding treatment NL), *Nothofagus* spp. wood mass increased by <10% (**Table 2**) (NB: isolated reductions in mass of the latter samples are outweighed by the increases). On the other hand, large mass increases of up to +36% occur in treatment NL for *Nothofagus* spp. wood and *S. officinarum* bagasse biochar shows changes of −9 to 41% (**Table 2**). *C. vagabunda* algae biochar again behaved differently, as its mass decreased by −41 to −52% (**Table 2**). This was consistently different to both the *Nothofagus* spp. wood and *S. officinarum* bagasse biochar ($p \leq 0.005$). There were statistically significant differences at 95% confidence between sample types, and treatments. An interaction between sample type and treatment ($p \leq 0.05$) was only observed for the 300°C samples, where mass

**TABLE 2 |** The proportional change following environmental exposure in sample mass, ash content, elemental abundance (%C, %O, %H, %N), expressed as % difference from starting values (as reported in **Table 1**), and the difference in stable isotope ratios ($\delta^{13}C$ and $\delta^{15}N$) after environmental exposure, expressed as ‰ deviation.

| Sample | Mass change | Ash change | %C change | %O change | %H change | %N change | $\delta^{13}C$ change | $\delta^{15}N$ change |
|---|---|---|---|---|---|---|---|---|
| *Nothofagus* wood 300°C NL | 31 ± 8 | 180** | 25.0 ± 11 | 39.4** | 36.4** | LD* | 0.2 ± 0.0 | LD* |
| *Nothofagus* wood 300°C L | 4 ± 0 | LD* | 7.1 ± 3 | 3.6** | 6.5** | LD* | 0.1 ± 0.0 | LD* |
| *Nothofagus* wood 300°C NL-LM | 5 ± 2 | LD* | 8.4 ± 10 | 8.5** | 11.1** | LD* | 0.1 ± 0.1 | LD* |
| *Nothofagus* wood 300°C L-LM | 6 ± 0 | LD* | 6.2 ± 3 | 9.5** | 10.6** | LD* | 0.1 ± 0.1 | LD* |
| *Nothofagus* wood 400°C NL | 36 ± 13 | 1 , 2 | 33.2 ± 11 | 29.9** | 25.8** | LD* | 0.2 ± 0.0 | LD* |
| *Nothofagus* wood 400°C L | −1 ± 2 | LD* | −0.9 ± 2 | 4.1** | 0.0** | LD* | 0.1 ± 0.0 | LD* |
| *Nothofagus* wood 400°C NL-LM | 7 ± 3 | LD* | 8.8 ± 1 | 9.3** | 8.6** | LD* | 0.1 ± 0.1 | LD* |
| *Nothofagus* wood 400°C L-LM | 2 ± 1 | LD* | 2.5 ± 2 | 0.9** | 0.8** | LD* | 0.1 ± 0.0 | LD* |
| *Nothofagus* wood 500°C NL | 32 ± 27 | LD* | 27.7 ± 29 | 54.7** | 46.8** | LD* | 0.1 ± 0.0 | LD* |
| *Nothofagus* wood 500°C L | 6 ± 1 | LD* | 7.4 ± 3 | 1.0** | 1.6** | LD* | 0.0 ± 0.1 | LD* |
| *Nothofagus* wood 500°C NL-LM | 7 ± 0 | LD* | 9.7 ± 5 | 6.6** | 9.5** | LD* | 0.2 ± 0.3 | LD* |
| *Nothofagus* wood 500°C L-LM | 5 ± 2 | LD* | 7.7 ± 1 | −0.3** | −0.9** | LD* | 0.1 ± 0.0 | LD* |
| *C. vagabunda* algae 300°C NL | −42 ± 1 | −65 ± 6 | −48.6 ± 3 | −40.7** | −45.7** | −49.7 ± 5.9 | 0.2 ± 0.3 | 0.1 , 0.2 |
| *C. vagabunda* algae 300°C L | −45 ± 0 | −75 ± 7 | −45.3 ± 6 | −37.8** | −46.2** | −45.9 ± 9.3 | 0.2 ± 0.1 | 0.2 , 0.2 |
| *C. vagabunda* algae 300°C NL-LM | −46 ± 0 | −82 ± 0 | −43.2 ± 4 | −36.8** | −42.2** | −42.5 ± 5.2 | 0.0 ± 0.2 | 0.2 , 0.2 |
| *C. vagabunda* algae 300°C L-LM | −49 ± 4 | −80 ± 1 | −47.2 ± 3 | −41.2** | −49.9** | −46.6 ± 1.3 | 0.0 ± 0.1 | 0.2 , 0.2 |
| *C. vagabunda* algae 400°C NL | −48 ± 1 | −76 ± 13 | −50.3 ± 6 | −38.3** | −38.0** | −50.4 ± 7.4 | 0.7 ± 0.2 | 0.3 , 0.0 |
| *C. vagabunda* algae 400°C L | −51 ± 1 | −83 ± 8 | −50.7 ± 5 | −43.5** | −41.4** | −50.5 ± 6.0 | 0.2 ± 0.1 | 0.1 , 0.1 |
| *C. vagabunda* algae 400°C NL-LM | −50 ± 0 | −81 ± 8 | −47.3 ± 4 | −44.1** | −40.4** | −47.2 ± 6.8 | 0.1 ± 0.3 | 0.2 , 0.1 |
| *C. vagabunda* algae 400°C L-LM | −52 ± 5 | −80 ± 2 | −50.2 ± 13 | −40.7** | −35.6** | −50.9 ± 15.2 | 0.4 ± 0.2 | 0.1 , 0.3 |
| *C. vagabunda* algae 500°C NL | −41 ± 4 | −70 ± 5 | −40.3 ± 2 | −30.0** | −30.3** | −39.5 ± 4.1 | 1.0 ± 0.2 | 0.1 , 0.3 |
| *C. vagabunda* algae 500°C L | −49 ± 0 | −70 ±, 7 | −47.2 ± 4 | −45.0** | −45.7** | −46.1 ± 5.6 | 0.6 ± 0.0 | 0.5 , 0.3 |
| *C. vagabunda* algae 500°C NL-LM | −48 ± 0 | −75 ± 0 | −45.9 ± 3 | −44.0** | −43.5** | −45.2 ± 4.7 | 0.4 ± 0.0 | 0.4 , 0.0 |
| *C. vagabunda* algae 500°C L-LM | −45 ± 1 | −73 ± 3 | −42.2 ± 4 | −39.7** | −40.4** | −40.8 ± 5.7 | 0.3 ± 0.2 | 0.4 , 0.3 |
| *S. officinarum* 300°C NL | 13 ± 2 | 200** | 7.0 ± 3 | 17.4** | 9.6** | LD* | 0.6 ± 0.3 | LD* |
| *S. officinarum* 300°C L | −6 ± 2 | LD* | −7.3 ± 6 | −0.7** | −4.0** | LD* | 0.6 ± 0.0 | LD* |
| *S. officinarum* 300°C NL-LM | 6 ± 1 | 69** | 5.1 ± 4 | 13.6** | 9.7** | LD* | 0.5 ± 0.1 | LD* |
| *S. officinarum* 300°C L-LM | −9 ± 0 | 43** | −8.7 ± 5 | −3.5** | −6.4** | LD* | 0.6 ± 0.2 | LD* |
| *S. officinarum* 400°C NL | 41 ± 15 | 6615** | 32.2 ± 20 | 44.6** | 29.9** | LD* | 0.4 ± 0.3 | LD* |
| *S. officinarum* 400°C L | 0 ± 2 | 2587** | 1.1 ± 0 | 8.5** | 5.5** | LD* | −0.1 ± 0.1 | LD* |
| *S. officinarum* 400°C NL-LM | 15 ± 3 | 3328** | 10.5 ± 5 | 26.1** | 15.5** | LD* | 0.1 ± 0.0 | LD* |
| *S. officinarum* 400°C L-LM | 4 ± 19 | 2208** | 1.5 ± 18 | 19.8** | 18.0** | LD* | 0.2 ± 0.0 | LD* |
| *S. officinarum* 500°C NL | 38 ± 25 | 1908** | 24.2 ± 22 | 100.7** | 61.3** | LD* | 0.4 ± 0.1 | LD* |
| *S. officinarum* 500°C L | −3 ± 4 | 478** | −4.6 ± 2 | 4.0** | −2.4** | LD* | 0.0 ± 0.1 | LD* |
| *S. officinarum* 500°C NL-LM | 26 ± 2 | 1082** | 21.2 ± 3 | 39.1** | 27.3** | LD* | 0.3 ± 0.1 | LD* |
| *S. officinarum* 500°C L-LM | −1 ± 4 | 438** | −2.1 ± 3 | 3.9** | 3.8** | LD* | 0.0 ± 0.0 | LD* |
| BEST biochar 550°C NL | 9 ± 0 | 274** | 2.8 ± 2 | 24.3** | 6.6** | LD* | −0.1 ± 0.1 | LD* |
| BEST biochar 550°C L | 2 ± 1 | LD* | −1.0 ± 1 | 8.2** | 0.4** | LD* | 0.0 ± 0.1 | LD* |
| BEST biochar 550°C NL-LM | −4 ± 3 | LD* | −8.7 ± 5 | 4.5** | −7.7** | LD* | 0.0 ± 0.0 | LD* |
| BEST biochar 550°C L-LM | 1 ± 2 | 159** | −1.3 ± 2 | 11.8** | 1.3** | LD* | −0.1 ± 0.1 | LD* |

*NB, values are the average of two replicates with the standard deviation presented as ± the average. LD*, At or below the limit of detection. **, Not replicated.*

gains in *Nothofagus* spp. wood biochar were greater than for other materials. At higher temperatures, there was no difference between the overall mass increases for *Nothofagus* spp. wood and *S. officinarum* bagasse biochar. *C. vagabunda* algae biochar showed no significant effect of treatment type at 95% confidence, and there was no clear difference in this between different temperatures, indicating that the mass losses in this sample type were consistent for all samples after 1 year. For the 300°C and 400°C *Nothofagus* spp. wood and *S. officinarum* bagasse biochar, treatment NL was associated with higher mass losses than other treatments ($p \leq 0.05$). At 500°C this effect was only evident for the *S. officinarum* bagasse biochar. Overall, *C. vagabunda* algae biochar showed a very different pattern of change to other sample types, and differences between treatments were most pronounced for samples produced at lower temperatures.

## Changes in Carbon, Nitrogen, Oxygen, and Hydrogen Concentration

Full results of measurements for all samples are presented in Supplementary Table S1, and summary data is presented in **Table 1**. For *Nothofagus* spp. wood, *S. officinarum* bagasse, and BEST biochar before environmental exposure, %C, concentrations clearly increased and %O and %H concentrations decreased as production temperature increased (**Table 1**), consistent with previous work (e.g., Ascough et al., 2008). *C. vagabunda* algae is different; although O is progressively lost at higher production temperatures, C and H show little change with production temperature after 300°C. Only *C. vagabunda* contained measureable quantities of nitrogen, which increased with initial charring at 300°C, thereafter remaining unchanged at production temperatures up to 500°C (**Table 1**).

For samples after environmental exposure, in all treatments except NL (exposed on the surface without litter cover) changes in carbon concentration relative to before exposure ranged from −1 to 33% in *Nothofagus* spp. wood, most *S. officinarum* bagasse, and BEST biochar (**Table 2**). Again, *C. vagabunda* algae is different; after environmental exposure C concentration decreases markedly, between −40 and −50%. There was no interaction between treatment and material type at any temperature (where $p \geq 0.1$ for the possibility of significant difference). There was no significant difference between carbon concentration increases in *Nothofagus* spp. wood, and *S. officinarum* bagasse except for treatment NL in 300°C samples ($p = 0.05$), where C increases in *Nothofagus* spp., wood, exceeded *S. officinarum* bagasse. Both were, however, consistently different to *C. vagabunda* biochar ($p \leq 0.01$). For at least some *Nothofagus* spp., wood, and *S. officinarum* bagasse samples prepared at 300 and 400°C, treatment NL showed higher C increases than other treatments ($p \leq 0.05$). This effect was not apparent in the 500°C samples).

After environmental exposure, oxygen concentration rises in *Nothofagus* spp., *S. officinarum*, and BEST biochar, in contrast with large decreases in oxygen in *C. vagabunda* algae biochar ($p \leq 0.05$). There are apparent differences between *Nothofagus* spp., and *S. officinarum* biochar prepared at 400 and 500°C, where oxygen concentration increases are greater in *S. officinarum* biochar (e.g., 55% vs. 100% change in treatment NL). For *C. vagabunda* algae biochar there is no clear effect of treatment upon sample oxygen content, whereas for *Nothofagus* spp., and *S. officinarum* biochar at all temperatures, oxygen increases in treatment NL are greatest. Oxygen increases for samples except *C. vagabunda* algae biochar appear somewhat larger in samples prepared at higher temperatures, although this correlation could not be tested.

After exposure, changes in hydrogen concentration broadly mirror those observed for %O, where the %H changes in *C. vagabunda* algae biochar (c.40% loss of starting amount) are significantly different to the overall H gains in other samples ($p \leq 0.001$). Changes in other samples are not significantly different from each other at any production temperature, and there is no clear effect of production temperature upon results for any specific material. For *C. vagabunda* algae biochar H change was not clearly different between treatments, whereas for other samples, increases in H were consistently greater in treatment NL. The net effect of %C, %O, and %H changes is that the pattern in O/C and H/C in all samples (i.e., a decrease with production temperature) is still clearly apparent (**Figure 2**).

There is little difference in %N in *C. vagabunda* algae biochar following environmental exposure; the majority of measured values do no change by greater than the limit of analytical uncertainty of ±0.5%, and there is no significant difference with production temperature or treatment ($p \geq 0.01$ for the possibility of a relationship).

## Stable Isotope Measurements ($\delta^{13}C$/ $\delta^{15}N$)

Full results of measurements for all samples are presented in Supplementary Table S1, and summary data is presented in **Table 1**. Decreases in *Nothofagus* spp. wood and *S. officinarum* $\delta^{13}C$ during charring are due to loss of cellulose (Ascough et al., 2008). Conversely, *C. vagabunda* algae shows a small increase in $\delta^{13}C$ of ∼1‰ above 400°C, this is greater than the analytical uncertainty of ±0.2‰ (**Table 2**). For the vast majority of samples, $\delta^{13}C$ following environmental exposure did not vary in excess of normal analytical uncertainty. The exception is an increase of up to 1.1% in *C. vagabunda* algae biochar produced at 400°C following exposure. Only *C. vagabunda* contained sufficient nitrogen to measure $\delta^{15}N$ values; these increased with charring to 300°C but were then constant to 500°C. The $\delta^{15}N$ of all *C. vagabunda* algae biochar decreased after environmental exposure by up to 0.5‰; this is greater than the analytical uncertainty of ±0.3‰ with no correlation to production temperature or treatment.

## GC-MS of Polycyclic Aromatic Hydrocarbons

The HyPy products consist of the <7 ring polycyclic aromatic hydrocarbons (PAHs) in the samples and comprise both those covalently bound to the biochar and present in the free (solvent extractable) state. The measured concentrations of PAHs in the samples are low overall and probably represent only a fraction of the labile biochar carbon (**Table 3**). Along with pyrene and phenanthrene a range of compounds known to result from incomplete combustion of biomass are detected (Simoneit, 2002).

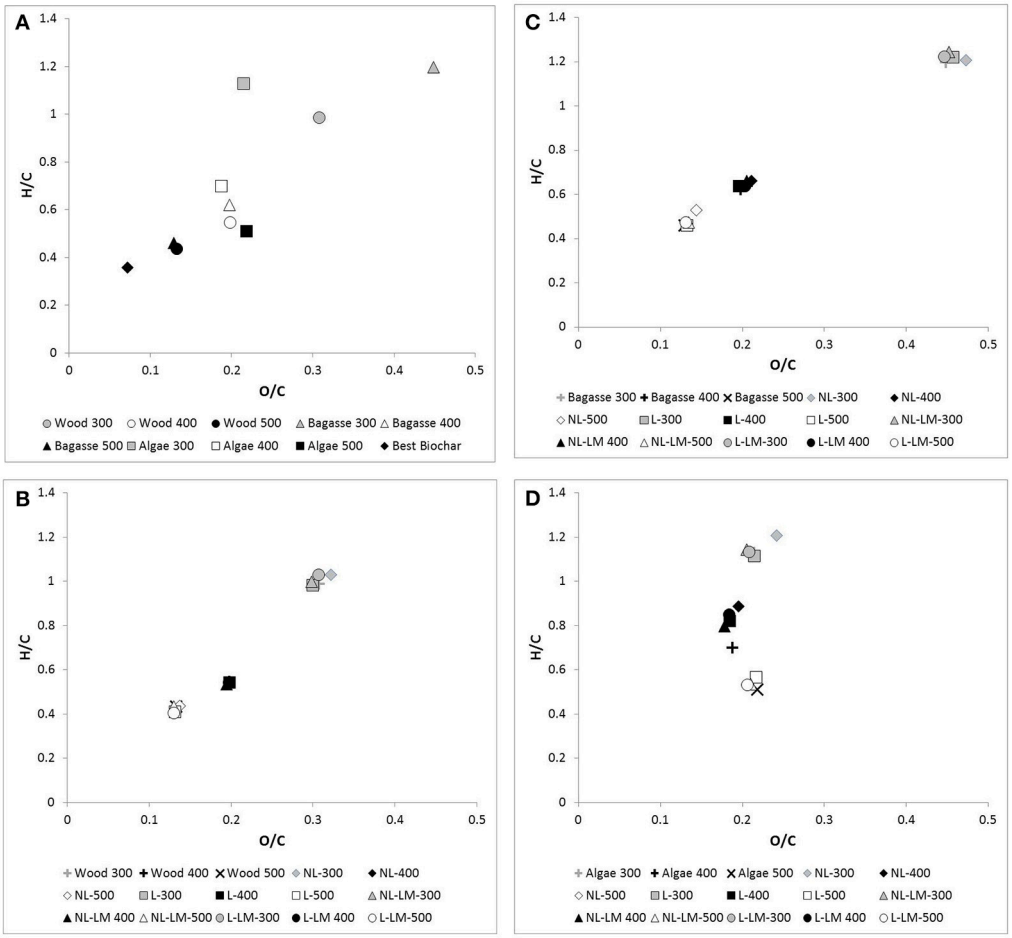


**FIGURE 2 |** O/C and H/C ratios of samples (Gray symbols, 300°C PyC; White symbols, 400°C samples; Black symbols, 500°C samples). **(A)** shows samples before environmental exposure: Circles, *Nothofagus* wood biochar; Triangles, *S. officinarum* biochar; Squares, *C. vagabunda* algae biochar; Diamonds, BEST Biochar. **(B)** (*Nothofagus* wood biochar), **(C)** (*S. officinarum* biochar), and **(D)** (*C. vagabunda* algae biochar) show biochar before and after environmental exposure: Crosses, original biochar; Diamonds, treatment NL; Squares, treatment L; Triangles, treatment NL-LM; Circles, treatment L-LM.

In freshly-produced *Nothofagus* spp. biochar, PAH concentration decreased with production temperature (**Table 3**); this trend was reversed following exposure. Extractable PAHs in *Nothofagus* spp. PyC are more abundant than in biochar produced from the other starting materials. In fresh *S. officinarum* bagasse biochar the total weight of PAHs increased with production temperature (**Table 3**), as does the ratio of 3+4:5+6 ring PAHs. Following exposure there was a slight increase in PAH abundance in all *S. officinarum* bagasse samples, which was largest in the 300°C *S. officinarum*. The pattern in ratio of 3+4:5+6 ring PAHs remains the same, although there is an anomalously high ratio (6.25) for 400°C samples in treatment NL.

In fresh *C. vagabunda* algae biochar PAH concentration also increased with production temperature. One difference from other samples is that naphthalene does not feature in the spectra of *C. vagabunda* algae samples either before or after environmental exposure. After exposure only the PAH concentration of the 400°C samples increases, particularly pyrene and fluoranthene. In BEST biochar the total content of PAHs is similar to that in *Nothofagus* spp. samples, although the absolute concentrations remain small. There is no effect of treatment upon PAH concentration.

## $^{13}$C-MAS-NMR

The changes over 300–500°C for lignocellulosic biomass comprise loss of cellulosic carbons at 60–105 ppm, lignin at 55 ppm, and aliphatic carbon (at 10–40 ppm), and increasing dominance of aromatic carbons at c. 129 ppm (**Figure 3**). In *S. officinarum* bagasse the process of aromatization is slower than in *Nothofagus* spp. wood, with peaks for lignin and aliphatic carbons at 400°C. Although *C. vagabunda* algae is substantially different to the other feedstocks (e.g., higher lipid concentration at 173 ppm), this sample follows the overall charring pattern above, and is dominantly aromatic at 500°C.

After environmental exposure there are no clear differences attributable to treatment. Instead, production temperature

**TABLE 3 |** The total weight (mg/g sample), 3:4 ring ratio and 3+4:5+6 ring ratio of extractable low molecular weight polycyclic aromatic hydrocarbons before and after environmental exposure.

| Sample | Total weight (mg/g sample) of PAHs | 3:4 ring ratio | 3+4:5+6 ring ratio |
|---|---|---|---|
| **BEFORE ENVIRONMENTAL EXPOSURE** | | | |
| *Nothofagus* wood | 0.00 | 0.00 | 0.00 |
| *Nothofagus* wood 300°C | 7.42 | 0.96 | 1.57 |
| *Nothofagus* wood 400°C | 9.25 | 0.84 | 1.29 |
| *Nothofagus* wood 500°C | 4.06 | 0.98 | 1.05 |
| Algae | 0.14 | 0.80 | 4.31 |
| *C. vagabunda* algae 300°C | 0.14 | 0.00 | 0.51 |
| *C. vagabunda* algae 400°C | 0.21 | 0.76 | 1.14 |
| *C. vagabunda* algae 500°C | 1.51 | 0.56 | 1.86 |
| *S. officinarum* | 0.12 | 0.96 | 8.21 |
| *S. officinarum* 300°C | 0.32 | 0.66 | 1.39 |
| *S. officinarum* 400°C | 0.73 | 1.45 | 3.26 |
| *S. officinarum* 500°C | 1.14 | 1.15 | 2.78 |
| BEST biochar 550°C | 4.55 | 0.78 | 1.96 |
| **AFTER ENVIRONMENTAL EXPOSURE** | | | |
| *Nothofagus* wood 300°C NL | 2.85 | 1.18 | 1.24 |
| *Nothofagus* wood 300°C L | 5.07 | 1.21 | 1.04 |
| *Nothofagus* wood 300°C NL-LM | 2.32 | 1.16 | 1.31 |
| *Nothofagus* wood 300°C L-LM | 2.78 | 1.23 | 1.44 |
| *Nothofagus* wood 400°C NL | 5.80 | 1.12 | 1.33 |
| *Nothofagus* wood 400°C L | 6.39 | 1.23 | 1.46 |
| *Nothofagus* wood 400°C NL-LM | 4.84 | 1.19 | 1.76 |
| *Nothofagus* wood 400°C L-LM | 4.43 | 1.01 | 1.55 |
| *Nothofagus* wood 500°C NL | 6.83 | 0.58 | 1.22 |
| *Nothofagus* wood 500°C L | 8.44 | 0.56 | 1.19 |
| *Nothofagus* wood 500°C NL-LM | 6.28 | 0.71 | 1.23 |
| *Nothofagus* wood 500°C L-LM | 5.49 | 0.67 | 1.05 |
| *C. vagabunda* algae 300°C NL | 0.17 | 0.00 | 18.52 |
| *C. vagabunda* algae 300°C L | 0.23 | 0.00 | 3.07 |
| *C. vagabunda* algae 300°C NL-LM | 0.18 | 0.00 | 11.78 |
| *C. vagabunda* algae 300°C L-LM | 0.37 | 0.35 | 6.08 |
| *C. vagabunda* algae 400°C NL | 1.78 | 0.24 | 1.99 |
| *C. vagabunda* algae 400°C L | 1.63 | 0.45 | 1.80 |
| *C. vagabunda* algae 400°C NL-LM | 0.88 | 0.71 | 1.36 |
| *C. vagabunda* algae 400°C L-LM | 2.00 | 0.98 | 2.49 |
| *C. vagabunda* algae 500°C NL | 1.67 | 0.68 | 1.75 |
| *C. vagabunda* algae 500°C L | 1.76 | 0.67 | 1.38 |
| *C. vagabunda* algae 500°C NL-LM | 1.07 | 0.85 | 1.68 |
| *C. vagabunda* algae 500°C L-LM | 0.92 | 0.82 | 2.11 |
| *S. officinarum* 300°C NL | 0.38 | 0.49 | 2.13 |
| *S. officinarum* 300°C L | 0.45 | 0.69 | 2.11 |
| *S. officinarum* 300°C NL-LM | 0.49 | 1.04 | 2.14 |
| *S. officinarum* 300°C L-LM | 0.35 | 0.52 | 2.59 |
| *S. officinarum* 400°C NL | 0.73 | 1.04 | 1.72 |
| *S. officinarum* 400°C L | 0.83 | 1.38 | 6.25 |
| *S. officinarum* 400°C NL-LM | 0.89 | 1.37 | 2.91 |
| *S. officinarum* 400°C L-LM | 1.05 | 1.28 | 2.25 |
| *S. officinarum* 500°C NL | 1.39 | 0.85 | 2.65 |
| *S. officinarum* 500°C L | 1.52 | 1.15 | 2.72 |
| *S. officinarum* 500°C NL-LM | 1.28 | 1.20 | 2.40 |
| *S. officinarum* 500°C L-LM | 1.58 | 1.34 | 2.87 |
| BEST biochar 550°C NL | 6.01 | 0.35 | 3.09 |
| BEST biochar 550°C L | 6.09 | 0.37 | 2.09 |
| BEST biochar 550°C NL-LM | 7.69 | 0.32 | 1.63 |
| BEST biochar 550°C L-LM | 5.18 | 0.25 | 1.37 |

*NB, values are the average of two replicates with the standard deviation presented as ± the average.*

has the biggest effect upon chemical changes. For samples produced at 300°C, cellulosic carbons are removed in preference to lignin, and many samples are oxidized, with peaks for carboxylic carbons at c.170 ppm, and signal at 150 ppm for oxygenated aromatics. Aromatic carbons increasingly dominate the spectra. Aliphatic signal is reduced, demonstrating the reduction in proportion of aliphatic carbons in the sample, relative to starting material. Remaining aliphatic carbons may be lipids, which are known to resist oxidation (Knicker, 2010). The aromatic peak in samples shifts closer to 130 ppm and narrows after exposure, meaning that the range of different forms of polyaromatic domains is reduced, possibly due to loss of smaller aromatics (**Figure 3**).

# DISCUSSION

## Biochar Chemistry Depends Upon Both Production Temperature and Feedstock

Production temperature is known to dictate the aromaticity of biochar/PyC, and determine the extent to which non-aromatic material (including oxygen and hydrogen) is removed from the sample (e.g., Ascough et al., 2008; Krull et al., 2009). A finding from this research, however, is that lignocellulosic and non-lignocellulosic biomasses have very different trajectories of chemical change during pyrolysis. In lignocellulosic biomass there is basically a linear relationship between temperature and carbon increase/ oxygen and hydrogen decrease, and aromaticity. At temperatures of c.500°C, samples become increasingly homogeneous. This is likely to have the effect that trajectories of environmental alteration for a specific environment are similar for different types lignocellulosic biomass (where the starting composition is similar) produced at a consistent temperature. This is borne out by the results for *Nothofagus* spp. and BEST wood biochars presented below. A difference is that the rate of aromatization in *S. officinarum* bagasse samples appears slower at lower temperatures than in *Nothofagus* spp. wood biochar or BEST Biochar. We posit that this is the basis for the different patterns of environmental alteration we observe for these samples.

During production of *C. vagabunda* algae biochar there appears to be a chemical factor that limits aromatization over the 300–500°C window. This could be the effect of chemical reactions involving the high ash concentration during pyrolysis (McBeath et al., 2015), meaning that the potential for environmental alteration of *C. vagabunda* algae biochar (i.e., non-lignocellulosic material) is greater, compared to lignocellulosic biomass, such as wood, for a given temperature. This is consistent with observations that non-woody biochar is less stable than plant-based material produced at an identical temperature (e.g., Singh et al., 2012). It is also important to consider that there may be physical differences between these types of materials that affect their survival potential in the environment, such as porosity, and micro/ macroscopic cracking. However, the physical structure of the biochars was not assessed in this study, so in the following discussion we focus on chemical factors.

The process of PyC production forms PAHs (e.g., Ballentine et al., 1996; Keiluweit et al., 2012), thought to form a proportion of the "semi-labile" fraction in PyC (McBeath et al., 2015). In *Nothofagus* spp. wood the highest temperature biochar has the lowest concentration of PAHs, indicating more extensive aromatization, which would raise the carbon content of the biochar, as observed in the results presented here. This would mean that the potential for environmental alteration is lower for a woody biomass such as the *Nothofagus* spp. biochar sample produced at the same temperature as *S. officinarum* bagasse and *C. vagabunda* algae samples, which display lower C contents The potential for alteration/ degradation appears linked to degree of aromaticity (Harvey et al., 2012) and O:C ratio (Spokas, 2010), meaning for the samples analyzed here, predicted alteration potential increases in the order BEST biochar< *Nothofagus* spp. Wood< *S. officinarum* bagasse< *C. vagabunda* algae. These predictions are confirmed by the results observed after environmental exposure of the samples.

## Characteristics of Environmental Alteration: Effects of Production Temperature

The results of the study, when considered in total, were consistent with the research hypothesis that material prepared at higher temperatures is less subject to alteration in the environment, supporting previous work (e.g., Zimmerman, 2010). For example, mass losses only displayed an interaction between sample type and treatment ($p \leq 0.05$) for samples prepared at 300°C, and treatment effects for both mass losses and changes in C concentration were stronger at lower temperatures. However, the effects we observed were relatively subtle, although also manifest in the $^{13}$C-MAS-NMR, and PAH results, as explained below. We posit that these effects are predominantly due to a decrease in less labile carbon vs. resistant polyaromatic domains in higher-temperature biochars. Despite this, some small changes in the $^{13}$C-MAS-NMR spectra of even samples produced at 500°C are observed, as the aromatic peak at c.130 ppm was slightly narrowed for all feedstock types and treatments. It is possible this reflects loss of a small proportion of the range of aromatic domains present in the samples before environmental exposure, most probably a fraction of the semi-labile component (*sensu* Bird et al., 2015). This is supported by the results of PAH measurement, where the greatest reduction in PAH concentration is seen for the lowest temperature biochar. The mechanism by which this could be achieved remains unclear, although growing evidence demonstrates microbial action resulting in degradation of indigenous biochar carbon over timescales on the order of a year (Ameloot et al., 2013; Farrell et al., 2013; Tilston et al., 2016; Bird et al., 2017). Increasing aromatization also increases resistance to oxidative processes, known to be one of the main agents of PyC alteration and degradation. This is shown in the O/C ratios where despite the loss of many oxygen-containing O-alkyl structures, this is

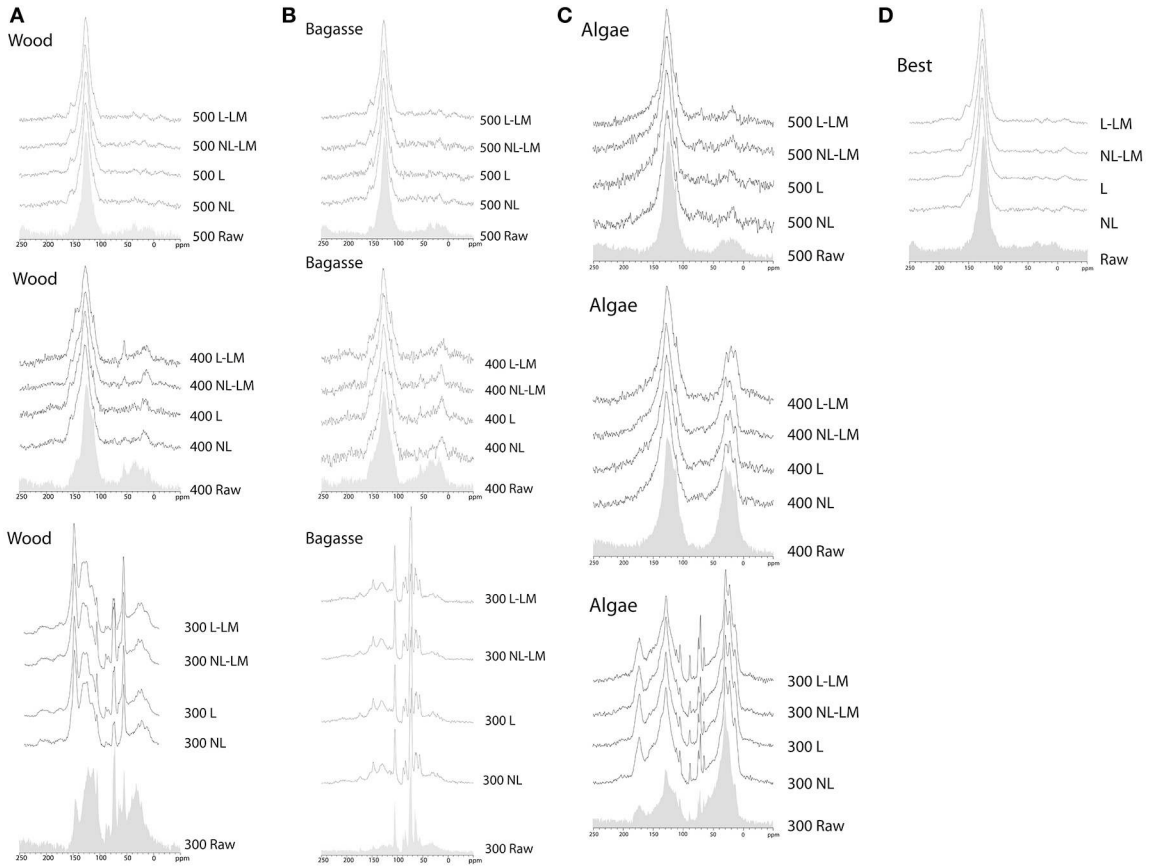


**FIGURE 3 |** $^{13}$C-MAS-NMR spectra of samples before and after exposure to environmental conditions. **(A)** *Nothofagus* wood biochar, **(B)** *S. officinarum* biochar, **(C)** Algae biochar, **(D)** BEST biochar. Spectra are given for uncharred (raw) material and samples prepared at 300°C, 400°C and 500°C emplaced in the four different treatments described in the text.

more than offset by the additional oxygen introduced to the structure of lower temperature (300–400°C) biochars after 1 year.

## Characteristics of Environmental Alteration: Effect of Feedstock

Differences in biochar chemistry after environmental exposure attributed to specific feedstock are relatively low between *Nothofagus* spp. wood PyC, and *S. officinarum* bagasse biochar, and although changes appear somewhat smaller in BEST Biochar, for all these sample types, changes in mass, C/O/H/N, and other characteristics are in the same direction. Changes in *C. vagabunda* algae biochar for these parameters are always in the opposite direction, however, and are consistently larger than those in other samples. The results therefore support the hypothesis that, although different types of woody biomass show relatively small differences in change with environmental exposure, at least at a gross scale, non-woody biomass is more susceptible to alteration than woody biomass (c.f. Hilscher et al., 2009; McBeath et al., 2014). This appears largely due to the removal of ash that is readily solubilised and/or physically migrated away from the sample. This ash contains essential plant nutrients (e.g., Na, Ca, Cl, Mg, K), and so this type of biochar may have a beneficial effect for soil fertility (e.g., Novak et al., 2009), although this will be over a restricted timescale. This type of biochar contains more labile carbon than the other samples, particularly aliphatic material indigenous to the sample and sorbed to its structure (Middelburg et al., 1997), and the C concentration decrease observed in the samples, potentially due to loss of labile C, is so large that any introduction of exogenous carbon, such as that observed in other samples (e.g., via soil microorganisms c.f. Steinbeiss et al., 2009; Bird et al., 2017), is not visible. It should be noted that along with complete degradation to $CO_2$, there is the possibility that some C is removed by solubilization and leaching during environmental exposure (Major et al., 2010; Abiven et al., 2011; Bird et al., 2017).

*C. vagabunda* algae biochar is the only sample in which $\delta^{15}$N and %N can be observed, although there is no effect of treatment or production temperature. There is a slight increase in $\delta^{15}$N overall, although this is very close to the limit of analytical precision. This may indicate that microbial action has removed lighter N isotopes via fractionation during decomposition (bonds involving $^{14}$N being broken more easily), possibly through decomposition of "black nitrogen" (Knicker, 2010; McBeath et al., 2015).

## Characteristics of Environmental Alteration: Effect of Depositional Environment

There is a clear effect of depositional environment on biochar alteration even after the relatively short timescale of this study. However, this is not consistent with the hypothesis that material in alkaline environments is more subject to alteration. Although for *C. vagabunda* algae biochar there is no effect from different treatments upon chemical changes, for other samples, increases in mass, and C/O/H concentrations are far more extensive in the material under the NL treatment. Mass increases due to ash and carbon increases are much greater in all samples under this treatment; the mass increase indicates the potential for a significant proportion of soil mineral ingress (c.f. Bird et al., 2008). Over time in the environment, it is evident that mineral material can strongly associate with both external and internal surfaces of PyC (Lehmann et al., 2011; Jaafar et al., 2015). This can be the result of abiotic processes such as water movement and biotic processes such as the movement of soil macrofauna. This interpretation is further supported by the increases in ash content in many samples, a phenomenon previously observed by Bird et al. (2014). An increase in sample carbon could result from removal of non-carbon elements (e.g., H), due to consumption by microbes. This labile carbon removal has been observed in incubations of the *Nothofagus* spp. wood charcoal samples (Bird et al., 2017). Conversely, increases in sample carbon concentration and mass could result from the ingress of exogenous carbon, e.g., fungi, soil biota, humic acids (Steinbeiss et al., 2009; Lehmann et al., 2011). For example, Mohan et al. (2014), and others demonstrate the sorption of organic compounds from the depositional environment onto the structure of PyC. Fungal ingress to samples equivalent to some of the material in this study has observational support in field (Bird et al., 2014), and laboratory (Ascough et al., 2010c) studies. The concept of an increase in mass due to introduction of exogenous carbon for the NL treatments is supported by the findings of Bird et al. (2017), using equivalent material to the *Nothofagus* spp. biochar described in the present study. Here, an increase in radiocarbon concentration of ∼0.5–1 pMC clearly demonstrates the addition of exogenous carbon to the radiocarbon-dead biochar. Using $\delta^{13}C$ measurements, the same study indicated a 5–10% contribution of exogenous carbon to the lower temperature biochars. This is also found in our results, where a decrease in $\delta^{13}C$ occurs overall, albeit to a lower extent than observed for the sample group analyzed by Bird et al. (2017) after 3 years. In this case, the larger %C increases observed in NL may be due to the higher oxygen availability for these samples on the soil surface, leading to unhindered access for microbiota, leading to decomposition of the more labile fraction of the biochar structure (containing non-C elements), raising the %C content as polyaromatic material, dominated by C remains behind. This use of biochar carbon by microbiota is consistent with the findings of Bird et al. (2017) for biochars inoculated with microbial material after drying following environmental exposure. Respiration of $CO_2$ from these samples was linked to both use of biochar carbon and some of the exogenous carbon from the deposition environment, using $\delta^{13}C$ measurements. This would explain why mass and %C increases on the same scale are not observed in the NL-LM treatment, even though this was also on the soil surface without litter. Here the limestone covering could physically (through reduced oxygen availability), or chemically (through increased pH) retard the ingress of microorganisms.

The ingress of exogenous carbon is supported by the $\delta^{13}C$ measurements, as the sample materials all have higher $\delta^{13}C$ values, by up to 15.4‰, than the surrounding leaf litter (−29‰). The $\delta^{13}C$ are small, but in the negative direction. Based on the observations of Bird et al. (2017), this ingress is limited to 1–2% carbon; therefore as the carbon increase for the NL treatment is so large, these low changes in $\delta^{13}C$ indicates use of indigenous sample carbon by microbiota inhabiting biochar surfaces.

Chemical changes in the samples following environmental exposure include oxidation of the biochar structure, which is most complete for samples under the NL treatment, where significant increases in oxygen concentration are observed. The results of the $^{13}C$-MAS-NMR measurement suggest that direct oxygenation of aromatic structures may be even more important than carboxylation in biochar/ PyC alteration, as signal at 150 ppm for oxygenated aromatics (Freitas et al., 1999) is present, while carboxylic peaks are small. Similarly, changes in the amounts of PAHs in samples after exposure indicate removal of pre-existing small-ring aromatics, and possibly removal of material that has been formed by cleavage from the larger aromatic skeleton of the biochar. However, the fact that these PAHs are extractable from the samples after environmental exposure points to these being sorbed to the sample structure, slowing their biodegradation and/or removal from site of formation after being cleaved from initially larger aromatic structures (c.f. Manilal and Alexander, 1991).

## CONCLUSIONS

It is clear that at a given production temperature, the chemistry of lignocellulosic and non-lignocellulosic material differs significantly, directly impacting its environmental behavior. In particular, the chemistry and alteration pathway of biochar/ PyC from non-lignocellulosic biomass is very different to that of lignocellulosic materials such as wood. While this reduces the carbon sequestration potential of this material, benefits lie in the direction of a short-term fertilization effect, as key soil nutrients are readily released into the soil environment. It is on this basis that high-N biomass has been proposed as a source of biochar (e.g., algae, poultry litter Chan et al., 2008), enhancing the physical and chemical benefits offered by the polyaromatic biochar structure itself. The requirement for continued biochar inputs to maintain this effect clearly depends upon environment and agricultural need, which is an important consideration for application of this type of material. Further, this heterogeneity in starting materials and corresponding environmental behavior means it is not possible to extend the results obtained on one sample type or one production temperature to different material; analyses must be performed on "like for like" material.

After 12 months of exposure in a tropical biome, alteration of biochar is observable, predominantly degradation of the "labile" component (*sensu* Bird et al., 2015). There is also

evidence for alteration of a proportion of the sample aromatic fraction, due to the rise in extractable 2–7 ring PAHs in some samples, potentially due to the degradation of larger aromatic structures. In this, oxidation may play a role, and we have identified direct oxygenation of aromatic structures as a possible mechanism, operating in conjunction with the more commonly-cited carboxylation (e.g., Cohen-Ofri et al., 2006). Despite this, a significant proportion of the non-aromatic material and small-ring aromatics remained, indicating this material was not yet accessible for degradation due to a physical or chemical protection mechanism.

In terms of depositional environment, it appears that oxygen availability and physical or chemical protection from sunlight and/or rainwater, is vital in determining the alteration trajectory of biochar, whereby buried material will be altered more slowly than that exposed on the soil surface, supporting the results of previous work (Zimmermann et al., 2012; Bird et al., 2017). A further implication of this work is that even for material with a very different $\delta^{13}C$ to the surrounding environment, changes due to the ingress of exogenous carbon are likely to be small. Carbon isotope values are a valuable source of (palaeo) environmental proxy data, and it appears that the $\delta^{13}C$ of biochar recovered for analysis from natural environmental deposits is not distorted by a large amount from the original sample $\delta^{13}C$. It is clearly important however, that non-PyC material is removed as far as possible; techniques such as hydropyrolysis (Ascough et al., 2009, 2010a; Meredith et al., 2012) are very useful in this regard.

## AUTHOR CONTRIBUTIONS

PA led preparation of the manuscript, undertook fieldwork, performed data analysis and interpretations, MB coordinated fieldwork and sample recovery, assisted with data analysis and interpretations, WM performed hydropyrolysis measurements, analysis of GC-MS measurements and scientific interpretations, CS coordinated chemical analyses, assisted with data analysis, and interpretation of analyses, DL coordinated chemical analyses and assisted with interpretations, ET performed chemical analyses, coordinated elemental and isotopic measurements and performed data interpretation, DA performed NMR measurements, data analysis and interpretations, AB performed GC-MS analyses and interpretation of results, LS performed hydropyrolysis measurements and interpretation of results. All authors had intellectual input to the study, and contributed to the preparation of the manuscript.

## ACKNOWLEDGMENTS

Overall financial support was provided by NERC (NE/F017456/1). Financial support for fieldwork was provided via the Carnegie Trust for the Universities of Scotland Small Grant Scheme. This publication represents a contribution from the Scottish Alliance for Geoscience, Environment, and Society (SAGES). Samples of 14C-depleted Nothofagus wood were kindly provided by Mr B. Wood (TRUenergy, Australia). We thank Barry Thornton (James Hutton Institute, UK) for the elemental analyses for oxygen and hydrogen, and Kerry Sayle (SUERC) for elemental and stable isotopic analyses of carbon and nitrogen. Stephanie Ascough (Imperial College, London) is thanked for assistance with statistical testing.

## SUPPLEMENTARY MATERIAL

The Supplementary Material for this article can be found online at: https://www.frontiersin.org/articles/10.3389/feart.2018.00061/full#supplementary-material

## REFERENCES

Abiven, S., Hengartner, P., Schneider, M. P. W., Singh, N., and Schmidt, M. W. I. (2011). Pyrogenic carbon soluble fraction is larger and more aromatic in aged charcoal than in fresh charcoal. *Soil Biol. Biochem.* 43, 1615–1617. doi: 10.1016/j.soilbio.2011.03.027

Ameloot, N., Graber, E. R., Verheijen, F. G. A., and De Neve, S. (2013). Interactions between biochar stability and soil organisms: review and research needs. *Eur. J. Soil Sci.* 64, 379–390. doi: 10.1111/ejss.12064

Ascough, P. L., Bird, M. I., Brock, F., Higham, T. F. G., Meredith, W., Snape, C., et al. (2009). Hydropyrolysis as a new tool for radiocarbon pretreatment and the quantification of black carbon. *Quat. Geochronol.* 4, 140–147. doi: 10.1016/j.quageo.2008.11.001

Ascough, P. L., Bird, M. I., Francis, S. M., Thornton, B., Midwood, A., Scott, A. C., et al. (2011). Variability in oxidative degradation of charcoal: influence of production variables and environmental exposure. *Geochim. Cosmochim. Acta* 75, 2361–2378. doi: 10.1016/j.gca.2011.02.002

Ascough, P. L., Bird, M. I., Meredith, W., Wood, R. E., Snape, C. E., Brock, F., et al. (2010a). Hydropyrolysis: implications for radiocarbon pretreatment and characterization of Black Carbon. *Radiocarbon* 52, 1336–1350. doi: 10.1017/S0033822200046427

Ascough, P. L., Bird, M. I., Scott, A. E., Collinson, M. E., Cohen-Ofri, I., Snape, C. E., et al. (2010b). Charcoal reflectance measurements: implications for structural characterization and assessment of diagenetic alteration. *J. Archaeol. Sci.* 37, 1590–1599. doi: 10.1016/j.jas.2010.01.020

Ascough, P., Bird, M. I., Wormald, P., Snape, C. E., and Apperley, D. (2008). Influence of pyrolysis variables and starting material on charcoal stable isotopic and molecular characteristics. *Geochim. Cosmochim. Acta* 72, 6090–6102. doi: 10.1016/j.gca.2008.10.009

Ascough, P. L., Sturrock, C. J. L., and Bird, M. I. (2010c). Investigation of growth responses in saprophytic fungi to charred biomass. *Isotopes Environ. Health Stud.* 46, 64–77. doi: 10.1080/10256010903388436

Ballentine, D. C., Macko, S. A., Turekian, V. C., Gilhooly, W. P., and Martincigh, B. (1996). Compound specific isotope analysis of fatty acids and polycyclic aromatic hydrocarbons in aerosols: implications for biomass burning. *Org. Geochem.* 25, 97–104. doi: 10.1016/S0146-6380(96)00110-6

Bird, M. I., and Ascough, P. L. (2012). Isotopes in pyrogenic carbon: a review. *Org. Geochem.* 42, 1529–1539. doi: 10.1016/j.orggeochem.2010.09.005

Bird, M. I., Ascough, P. L., Young, I. M., and Wood, C. V. (2008). X-ray ray Microtomographic microtomographic Imaging imaging of Charcoalcharcoal. *J. Archaeol. Sci.* 35, 2698–2706. doi: 10.1016/j.jas.2008.04.018

Bird, M. I., Levchenko, V., Ascough, P. L., Meredith, W., Wurster, C. M., Williams, A., et al. (2014). The efficiency of charcoal decontamination for radiocarbon

dating by three pre-treatments–ABOX, ABA and hypy. *Quat. Geochronol.* 22, 25–32. doi: 10.1016/j.quageo.2014.02.003

Bird, M. I., McBeath, A., Ascough, P. L., Levchenko, V., Wurster, C. M., Munksgaard, N. C., et al. (2017). Loss and gain of carbon during char degradation. *Soil Biol. Biochem*. 106, 80–89. doi: 10.1016/j.soilbio.2016.12.012

Bird, M. I., Wurster, C. M., de Paula Silva, P. H., Bass, A., and de Nys, R. (2011). Algal biochar – production and properties. *Bioresour. Technol.* 102, 1886–1891. doi: 10.1016/j.biortech.2010.07.106

Bird, M. I., Wynn, J. G., Saiz, G., Wurster, C. M., and McBeath, A. (2015). The pyrogenic carbon cycle. *Annu. Rev. Earth Planet. Sci.* 43, 9–1. doi: 10.1146/annurev-earth-060614-105038

Braadbaart, F., Poole, I., and Van Brussel, A. A. (2009). Preservation potential of charcoal in alkaline environments: an experimental approach and implications for the archaeological record. *J. Archaeol. Sci.* 36, 1672–1679. doi: 10.1016/j.jas.2009.03.006

Bruun, S., Jensen, E. S., and Jensen, L. S. (2008). Microbial mineralization and assimilation of black carbon: Dependency on degree of thermal alteration. *Org. Geochem.* 39, 839–845. doi: 10.1016/j.orggeochem.2008.04.020

Carcaillet, C. (2001). Are Holocene wood-charcoal fragments stratified in alpine and subalpine soils? Evidence from the Alps based on AMS C-14 dates. *Holocene* 11, 231–242. doi: 10.1191/095968301674071040

Chan, K. Y., Van Zwieten, L., Meszaros, I., Downie, A., and Joseph, S. (2008). Using poultry litter biochars as soil amendments. *Soil Res.* 46, 437–444. doi: 10.1071/SR08036

Cheng, C.-H., Lehmann, J., and Engelhard, M. H. (2008a). Natural oxidation of black carbon in soils: changes in molecular form and surface charge along a climosequence, Geochimica et Cosmochimica. *Acta* 72, 1598–1610. doi: 10.1016/j.gca.2008.01.010

Cheng, C.-H., Lehmann, J., Thies, J. E., and Burton, S. D. (2008b). Stability of black carbon in soils across a climatic gradient. *J. Geophys. Res.* 113:G02027. doi: 10.1029/2007JG000642

Cohen-Ofri, I., Weiner, L., Boaretto, E., Mintz, G., and Weiner, S. (2006). Modern and fossil charcoal: aspects of structure and diagenesis. *J. Archaeol. Sci.* 33, 428–439. doi: 10.1016/j.jas.2005.08.008

Deckers, J. A., Nachtergaele, F., and Spaargaren, O. C. (1998). *World Reference Base for Soil Resources: Introduction,* Vol. 1. Leuven: Acco.

DeLuca, T. H., and Aplet, G. H. (2008). Charcoal and carbon storage in forest soils of the Rocky Mountain west. *Front. Ecol. Environ.* 6, 18–24. doi: 10.1890/070070

Donato, D. C., Campbell, J. L., Fontaine, J. B., and Law, B. E. (2009). Quantifying char in postfire woody detritus inventories. *Fire Ecol.* 5, 104–115. doi: 10.4996/fireecology.0502104

Farrell, M., Kuhn, T. K., Macdonald, L. M., Maddern, T. M., Murphy, D. V., Hall, P. A., et al. (2013). Microbial utilisation of biochar-derived carbon. *Sci. Total Environ*. 465, 288–297. doi: 10.1016/j.scitotenv.2013.03.090

Freitas, J. C. C., Bonagamba, T. J., and Emmerich, F. G. (1999). 13C high-resolution solid-state NMR study of peat carbonization. *Energy Fuels* 11, 53–59. doi: 10.1021/ef980075c

Hammes, K., and Schmidt, M. W. I. (2009). "Changes of biochar in soil," in *Biochar for Environmental Management*, eds J. Lehmann, and S. Joseph (London: Earthscan), 169–182.

Harvey, O. R., Kuo, L. J., Zimmerman, A. R., Louchouarn, P., Amonette, J. E., and Herbert, B. E. (2012). An index-based approach to assessing recalcitrance and soil carbon sequestration potential of engineered black carbons (biochars). *Environ. Sci. Technol.* 46, 1415–1421. doi: 10.1021/es2040398

Hilscher, A., Heister, K., Siewert, C., and Knicker, H. (2009). Mineralisation and structural changes during the initial phase of microbial degradation of pyrogenic plant residues in soil. *Org. Geochem.* 40, 332–342. doi: 10.1016/j.orggeochem.2008.12.004

Huston, M. A., and Wolverton, S. (2009). The global distribution of net primary production: resolving the paradox. *Ecol. Monogr.* 79, 343–377. doi: 10.1890/08-0588.1

Isbell, R. (2002). *The Australian Soil Classification. Revised Edition,* Vol. 4. Collingwood, VIC: CSIRO Publishing.

Jaafar, N. M., Clode, P. L., and Abbott, L. K. (2015). Soil microbial responses to biochars varying in particle size, surface and pore properties. *Pedosphere* 255, 770–780. doi: 10.1016/S1002-0160(15)30058-8

Keiluweit, M., Kleber, M., Sparrow, M. A., Simoneit, B. R., and Prahl, F. G. (2012). Solvent-extractable polycyclic aromatic hydrocarbons in biochar: influence of pyrolysis temperature and feedstock. *Environ. Sci. Technol.* 46, 9333–9341. doi: 10.1021/es302125k

Knicker, H. (2010). "Black nitrogen" – an important fraction in determining the recalcitrance of charcoal. *Orga. Geochem.* 41, 947–950. doi: 10.1016/j.orggeochem.2010.04.007

Krull, E. S., Baldock, J. A., Skjemstad, J. O., and Smernik, R. J. (2009). "Characteristics of biochar: organo-chemical properties," in *Biochar for Environmental Management,* eds J. Lehmann and S. Joseph (Routledge: Earthscan Publications Ltd.), 53–65.

Kuhlbusch, T. A. J. (1998). Black carbon and the carbon cycle. *Science* 280, 1903–1904. doi: 10.1126/science.280.5371.1903

Lehmann, J., da Silva, J. P., Steiner, C., Nehls, T., Zech, W., and Glaser, B. (2003). Nutrient availability and leaching in an archaeological Anthrosol and a Ferralsol of the Central Amazon basin: fertilizer, manure and charcoal amendments. *Plant Soil* 249, 343–357. doi: 10.1023/A:1022833116184

Lehmann, J., Gaunt, J., and Rondon, M. (2006). Bio-char sequestration in terrestrial ecosystems. *Mitig. Adapt. Strat. Glob. Change* 11, 395–419. doi: 10.1007/s11027-005-9006-5

Lehmann, J., Rillig, M. C., Thies, J., Masiello, C. A., Hockaday, W. C., and Crowley, D. (2011). Biochar effects on soil biota – a review. *Soil Biol. Biochem.* 43, 1812–1836. doi: 10.1016/j.soilbio.2011.04.022

Major, J., Lehmann, J., Rondon, M., and Goodale, C. (2010). Fate of soil-applied black carbon: downward migration, leaching and soil respiration. *Glob. Chang. Biol.* 16, 1366–1379. doi: 10.1111/j.1365-2486.2009.02044.x

Manilal, V. B., and Alexander, M. (1991). Factors affecting the microbial degradation of phenanthrene in soil. *Appl. Microbiol. Biotechnol.* 35, 401–405. doi: 10.1007/BF00172733

McBeath, A. V., Smernik, R. J., Krull, E. S., and Lehmann, J. (2014). The influence of feedstock and production temperature on biochar carbon chemistry: a solid-state 13C NMR study. *Biomass Bioenergy* 60, 121–129. doi: 10.1016/j.biombioe.2013.11.002

McBeath, A. V., Wurster, C. M., and Bird, M. I. (2015). Influence of feedstock properties and pyrolysis conditions on biochar carbon stability as determined by hydrogen pyrolysis. *Biomass Bioenergy* 73, 155–173. doi: 10.1016/j.biombioe.2014.12.022

Meredith, W., Ascough, P. L., Bird, M. I., Large, D. J., Snape, C. E., Sun, Y., et al. (2012). Assessment of hydropyrolysis as a method for the quantification of black carbon using standard reference materials. *Geochim. Cosmochim. Acta* 97, 131–147. doi: 10.1016/j.gca.2012.08.037

Meredith, W., Ascough, P. L., Bird, M. I., Large, D. J., Snape, C. E., Song, J., et al. (2013). Direct evidence from hydropyrolysis for the retention of long alkyl moieties in soil black carbon fractions isolated by acid dichromate oxidation. *J. Anal. Appl. Pyrolysis* 103, 232–239. doi: 10.1016/j.jaap.2012.11.001

Middelburg, J. J., Nieuwenhuize, J., Lubberts, R. K., and van de Plassche, O. (1997). Organic carbon isotope systematics of coastal marshes. *Estuar. Coast. Shelf Sci.* 45, 681–687. doi: 10.1006/ecss.1997.0247

Mohan, D., Sarswat, A., Ok, Y. S., and Pittman, C. U. (2014). Organic and inorganic contaminants removal from water with biochar, a renewable, low cost and sustainable adsorbent a critical review. *Bioresour. Technol.* 160, 191–202. doi: 10.1016/j.biortech.2014.01.120

Novak, J. M., Busscher, W. J., Laird, D. L., Ahmedna, M., Watts, D. W., and Niandou, M. (2009). Impact of biochar amendment on fertility of a southeastern coastal plain soil. *Soil Sci.* 174, 105–112. doi: 10.1097/SS.0b013e3181981d9a

Preston, C. M., and Schmidt, M. W. I. (2006). Black (pyrogenic) carbon in boreal forests: a synthesis of current knowledge and uncertainties. *Biogeosci. Discuss* 3, 211–271. doi: 10.5194/bgd-3-211-2006

Santín, C., Doerr, S. H., Kane, E. S., Masiello, C. A., Ohlson, M., de la Rosa, J. M., et al. (2016). Towards a global assessment of pyrogenic carbon from vegetation fires. *Glob. Chang. Biol.* 22, 76–91. doi: 10.1111/gcb.12985

Santín, C., Doerr, S. H., Merino, A., Bucheli, T. D., Bryant, R., Ascough, P., et al. (2017). Carbon sequestration potential and physicochemical properties differ between wildfire charcoals and slow-pyrolysis biochars. *Sci. Rep.* 7:11233. doi: 10.1038/s41598-017-10455-2

Schmidt, M. W. I., and Noack, A. G. (2000). Black carbon in soils and sediments: analysis, distribution, implications, and current challenges. *Global Biogeochem. Cycles* 14, 777–793. doi: 10.1029/1999GB001208

Simoneit, B. R. T. (2002). Biomass burning - a review of organic tracers for smoke from incomplete combustion. *Appl. Geochem.* 17, 129–162. doi: 10.1016/S0883-2927(01)00061-0

Singh, B. P., Cowie, A. L., and Smernik, R. J. (2012). Biochar carbon stability in a clayey soil as a function of feedstock and pyrolysis temperature. *Environ. Sci. Technol.* 46, 11770–11778. doi: 10.1021/es302545b

Spokas, K. A. (2010). Review of the stability of biochar in soils: predictability of O:C molar ratios. *Carbon Manage.* 1, 289–303. doi: 10.4155/cmt.10.32

St John, T. V. (1980). Influence of litterbags on growth of fungal vegetative structures. *Oecologia* 46, 130–132. doi: 10.1007/BF00346977

Steinbeiss, S., Gleixner, G., and Antonietti, M. (2009). Effect of biochar amendment on soil carbon balance and soil microbial activity. *Soil Biol. Biochem.* 41, 1301–1310. doi: 10.1016/j.soilbio.2009.03.016

Tilston, E. L., Ascough, P. L., Garnett, M. H., and Bird, M. I. (2016). Quantifying charcoal degradation and negative priming of soil organic matter with a radiocarbon-dead tracer. *Radiocarbon* 58, 905–919. doi: 10.1017/RDC.2016.45

Torello-Raventos, M., Feldpausch, T. R., Veenendaal, E., Schrodt, F., Saiz, G., Domingues, T. F., et al. (2013). On the delineation of tropical vegetation types with an emphasis on forest/savanna transitions. *Plant Ecol. Divers.* 6, 101–137. doi: 10.1080/17550874.2012.762812

Wang, J., Xiong, Z., and Kuzyakov, Y. (2016). Biochar stability in soil: meta-analysis of decomposition and priming effects. *GCB Bioenergy* 8, 512–523. doi: 10.1111/gcbb.12266

Zimmerman, A. R. (2010). Abiotic and microbial oxidation of laboratory-produced black carbon (biochar). *Environ. Sci. Technol.* 44, 1295–1301. doi: 10.1021/es903140c

Zimmermann, M., Bird, M. I., Wurster, C., Saiz, G., Goodrick, I., Barta, J., et al. (2012). Rapid degradation of pyrogenic carbon. *Glob. Chang. Biol.* 18, 3306–3316. doi: 10.1111/j.1365-2486.2012.02796.x

**Conflict of Interest Statement:** The authors declare that the research was conducted in the absence of any commercial or financial relationships that could be construed as a potential conflict of interest.

frontiers in Earth Science

ORIGINAL RESEARCH
published: 08 May 2018
doi: 10.3389/feart.2018.00052

# Physical Processes Dictate Early Biogeochemical Dynamics of Soil Pyrogenic Organic Matter in a Subtropical Forest Ecosystem

*Jason M. Stuart*[1], *Russell Anderson*[1], *Patrick Lazzarino*[2], *Kevin A. Kuehn*[3] *and Omar R. Harvey*[1,2]*

[1] Department of Geography and Geology, University of Southern Mississippi, Hattiesburg, MS, United States, [2] School of Geology, Energy and the Environment, Texas Christian University, Fort Worth, TX, United States, [3] Department of Biological Sciences, University of Southern Mississippi, Hattiesburg, MS, United States

Quantifying links between *py*OM dynamics, environmental factors and processes is central to predicting ecosystem function and response to future perturbations. In this study, changes in carbon (*TC*), nitrogen (*TN*), pH, and relative recalcitrance ($R_{50}$) for pine- and cordgrass-derived *py*OM were measured at 3–6 weeks intervals throughout the first year of burial in the soil. Objectives were to (1) identify key environmental factors and processes driving early-stage *py*OM dynamics, and (2) develop quantitative relationships between environmental factors and observed changes in *py*OM properties. The study was conducted in sandy soils of a forested ecosystem within the Longleaf pine range of the United States with a focus on links between changes in *py*OM properties, fire history (*FH*), cumulative precipitation ($P_{cum}$), average temperature ($T_{avg}$) and soil residence time (*SRT*). $P_{cum}$, *SRT* and $T_{avg}$ were the main factors controlling TC and TN accounting for 77–91% and 64–96% of their respective variability. Fire history, along with $P_{cum}$, *SRT* and $T_{avg}$, exhibited significant controlling effects on *py*OM pH and $R_{50}$—accounting for 48–91% and 88–93% of respective variability. Volatilization of volatiles and leaching of water-soluble components (in summer) and the sorption of exogenous organic matter (fall through spring) were most plausibly controlling *py*OM dynamics in this study. Overall, our results point to climatic and land management factors and physicochemical process as the main drivers of *py*OM dynamics in the pine ecosystems of the Southeastern US.

**Keywords: *py*OM dynamics, fire-derived soil carbon, forest soils, recalcitrance, priming effects**

OPEN ACCESS

***Edited by:***
*Cristina Santin,*
*Swansea University, United Kingdom*

***Reviewed by:***
*Sasha Wagner,*
*Northeastern University, United States*
*Melissa R. A. Pingree,*
*University of Idaho, United States*

***Correspondence:**
*Omar R. Harvey*
*omar.harvey@tcu.edu*

***Specialty section:***
*This article was submitted to Biogeoscience, a section of the journal Frontiers in Earth Science*

***Received:*** *04 December 2017*
***Accepted:*** *18 April 2018*
***Published:*** *08 May 2018*

***Citation:***
*Stuart JM, Anderson R, Lazzarino P, Kuehn KA and Harvey OR (2018) Physical Processes Dictate Early Biogeochemical Dynamics of Soil Pyrogenic Organic Matter in a Subtropical Forest Ecosystem. Front. Earth Sci. 6:52. doi: 10.3389/feart.2018.00052*

## INTRODUCTION

Current evidence suggests that despite a relatively small annual global production rate (40–259 Gt/yr; Bird et al., 2015; Santin et al., 2015), carbon in the fire-derived/pyrogenic organic matter (*py*OM) pool accounts for a significant quantity (2–45%) of the total organic carbon in terrestrial systems (Skjernstad et al., 1999; Skjemstad et al., 2002; Lehmann et al., 2008; Reisser et al., 2016). There is fairly widespread consensus that the significant quantity of terrestrial carbon held in the *py*OM pool is largely attributable to a comparatively higher innate resistance/recalcitrance to abiotic/biotic degradation and, longer turnover times of pyrogenic carbon compared to its non-pyrogenic counterpart (Schmidt and Noack, 2000; Hammes et al., 2008). For example,

turnover times for pyrogenic carbon are on the order of decades to thousands of years, compared to a few years for its non-pyrolysed counterpart (Hammes et al., 2008; Liang et al., 2008; Carvalhais et al., 2014; de la Rosa et al., 2018).

The recognition of *py*OM being relatively more resistant to abiotic and biotic transformation has led to increased interest in the global *py*OM pool as a potential carbon sink and carbon sequestration strategy (Lehmann et al., 2006). Current estimates for carbon sequestration potential in the *py*OM pool are as high as $9.5 \times 10^9$ tons C/yr—comparable to estimated carbon emission from fossil fuel burning ($9.1 \times 10^9$ tons C/yr; Lehmann et al., 2006). However, it is now well-known that this sequestration potential will vary with *py*OM composition/properties as well as field/environmental conditions. The composition/properties of *py*OM have been extensively studied and are known to be a heterogeneous mix of thermally-altered carbon-, hydrogen-, nitrogen-, oxygen-, and sulfur-containing organic structures with the degrees of heterogeneity or thermal alteration varying systematically across feedstock chemistry and pyrolysis conditions (e.g., Zimmerman, 2010; Harvey et al., 2012). Increasing degrees of thermal alteration favor increasingly condensed carbon- and/or nitrogen-rich structures of higher innate environmental recalcitrance/stability (Knicker et al., 2008; Knicker, 2010; Zimmerman, 2010; Harvey et al., 2012).

Current understanding of the impact of variations in environmental conditions on *py*OM behavior is far less clear than that for feedstock chemistry or pyrolysis conditions. Results on the biogeochemical trajectory of key *py*OM properties and, most importantly, the environmental factors driving that trajectory are still unclear. For example, Mukherjee et al. (2014) reported increases of up to 124, 143, and 43% in *py*OM-associated carbon, nitrogen and exchange capacity, respectively—after burying different *py*OMs for 15 months in two distinct soils (a sandy Entisol used for agriculture and a forested Spodosol) in Florida. The observed differences in *py*OM behavior were attributed to differences in soil composition and structure. In contrast, while Sorrenti et al. (2016) and de la Rosa et al. (2018) observed increases in *py*OM-associated nitrogen (four-fold) after soil burial of *py*OM for 24–48 months, they both reported decreases in *py*OM-associated carbon (11–27%). Both studies were conducted in inceptisols (in the case of Sorrenti et al. (2016)—a sandy loam in Italy and in the case of de la Rosa et al.—a sandy clay loam in Spain). Except noting that hydrologic properties of *py*OM were linked to surface changes induced by environmental exposure, Sorrenti et al. (2016) did not discuss specific environmental factors driving observed changes. On the other hand, de la Rosa et al. (2018) noted climatic conditions (in particular rainfall and temperature) and soil characteristics as the key drivers of the observed changes in *py*OM-associated carbon and nitrogen.

Whilst it is intuitive—and of great qualitative value—that environmental factors such as ecosystem type, soil properties, temperature, nutrient availability and moisture conditions drives *py*OM dynamics (Cheng et al., 2008; O'Neill et al., 2009; Khodadad et al., 2011; Bird et al., 2015); quantitative assessments of the individual and interactive contributions of these factors are necessary for predicting the behavior and ecosystem value of *py*OM over time and space. Such assessments remain sparse and, to our knowledge, are currently exclusively obtained via meta-analysis type studies. Recent meta-analytical studies directly addresses important environmental factors driving; (1) the environmental persistence of *py*OM, its priming effects on native soil organic matter (SOM; Wang et al., 2016) and (2) its global distribution in carbon stocks (Reisser et al., 2016). Wang et al. (2016) found that for a given *py*OM, experimental duration (soil residence time, *SRT*) and soil clay content controlled the degradation rate of *py*OM, and its priming effect—with higher *py*OM degradation rates and positive *py*OM priming of native SOM favored at $SRT < 0.5$ years and soil clay contents $\leq$9%. Reisser et al. (2016) found that, globally, the largest *py*OM-associated carbon stocks generally occurred in areas of warmer climates ($\geq$10°C) and soils having high clay contents (>50%) and/or pH > 7. Higher *py*OM-associated carbon in warmer climates was attributed to higher temperature-promoted biomass production and fire probability; and in high clay content, high pH soils due to protection via organo-mineral interactions leading to less *py*OM degradation (Reisser et al., 2016).

As demonstrated through the work of both Wang et al. (2016) and Reisser et al. (2016), global meta-analysis-type studies can provide valuable insights into the environmental factors that drive *py*OM dynamics at the global scale. It is also equally important to recognize that such studies represent the global/on-average case and are not necessarily directly transferrable (or downscalable) to explaining *py*OM dynamics at local or regional scales. That is, factors determined to be driving *py*OM dynamics at the global scale may not necessarily explain variability at finer scales—especially, when spatial and/or temporal variability in potential environmental drivers differ from that captured in global assessment.

It is reasonable to expect spatial variability in the (i) fire and landuse, (ii) climatic, and (iii) pedogenic drivers of *py*OM dynamics, identified by Reisser et al. (2016), at the local and regional scales. With season-to-season variability in rainfall and temperature, changes in landuse and land/fire management, as well as projected climate shifts, environmental drivers of *py*OM dynamics can also be expected to change on short- and long-term temporal scales. For example, with climate change projected to induce regional shifts in temperatures and precipitation, the fire regimes, the amount of *py*OM produced, the soil moisture, biota, and consequently *py*OM biogeochemical cycling are expected to be altered (Flannigan et al., 2000; Santin et al., 2015). Identifying region specific drivers of *py*OM dynamics and developing quantitative relationships between them and the properties and processes they drive are central to predicting impacts of environmental change on ecosystem functions such as carbon sequestration and nutrient cycling.

In this study, we tracked early dynamics of *py*OM from two isotopically distinct sources at 3–6 weeks intervals throughout the first year of burial in coarse textured ultisols located in a forested ecosystem within the Longleaf pine range of the Southeastern United States. The objectives of the study were to (1) identify key environmental factors and processes driving early-stage biogeochemical alteration in *py*OM in such an ecosystem, and

(2) develop quantitative relationships between environmental factors and observed changes in *py*OM properties to explain early-stage dynamics of *py*OM. Focus was placed specifically on the relationship between fire history (*FH*; burnt vs. unburnt), cumulative precipitation ($P_{cum}$), average temperature ($T_{avg}$), soil residence time (*SRT*) and early-stage temporal variability in *py*OM-associated carbon, *py*OM-associated nitrogen, *py*OM pH and *py*OM stability/degradability. The underlying hypothesis was that in its early stages, *py*OM dynamics in sandy-textured (low CEC, low organic matter) soils is analogous to initial stages of soil formation whereby climatic effects (e.g., precipitation and temperature) and the innate properties of the parent material (rock type in the case of soils; in our case, pine- vs. cordgrass-derived pyOM) dictates outcome.

# MATERIALS AND METHODS

## Study Site, Sampling, and Soil Description

The study was conducted at the Lake Thoreau Environmental Center (LTEC; 31.3466° N, 89.4223° W), a 121-hectare facility owned and operated by The University of Southern Mississippi in a manner that parallels historic and current forest management practices across the Southeastern US. The LTEC is located within the pine-belt of Mississippi and the wider Longleaf pine range of the Southeastern United States. It is representative of the region in terms of vegetative cover (∼52% pine forest), fire management (2 year prescribed-burning cycle vs. no burning), surface soils (coarse textured ultisols formed from coastal plain sediments; Soil Survey Staff, 2018), mean annual temperature (15–21°C; Markewitz et al., 2002), mean annual rainfall/precipitation (1,020–1,520 mm; Markewitz et al., 2002) and Koppen-Geiger Climate Classification (humid subtropical; Kottek et al., 2006). Average seasonal temperatures at the LTEC are 32.1, 25.5, 16.2, and 25.2°C for the summer, fall, winter, and spring seasons, respectively with average monthly precipitation values for the same seasons of 112, 105, 139, and 147 mm, respectively.

A total of six sampling locations, along two converging transects, were selected for use in this study (**Figure 1**). Four sampling locations were in an area (herein referred to as the Burnt Zone) with a consistent two-year prescribed burning cycle since the mid 1960's; the most recent burn occurring in January of 2014—prior to the start of the study in the Summer of 2014 (May 31, 2014). The remaining two sampling locations were in an area (herein referred to as the unburnt zone) that has no history of ever being burnt or systematically managed in the last 50 years—besides infrequent grazing from miniature cattle in a small subsection. Sampling locations in the burnt zone are designated with a "B" and those in the unburnt zone are designated with a "U" (see **Figure 1** for complete sampling designations). At the time of the study, the sample sites within the unburnt zone were not being grazed and had very heavily vegetated understories and shrub layers as well as thick litter layers on the forest floor.

Elevation for the study area varied from 88 to 100 m above sea level with overall downhill sloping from NE to SW (i.e., from B4 to B1). Soils at the study site are alluvial in origin and with the exception of B2, were mapped in the US Soil Survey as being from the Freestone-McLaurin-Susquehanna association. The Freestone-McLaurin-Susquehanna association is characterized by a moderately well-drained upper profile—typical of the predominantly coarse-textured ultisols found in the Long leaf pine range. Soils at sampling location B2 were mapped as the Prentiss series (also typical of the region) and comprising also of moderately well-drained upper profile. The textures of soils in the upper 10 cm at the sample locations were determined via the hydrometer method of Gee and Bauder (1986) to be sandy clay loam (B1, B2, B3, U1, U2) or borderline sandy clay loam/clay loam (B4; Supplementary Figure 1).

At each of the six sampling location, samples of pine-derived (P, *Pinus taeda*) and cordgrass-derived (CG, *Spartina alterniflora*) *py*OM were placed in polypropylene litterbags and buried in a gridded design at a depth of ∼8 cm below the soil surface (Supplementary Figure 2). A total of 11 P and 11 CG *py*OM-containing litterbags were buried at each sampling location. One litterbag each of P and CG *py*OM were removed on each sampling excursion, which occurred at 21, 42, 63, 84, 105, 126, 147, 217, 294, 322, and 350 days after burial. Samples collected on each excursion were split 2:1, with two-thirds of each sample being dried (75°C for 24 h) and used for immediate analysis of pH, electrical conductivity (EC), relative recalcitrance ($R_{50}$), total carbon content and total nitrogen content, while one-third of the sample was frozen and subsampled for use in ergosterol, and $\delta^{13}C$ and $\delta^{15}N$ isotopic analysis.

## Preparation of *py*OM

Pine-derived *py*OM was produced from pine needles collected from the study site, while cordgrass-derived *py*OM was produced from cordgrass straw collected from USM's Gulf Coast Research Laboratory. Prior to pyrolysis, needles and grass were dried at 60°C to constant weight and cut into ∼2 cm pieces. Pyrolysis of plant material was performed in a muffle furnace (ramp rate = 25°C/min) under oxygen-limited conditions at 450°C for a total of 1 h. The 450°C was representative of average temperature conditions for a typical vegetation fire in the southeastern United States (Alexis et al., 2007). Upon cooling and removal from the furnace, the *py*OM material was separated into a fine (<250 μm) and a coarse (250–500 μm) fraction. Approximately 1.5 g of the coarse *py*OM material was placed into litterbags (8 × 8 cm). The litterbags used were made from needle-punched polypropylene material with apparent openings of 210 μm (small enough to contain the coarse fraction of the *py*OM, yet large enough to allow environmental interaction with the *py*OM).

## Post-burial *py*OM and Soil Analysis

Pyrogenic organic matter collected on each sampling excursion was analyzed for total carbon content (TC), total nitrogen (TN), pH and relative recalcitrance ($R_{50}$). Samples from selected excursions were analyzed for fungal ergosterol, base-extractable organic carbon (BEOC) and $\delta^{13}C$ and $\delta^{15}N$ isotopic signature.

Carbon and nitrogen content was determined in triplicate by combustion elemental analysis (Costech elemental combustion analyzer) using 2–3 mg of *py*OM tightly wrapped in tin capsules

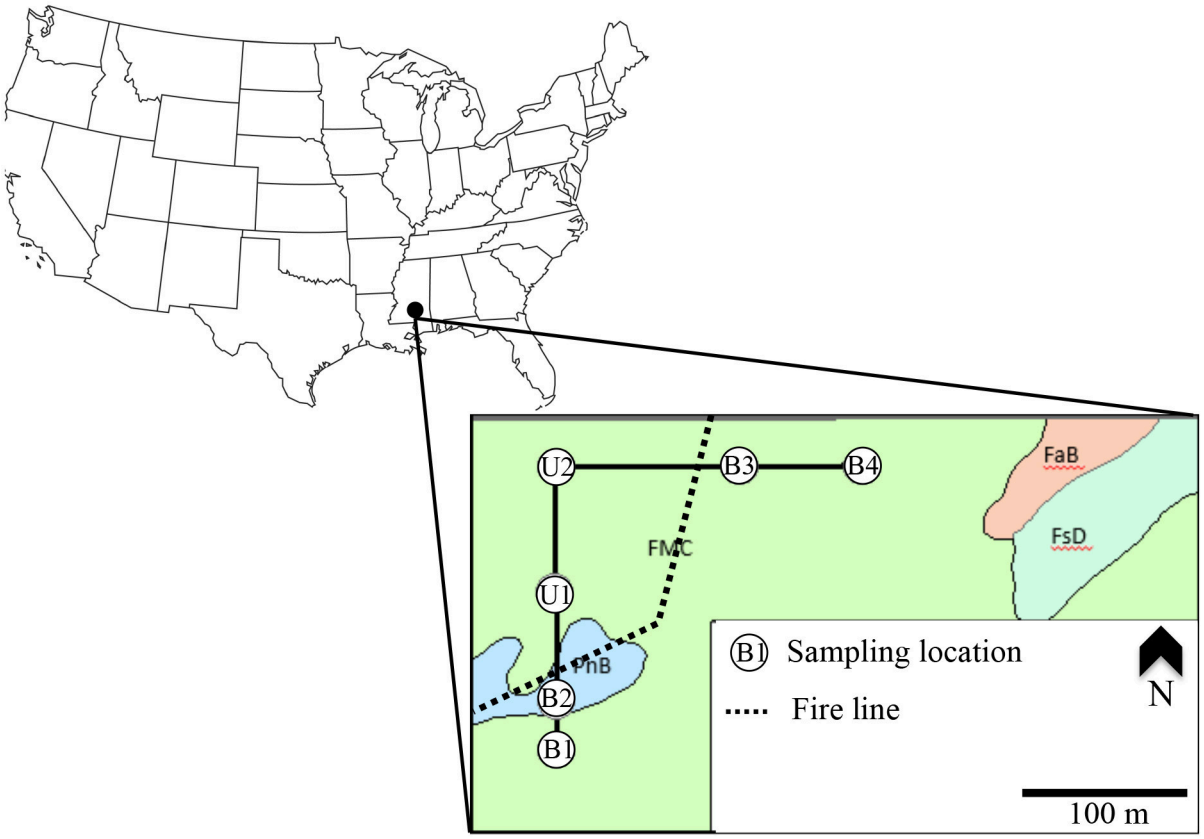


**FIGURE 1 |** Map of study area showing sampling locations, fire line separating the unburnt and burnt zone, and map unit level classification of soils per US Soil Survey (FMC, Freestone-McLaurin-Susquehanna association; PnB, Prentiss fine sandy loam, 2–5% slope; FaB, Faulkner silt loam, 2–5% slope; Soil Survey Staff, 2018).

combusted and compared to acetanilide as a standard (Sarkhot et al., 2012).

Base-extractable organic carbon (BEOC) of *py*OM samples was determined using UV-visible spectrophotometry. Between 150 and 151 mg of *py*OM was placed in 30 ml of 0.5M NaOH solution before being heated for 2 h at 80°C. After heating, the *py*OM: NaOH suspension was cooled, filtered (0.2 μm) and the absorbance measured at 365 nm then compared to a 4-point standard curve of absorbance vs. dissolved organic carbon content from heated-persulfate oxidation method (Shimadzu Scientific Instruments, Columbia, Maryland; Raimbault et al., 1999; Harvey et al., 2009).

For *py*OM pH and EC, 5 ml of de-ionized water was mixed with 50 mg of sample, creating a 1:100 *py*OM: water suspension. This solution was allowed to equilibrate for 12 h before measuring the pH and EC of the extractant (Accumet pH/EC submersible probe).

Relative recalcitrance of the *py*OM was determined by thermogravimetric analysis (TGA; SDTQ600, TA Instruments, New Castle, DE) and the use of the $R_{50}$ index as described by Harvey et al. (2012). Thermal analysis began at an oven temperature of 20°C, increasing at a ramp rate of 10°C per minute until 700°C, at which point no further weight loss was observed. The $R_{50}$ value of the *py*OM is a measure of the innate resistance of the *py*OM material to abiotic and biotic oxidation, and was calculated as:

$$R_{50} = \frac{T_{50,\,pyOM}}{T_{50,\,graphite}} \quad (1)$$

where $T_{50,pyOM}$ and $T_{50,graphite}$ are the temperature values corresponding to 50% oxidation of *py*OM material and graphite (<149 μm, purity 99.9995%; Alfa Aesar, Ward Hill, MA), respectively, and were obtained via use of TGA mentioned above.

The fungal biomass associated with *py*OM samples were estimated using ergosterol concentrations (Kuehn et al., 2011). Ergosterol was extracted from *py*OM samples (∼60 mg) by refluxing in alcoholic KOH (4% KOH in 95% methanol) for 30 min. The resultant extract was partitioned into *n*-pentane and evaporated to dryness under a stream of nitrogen gas. Ergosterol in dried samples was then re-dissolved by sonication in 0.5 ml of methanol and stored, tightly capped, in 1.5 ml screw cap high pressure liquid chromatography (HPLC) vials at ∼20°C until analyzed. Separation and analysis of ergosterol was done using HPLC according to procedures from Kuehn et al. (2011).

Carbon and nitrogen ($\delta^{13}C$ and $\delta^{15}N$) isotopic signature of the *py*OM were determined by EA-IRMS using 2–3 mg of sample

and an elemental analyzer (EA) interfaced to a Thermo-Electron Delta V Advantage isotope ratio mass spectrometer (IRMS). Values for $\delta^{13}C$ were reported relative to the Vienna PeeDee Belemnite standard and values for $\delta^{15}N$ to atmospheric nitrogen.

In addition to *py*OM, soils were collected (to a depth of ∼3 cm) from directly beneath the litterbags on each of the following sampling excursions. The collected soil samples were air-dried to constant weight, grounded to <2 mm and used for soil pH and soil organic carbon (SOC) analyses. Soil pH and SOC was determined using the same procedures as described above for *py*OM albeit samples for SOC analyses were done using 20 mg of sample. It is worth noting that in these soils TC = SOC because of the lack of inorganic carbon—verified by the lack of fizzing in response to HCl additions and supported by the acidic soil pH.

## Precipitation and Temperature Data

The LTEC maintains a weather station (∼600 m west of the study site) with research grade sensors for monitoring precipitation (Tipping bucket rain gauge; model: TE525WS—Texas Electronics) and temperature (HygroClip2 HC2s3—Rotronic Instrument) as well as other climatic parameters (relative humidity, barometric pressure, solar irradiance and wind speed/direction) on 1-min temporal scales. For this study, 1-min averaged precipitation and temperature data were aggregated to obtain daily precipitation and average air temperatures for every day of the study. Daily values were further aggregated through addition or averaging to obtain cumulative precipitation ($P_{cum}$) and average maximum daily temperature ($T_{avg}$), respectively for each sampling day. It is these latter $P_{cum}$ and $T_{avg}$ that are utilized in all our analyses.

## Data Analysis and Modeling

Data analysis was conducted in two phases. The first phase of analysis was executed using two-way analysis of variance and was focused on assessing the relative importance of time (as *SRT*) and sample site in driving observed changes in *py*OM properties of both pine- and cordgrass-derived *py*OM within a given fire history/zone (i.e., burnt vs. unburnt). The goal of this initial analysis was to screen if measured changes in *py*OM properties at the study site were controlled primarily by temporally- or spatially-driven environmental factors (e.g., soil properties) and, therefore, data within a given fire zone could be aggregated across space or time. Two-way analysis was done using Graphpad Prism (version 7.0).

The second phase of data analysis was executed using generalized linear modeling (GLM) and was focused on identifying and then modeling statistically significant ($p < 0.05$) main and/or interactive effects of environmental co-factors (soil residence time, *SRT* (in days); cumulative precipitation, $P_{cum}$(in mm); average maximum daily temperature, $T_{avg}$(in °C); and fire history, *FH*; burnt vs. unburnt) on changes in *py*OM properties (TC, TN, pH, and $R_{50}$). Three initial GLM models were fitted to respective datasets for cordgrass- and pine-derived *py*OM:

1) A main-effects only model with a linear predictor component of the form, $Y = \beta_0 + \beta_1(SRT) + \beta_2(P_{cum}) + \beta_3(T_{avg}) + \beta_4(FH) + \varepsilon$;
2) An interaction-effects only model with a linear predictor component of the form, $Y = \beta_0 + \beta_1(SRT \times P_{cum}) + \beta_2(SRT \times T_{avg}) + \beta_3(SRT \times FH) + \beta_4(P_{cum} \times T_{avg}) + \beta_5(P_{cum} \times \mathrm{FH}) + \beta_6(T_{avg} \times FH) + \varepsilon$; and
3) A combined-effects model with a linear predictor component of the form, $Y = \beta_0 + \beta_1(SRT) + \beta_2(P_{cum}) + \beta_3(T_{avg}) + \beta_4(FH)\ \beta_5(SRT \times P_{cum}) + \beta_6(SRT \times T_{avg}) + \beta_7(SRT \times FH) + \beta_8(P_{cum} \times T_{avg}) + \beta_9(P_{cum} \times \mathrm{FH}) + \beta_{10}(T_{avg} \times FH) + \varepsilon$;

where, $Y$ is the *py*OM property of interest, $\beta_0$ is the model intercept; $\beta_{1...}\beta_n$ are fitted values for contributions of each predictor to $Y$ and $\varepsilon$ is the error term. Values for *FH* were set to 1 for burnt zone and 0 for the unburnt zone. Each model was fitted in two iterations with a normal random component and an identity link function. The first iteration involved all possible predictors (as outlined above) while the second iteration involved only predictors that were identified from the first iteration as having significant $\beta_n$ values (i.e., $p < 0.05$). Main-effects, interaction-effects and combined-effects models from the second iteration were compared via ANOVA; with the best model being selected as that with the lowest AIC (Akiake Information Criterion) and best fit/trace ($R^2$) to the measured data. All statistical analyses were done using the GLM function from statistical package in R-Gui (R-Core Team, 2017).

# RESULTS

## Overall Effects of Time and Space on *py*OM Dynamics

Initial properties of the pine- and cordgrass derived *py*OM are summarized in **Table 1**. Two-way analysis of variance examining the effect of time and sampling site on changes in *py*OM properties indicated that time (*SRT*) accounted for 80–92% of total variability in *py*OM-associated organic carbon, 38–79% in *py*OM-associated nitrogen and 81–91% in *py*OM pH over the course of the study. By comparison, sampling site accounted for 0.005–2.53, 0.08–13, and 1–3% of variability in *py*OM-associated carbon, nitrogen and pH respectively. Interactive effects between time and sampling site were also much (4–49 times) lower than time effects alone in all cases; except for TN in the unburnt zone where the effect of time alone and interactive effects were equal (Supplementary Table 1). The much higher variability in *py*OM-associated carbon, nitrogen and pH accounted for by time (compared to location or interactive effects) pointed to temporally variable environmental, rather than location-based, factors being the primary drivers of *py*OM dynamics in this study. This also indicated that in contrast to other studies (Kane et al., 2010; Kasin and Ohlson, 2013), variations in early-stage *py*OM dynamics due to location-based parameters such as elevation, soil type and position in landscape would not be important in our study. Of such, properties associated with a given *py*OM source and within a given fire zone could be considered as replicates (i.e., properties at U1 and U2 are replicates for unburnt treatment while B1, B2, B3, and B4 are replicates for burnt treatments) and can be spatially-aggregated based on *py*OM feedstock and fire history without any significant loss in the amount of variability captured in the study.

**TABLE 1 |** Selected properties of *py*OM at the time of burial.

| | Total Carbon, $TC_0$ (%) | Total Nitrogen, $TN_0$ (%) | Ash Content (%) | pH *py*OM |
|---|---|---|---|---|
| Pine-derived pyOM | 64.0 ± 1.07 | 0.67 ± 0.02 | 13.8 | 6.25 ± 0.03 |
| Cordgrass-derived pyOM | 64.0 ± 1.64 | 1.44 ± 0.01 | 14.3 | 7.89 ± 0.12 |

## Temporal Trends in *py*OM-Associated Carbon and Nitrogen

Spatially-aggregated, temporal trends in relative total carbon and nitrogen content associated with pine- or cordgrass-derived *py*OM in the unburnt and burnt zones are presented in **Figures 2**, **3**. Over the study period, carbon content associated with *py*OM varied between 0.75 and 1.25 times that of initial values in both fire zones and across both *py*OM source. Interestingly, relative changes in carbon content associated with pine-derived *py*OM followed that of cordgrass-derived *py*OM throughout the study irrespective of fire history. Summer was characterized by a continued decrease (15–25% loss of initial) in *py*OM-associated carbon across both *py*OM sources and fire history. Fall through winter was characterized by an apparent re-accumulation of carbon, lost during summer, while spring was characterized by an additional 17–25% increase in *py*OM-associated carbon, relative to the initial carbon content.

Like *py*OM-associated carbon, temporal trends in *py*OM-associated nitrogen for pine- vs. cordgrass-derived *py*OM were comparable in summer- decreasing slightly to ∼0.96 times the initial (**Figure 3**). However, thereafter, the dynamics of *py*OM-associated nitrogen for pine- and cord-grass derived *py*OM followed very different trajectories within a given fire zone. For pine-derived *py*OM, no further changes in associated nitrogen content were observed over fall, winter and spring in either the unburnt or burnt zones. In contrast, for cordgrass-derived *py*OM, an increase of up to 1.3 times in initial *py*OM-associated nitrogen was observed through Fall, peaking in winter at 1.2–1.3 times initial values and remaining stable thereafter until the end of the study in spring.

Precipitation ($P_{cum}$), soil residence time (*SRT*), average temperature ($T_{avg}$) and the interaction between $P_{cum}$ and *SRT* were found (through GLM analyses) to be the significant ($p < 0.05$) drivers of relative *py*OM-associated carbon content. For observed changes in *py*OM-associated nitrogen, significant drivers were $P_{cum}$, *SRT*, the interactive effects between $P_{cum}$ and *SRT*, interactions between $T_{avg}$ and *SRT* and that between $T_{avg}$ and $P_{cum}$. The final generalized linear model for *py*OM-associated organic carbon was,

$TC_t/TC_0 = 2.84 \times 10^{-4}(P_{cum}) - 1.64 \times 10^{-3}(SRT) - 5.67 \times 10^{-3}(T_{avg}) + 1.11 \times 10^{-6}\ (SRT \times P_{cum}) + 1.123$, was applicable across fire history (burnt vs. unburnt zone) and *py*OM source (cordgrass vs. pine), and captured 77–91% of variability in measured values (**Figure 2** and Supplementary Figure 3).

The final models for *py*OM-associated nitrogen had the same driving factors/parameters for cordgrass- vs. pine-derived *py*OM but different estimates for constants (i.e., $\beta_i$). In the case cordgrass-derived *py*OM, changes in associated nitrogen in both the burnt and unburnt zone could be modeled as:

$TN_t/TN_0 = -2.62 \times 10^{-2}\ (P_{cum}) + 8.31 \times 10^{-2}\ (SRT) + 4.93 \times 10^{-6}\ (SRT \times P_{cum}) - 2.65 \times 10^{-3}\ (SRT \times T_{avg}) + 8.09 \times 10^{-4}\ (P_{cum} \times T_{avg}) + 1.117$, capturing 83–96% of the observed variability in measured values (**Figure 3** and Supplementary Figure 4). In the case of pine-drived *py*OM, changes in associated nitrogen could be modeled as:

$TN_t/TN_0 = -8.98 \times 10^{-3}\ (P_{cum}) + 2.68 \times 10^{-2}\ (SRT) + 1.87 \times 10^{-6}\ (SRT \times P_{cum}) - 9.20 \times 10^{-4}\ (SRT \times T_{avg}) + 2.95 \times 10^{-4}\ (P_{cum} \times T_{avg}) + 1.028$, capturing 64–79% of the observed variability in measured values (**Figure 3** and Supplementary Figure 4).

## Temporal Changes in *py*OM PH and Stability

Throughout summer and fall, the pH of the pine-derived *py*OM remained relatively stable at 6.49 ± 0.24 in the burnt and unburnt zones, before decreasing through winter and early spring to 5.42 ± 0.18 in the burnt zone and 5.03 ± 0.10 in the unburnt zone (**Figure 4**). As spring progressed, pH of pine-derived *py*OM rebounded to 6.36 ± 0.14 by the end of the study on day 350. For cordgrass-derived *py*OM, pH decreased with time from 7.89 ± 0.04 at the start of the experiment in summer to 5.94 ± 0.11 and 4.91 ± 0.07 in the burnt and unburnt zone, respectively, by early spring (day 294). As spring progressed, as with pine-derived *py*OM, the pH of cordgrass-derived *py*OM also rebounded—reaching 7.15 ± 0.10 in the burnt zone and 5.96 ± 0.03 in the unburnt zone by the end of the study on day 350.

Results from GLM analyses indicated that $T_{avg}$, its interaction with *FH*, *SRT,* and $P_{cum}$, and the interaction between $P_{cum}$ and *SRT* were the major factors driving observed changes in the pH of both cordgrass- and pine-derived *py*OM. For cordgrass-derived *py*OM the observed changes in both the unburnt and burnt zone could be modeled as;

$pH_{pyOM} = 3.05 \times 10^{-1}\ (T_{avg}) + 1.68 \times 10^{-2}\ (FH \times T_{avg}) + 1.52 \times 10^{-5}\ (SRT \times P_{cum}) + 1.40 \times 10^{-3}\ (SRT \times T_{avg}) - 6.60 \times 10^{-4}\ (P_{cum} \times T_{avg})$, while changes in pH for the pine-derived *py*OM could be modeled as;

$pH_{pyOM} = 1.46 \times 10^{-1}\ (T_{avg}) - 3.67 \times 10^{-3}\ (FH \times T_{avg}) + 4.35 \times 10^{-6}\ (SRT \times P_{cum}) + 5.55 \times 10^{-4}\ (SRT \times T_{avg}) - 2.21 \times 10^{-4}\ (P_{cum} \times T_{avg}) + 2.699$. The models accounted for 87–94 and 48–61% of the variability observed across fire history in cordgrass- and pine-derived pyOM, respectively (Supplementary Figure 5).

Relative recalcitrance/stability, $R_{50}$, values of the pine- and cordgrass-derived *py*OM are shown in **Figure 5**. These values showed an initial difference in the recalcitrance of pine- and cordgrass-derived *py*OM, with $R_{50}$ values starting at 0.524 and

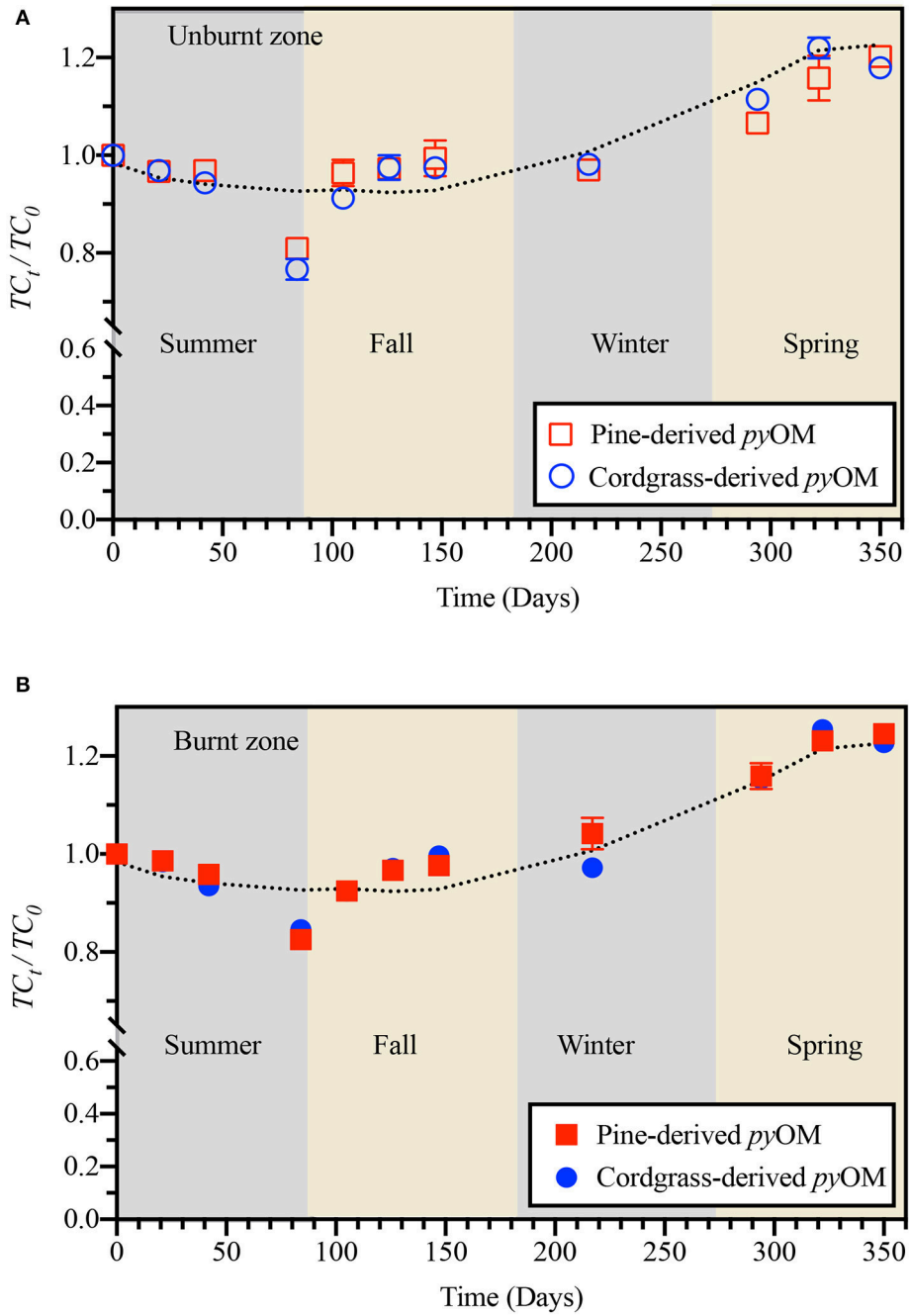


**FIGURE 2 |** Temporal variation in relative *py*OM-associated carbon for pine- and cordgrass-derived pyrogenic organic matter buried to a soil depth of 8 cm in either the **(A)** unburnt or **(B)** burnt fire management zone. Values are based on ash-free carbon content of *py*OM at sampling, relative to that of the initial material. Lines indicate model trace from generalized linear modeling.

0.476, respectively. The relative recalcitrance, $R_{50}$, of pine-derived pyOM generally decreased with increasing soil residence time. The $R_{50}$ of pine-derived pyOM in burned and unburned areas stabilized after ~200 days ($R_{50}$ = 0.512 and 0.518, respectively). Irrespective of fire history, the $R_{50}$ values of the cordgrass-derived *py*OM increased in a logarithmic pattern with time but also converged around 0.508 and 0.518 – similar to the pine-derived *py*OM. Not only were the trajectories in $R_{50}$ values of pine- and cordgrass-derived *py*OM different, but the rates of change varied as well. For pine-derived *py*OM the sigmoidal decrease in $R_{50}$ occurred around late summer-early fall and reaching a minimum in winter. For cordgrass-derived *py*OM, the increasing segment of the $R_{50}$-time relationship reached a maximum $R_{50}$ around late fall-early winter.

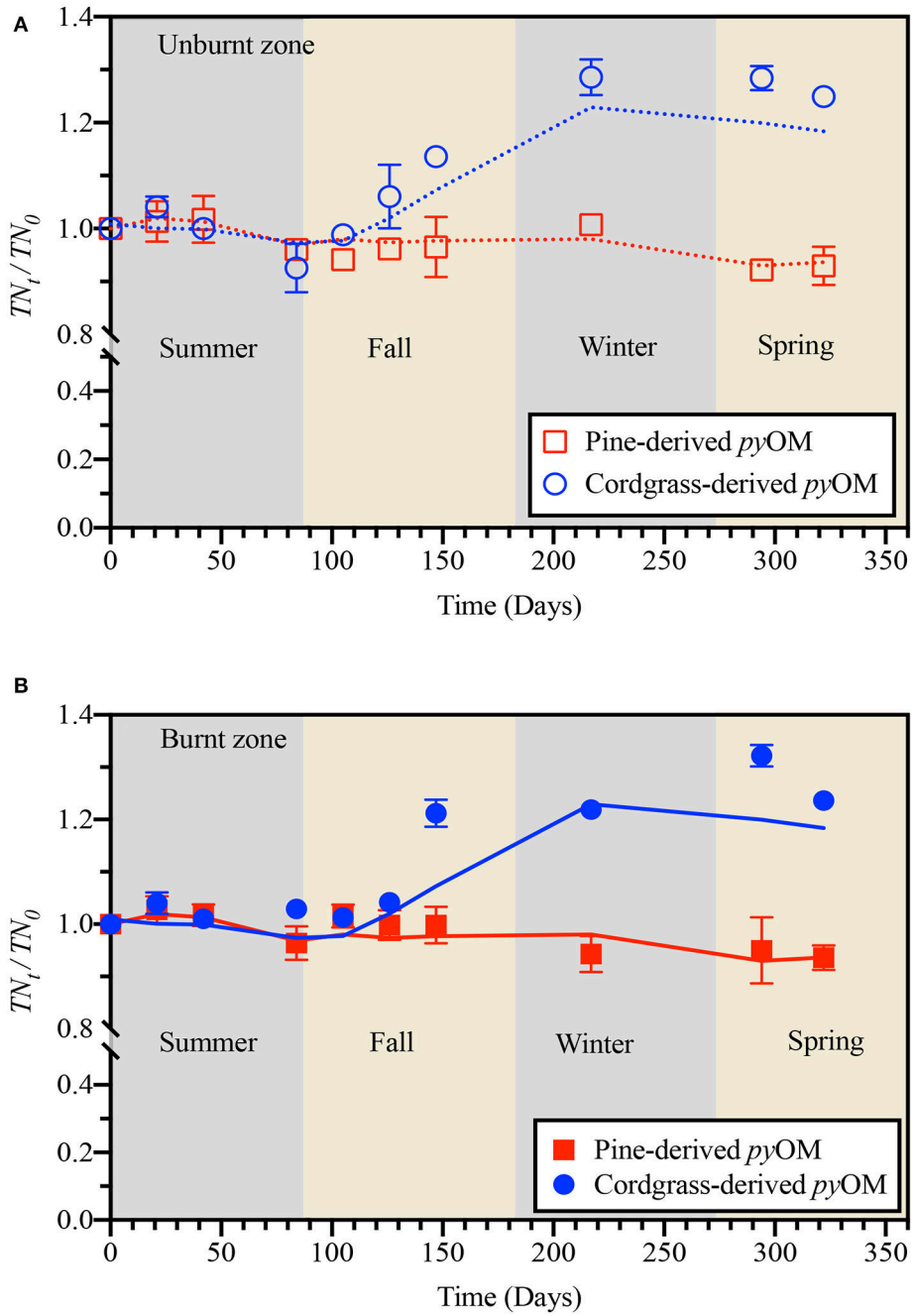


**FIGURE 3 |** Temporal variation in relative *py*OM-associated nitrogen for pine- and cordgrass-derived pyrogenic organic matter buried to a soil depth of 8 cm in either the **(A)** unburnt or **(B)** burnt fire management zone. Values are based on ash-free nitrogen content of *py*OM at sampling, relative to that of the initial material. Lines indicate model trace from generalized linear modeling.

Generalized linear modeling of changes in $R_{50}$ was possible for cordgrass-derived but could not be successfully applied to pine-derived *py*OM. In the case of cordgrass-derived *py*OM, variability in $R_{50}$ in both the burnt and unburnt zone was shown to be predominantly driven by interaction-only effects (between *FH* and $T_{avg}$, *SRT* and $P_{cum}$, *SRT* and $T_{avg}$, *SRT* and $T_{avg}$) and could be modeled as,

$$R_{50} = -3.57 \times 10^{-4}\,(FH \times T_{avg}) - 1.06 \times 10^{-7}\,(SRT \times P_{cum}) - 1.38 \times 10^{-5}\,(SRT \times T_{avg}) + 7.16 \times 10^{-6}\,(P_{cum} \times T_{avg}) + 0.480,$$

with the model accounting for 88–93% of variability in both cases (Supplementary Figure 6). However, such an assessment was not possible for pine-derived *py*OM—because none of the tested co-factors in our main-effects only, interactions-only or mixed effects models were significant at the $p = 0.05$ level.

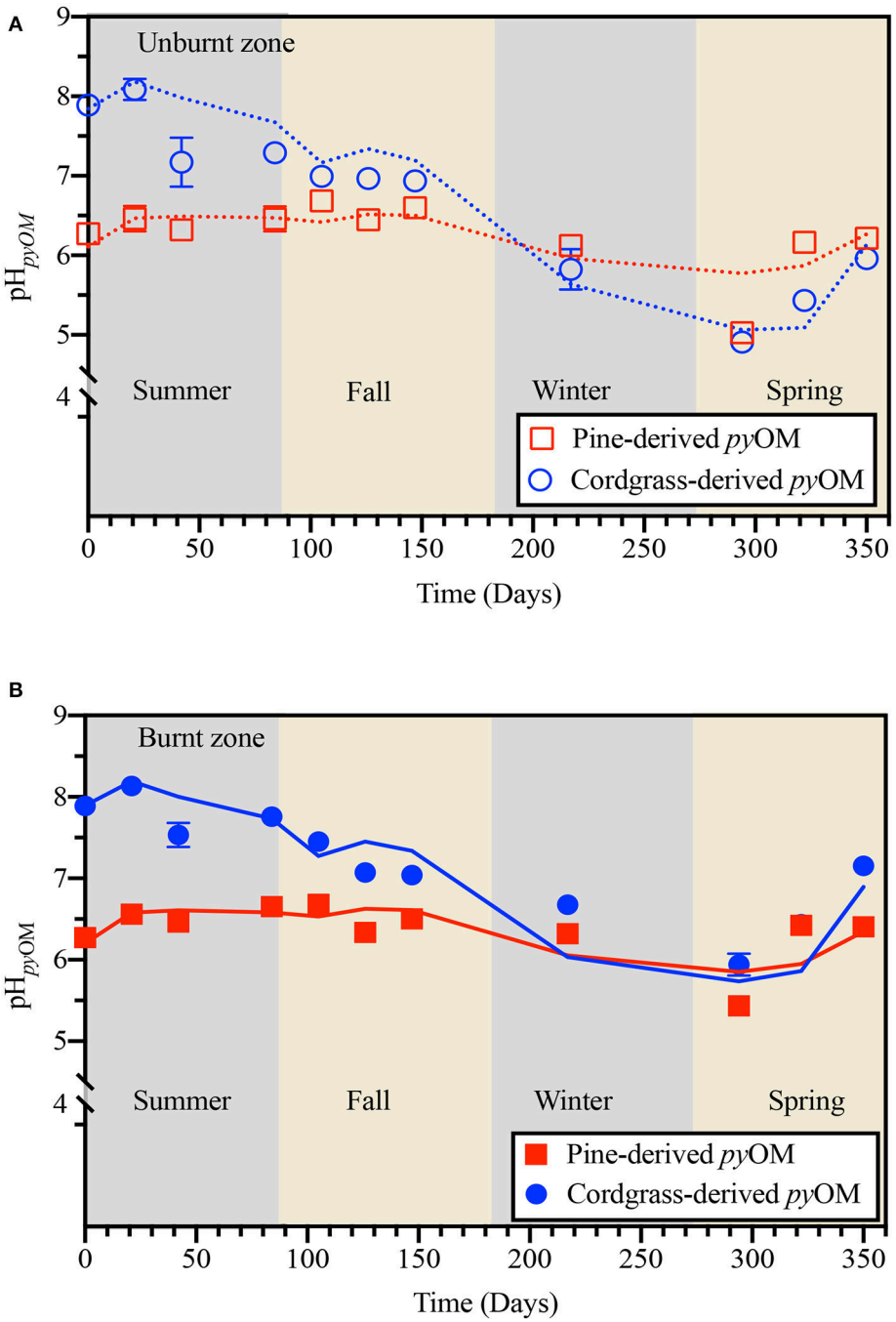


**FIGURE 4 |** Temporal variation in the pH of pine- and cordgrass-derived pyrogenic organic matter (pH$_{pyOM}$) buried to a soil depth of 8 cm in either the **(A)** unburnt or **(B)** burnt fire management zone. Values are based on a 1:100 *py*OM: water ratio. Lines indicate model trace from generalized linear modeling.

## Impact on Soil Properties

Soils immediately below the buried pine- and cordgrass-derived *py*OM did not show significant difference in pH across feedstock but were more acidic in the unburnt (pH = 5.74 ± 0.05) than burnt zone (pH = 6.00 ± 0.04; Supplementary Figure 7). By the first sampling excursion, the pH of the soil immediately beneath the litterbag in the unburnt zone increased to 5.92 ± 0.03 (in both pine- and cordgrass-derived *py*OM) and in the burnt zone to 6.12 ± 0.03 (cordgrass-derived *py*OM). This increase in pH was accompanied by a decrease in the electrical conductivity of the *py*OM from 523 ± 2.29 to 21.7 ± 1.38 and 23.2 ± 3.40 μS cm$^{-1}$ in the burnt and unburnt zone, respectively—with 66–79% of this decrease occurring within the first 21 days (Supplementary Figure 8). The concomitant decline in soil pH

and *py*OM electrical conductivity continued over the fall and winter excursions. In the spring sample excursions, the pH of the soil immediately below the litterbags increased to it initial values.

As with soil pH, SOC content immediately beneath the buried *py*OM litterbags were similar under pine- and cordgrass-derived *py*OM; averaging 2.08 ± 0.07 wt% in the burnt zone and 1.47 ± 0.07 wt% in the unburnt zone (Supplementary Figure 9). In samples from excursions during the latter part of the fall into winter, there was evidence of a comparatively lower SOC content, compared to samples from other excursions.

# DISCUSSION

## Dynamics of *py*OM-Associated Carbon and Nitrogen

Early stage decreases in *py*OM-associated carbon and nitrogen, such as that observed during the summer season of the study, has been attributed to loss of labile components of *py*OM via microbially-mediated degradation, volatilization and/or precipitation-induced leaching (Rajkovich et al., 2012; Norwood et al., 2013; Mukherjee et al., 2014; Sorrenti et al., 2016). At first glance, the microbially-mediated degradation of labile components in *py*OM during summer seemed plausible and was supported to some extent by the fact that most of the loss in carbon and nitrogen (between sampling days 42 and 84) coincided with a 4–5°C increase in air temperature from 31 to 36°C (Supplementary Figure 10). These temperatures, as well as their observed increase during periods of highest carbon and nitrogen loss, were well within the range for optimal soil microbial activity and (all else being constant) would be expected to trigger increased microbial activity (Andersson and Nilsson, 2001; Liang et al., 2003).

Volatilization and/or precipitation-induced leaching/flushing of water-soluble organic components for the observed decrease in *py*OM-associated carbon and nitrogen were also plausible. With the observed increase in $T_{avg}$ over the summer, the volatilization of volatile organic compounds (VOCs) formed during *py*OM formation can be expected; and has been previously linked to the loss of $CO_2$-C from *py*OM with subsequent oxidation of the *py*OM surface (Bruun et al., 2008; Steiner et al., 2008; Rajkovich et al., 2012). Potential support for precipitation-induced leaching/flushing was provided by the occurrence of several rainfall events (ranging in size from 2.54 to 43 mm) during this period (Supplementary Figure 10). As noted earlier, these events were accompanied by sharp declines in the electrical conductivity of the buried *py*OM, indicative of the flushing of salts from the materials (Supplementary Figure 8). It is therefore plausible that rain-induced flushing of salts from *py*OM would also trigger the concomitant leaching of water-soluble carbon and nitrogen from the *py*OM as well.

Direct evidence from $\delta^{13}C$ isotopic signatures of the residual *py*OM was more supportive of precipitation-induced leaching of water-soluble organic components (than the microbial-mediated degradation) as significant driver for observed organic carbon loss in this study. The average $\delta^{13}C$ in pine- and cordgrass-derived *py*OM on day 21 was −28.4 ± 0.05 and −23.9 ± 0.22 ‰ respectively and did not change significantly in the unburnt or burnt zones between days 21 and 84—when *py*OM-associated carbon loss was observed (**Figure 6**). This lack of evidence for a significant shift in the $\delta^{13}C$ signature of *py*OM-associated carbon was inconsistent with expectations for the microbial-mediated oxidation in aerobic surface soils such as those in the study. In such soils, microbial degradation is accompanied by $^{12}C$ enrichment of released $CO_2$ and $^{13}C$ enrichment of the residual OM (Ågren et al., 1996; Feng, 2002; Wang et al., 2015). Conversely, the leaching of water-soluble organic components from *py*OM without significant microbial transformation can be expected to have little or no effect on $\delta^{13}C$ signature (Cleveland et al., 2004). The role of carbon mineralization via the volatilization of VOCs could not be ruled out as significant contributor to the observed loss of *py*OM-associated carbon. In fact, given (1) the lack of isotopic support for microbial mineralization and (2) that $P_{cum}$, *SRT* and $T_{avg}$ (i.e., the GLM model in **Figure 2**) accounted for only 6 of 15–25% of *py*OM-associated carbon lost in the first 84 days (∼3 months), it was quite justifiable that of the three potential processes; volatilization was the process that would account for the greatest loss of *py*OM-associated carbon observed in this study.

The scenario would be somewhat different for losses of *py*OM-associated nitrogen. As the model fit in **Figure 3** indicates—unlike for *py*OM-associated carbon - losses in *py*OM-associated nitrogen during summer could be fully accounted for by leaching (i.e., variations in $P_{cum}$, *SRT,* and $T_{avg}$). The fact that losses in *py*OM-associated nitrogen were accompanied by an approximate 0.5‰ enrichment in the $^{15}N$ signature of the residual *py*OM (**Figure 7**) suggested that the water-soluble nitrogen lost from *py*OM during leaching would be more depleted in $^{15}N$ than the residual *py*OM fraction remaining. $^{15}N$-enrichment in soils has also been attributed to adsorption of microbially processed organic matter and/or increased abundance of soil fungi (Natelhoffer and Fry, 1988; Etcheverría et al., 2009; Wallander et al., 2009). However, neither of these mechanisms was well-supported by our data. Firstly, the net loss of nitrogen, observed during summer, would rule out adsorption as important contributor to $^{15}N$ enrichment. Secondly, there was no evidence for significant fungal colonization of *py*OM during the early stages of experiment associated with summer losses of *py*OM-associated nitrogen. In fact, temporal trends in ergosterol content of *py*OM pointed to summer as being the least biotically-active period—from a fungal perspective—in the study (Supplementary Figure 6). For instance, it is well-known that fungi are the primary degraders of *py*OM in forest soils (Steinbeiss et al., 2009), and as such the ergosterol in fungal cells is widely used as a biomarker for fungal activity (Djajakirana et al., 1996; Mille-Lindblom et al., 2004). However, the fact that measured ergosterol content of *py*OM was significantly lower in summer (2–5 $\mu g\ g^{-1}$ of *py*OM) than in spring (13 $\mu g\ g^{-1}$ of *py*OM) was consistent with the lowest fungal/biotic activity coinciding with greatest and only occurrence of losses in *py*OM-associated carbon (Supplementary Figure 11).

The re-accumulation of *py*OM-associated carbon and nitrogen we observed throughout fall and into spring was consistent with both the trajectory and magnitudes reported by

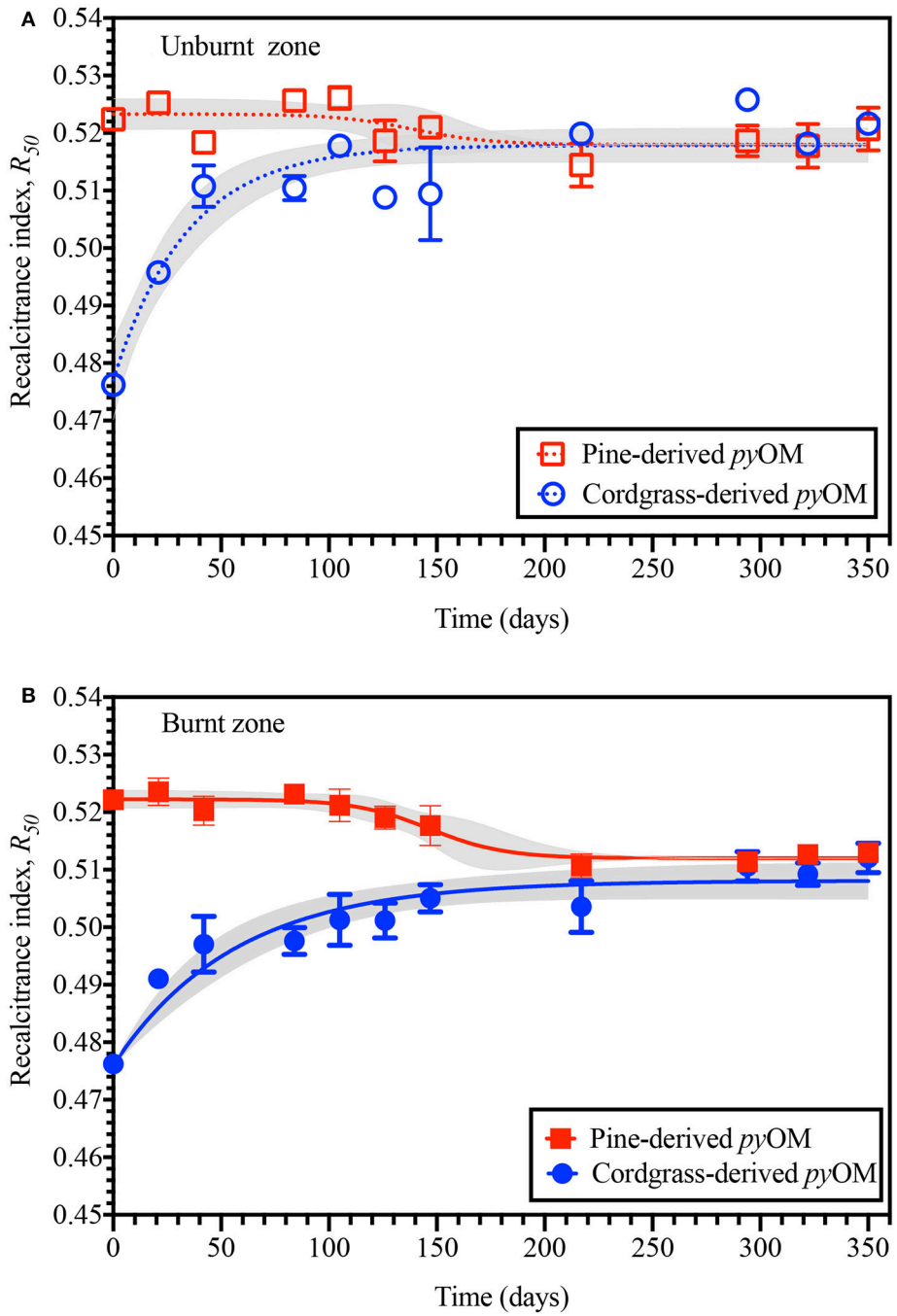


**FIGURE 5 |** Temporal variation in the relative recalcitrance ($R_{50}$) of pine- and cordgrass-derived pyrogenic organic matter buried to a soil depth of 8 cm in either the **(A)** unburnt or **(B)** burnt fire management zone. Values are based on the thermal oxidation of the respective *py*OM to that of graphite.

Mukherjee et al. (2014). In their study, Mukherjee et al. (2014) found that the burial of oak, pine and grass *py*OM (produced at ≥400°C) for a soil residence time of 15 months (May 1, 2009 to September 1, 2010) resulted in an increase of up to 124 and 143% in associated carbon and nitrogen, respectively. They attributed the observed increases to variations in the two soils and *py*OM type studied. Interestingly, the experiments of Mukherjee et al. (2014) were also conducted within the Long leaf pine region about 490 miles east of our site, under comparable average temperatures and cumulative rainfall but in very different soils. That our study conditions differed from Mukherjee et al. (2014) primarily in soil types but yielded similar overall trends in *py*OM dynamics brings into question the overall importance of soil type in *py*OM carbon and nitrogen dynamics in the

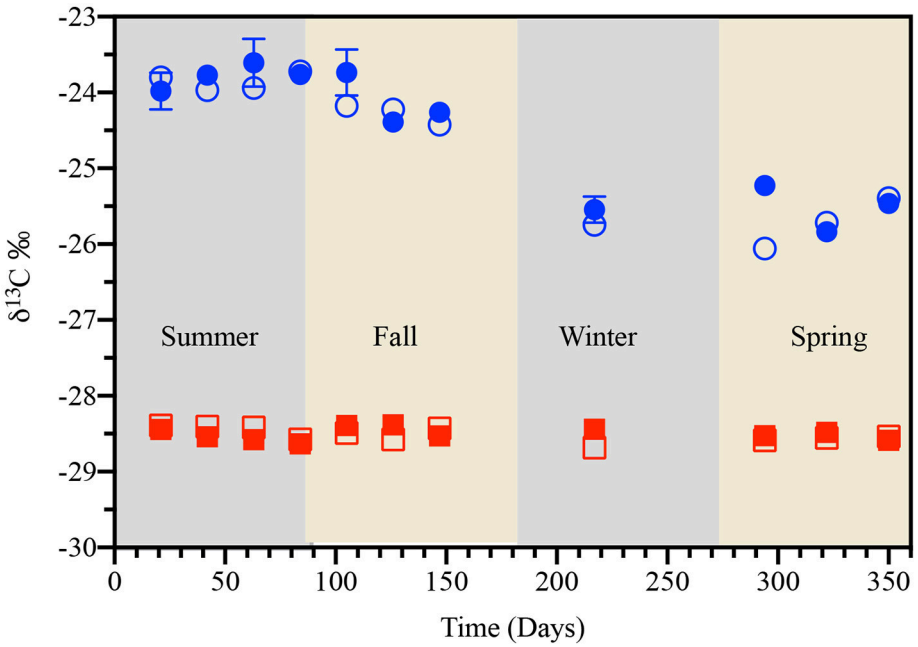


**FIGURE 6 |** Temporal variation in the carbon isotope signature ($\delta^{13}C$) of pine- (red squares) and cordgrass-derived (blue circles) pyrogenic organic matter buried to a soil depth of 8 cm in either the unburnt (open symbols) or burnt (filled symbols) fire management zone. Values of $\delta^{13}C$ are for sampling locations U1 (unburnt values), averages of B1 and B3 (burnt values), and are reported relative to the Vienna PeeDee Belemnite standard.

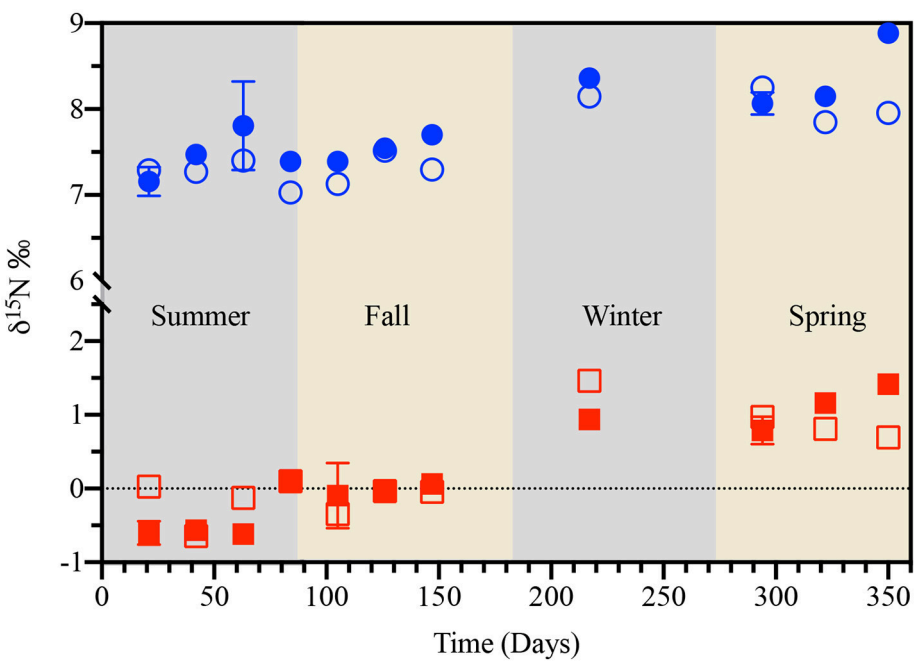


**FIGURE 7 |** Temporal variation in the nitrogen isotope signature ($\delta^{15}N$) of pine- (red squares) and cordgrass-derived (blue circles) pyrogenic organic matter buried to a soil depth of 8 cm in either the unburnt (open symbols) or burnt (filled symbols) fire management zone. Values of $\delta^{15}N$ are for sampling locations U1 (unburnt values), averages of B1 and B3 (burnt values), and are reported relative to the international atmospheric $N_2$ standard.

forested ecosystems of this area and most likely the region. Particularly, since like the spodosol and entisol of Mukherjee et al. (2014) and the ultisol at our site, the surface soils of the region are predominantly coarse (sandy) textured, with low pH, low organic matter and low retention capacities (Shaw et al., 2004; Novak et al., 2009). Other studies have also reported either

the accumulation of carbon (Kasin and Ohlson, 2013; Dong et al., 2017) or nitrogen (Sorrenti et al., 2016; de la Rosa et al., 2018), but not both, after the field aging of *py*OM for up to 5 years. It is also interesting to note that for studies having similar trajectories in *py*OM carbon and nitrogen dynamics, there were suggestions of similar climate—either similar Koppen-Geiger climate classification (continental climate; Kasin and Ohlson, 2013; Dong et al., 2017) or similar annual precipitations and temperatures (Sorrenti et al., 2016; de la Rosa et al., 2018). In all these cases, carbon or nitrogen accumulations in *py*OM were attributed to the sorption of exogenous components (inorganic or organic) and/or microbial/fungal colonization.

Our data showing accumulations of *py*OM-associated carbon and nitrogen, from fall through spring, was consistent with this latter explanation of exogenous carbon and nitrogen sorption to and/or the microbial colonization of the *py*OM. Specifically, the climate-driven leaching of microbially "reworked" exogenous water-soluble organic matter and its subsequent sorption to the *py*OM. Firstly, the fact that both carbon and nitrogen accumulations could be effectively modeled by considering only variations in $P_{cum}$, $T_{avg}$, and *SRT* points to the critical role of climatic conditions (**Figures 2**, **3**). Secondly, the exceedance of the initial carbon and nitrogen values as shown in **Figures 2**, **3** for this period coupled with an accompanying $^{13}C$ depletion in carbon (from $\delta^{13}C = -23.9$ to $-25.7$‰; **Figure 6**) associated with cordgrass-derived *py*OM was reflective of an exogenous source that is isotopically lighter than cordgrass. Thirdly, the presence of $^{15}N$ enrichment in cordgrass *py*OM was reflective of the associated exogenous N being isotopically heavier than the residual *py*OM—consistent with microbial processing of this nitrogen prior to its interaction with *py*OM (**Figure 7**). The fact that nitrogen accumulation was only apparent in cordgrass-derived *py*OM suggested the preferential association of this exogenous nitrogen with functional groups that are more prevalent in the cordgrass- than the pine-derived *py*OM.

Increasing quantities of base-extracted organic carbon (BEOC) associated with both pine- and cordgrass-derived *py*OM, over the course of the study, further supported an exogenous origin for the re-accumulated *py*OM-associated carbon (Supplementary Figure 12). The increasing trends in BEOC with *SRT* also suggested that the plateau in carbon re-accumulation on *py*OM around late fall or winter was more reflective of a lowered availability of "labile" carbon rather than saturation of the *py*OM sorption capacity. A lowered availability of organic carbon in late fall and winter was attributable to lowered temperatures and rainfall favoring a decrease in microbial processing of organic matter, leaching and subsequently a decrease in water-soluble organic matter available for sorption. The lack of $\delta^{13}C$ depletion (or enrichment) for the pine-derived *py*OM ($\delta^{13}C = -28.3$‰; **Figure 6**) pointed to leachate from pine needles, fungal biomass and other similarly $^{13}C$-depleted components of litter/soil organic matter as possible sources (McDowell and Likens, 1988; Qualls and Haines, 1991; Wallander et al., 2009) Increasing availability of this more $^{13}C$-depleted carbon—due to needle shedding, senescence and biotic degradation—would account for the re-accumulation of *py*OM-associated carbon in early to mid-fall (**Figure 2**). Lower temperatures and rainfall, as well as lower biotic activity would explain the reduce availability and hence plateauing in carbon re-accumulation during the latter parts of fall into winter. The return of higher temperatures and rainfall would explain further increases in *py*OM-associated carbon content (from 1 to 1.25 times initial values) observed during spring. As temperature increases in spring, an increase in biotic activity, resulting in more water-soluble organic matter being available for association with *py*OM via for sorption—as in fall. However, as opposed to fall when microbial processing of senescenced plant biomass would drive availability of exogenous carbon, in spring root exudates released to enhance nutrient uptake (as plant shift from dormancy to active growth) would be a potential source of exogenous carbon available for sorption (Mergel et al., 1998; Nardi et al., 2000; Richardson et al., 2011; Keiluweit et al., 2015).

It is worth noting that although increased *py*OM-associated ergosterol was observed with time in all but our pine-derived pyOM in the unburnt zone (Supplementary Figure 11) the role of fungal colonization in observed *py*OM dynamics is not unequivocal. For instance, the range of ergosterol values were well within expectations for mineral soils without fungal colonization (Sung et al., 1995; Djajakirana et al., 1996; Frostegård and Bååth, 1996). Therefore, it is quite plausible that the observed increase ergosterol with *SRT* was exogenous and a result of its sorption to the *py*OM rather than colonization by fungi. Such persistence is not unexpected given the likely protection of fungal biomass by forest litter from sunlight (Mille-Lindblom et al., 2004).

## Dynamics of *py*OM pH and Stability

The differences observed in initial pH in the study was attributable to differences in source material (i.e., pine- vs. cordgrass-derived *py*OM; de la Rosa et al., 2018). The generally lower pH values and lower pH-sensitivity of pine-derived *py*OM, compared to its cordgrass-derived counterpart, was reflective of the acidic conditions typical of the soils in pine forest ecosystems. Cordgrass, on the other hand, is native to coastal regions where pH is usually more basic and more reflective of seawater pH (around pH 8–8.2). The pH of a basic material in an acidic environment is expected to decline as it adjusts to equilibrium conditions, thus the observed decline in pH in cordgrass-derived *py*OM. Declines in *py*OM pH with aging/*SRT* has been widely observed and is attributable to the weathering-induced oxidation of basic to acidic functionalities (e.g., alcohols to carboxyls), the dissolution of carbonates or (oxy)hydroxides and/or the leaching and exchange of basic cations with $H^+$ or acidic cations (Joseph et al., 2010; Yao et al., 2010; Spokas et al., 2012; Sorrenti et al., 2016; de la Rosa et al., 2018). All three of these mechanisms were quite plausible in our study given the observed flushing of salts and observations by others indicating increased ion exchange with aging of *py*OM (Cheng et al., 2008; Mukherjee et al., 2014). The fact that the largest declines in *py*OM pH (1–2 pH units; fall through early spring) coincided with period of accumulation for exogenous carbon and nitrogen further points to the acidic nature of the exogenous organic matter being leached from litter and partitioned to the *py*OM.

The fact that the decline in pH at day 217 was seen in both types of *py*OM and is associated with the transition from winter to spring, suggested that the change was likely linked to a seasonally-driven shift in environmental conditions. The most likely trigger is the occurrence of several large precipitation events throughout winter into early spring (between days 210 and 240; Supplementary Figure 10). This period represented the most intense period of precipitation, resulting in an influx of more acidic exogenous materials and the observed decline in pH of both pine- and cordgrass-derived *py*OM between sampling day 217 and 294. This would also be consistent with results from GLM indicative of $P_{cum}$, $T_{avg}$, and *SRT* being significant parameters in explaining observed variations in the pH of *py*OM. The rebound of *pyOM* pH back to more circumneutral conditions (pH 6.0–7.2) by the end of the study was congruent with eventual loss of acidic exogenous materials via their neutralization through the ingress of basic cations mobilized by root exudates into the *py*OM. The difference in the absolute magnitudes of pH declines and subsequent rebound observed across fire history can be reasonably explained as a fire-induced soil buffering effect; where previous burning imparts a higher soil buffering capacity to soils in the burnt zone (Mukherjee et al., 2014; Wang et al., 2014; Shi et al., 2017, 2018). The source of this buffering would be increased cation exchange capacity and basic cation content arising from higher soil carbon and ash-contained basic cations contents accumulating over progressive burns. Therefore, these soils are better able to resist decreases in pH arising from ingress of exogenous organic matter and/or $H^+$. This fire-induced buffering effect would also explain the significance of *FH* (specifically its interaction with $T_{avg}$), as identified via GLM, as an important parameter in explaining observed variability in pH. We posit that as $T_{avg}$ decreases and plants shift into dormancy, the interaction of precipitation with senesced/senescing plant matter results in the leaching of exogenous organic matter (and $H^+$) that flushes basic cations and gets sorbed to *py*OM reducing its pH. A rebounding of $T_{avg}$ in spring, the return of active plant growth and the associated release of root exudates triggered the release of basic cations from minerals with the leaching and ingress of these basic cations into *py*OM triggering its increase in pH observed in the latter part of the study.

Measured $R_{50}$ values provided a proxy for the bulk recalcitrance (relative to graphite) of the *py*OM remaining in the soil (Harvey et al., 2012). Since the exogenous carbon and nitrogen interacting with the *py*OM was soil dissolved organic matter leached from the same source; the observed changes in $R_{50}$ were reflective of changes in the innate recalcitrance of the original *py*OM material and/or the induced effects of the exogenous OM. Of such, observed $R_{50}$ provided insights into the overall recalcitrance or so called "quality" of the remaining *py*OM.

The different temporal trajectories in $R_{50}$ observed in pine- vs. cordgrass-derived *py*OM can be reasonably explained by considering differences in feedstock structure and effect of associated water-soluble and exogenous OM. The interactions of these factors and subsequent impacts on recalcitrance ($R_{50}$) are summarized in **Figure 8**. Initial differences observed in $R_{50}$ were attributable to structural differences between the pine- and cordgrass-derived *py*OM (mainly the higher fraction of lignin in wood vs. grass feedstocks) that has been well-recognized in a number of previous studies (e.g., McBeath and Smernik, 2009; Harvey et al., 2012). Over the summer, the lack of a significant change in $R_{50}$ values for pine-derived *py*OM indicated that the associated flushing of water-soluble OM (and salts) from this *py*OM had no significant effect on its relative recalcitrance. This was consistent with the leached water-soluble components of pine-derived *py*OM having comparable recalcitrance as the remaining residual *py*OM component. By comparison, the increase in $R_{50}$ values for the cordgrass-derived *py*OM—over the same period—was consistent with the flushed water-soluble OM components of this *py*OM being of lower recalcitrance than the remaining residual *py*OM.

The decline in $R_{50}$ of pine-derived *py*OM with the onset and subsequent increase in the accumulation of exogenous OM (in the *py*OM), over fall and winter, was reflective of this exogenous OM being of lower recalcitrance than the residual *py*OM component. Therefore as the amount of exogenous OM associated with the pine-derived *py*OM increased, its negative effect on $R_{50}$ was enhanced until an apparent plateauing point was reached in the latter part of winter. In contrast, the corresponding increase in $R_{50}$ for cordgrass-derived *py*OM observed over fall and winter was congruent with exogenous OM having a positive effect (i.e., $R_{50}$ of exogenous OM is greater than that for residual *py*OM) on the overall recalcitrance of the cordgrass-derived *py*OM; with this positive effect on recalcitrance also reaching a plateauing point in late winter.

Similarities in the timing and $R_{50}$ values at which plateauing occurred in cordgrass- and pine-derived *py*OM, within a given fire history, pointed to a common "equilibrium" $R_{50}$ ($R_{50,\,eq}$). In addition to being reflective of the overall effect of residual *py*OM and exogenous OM on *py*OM recalcitrance, this $R_{50,\,eq}$ provide some interesting insights into overall *py*OM recalcitrance as it pertains to, 1) fire history at the study site and 2) potential priming effects of exogenous OM on *py*OM recalcitrance. Lower values for $R_{50,\,eq}$ in the burnt vs. unburnt zone suggested that *py*OM was likely to have a comparatively lower persistence in soils with longer fire histories (**Figure 8**). Lower persistence of *py*OM in soils with a history of fires have been attributed to the presence of microbial populations that are well-adapted to utilizing fire-derived carbon (Khodadad et al., 2011; Masiello et al., 2013). However, our results suggested that leaching and the modifying effects of exogenous OM are also important factors in *py*OM persistence. For instance, in the case of cordgrass-derived *py*OM the difference in $R_{50,\,eq}$ between the burnt and unburnt zones was established during the *py*OM flushing stage—indicative of leaching differences. By comparison, in pine-derived *py*OM, the precedence for the observed difference in $R_{50,\,eq}$ between the burnt and unburnt zones was established during the stage of accumulation of exogenous OM—indicative of differences in the interaction between *py*OM and exogenous OM in the fire zones being an important factor.

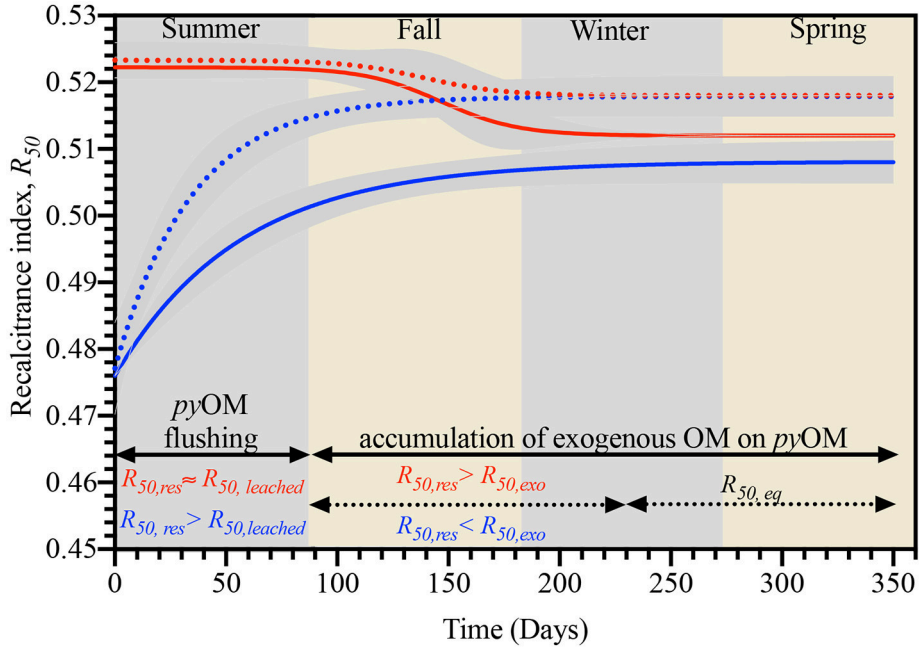


**FIGURE 8 |** Relationship between recalcitrance ($R_{50}$) and processes (*py*OM flushing and accumulation of exogenous OM) controlling biogeochemical dynamics of, pine- (red lines) and cordgrass-derived (blue lines) *py*OM buried in either the unburnt (broken lines) or burnt (solid lines) fire management zone.

In terms of potential priming effects, the higher residual $R_{50}$ ($R_{50,\ res}$) at the end of summer for pine-derived materials compared to the corresponding $R_{50,\ eq}$ (i.e., $R_{50,\ res} > R_{50,\ eq}$) is consistent with exogenous OM reducing the overall recalcitrance of *py*OM and hence favor positive priming (**Figure 8**). In contrast, the reverse situation ($R_{50,\ res} < R_{50,\ eq}$) existed for the cordgrass-derived *py*OM, indicative of exogenous OM in the study area increasing overall recalcitrance of *py*OM and hence is most likely to result in negative priming of *py*OM. The higher absolute magnitude of $R_{50,\ res}$ minus $R_{50,\ eq}$ in burnt vs. unburnt fire zones suggest that the priming effects of exogenous OM on *py*OM degradability would be more pronounced in soils with an history of fire/*py*OM input.

## Temporal Changes in Soil Within the Vicinity of the *py*OM

The overall acidic pH conditions of the soils were consistent with expectations, for soils within a pine forest ecosystem (Falkengren-Grerup, 1987) while the higher pH conditions observed in burnt vs. unburnt soils were consistent with the presence of basic salts (e.g., CaO and $CaCO_3$)—produced as components in the ash byproduct of plant biomass pyrolysis (Bodí et al., 2014; Wang et al., 2014 and references therein). The concomitant increase in the pH of the soil immediately beneath the litter bags, with loss in *py*OM electrical conductivity, after the first excursion was consistent with *in-situ* flushing of basic salts from ash (13–14 wt%) within the *py*OM into the immediate soil. The role of ash components in early soil pH modification was well-supported by evidence from temporal changes in the electrical conductivity of CG-derived *py*OM consistent with enhanced *in-situ* flushing of the *py*OM within the first 21 days of the study (Supplementary Figure 8). For example, over the course of the study the electrical conductivity of the CG-derived *py*OM decreased from 523 ± 2.29 μS $cm^{-1}$ to 21.7 ± 1.38 and 23.2 ± 3.40 μS $cm^{-1}$ in the burnt and unburnt zone, respectively. However, 66–79% of this decrease in electrical conductivity occurred within the first 21 days—congruent with the vast majority of basic salts being leached from the *py*OM during this period into the soil below.

The continued decline in soil pH and *py*OM electrical conductivity observed for the fall and winter excursions reflected continued leaching and the loss of basic salts from the soils immediately below the litterbags. The subsequent increase in soil pH for the spring sample excursions suggested either a latter influx of basic salts into, or loss of acidic components from, the soil immediately below the *py*OM. However, the lack of an accompanying decrease in *py*OM electrical conductivity evidence would exclude ash from the *py*OM as the source of the observed increase in soil pH in the spring. The actual source of this increase in soil pH is unclear at this time but is likely linked to temperature- and precipitation-enhanced process(es)—in particular the root exudate enhanced mobilization of base cations from minerals as plants return to active growth from dormancy.

Higher SOC content in the burnt zone was consistent with the migration and storage of *py*OM from previous burning events below the soil surface (Supplementary Figure 9). The lower SOC content in samples from late fall and winter, compared to the other seasons, was congruent with decreasing soil pH trends and

suggest an association of leaching with lower SOC immediately below the buried litterbag (Supplementary Figure 4).

## SUMMARY AND CONCLUDING REMARKS

In an effort to better understand the factors driving early-stage *py*OM dynamics we studied the chemical evolution of freshly produced cordgrass- and pine-derived *py*OM over the first year post-burial in pine-forest soils with similar origins (parent material and texture) but very different fire management histories. Results from the study indicated that spatially-driven factors had little to no effect on *py*OM dynamics in the short-term (up to 1 year). By comparison, temporally-variable factors such *SRT*, $P_{cum}$, $T_{avg}$ and to a lesser degree the land management factor, *FH* were found to be the primary contributors to observed variation in the biogeochemical dynamics—specifically *py*OM-associated carbon content, nitrogen content, pH and bulk recalcitrance—of *py*OM from different sources. Interestingly, we found no evidence to support microbially-driven mineralization of *py*OM as an important driver of *py*OM dynamics in this study. Instead, the volatilization of VOCs and/or the leaching of water-soluble components from the *py*OM were most plausibly controlling *py*OM dynamics in the first 3 months (i.e., summer) of the study; while in the next 9 months (i.e., fall through spring), the dynamics of *py*OM was likely controlled by availability of exogenous organic matter and its interaction with *py*OM.

The volatilization of VOCs and the flushing of water-soluble components from *py*OM (including water-soluble organic matter) during the first 3 months resulted in (1) a decrease in *py*OM-associated carbon, (2) minimal effect on *py*OM-associated nitrogen or the overall stability of pine-derived *py*OM but (3) increased the overall stability of cordgrass-derived *py*OM. The increasing availability of labile exogenous organic matter (from needle fall and senescence in fall and root exudates in spring) resulted in a re-accumulation/accumulation of *py*OM-associated carbon and nitrogen (for cordgrass-derived *py*OM) in fall through to spring. Interaction of this exogenous organic matter with *py*OM caused an initial decrease and increase in the recalcitrance of pine-derived and cordgrass-derived *py*OM, respectively - with an eventual convergence in recalcitrance for both *py*OMs by mid-winter. A higher recalcitrance convergence point in the unburnt zone was congruent with a longer potential persistence of *py*OM in these soils compared to that in the burnt zone. The decreasing effect of exogenous organic matter on *py*OM recalcitrance suggests that native non-pyrogenic organic matter in the study area is likely to have a positive priming effect on any eventual microbial degradation.

The overall lack of evidence to support a significant microbiological influence—contrasted against that for volatilization, leaching of water-soluble *py*OM, and sorption of exogenous organic matter—pointed overwhelmingly to physicochemical (rather than microbiological) processes as the primary drivers of early *py*OM dynamics in our study system. Such results suggest that models of *py*OM behavior (especially in the early stages) in humid subtropical systems may need to adopt a multifactorial approach in determining the factors dictating *py*OM dynamics.

## AUTHOR CONTRIBUTIONS

All authors were involved in the design of experiments and planning of analysis. JS and RA conducted field experiments; JS, PL, and KK conducted laboratory analyses; OH and JS wrote the manuscript.

## ACKNOWLEDGMENTS

Funding for this project was primarily through startup funds provided to OH by the University of Southern Mississippi and Texas Christian University. The authors are grateful to Drs. Michael Davis and Andy Reece for allowing access to the LTEC and weather station data, respectively. Dr. Ren Zhang at the Baylor University Stable Isotope Laboratory performed isotopic analysis on a fee basis. Stable isotope analysis was supported through an internal grant to OH from TCU's Andrew's Institute for Mathematics and Science Education.

## SUPPLEMENTARY MATERIAL

The Supplementary Material for this article can be found online at: https://www.frontiersin.org/articles/10.3389/feart.2018.00052/full#supplementary-material

## REFERENCES

Ågren, G. I., Bosatta, E., and Balesdent, J. (1996). Isotope discrimination during decomposition of organic matter: a theoretical analysis. *Soil Sci. Soc. Am. J.* 60, 1121–1126. doi: 10.2136/sssaj1996.03615995006000040023x

Alexis, M. A., Rasse, D. P., Rumpel, C., Bardoux, G., Pechot, N., Schmalzer, P., et al. (2007). Fire impact on C and N losses and charcoal production in a scrub oak ecosystem. *Biogeochemistry* 82, 201–216.

Andersson, S., and Nilsson, S. I. (2001). Influence of ph and temperature on microbial activity, substrate availability of soil-solution bacteria and leaching of dissolved organic carbon in a mor humus. *Soil Biol. Biochem.* 33, 1181–1191. doi: 10.1016/S0038-0717(01)00022-0

Bird, M. I., Wynn, J. G., Saiz, G., Wurster, C. M., and McBeath, A. (2015). The pyrogenic carbon cycle. *Annu. Rev. Earth Planet. Sci.* 43, 273–298. doi: 10.1146/annurev-earth-060614-105038

Bodí, M. B., Martin, D. A., Balfour, V. N., Santín, C., Doerr, S. H., Pereira, P., et al. (2014). Wildland fire ash: production, composition and Eco-Hydro-geomorphic effects. *Earth Sci. Rev.* 130, 103–127. doi: 10.1016/j.earscirev.2013.12.007

Bruun, S., Jensen, E. S., and Jensen, L. S. (2008). Microbial mineralization and assimilation of black carbon: dependency on degree of thermal alteration. *Org. Geochem.* 39, 839–845. doi: 10.1016/j.orggeochem.2008.04.020

Carvalhais, N., Forkel, M., Khomik, M., Bellarby, J., Jung, M., Migliavacca, M., et al. (2014). Global covariation of carbon turnover times with climate in terrestrial ecosystems. *Nature* 514, 213–217. doi: 10.1038/nature13731

Cheng, C.-H., Lehmann, J., Thies, J. E., and Burton, S. D. (2008). Stability of black carbon in soils across a climatic gradient. *J. Geophys. Res.* 113:G02027. doi: 10.1029/2007JG000642

Cleveland, C. C., Neff, J. C., Townsend, A. R., and Hood, E. (2004). Composition, dynamics, and fate of leached dissolved organic matter in terrestrial

ecosystems: results from a decomposition experiment. *Ecosystems* 7, 175–285. doi: 10.1007/s10021-003-0236-7

de la Rosa, J. M., Rosado, M., Paneque, M., Miller, A. Z., and Knicker, H. (2018). Effects Of aging under field conditions on biochar structure and composition: implications for biochar stability in soils. *Sci. Tot. Environ.* 613–614, 969–976. doi: 10.1016/j.scitotenv.2017.09.124

Djajakirana, G., Joergensen, R. G., and Meyer, B. (1996). Ergosterol and microbial biomass relationship in soil. *Biol. Fertil. Soils* 22, 299–304. doi: 10.1007/BF00334573

Dong, X., Li, G., Lin, Q., and Zhao, X. (2017). Quantity and quality changes of biochar aged for 5 years in soil under field conditions. *Catena* 159, 136–143. doi: 10.1016/j.catena.2017.08.008

Etcheverría, P., Huygens, D., Godoy, R., Borie, F., and Boeckx, P. (2009). Arbuscular mycorrhizal fungi contribute to 13c and 15n enrichment of soil organic matter in forest soils. *Soil Biol. Biochem.* 41, 858–861. doi: 10.1016/j.soilbio.2009.01.018

Falkengren-Grerup, U. (1987). Long-term changes in ph of forest soils in southern sweden. *Environ. Pollut.* 43, 79–90. doi: 10.1016/0269-7491(87)90067-4

Feng, X. (2002). A theoretical analysis of carbon isotope evolution of decomposing plant litters and soil organic matter. *Global Biogeochem. Cycles* 16, 66–1. doi: 10.1029/2002GB001867

Flannigan, M. D., Stocks, B. J., and Wotton, B. M. (2000). Climate change and forest fires. *Sci. Tot. Environ.* 262, 221–229. doi: 10.1016/S0048-9697(00)00524-6

Frostegård, A., and Bååth, E. (1996). The use of phospholipid fatty acid analysis to estimate bacterial and fungal biomass in soil. *Biol. Fertil. Soils* 22, 59–65. doi: 10.1007/BF00384433

Gee, G. W., and Bauder, J. W. (1986). "Particle-size analysis, in *Methods of Soil Analysis; Part 1 Physical and Mineralogical Methods, 2nd Edn,* ed A. Klute (Madison: American Society of Agronomy).

Hammes, K., Torn, M. S., Lapenas, A. G., and Schmidt, M. W. I. (2008). Centennial black carbon turnover observed in a russian steppe soil. *Biogeosciences* 5, 1339–1350. doi: 10.5194/bg-5-1339-2008

Harvey, O. R., Herbert, B. E., Harris, J. P., Stiffler, E. A., and Crenwelge, J.-A. (2009). A new spectrophotometric method for rapid semiquantitative determination of soil organic carbon. *Soil Sci. Soc. Am. J.* 73, 822–830. doi: 10.2136/sssaj2008.0268

Harvey, O. R., Kuo, L. J., Zimmerman, A. R., Louchouarn, P., Amonette, J. E., and Herbert, B. E. (2012). An index-based approach to assessing recalcitrance and soil carbon sequestration potential of engineered black carbons (Biochars). *Environ. Sci. Technol.* 46, 1415–1421. doi: 10.1021/es2040398

Joseph, S. D., Camps-Arbestain, M., Lin, Y., Munroe, P., Chia, C. H., Hook, J., et al. (2010). An investigation into the reactions of biochar in soil. *Soil Res.* 48, 501–515. doi: 10.1071/SR10009

Kane, E. S., Hockaday, W. C., Turetsky, M. R., Masiello, C. A., Valentine, D. W., Finney, B. P., et al. (2010). Topographic controls on black carbon accumulation in alaskan black spruce forest soils: implications for organic matter dynamics. *Biogeochemistry* 100, 39–56. doi: 10.1007/s10533-009-9403-z

Kasin, I., and Ohlson, M. (2013). An experimental study of charcoal degradation in a boreal forest. *Soil Biol. Biochem.* 65, 39–49. doi: 10.1016/j.soilbio.2013.05.005

Keiluweit, M., Bougoure, J. J., Nico, P. S., Pett-Ridge, J., Weber, P. K., and Kleber, M. (2015). Mineral protection of soil carbon counteracted by root exudates. *Nat. Clim. Chang.* 5, 588–595. doi: 10.1038/nclimate2580

Khodadad, C. L. M., Zimmerman, A. R., Green, S. J., Uthandi, S., and Foster, J. S. (2011). Taxa-specific changes in soil microbial community composition induced by pyrogenic carbon amendments. *Soil Biol. Biochem.* 43, 385–392. doi: 10.1016/j.soilbio.2010.11.005

Knicker, H. (2010). "Black Nitrogen" – an important fraction in determining the recalcitrance of charcoal. *Organ. Geochem.* 41, 947–950. doi: 10.1016/j.orggeochem.2010.04.007

Knicker, H., Hilscher, A., González-Vila, F. J., and Almendros, G. (2008). A new conceptual model for the structural properties of char produced during vegetation fires. *Organ. Geochem.* 39, 935–939. doi: 10.1016/j.orggeochem.2008.03.021

Kottek, M., Grieser, J., Beck, C., Rudolf, B., and Rubel, F. (2006). World map of the köppen-geiger climate classification updated. *Meteorologische Zeitschrift* 15, 259–263. doi: 10.1127/0941-2948/2006/0130

Kuehn, K. A., Ohsowski, B. M., Francoeur, S. N., and Neely, R. K. (2011). Contributions of fungi to carbon flow and nutrient cycling from standing dead typha angustifolia leaf litter in a temperate freshwater marsh. *Limnol. Oceanogr.* 56, 529–539. doi: 10.4319/lo.2011.56.2.0529

Lehmann, J., Gaunt, J., and Rondon, M. (2006). Bio-char sequestration in terrestrial ecosystems – a review. *Mitigat. Adapt. Strateg. Global Change* 11, 403–427. doi: 10.1007/s11027-005-9006-5

Lehmann, J., Skjemstad, J., Sohi, S., Carter, J., Barson, M., Falloon, P., et al. (2008). Australian climate–carbon cycle feedback reduced by soil black carbon. *Nat. Geosci.* 1, 832–835. doi: 10.1038/ngeo358

Liang, B., Lehmann, J., Solomon, D., Sohi, S., Thies, J. E., Skjemstad, J. O., et al. (2008). Stability of biomass-derived black carbon in soils. *Geochim. Cosmochim. Acta* 72, 6069–6078. doi: 10.1016/j.gca.2008.09.028

Liang, C., Das, K. C., and McClendon, R. W. (2003). The influence of temperature and moisture contents regimes on the aerobic microbial activity of a biosolids composting blend. *Bioresour. Technol.* 86, 131–137. doi: 10.1016/S0960-8524(02)00153-0

Markewitz, D., Sartori, F., and Craft, C. (2002). Soil change and carbon storage in longleaf pine stands planted on marginal agricultural lands. *Ecol. Appl.* 12, 1276–1285. doi: 10.1890/1051-0761(2002)012[1276:SCACSI]2.0.CO;2

Masiello, C. A., Chen, Y., Gao, X., Liu, S., Cheng, H. Y., Bennett, M. R., et al. (2013). Biochar and microbial signaling: production conditions determine effects on microbial communication. *Environ. Sci. Technol.* 47, 11496–11503. doi: 10.1021/es401458s

McBeath, A. V., and Smernik, R. J. (2009). Variation in the degree of aromatic condensation of chars. *Organ. Geochem.* 40, 1161–1168. doi: 10.1016/j.orggeochem.2009.09.006

McDowell, W. H., and Likens, G. E. (1988). Origin, composition, and flux of dissolved organic carbon in the hubbard brook valley. *Ecol. Monogr.* 58, 177–195. doi: 10.2307/2937024

Mergel, A., Timchenko, A., and Kudeyarov, V. (1998). "Role of plant root exudates in soil carbon and nitrogen transformation," in *Root Demographics And Their Efficiencies in Sustainable Agriculture, Grasslands and Forest Ecosystems: Proceedings of the 5th Symposium of the International Society of Root Research, Held 14–18 July 1996 At Madren Conference Center, Clemson University, Clemson, South Carolina, USA.* ed J. E. Box (Dordrecht: Springer).

Mille-Lindblom, C., Von Wachenfeldt, E., and Tranvik, L. J. (2004). Ergosterol as a measure of living fungal biomass: persistence in environmental samples after fungal death. *J. Microbiol. Methods* 59, 253–262. doi: 10.1016/j.mimet.2004.07.010

Mukherjee, A., Zimmerman, A. R., Hamdan, R., and Cooper, W. T. (2014). physicochemical changes in pyrogenic organic matter (biochar) after 15 months of field aging. *Solid Earth* 5, 693–704. doi: 10.5194/se-5-693-2014

Nardi, S., Concheri, G., Pizzeghello, D., Sturaro, A., Rella, R., and Parvoli, G. (2000). Soil organic matter mobilization by root exudates. *Chemosphere* 41, 653–658. doi: 10.1016/S0045-6535(99)00488-9

Natelhoffer, K. J., and Fry, B. (1988). Controls on natural Nitrogen-15 and Carbon-13 abundances in forest soil organic matter. *Soil Sci. Soc. Am. J.* 52, 1633–1640. doi: 10.2136/sssaj1988.03615995005200060024x

Norwood, M. J., Louchouarn, P., Kuo, L.-J., and Harvey, O. R. (2013). Characterization and biodegradation of water-soluble biomarkers and organic carbon extracted from low temperature chars. *Organ. Geochem.* 56, 111–119. doi: 10.1016/j.orggeochem.2012.12.008

Novak, J. M., Busscher, W. J., Laird, D. L., Ahmedna, M., Watts, D. W., and Niandou, M. A. S. (2009). Impact of biochar amendment on fertility of a southeastern coastal plain soil. *Soil Sci.* 174, 105–112. doi: 10.1097/SS.0b013e3181981d9a

O'Neill, B., Grossman, J., Tsai, M. T., Gomes, J. E., Lehmann, J., Peterson, J., et al. (2009). Bacterial community composition in brazilian anthrosols and adjacent soils characterized using culturing and molecular identification. *Microb. Ecol.* 58, 23–35. doi: 10.1007/s00248-009-9515-y

Qualls, R. G., and Haines, B. L. (1991). Geochemistry of dissolved organic nutrients in water percolating through a forest ecosystem. *Soil Sci. Soc. Am. J.* 55, 1112–1123. doi: 10.2136/sssaj1991.03615995005500040036x

R-Core Team (2017). *R: A Language And Environment For Statistical Computing.* Available online at: https://www.R-Project.Org/ (Accessed January 29, 2018).

Raimbault, P., Pouvesle, W., Diaz, F., Garcia, N., and Sempéré, R. (1999). Wet-Oxidation and automated colorimetry for simultaneous determination of

organic carbon, nitrogen and phosphorus dissolved in seawater. *Mar. Chem.* 66, 161–169. doi: 10.1016/S0304-4203(99)00038-9

Rajkovich, S., Enders, A., Hanley, K., Hyland, C., Zimmerman, A. R., and Lehmann, J. (2012). Corn growth and nitrogen nutrition after additions of biochars with varying properties to a temperate soil. *Biol. Fertil. Soils,* 48, 271–284. doi: 10.1007/s00374-011-0624-7

Reisser, M., Purves, R. S., Schmidt, M. W. I., and Abiven, S. (2016). Pyrogenic carbon in soils: a literature-based inventory and a global estimation of its content in soil organic carbon and stocks. *Front. Earth Sci.* 4:80. doi: 10.3389/feart.2016.00080

Richardson, A. E., Lynch, J. P., Ryan, P. R., Delhaize, E., Smith, F. A., Smith, S. E., et al. (2011). Plant and microbial strategies to improve the phosphorus efficiency of agriculture. *Plant Soil* 349, 121–156. doi: 10.1007/s11104-011-0950-4

Santin, C., Doerr, S. H., Preston, C. M., and Gonzalez-Rodriguez, G. (2015). Pyrogenic organic matter production from wildfires: a missing sink in the global carbon cycle. *Glob. Change Biol.* 21, 1621–1633. doi: 10.1111/gcb.12800

Sarkhot, D. V., Berhe, A. A., and Ghezzehei, T. A. (2012). Impact of biochar enriched with dairy manure effluent on carbon and nitrogen dynamics. *J. Environ. Qual.* 41, 1107–1114. doi: 10.2134/jeq2011.0123

Schmidt, M. W. I., and Noack, A. G. (2000). Black carbon in soils and sediments: analysis, distribution, implications, and current challenges. *Global Biogeochem. Cycles* 14, 777–793. doi: 10.1029/1999GB001208

Shaw, J. N., West, L. T., Bosch, D. D., Truman, C. C., and Leigh, D. S. (2004). Parent material influence on soil distribution and genesis in a paleudult and kandiudult complex, southeastern USA. *Catena* 57, 157–174. doi: 10.1016/j.catena.2003.10.016

Shi, R. Y., Hong, Z. N., Li, J. Y., Jiang, J., Baquy, M. A., Xu, R. K., et al. (2017). Mechanisms for increasing the ph buffering capacity of an acidic ultisol by crop residue-derived biochars. *J. Agric. Food Chem.* 65, 8111–8119. doi: 10.1021/acs.jafc.7b02266

Shi, R. Y., Li, J. Y., Jiang, J., Kamran, M. A., Xu, R. K., and Qian, W. (2018). Incorporation of corn straw biochar inhibited the re-acidification of four acidic soils derived from different parent materials. *Environ. Sci. Pollut. Res.* doi: 10.1007/s11356-018-1289-7

Skjemstad, J. O., Reicosky, D. C., Wilts, A. R., and McGowan, J. A. (2002). Charcoal carbon in, U.S. agricultural soils. *Soil Sci. Soc. Am. J.* 66, 1249–1255. doi: 10.2136/sssaj2002.1249

Skjernstad, J. O., Taylor, J. A., and Smernik, R. J. (1999). Estimation of charcoal (Char) in soils. *Commun. Soil Sci. Plant Anal.* 30, 2283–2298. doi: 10.1080/00103629909370372

Soil Survey Staff (2018). *Natural Resources Conservation Service, United States Department of Agriculture. Web Soil Survey.* Available online at: https://Websoilsurvey.Sc.Egov.Usda.Gov/ (Accessed April 14, 2018).

Sorrenti, G., Masiello, C. A., Dugan, B., and Toselli, M. (2016). Biochar physico-chemical properties as affected by environmental exposure. *Sci. Tot. Environ.* 563–564, 237–246. doi: 10.1016/j.scitotenv.2016.03.245

Spokas, K. A., Novak, J. M., and Venterea, R. T. (2012). Biochar's role as an alternative n-fertilizer: ammonia capture. *Plant Soil,* 350, 35–42. doi: 10.1007/s11104-011-0930-8

Steinbeiss, S., Gleixner, G., and Antonietti, M. (2009). Effect of biochar amendment on soil carbon balance and soil microbial activity. *Soil Biol. Biochem.* 41, 1301–1310. doi: 10.1016/j.soilbio.2009.03.016

Steiner, C., Glaser, B., Geraldes Teixeira, W., Lehmann, J., Blum, W. E. H., and Zech, W. (2008). Nitrogen retention and plant uptake on a highly weathered central amazonian ferralsol amended with compost and charcoal. *J. Plant Nutrit. Soil Sci.* 171, 893–899. doi: 10.1002/jpln.200625199

Sung, S.-J. S., White, L. M., Marx, D. H., and Otrosina, W. J. (1995). Seasonal ectomycorrhizal fungal biomass development on loblolly pine (*Pinus Taeda*, L.) seedlings. *Mycorrhiza* 5, 439–447.

Wallander, H., Mörth, C.-M., and Giesler, R. (2009). Increasing abundance of soil fungi is a driver for 15n enrichment in soil profiles along a chronosequence undergoing isostatic rebound in northern sweden. *Oecologia* 160, 87–96. doi: 10.1007/s00442-008-1270-0

Wang, G., Jia, Y., and Li, W. (2015). Effects of environmental and biotic factors on carbon isotopic fractionation during decomposition of soil organic matter. *Sci. Rep.* 5:11043. doi: 10.1038/srep11043

Wang, J., Xiong, Z., and Kuzyakov, Y. (2016). biochar stability in soil: meta-analysis of decomposition and priming effects. *GCB Bioenergy* 8, 512–523. doi: 10.1111/gcbb.12266

Wang, T., Arbestain, M. C., Hedley, M., Singh, B. P., Calvelo-Pereira, R., and Wang, C. (2014). Determination of Carbonate-C in biochars. *Soil Res.* 52, 495–504. doi: 10.1071/SR13177

Yao, F. X., Arbestain, M. C., Virgel, S., Blanco, F., Arostegui, J., Maciá-Agull,ó, J. A., et al. (2010). Simulated geochemical weathering of a mineral Ash-Rich biochar in a modified soxhlet reactor. *Chemosphere* 80, 724–732. doi: 10.1016/j.chemosphere.2010.05.026

Zimmerman, A. R. (2010). Abiotic and microbial oxidation of laboratory-produced black carbon (Biochar). *Environ. Sci. Technol.* 44, 1295–1301. doi: 10.1021/es903140c

**Conflict of Interest Statement:** The authors declare that the research was conducted in the absence of any commercial or financial relationships that could be construed as a potential conflict of interest.

frontiers in Earth Science

ORIGINAL RESEARCH
published: 10 October 2018
doi: 10.3389/feart.2018.00127

# Fire as a Removal Mechanism of Pyrogenic Carbon From the Environment: Effects of Fire and Pyrogenic Carbon Characteristics

*Stefan H. Doerr*[1]*, *Cristina Santín*[1,2], *Agustín Merino*[3], *Claire M. Belcher*[4] and *Greg Baxter*[5]

[1] Department of Geography, College of Science, Swansea University, Swansea, United Kingdom, [2] Department of Biosciences, College of Science, Swansea University, Swansea, United Kingdom, [3] Department of Soil Science and Agricultural Chemistry, University of Santiago de Compostela, Lugo, Spain, [4] Wildfire Lab, Hatherly Laboratories, University of Exeter, Exeter, United Kingdom, [5] Wildfire Operations Research, FPInnovations, Hinton, AB, Canada

Pyrogenic carbon (PyC, charcoal) is produced during vegetation fires at a rate of ~116–385 Tg C $yr^{-1}$ globally. It represents one of the most degradation-resistant organic carbon pools, but its long-term fate and the processes leading to its degradation remain subject of debate. A frequently highlighted potential loss mechanism of PyC is its consumption in subsequent fires. However, only three studies to date have tested this hypothesis with reported losses of <8–37%, with the effects of PyC chemical characteristics and fire conditions on PyC loss in wildfires remaining unexplored. To address this, we placed materials with different degrees of thermal and chemical recalcitrance (A: wildfire charcoal, B: slash-pile charcoal, C: pine wood and D: cedar wood) on the ground surface just prior to a high-intensity and a low-intensity boreal forest wildfire. Mass losses were highly variable and dependent on fire- and sample characteristics. Mass losses across both fires (as % of dry weight) were for A: 66.5 ± 25.2, B: 41.7 ± 27.2, C: 78.2 ± 14.9, and D: 83.8 ± 18.9. Mass loss correlated significantly with maximum temperature ($T_{max}$) recorded on sample surfaces ($r = 0.65$, $p = 0.01$), but only weakly ($r = 0.33$) with time >300°C. Mass losses also showed a significant negative correlation ($r = -0.38$, $p = 0.05$) with thermal recalcitrance (T50) determined using Differential Scanning Calorimetry (DSC) and $T_{max}$ with charcoal reflectance (Ro) determined after the fires ($r = 0.46$, $p = 0.05$). Losses in the high-intensity fire were significantly higher ($p = 0.05$) than in the low-intensity fire, but the latter had a higher rate of conversion of fuel to PyC. Our results demonstrate that exposure to fire can indeed be a significant removal mechanism for PyC that remains exposed on the ground after a previous fire. The losses found, however, are likely to represent an extreme upper range as most PyC produced in a fire would not remain exposed on the ground surface by the time the next fire occurs. Our data also demonstrate, for real wildfire conditions, the (i) contrasting resistance of different PyC types to combustion and (ii) contrasting net PyC losses between different fire intensities. The DSC and reflectance (Ro) results support the usefulness of these analyses in reflecting thermal degradation resistance and temperature exposure under actual wildfire conditions.

**Keywords: black carbon, boreal forest, carbon balance, charcoal, charcoal reflectance, wildfire, management burn, thermal analysis**

OPEN ACCESS

***Edited by:***
*Satish Myneni,*
*Princeton University, United States*

***Reviewed by:***
*Ronny Lauerwald,*
*Free University of Brussels, Belgium*
*Dimitris Poursanidis,*
*Foundation for Research and Technology Hellas, Greece*

***Correspondence:**
*Stefan H. Doerr*
*s.doerr@swan.ac.uk*

***Specialty section:***
*This article was submitted to Biogeoscience, a section of the journal Frontiers in Earth Science*

***Received:*** *15 December 2017*
***Accepted:*** *10 August 2018*
***Published:*** *10 October 2018*

***Citation:***
*Doerr SH, Santín C, Merino A, Belcher CM and Baxter G (2018) Fire as a Removal Mechanism of Pyrogenic Carbon From the Environment: Effects of Fire and Pyrogenic Carbon Characteristics. Front. Earth Sci. 6:127. doi: 10.3389/feart.2018.00127*

## INTRODUCTION

Pyrogenic carbon (PyC, also known as charcoal, pyrogenic organic matter or black carbon) is a ubiquitous organic residue resulting from the incomplete combustion of organic fuels during vegetation fires (both natural and anthropogenic fires). It comprises a continuum of pyrogenic organic compounds ranging from partly charred material to soot (Santín et al., 2016a). Its chemical properties result in some of the PyC materials being highly resistant to biological breakdown, making PyC one of Earth's most degradation-resistant organic carbon pools. Estimates of its mean residence time range from decades or centuries (e.g., Steinbeiss et al., 2009; Bird et al., 2015) to millennia (e.g., Thevenon et al., 2010; de Lafontaine et al., 2011), and, importantly, consistently one or two orders of magnitude longer than those of their unburnt precursors (Bruun and EL-Zehery, 2012; Santos et al., 2012; Naisse et al., 2014). The most recent estimates of PyC global production range from between 63 and 140 Tg C $yr^{-1}$ (Bird et al., 2015) and 116–385 Tg C $yr^{-1}$ (Santín et al., 2016a), which is equivalent to ∼0.1–0.6% of the annual terrestrial net primary productivity (Huston and Wolverton, 2009).

Production of PyC and its subsequent fate, therefore, have important implications for the global carbon cycle (Landry and Matthews, 2017). However, its long-term fate in the environment and the specific biotic and abiotic processes leading to its degradation remain the subject of much debate (Bird et al., 2015; Santín et al., 2016a). A potentially major mechanism highlighted in the literature for the abiotic terrestrial breakdown of PyC has been its *in situ* combustion in subsequent fires (e.g., Ohlson and Tryterud, 2000; Czimczik et al., 2005; Preston and Schmidt, 2006; Czimczik and Masiello, 2007; Kane et al., 2010; Foereid et al., 2011). PyC produced in a fire and not transported off site by wind or water, or protected through its transfer to sufficient depths below litter or soil surface layers, can act as fuel and be subject to combustion in subsequent fires. This abiotic loss mechanism for PyC could be particularly important in environments with short fire-return intervals, low bioturbation and topography, which limit, respectively, its vertical movement and off-site transport.

The efficacy of this proposed loss mechanism, however, has remained largely untested and was based, until recently, on little more than speculation. Indeed, to our knowledge, this "fire loss" hypothesis has, to date, been tested empirically in only the following three studies. In a high-intensity experimental boreal forest fire, Santín et al. (2013) found median losses of charcoal pieces (2–4 cm size) placed in the forest floor layer (∼2 cm depth) to be <15%. Saiz et al. (2014) reported mean losses of <8% for charcoal pieces (0.5–1.5 cm size) placed on the soil surface in a prescribed fire in an open savannah woodland. Using coniferous fuels typical of the western US, Tinkham et al. (2016) found that repeated burning of litter beds in the laboratory reduced the PyC mass (>6 mm size) formed in the first fire, by 37% in the subsequent fire.

Given that vegetation fires as well as PyC materials vary widely in their characteristics, the current study aimed to explore the role of fire and PyC characteristics as potentially important variables in determining PyC removal rates during fires. We hypothesized that PyC with different degrees of carbonization exposed to fires of contrasting intensities would result in different PyC losses during burning. Thus, two different types of PyC (wildfire and slash-pile charcoal from jack pine wood) and, for comparison, uncharred wood (jack pine and western red cedar), were exposed to two contrasting types of wildfires: a high-intensity crown fire and a low-intensity surface fire. Temperature exposure of the samples during the fires was determined using thermocouples attached to sample surfaces, and the chemical and physical characteristics of the exposed and, where relevant, reference (unburnt) samples determined using thermogravimetric-differential scanning calorimetry, elemental- and charcoal surface reflectance analyses.

## MATERIALS AND METHODS

### Study Area and Experimental Setup

Field experiments were carried out in the Great Slave Lake region of the Canadian Northwest Territories in summer 2015. This boreal region has a dry, sub-humid continental climate with an annual precipitation of ∼300 mm, a wildfire season usually between May and September, and a fire recurrence interval in the region of 150 to 200 years. The forest is dominated by black spruce (*Picea mariana*) and jack pine (*Pinus banksiana*) with often thick organic soil layers. The topography is largely flat with an elevation between 100 and 200 m.a.s.l. (Alexander et al., 2004; Stocks et al., 2004).

Two types of PyC and two types of uncharred wood materials were used in the fire exposure experiments (**Figures 1A,B**):

(A) Wildfire charcoal generated during an experimental wildfire (June, 2012) in a mature jack pine stand in this region and collected in June 2013 (61°34'55" N; 117°11'55" W, see Santín et al. (2015), for site and fire characteristics).
(B) Charcoal from a jack pine slash-pile (a pile of slash generated in clearing/harvesting) burn in the winter of 2011/12 and collected in June 2012 at a site adjacent to where wildfire charcoal was sampled. Due to its production in a long-burning slash pile fire, this type of charcoal was speculated in previous work (Santín et al., 2013) to exhibit a higher degree of charring and therefore greater resistance to combustion when exposed to a subsequent fire than wildfire charcoal.
(C) Unburned jack pine down wood (small dead branches) collected in 2012 from an unburned area in the same study region.
(D) Unburned blocks cut from western red cedar (*Thuja plicata*) wood were included for comparison as a low-density wood used in a complementary study focusing specifically on charcoal reflectance (Belcher et al., 2018).

A–C pieces were 2–3 cm in diameter and 2–4 cm in length. D blocks were 3 × 3 × 3 cm. All were free of bark. Sets were made with one piece of each type (A+B+C+D), and the four pieces were linked together by thin wire and with a metal label added to facilitate relocation after fire (**Figure 1B**). A total of 30 sets were placed onto the forest floor <24 h prior to exposure to two types


**FIGURE 1 | (A)** A sample set placed on the forest floor prior to the high-intensity fire. The samples are connected by a thin wire to facilitate relocation. The thicker wires are thermocouples. (N.B. The pine wood sample appears dark, but was free of bark. The wildfire charcoal is not visible and was located just below the image frame.) **(B)** Examples of charred samples after the high-intensity fire. **(C)** The high intensity fire. **(D)** Sampling after the low-intensity fire where much of the standing vegetation remained unaffected. The figure is published with the consent of the depicted individual (the lead author) in **(D)**.

of boreal wildfire conditions: a high-intensity crown fire and a low-intensity surface fire (i.e., 15 sets for each fire). Individual pieces were situated at least 5 cm apart (**Figure 1A**).

K-type thermocouples ($\leq$ 1 mm diameter) were attached directly to the surface of the samples and connected to data loggers (Lascar, Easylog) buried in the adjacent soil to record the temperature at the sample surface-flame interface during the fire (at 10 s intervals). Given the limited number of loggers available, we chose to attach thermocouples to only one type of charcoal (A: wildfire charcoal) on the basis that any differences in temperature/duration data between the two types of charcoal might be expected to be less than between the charcoal and the contrasting types of wood. All B, C, and D samples had thermocouples attached.

Immediately after the fires samples were identified (**Figure 1B**), thermocouples and loggers removed and samples placed in sealed containers for subsequent laboratory analysis.

## Wildfire Burn Experiments

(1) The high-intensity crown fire was an experimental fire conducted on 15/6/2015 as part of the Canadian Boreal Community FireSmart Project at Ft. Providence, (61°34'55" N; 117°10'13" W) and aimed at simulating wildfire conditions. The experimental plot (~2,000 $m^2$) was a mature stand of black spruce and jack pine, originating from a stand-replacing wildfire in 1931, with a tree density (live and dead, >1.5 m high) of approximately 5,500 stems $ha^{-1}$ and an average canopy tree height of 11 m (a typical mature stand height in this boreal region). The understorey was very sparse, the forest floor composed of litter, mosses and lichens, with some down wood present. Fifteen sets of A-D samples (**Figures 1A,B**) were placed randomly at least 1 m apart from each other within an area of 15 × 15 m. The fire was fast moving with a total burn time of <5 mins and flame lengths >5 m above canopy height (**Figure 1C**). The overall fireline intensity was estimated as ~8,000 kW $m^{-1}$, which is within the typical range of high-intensity boreal crown fires in Canada (de Groot et al., 2009). The fire resulted in the homogenous and complete consumption of the canopy, thin branches and the understory, with no unburnt or low severity patches remaining within the plot.

(2) The low-intensity fire was situated ~170 km east of the high-intensity fire site (60°49′38″ N; 114°24′28″ W). It was a slow-moving, surface wildfire (Fire 28, Hay River) affecting a mixed black spruce and jack pine stand of comparable stand characteristics to the high-intensity fire, but with a peaty soil layer of up 50 cm depth. This lightning-caused wildfire burnt across the site on 29/6/2017 during calm atmospheric conditions, advancing at <5 m $h^{-1}$. This allowed sufficient time to place samples and thermocouples with loggers ahead of one of the flanks of the fire. Fifteen sets of A-D samples were placed 2 m apart along a transect parallel to the fire front. This surface fire led to the patchy smoldering combustion of the forest floor to a depth of up to 30 cm (**Figure 1D**), charring of trees to ~1 m height and the

"torching" of a few individual trees, with some areas remaining unburned. The fireline intensity was estimated to not exceed 500 kW $m^{-1}$ based on flame-length/intensity relationships for jack pine forest (Cruz and Alexander, 2010). Due to the patchy nature of this burn, not all samples were exposed to fire and, but in some cases, deep burning of the organic soil layer also led to the destruction of loggers and loss of data.
Further details about the fires are given in **Table 1**.

## Laboratory Analyses

The air-dry weight of all samples ($N = 120$) was determined before and after exposure to fire, and mass loss calculated as:

$$Mass\ loss\ (\%) = 100^{*}(1 - \frac{\text{postfire weight}}{\text{prefire weight}})$$

Of the total 120 samples, 90 had thermocouples attached, and of those, 19 loggers were lost or did not record properly during the fires. A subset of 40 samples (5 of each type A-D for each fire) spanning a representative range of mass losses and temperature/duration records, and pre-fire reference samples ($n = 1$–5 for each type A–D) were selected for further analyses to allow the potential relationships between mass loss, sample characteristics, and temperature exposure during the fires to be examined.

### Differential Scanning Calorimetry (DSC)

These analyses were carried out using a Mettler Toledo instrument to determine the thermolability (Merino et al., 2014) of the different samples before and after the exposure to the fires. Approximately 4 mg of ground sample was placed in aluminum pans under a flow of dry air (under $O_2$ flux; flow rate, 50 mL $s^{-1}$) at a scanning rate of 10°C $min^{-1}$. The temperature ranged between 50 and 600°C. Samples of indium (mp: 156.6°C) were used to calibrate the calorimeter. Samples were analyzed in duplicate. The heat of combustion (Q) was determined by integrating the DSC thermographs with respect to time over the exothermic region (150<T<600°C). The region T< 150°C was not considered as it is dominated by endothermic reactions associated with water loss. The areas under the thermographs were divided into three temperature regions representing different levels of resistance of the organic material to thermal oxidation (Merino et al., 2014, 2015): between 150 and 375°C (Q1), between 375 and 475°C (Q2) and between 475 and 600°C (Q3). The temperature at which 50% of the total energy is released under the given conditions ($T_{50}$) was also determined (Rovira et al., 2008).

### Elemental Composition

Total carbon (C), nitrogen (N) and hydrogen (H) contents (%) were determined using a LECO elemental analyzer. Values reported were corrected by mineral ash content (as determined by DSC): e.g., C ash-corrected = (C*100)/Total OM loss.

The percentage of the C remaining in samples after fire ($\%C_{rem}$) compared to their initial C content was also calculated as follows using the ash-corrected C% values:

$$\%\text{Crem} = 100 * \frac{\text{postfire C concentration } (\text{g/g}) * \text{postfire mass (g)}}{\text{prefire C concentration } (\text{g/g}) * \text{prefire mass(g)}}$$

For the cedar and pine wood pieces (C & D sample types) that were fully charred following fire, this figure is equivalent to the conversion rate of fire-affected C to PyC (%PyC). This rate quantifies the fraction of fire-affected C that is retained as PyC in charred material rather than emitted to the atmosphere (Santín et al., 2015).

**TABLE 1 |** Experimental conditions and resulting PyC losses in previous- and the current studies (n.d., no data; T, ambient air temperature, and RH, relative humidity immediately prior to ignition).

| Study | Environment | PyC source and size of pieces | Surface fuel load (kg $m^{-2}$) | PyC size range and location | Atmospheric conditions (T, RH, wind speed) & fire intensity | Mean PYC losses (% mass) |
|---|---|---|---|---|---|---|
| Saiz et al., 2014 | Savanna | *Acacia aneura,* ~700°C slash burn charcoal | 0.8–1.0 | ~0.5–1.5 cm soil surface | 26–36°C; 17–45%; ~5 m $s^{-1;}$ n.d. | <8 |
| Santín et al., 2013 | Boreal forest | *Pinus banksiana,* slash-pile charcoal | 9.4 | 2–4 cm inside litter | 28°C; 22%; 3 m $s^{-1}$, ~8,000 kW $m^{-1}$ | 23 (median <15) |
| Tinkham et al., 2016 | Laboratory | *Pseudotsuga menziesii, Pinus monticola, P. contorta* wood chips, experimental lab burn* | 2.1 | < 6 mm−7 cm inside litter | 17°C; 36%; <1 m $s^{-1}$; n.d. | 36* |
| This study (high-intensity fire) | Boreal forest | *Pinus banksiana,* slash-pile charcoal) | >7 | 1–3 cm litter surface | 28°C; ~32%; ~2.5 m $s^{-1}$, 6,000–8,000 kW $m^{-1}$ | 64 |
| | | *Pinus banksiana,* wildfire charcoal | | | | 84 |
| This study (low-intensity fire) | Boreal forest | *Pinus banksiana,* slash-pile | >10 | 1–3 cm litter surface | ~28°C; ~25%; <1 m $s^{-1}$, <500 kW $m^{-1}$ | 17 |
| | | *Pinus banksiana,* wildfire charcoal | | | | 50 |

**PyC was quantified only in the fraction >6 mm using a method which only considers part of the PyC spectrum.*

### Charcoal Reflectance

Charcoals have been observed to have varying abilities to reflect light when studied under oil using a reflectance microscope, which has been shown to evolve throughout pyrolysis (e.g., Belcher and Hudspith, 2016). Therefore, we anticipated that charcoal reflectance might vary between the types of fires that created or modified the PyC examined in this study. In order to assess this, the PyC samples were sliced into sections using a band saw and embedded in polyester resin, then ground and polished using a Buehler MetaServ 250 grinder–polisher (Buehler, Neckar, Germany). The samples were placed in the resin such that the top surface exposed to the fire was the polished face following the method described in Belcher and Hudspith (2016). The polished samples were analyzed under oil (RI 1.514) at 238°C, using a Zeiss Axio-Scope A1 optical microscope, with a TIDAS-MSP 200 microspectrometer (SMCS Ltd, Baldock, UK). Thirty manual photometric reflectance measurements were taken at cell-wall junctions across the polished surface of all 35 sufficiently sized post-fire samples and the mean charcoal reflectance (Ro%) calculated for each sample.

## Statistical Analysis

Statistical analyses were performed with the software IBM SPSS Statistics 20. The level of significance used for all tests was 5% (i.e., $\alpha = 0.05$). Pearson product-moment correlation coefficients (r) were calculated to test linear correlations between pairs of variables. Variables examined were: mass loss (%), TG-DSC parameters (T50, Q1, Q3), C, N, H contents (%), initial C remaining (%Ci), and Ro (%), as well as maximum temperature recorded on samples (Tmax), time >300°C (s), integral of duration >300°C (°Cs). The threshold of 300°C was chosen because is widely considered the temperature above which charring begins in woody fuels (Drysdale, 2011), the main chemical transformations of biomass-derived materials during heating start around 200–300°C (Keiluweit et al., 2010), and it having been used in previous studies focusing on PyC (e.g., Santín et al., 2016b, 2017).

To analyze the differences in mass loss (%) between sample types, one-factor ANOVA was performed using sample type as the independent factor. Before the ANOVAs, the equality of variances for the studied groups was tested by the Levene's homoscedasticity test and the *post-hoc* Duncan's multiple range test (groups had equal variances) were performed to identify classes with significantly different means.

# RESULTS

## Sample Properties Before the Fires

The two unburned wood samples used in this study (types C and D) showed the lowest % C, the highest contents of thermolabile biomass and the lowest thermal recalcitrance (Q1 >33%; T50 <420°C), with the cedar wood (D) being more thermolabile than the pine wood (**Table 2**, **Figure 2**). In comparison, both charcoal types (A and B) showed much higher C content and thermal recalcitrance, and lower thermolability (Q1 <21%; T50 >447°C). As expected, the slash-pine charcoal (B) presented, by far, the highest C% and thermal recalcitrance of all the samples before fire (**Table 2**).

**TABLE 2 |** Arithmetic mean values and standard deviation (italicized) of elemental composition and outcomes of thermal analysis (Differential Scanning Calorimetry; DSC) before and after fire, and of mass loss and reflectance (Ro) after fire, of the four different sample types of samples for the high-intensity (H) and low-intensity (L) fires.

| | Pre-fire | | | | | | | Post-fire | | | | | | | |
|---|---|---|---|---|---|---|---|---|---|---|---|---|---|---|---|
| | C (%) | N (%) | H (%) | T50 (°C) | Q1 (%) | Q3 (%) | | C (%) | N (%) | H (%) | T50 (°C) | Q1 (%) | Q3 (%) | Ro (%) | Mass loss (%) |
| Wildfire charcoal | 72.5 | 0.23 | 2.9 | 447 | 20.5 | 43.8 | H | 80.2 | 0.26 | 2.31 | 486 | 9.5 | 50.6 | 1.73 | 77.9 |
| | *0.9* | *0.03* | *0.2* | *4.1* | *0.1* | *3.6* | | *4.3* | *0.03* | *1.04* | *14.5* | *1.0* | *12.3* | *0.74* | *14.1* |
| | | | | | | | L | 78.8 | 0.43 | 2.43 | 468 | 14.1 | 43.9 | 0.92 | 53.7 |
| | | | | | | | | *6.4* | *0.30* | *0.51* | *19.0* | *6.6* | *14.0* | *0.36* | *31.0* |
| Slash-pile charcoal | 80.2 | 0.16 | 2.6 | 510 | 6.4 | 71.4 | H | 86.8 | 0.11 | 1.29 | 523 | 6.9 | 76.4 | 2.80 | 52.9 |
| | *n.a* | *n.a* | *n.a* | *n.a* | *n.a* | *n.a* | | *2.0* | *0.17* | *0.24* | *22.5* | *1.8* | *9.1* | *0.54* | *19.4* |
| | | | | | | | L | 85.8 | 0.17 | 1.36 | 519 | 5.9 | 76.3 | 2.37 | 24.8 |
| | | | | | | | | *2.2* | *0.14* | *0.24* | *14.7* | *1.4* | *5.8* | *0.98* | *22.7* |
| Pine wood | 46.1 | 0.07 | 5.4 | 417 | 33.8 | 25.8 | H | 76.3 | 0.29 | 2.74 | 470 | 13.8 | 46.9 | 1.47 | 89.0 |
| | *n.a* | *n.a* | *n.a* | *n.a* | *n.a* | *n.a* | | *2.2* | *0.03* | *0.36* | *7.1* | *2.5* | *4.8* | *0.26* | *6.6* |
| | | | | | | | L | 73.2 | 0.38 | 2.83 | 459 | 18.4 | 39.6 | 0.97 | 65.9 |
| | | | | | | | | *2.3* | *0.06* | *0.41* | *10.4* | *4.2* | *6.9* | *0.27* | *9.0* |
| Cedar wood | 50.9 | 0.23 | n.d. | 395 | 40.5 | 4.6 | H | 75.6 | 0.32 | 2.65 | 458 | 19.1 | 35.2 | 1.46 | 96.2 |
| | *0.2* | *0.04* | | *1.3* | *0.5* | *1.6* | | *3.6* | *0.03* | *0.20* | *3.1* | *3.6* | *3.7* | *0.34* | *3.8* |
| | | | | | | | L | 72.9 | 0.34 | 2.75 | 453 | 21.1 | 32.5 | 1.33 | 70.4 |
| | | | | | | | | *1.2* | *0.09* | *0.28* | *10.5* | *5.2* | *7.1* | *0.16* | *19.3* |

*T50 index: loss of 50% of energy during DSC; Q1 and Q3: percentage contributions of combustion heats obtained by DSC analysis. Note that mean mass loss values given here represent a subset of samples analyzed for specific characteristics given in this table. Mean mass losses for all samples are given in* ***Table 4.***

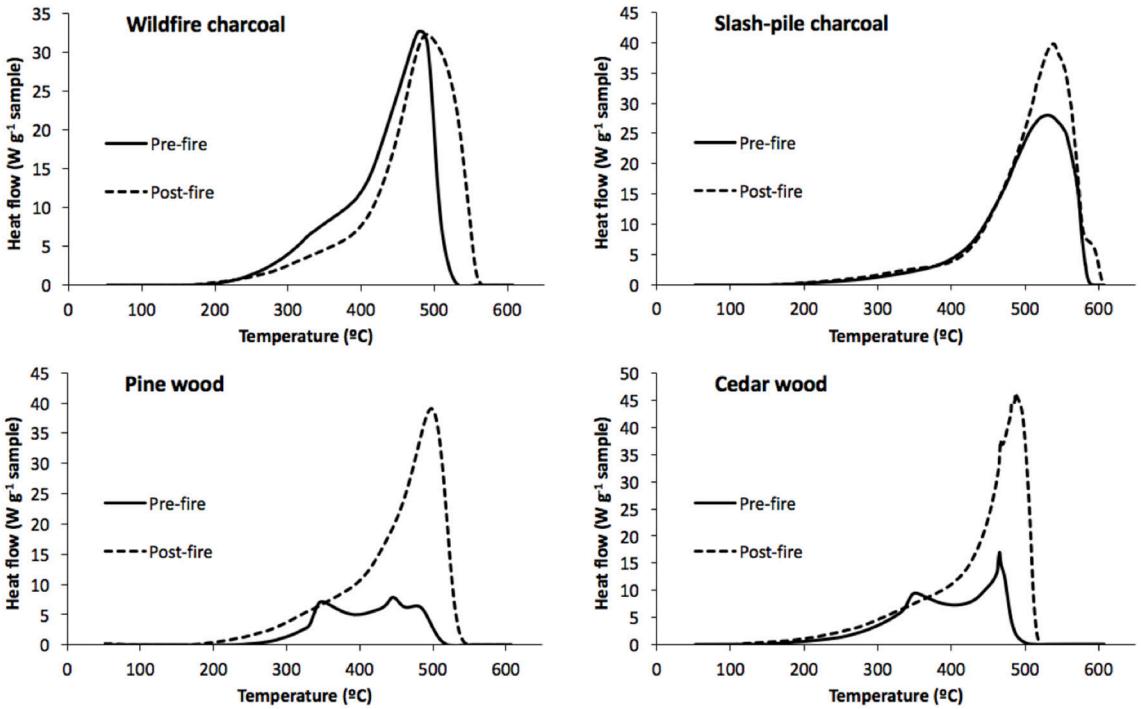


**FIGURE 2 |** Comparison of the differential scanning calorimetry curves (arithmetic mean values of 5 samples each) of the four samples types before and after the fire.

**TABLE 3 |** Pearson product-moment correlation coefficients (r) between selected chemical and reflectance characteristics of the studied samples, and key fire parameters.

| | MaxT | IntSecs > 300°C | Mass loss% | Ro% | C% | H% | T50 |
|---|---|---|---|---|---|---|---|
| MaxT | 1 | 0.228 | 0.644** | 0.462* | 0.351 | −0.486** | 0.374 |
| IntSecs>300°C | | 1 | 0.483** | 0.548** | 0.168 | −0.322 | 0.216 |
| Mass loss% | | | 1 | −0.148 | −0.418** | 0.190 | −0.379* |
| Ro% | | | | 1 | 0.768** | −0.785** | 0.722** |
| C% | | | | | 1 | −0.900** | 0.908** |
| H% | | | | | | 1 | −0.856** |
| T50 | | | | | | | 1 |

*Only the most relevant correlations are shown here. For correlations among other variables analyzed see **Table S1**. Number of samples: 28–47 (see **Table S1**)*
**Significant at the 0.05 level.*
***Significant at the 0.01 level.*

## Mass Losses and Their Correlations With Temperature/Duration Records

Considering data from both fires together ($N = 101$), wildfire charcoal (type A), exhibited a significantly higher mean mass loss (66.5 ± 25.2%) compared to slash-pile charcoal (Type B, 41.7 ± 27.2%). Pine wood (type C) showed higher mean mass losses (78.2 ± 14.9%) compared to both charcoal types A&B, and cedar wood (type D) the greatest losses (83.8 ± 18.9%). However, given the high variability in the data, the differences between mean mass losses between the groups of wildfire charcoal, pine wood and cedar wood were not significant.

For the combination of all the samples with temperature data associated ($N = 71$) and of the three fire parameters analyzed, $T_{max}$ showed the strongest positive correlation ($r = 0.64$) with mass loss (**Table 3**, **Figure 3**). Correlation between mass loss and the integral >300°C was also significant, but weaker ($r = 0.48$). No significant correlation was found between mass loss and time >300°C ($r = 0.33$) (**Supplementary Table 1**).

When comparing the two fires (**Figure 4**), the mean maximum temperature ($T_{max}$) recorded on all samples in the high-intensity fire was 855°C (range 661–1005°C; $N = 39$), whereas in the low-intensity fire it was only 434°C (range 40–792°C; $N = 32$). Indeed nearly all $T_{max}$ values recorded on samples in the high-intensity fire exceed those of low-intensity fire (**Figure 4**). The high-intensity fire also exhibited longer mean residence times (>300°C) than the low-intensity fire,

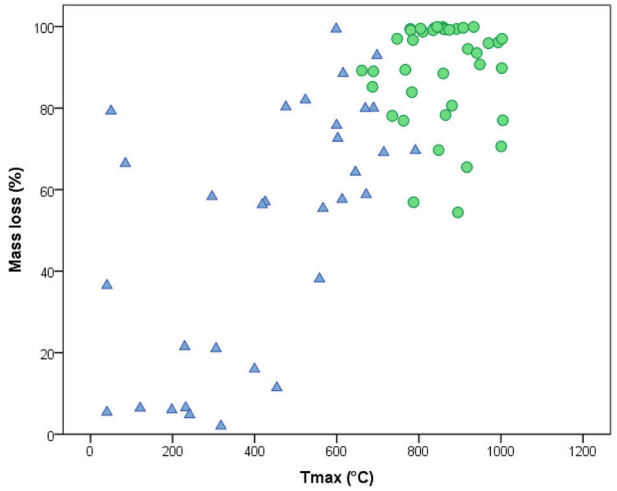


**FIGURE 3 |** Mass loss versus maximum temperature recorded for all cedar wood, pine wood and wildfire charcoal samples ($N = 71$; slash-pile charcoal samples did not have temperature data associated). Green circles, high-intensity fire; blue circles, low-intensity fire.

although these differences between fires were less pronounced (**Figure 4**). Mean sample exposure durations >300°C were 245 s (range 70–570 s) and 142 s (0–620 s) for the high- and low-intensity fire respectively, and the mean integrals >300°C were 53,656°C s (range 20,689–122,798°C s) and 18,589°C s (range 0–99,327°C s) for these respective fires. All samples exposed to the high-intensity fire, and most samples exposed to the low-intensity fire experienced mass losses, with these mean losses being significantly higher in the wood pieces (80.7 ± 16.8%; $n = 49$) than in charcoal pieces (54.7 ± 28.5%; $n = 52$) and in the high-intensity than in the low-intensity fire (80.4 ± 18.6%; $n = 47$ vs. 53.7 ± 27.4%; $n = 54$). These significant differences in losses between fire types agree with their contrasting temperature records (**Table 4**, **Figure 4**). Regarding the differences in mass losses between the two fires for the different sample types, mass losses were consistently smaller in the low-intensity than in the high-intensity fire and in both cases following the order D>C>A>B (**Figure 5**). The variability of these losses was higher in the low-intensity fire in all cases except type D, the slash-pile charcoal (**Figure 5**).

## Thermal-, Elemental-, and Reflectance Characteristics

Results of the elemental-, DSC- and reflectance analyses for each fire are given in **Table 2**, and DSC curves for each sample type in **Figure 2**. As highlighted before, the DSC analyses show that, prior to the fires, the slash-pile charcoal was the most thermally recalcitrant (i.e., least thermolabile) material used in this experiment (mean T50 = 510°C) followed by wildfire charcoal (447°C), pine wood (417°C), and cedar wood (395°C). This order is reflected also in the increasing values for Q1 and decreasing values for Q3 (**Table 2**).

After sample exposure to fire, the same order is retained, but with substantial increases in thermal recalcitrance for the wood samples following charring, and only modest increases for the charcoal samples (**Table 2**, **Figure 2**). These increases in recalcitrance were greater in the high- than the low-intensity fire, which matches the greater thermal exposure of the samples in the former (**Table 4**).

The C concentration also increased in all sample types following fire exposure, but this change was much more pronounced for the wood samples than charcoal samples (**Table 2**). Given that exposure to fire does not only lead to mass- and therefore C losses through combustion, but also to relative enrichment in C in the remaining PyC through pyrolysis, we also calculated the % of PyC remaining in relation to the total C content of the samples prior to exposure (**Table 4**). Mean values of PyC% remaining were, respectively for high- and low-intensity fires: 26.2 vs. 48.3 (wildfire charcoal), 44.8 vs. 80.8 (slash charcoal), 15.7 vs. 54.2 (pine wood) and 8.2 vs. 30.8 (cedar wood). As highlighted in the methodology, for the fully charred wood samples C&D, this parameter represents the fuel C to PyC conversion rate used in Santín et al. (2015). It is interesting to note that the low-intensity fire resulted in a higher mean PyC production ratio (54.2 and 30.8%) than the high-intensity fire (15.7 and 8.2%) for the pine and cedar wood samples respectively.

Regarding N and H concentrations, N increased and H decreased after fire for most sample types (**Table 2**). Charcoal reflectance (Ro) following the fires was highest for slash-pile charcoal with values for the other sample types being around half this value (**Table 2**). Values following the high-intensity fire overall exceed those following the low-intensity fire with respectively mean Ro values of 2.80 vs. 2.37 (slash charcoal), 1.73 vs. 0.92 (wildfire charcoal), 1.47 vs. 0.97 (pine wood), and 1.46 vs. 1.33 (cedar wood).

## Correlations Between Sample Characteristics, Charcoal Reflectance and Fire Properties

When considering all samples exposed to the fires together, significant correlations were found between some sample chemical and reflectance characteristics, and with fire properties (**Table 3**). For example, T50 showed positive correlations with C% ($r = 0.91$), Ro ($r = 0.72$) and a negative correlation with mass loss (−0.38) and with H% ($r = -0.86$). C% correlated with Ro ($r = 0.72$) and mass loss (−0.42). Maximum temperature at the fuel-flame interface ($T_{max}$) showed not only a positive correlation with mass loss ($r = 0.64$) as presented in more detail above, but also with Ro ($r = 0.46$) and H% ($r = -0.49$). The duration integral of exposure >300°C was similarly well correlated to Ro ($r = 0.55$), and weaker (but still significantly) correlated to mass loss than $T_{max}$ ($r = 0.48$). All other relationships between fire characteristics, including exposure duration >300°C, showed weaker and non-significant relationships with sample chemical and reflectance characteristics (**Table S1**).

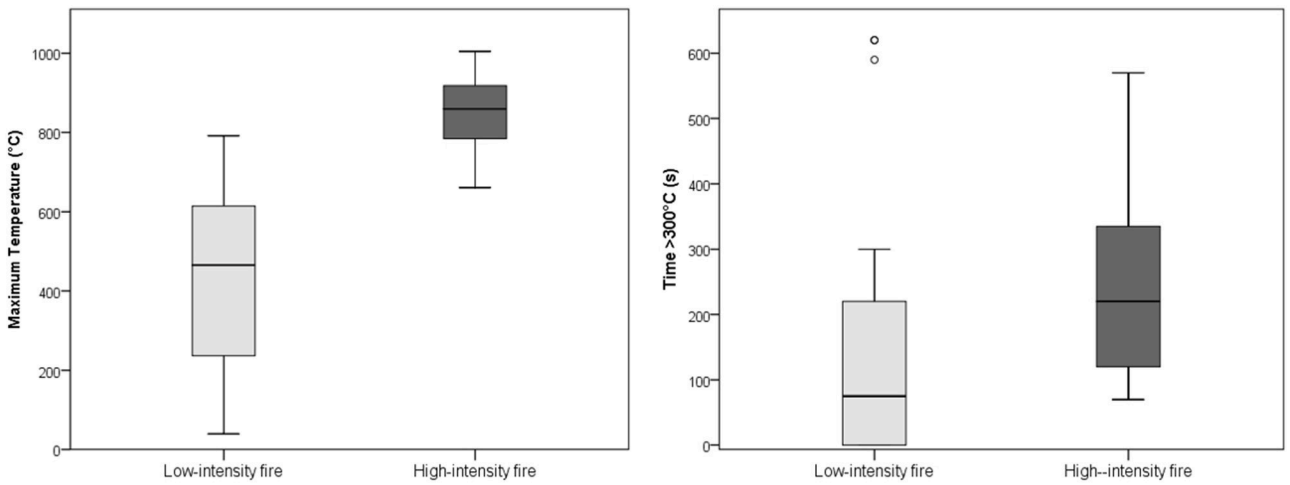


**FIGURE 4 |** Maximum temperatures (°C) (left) and residence times of T > 300°C (right) recorded at the sample-flame interface during the low- and high-intensity fires for all sample types combined ($N = 71$). Circles indicate outliers.

**TABLE 4 |** Mean values (*and range*) of temperature characteristics, mass losses and % PyC remaining, separated by sample and fire types.

| | Tmax (°C) | Time >300°C (s) | Integral >300°C (°Cs) | Mass loss (%) | *PyC remaining (%)* |
|---|---|---|---|---|---|
| **HIGH-INTENSITY FIRE** | | | | | |
| Wildfire charcoal ($n = 12$; *6*) | 882 | 283 | 61197 | 82 | 26.2 |
| | *(735–1005)* | *(70–410)* | *(20689–101113)* | *(54–100)* | *(6.0–53.6)* |
| Slash-pile charcoal ($n = 15$; *5*) | n.d. | n.d. | n.d. | 63 | 44.8 |
| | | | | *(33–100)* | *(19.4–73.7)* |
| Pine wood ($n = 13$; *5*) | 833 | 249 | 53,132 | 86 | 15.7 |
| | *(661–1003)* | *(80–570)* | *(21406–122798)* | *(57–100)* | *(5.1–31.7)* |
| Cedar wood ($n = 14$; *3*) | 851 | 208 | 47681 | 98 | 8.2 |
| | *(747–1002)* | *(90–460)* | *(22932–97238)* | *(90–100)* | *(4.7–14.2)* |
| **LOW-INTENSITY FIRE** | | | | | |
| Wildfire charcoal ($n = 10$; *5*) | 390 | 16 | 13685 | 56 | 48.3 |
| | *(50–603)* | *(0–590)* | *(0–43290)* | *(2–82)* | *(17.2–97.1)* |
| Slash-pile charcoal ($n = 15$; *5*) | n.d. | n.d. | n.d. | 17 | 80.8 |
| | | | | *(12–64)* | *(39.5–100)* |
| Pine wood ($n = 11$; *5*) | 432 | 90 | 14286 | 41 | 54.2 |
| | *(85–715)* | *(0–300)* | *(0–51011)* | *(5–80)* | *(31.5–65.8)* |
| Cedar wood ($n = 11$; *4*) | 475 | 172 | 27349 | 55 | 30.8 |
| | *(40–792)* | *(0–620)* | *(0–99327)* | *(5–99)* | *(16.3–44.1)* |

*% PyC remaining is the fraction of C remaining compared to the total C content of the samples prior to fire exposure. (The post-fire wood samples selected for chemical analysis were fully charred, therefore all the C in them is considered PyC). Sample size (n) applies to all parameters except for PyC remaining where the second italicized figure applies.*
*n.d., no data.*

# DISCUSSION

## Mass Losses Compared to Previous Studies

The only two previous studies examining PyC recombustion under field conditions reported mean mass losses of <8% for charcoal pieces of ∼0.5–1.5 cm (Saiz et al., 2014) and of 23% (median value <15%) for charcoal pieces of 2–4 cm (Santín et al., 2013). In the current study, mass losses were substantially higher except for the slash-pile charcoal exposed to the low intensity fire, which had a mean loss of 17.0% (median 11.8%) (**Table 4**). In the high-intensity fire, slash-pile charcoal showed mean losses of 63.6% (median 58.6). Wildfire charcoal exhibited losses of 84.0% (median 81.9%) and 49.7% (median 58.6%) in the high- and low-intensity fires, respectively (**Table 4**). Thus, all losses recorded here across the two types of PyC and fires (i) exceed those previously reported from *in-situ* field studies and, except for the slash-pile charcoal in the low intensity fire, (ii) exceed also the mean losses of 36% for PyC fragments >6 mm reported in the laboratory study by Tinkham et al. (2016). The data presented in

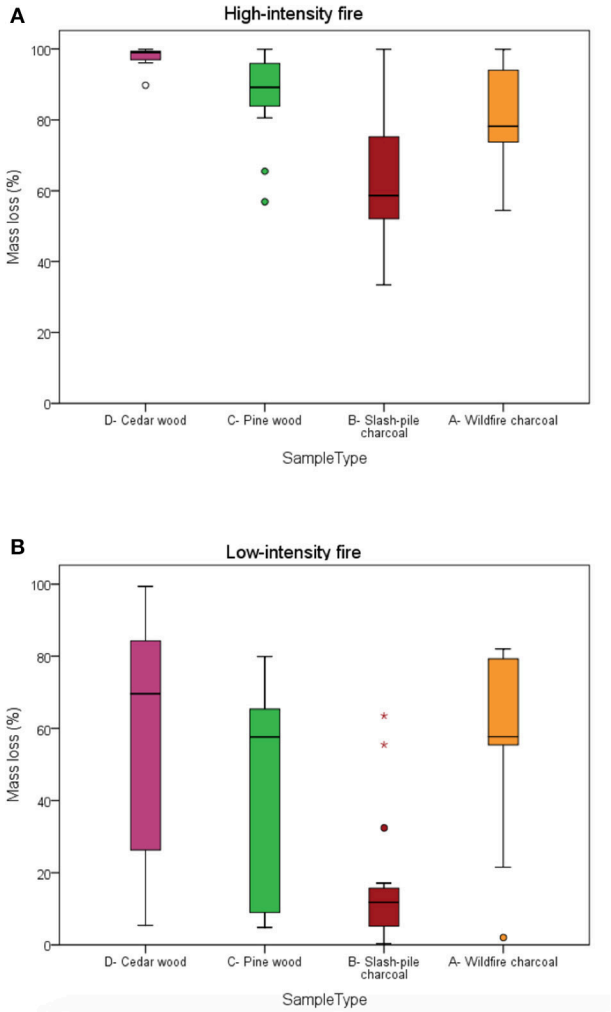


**FIGURE 5 |** Mass losses for the different type of samples for the **(A)** high - and **(B)** low-intensity fire. Circles and stars indicate outliers. Total $N = 101$.

**Table 1** allows comparison of the current study with fire and PyC characteristics in these previous studies.

The comparatively low losses in the study by Saiz et al. (2014) (<8%; **Table 1**) could be a reflection of a relatively high thermal resistance of their PyC combined with a low capacity of the fire to lead to PyC combustion. The source material, *Acacia aneura*, has roughly twice the density (1 g $cm^{-3}$) of pine wood and was produced in a slash burn, which typically have much longer flame residence times than wildfire and therefore lead to a greater thermal degradation resistance of the charcoal produced than in a wildfire (Massman et al., 2008). The fire, although considered intense in the context of savanna fires, had the lowest fuel load and highest wind speed of all experimental fires listed in **Table 1** and hence is likely to have led to a burn of comparatively low intensity and flame residence time.

The experimental crown fire examined by Santín et al. (2013) was carried out in the same fuel complex and study region as the current study and used the same source of slash-pile charcoal. Fuel load, atmospheric conditions and fireline intensity (∼8,000 kW $m^{-2}$) were also broadly comparable to the high intensity fire of current study (**Table 1**). The main difference between these two studies is that, in the current study, PyC pieces were placed on the forest floor surface, whereas in Santín et al. (2013) they were placed at ∼2 cm depth in the forest floor layer. In the 2013 study, this could have resulted in the initial protection from thermal exposure of the charcoal pieces until the litter layer itself was consumed to this depth. This may have contributed to the substantially lower combustion of the slash-charcoal of 23% reported by Santín et al. (2013) compared to the 64% in the high-intensity fire of the current study (**Table 1**).

The mass losses of both slash-pile charcoal in the high-intensity fire and of wildfire charcoal in both fires of the current study are substantially greater than the 36% found in the laboratory burns of Tinkham et al. (2016) (**Table 1**). Their experiment, however, is not directly comparable to the current study not only due to it being carried out under laboratory conditions using masticated fuels. They also considered only PyC pieces >6 mm and within those, only the fraction that is resistant to chemical degradation based on the CTO375 method (Hatten and Zabowski, 2009). In addition, the sample placement on the litter surface, the substantially higher fuel loads and warmer and drier atmospheric conditions in the current study are all more conducive to a greater combustion completeness than those in the laboratory burn by Tinkham et al. (2016).

## Mass Losses and Their Correlations With Temperature/Duration Records

Our research design allowed us to link PyC losses directly to temperature recorded on the fuel-flame interface of the respective PyC pieces. That mass losses show a reasonably strong correlation with $T_{max}$ ($r = 0.65$; **Table 3**) is perhaps not surprising. The thermocouple tip (≤ 1 mm diameter) reflects the temperature at the fuel-flame interface, which is influenced by the energy received from the surrounding combustion combined with that released from the burning PyC piece itself. $T_{max}$ could therefore be expected to be at least somewhat related to the mass loss of a PyC piece, with higher temperatures reflecting greater losses. What may be surprising is that mass losses are only weakly correlated with exposure duration >300°C ($r = 0.33$, not significant; **Table S1**). Three Hundred degree is widely considered the threshold above which charring begins in woody fuels (Drysdale, 2011) and hence the duration above this threshold could be expected to correlate more closely with mass loss than $T_{max}$. Given that the correlation between mass loss and the integral >300°C was stronger ($r = 0.48$) than for time >300°C (and significant), suggests that the faster rate of combustion associated with the process that generates higher temperature readings in thermocouples is more important in the overall mass loss process observed here than the total time during which mass loss occurs. This notion is supported by a study examining organic matter in a soil block affected by experimental laboratory burns, where the time >300°C also showed no correlation with C loss (Merino et al., 2018).

The fact that the samples exposed to the high-intensity fire recorded substantially higher mean values for $T_{max}$, the time integral (s) >300°C and exposure duration >300°C than the lower intensity fire (**Table 4**) provide not only an additional set of measures confirming the contrasting intensities of these fires. It also suggests that once combustion of individual PyC pieces begins, the greater rate of thermal energy release during the more intense fire facilitates a greater rate of loss of individual PyC pieces. This, together with the fact that exposure duration >300°C showed only a weak (and not significant) correlation with mass loss (**Table S1**), suggest that the energy released from the combustion of the surrounding fuel may be a more important factor in PyC mass loss than that released from the combustion of a PyC piece itself.

## Mass Losses, PyC Characteristics and Thermal Recalcitrance

Our data also allows PyC losses in a fire to be evaluated in relation to the specific PyC characteristics. The importance of considering PyC type when evaluating potential losses in fires is clearly highlighted by our finding that slash-pile charcoal, which exhibits higher thermal degradation resistance according to the DSC analysis (**Table 2**), indeed exhibited a significantly lower mass loss under actual wildfire conditions (41.7 ± 27.2%; mean of both fires combined) compared to wildfire charcoal (66.5 ± 25.2%). This supports the speculation made by Santín et al. (2013), that the slash-pile charcoal placed in their fire could be expected to be more thermally resistant and may therefore have given lower rates of losses than if wildfire charcoal had been used. Prior to the new fire exposure, the slash-pile charcoal was more thermally recalcitrant (mean T50 = 510°C) than wildfire charcoal (447°C; **Table 2**) due to its origin in a pile burn, which generates prolonged burning conditions with restricted oxygen supply compared to typical wildfires (Santín and Doerr, 2016). This difference in thermal resistance is also reflected in the higher C content and lower values of Q1, and higher values of Q3 for the slash-pile compared to the wildfire charcoal (**Table 2**). Following fire exposure, both charcoal types exhibit an additional, albeit small, increase in mean values of T50, C%, and Q3 (**Table 2**, **Figure 2**). This suggests that the exposure of this charcoal to a new fire has led to its further increased thermal recalcitrance, particularly in the high-intensity fire, which can be expected to lower the susceptibility to combustion of this remaining PyC in a subsequent fire. Unsurprisingly, the wood pieces that were exposed to the high-intensity fire showed greater mass loss than in the low-intensity fire.

It is noteworthy that the low-intensity fire led to a higher PyC production rate than the high-intensity fire (as reflected by percentage PyC remaining for the wood samples; **Table 4**). This could suggest that more intense fires produce less PyC in relation to fuel consumed and hence emit a greater proportion of C to the atmosphere than is converted to PyC and remains *in situ* for a given amount of fuel affected by burning (Santín et al., 2015).

The significant correlations between chemical characteristics of samples, and their relationship with fire properties (**Table 3**), are also noteworthy. For example, they provide valuable evidence from real wildfires that some chemical parameters, which are often utilized to indicate thermal and chemical recalcitrance (C%, T50, Q3) are well correlated (**Table 3**) and indeed provide useful indicators of the resistance of PyC materials to combustion in field-scale fire conditions.

Furthermore, our data support the notion that charcoal reflectance (Ro) can be related to post-fire chemical recalcitrance parameters such as resistance to dichromate etch and the size of polyaromatic units remaining used in other studies (Ascough et al., 2010, 2011). The significant correlations relationships of Ro% with T50 ($r = 0.72$) and C% (0.77; **Table 3**), as well as with other DSC parameters (**Table S1**), suggest that Ro may be a useful indicator of charcoal resistance to thermal degradation. This is important because it implies that PyC exhibiting higher Ro% will not only be more chemically inert in the post-fire environment (e.g., Ascough et al., 2010; Belcher et al., 2018), but also that such PyC will be more resistant to thermal degradation in subsequent fires. The potential of this additional metric for exploring charcoal recalcitrance, its resistance to thermal degradation in future wildfires, and more generally fire effects on C storage in wood and charcoal, is explored in more detail in Belcher et al. (2018). The results also highlight that the DSC analysis methods used here provide a relatively rapid and economic approach for the assessment of the resistance of PyC to removal from subsequent fires.

## Significance and Implications for Wildfire as a PyC Production and Removal Mechanism

The data presented here add to the still small, but growing body of evidence for the relevance of fire as a removal mechanism of any PyC exposed at the ground surface. Whilst experimental conditions and PyC analysis methods are not fully comparable across the four studies examining this process experimentally to date (**Table 1**), the current study stands out with the highest overall PyC losses from recombustion reported to date. The mean losses of 82 and 56% for wildfire charcoal in the high- and low-intensity boreal wildfires found here respectively, suggest that fire can indeed be a significant removal mechanism for any PyC that was produced in previous fires and remains exposed at the ground surface. These values, however, should be considered as a being in the extreme upper range of what might be expected under natural conditions for the following reasons. First, the PyC pieces were placed on the surface and not inside the litter layer. Under most natural situations, PyC would be subject to bioturbation and burial in the soil or within the accumulating litter, resulting in reduced exposure to thermal energy and hence combustion. This may be particularly relevant in the North American boreal region where the typical intervals between fires is relatively long, ranging from 150 to 200 years (Stocks et al., 2003; Balshi et al., 2009). Second, the pieces used here were within a size range of 1–3 cm, which represents only a fraction of the full size-range of PyC in the environment (Santín et al., 2015). For example, PyC present on the surface of larger pieces of down wood or standing timber could be expected to show lower losses due to their relatively smaller fuel surface area/volume ratio. To

further improve our understanding of the role of wildfire as a removal mechanism of PyC, we need not only more experimental data on PyC recombustion from different types of fires and environments, but critically also a better understanding of the fate and movement of PyC between fires [see review by (Abney and Behre, 2018)] in order to assess how much of the PyC produced in a given fire is likely to be exposed to combustion in a subsequent fire.

What this study has demonstrated for the first time under field conditions is (i) the contrasting resistance of different types of PyC to combustion even when produced from the same material (in this case pine wood), and (ii) the contrasting net PyC losses different types of fire can cause. The significantly greater losses found for wildfire PyC compared to slash-pile PyC found here also match what would be expected based on the chemical and reflectance characteristics of the PyC types used here (**Table 2**) and supports the usefulness of these characteristics in reflecting thermal degradation resistance under field conditions.

The results of this study also demonstrate that wildfire charcoals do present different chemical characteristics and resistance to combustion than other types of man-made PyC such as the slash-pile charcoal used here. The latter may be more comparable to the more degradation resistant charcoal produced in kilns or, to some extent, also to biochar than to wildfire charcoal, confirming the need for considering their direct comparability with caution as highlighted by Santín et al. (2017) in their study comparing wildfire charcoal and biochar. This is especially relevant in the context of the C sequestration abilities of different PyC materials (Santín et al., 2017).

Based on the results presented here, it could be argued that more intense flaming fires that lead to higher temperatures at the fuel-flame interface will produce new PyC of higher recalcitrance compared to lower-intensity (and "cooler") flaming fires. However, as also seen here, more intense flaming fires are likely to also produce less PyC in relation to fuel consumed, but (ii) potentially also consume overall more of any old PyC that may be available for combustion. If these notions prove to be widely applicable, they have implications for the accounting of PyC production and fate in local- to global-scale carbon budget modeling of fires.

In this context, it is important to consider that deep-burning smoldering fires, that would also be considered as low-intensity, would not fit this pattern as they lead to relatively complete combustion of the affected fuel (Rein, 2013), which would include any PyC present. To what degree fire intensity (or indeed fire behavior in general) and other factors such as fuel characteristics, PyC redistribution and its breakdown in the landscape between fires, influence (i) the total amount of PyC present in the landscape and (ii) its resistance to biotic and abiotic degradation, remains poorly understood today. Recent work by Hudspith et al. (2017), for example, has highlighted important differences between specific fuel types in how much charcoal they produce under comparable laboratory burn conditions. Further work representative of a range of environmental and fire behavior characteristics is clearly needed to provide a more complete understanding of the production and fate of PyC, and its role in the global carbon cycle. Developing this understanding is particularly relevant given that human-induced climate- and land cover changes are leading to large-scale changes in fuel characteristic, fire occurrence, and fire severity (Jolly et al., 2015; Abatzoglou and Williams, 2016). These shifts will affect the overall role of fire in the global carbon balance, which in turn will be affected by the balance of PyC production and its fate (Bird et al., 2015; Santín et al., 2016a).

## AUTHOR CONTRIBUTIONS

SD, CS, and CB conceived the work. SD, CS, and GB carried out the field experimentation, AM conducted the thermal and chemical-, and CB the reflectance analyses. All authors contributed substantially to the interpretation of the data and to drafting the manuscript. All authors gave final approval of the version submitted and agree to be accountable for all aspects of the work in ensuring that questions related to the accuracy or integrity of any part of the work are appropriately investigated and resolved.

## FUNDING

Fieldwork and sample analysis was supported a Leverhulme Trust grant to SD (RPG-2014-095) and a European Research Council Starter Grant ERC-2013-StG-335891-ECOFLAM to CB. During manuscript preparation, SD was supported by a Leverhulme Trust Fellowship (RF-2016-456\2) and CS by a Sêr Cymru Fellowship co-funded by European Union's Horizon 2020 research and innovation programme (Marie Skłodowska-Curie grant agreement No 663830).

## ACKNOWLEDGMENTS

Special thanks go to Westly Steed and the Department of Environment and Natural Resources, Government of the Northwest Territories, Canada for supporting the field work. Thanks also the staff of FPInnovations, Alberta Environment and Sustainable Resource Development and the residents of Fort Providence for their support during fieldwork.

## SUPPLEMENTARY MATERIAL

The Supplementary Material for this article can be found online at: https://www.frontiersin.org/articles/10.3389/feart.2018.00127/full#supplementary-material

## REFERENCES

Abatzoglou, J. T., and Williams, A. P. (2016). Impact of anthropogenic climate change on wildfire across western US forests. *Proc. Natl. Acad. Sci. U.S.A.* 113, 11770–11775. doi: 10.1073/pnas.1607171113

Abney, R. B., and Behre, A. A. (2018). Pyrogenic carbon erosion: implications for stock and persistence of pyrogenic carbon in soil. *Front. Earth Sci. Biogeosci.* 6:26. doi: 10.3389/feart.2018.00026

Alexander, M. E., Stefner, C. N., Mason, J. A., Stocks, B. J., and Hartley, G. R. (2004). *Characterizing the Jack Pine—Black Spruce Fuel Complex of the International*

*Crown Fire Modelling Experiment (ICFME)*. Sault Ste. Marie: Canadian Forest Service.

Ascough, P. L., Bird, M. I., Francis, S. M., Thornton, B., Midwood, J., Scott, A. C., et al. (2011). Variability in oxidative degradation of charcoal: influence of production conditions and environmental exposure. *Geochim. Cosmochim. Acta* 75, 2361–2378. doi: 10.1016/j.gca.2011.02.002

Ascough, P. L., Bird, M. I., Scott, A. C., Collinson, M. E., Cohen-Ofri, I., Snape, C. E., et al. (2010). Charcoal reflectance measurements: implications for structural characterization and assessment of diagenetic alteration. *J. Archaeol. Sci.* 37, 1590–1599. doi: 10.1016/j.jas.2010.01.020

Balshi, M. S., McGuire, A. D., Duffy, P., Flannigan, M., Walsh, J., and Melillo, J. (2009). Assessing the response of area burned to changing climate in western boreal North America using a multivariate adaptive regression splines (MARS) approach. *Glob. Change Biol.* 15, 578–600. doi: 10.1111/j.1365-2486.2008.01679.x

Belcher, C. M., and Hudspith, V. A. (2016). The formation of charcoal reflectance and its potential use in post-fire assessments. *Int. J. Wildl. Fire* 25, 775–779. doi: 10.1071/WF15185

Belcher, C. M., New, S. L., Santín, C., Doerr, S. H., Grosvenor, M. J., Dewhirst, R., et al. (2018). What can charcoal reflectance tell us about energy release in wildfires and charcoal properties? *Front. Earth Sci. Biogeosci.* 6:169. doi: 10.3389/feart.2018.00169

Bird, M. I., Wynn, J. G., Saiz, G., Wurster, C. M., and McBeath, A. (2015). The pyrogenic carbon cycle. *Annu. Rev. Earth Planet. Sci.* 43, 273–298. doi: 10.1146/annurev-earth-060614-105038

Bruun, S., and EL-Zehery, N. (2012). Biochar effect on the mineralization of soil organic matter. *Pesq. Agropec. Bras.* 47, 665–671. doi: 10.1590/S0100-204X2012000500005

Cruz, M. G., and Alexander, M. E. (2010). Assessing crown fire potential in coniferous forests of western North America: a critique of current approaches and recent simulation studies. *Int. J. Wildl. Fire* 19, 377–398. doi: 10.1071/WF08132

Czimczik, C. I., and Masiello, C. A. (2007). Controls on black carbon storage in soils. *Glob. Biogeochem. Cycles* 21, 1–8. doi: 10.1029/2006GB002798

Czimczik, C. I., Schmidt, M. W. I., and Schulze, E. D. (2005). Effects of increasing fire frequency on black carbon and organic matter in Podzols of Siberian Scots pine forests. *Eur. J. Soil Sci.* 56, 417–428. doi: 10.1111/j.1365-2389.2004.00665.x

de Groot, W. J., Pritchard, J. M., and Lynham, T. J. (2009). Forest floor fuel consumption and carbon emissions in Canadian boreal forest fires. *Can. J. For. Res.* 39, 367–382. doi: 10.1139/X08-192

de Lafontaine, G., Couillard, P. L., and Payette, S. (2011). Permineralization process promotes preservation of Holocene macrofossil charcoal in soils. *J. Quat. Sci.* 26, 571–575. doi: 10.1002/jqs.1529

Drysdale, D. (2011). *An Introduction to Fire Dynamics*, *3rd Edn*. Chichester, UK: Wiley.

Foereid, B., Lehmann, J., and Major, J. (2011). Modeling black carbon degradation and movement in soil. *Plant Soil* 345, 223–236. doi: 10.1007/s11104-011-0773-3

Hatten, J. A., and Zabowski, D. (2009). Changes in soil organic matter pools and carbon mineralization as influenced by fire severity. *Soil Sci. Soc. Am. J.* 73, 262–273. doi: 10.2136/sssaj2007.0304

Hudspith, V. A., Belcher, C. M., Barnes, J., Dash, C. B., Kelly, R., and Hu, F. S. (2017). Charcoal reflectance suggests heating duration and fuel moisture affected burn severity in four Alaskan tundra wildfires. *Int. J. Wildl. Fire* 26, 306–316. doi: 10.1071/WF16177

Huston, M. A., and Wolverton, S. (2009). The global distribution of net primary production: resolving the paradox. *Ecol. Monogr.* 79, 343–377. doi: 10.1890/08-0588.1

Jolly, W. M., Cochrane, M. A., Freeborn, P. H., Holden, Z. A., Brown, T. J., Williamson, G. J., et al. (2015). Climate-induced variations in global wildfire danger from 1979 to 2013. *Nat. Commun.* 6:7537. doi: 10.1038/ncomms8537

Kane, E. S., Hockaday, W. C., Turetsky, M. R., Masiello, C. A., Valentine, D. W., Finney, B. P., et al. (2010). Topographic controls on black carbon accumulation in Alaskan black spruce forest soils: implications for organic matter dynamics. *Biogeochemistry* 100, 39–56. doi: 10.1007/s10533-009-9403-z

Keiluweit, M., Nico, P. S., Johnson, M. G., and Kleber, M. (2010). Dynamic molecular structure of plant biomass-derived black carbon (biochar). *Environ. Sci. Technol.* 44, 1247–1253. doi: 10.1021/es9031419

Landry, J.-S., and Matthews, H. D. (2017). The global pyrogenic carbon cycle and its impact on the level of atmospheric CO 2 over past and future centuries. *Glob. Chang. Biol.* 23, 3205–3218. doi: 10.1111/gcb.13603

Massman, W. J., Frank, J. M., and Reisch, N. B. (2008). Long-term impacts of prescribed burns on soil thermal conductivity and soil heating at a Colorado Rocky Mountain site: a data/model fusion study. *Int. J. Wildl. Fire* 17, 131–146. doi: 10.1071/WF06118

Merino, A., Chávez-vergara, B., Salgado, J., Fonturbel, M. T., García-oliva, F., and Vega, J. A. (2015). Variability in the composition of charred litter generated by wildfire in different ecosystems. *Catena* 133, 52–63. doi: 10.1016/j.catena.2015.04.016

Merino, A., Ferreiro, A., Salgado, J., Fontúrbel, M. T., Barros, N., Fernández, C., et al. (2014). Use of thermal analysis and solid-state 13C CP-MAS NMR spectroscopy to diagnose organic matter quality in relation to burn severity in Atlantic soils. *Geoderma* 226–227, 376–386. doi: 10.1016/j.geoderma.2014.03.009

Merino, A., Fonturbel, M. T., Fernández, C., Chávez-vergara, B., Salgado, J., García-oliva, F., and Vega, J. (2018). Inferring changes in soil organic matter in soil burn severities after wildfire in temperate climates. *Sci. Total Environ.* 627, 622–632. doi: 10.1016/j.scitotenv.2018.01.189

Naisse, C., Girardin, C., Davasse, B., Chabbi, A., and Rumpel, C. (2014). Effect of biochar addition on C mineralisation and soil organic matter priming in two subsoil horizons. *J. Soil Sediments* 15, 825–832. doi: 10.1007/s11368-014-1002-5

Ohlson, M., and Tryterud, E. (2000). Interpretation of the charcoal record in forest soils: forest fires and their production and deposition of macroscopic charcoal. *Holocene* 10, 519–525. doi: 10.1191/095968300667442551

Preston, C. M., and Schmidt, M. W. I. (2006). Black (pyrogenic) carbon in boreal forests: a synthesis of current knowledge and uncertainties. *Biogeoscience* 3, 211–271. doi: 10.5194/bgd-3-211-2006

Rein, G. (2013). "Smouldering fires and natural fuels," in *Fire Phenomena in the Earth System–An Interdisciplinary Approach to Fire Science,* ed C. Belcher (London: Wiley and Sons), 15–34.

Rovira, P., Kurz-Besson, C., Coûteaux, M. M., and Ramón Vallejo, V. (2008). Changes in litter properties during decomposition: a study by differential thermogravimetry and scanning calorimetry. *Soil Biol. Biochem.* 40, 172–185. doi: 10.1016/j.soilbio.2007.07.021

Saiz, G., Goodrick, I., Wurster, C. M., Zimmermann, M., Nelson, P. N., and Bird, M. I. (2014). Charcoal re-combustion efficiency in tropical savannas. *Geoderma* 219–220, 40–45. doi: 10.1016/j.geoderma.2013.12.019

Santín, C., and Doerr, S. H. (2016). Fire effects on soils: the human dimension. *Proc. R. Soc. B Biol. Sci.* 371:20150171. doi: 10.1098/rstb.2015.0171

Santín, C., Doerr, S. H., Kane, E. S., Masiello, C. A., Ohlson, M., de la Rosa, J. M., et al. (2016a). Towards a global assessment of pyrogenic carbon from vegetation fires. *Glob. Chang. Biol.* 22, 76–91. doi: 10.1111/gcb.12985

Santín, C., Doerr, S. H., Merino, A., Bryant, R., and Loader, N. J. (2016b). Forest floor chemical transformations in a boreal forest fire and their correlations with temperature and heating duration. *Geoderma* 264, 71–80. doi: 10.1016/j.geoderma.2015.09.021

Santín, C., Doerr, S. H., Merino, A., Bucheli, T. D., Bryant, R., Ascough, P., et al. (2017). Carbon sequestration potential and physicochemical properties differ between wildfire charcoals and slow-pyrolysis biochars. *Sci. Rep.* 7:11233. doi: 10.1038/s41598-017-10455-2

Santín, C., Doerr, S. H., Preston, C., and Bryant, R. (2013). Consumption of residual pyrogenic carbon by wildfire. *Int. J. Wildl. Fire* 22, 1072–1077. doi: 10.1071/WF12190

Santín, C., Doerr, S. H., Preston, C. M., and González-Rodríguez, G. (2015). Pyrogenic organic matter production from wildfires: a missing sink in the global carbon cycle. *Glob. Change Biol.* 21, 1621–1633. doi: 10.1111/gcb.12800

Santos, F., Torn, M. S., and Bird, J. (2012). Biological degradation of pyrogenic organic matter in temperate forest soils. *Soil Biol. Biochem.* 51, 115–124. doi: 10.1016/j.soilbio.2012.04.005

Steinbeiss, S., Gleixner, G., and Antonietti, M. (2009). Effect of biochar amendment on soil carbon balance and soil microbial activity. *Soil Biol. Biochem.* 41, 1301–1310. doi: 10.1016/j.soilbio.2009.03.016

Stocks, B. J., Alexander, M. E., Wotton, B. M., Stefner, C. N., Flannigan, M. D., Taylor, S. W., et al. (2004). Crown fire behaviour in a northern jack pine - black spruce forest. *Can. J. For. Res.* 34, 1548–1560. doi: 10.1139/x04-054

Stocks, B. J., Mason, J., Todd, J. B., Bosch, E. M., Wotton, B. M., Amiro, B. D., et al. (2003). Large forest fires in Canada, 1959–1997. *J. Geophys. Res.* 108:8149. doi: 10.1029/2001JD000484

Thevenon, F., Williamson, D., Bard, E., Anselmetti, F. S., Beaufort, L., and Cachier, H. (2010). Combining charcoal and elemental black carbon analysis in sedimentary archives: implications for past fire regimes, the pyrogenic carbon cycle, and the human-climate interactions. *Glob. Planet. Change* 72, 381–389. doi: 10.1016/j.gloplacha.2010.01.014

Tinkham, W. T., Smith, A. M. S., Higuera, P. E., Hatten, J. A., Brewer, N. W., and Doerr, S. H. (2016). Replacing time with space: using laboratory fires to explore the effects of repeated burning on black carbon degradation. *Int. J. Wildl. Fire* 25, 242–248. doi: 10.1071/WF15131

**Conflict of Interest Statement:** The authors declare that the research was conducted in the absence of any commercial or financial relationships that could be construed as a potential conflict of interest.

The reviewer, RL, declared a shared affiliation, with no collaboration, with one of the authors, CB, to the handling editor at time of review.

frontiers in Earth Science

ORIGINAL RESEARCH
published: 24 April 2018
doi: 10.3389/feart.2018.00043

# Production and Composition of Pyrogenic Dissolved Organic Matter From a Logical Series of Laboratory-Generated Chars

*Kyle W. Bostick[1], Andrew R. Zimmerman[1]*, Andrew. S. Wozniak[2], Siddhartha Mitra[3] and Patrick G. Hatcher[4]*

[1] Department of Geological Sciences, University of Florida, Gainesville, FL, United States, [2] School of Marine Science and Policy, College of Earth, Ocean, and Environment, University of Delaware, Newark, DE, United States, [3] Department of Geological Sciences, East Carolina University, Greenville, NC, United States, [4] Department of Chemistry and Biochemistry, Old Dominion University, Norfolk, VA, United States

Though pyrogenic carbon (pyC) has been assumed to be predominantly stable, degradation and transfers of pyC between various pools have been found to influence its cycling and longevity in the environment. Dissolution via leaching may be the main control on loss processes such as microbial or abiotic oxidation, mineral sorption, or export to aquatic systems. Yet, little is known about the controls on pyrogenic dissolved organic matter (pyDOM) generation or composition. Here, the yield and composition of pyDOM generated through batch leaching of a thermal series of oak and grass biochars, as well as several non-pyrogenic reference materials, was compared to that of their parent solids. Over 17 daily leaching cycles, biochars made from oak at 250–650°C released decreasing amounts of C on both a weight (16.9–0.3%, respectively) and C yield basis (7.4–0.2% C, respectively). Aryl-C represented an estimated 32–82% of C in the parent solids (identified by $^{13}$C-NMR), but only 7–38% in the leachates (identified by $^{1}$H-NMR), though both increased with pyrolysis temperature. PyC, often operationally defined as condensed aromatic carbon (ConAC), was quantified using the benzenepolycarboxylic acid (BPCA) method. Tri- and tetra-carboxylated BPCAs were formed from non-pyrogenic reference materials, thus, only penta- and hexa-carboxylated BPCAs were used to derive a BPCA-C to ConAC conversion factor of 7.04. ConAC made up 24–57% of the pyrogenic solid C (excluding the 250°C biochar), but only about 9–23% of their respective leachates' DOC, though both proportions generally increased with pyrolysis temperature. Weighted BPCA compound distributions, or the BPCA Aromatic Condensation (BACon) Index, indicate that ConAC cluster size increased in pyrogenic solids but not in leachates. Additional evidence presented suggests that both aromatic cluster size and O-containing functional group contents in the pyrogenic solid control pyC solubility. Overall, pyDOM was found to be compositionally dissimilar from its parent chars and contained a complex mixture of organic compound groups. Thus, it is expected that estimates of dissolved pyC production and export, made only by detection of ConAC, are too low by factors of 4–11.

**Keywords: dissolved organic matter (DOM), pyrogenic carbon, biochar, charcoal, benzenepolycarboxylic acid (BPCA), leaching, fire, black carbon**

OPEN ACCESS

***Edited by:***
*Samuel Abiven,*
*Universität Zürich, Switzerland*

***Reviewed by:***
*Melanie Bläsing,*
*Universität Bonn, Germany*
*Sasha Wagner,*
*Northeastern University, United States*

***Correspondence:**
*Andrew R. Zimmerman*
*azimmer@ufl.edu*

***Specialty section:***
*This article was submitted to Biogeoscience, a section of the journal Frontiers in Earth Science*

***Received:*** *23 January 2018*
***Accepted:*** *09 April 2018*
***Published:*** *24 April 2018*

***Citation:***
*Bostick KW, Zimmerman AR, Wozniak AS, Mitra S and Hatcher PG (2018) Production and Composition of Pyrogenic Dissolved Organic Matter From a Logical Series of Laboratory-Generated Chars. Front. Earth Sci. 6:43. doi: 10.3389/feart.2018.00043*

## INTRODUCTION

Pyrogenic organic matter (pyOM), is a physically- and chemically-diverse suite of carbonaceous products generated during the incomplete combustion of biomass (e.g., charcoal and soot). Given that climate change is likely to increase the frequency and intensity of wildfires (Bowman et al., 2009) and the growing interest in the application of pyrolyzed waste agricultural biomass (biochar) to agricultural soils (Spokas et al., 2012), pyOM may become more abundant in the bio- and geosphere in the future. Therefore, a more complete understanding of the global cycling of pyrogenic carbon (pyC), often referred to as "black carbon" (BC), is needed. While we are beginning to better quantify the global production of pyC from wildfires and anthropogenic burning, we have a poor understanding of its mobility and geochemical fate in the environment.

PyOM has been generally characterized as a recalcitrant form of organic matter. However, using today's pyC production rate via natural and anthropogenic biomass burning (50–300 Tg yr-1, Kuhlbusch and Crutzen, 1996; Forbes et al., 2006; Bird et al., 2015), soil C would be 25–125% pyC after just 7,000 years (Masiello, 2004). A current estimate of soil pyC (in the uppermost 2 m) is ∼200,000 Tg (Reisser et al., 2016). Since soil C is only ∼10% pyC, on average (e.g., Bird et al., 1999; Hammes et al., 2007; Cusack et al., 2012), significant pyC losses must occur.

PyOM releases pyrogenic dissolved organic carbon (pyDOC) into aqueous solution via dissolution or "leaching." For example, one leaching experiment recorded losses of about 0.3% of the initial C in fresh and aged chars over a period of only 6 h (Abiven et al., 2011). Another laboratory leaching study examining the effects of repeated leaching estimated that up to 3.7% of biochar C could be lost to dissolution annually in sandy soils (Mukherjee and Zimmerman, 2013; Zimmerman and Gao, 2013). It is likely, though not yet adequately shown, that both abiotic (e.g., chemical oxidation and photooxidation) and biotic degradation (microbial enzymatic attack) enhances the production of water-soluble constituents of pyOM (Abiven et al., 2011; Mukherjee and Zimmerman, 2013) and even more pyDOC may be released than these studies suggest. Furthermore, the effects of bulk DOC on pyC solubility has been investigated to a minor extent (Wagner et al., 2017).

The production of pyOM converts labile C (biomass) into recalcitrant forms that can be stored in the geosphere, making it an important component in the global C cycle with implications for atmospheric $CO_2$ concentrations, and thus, climate variations through time. An improved understanding of the composition, mobility, and stability of pyrogenic dissolved organic matter (pyDOM) in the environment is thus essential.

## Pyrogenic Organic Matter Chemistry

The chemical composition of pyOM solids has been recognized to be highly complex (Schneider et al., 2010, 2013; Cao et al., 2012), though it can be generalized as biphasic, consisting of both a condensed aromatic portion and a more aliphatic, non-condensed portion (Hockaday et al., 2007). Because the condensed aromatic property of pyOM has often been used to quantify pyC, we coin the term "ConAC" (condensed aromatic carbon) to refer only to this portion rather than the chemically ambiguous term "black carbon." In biochars and charcoals, the proportion of ConAC varies with biomass type and charring conditions, but it generally increases with the temperature and duration of pyrolysis (Schneider et al., 2010, 2013; McBeath et al., 2011; Wolf et al., 2013).

Variations in parent solid composition are assumed to dictate the leachability and production of pyDOM from biochars and charcoals. Experiments have shown that chars produced at lower temperatures (e.g., <400°C) contain more readily soluble constituents than those produced at higher temperature (e.g., >400°C) (Mukherjee and Zimmerman, 2013). Feedstock has also been shown to affect pyDOM production; in an aqueous leaching study, Wagner et al. (2017) found that rice straw chars produce about 5.5 times as much pyDOC as chestnut wood chars relative to their C content. Environmental exposure may also affect the abundance and composition of leached pyDOM. For example, ∼50 times more ConAC was released from aged chestnut wood chars than from freshly made chars (Abiven et al., 2011). Similar results were observed by Roebuck et al. (2017). Using Fourier-transform ion cyclotron resonance mass spectrometry (FTICR-MS), Hockaday et al. (2006) estimated that the water-soluble portion of soil charcoal contained 1,200 unique formulas corresponding to condensed aromatic ring structures that constituted about 65% of the total peaks observed. In marine DOM, these condensed aromatic compounds consist of only seven fused aromatic rings, on average, and are substituted with oxygen-containing functional groups (e.g., carboxyl, hydroxyl, and aliphatic, Koch and Dittmar, 2006). A significant portion of the oxygenated polycyclic aromatic hydrocarbons in marine DOM are thought to be pyrogenic (Hockaday et al., 2006), though this is based only on the similarities in structure derived from O/C and H/C ratios. In addition to condensed aromatic hydrocarbons, pyDOM must also contain aliphatic and non-condensed aromatic OM, though this is seldom investigated in detail or even acknowledged in the context of the global pyC cycle. Thus, improvements are needed in our ability to account for all components of pyDOM in the environment and distinguish it from non-pyrogenic DOM.

## Pyrogenic Carbon Quantification Method

Quantification of pyC in soils, sediments, and DOM has been performed using a variety of methods that rely on the general properties of pyrogenic materials including morphology, light absorption, thermochemical stability, and chemical composition (Hammes et al., 2007). Of these, the method most commonly used for pyDOC analysis involves the acid-mediated oxidation of ConAC constituents of pyDOM into smaller, quantifiable molecular markers (i.e., benzenepolycarboxylic acids or BPCAs). These BPCA molecules consist of a central benzene ring with two to six carboxylic acid functional groups. Historically, only compounds that can produce three to six carboxyl substitutions are quantified as ConAC. However, because not all ConAC is converted to BPCA carbon (BPCA-C), total ConAC is calculated via a conversion factor, and is assumed to be exclusively pyrogenic. The method also provides structural information

about ConAC in the form of BPCA molecular distribution. Production of BPCAs with higher levels of carboxylation (e.g., benzenepentacarboxylic acids and benzenehexacarboxylic acids, B5CA and B6CA) are thought to indicate greater aromatic condensation or aromatic "cluster size" (Ziolkowski and Druffel, 2009, 2010; Schneider et al., 2010, 2011).

Using this BPCA method, substantial quantities of "pyDOC" (reported as dissolved black carbon, DBC) have been reported in aquatic systems and rivers (Dittmar et al., 2012b; Jaffé et al., 2013), subtropical wetlands (Ding et al., 2014), intertidal systems (Dittmar et al., 2012b), glacial melt systems (Nakane et al., 2017), and open marine environments (Ziolkowski et al., 2011). Jaffé et al. (2013) calculated that "pyDOC" comprises from 0.1 to 17.5% of global riverine DOC. Despite this, total DOC and "pyDOC" concentrations were highly correlated in this and several other BPCA-based studies (e.g., Dittmar et al., 2012b; Ding et al., 2013, 2014) suggesting that pyDOC represents a relatively constant proportion of riverine DOC globally (∼10% pyDOC/DOC). This conclusion is potentially problematic since one would expect this ratio to vary with regional climate, burning regimes, and soil characteristics.

While the BPCA method has been adapted and improved recently to reduce artifacts Brodowski et al. (2005), some caveats and assumptions still must be considered. This method does not target aliphatic or other non-condensed compounds in pyDOM, as they likely do not form BPCA compounds upon nitric acid oxidation. Aliphatic and O-containing components are likely to be more soluble than the condensed aromatic fraction, thus may represent a large portion of pyDOM, as directly identified using FTICR-MS (Podgorski et al., 2012; Ward et al., 2014). It is also unclear if the BPCA method quantifies pyC, exclusively. The method may result in some non-pyrogenic DOC (such as humic substances) being identified as pyrogenic (Kappenberg et al., 2016; Zimmerman and Mitra, 2017). Aside from the potential for false positives, other difficulties arise from the choice of conversion factor and methods used to convert measured BPCA-C of a sample to the amount of ConAC. These range from 2.3 to 4.4 ((Glaser et al., 1998; Ziolkowski and Druffel, 2009), respectively) using gas chromatography method (GC) which requires a derivatization step, and about 3 based on FTICR-MS and HPLC (Dittmar, 2008). Another conversion factor would be needed if not all pyC were condensed aromatics. Clearly, the abilities and limitations of the BPCA method to quantify pyC, particularly in dissolved form, must be further explored.

While many natural DOM samples have been analyzed using the BPCA method, to our knowledge, only two studies examined well-characterized pyrogenic solid leachates (Abiven et al., 2011; Wagner et al., 2017). Here, pyDOM was extracted using batch leaching experiments on a series of biochars as well as several non-pyrogenic reference materials. Specific objectives of this study were to: (1) determine how pyDOC and BPCA production vary with pyrogenic solid type (range of pyrolysis temperatures and feedstock types) and over the course of leaching, and (2) examine how pyDOM composition relates to its parent pyrogenic solid type (using the BPCA technique as well as $^{13}$C- and $^{1}$H-NMR analysis).

We hypothesize that pyDOC production, i.e., solubility, will be controlled by both abundance of O-containing functional groups and ConAC cluster size (as evidenced by $^{13}$C-NMR and $^{1}$H-NMR group, and BPCA molecular distributions, respectively). Further, we expect that the chemical composition of the produced pyDOM will be different from that of its parent solid phase, reflecting relative compound solubility instead of parent phase abundance. Specifically, we hypothesize that the biochar leachates should contain more O-containing function groups and less condensed aromatic content (or at least smaller aromatic clusters) than their respective solids. In testing these hypotheses, we hope to clarify the inferences that can be made using BPCA biomarkers in regards to natural DOM samples, as well as to improve our understanding of the mechanisms involved in pyC production and fate.

# METHODS AND MATERIALS

## Materials

### Parent Solids

Biochars were produced from laurel oak wood (*Quercus hemisphaerica*) by combustion at 250°C in a furnace (Oak-250) and by pyrolysis under flowing nitrogen gas (held at peak temperatures of 400, 525, and 650°C for 3 h, hereby denoted as Oak-400, Oak-525, and Oak-650). Using the same pyrolysis technique, biochars were prepared from dwarf Fakahatchee grass sheaths (*Tripsacum floridanum*) at 400 and 650°C (i.e., Grass-400 and Grass-650). Lastly, laurel oak wood was pyrolyzed at 650°C for 24 h (Oak-650-24 h). Physiochemical data on these biochars have been reported previously (Zimmerman, 2010; Mukherjee et al., 2011). Non-pyrolyzed reference materials included the wood, the grass, and pyrogenic-free leaf-litter compost. A mortar, pestle, and sieve were used to achieve solid samples with a semi-uniform 0.25–2.0 mm particle size. Additional reference materials analyzed included pristine multiwall carbon nanotubes (750 nm diameter; from SinoNano Tech Corp.) and graphene oxide (from JCNANO) which were considered semi-pure forms of condensed aromatics.

## Experimental and Analytical Methods

Approximately 1 g of each solid sample was added to 40 ml of MilliQ Nanopure water (18.1 MΩ) in a 250 ml glass flask (all glassware throughout the experiment was pre-cleaned via combustion at 500°C for 3 h). These flasks were placed on a platform shaker and agitated at 120 rpm in the dark. After 24 h, the overlying supernatants were removed and stored in a refrigerator at 4°C. The 40 ml of water was replaced in each flask and they were returned to the shaker-table and agitated for another 24 h (day 2). Then, the 40 ml supernatants of each sample were combined with the previous leachate. These day 1- and 2- combined leachates were designated "Early" pyDOM leachates. This process was repeated, but with 100 ml additions, for 13 more 24 h periods. On days 16 and 17, the corresponding 40 ml supernatant were combined and designated "Late" pyDOM leachates.

All "Early" and "Late" leachates were pre-filtered through combusted (450°C) Fisherbrand G2 glass fiber filters (1.0 μm

particle retention), then vacuum-filtered using a 0.45 μm mixed cellulose ester filter (Millipore). All filtrates were analyzed for DOC on a Shimadzu TOC-$V_{CSN}$ after acidification to pH 2 with trace metal grade hydrochloric acid and sparging for 2 min with $N_2$ to remove dissolved inorganic C. Standard curves were generated using concentrations of potassium biphthalate solutions ranging from 0.4 to 40.0 mg $L^{-1}$ ($C_8H_5KO_4$; Sigma-Aldrich, >99.95%).

## Solid Phase Extraction

Prior to BPCA analyses, pyDOM leachates were concentrated using solid phase extraction (SPE), following Dittmar (2008) and Dittmar et al. (2008). Agilent PPL cartridges (3 ml, 100 mg) were rinsed with at least 10 ml HPLC-grade methanol. Aliquots of each leachate (20 ml) were acidified to pH 2 with trace metal grade HCl and pipetted through the PPL at a rate not exceeding 10 ml $min^{-1}$. The appropriate flow rate was achieved using a glass manifold connected to a vacuum pump. After leachates were loaded onto PPL cartridges, 30 ml of dilute trace metal grade hydrochloric acid (0.01 N) was slowly passed through each PPL to ensure the removal of salts. The PPL cartridges were dried and sealed under nitrogen gas (foil-wrapped in individual $N_2$-filled zip-top bags) and stored in a −20°C freezer until elution with 8 ml HPLC-grade methanol.

## BPCA Analysis

Following Dittmar (2008), eluents were blown down to 0.5 ml under $N_2$ gas at 45°C, and transferred in methanol into ampules (Wheaton: 1 ml, gold band, pre-scored) via glass pipettes and blown to dryness. For solids, ≤5.0 mg of finely powdered sample were weighed into glass ampules. Approximately 0.5 ml concentrated nitric acid was added to each ampoule. Then, ampoules were flame-sealed, and placed into Teflon-lined Parr steel bombs that were held in a 170°C furnace for 9 h. Approximately 3 ml tap water was added to the Teflon liner to prevent the ampoules from rupturing.

## High Performance Liquid Chromatography Analysis

Following acid oxidation, samples were dried under $N_2$ gas at 45°C, and methanol-transferred into 2 ml high-recovery HPLC vials (Fisherbrand, 60180-508, with PTFE septa). BPCA compounds were detected on a Shimadzu HPLC (LC-20 Prominence Series) equipped with a C18 column (3.5 μm, 2.1 × 150 mm, Waters Sunfire) and a diode array detector (DAD) (Surveyor, Thermo-Scientific, SPD-M20A) with a binary gradient program as described in the SI section.

## Solid-State $^{13}$C NMR Spectroscopy (Solids)

Solid biochar and reference materials samples were transferred to a 4 mm rotor covered with a Vespel cap for solid-state $^{13}$C NMR analysis using a multiple cross-polarization magic angle spinning (multiCPMAS) pulse sequence (Johnson and Schmidt-Rohr, 2014). Experiments were conducted on a Bruker Avance II instrument with $^1$H resonating at 400 MHz and $^{13}$C resonating at 100 MHz. Samples were spun at the magic angle (54.7°) and at a frequency of 18 MHz. The continuous pulses were optimized at 0.5 s and a 1 s recycle delay was used. All sample spectra (1,600 co-added scans) were baseline-corrected and calibrated to a glycine external standard (176.03 ppm).

To simplify data comparisons, sample spectra were divided into chemical shift ranges characteristic of carbon moieties typical of natural OM and chars. "Alkyl-C" 0-110 ppm, consists of methyl, methylene, alkyl-O, and di-O-alkyl C. "Aryl-C" refers to 110–146 ppm: C in aromatic rings (C=C, Ar-C-H). "O-aryl C" refers to 146–165 ppm: C in aromatic rings attached to O atoms including phenolic groups. Lastly, "carbonyl C" refers to the sum of 165–220 ppm: carboxyl, amide, ester, aldehyde and ketone C. More in-depth categorization of these $^{13}$C NMR groups can be found in Table S3. The relative contributions (% of total spectral signal) from major C moieties present in each sample were obtained by integrating the spectral signal over each chemical shift region using Bruker Topspin software, and divided by that of the entire spectral region (0–220 ppm).

## $^1$H-NMR Spectroscopy (Leachates)

Leachates were diluted with $D_2O$ (100% atomic D, Acros Organics) at a volumetric ratio of 9:1 (i.e., $H_2O$:$D_2O$) immediately prior to $^1$H NMR analysis. Deuterated solution $^1$H NMR spectra were obtained on a Bruker Biospin Avance III 400 MHz NMR with a BBI probe using a water suppression technique following previous studies (e.g., Wozniak et al., 2013; Willoughby et al., 2016) at Old Dominion University's COSMIC facility. Each sample was scanned at least 4,000 times to obtain an integrated spectrum detecting non-exchangeable H. Scan numbers were increased for samples with lower DOM concentrations to ensure a high enough signal to noise ratio for data interpretation.

The signals obtained from $^1$H NMR spectra were integrated over specific chemical shift regions that are characteristic of H chemical environments. The region between 0.60 and 1.80 ppm is referred to as "Alkyl-C" and includes signal from methyl-H ($\underline{H}_3$C), methylene H ($\underline{H}_2$C), and H in alkyl groups that have heteroatoms bound to beta C (H$\underline{C}$-C-CX, where X is O, N, S, etc.). The region between 1.85 and 4.4 ppm is referred to as "Oxygenated-C" and includes signal from: H bound to C that have alpha C that are doubly bonded to C, O, N, or S (H$\underline{C}$-C=Y, where Y is C, O, N, or S including carbonyl and carboxyl functional groups), H bound to C bound to N, S (H$\underline{C}$-Z, where Z is N or S), and carbohydrate and alcohol groups (H$\underline{C}$-OR). The region between 6.50 and 8.30 ppm is referred to as "Aryl-C" and corresponds to H attached to aromatic C (Ar-$\underline{H}$). Lastly, hydrogens in acetic acid/acetate (1.9–2.1 ppm), methanol (3.2–3.4 ppm) and formic acid (8.1–8.3 ppm) appeared in all spectra as sharp peaks indicative of their identification as pure compounds. Signal corresponding to these three regions was summed and reported as "low molecular weight-C" (LMW-C) compounds and subtracted from the Alkyl-C, Oxygenated-C, Aryl-C regions to which their chemical shifts correspond. Detailed information on categorization of these $^1$H NMR groups can be found in Table S4. It is important to note that exchangeable H such as those in carboxylic acid groups (COO$\underline{H}$) readily exchange with deuterium in the $D_2O$ required for analysis and therefore go undetected. Additionally, H signal between 4.40 and 5.00 ppm, which includes some amine and ester H, is not considered

because signal in this region is obscured by the water suppression technique. Spectral signals in each chemical shift region were integrated using Bruker Topspin software.

For comparison to the DOC values and $^{13}$C NMR data, the $^{1}$H NMR spectral integrations which are quantitative for H signal, were converted to a C basis by dividing each integrated area by H/C ratios typical of the H environments in that chemical shift region (following, e.g., Decesari et al., 2007): $H/C_{\underline{H}3C} = 3$, $H/C_{\underline{H}2C} = 2$, $H/C_{\underline{H}C-C-CX} = 2$, $H/C_{\underline{H}C=C-Y,\underline{H}C-Z} = 2$, $H/C_{\underline{H}C-OR} = 1.1$, $H/C_{\underline{H}C=C} = 0.4$, $H/C_{\underline{H}-Ar} = 0.3$, $H/C_{\underline{H}C=O} = 1$. The relative contribution of each chemical shift region was then calculated as the C-basis area divided by the sum of all C basis areas.

## Data Analysis

The molecular distributions of BPCA molecular markers have been used to infer the degree of aromatic condensation (or aromatic cluster size) in pyOM (Hammes et al., 2007; Schneider et al., 2009, 2010; Ziolkowski and Druffel, 2010; Ziolkowski et al., 2011). Smaller condensed clusters produce benzenetricarboxylic acids (B3CAs) and benzenetetracarboxylic acids (B4CAs); whereas benzenepentacarboxylic acid (B5CA) and benzenehexacarboxylic acid (B6CA) are thought to only form from the central aromatic rings of large aromatic clusters (Schneider et al., 2009; Ziolkowski and Druffel, 2010; Ziolkowski et al., 2011). Thus, greater proportions of B5CA and B6CA have been suggested to indicate higher degrees of condensation in each sample.

Following Ziolkowski and Druffel (2010) and Schneider et al. (2011), we calculate the average number of carboxyl groups present among the BPCA compounds produced by a sample (Equation 1):

$$\mathrm{BACon} = \frac{(6)\cdot[\mathrm{B6CA}]}{\sum[\mathrm{BPCA}]} + \frac{(5)\cdot[\mathrm{B5CA}]}{\sum[\mathrm{BPCA}]} + \frac{(4)\cdot[\mathrm{B4CA}]}{\sum[\mathrm{BPCA}]} + \frac{(3)\cdot[\mathrm{B3CA}]}{\sum[\mathrm{BPCA}]} \quad (1)$$

where $\Sigma$[BPCA] is the sum of B3CAs, B4CAs, B5CA, and B6CA molar abundance. This BPCA Aromatic Condensation (BACon) Index spans from 3.0 (least condensed; produces only B3CAs) to 6.0 (fully condensed; produces only B6CAs; Ziolkowski and Druffel, 2010).

Oak-400 and Oak-650 leachates were produced in triplicate to gauge the variability in pyDOC production and BPCA analysis reproducibility. All DOC analyses were run in quintuplicate and were re-run if coefficients of variation were >5%. Bar chart values display the average value of these replicates and error bars represent one standard deviation of values observed. Correlation and statistics between parameters were calculated using the Microsoft Excel (MS, 2010) data analysis tool pack.

# RESULTS

## Chemistry of Parent Pyrogenic and Reference Solids

Elemental composition (i.e., %OC, %H, %N, %O, and %ash and %volatile matter) of biochars and reference solid materials are provided in Table S1. Compared to their non-pyrolyzed feedstocks, pyrolyzed products were more C-rich and relatively depleted in N, H, and O. In general, these heteroatoms were progressively lost with increased heating temperature and duration. Consequently, high-temperature biochars (525–650°C) were much more carbonaceous (~80–94% C) than low-temperature (250–400 °C) chars (~56–71% C). These elemental trends are commonly observed in pyrogenic solids (Baldock and Smernik, 2002; Czimczik et al., 2002; Zimmerman, 2010). While the organic C yield was measured only in the "Early" and "Late" leachate (**Figure 1**), the proportion of total C lost during the entire leaching of the pyrogenic solids (soluble C) was estimated to have ranged from 0.2% (Oak-650, 24 h) to 7.4% (Oak-250) (see Table S2).

### $^{13}$C NMR Analysis of Parent Solids

Trends in biomass and biochar solid functional group composition, as determined by $^{13}$C-NMR (**Figure 2** and

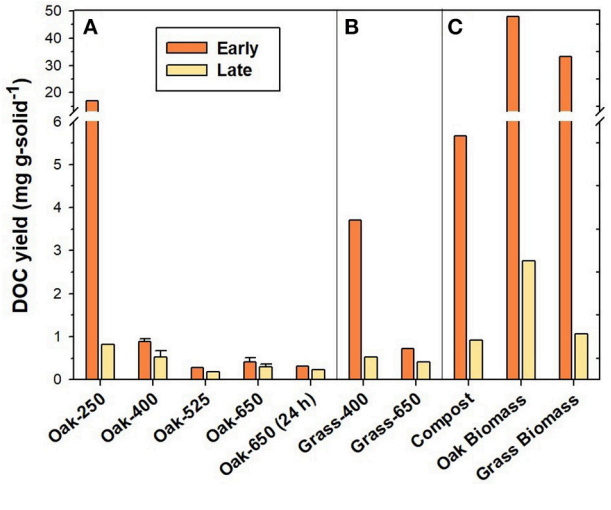


**FIGURE 1 |** DOC yield from "Early" and "Late" leachates of **(A)** oak biochar thermal series, **(B)** grass biochars, and **(C)** reference materials.

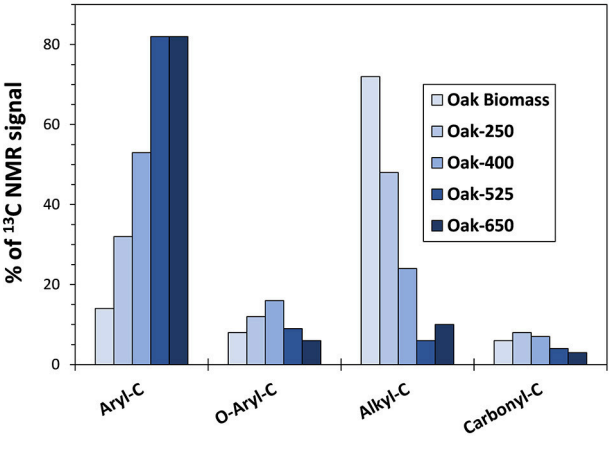


**FIGURE 2 |** Solid State $^{13}$C-NMR functional group abundances for non-pyrolyzed oak biomass and oak biochar (parent solid) thermal series. See the text for chemical group assignments.

Table S3) were like those observed previously (Hockaday et al., 2007; McBeath et al., 2011, 2014; Cao et al., 2012; Kim et al., 2012; Li et al., 2013). As expected, oak biochars became increasingly rich in aromatic-C with increasing pyrolysis temperature (from 32 to 82% of the identified functional groups), a property also seen in grass biochars (data not shown). Correspondingly, higher temperature biochars contained less oxygenated and aliphatic functional groups (methyl, O-alkyl, and carboxyl groups) than lower temperature ones. However, grass biochars had less aromatic C and more O-containing functional groups than oak biochars made at the same temperature (e.g., 19% less aryl C for 400°C biochar).

### BPCA Analysis of Parent Solids

The proportion of OC in parent pyrogenic solids that yielded BPCA-C ranged from 7.0 to 12.1% (**Figure 3**). As expected, given the $^{13}$C-NMR-determined increase in aromaticity, BPCA-C yield generally increased with pyrolysis temperature. However, the portion of BPCA-C produced by Oak-650 (24 h) was lower, a trend comparable to that of other charcoal BPCA studies (e.g., Hammes et al., 2006; Schneider et al., 2010) where less of the C in very high-temperature chars and soots (800–1,000°C) was converted to BPCA-C than from intermediate temperature chars. However, graphene oxide and carbon nanotubes showed the highest yields of BPCA-C (20.4 and 15.1%, respectively), similar to other graphitic materials (Dittmar, 2008; Ziolkowski and Druffel, 2009; Schneider et al., 2010); This is likely because they contain relatively more ConAC, but also, the B5CA and B6CA which they produce are less likely to be nitrated during digestion than B3CA and B4CA (Ziolkowski et al., 2011) and thus, not quantified. Thus, it appears that turbostratic graphene structures have lower conversion efficiencies (pyC to BPCA-C) than that of graphene oxide sheets.

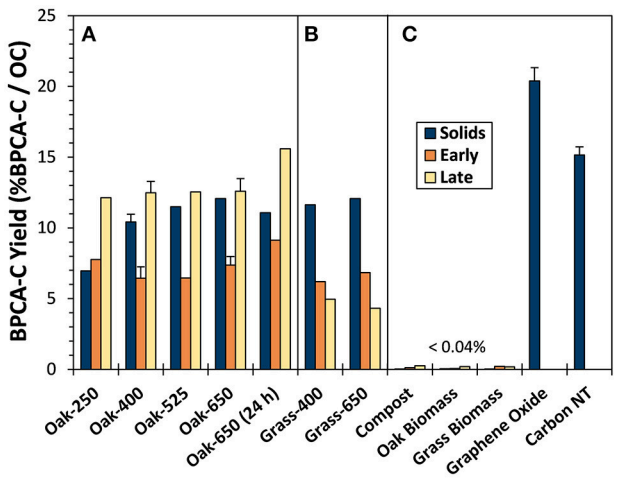


**FIGURE 3 |** BPCA-C yield from **(A)** oak char thermal series, **(B)** grass chars, and **(C)** reference material solids and leachates during days 1 and 2 ("Early") and days 16 and 17 ("Late").

The degree of carboxylation in BPCAs from biochar solids, as represented by the BACon Index, increased with pyrolysis temperature (3.7–4.8 for the oak series and 4.3–4.8 for the grass series) (**Figure 4**). These trends in BACon suggest an increase in ConAC cluster size as chars become more thermally mature, (as observed by others Hammes et al., 2007; Schneider et al., 2010). The highest BACon values calculated were produced by the highly condensed graphene oxide (5.7) and carbon nanotubes (5.2), and were like that of another carbon nanotube BPCA study (e.g., about 5.7, Ziolkowski and Druffel, 2009).

Biomass and compost yielded low amounts of BPCAs (<0.05% BPCA-C OC$^{-1}$), suggesting that BPCAs are not exclusive indicators of pyrogenic materials. However, only B3CAs and a few B4CAs were produced from non-pyrolyzed biomass, resulting in BACon values between 3.2 and 3.3, and indicating that if aromatic clusters do exist in these non-pyrogenic solids, they are likely very small or that the digestion step transforms some portion of biomass components into B3CAs and B4CAs.

## Yield and Composition of Pyrogenic and Reference Solid Leachates

### DOC Yield

Non-pyrolyzed plant biomass produced 33.1–47.9 mg C g-solid$^{-1}$ in "Early" leachates (**Figure 1**). The "Early" compost leaching yielded considerably less DOC than the oak and grass biomass leachates (about 80% less) as it had probably been leached by rainfall in the field prior to collection. The DOC yield in "Early" leachates of low-temperature biochar (Oak-250) was on the same order of magnitude (16.9 mg C g-solid$^{-1)}$ as the biomass materials. Biochars produced at higher temperatures had DOC yields that were one to two orders of magnitude lower than those of biomass leachates, ranging from only 0.3 to 0.9 mg C g-solid$^{-1}$ for oak biochars and 0.7– 3.7 mg C g-solid$^{-1}$ for grass biochars made at 400–650°C (**Figure 3**). After 16 days of leaching, the "Late" DOC yield had decreased by about 95% for the low-temperature biochars by 25–40% for high-temperature biochars, compared to their "Early" leachate DOC yield.

These py-DOC production trends are similar to those observed previously in other biochar leaching experiments (Mukherjee and Zimmerman, 2013) and were anticipated given the greater abundance of more-soluble components in low temperature and grass chars (e.g., more O-rich functional groups as determined via $^{13}$C-NMR and elemental analyses and lesser condensed fraction as determined by BPCA analysis).

The observation that the most leachable (low T) biochars showed the greatest decreases in pyDOC production over time (with leaching extent), while less leachable chars retained their C loss rates, suggests that, over time, pyDOM production rates from different charcoal types may become similar to each other due to rapid loss of highly leachable portions and environmental oxidation of less leachable portions (making them more soluble).

### $^{1}$H-NMR Analysis of pyDOM

$^{1}$H-NMR analysis of biochar leachates revealed generally increasing proportions of aromatic and alkyl components with increasing pyrolysis temperature of their parent solids (**Figure 5**,

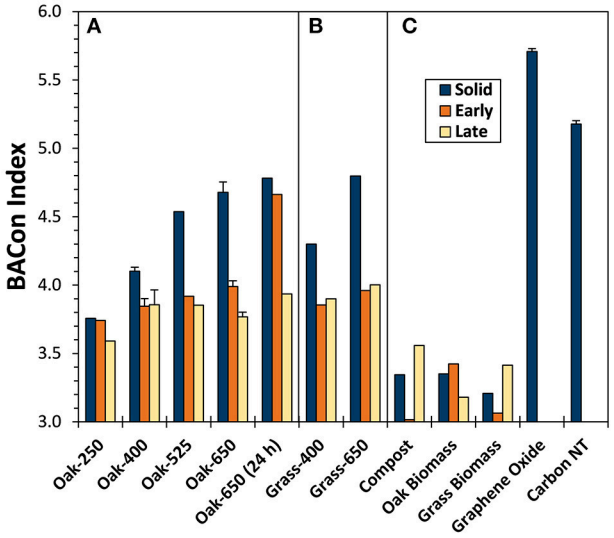


**FIGURE 4 |** BPCA aromatic condensation (BACon) index values for biochar solids and "Early" and "Late" leachates of **(A)** oak char thermal series, **(B)** grass chars, and **(C)** reference materials.

Table S4). Correspondingly, proportions of oxygenated functional groups (e.g., ether, ester, carbohydrate, and alcohol groups) decreased with increasing parent thermal maturity. The same relationship between aromaticity and temperature was observed in grass biochar leachates (Table S4). However, the aromatic portion was much higher in grass biochar leachates than in oak biochar leachates (e.g., 22% vs. 10% aryl C for Grass-400 and Oak-400 leachate, respectively). An exception to these trends was the "Early" leachate of Oak-250, which was more aromatic than the higher temperature biochars. This is most likely because of contributions from the ligninaceous components of the wood biomass that remained at this low treatment temperature. Aromatic compounds made up 14% of the $^{13}$C-NMR signal of non-pyrolyzed oak biomass and 10% of the $^{13}$C-NMR signal of non-pyrolyzed grass biomass. Among these, low molecular weight oligomers of lignin may be among the more soluble components in wood. The LMW-C compounds become much more abundant in leachates upon heating of parent solids from 250 to 400°C while contributions from aryl-C are decreased considerably (**Figure 5**) suggesting that phenolic compounds from lignin may be the predominant source of the LMW-C compounds. The LMW-C compounds may have been mineralized to carbon dioxide or volatilized upon pyrolysis at higher temperatures.

## BPCA-C Yield From pyDOM and Reference Leachates

The proportions of total C converted to BPCA (i.e., the BPCA-C yield) in "Early" and "Late" biochar leachates were similar to that of solid biochars, with most in the range of 7–12% BPCA-C/OC (**Figure 3**, Tables S2, S5). However, some differences were apparent. Oak biochar "Late" leachates were always somewhat enriched in BPCA-producing compounds compared to either their parent solids or "Early" leachates (by 20 and 43% on average, respectively). This may be attributed to the presence of non-condensed OM in the solids and "Early" leachates that was progressively lost with leaching. In contrast, this increase in %BPCA-C/DOC with leaching did not occur in the grass biochars, possibly because the non-condensed OM of grass chars, being much more abundant, was still being released even after many leaching cycles. While BPCA-C yield from non-pyrogenic reference leachates were low on a per DOC basis (<0.04%), compost and the biomasses produced as much BPCA-C as oak-400 on a per g parent solid basis.

## Molecular Distribution of BPCA in pyDOM

Trends in the varying proportions of the eight BPCA compounds produced upon oxidation of the biochar leachates (Table S5) are represented by their BACon values (**Figure 4**). Pyrogenic leachates usually had lower BACon values than their parent solids. BACon values of "Early" and "Late" leachates were, in most cases, quite similar, as were those of grass and oak biochar leachates from parent solids of the same charring temperature (BACon values ≈ 3.8). Unlike the parent solids, biochar leachate BACon values increased only slightly with parent solid pyrolysis temperature (e.g., from 3.7 to 4.0 for "Early" Oak-250 and Oak-650, respectively). Thus, it can be inferred that the size of aromatic clusters in pyDOM were relatively constant, even as the ConAC content and aromatic cluster size of its parent solids increased with thermal maturity.

The "Early" leachate of Oak-650 (24 h) had an anomalously high BACon value for which we have no explanation other than to speculate that a small amount of colloidal pyOM with composition very similar to the parent biochar solid may have entered the filtrate. This proposed shift in composition would have been all the more likely in this sample of very low DOC content.

The pyDOM produced in this study had BACon values that were similar to that of aged chestnut char leachate described previously (about 4.0, Abiven et al., 2011). Further, BACon values of char leachates (e.g., this study, Abiven et al., 2011; Roebuck et al., 2017; Wagner et al., 2017) resembled those of natural DOM from the Gulf of Mexico (about 4.3, Dittmar, 2008), ultrafiltered Amazon River water (about 4.0, Ziolkowski and Druffel, 2010), and the open ocean (about 3.8, Ziolkowski and Druffel, 2010). A possible explanation is that condensed OM is uniformly susceptible to degradation, regardless of cluster size. Alternatively, several environmental degradation pathways could affect BACon values of DOM in opposing ways. Photodegradation may oxidize larger aromatic clusters into smaller aromatic clusters, resulting in lower BACon values, while preferential microbial consumption of smaller aromatic clusters may result in a higher BACon value.

As with their parent solids, the reference biomass and compost leachates contained only B3CAs and B4CAs (about 0.05–0.2% in "Early" and about 0.2–0.3% BPCA-C/DOC in "Late" leachates). While these BPCA-C yields were very low on an OC basis, their increase over time is notable. Furthermore, on a weight basis,

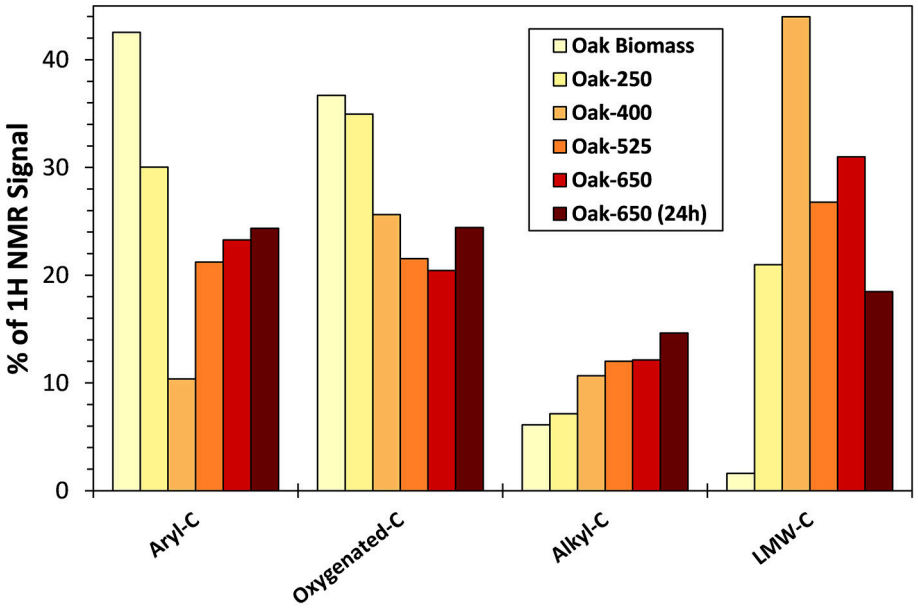


**FIGURE 5 |** $^{1}$H-NMR functional group abundances in "Early" leachates of oak biomass and its biochar thermal series, calculated on a carbon basis. See the text for chemical group assignments.

amounts of B3CAs and B4CAs produced from non-pyrogenic leachates were similar to that of parent pyrogenic materials (discussed further below).

# DISCUSSION

## Pyrogenic C Quantification Implications

### Non-pyrogenic BPCA Production

In this study, solid non-pyrogenic solids (oak biomass, grass biomass, and compost) and their leachates were shown to produce B3CAs and B4CAs upon nitric acid digestion. The production of BPCAs from the oxidation of natural "humic" substances, using both $HNO_3$ and alkaline-$KMnO_4$ techniques, has long been noted, and was proposed to have been produced by the destruction of aromatic rings with oxygen-containing side chains, as well as from ConAC (Hansen and Schnitzer, 1967; Stevenson, 1994). More recently, it was suggested that even aromatic rings with aliphatic side chains (e.g., retene) can produce BPCA-C (Ziolkowski et al., 2011). Perhaps this is why Kappenberg et al. (2016) observed BPCA production (even B6CA) from pyC-free corn stalks (*Zea mays*) and leaves of pepper plants (*Capsicum annuum*), when enough sample was processed (>8.7 mg C). This may also explain why, using total BPCA as an indicator, the greatest concentrations of "pyDOC" have been reported for peat-influenced sloughs and rivers that contain large amounts of humic-like DOM (Ziolkowski and Druffel, 2010; Jaffé et al., 2013).

An additional issue is that many B3CAs and B4CAs (produced by less condensed pyC) are more likely nitrated during the nitric acid digestion step. As these are not quantified by HPLC-DAD, this further complicates the usage of B3CA+B4CA-C as a marker of ConAC. More investigations are needed to identify the organic matter fraction targeted by total BPCA analysis.

In our study, B5CA and B6CA was not produced from reference materials (even when digesting samples with more than 5 mg C). Thus, we agree with Kappenberg et al. (2016) that B5CA+B6CA-C, and only B5CA+B6CA-C, can be used as a quantitative marker for ConAC, and by inference, the condensed aromatic portion of pyC, as we have done below.

### Estimating ConAC From B5CA+B6CA-C

The B5CA+B6CA-C yields from oak biochar solids ranged from 2.5 to 7.1% (**Figure 6**, left axis). Unlike total BPCA-C yield, B5CA+B6CA-C yield from the biochar solids was consistently greater than that of their leachates, which ranged from 0.9% (Oak-250) to 4.4% (Oak-650, 24 h). In addition, both solid and leachate B5CA+B6CA-C yields increased more consistently with pyrolysis temperature than total BPCA-C yield. Finally, B5CA+B6CA-C yields of "Early" and "Late" leachates were more similar than those of total BPCA-C. These trends, along with the lack of production of B5CA and B6CA from solids and leachates of non-pyrolyzed biomass, suggest that B5CA and B6CA are indeed better markers for pyrogenic C than total BPCAs. However, because B5CA and B6CA likely do not form from non-condensed or the small (<5 aromatic rings) condensed clusters of pyrogenic OM, it is certainly a more conservative estimate of ConAC and potentially pyC.

We used the B5CA+B6CA-C yield from graphene oxide (14.2%), assumed to only contain condensed aromatic C, to generate a conversion factor to calculate the ConAC content of each pyrogenic sample (i.e., $^{100}/_{14.2} = 7.04$). Using this approach, the ConAC content of the solid biochars was calculated to

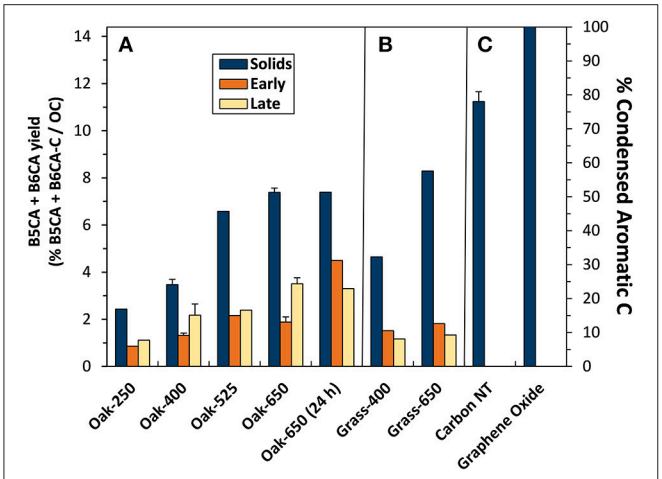


**FIGURE 6 |** Benzene penta- and hexa-carboxylated acid (B5CA + B6CA)-C yield (left axis) and calculated condensed aromatic C abundance (right axis) in biochar solids and "Early" and "Late" leachates of **(A)** oak char thermal series, **(B)** grass chars, and **(C)** reference materials.

range from 16% in Oak-250 to 51% in Oak-650 (**Figure 6**, right axis). These ConAC proportions (as quantified with B5CAs and B6CAs) represent approximately half of the aryl-C content indicated by $^{13}$C-NMR analysis, suggesting that about half of the aromatics in biochars may be non-condensed aromatics (e.g., lignin oligomers). For example, whereas $^{13}$C-NMR assigned 53% of the C in Oak-400 as aromatic, 24.2% was estimated to be ConAC using the B5CA+B6CA-C calculation method. Similarly, pyrogenic oak leachates C ranged from about 6 to 31% ConAC (in "Early" Oak-250 to "Early" Oak-650 (24 h) respectively), with "Late" leachates falling in a similar range. The ConAC content of leachates was also approximately half that assigned by $^{1}$H-NMR as aromatic C. The other half of aromatic C in leachates and solids could be in the form of non-condensed or small (cluster sizes <5 aromatic rings) condensed structures that do not form B5CA+B6CA-C or from olefinic carbons that overlap the aromatic C region of the NMR spectrum but do not form BPCAs. From these calculations, it can be further estimated that, whereas the biochars released 0.2–7.4% of their C during the experiment, only 0.1–3.0% of the solid ConAC was lost via dissolution.

### Estimating pyDOC From ConAC

BPCA-C analysis detected 14.2% of the ConAC in graphene oxide (C is composed of 100% ConAC), arriving at a multiplication factor of 7.04 required to convert B5CA+B6CA-C amounts to ConAC. However, based on the finding that ConAC represented 5–24% of the total pyDOC, an additional multiplication factor of 4–20 is still required to convert ConAC to total pyDOC. However, if one was using this ConAC to pyDOC conversion factor, one would need to assume that all ConAC is pyrogenic. In addition to the large margins of error that would thus be expected to be associated with these ConAC to pyDOC conversion factors, further caution should be exercised because different pyrogenic solids (biochars) were shown to produce pyDOM with different non-ConAC:ConAC ratios. To make pyDOM quantification even more difficult, in nature, the non-ConAC:ConAC ratio in pyDOM is also likely to be altered by variable abiotic and biotic degradation, timing and extent of leaching, variable mineral/particulate interactions, and a variety of other factors. Together, these uncertainties will make the elucidation of the pyDOM cycle a very challenging task.

## Controls on PyDOM Release

An overall finding of this study is that pyrogenic leachates are compositionally dissimilar to their respective parent solids. Although the similar yield of total BPCA-C from parent solids and leachates (**Figure 3**) suggests a similar ConAC content, a closer examination of the molecular distribution of BPCA compounds shows that this resulted from the co-occurrence of decreases in the abundance of B3CA- and B4CA-producing compounds (Figure S1) and increases in the abundance of B5CA- and B6CA-producing compounds (**Figure 6**) in the leachates with increasing thermal maturity of their pyrogenic parent solids. Moreover, the proportion of B5CA+B6CA-C, and calculated BACon values and ConAC contents were greater in parent solids than their leachates (**Figures 4**, **6**). Higher temperature (525–650°C) biochar leachates produced only about half as much B5CA+B6CA-C as their parent solids (on a per OC basis) with no consistent trends distinguishing "Early" and "Late" leachates.

Distributions of non-aromatic constituents (10–56% of pyrogenic solid C vs. 63–88% of their leachates) also suggested that pyDOM is of different composition than its solid pyOM parent. For example, while aliphatic-C represented similar proportions of total C in the pyrogenic solids and their leachates (10–30% excluding the 250°C biochar), this proportion decreased in the solids and increased in the leachates along the pyrolysis temperature gradient. Leachates of Oak-250 biochar had anomalously high aryl-C relative abundance, while its parent solid did not. However, these differences could have been driven by the pattern of LMW compounds that were separately quantified in the leachates but not the solids. Caution should be used when interpreting $^{1}$H-NMR aromaticity data, especially when samples contain large condensed moieties, as these are largely undersaturated with hydrogen and are difficult to quantify as aryl-C. Finally, it must be noted that comparisons between $^{13}$C-NMR and $^{1}$H-NMR data are imperfect because functional group classifications are not identical.

In order to further examine the controls on the solubility of BPCA-producing components in pyC, solid-liquid distribution coefficients, defined here as the ratio of the amount of a component in the solid to the amount in its leachate, were calculated for both the bulk pyC and ConAC yielding B5CA-C and B6CA-C (i.e., $K_{D,\ pyC}$ and $K_{D,\ ConAC}$, respectively). Thus, a greater $K_D$ indicates relatively lower solubility.

The first notable result was that the $K_{D,pyC}$ and $K_{D,\ ConAC}$ varied by about 1 and 2 orders of magnitude, respectively (**Figure 7**), again illustrating the wide variations in biochar-C solubility and the distinction between production of total pyC and ConAC. The significant negative correlation of both $K_{D,pyC}$ and $K_{D,\ ConAC}$ with % oxygenated C in parent solids (**Figures 7A,B**), and their positive correlation with BACon value of parent solids (**Figures 7C,D**) show that both functional

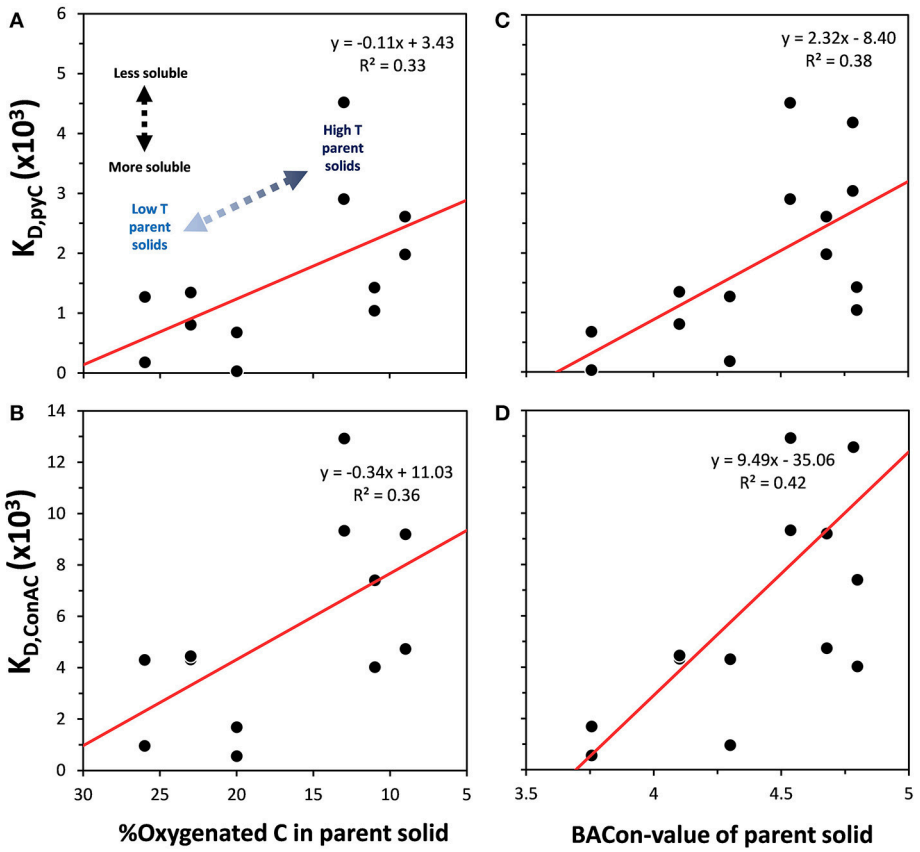


**FIGURE 7 |** Relationship between the solid-liquid distribution coefficients of bulk pyC and ConAC compounds yielding B5CA-C and B6CA-C (i.e., $K_{D,\ pyC}$ and $K_{D,\ ConAC}$, respectively) in "Early" and "Late" leachates and %C in parent solid O-containing functional groups (**A,B**, respectively), and aromatic cluster size as indicated by the BACon Index (**C,D**, respectively). All linear correlations are statistically significant ($p < 0.05$).

group content and aromatic cluster size control pyC solubility. The data generated here do not support a greater role of either factor or a greater influence on either the condensed or non-condensed portion of pyC (all correlation coefficients were similar: 0.33–0.42). A further indication that bulk pyC and ConAC solubility are controlled by similar factors is the strong correlation between the $K_{D,pyC}$ and each $K_{D,\ BPCA-C}$ (i.e., partitioning coefficients of compounds that produce each BPCA) (Figure S2, $r^2 \sim 0.80$, $p < 0.05$). Besides functional group content and aromatic cluster size, other processes that may result in the decrease in solubility with thermal maturity for both pyC and BPCA-producing compounds, include: (1) volatilization and removal of readily-soluble components from the pyOM pores with increasing pyrolysis temperature, (2) a co-dependence of solubility on the presence of inorganic ions or colloids, and (3) the mutual assistance of condensed and non-condensed pyOM in their solubilization. This latter explanation may be similar to the proposal that non-pyOM assists in the solubilization of condensed portions of pyC (Wagner et al., 2017). A final observation is that while B5CA- and B6CA-producing compounds were much less soluble than bulk pyC (slopes of ~4 in Figure S2), B3CA- and B4CA-producing compounds were similar to or less soluble than the bulk pyC.

These findings have implications for the use of BPCAs as pyrogenic C markers in natural samples. First, solid pyC solubility varied greatly along the thermal gradient; a fire's temperature will make a substantial difference in how representative the BPCA method is for quantifying its pyC content and its pyDOC products. While it would be optimal for a dissolved phase chemical marker to have the same solubility as the solid component it traces, the use of B3CAs and B4CAs has a number of disadvantages including their generation from non-pyrogenic processes, as noted above.

## Environmental Significance

These results show that pyrogenic materials (as modeled by laboratory-made biochars) are diverse in both their composition and propensity to release pyDOM. The estimated pyC losses ranged from about 7.5% for lightly-charred (250°C) biomass to 0.2% for higher temperature biochars during the current experiment. The biochar:water ratio (1 g biochar in daily leachings totaling 870 ml over 17 days, see Table S1) is similar to the average global precipitation rate passing through a half meter of soil of an average pyC content (see SI section on "biochar:water ratio"). As a result, if one considers our experiments as having substituted agitation for time, these C

releases (0.2–7.5% on a pyC basis) may be on the order of annual C released by biochars in an average soil. In nature, these loss rates might be expected to continue indefinitely due to equilibrium partitioning of compounds between solid and dissolved phases and due to ongoing abiotic and enzymatic oxidation within soils, which assists in solubilizing pyC. PyDOC yields from biochars aged for 9 months in Florida humid air and precipitation, but not sunlight, was found to be similar to those of their unaged counterparts (Mukherjee and Zimmerman, 2013). Additionally, mobilized pyDOC was detected in rivers draining Brazil's Atlantic forest even 40 years after cessation of widespread slash-and-burning (Dittmar et al., 2012a). Given that wildfires are typically in the upper range of the temperatures (500–700°C) used to produce our biochars (Santin et al., 2015), and 60% of riverine organic DOC derives largely from forested (not grassy) catchments (Hedges et al., 1997), we have weighted the results (30% Oak-400, 30% Oak-650, 20% Grass-400, 20% Grass-650) to arrive at a global estimate of annual pyDOC release from pyrogenic solids of about 0.9% of the total pyC pool (calculation shown in SI section). This is probably an underestimate if one considers that our experiments did not allow for charcoal surface colonization by microbial and associated enzymatic oxidation or photodegradation, which would solubilize formerly insoluble pyC.

Construction of a simple pyC cycling box model can help to identify "knowns" and "unknowns" in our understanding of pyDOC transfers between soil and fluvial reservoirs. Using the commonly-cited soil organic carbon (SOC) stock of 1,600 Pg C (upper 1 m of soil, Eswaran et al., 1993) and a median value of pyC/SOC measurements of 10% (e.g., Bird et al., 1999; Hammes et al., 2007; Cusack et al., 2012), the pyC soil stock can be estimated as 160 Pg (**Figure 8**). Using our estimate of 0.9% annual pyC leaching, a flux to soil porewater of 1,440 Tg $y^{-1}$ pyC is calculated. Using the finding that "pyDOC" represents a constant fraction of about 10.6% of riverine DOC globally (Ding et al., 2013, 2014; Jaffé et al., 2013) and the annual total riverine DOC export of 250 Tg C $yr^{-1}$ (Hedges et al., 1997), an annual riverine "pyDOC" export of 27 Tg C $y^{-1}$ is calculated (**Figure 8**). However, the "pyDOC" concentrations measured in these studies were based on BPCA analysis, which, as previously mentioned, only detects ConAC. Because BPCA-C represents only about 13.3% of total pyDOC (averaged using the same weighting, as above), we can apply a multiplication factor of 7.5 ($^{100}/_{13.3}$) to scale this leached ConAC flux up to approximately 203 Tg pyDOC delivered to rivers annually.

Several overall conclusions can be made from this box modeling exercise (**Figure 8**). First, as the pyC leaching flux is much greater than the riverine C flux, much of the leached pyDOC (>86%) must be lost in transit. In addition to microbial oxidation, other potential fates of pyDOC include photolytic oxidation and sorption to minerals or particulate OM (i.e., in soil, the vadose zone, or in rivers). However, these processes are yet to be comprehensively quantified.

The results of this study also highlight the chemical diversity of pyDOM, both in the range of compound types leached, and the variations that may be attributed to the different types of pyrogenic parent solids. The majority of pyDOC, especially in "Early" leachates, is not ConAC, which may change our perspective of the overall solubility/lability of pyDOM and our endeavors to quantify it. In nature, these non-ConAC moieties (e.g., pyrogenic alcohols, carbohydrates, aliphatic, and LMW components) are likely more labile than the aromatic components of pyDOM (as inferred from Kalbitz et al., 2003), and thus may fuel heterotrophy in groundwater and surface water systems. Thus, occurrence of fire and the functioning and health of aquatic ecosystems within a watershed may be linked on short timescales.

As for the condensed aromatic portion of pyDOM, it has long been demonstrated that ConAC compounds can be biodegraded by bacteria, lignolytic (Field et al., 1992), and non-lignolytic

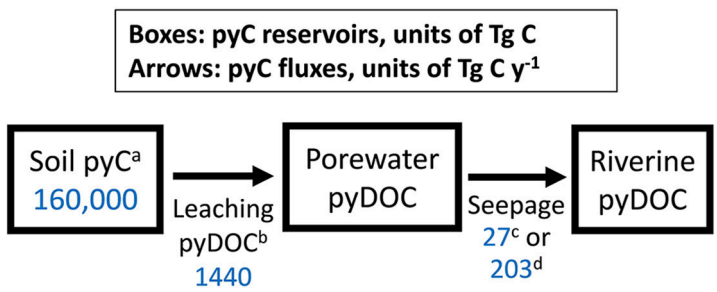


Sources and calculation methods of values shown [and ranges]

a. pyC/SOC = 10% (Mitra *et al.*, 2014) of 1600 Pg C, (Eswaran *et al.*, 1993) [575-3101 Pg C, Todd-Brown *et al.*, 2013].
b. 0.9%* of pyC [0.2 – 7.4%, this study].
c. pyDOC/DOC = 10.6% (Jaffé *et al.*, 2013) of 250 Tg $y^{-1}$ DOC (Hedges *et al.*, 1997).
d. Conversion of ConAC of #3 (above) to total pyC using factor of 13.3* [6.9 – 18.7, this study].

*weighted as described in manuscript

**FIGURE 8 |** Box model of pyC transfer from terrestrial to fluvial systems.

fungi (Karich et al., 2017), photodegraded (Fasnacht and Blough, 2002; Saeed et al., 2011; Stubbins et al., 2012), and even completely mineralized (Haemmerli et al., 1986; Cerniglia and Heitkamp, 1990; Bezalel et al., 1996a,b,c). The absence of these microbial groups and light may, perhaps, explain the persistence of ConAC in the marine environment where it has been found to be the oldest component of marine DOM (radiocarbon ages of approximately 18,000 ± 3,000 years bp, Ziolkowski and Druffel, 2010; Stubbins et al., 2012). As a long-lived C sink, further investigation of the source and fate of long-lived marine ConAC compounds is needed, especially since non-thermogenic processes can also produce ConAC (Chen et al., 2014).

## CONCLUSIONS

By analyzing the leachates of a series of pyrogenic solids generated from both hardwood and grass feedstock with systematic increases in pyrolysis temperature, this study improves our understanding of pyDOM composition and the BPCA method commonly used to quantify pyDOC. The finding that pyrogenic materials are diverse in composition and solubility and that a large portion of pyDOC is non-condensed has implications for pyDOC as it is currently quantified. Pyrogenic OM was shown in this study to be compositionally diverse, dissimilar to its parent pyrogenic solid, and more than half of pyDOC was non-condensed aromatic C. Because of this, we recommend that researchers using the BPCA method state explicitly that they are quantifying ConAC and not pyDOC in their future studies to minimize confusion.

A further implication is that inferences as to pyC source drawn from pyDOM chemical composition may be made only with extreme caution. The solubility of pyC is controlled by parent solid O-containing functional group content and degree of aromatic condensation but is also likely to be highly altered by photolytic, enzymatic, and sorptive processes during mobilization. Future work should examine the effects of these processes on pyDOM mobility and composition as well as the initial solubilization of pyC. The ultimate goal would be to balance the global pyC cycle (**Figure 8**) so that the role of fire and human influence on it (i.e., whether through climate change or intentional pyC production and soil amendment) can be fully understood and incorporated into global C cycling models. Before global-scale inferences can be made about the cycling of pyC, it is important to establish a fundamental understanding of the yield and character of soluble components produced by different pyrogenic materials.

## AUTHOR CONTRIBUTIONS

KB and AZ conducted all biochar manufacturing, leaching, DOC analyses, and BPCA analyses. $^{13}$C-NMR and $^{1}$H-NMR analyses were conducted by AW and PH. All authors listed have made a substantial, direct, and intellectual contribution to the current work, and approved it for this publication.

## FUNDING

This work was funded by the U.S. National Science Foundation - Geobiology and Low-Temperature Geochemistry Program (EAR-1451367). Publication of this article was funded in part by the University of Florida Open Access Publishing Fund.

## ACKNOWLEDGMENTS

We thank Dr. Jason Curtis for his help with elemental analyses. Additionally, we thank the UF Geological Science department engineer Dow Van Arnam for helping with construction and maintenance of laboratory apparatus. Alex Goranov and Jim Hall assisted with NMR measurements.

## SUPPLEMENTARY MATERIAL

The Supplementary Material for this article can be found online at: https://www.frontiersin.org/articles/10.3389/feart.2018.00043/full#supplementary-material

## REFERENCES

Abiven, S., Hengartner, P., Schneider, M. P. W., Singh, N., and Schmidt, M. W. I. (2011). Pyrogenic carbon soluble fraction is larger and more aromatic in aged charcoal than in fresh charcoal. *Soil Biol. Biochem.* 43, 1615–1617. doi: 10.1016/j.soilbio.2011.03.027

Baldock, J. A., and Smernik, R. J. (2002). Chemical composition and bioavailability of thermally, altered *Pinus resinosa* (Red Pine) wood. *Org. Geochem.* 33, 1093–1109. doi: 10.1016/S0146-6380(02)00062-1

Bezalel, L., Hadar, Y., and Cerniglia, C. E. (1996a). Mineralization of polycyclic aromatic hydrocarbons by the white rot fungus *Pleurotus ostreatus*. *Appl. Environ. Microbiol.* 62, 292–295.

Bezalel, L., Hadar, Y., Fu, P. P., Freeman, J. P., and Cerniglia, C. E. (1996b). Initial oxidation products in the metabolism of pyrene, anthracene, fluorene, and dibenzothiophene by the white rot fungus *Pleurotus ostreatus*. *Appl. Environ. Microbiol.* 62, 2554–2559.

Bezalel, L., Hadar, Y., Fu, P. P., Freeman, J. P., and Cerniglia, C. E. (1996c). Metabolism of phenanthrene by the white rot fungus *Pleurotus ostreatus*. *Appl. Environ. Microbiol.* 62, 2547–2553.

Bird, M. I., Moyo, C., Veenendaal, E. M., Lloyd, J., and Frost, P. (1999). Stability of elemental carbon in a savanna soil. *Global Biogeochem. Cycles* 13, 923–932. doi: 10.1029/1999GB900067

Bird, M. I., Wynn, J. G., Saiz, G., Wurster, C. M., and McBeath, A. (2015). The pyrogenic carbon cycle. *Annu. Rev. Earth Planet. Sci.* 43, 273–298. doi: 10.1146/annurev-earth-060614-105038

Bowman, D. M., Balch, J. K., Artaxo, P., Bond, W. J., Carlson, J. M., and Cochrane, M. A. (2009). Fire in the Earth system. *Science* 324, 481–484. doi: 10.1126/science.1163886

Brodowski, S., Rodionov, A., Haumaier, L., Glaser, B., and Amelung, W. (2005). Revised black carbon assessment using benzene polycarboxylic acids. Org. Geochem. 36, 1299–1310. doi: 10.1016/j.orggeochem.2005.03.011

Cao, X., Pignatello, J. J., Li, Y., Lattao, C., Chappell, M. A., Chen, N., et al. (2012). Characterization of wood chars produced at different temperatures using advanced solid-state 13C NMR spectroscopic techniques. *Energy Fuels* 26, 5983–5991. doi: 10.1021/ef300947s

Cerniglia, C. E., and Heitkamp, M. A. (1990). Polycyclic aromatic hydrocarbon degradation by mycobacterium. *Methods Enzymol.* 188, 148–153. doi: 10.1016/0076-6879(90)88027-8

Chen, H. M., Abdulla, H. A. N., Sanders, R. L., Myneni, S. C. B., Mopper, K., and Hatcher, P. G. (2014). Production of black carbon-like and aliphatic molecules from terrestrial dissolved organic matter in the presence of sunlight and iron. *Environ. Sci. Technol. Lett.* 1, 399–404. doi: 10.1021/ez5002598

Cusack, D. F., Chadwick, O. A., Hockaday, W. C., and Vitousek, P. M. (2012). Mineralogical controls on soil black carbon preservation. *Global Biogeochem. Cycles* 26, 1–10. doi: 10.1029/2011GB004109

Czimczik, C. I., Preston, C. M., Schmidt, M. W. I., Werner, R. A., and Schulze, E.-D. (2002). Effects of charring on mass, organic carbon, and stable carbon isotopic composition of wood. *Org. Geochem.* 33, 1207–1223. doi: 10.1016/S0146-6380(02)00137-7

Decesari, S., Mircea, M., Cavalli, F., Fuzzi, S., Moretti, F., Tagliavini, E., et al. (2007). Source attribution of water-soluble organic aerosol by nuclear magnetic resonance spectroscopy. *Environ. Sci. Technol.* 41, 2479–2484. doi: 10.1021/es061711l

Ding, Y., Cawley, K. M., da Cunha, C. N., and Jaffe, R. (2014). Environmental dynamics of dissolved black carbon in wetlands. *Biogeochemistry* 119, 259–273. doi: 10.1007/s10533-014-9964-3

Ding, Y., Yamashita, Y., Dodds, W. K., and Jaffé, R. (2013). Dissolved black carbon in grassland streams: is there an effect of recent fire history? *Chemosphere* 90, 2557–2562. doi: 10.1016/j.chemosphere.2012.10.098

Dittmar, T. (2008). The molecular level determination of black carbon in marine dissolved organic matter. *Org. Geochem.* 39, 396–407. doi: 10.1016/j.orggeochem.2008.01.015

Dittmar, T., de Rezende, C. E., Manecki, M., Niggemann, J., Ovalle, A. R. C., Stubbins, A., et al. (2012a). Continuous flux of dissolved black carbon from a vanished tropical forest biome. *Nat. Geosci.* 5, 618–622. doi: 10.1038/ngeo1541

Dittmar, T., Koch, B., Hertkorn, N., and Kattner, G. (2008). A simple and efficient method for the solid-phase extraction of dissolved organic matter (SPE-DOM) from seawater. *Limnol. Oceanogr. Methods* 6, 230–235. doi: 10.4319/lom.2008.6.230

Dittmar, T., Paeng, J., Gihring, T. M., Suryaputra, I., and Huettel, M. (2012b). Discharge of dissolved black carbon from a fire-affected intertidal system. *Limnol. Oceanogr.* 57, 1171–1181. doi: 10.4319/lo.2012.57.4.1171

Eswaran, H., Van Den Berg, E., and Reich, P. (1993). Organic carbon in soils of the World. *Soil Sci. Soc. Am. J.* 57, 192–194. doi: 10.2136/sssaj1993.03615995005700010034x

Fasnacht, M. P., and Blough, N. V. (2002). Aqueous photodegradation of polycyclic aromatic hydrocarbons. *Environ. Sci. Technol.* 36, 4364–4369. doi: 10.1021/es025603k

Field, J. A., de Jong, E., Feijoo Costa, G., and de Bont, J. A. M. (1992). Biodegradation of polycyclic aromatic hydrocarbons by new isolated of white-rot fungi. *Appl. Environ. Microbiol.* 58, 2219–2226.

Forbes, M. S., Raison, R. J., and Skjemstad, J. O. (2006). Formation, transformation and transport of black carbon (charcoal) in terrestrial and aquatic ecosystems. *Sci. Total Environ.* 370, 190–206. doi: 10.1016/j.scitotenv.2006.06.007

Glaser, B., Haumaier, L., Guggenberger, G., and Zech, W., (1998). Black carbon in soils: the use of benzenecarboxylic acid as specific markers. *Organ. Geochem.* 29, 811–819. doi: 10.1016/S0146-6380(98)00194-6

Haemmerli, S. D., Leisola, M. S., Sanglard, D., and Fiechter, A. (1986). Oxidation Of Benzo(A)Pyrene by extracellular ligninases OF phanerochaete-chrysosporium - veratryl alcohol and stability of ligninase. *J. Biol. Chem.* 261, 6900–6903.

Hammes, K., Schmidt, M. W. I., Smernik, R. J., Currie, L. A., Ball, W. P., Nguyen, T. H., et al. (2007). Comparison of quantification methods to measure fire-derived (black/elemental) carbon in soils and sediments using reference materials from soil, water, sediment and the atmosphere. *Global Biogeochem. Cycles* 21, 1–18. doi: 10.1029/2006GB002914

Hammes, K., Smernik, R., Skjemstad, J., Herzog, A., Vogt, U., Schmidt, M., et al. (2006). Synthesis and characterisation of laboratory-charred grass straw (*Oryza saliva*) and chestnut wood (*Castanea sativa*) as reference materials for black carbon quantification. *Org. Geochem.* 37, 1629–1633. doi: 10.1016/j.orggeochem.2006.07.003

Hansen, E. H., and Schnitzer, M. (1967). The alkaline permanganate oxidation of Danish illuvial organic matter. *Soil Sci. Soc. Am. J.* 30, 745–748. doi: 10.2136/sssaj1966.03615995003000060025x

Hedges, J. I., Keil, R. G., and Benner, R. (1997). What happens to terrestrial organic matter in the ocean? *Org. Geochem.* 27, 195–212. doi: 10.1016/S0146-6380(97)00066-1

Hockaday, W. C., Grannas, A. M., Kim, S., and Hatcher, P. G. (2006). Direct molecular evidence for the degradation and mobility of black carbon in soils from ultrahigh-resolution mass spectral analysis of dissolved organic matter from a fire-impacted forest soil. *Org. Geochem.* 37, 501–510. doi: 10.1016/j.orggeochem.2005.11.003

Hockaday, W. C., Grannas, A. M., Kim, S., and Hatcher, P. G. (2007). The transformation and mobility of charcoal in a fire-impacted watershed. *Geochim. Cosmochim. Acta* 71, 3432–3445. doi: 10.1016/j.gca.2007.02.023

Jaffé, R., Ding, Y., Niggemann, J., Vähätalo, A. V., Stubbins, A., Spencer, R. G., et al. (2013). Global charcoal mobilization from soils via dissolution and riverine transport to the oceans. *Science* 340, 345–347. doi: 10.1126/science.1231476

Johnson, R. L., and Schmidt-Rohr, K. (2014). Quantitative solid-state C-13 NMR with signal enhancement by multiple cross polarization. *J. Magn. Reson.* 239, 44–49. doi: 10.1016/j.jmr.2013.11.009

Kalbitz, K., Schmerwitz, J., Schwesig, D., and Matzner, E. (2003). Biodegradation of soil-derived dissolved organic matter as related to its properties. *Geoderma* 113, 273–291. doi: 10.1016/S0016-7061(02)00365-8

Kappenberg, A., Blaesing, M., Lehndorff, E., and Amelung, W. (2016). Black carbon assessment using benzene polycarboxylic acids, limitations for organic-rich matrices. *Org. Geochem.* 94, 47–51. doi: 10.1016/j.orggeochem.2016.01.009

Karich, A., Ullrich, R., Scheibner, K., and Hofrichter, M. (2017). Fungal unspecific peroxygenases oxidize the majority of organic EPA priority pollutants. *Front. Microbiol.* 8:1463. doi: 10.3389/fmicb.2017.01463

Kim, K. H., Kim, J. Y., Cho, T. S., and Choi, J. W. (2012). Influence of pyrolysis temperature on physicochemical properties of biochar obtained from the fast pyrolysis of pitch pine (*Pinus rigida*). *Bioresour. Technol.* 118, 158–162. doi: 10.1016/j.biortech.2012.04.094

Koch, B. P., and Dittmar, T. (2006). From mass to structure: an aromaticity index for high-resolution mass data of natural organic matter. *Rapid Commun. Mass Spectrom.* 20, 926–932. doi: 10.1002/rcm.2386

Kuhlbusch, T., and Crutzen, P. (1996). "Chapter 16: black carbon, the global carbon cycle, and atmospheric carbon dioxide," in *Biomass Burning and Global Change*, ed J. Levine (Cambridge, MA: The MIT Press), 160–169.

Li, X. M., Shen, Q., Zhang, D., Mei, X., Ran, W., Xu, Y., et al. (2013). Functional groups determine biochar properties (pH and EC) as studied by two-dimensional C-13 NMR correlation spectroscopy. *PLoS ONE* 8:e65949. doi: 10.1371/journal.pone.0065949

Masiello, C. A. (2004). New directions in black carbon organic geochemistry. *Mar. Chem.* 92, 201–213. doi: 10.1016/j.marchem.2004.06.043

McBeath, A. V., Smernik, R. J., Krull, E. S., and Lehmann, J. (2014). The influence of feedstock and production temperature on biochar carbon chemistry: a solid-state C-13 NMR study. *Biomass Bioenergy* 60, 121–129. doi: 10.1016/j.biombioe.2013.11.002

McBeath, A. V., Smernik, R. J., Schneider, M. P. W., Schmidt, M. W. I., and Plant, E. L. (2011). Determination of the aromaticity and the degree of aromatic condensation of a thermosequence of wood charcoal using NMR. *Org. Geochem.* 42, 1194–1202. doi: 10.1016/j.orggeochem.2011.08.008

Mukherjee, A., and Zimmerman, A. R. (2013). Organic carbon and nutrient release from a range of laboratory-produced biochars and biochar-soil mixtures. *Geoderma* 193, 122–130. doi: 10.1016/j.geoderma.2012.10.002

Mukherjee, A., Zimmerman, A. R., and Harris, W. (2011). Surface chemistry variations among a series of laboratory-produced biochars. *Geoderma* 163, 247–255. doi: 10.1016/j.geoderma.2011.04.021

Nakane, M., Ajioka, T., and Yamashita1, Y. (2017). Distribution and sources of dissolved black carbon in surface waters of the Chukchi Sea, Bering Sea, and the North Pacific Ocean. *Front. Earth Sci.* 5:34. doi: 10.3389/feart.2017.00034

Podgorski, D. C., Hamdan, R., McKenna, A. M., Nyadong, L., Rodgers, R. P., Marshall, A. G., et al. (2012). Characterization of pyrogenic black carbon by desorption atmospheric pressure photoionization fourier transform ion cyclotron resonance mass spectrometry. *Anal. Chem.* 84, 1281–1287. doi: 10.1021/ac202166x

Reisser, M., Purves, R. S., Schmidt, M. W. I., and Abiven, S. (2016). Pyrogenic Carbon in soils: a literature-based inventory and a global estimation of its content in soil organic carbon and stocks. *Front. Earth Sci.* 4:80. doi: 10.3389/feart.2016.00080

Roebuck, J. A., Podgorksi, D. C., Wagner, S., and Jaffe, R. (2017). Photodissolution of charcoal and fire-impacted soil as a potential source of dissolved

black carbon in aquatic environments. *Org. Geochem.* 112, 16–21. doi: 10.1016/j.orggeochem.2017.06.018

Saeed, T., Ali, L. N., Al-Bloushi, A., Al-Hashash, H., Al-Bahloul, M., Al-Khabbaz, A., et al. (2011). Effect of environmental factors on photodegradation of polycyclic aromatic hydrocarbons (PAHs) in the water-soluble fraction of Kuwait crude oil in seawater. *Mar. Environ. Res.* 72, 143–150. doi: 10.1016/j.marenvres.2011.07.004

Santin, C., Doerr, S. H., Preston, C. M., and Gonzalez-Rodriguez, G. (2015). Pyrogenic organic matter production from wildfires: a missing sink in the global carbon cycle. *Glob. Chang. Biol.* 21, 1621–1633. doi: 10.1111/gcb.12800

Schneider, M. P. W., Hilf, M., Vogt, U. F., and Schmidt, M. W. I. (2010). The benzene polycarboxylic acid (BPCA) pattern of wood pyrolyzed between 200°C and 1000°C. *Org. Geochem.* 41, 1082–1088. doi: 10.1016/j.orggeochem.2010.07.001

Schneider, M. P. W., Pyle, L. A., Clark, K. L., Hockaday, W. C., Masiello, C. A., and Schmidt, M. W. I. (2013). Toward a "molecular thermometer" to estimate the charring temperature of wild land charcoals derived from different biomass sources. *Environ. Sci. Technol.* 47, 11490–11495. doi: 10.1021/es401430f

Schneider, M. P. W., Smittenberg, R. H., Dittmar, T., and Schmidt, M. W. I. (2009). Analysis of black carbon molecular markers by two chromatographic methods (GC-FID and HPLC-DAD). *Geochim. Cosmochim. Acta* 73, A1181.

Schneider, M. P. W., Smittenberg, R. H., Dittmar, T., and Schmidt, M. W. I. (2011). Comparison of gas with liquid chromatography for the determination of benzenepolycarboxylic acids as molecular tracers of black carbon. *Org. Geochem.* 42, 275–282. doi: 10.1016/j.orggeochem.2011.01.003

Spokas, K. A., Cantrell, K. B., Novak, J. M., Archer, D. W., Ippolito, J. A., Collins, H. P., et al. (2012). Biochar: a synthesis of its agronomic impact beyond carbon sequestration. *J. Environ. Qual.* 41, 973–989. doi: 10.2134/jeq2011.0069

Stevenson, F. J. (1994). *Humus Chemistry: Genesis, Composition, Reactions*. New York, NY: John Wiley & Sons.

Stubbins, A., Niggemann, J., and Dittmar, T. (2012). Photo-lability of deep ocean dissolved black carbon. *Biogeosciences* 9, 1661–1670. doi: 10.5194/bg-9-1661-2012

Wagner, S., Ding, Y., and Jaffé, R. (2017). A new perspective on the apparent solubility of dissolved black carbon. *Front. Earth Sci.* 5:75. doi: 10.3389/feart.2017.00075

Ward, C. P., Sleighter, R. L., Hatcher, P. G., and Cory, R. M. (2014). Insights into the complete and partial photooxidation of black carbon in surface waters. *Environ. Sci. Process. Impacts* 16, 721–731. doi: 10.1039/C3EM00597F

Willoughby, A. S., Wozniak, A. S., and Hatcher, P. G. (2016). Detailed source-specific molecular composition of ambient aerosol organic matter using ultrahigh resolution mass spectrometry and H-1 NMR. *Atmosphere* 7, 24. doi: 10.3390/atmos7060079

Wolf, M., Lehndorff, E., Wiesenberg, G. L. B., Stockhausen, M., Schwark, L., and Amelung, W. (2013). Towards reconstruction of past fire regimes from geochemical analysis of charcoal. *Org. Geochem.* 55, 11–21. doi: 10.1016/j.orggeochem.2012.11.002

Wozniak, A. S., Shelley, R. U., Sleighter, R. L., Abdulla, H. A.N., Morton, P. L., Landing, W. M., et al. (2013). Relationships among aerosol water soluble organic matter, iron and aluminum in European, North African, and Marine air masses from the 2010 US GEOTRACES cruise. *Mar. Chem.* 154, 24–33. doi: 10.1016/j.marchem.2013.04.011

Zimmerman, A. (2010). Abiotic and microbial oxidation of laboratory-produced black carbon (biochar). *Environ. Sci. Technol.* 44, 1295–1301. doi: 10.1021/es903140c

Zimmerman, A. R., and Gao, B. (2013). "The stability of biochar in the environment," in *Biochar and Soil Biota*, eds N. Ladygina and F. Rineau (Boca Raton, FL: CRC Press; A Taylor and Francis Group Co.).

Zimmerman, A. R., and Mitra, S. (2017). Trial by fire: on the terminology and methods used in pyrogenic organic carbon research. *Front. Earth Sci.* 5:95.doi: 10.3389/feart.2017.00095

Ziolkowski, L. A., Chamberlin, A. R., Greaves, J., and Druffel, E. R. M. (2011). Quantification of black carbon in marine systems using the benzene polycarboxylic acid method: a mechanistic and yield study. *Limnol. Oceanogr. Methods* 9, 140–149. doi: 10.4319/lom.2011.9.140

Ziolkowski, L. A., and Druffel, E. R. M. (2009). The feasibility of isolation and detection of fullerenes and carbon nanotubes using the benzene polycarboxylic acid method. *Mar. Pollut. Bull.* 59, 213–218. doi: 10.1016/j.marpolbul.2009.04.018

Ziolkowski, L. A., and Druffel, E. R. M. (2010). Aged black carbon identified in marine dissolved organic carbon. *Geophys. Res. Lett.* 37. doi: 10.1029/2010GL043963

**Conflict of Interest Statement:** The authors declare that the research was conducted in the absence of any commercial or financial relationships that could be construed as a potential conflict of interest.

frontiers in Earth Science

ORIGINAL RESEARCH
published: 16 October 2017
doi: 10.3389/feart.2017.00080

# Impact of a Historical Fire Event on Pyrogenic Carbon Stocks and Dissolved Pyrogenic Carbon in Spodosols in Northern Michigan

*Fernanda Santos[1*†], Sasha Wagner[2†], David Rothstein[1], Rudolf Jaffe[2] and Jessica R. Miesel[1]*

[1] Department of Forestry, Michigan State University, East Lansing, MI, United States, [2] Department of Chemistry and Biochemistry, Southeast Environmental Research Center, Florida International University, North Miami, FL, United States

OPEN ACCESS

**Edited by:**
*Cristina Santin,*
*Swansea University, United Kingdom*

**Reviewed by:**
*Youhei Yamashita,*
*Hokkaido University, Japan*
*Derrick Y. F. Lai,*
*The Chinese University of Hong Kong, Hong Kong*

***Correspondence:**
*Fernanda Santos*
*fsantos.soils@gmail.com*

**†Present Address:**
*Fernanda Santos, School of Natural Sciences, University of California-Merced, Merced, CA, United States*
*Sasha Wagner, Marine Sciences Department, Skidaway Institute of Oceanography, University of Georgia, Savannah, GA, United States*

**Specialty section:**
*This article was submitted to Biogeoscience, a section of the journal Frontiers in Earth Science*

**Received:** *29 May 2017*
**Accepted:** *29 September 2017*
**Published:** *16 October 2017*

**Citation:**
*Santos F, Wagner S, Rothstein D, Jaffe R and Miesel JR (2017) Impact of a Historical Fire Event on Pyrogenic Carbon Stocks and Dissolved Pyrogenic Carbon in Spodosols in Northern Michigan. Front. Earth Sci. 5:80. doi: 10.3389/feart.2017.00080*

Inventories of fire-derived (pyrogenic) C (PyC) stocks in soils remain incomplete for many parts of the world, yet are critical to reduce uncertainties in global PyC estimates. Additionally, PyC dynamics in soils remain poorly understood. For example, dissolved PyC (DPyC) fluxes from soil horizons, as well as the influence of historical fire events on these fluxes and soil PyC stocks remain poorly quantified. In this study, we examined stock and concentration differences in soil PyC and leached DPyC, respectively, between two forest types in the Great Lakes region (USA): (1) a red pine (*Pinus resinosa*) forest planted after the site had experienced post-logging slash burning in the late nineteenth century (100 year-burned site), and (2) a sugar maple (*Acer saccharum*) forest that showed no evidence of burning in the past 250 years (unburned site). We hypothesized that the 100 year-burned site would have greater PyC stocks and concentrations of DPyC compared to the unburned site. We measured PyC in soil, as well as DPyC in soil water leaching from O and E horizons following a spring snowmelt event in both 100 year-burned and unburned sites. Additionally, we measured DPyC drained from B horizons in 100 year-burned site. In organic horizons, PyC stocks were 1.8 (Oi) and 2.3 (Oe) times greater in the 100 year-burned site than in the unburned site. Contrary to our initial hypothesis, DPyC concentrations did not differ between sites. On average, DPyC leached from all sites contributed 3.11 $\pm$ 0.27% of the total dissolved organic carbon pool. In the 100 year-burned site, a significant decline in concentrations of DPyC leaving the B horizon was attributed to the immobilization of this C pool in the Al and Fe oxides-rich subsoil. Even though PyC stock in O horizons was higher in 100 year-burned than in unburned site, our results did not support our initial hypothesis that the 100 year-burned site would have greater DPyC concentrations than the unburned site, suggesting that any differences in DPyC resulting from a single fire event are either not detectable after >100 years post-burn, and/or that the release of DPyC is a continuous, long-term process resulting from the degradation of historically accumulated PyC.

**Keywords: dissolved pyrogenic carbon, pyrogenic carbon stock, carbon leaching, spodosols, historical fire, Michigan, temperate forest**

## INTRODUCTION

Pyrogenic carbon (PyC) is a thermally-altered form of organic carbon (C) produced during fires (Goldberg, 1985; Bird et al., 2015). Interest in understanding the importance of PyC to the global soil C dynamics has increased in part because PyC is thought to contribute to long-term C sequestration in soils, owed to its apparent stability in soils on decades to millennial residence time scales (Santos et al., 2012; Singh et al., 2012; Fang et al., 2014). Global storage of soil PyC has been estimated at 200 Pg (uppermost 2 m), with PyC accounting for up to 60% of soil organic C worldwide (Forbes et al., 2006; Reisser et al., 2016). Limited data on PyC stocks and dynamics in many ecosystems and subsoil horizons, however, still hinder a better understanding of PyC stabilization processes and accurate estimations of the global PyC budget. Despite the apparent stability of PyC in soils, there is growing evidence that a fraction of PyC is subjected to redistribution in the landscape and lost from soils via erosion (Rumpel et al., 2006, 2009; Boot et al., 2015; Güereña et al., 2015; Cotrufo et al., 2016) and can be vertically transported to lower soil depths via translocation (Dai et al., 2005; Leifeld et al., 2007) and leaching (Hockaday et al., 2006, 2007; Major et al., 2010). This suggests that PyC is much more dynamic in soils than previously thought. For example, large fluxes of dissolved PyC (DPyC, $<0.7\,\mu m$ particle size) in a tropical river were reported to increase during heavy rain and derive from charcoal remaining in surface soils from historical fires rather than from recent burning (Marques et al., 2017). Thus, quantifying the relative impact of historical fires on PyC stocks and export from soils is essential to understand the impact of fires on PyC stabilization in and mobilization mechanisms from soils.

Although much of the existing soil PyC stocks data reported in the literature is restricted to the uppermost 30 cm depth (Bird et al., 2015), a significant proportion of PyC could be stored below 30 cm depth (subsoils) in forest ecosystems. Subsoils have been reported to store up to 63% of the total C stored in soils worldwide (Batjes, 1996; Jobbagy and Jackson, 2000), but only few studies have reported PyC stocks in lower soil horizons of fire-impacted forest ecosystems (Czimczik et al., 2005; Soucémarianadin et al., 2014; Jauss et al., 2017; Koele et al., 2017). For example, in a Canadian boreal forest, 12–46% of the total PyC stock in podzols was found in the entire mineral horizon (Ae, Bf, Bfc, BC, and C) (Soucémarianadin et al., 2014). In a study conducted in a boreal forest in Siberia, on the other hand, PyC in mineral soils (depth >1 m) contributed very little (<1%) to the total stocks in podzols (Czimczik et al., 2005). In a recent inventory of PyC in Amazon basin forest soils, 50% of PyC in the soil profile was measured at depths ranging from 44 to 71 cm (Koele et al., 2017). Incomplete available datasets on PyC pools for the entire soil profile limit accurate estimations of the global PyC budget and the assessment of how fire impacts PyC storage in deep soils.

PyC loss from soils via leaching is one of the major gaps in PyC research (Bird et al., 2015; Santín et al., 2016), limiting our understanding of PyC transport pathways across ecosystems and the role of PyC in the global C cycle (Santín et al., 2016). In aquatic systems, DPyC is typically reported as a measure of dissolved poly-condensed aromatic C (Dittmar, 2008) and has been shown to correlate with dissolved organic carbon (DOC) (Ding et al., 2013, 2014; Jaffé et al., 2013; Güereña et al., 2015). Few studies have examined the export pathways for the transport of DPyC from terrestrial to aquatic ecosystems (Güereña et al., 2015; Cotrufo et al., 2016; Marques et al., 2017). While a study conducted in mixed tropical highland forest and agricultural catchments dominated by Nitisols showed that subsurface transport was more important than erosion in driving the movement of DPyC from soils to streams (Güereña et al., 2015), a study conducted in a savanna Oxisol showed that leaching accounted for less than 1% of the annual DPyC losses (detected based on $^{13}C$ stable isotope approaches) one and two years after the addition of charcoal to tropical soil (Major et al., 2010). No study, however, has reported fluxes of DPyC from organic and mineral soil horizons in temperate ecosystems, limiting our understanding of PyC contribution to C stabilization in subsoils and mobilization of DPyC to aquatic systems. Moreover, the role of historical fire events in controlling the fluxes of terrestrially-derived DPyC to aquatic ecosystems remains unclear. Accurate estimations of DPyC fluxes from soils and a clearer picture of the role of historical fires in driving these fluxes are essential to understand PyC dynamics in soils, and to predict the impact of fires on PyC export from soils to aquatic systems.

Although it would be plausible to expect that recent fires would be the major factor driving the export of DPyC from land to aquatic systems, recent studies do not support this hypothesis (Dittmar et al., 2012; Ding et al., 2013; Myers-Pigg et al., 2015; Wagner et al., 2015). For example, there was no correlation between DPyC concentrations in streams and fire frequency in the grassland ecosystem watersheds in Kansas (Ding et al., 2013). In another study, DPyC fluxes in burned watersheds were not greater than those in unburned sites when measured 1 year after a wildfire event in Colorado (Wagner et al., 2015). The difficulty in linking DPyC with fire events in watersheds suggests that other variables interact to drive the transport of DPyC from soils to fluvial systems, including fire characteristics (i.e., size, severity, and intensity), soil physical and chemical properties, landscape geomorphology, ecosystem type, the time elapsed since the fire event, and hydrology (Cotrufo et al., 2016; Reisser et al., 2016). Despite evidence for the uncoupled relationship between DPyC in rivers and forest fires, no study has yet investigated the direct impact of a single fire event on DPyC leached from different soil horizons in temperate forest ecosystems.

The concentration of DPyC in soil solution percolating through the soil system could be influenced by the amount of PyC stored in organic horizons and formation of chemical associations with reactive minerals in subsoils. In forest soils, organic horizons are the major source of DOC moving downward to lower soil depths, where part of the DOC pool can be retained due to its chemical associations with mineral surfaces (Kaiser and Guggenberger, 2000; Kalbitz et al., 2000; Kleber et al., 2015). Whether PyC stocks in topsoil (above 30 cm depth) influences DPyC concentrations in forest soils impacted by a historic fire remains largely unknown, but could provide insights

on the mechanisms driving the vertical downward mobilization of DPyC.

Here, we investigated how a historical fire in the Upper Peninsula of Michigan (USA) influenced stocks of PyC and its downward movement through the soil profile as DPyC. In this study, we report PyC stocks in the area of the Upper Peninsula of Michigan that either burned, or did not burn, in the extensive post-logging fires associated with Euro-American settlement of this region in the late nineteenth century (Whitney, 1987). Additionally, we explored the relative importance of charcoal stocks on the fluxes of DPyC leached from soils by taking advantage of the experimental sites mentioned above. These site characteristics present unique opportunities to: (1) quantify the stocks of PyC, as well as concentrations of DPyC leached through different soil horizons and (2) determine whether soils with a charcoal layer >100 years old would (a) result in higher PyC stocks in both organic and mineral soils; and (b) release more DPyC into soil leachates than forest soils that had not burned for at least the past 250 years. We hypothesized that PyC stocks and DPyC concentrations would be greater in sites with a history of more recent fire (hereafter referred to as 100 year-burned sites), compared to sites that have remained unburned for at least two centuries (hereafter referred to as unburned sites).

# MATERIALS AND METHODS

## Field Sites and Experimental Design

Our study was located in the eastern Upper Peninsula of Michigan (USA, 46°19′N, 85°02′W, **Figure 1A**), in adjacent areas representing two contrasting forest cover types: red pine (*Pinus resinosa*) forests planted in the 1930s, and naturally regenerated (i.e., unplanted) sugar-maple (*Acer saccharum)* forests. The study area has been described in detail by Schaetzl and Rothstein (2016). General Land Office (GLO) survey data from 1850 show that pre-settlement vegetation of all our study sites consisted of mature beech (*Fagus grandifolia*)—sugar maple—hemlock (*Tsuga canadensis*) forest, which was harvested during the late nineteenth to early twentieth century (Comer et al., 1995). GLO survey records of the same area from 1938, together with the presence of a distinct charcoal layer (<0.5 cm thick) in the red pine forest sites, clearly indicate that areas planted to red pine in the 1930s experienced severe slash fires during the logging era, prior to the establishment of the red pine plantations. In contrast, there is no visible charcoal in the sugar maple sites, and no indication of burning in the GLO records for at least the past 250 years. Thus, we highlight that these two different forest types (planted and unplanted) developed *after* the time of these major disturbances. Three distinct stands were selected for each forest type. In this paper, we refer to red pine and sugar maple sites as "100 year-burned" and "unburned," respectively. The sites are characterized by a mean annual temperature and precipitation of 4.7°C and 812 mm, respectively. The soils are strongly developed, well-drained spodosols, developed on deep outwash sands and classified as sandy, isotic, frigid Typic Haplorthods (Schaetzl et al., 2015; Schaetzl and Rothstein, 2016). Pictures of the vertical soil profiles typically found in the sites are shown in **Figures 1B,C**.

## PyC Measurements

### PyC in Organic and Mineral Soils

Zero-tension lysimeters (ZTLs) were installed underneath each soil horizon (O, E, and B), as described in Schaetzl and Rothstein (2016). Organic (Oi and Oe) and mineral (E and B) soil horizons overlying the ZTLs were sampled from nine pits per forest type, totaling 18 pits. Organic horizons were collected within a 930 $cm^2$ diameter sampling frame. All soil samples were air-dried, and mineral soils were sieved to 2-mm particle-size. Prior to analyses, samples were dried to constant mass at 60°C and ball milled. Total C content was determined by dry combustion using an elemental analyzer (Costech Analytical Technologies, Inc., Valencia, CA).

To examine changes in PyC stocks in soils with depth, PyC in soil horizons overlying and underneath the ZTLs was measured using a thermo-chemical digestion method (Kurth, MacKenzie and DeLuca, KMD) described by Kurth et al. (2006) and later modified for organic samples (Maestrini and Miesel, 2016). Briefly, 1 g of soil along with 10 mL of 1 M nitric acid and 20 mL of 30% hydrogen peroxide were added to glass tubes and digested in an aluminum block heater at 100°C for 16 h. For organic samples, pulverized quartz sand was mixed with the sample to achieve a 10% mass ratio (Maestrini and Miesel, 2016). After the digestion, the samples were cooled and vacuum-filtered through glass funnels lined with pre-weighed Whatman filter paper (grade 2) to recover the post-digested fine soil material. Filters with digested materials were dried at 60°C for 24 h and weighed to determine dry mass. The digested materials were separated from the filters and re-homogenized prior to analyzing for total C by dry combustion. PyC was assumed to comprise the total OC in the digested material, although we acknowledge that the KMD method can overestimate PyC in non-pyrolyzed organic samples by ∼5% (Maestrini and Miesel, 2016). We used PyC concentration (Table S1), litter mass, and sampling area data to calculate PyC stocks (g $m^{-2}$) in the O horizon. In the unburned site, one of the Oe horizons was not measured for PyC (missing sample). Additionally, in most cases PyC in BC horizons was not reported due to low C detection. To calculate stocks (g PyC $m^{-2}$) in the mineral horizon, we used PyC concentration, bulk density, and thickness of the soil horizon. In the 100 year-burned site, one sample from the E horizon was identified as an outlier and removed from the analysis. Because lysimeters were specifically placed underneath the upper B horizon, we report soil PyC stocks for both upper and lower B horizons in the two sites.

To provide information on the quality of PyC in Oi and Oe horizons, which we assume to be the main sources of DPyC entering in the soil system, we limited our sample size to three pits per forest type (totaling 6 pits). We used benzene polycarboxylic acids (BPCAs) as specific markers for PyC as described by Wiedemeier et al. (2013), and used the equivalent of 0.5 mg OC per sample as recommended by Kappenberg et al. (2016). Briefly, the ball-milled sample was digested at 170°C under pressure for 8 h in 70% nitric acid. The digested solution was filtered and phthalic acid was added to the solution as an internal check standard. The filtrate was cleaned in cation exchange resins, freeze-dried and subsequently redissolved in HPLC-grade water. These clean-up steps are required to remove

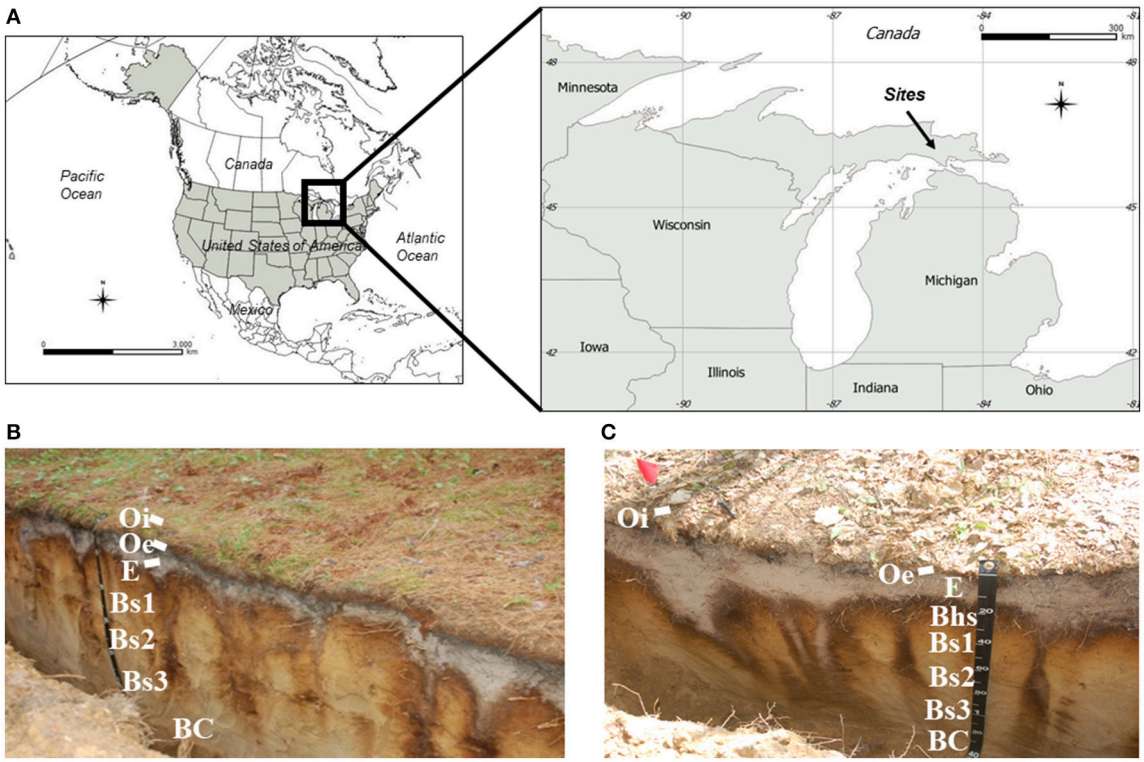


**FIGURE 1 |** Map showing the location of the sites in the eastern Upper Peninsula of Michigan (USA), **(A)** and schematic figures of soil vertical profiles typically found in 100-year burned **(B)** and unburned sites **(C)**. Spodic horizons: Bs, sesquioxides of Al and Fe; and Bhs, mixture of Bs and Bh (organic matter accumulation).

metals and other interfering compounds from soil-derived BPCAs prior to analysis (Wiedemeier et al., 2013). The cation exchange procedure results in very small losses of BPCAs which do not impact overall data trends (Wiedemeier et al., 2013). Individual BPCAs were separated from the redissolved solution using a reversed stationary phase column using standard gradient conditions and quantified using multiple-point calibration with external standard solutions of BPCAs. PyC contents in these samples are reported as a sum of individual BPCA monomers (B6CA, B5CA, B4CA, and B3CA), each representing a BPCA with a particular number of carboxylic groups (e.g., B3CA represents BPCA with three carboxylic groups). The relative proportion of each individual BPCA reflects the level of PyC aromatic condensation, which mirrors the size of the original polycyclic structures (Schmidt et al., 2017). The amount of PyC as BPCAs in those soils (Table S2), as well as the distribution of each individual BPCA in soil PyC (Figure S1) are reported in the Supplemental Material.

## PyC in Soil Solution

On April 28th, 2014, we sampled soil solution from three stands per forest type, within an area of approximately 17 $km^2$. Leachates drained from the O, E, and B horizons were collected in pre-cleaned bottles and stored at −20°C until further analysis. Although the entire site had 54 ZTLs installed, we collected soil leachates from 18 ZTLs that had not been affected by a manipulation experiment out of the scope of this study. The concentration of dissolved organic C (DOC, mg $L^{-1}$) was measured on a TOC-Vcpn analyzer (Shimadzu Corp., Kyoto, Japan). PyC in leachate was measured using the BPCA method (Dittmar, 2008; Ding et al., 2013), which may slightly overestimate DPyC (Wagner et al., 2017). Here, we report DPyC data in O and E horizons for both 100 year-burned and unburned sites. Due to lack of replication, we only report DPyC data in the B horizon for the 100 year-burned site. Briefly, we filtered leachates through pre-combusted (450°C, 5 h) fiberglass filters (Whatman GF/F 0.7 µm pore size) and extracted dissolved organic matter (DOM) by solid-phase extraction (SPE, 5 g Bond Elut PPL, Agilent, Dittmar, 2008; Dittmar et al., 2008) by passing samples through pre-rinsed (with MeOH) SPE cartridges. The cartridges were dried under $N_2$, after which DOM was eluted with 20 mL MeOH. Aliquots of the MeOH-extracted DOM were transferred to 2 mL glass ampules and dried under $N_2$ until MeOH was completely evaporated. Each ampule received 0.5 mL of concentrated $HNO_3$ and was then flame-sealed. DOM was oxidized at 160°C for 6 h (Ding et al., 2013). Since BPCA oxidation conditions were optimized in each laboratory to maximize the greatest percent carbon recovery, oxidation times and temperatures are different for the analysis of DPyC (at Florida International University) and soil PyC (at Colorado State University). After oxidation, the concentrated $HNO_3$ was dried under $N_2$ at 50°C. The solid residue remaining in the ampules was re-dissolved in mobile phase for high pressure liquid chromatography (HPLC) analysis

of BPCAs (Dittmar, 2008) using an HPLC system coupled with a diode array detector (Surveyor, Thermo Scientific) and a Sunfire C18 reversed phase column (3.5 μm, 2.1 × 150 mm; Waters Corporation). BPCAs generated from DPyC were separated and quantified using a gradient elution method with a mobile phase A (4 mM tetrabutylammonium bromide, 50 mM sodium acetate, 10% MeOH) and mobile phase B (100% MeOH) (Dittmar, 2008). Non-pyrogenic organic materials do not produce BPCAs following the procedure described in the current study (Dittmar, 2008; Kappenberg et al., 2016), therefore we presume the DPyC reported in our study to be fire-derived. To calculate flux (g $m^{-2}$), DPyC concentration (mg $L^{-1}$) was multiplied by the total volume per unit area (L $m^{-2}$) of leachate collected in one single snowmelt event (**Figures 3A,B**). The distribution of each individual BPCA in DPyC (Figure S2) is reported in the Supplemental Material.

## Statistical Analyses

Data were transformed (log10) to normality and homogeneity of variance when necessary, and outliers were identified using Grubb's test. Comparisons between 100 year-burned and unburned sites for DPyC concentrations and fluxes, as well as PyC stocks in soils were performed using *t*-test at $p < 0.05$ significance level. Analyses were conducted using SigmaPlot v.12 (Systat Software, Inc., Chicago, IL), SPSS v.24 (IBM SPSS statistics for Windows), and software R 3.4.0 (R Development Core Team; http://www.R-project.org/).

# RESULTS

## PyC Stocks in 100 Year-Burned and Unburned Sites

One hundred year-burned sites had significantly greater PyC stocks in the Oi (17.0 ± 2.1 g $m^{-2}$) and Oe (39.8 ± 6.1 g $m^{-2}$) horizons compared to unburned sites (Oi: 9.7 ± 0.8 g $m^{-2}$, Oe: 17.0 ± 0.8 g $m^{-2}$, $P < 0.01$, **Figure 2**). In the 100 year-burned site, PyC stocks were significantly greater in the Oe horizon (39.8 ± 6.1 g $m^{-2}$) than in Oi horizon (17.0 ± 2.1 g $m^{-2}$, $P = 0.002$, **Figure 2**). In E and B horizons, total stocks averaged 83.8 ± 6.7 and 400 ± 33 g $m^{-2}$, respectively, across both sites. Differences in mineral soil PyC stocks between the two sites were not statistically significant ($P = 0.296$ and 0.364 for E and B horizon, respectively), even though the average PyC stocks in E and B soil horizons were greater in the 100 year-burned site than in the unburned site (**Figure 2**).

## Dissolved PyC Leached from Organic and Mineral Soil Horizons

DPyC concentrations averaged 0.75 ± 0.13 and 1.24 ± 0.33 mg $L^{-1}$ in 100 year-burned and unburned sites, respectively; however, there was no statistically significant difference between 100 year-burned and unburned sites (**Figure 3A**). Differences between horizons were only statistically significant between E and B horizons in the 100 year-burned site, with the E horizon yielding greater DPyC concentrations than the B horizon ($P = 0.013$, **Figure 3A**). In both sites, DPyC fluxes averaged 0.081 ± 0.032 and 0.052 ± 0.020 g $m^{-2}$ in the O and E horizons, respectively (**Figure 3B**). For flux values, we found no significant difference between E and B horizons in the 100 year-burned site. Differences in DPyC fluxes and proportion of DPyC in DOC leached from O and E horizons between 100 year-burned and unburned sites were not statistically significant; however, we noted that the proportion of DPyC in DOC in E horizon was slightly higher in the 100 year-burned site than in unburned site and this difference was marginally significant (**Figure 3C**, $P = 0.057$).

# DISCUSSION

Our results provided evidence for a persistence of PyC input in soils caused by a single fire event in the 100 year-burned red pine sites. The PyC stocks measured in the O horizons were within the range of those reported for a conifer forest soil sampled 1 year after burning (Pingree et al., 2012), but lower than those reported for unburned sites in subalpine forest soil in Colorado (Buma et al., 2014). PyC stocks reported in this study are also lower than those reported for southern boreal forest soils in Minnesota sampled 1–2 months after burning and measured using solid-state $^{13}C$ NMR (Miesel et al., 2015). Although the study by Miesel et al. (2015) used a different technique to measure soil PyC stocks, making direct comparisons of soil PyC stocks difficult, this is the only publication that reports PyC stock data for soils within the same region as our study site. PyC stocks presented here for E horizons are lower than those reported for the top 30 cm of sandy podzols (which included both Ae and B horizons) under a black spruce forest (Soucémarianadin et al., 2014) and the uppermost 10 cm of a subalpine (Buma et al., 2014) and a southern boreal forest soil (Miesel et al., 2015). PyC stocks measured for B horizon in our study were 3.1- to 3.5-fold greater than those reported by Soucémarianadin et al. (2014) 3–5 years after the fire. It is possible that (1) these stocks in the B horizons result from great amounts of PyC generated immediately after fire in the 100-year burned site, and that (2) that particulate PyC vertically moved to lower soil dephs via translocation over time (Dai et al., 2005; Leifeld et al., 2007; Koele et al., 2017). Further studies are needed to determine the major factors driving the stocks and transport rates of PyC to lower soil depths. Currently, little PyC stock data exists for B horizons in forest soils (Bird et al., 2015). As such, our study contributes to the fill this gap in PyC literature by providing a complete PyC stock dataset for a temperate forest soil.

Because our data show that a single fire event that occurred >100 years prior to sample collection significantly increased PyC stocks in organic horizons, we expected the increased soil PyC content to translate to higher concentrations and fluxes of DPyC in melt waters leached from the same fire-impacted soils. However, contrary to our hypothesis, concentrations and fluxes of DPyC mobilized from the O and E horizons did not reflect differences in fire recent history between the two sites studied here, even though a visible PyC layer was retained in the 100 year-burned site soils for approximately 100 years, and as evidenced by greater PyC stocks in the Oe horizon of the 100 year-burned site relative to the unburned site (**Figure 2**). The contribution of DPyC to total DOC reported in this study was much greater (from 1.77 to 5.51% across sites) than that reported for DPyC

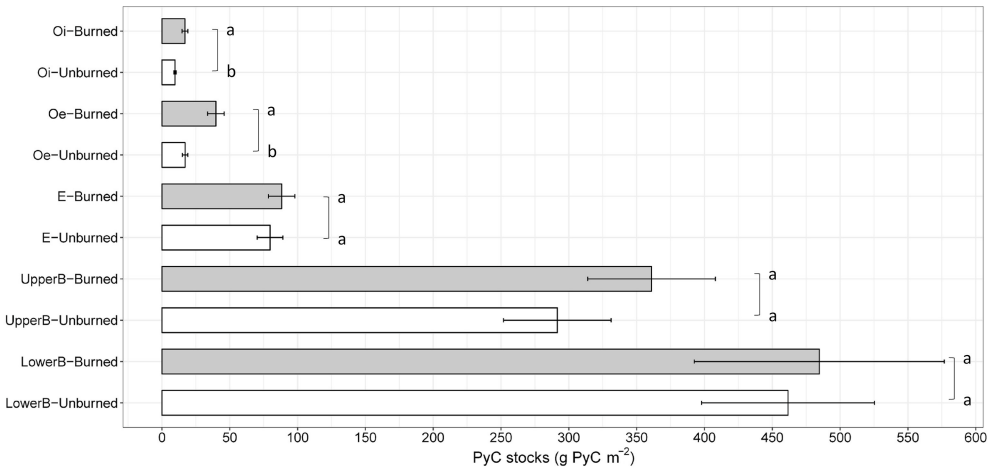


**FIGURE 2 |** Pyrogenic carbon (PyC) stocks (g m$^{-2}$) in organic (Oi and Oe) and mineral horizons E and B in burned and unburned sites, determined by the KMD method. Values shown are means ± standard error. Similar letters denote no statistically significant differences ($P < 0.05$). Number of replicates: Oi-Burned and -Unburned ($n = 9$), Oe-Burned and -Unburned ($n = 8$), E-Burned ($n = 8$), and -Unburned ($n = 9$), UpperB-Burned and -Unburned ($n = 9$), and LowerB-Burned and -Unburned ($n = 9$).

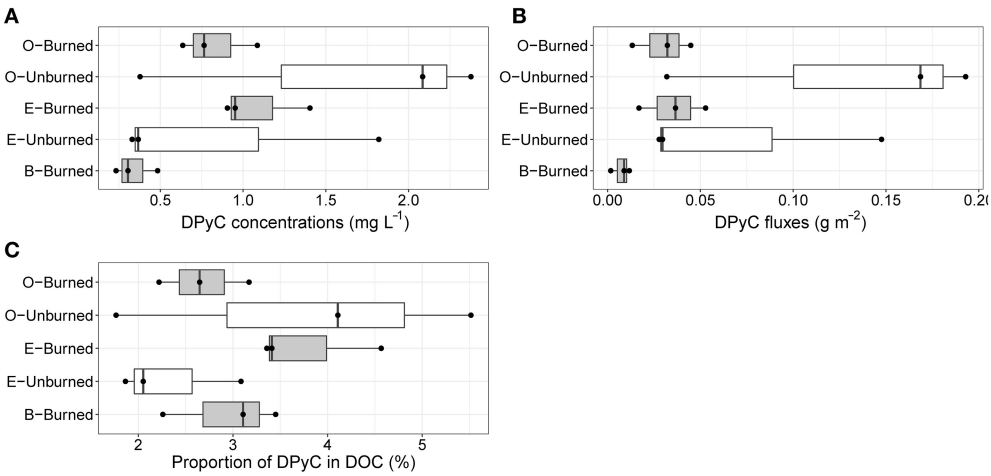


**FIGURE 3 |** Box-plot of DPyC concentration (**A**, mg L$^{-1}$), flux (**B**, g m$^{-2}$), and proportion of DPyC in total DOC (**C**, %) in soil solution drained from the O, E, and B horizons in burned sites and from the O and E horizons in unburned sites. DPyC was determined by the BPCA-DOC method. BPCA-based DPyC data for the B horizon in unburned sites are missing in **(A–C)** due to lack of replication. Dark circles are individual data points. Statistically significant differences in **(A)** between E and B horizons in burned sites ($P = 0.013$).

leached from the first 15 cm (0.02%) and 30 cm (0.017%) depths of a savanna oxisol 2 years after PyC application as charcoal (Major et al., 2010). We speculate that these differences are likely due to the timing of the leachate sampling, soil properties, and the physicochemical characteristics of PyC. Interestingly, our values are within the observed range of % DPyC reported in riverine systems (from 0.1 to 17.5%, Jaffé et al. (2013)).

We offer two explanations for the apparent uncoupling between DPyC concentrations and the abundance of PyC produced in the logging-era fire: First, DPyC concentrations and fluxes were likely influenced by the time and duration of our single sampling event, as soil leachates were sampled at a time when snowmelt occurred earlier at the unburned site because of the absence of leaves in the deciduous-dominated forest. As a result, more melt water moved through the unburned sites compared to the 100 year-burned sites. It is also possible that we may have missed the peak flux of DPyC associated with spring snowmelt. In-stream concentrations of DPyC can vary significantly with discharge in response to spring snow melt, likely driven by variations in hydrological flow paths which connect different soil horizons to the stream (Guggenberger et al., 2008; Stubbins et al., 2015; Wagner et al., 2015). Therefore, concentrations of DPyC mobilized from different soil horizons likely also undergo similar hysteresis patterns during a flushing

event. Although capturing variations in DPyC concentrations leached from each soil horizon over the entire duration of spring snow melt at these sites was outside the scope of the current study, our results highlight the importance of closing this knowledge gap in future research endeavors. Second, it is possible that much of the easily-mobilized forms of PyC were lost to leaching during the first stages of PyC decomposition in soils (Hammes et al., 2008). As such, we may have missed the initial pulse of DPyC derived from fresh charcoal deposited in soils immediately after the original burn event some 100 years prior. Since soil DPyC did not vary predictably between 100 year-burned and unburned sites, this observation is in agreement with previous suggestions (Dittmar et al., 2012; Ding et al., 2013), that concentrations of DPyC alone may not be a suitable proxy for the occurrence of historic fire events.

In the current study, B soil horizons exhibited greater Fe and Al oxide contents compared to the E soil horizons (Schaetzl and Rothstein, 2016). PyC has been shown to interact with, and possibly bind to, Fe and Al hydroxides (Brodowski et al., 2005; Santos et al., 2012; Solomon et al., 2012; Soucémarianadin et al., 2014). Therefore, the Fe and Al concentrations in the B soil horizons likely influenced the amount of soil PyC stored in those horizons, consistent with previous studies (see above). It is also possible that DPyC was in part retained in the B horizons via sorption to Fe and Al hydroxides, as concentrations decreased significantly from the E to the B horizons for DPyC measured in soil solutions leached from 100 year-burned site soils. This sharp decrease in DPyC concentrations has been also observed by previous studies for DOC (Kaiser and Guggenberger, 2000). Taken together, our observations are consistent with previous studies that propose mineral adsorption as a stabilization mechanism for PyC (Czimczik and Masiello, 2007; Cusack et al., 2012).

Although further studies are needed to determine the mechanisms driving this relationship, we found similarities in the relative proportion of BPCAs between DPyC in soil solution leached from the O and E horizons (Figure S2) and in the soluble fraction of aged charcoal leached in laboratory (Abiven et al., 2011). This finding suggests that DPyC released from spodosols is influenced by aging and oxidation of soil PyC remaining in soil on a timescale of 100 years, which is also consistent with previous observations of PyC-like compounds in leachates sampled from a spodosol affected by a historic fire in northern Michigan (Hockaday et al., 2006).

It is possible that atmospheric PyC deposition from recent and historical fire events also contributed to: (a) the amount of PyC observed in the forest floor of both forest cover types, and (b) the concentration of DPyC in soil solution. Although annual PyC deposition fluxes (19.3–24.4 mg $m^{-2}$ $year^{-1}$) estimated for a single site in northern Michigan were considered small relative to soil PyC stock estimated for that site, these flux estimations did not take into account wet deposition of PyC during wintertime (Santos et al., 2014). A significant proportion of atmospheric PyC can be deposited onto snow during the winter and released during snowmelt (Lazarcik et al., 2017), becoming part of the soil DOC pool. For instance, results from a study conducted in New Hampshire, US, reported up to 62% losses of atmospheric PyC from snowpack within the first 24% of the snowmelt (Lazarcik et al., 2017). Over time, some of this atmospheric PyC could have migrated vertically to lower soil depths, becoming either retained in mineral soils or part of the DPyC pool. Thus, it may be possible that a proportion of the DPyC we observed in this study was derived from a pulse of atmospheric PyC that percolated into the soil with snowmelt, especially in the unburned site. Because wet deposition can be a significant source of DOC in watersheds, with annual wet deposition of DOC ranging between 3 and 13 kg C $ha^{-1}$ $year^{-1}$ (Iavorivska et al., 2017), the role of atmospheric deposition as an input of DPyC mobilized in soils warrants further research.

We cannot exclude the possibility that an ancient forest fire event (>250 years ago) may have contributed to the PyC and DPyC values we reported for the unburned sites. This would be consistent with observations of a continuous, long-term release of DPyC resulting from the degradation of historically accumulated PyC (Dittmar et al., 2012; Marques et al., 2017).

Finally, we acknowledge the limitations of this study, which prevents us from extrapolating current results to different field conditions. Due to budget limitations, the DPyC data reported here was collected from a single sampling date during spring snowmelt at our study site; therefore, variability in DPyC fluxes from different soil horizons across larger spatial and temporal scales between these contrasting forest types is still not understood. Future studies should focus on the collection of soil water samples at different times of the year and under different flow regimes to provide a more comprehensive dataset across which mobilization of DPyC from 100 year-burned and unburned landscapes can be robustly compared.

## CONCLUSION

This study provides a preliminary look at the relationship between PyC stored in soils and the soluble fraction of DPyC, which is mobilized from different soil horizons during flushing events. Our results suggest that a single major fire event that occurred >100 years ago, which generated a substantial visible charcoal layer in the Oe horizon, had little to no detectable effect on concentrations of DPyC leached from soils relative to soils that have not experienced a similar fire event for the past 250 years. Based on the results of this study, we recommend three research directions that should be further explored to close critical knowledge gaps in our understanding of the PyC cycle this and similar systems: (1) dominant processes that constrain the links between soil PyC and DPyC; (2) the role of biotic and abiotic processes in facilitating the mobilization of PyC to lower soil depths; (3) the contribution of reactive Al and Fe oxides and oxyhydroxides in the retention of DPyC in subsoils.

## AUTHOR CONTRIBUTIONS

FS, DR, and JM led efforts in devising the study objectives and approach, and in writing the manuscript. FS and SW conducted DPyC measurements and analyzed DPyC data. DR established the original study site, provided soil and leachate

samples, and provided the background data. RJ provided support with DPyC and soil PyC measurements, and data interpretation. JM provided support for DOC-SPE extraction and soil PyC measurements. All authors provided input and revisions in constructing the final version of the manuscript.

## ACKNOWLEDGMENTS

We thank two reviewers for their constructive and helpful comments. Rodney Simpson and the EcoCore Analytical Facility (Colorado State University) for soil BPCA analysis, Dominic Uhelski for assistance with KMD digestions and data, as well as Mike Cook and Mike Luehmann for collecting the soil leachates. This project was supported by Michigan State University, the Department of Forestry Fred Arnold fund (awarded to JM), with partial support provided through the Scientist Exchange Program of the Novus Research Coordination Network NSF DEB-1145815 (awarded to FS). Establishment of the original study site, lysimeter installation and soil sample collection was supported by National Science Foundation (grant EAR1053373), Michigan State University AgBioResearch, and USDA National Institute of Food and Agriculture (McIntire Stennis Project MICL06006) awards to DR. Additional support was provided through Florida International University for the BPCA measurements for both DPyC and PyC, funded through the George Barley Fund (awarded to RJ). SW and RJ thank the NSF through the FCE LTER (DEB-1237517) for additional financial support of this work. This is contribution number 846 from the Southeast Environmental Research Center in the Institute of Water & Environment at Florida International University.

## SUPPLEMENTARY MATERIAL

The Supplementary Material for this article can be found online at: https://www.frontiersin.org/articles/10.3389/feart.2017.00080/full#supplementary-material

## REFERENCES

Abiven, S., Hengartner, P., Schneider, M. P., Singh, N., and Schmidt, M. W. (2011). Pyrogenic carbon soluble fraction is larger and more aromatic in aged charcoal than in fresh charcoal. *Soil Biol. Biochem.* 43, 1615–1617. doi: 10.1016/j.soilbio.2011.03.027

Batjes, N. H. (1996). Total carbon and nitrogen in the soils of the world. *Eur. J. Soil Sci.* 47, 151–163. doi: 10.1111/j.1365-2389.1996.tb01386.x

Bird, M. I., Wynn, J. G., Saiz, G., Wurster, C. M., and McBeath, A. (2015). The pyrogenic carbon cycle. *Annu. Rev. Earth Planet. Sci.* 43:273–298. doi: 10.1146/annurev-earth-060614-105038

Boot, C. M., Haddix, M., Paustian, K., and Cotrufo, M. F. (2015). Distribution of black carbon in ponderosa pine forest floor and soils following the high park wildfire. *Biogeosciences* 12:3029–3039. doi: 10.5194/bg-12-3029-2015

Brodowski, S., Amelung, W., Haumaier, L., Abetz, C., and Zech, W. (2005). Morphological and chemical properties of black carbon in physical soil fractions as revealed by scanning electron microscopy and energy-dispersive X-ray spectroscopy. *Geoderma* 128, 116–129.doi: 10.1016/j.geoderma.2004.12.019

Buma, B., Poore, R. E., and Wessman, C. A. (2014). Disturbances, their interactions, and cumulative effects on carbon and charcoal stocks in a forested ecosystem. *Ecosystems* 17, 947–959. doi: 10.1007/s10021-014-9770-8

Comer, P. J., Albert, D. A., Wells, H. A., Hart, B. L., Raab, J. B., Price, D. L., et al. (1995). Michigan's presettlement vegetation, as interpreted from the general land office Surveys 1816–1856. Michigan Natural Feature Inventory, Lansing

Cotrufo, M. F., Boot, C. M., Kampf, S., Nelson, P. A., Brogan, D. J., Covino, T., et al. (2016). Redistribution of pyrogenic carbon from hillslopes to stream corridors following a large montane wildfire. *Glob. Biogeochem. Cycles* 30, 1348–1355. doi: 10.1002/2016GB005467

Cusack, D. F., Chadwick, O. A., Hockaday, W. C., and Vitousek, P. M. (2012). Mineralogical controls on soil black carbon preservation. *Glob. Biogeochem. Cycles* 26:GB2019. doi: 10.1029/2011GB004109

Czimczik, C. I., and Masiello, C. A. (2007). Controls on black carbon storage in soils. *Glob. Biogeochem. Cycles* 21, 1–8. doi: 10.1029/2006GB002798

Czimczik, C. I., Schmidt, M. W. I., and Schulze, E. D. (2005). Effects of increasing fire frequency on black carbon and organic matter in Podzols of Siberian Scots pine forests. *Eur. J. Soil Sci.* 56, 417–428. doi: 10.1111/j.1365-2389.2004.00665.x

Dai, X., Boutton, T. W., Glaser, B., Ansley, R. J., and Zech, W. (2005). Black carbon in a temperate mixed-grass savanna. *Soil Biol. Biochem.* 37, 1879–1881. doi: 10.1016/j.soilbio.2005.02.021

Ding, Y., Cawley, K. M., da Cunha, C. N., and Jaffé, R. (2014). Environmental dynamics of dissolved black carbon in wetlands. *Biogeochemistry* 119, 259–273. doi: 10.1007/s10533-014-9964-3

Ding, Y., Yamashita, Y., Dodds, W. K., and Jaffé, R. (2013). Dissolved black carbon in grassland streams: is there an effect of recent fire history? *Chemosphere* 90, 2557–2562. doi: 10.1016/j.chemosphere.2012.10.098

Dittmar, T. (2008). The molecular level determination of black carbon in marine dissolved organic matter. *Org. Geochem.* 39, 396–407. doi: 10.1016/j.orggeochem.2008.01.015

Dittmar, T., De Rezende, C. E., Manecki, M., Niggemann, J., Ovalle, A. R. C., Stubbins, A., et al. (2012). Continuous flux of dissolved black carbon from a vanished tropical forest biome. *Nat. Geosci.* 5:618–622. doi: 10.1038/ngeo1541

Dittmar, T., Koch, B., Hertkorn, N., and Kattner, G. (2008). A simple and efficient method for the solid-phase extraction of dissolved organic matter (SPE-DOM) from seawater. *Limnol. Oceanogr. Methods* 6, 230–235. doi: 10.4319/lom.2008.6.230

Fang, Y., Singh, B., Singh, B. P., and Krull, E. (2014). Biochar carbon stability in four contrasting soils. *Eur. J. Soil Sci.* 65, 60–71. doi: 10.1111/ejss.12094

Forbes, M. S., Raison, R. J., and Skjemstad, J. O. (2006). Formation, transformation and transport of black carbon (charcoal) in terrestrial and aquatic ecosystems. *Sci. Total Environ.* 370, 190–206. doi: 10.1016/j.scitotenv.2006.06.007

Goldberg, E. D. (1985). *Black Carbon in the Environment: Properties and Distribution*. New York, NY: John Wiley & Sons.

Güereña, D. T., Lehmann, J., Walter, T., Enders, A., Neufeldt, H., Odiwour, H., et al. (2015). Terrestrial pyrogenic carbon export to fluvial ecosystems: lessons learned from the white Nile watershed of East Africa. *Glob. Biogeochem. Cycles* 29, 1911–1928. doi: 10.1002/2015GB005095

Guggenberger, G., Rodionov, A., Shibistova, O., Grabe, M., Kasansky, O. A., Fuchs, H., et al. (2008). Storage and mobility of black carbon in permafrost soils of the forest tundra ecotone in Northern Siberia. *Glob. Chang. Biol.* 14, 1367–1381. doi: 10.1111/j.1365-2486.2008.01568.x

Hammes, K., Torn, M. S., Lapenas, A. G., and Schmidt, M. W. I. (2008). Centennial black carbon turnover observed in a Russian steppe soil. *Biogeosciences* 5, 1339–1350. doi: 10.5194/bg-5-1339-2008

Hockaday, W. C., Grannas, A. M., Kim, S., and Hatcher, P. G. (2006). Direct molecular evidence for the degradation and mobility of black carbon in soils from ultrahigh-resolution mass spectral analysis of dissolved organic matter from a fire-impacted forest soil. *Org. Geochem.* 37, 501–510. doi: 10.1016/j.orggeochem.2005.11.003

Hockaday, W. C., Grannas, A. M., Kim, S., and Hatcher, P. G. (2007). The transformation and mobility of charcoal in a fire-impacted watershed. *Geochim. Cosmochim. Acta* 71:3432–3445. doi: 10.1016/j.gca.2007.02.023

Iavorivska, L., Boyer, E. W., and Grimm, J. W. (2017). Wet atmospheric deposition of organic carbon: an underreported source of carbon to watersheds in the northeastern United States. *J. Geophys. Res. Atmos.* 122, 3104–3115. doi: 10.1002/2016JD026027

Jaffé, R., Ding, Y., Niggemann, J., Vähätalo, A. V., Stubbins, A., Spencer, R. G., et al. Dittmar (2013). Global charcoal mobilization from soils via dissolution and riverine transport to the oceans. *Science* 340, 345–347. doi: 10.1126/science.1231476

Jauss, V., Sullivan, P. J., Sanderman, J., Smith, D. B., and Lehmann, J. (2017). Pyrogenic carbon distribution in mineral topsoils of the northeastern United States. *Geoderma* 296, 69–78. doi: 10.1016/j.geoderma.2017.02.022

Jobbagy, E. G., and Jackson, R. B. (2000). The vertical distribution of soil organic carbon and its relation to climate and vegetation. *Ecol. Appl.* 10, 423–436. doi: 10.1890/1051-0761(2000)010[0423:TVDOSO]2.0.CO;2

Kaiser, K., and Guggenberger, G. (2000). The role of DOM sorption to mineral surfaces in the preservation of organic matter in soils. *Org. Geochem.* 31, 711–725. doi: 10.1016/S0146-6380(00)00046-2

Kalbitz, K., Solinger, S., Park, J. H., Michalzik, B., and Matzner, E. (2000). Controls on the dynamics of dissolved organic matter in soils: a review. *Soil Sci.* 165, 277–304. doi: 10.1097/00010694-200004000-00001

Kappenberg, A., Bläsing, M., Lehndorff, E., and Amelung, W. (2016). Black carbon assessment using benzene polycarboxylic acids: limitations for organic-rich matrices. *Org. Geochem.* 94, 47–51. doi: 10.1016/j.orggeochem.2016.01.009

Kleber, M., Eusterhues, K., Keiluweit, M., Mikutta, C., Mikutta, R., and Nico, P. S. (2015). Mineral-organic associations: formation, properties, and relevance in soil environments. *Adv. Agron.* 130, 1–140. doi: 10.1016/bs.agron.2014.10.005

Koele, N., Bird, M., Haig, J., Marimon-Junior, B. H., Marimon, B. S., Phillips, O. L., et al. (2017). Amazon Basin forest pyrogenic carbon stocks: first estimate of deep storage. *Geoderma* 306, 237–243. doi: 10.1016/j.geoderma.2017.07.029

Kurth, V. J., Mackenzie, M. D., and Deluca, T. H. (2006). Estimating charcoal content in forest mineral *Soils* 137, 135–139. doi: 10.1016/j.geoderma.2006.08.003

Lazarcik, J., Dibb, J. E., Adolph, A. C., Amante, J. M., Wake, C. P., Scheuer, E., et al. (2017). Major fraction of black carbon is flushed from the melting New Hampshire snowpack nearly as quickly as soluble impurities. *J. Geophys. Res. Atmos.* 122, 537–553. doi: 10.1002/2016JD025351

Leifeld, J., Fenner, S., and Müller, M. (2007). Mobility of black carbon in drained peatland soils. *Biogeosciences* 4, 425–432. doi: 10.5194/bg-4-425-2007

Maestrini, B., and Miesel, J. R. (2016). Modification of the weak nitric acid digestion method for the quantification of black carbon in organic matrices. *Org. Geochem.* 103, 1–4. doi: 10.1016/j.orggeochem.2016.10.010

Major, J., Lehmann, J., Rondon, M., and Goodale, C. (2010). Fate of soil-applied black carbon: downward migration, leaching and soil respiration. *Glob. Chang. Biol.* 16, 1366–1379. doi: 10.1111/j.1365-2486.2009.02044.x

Marques, J. S. J., Dittmar, T., Niggemann, J., Almeida, M. G., Gomez-Saez, G. V., and Rezende, C. E. (2017). Dissolved Black Carbon in the Headwaters-to-Ocean Continuum of Paraíba do Sul River. *Front. Earth Sci.* 5:11. doi: 10.3389/feart.2017.00011

Miesel, J. R., Hockaday, W. C., Kolka, R. K., and Townsend, P. A. (2015). Soil organic matter composition and quality across fire severity gradients in coniferous and deciduous forests of the southern boreal region. *J. Geophys. Res. Biogeosci.* 120, 1124–1141. doi: 10.1002/2015JG002959

Myers-Pigg, A. N., Louchouarn, P., Amon, R. M., Prokushkin, A., Pierce, K., and Rubtsov, A. (2015). Labile pyrogenic dissolved organic carbon in major Siberian Arctic rivers: implications for wildfire-stream metabolic linkages. *Geophys. Res. Lett.* 42, 377–385. doi: 10.1002/2014GL062762

Pingree, M. R. A., Homann, P. S., Morrissette, B., and Darbyshire, R. (2012). Long and short-term effects of fire on soil charcoal of a conifer forest in Southwest Oregon. *Forests* 3, 353–369. doi: 10.3390/f3020353

Reisser, M., Purves, R. S., Schmidt, M. W. I., and Abiven, S. (2016). Pyrogenic carbon in soils: a literature-based inventory and a global estimation of its content in soil organic carbon and stocks. *Front. Earth Sci.* 4, 1–14. doi: 10.3389/feart.2016.00080

Rumpel, C., Alexis, M., Chabbi, A., Chaplot, V., Rasse, D. P., Valentin, C., et al. (2006). Black carbon contribution to soil organic matter composition in tropical sloping land under slash and burn agriculture. *Geoderma* 130, 35–46. doi: 10.1016/j.geoderma.2005.01.007

Rumpel, C., Ba, A., Darboux, F., Chaplot, V., and Planchon, O. (2009). Erosion budget and process selectivity of black carbon at meter scale. *Geoderma* 154, 131–137. doi: 10.1016/j.geoderma.2009.10.006

Santín, C., Doerr, S. H., Kane, E. S., Masiello, C. A., Ohlson, M., de la Rosa, J. M., et al. (2016). Towards a global assessment of pyrogenic carbon from vegetation fires. *Glob. Chang. Biol.* 22, 76–91. doi: 10.1111/gcb.12985

Santos, F., Fraser, M. P., and Bird, J. A. (2014). Atmospheric black carbon deposition and characterization of biomass burning tracers in a northern temperate forest. *Atmos. Environ.* 95, 383–390. doi: 10.1016/j.atmosenv.2014.06.038

Santos, F., Torn, M. S., and Bird, J. A. (2012). Biological degradation of pyrogenic organic matter in temperate forest soils. *Soil Biol. Biochem.* 51, 115–124. doi: 10.1016/j.soilbio.2012.04.005

Schaetzl, R. J., and Rothstein, D. E. (2016). Temporal variation in the strength of podzolization as indicated by lysimeter data. *Geoderma* 282:26–36. doi: 10.1016/j.geoderma.2016.07.005

Schaetzl, R. J., Luehmann, M. D., and Rothstein, D. (2015). Pulses of podzolization: the relative Importance of spring snowmelt, summer storms, and fall rains on spodosol development. *Soil Sci. Soc. Am. J.* 79, 117–131. doi: 10.2136/sssaj2014.06.0239

Schmidt, M. W. I., Hilf, M. D., and Wiesenberg, G. L. B. (2017). "15 Analysis of biochars using benzene polycarboxylic acids," in *Biochar A Guide to Analytical Methods*, eds B. Singh, M. Camps-Arbestain, and J. Lehmann (Boca Raton, FL: CSIRO Publishing), 162.

Singh, N., Abiven, S., Torn, M. S., and Schmidt, M. W. I. (2012). Fire-derived organic carbon in soil turns over on a centennial scale. *Biogeosciences* 9, 2847–2857. doi: 10.5194/bg-9-2847-2012

Solomon, D., Lehmann, J., Wang, J., Kinyangi, J., Heymann, K., Lu, Y. et al. (2012). Micro- and nano-environments of C sequestration in soil: a multi-elemental STXM-NEXAFS assessment of black C and organomineral associations. *Sci. Total Environ.* 438, 372–388. doi: 10.1016/j.scitotenv.2012.08.071

Soucémarianadin, L. N., Quideau, S. A., and MacKenzie, M. D. (2014). Pyrogenic carbon stocks and storage mechanisms in podzolic soils of fire-affected Quebec black spruce forests. *Geoderma* 217–218, 118–128. doi: 10.1016/j.geoderma.2013.11.010

Stubbins, A., Spencer, R. G., Mann, P. J., Holmes, R. M., McClelland, J. W., Niggemann, J., et al. (2015). Utilizing colored dissolved organic matter to derive dissolved black carbon export by arctic rivers. *Front. Earth Sci.* 3:63. doi: 10.3389/feart.2015.00063

Wagner, S., Cawley, K. M., Rosario-Ortiz, F. L., and Jaffé, R. (2015). In-stream sources and links between particulate and dissolved black carbon following a wildfire. *Biogeochemistry* 124, 145–161. doi: 10.1007/s10533-015-0088-1

Wagner, S., Ding, Y., and Jaffé, R. (2017). A new perspective on the apparent solubility of dissolved black carbon. *Front. Earth Sci.* 5:75. doi: 10.3389/feart.2017.00075

Whitney, G. G. (1987). An ecological history of the Great Lakes forest of Michigan. *J. Ecol.* 75, 667–684. doi: 10.2307/2260198

Wiedemeier, D. B., Hilf, M. D., Smittenberg, R. H., Haberle, S. G., and Schmidt, M. W. (2013). Improved assessment of pyrogenic carbon quantity and quality in environmental samples by high-performance liquid chromatography. *J. Chromatogr. A* 1304, 246–250. doi: 10.1016/j.chroma.2013.06.012

**Conflict of Interest Statement:** The authors declare that the research was conducted in the absence of any commercial or financial relationships that could be construed as a potential conflict of interest.

The reviewer, YY, declared a past co-authorship with one of the authors, RJ, to the handling editor.

frontiers in Earth Science

REVIEW
published: 20 March 2018
doi: 10.3389/feart.2018.00026

# Pyrogenic Carbon Erosion: Implications for Stock and Persistence of Pyrogenic Carbon in Soil

*Rebecca B. Abney*[1,2]* *and Asmeret Asefaw Berhe*[1]

[1] *Environmental Systems, Life and Environmental Sciences, University of California, Merced, Merced, CA, United States,*
[2] *School of Public and Environmental Affairs, Indiana University, Bloomington, IN, United States*

Pyrogenic carbon (PyC) constitutes an important pool of soil organic matter (SOM), particularly for its reactivity and because of its assumed long residence times in soil. In the past, research on the dynamics of PyC in the soil system has focused on quantifying stock and mean residence time (MRT) of PyC in soil, as well as determining both PyC stabilization mechanisms and loss pathways. Much of this research has focused on decomposition as the most important loss pathway for PyC from soil. However, the low density of PyC and its high concentration on the soil surface after fire indicates that a significant proportion of PyC formed or deposited on the soil surface is likely laterally transported away from the site of production by wind and water erosion. Here, we present a synthesis of available data and literature to compare the magnitude of the water-driven erosional PyC flux with other important loss pathways, including leaching and decomposition, of PyC from soil. Furthermore, we use a simple first-order kinetic model of soil PyC dynamics to assess the effect of erosion and deposition on residence time of PyC in eroding landscapes. Current reports of PyC MRT range from 250 to 660 years. Using a specific example-based model system, we find that ignoring the role of erosion may lead to the under- or over-estimation of PyC MRT on the centennial time scale. Furthermore, we find that, depending on the specific landform positions, timescales considered, and initial concentrations of PyC in soil, ignoring the role of erosion in distributing PyC across a landscape can lead to discrepancies in PyC concentrations on the order of several 100 g PyC $m^{-2}$. Erosion is an important PyC flux that can act as a significant control on the stock and residence time of PyC in the soil system.

**Keywords: soil carbon stabilization, erosion, fire, persistence, pyrogenic carbon**

OPEN ACCESS

***Edited by:***
*Samuel Abiven,*
*Universität Zürich, Switzerland*

***Reviewed by:***
*Stefan Doerr,*
*Swansea University, United Kingdom*
*Laure Nalini Soucemarianadin,*
*École Normale Supérieure, France*

***Correspondence:**
*Rebecca B. Abney*
*rebabney@iu.edu*

***Specialty section:***
*This article was submitted to Biogeoscience, a section of the journal Frontiers in Earth Science*

***Received:*** *30 November 2017*
***Accepted:*** *05 March 2018*
***Published:*** *20 March 2018*

***Citation:***
*Abney RB and Berhe AA (2018) Pyrogenic Carbon Erosion: Implications for Stock and Persistence of Pyrogenic Carbon in Soil. Front. Earth Sci. 6:26. doi: 10.3389/feart.2018.00026*

## INTRODUCTION

### Fires and Production of Pyrogenic Carbon

Fire is a major environmental perturbation and driver of biogeochemical processes across a diversity of landscapes worldwide. Globally, over 400 million hectares are burned annually (Andela et al., 2017), and in the US alone, wildfires consume over 2.6 million hectares per year in over 74,000 wildfires (National Interagency Fire Center, 2015). The amount and properties of organic matter

(OM) left behind in and on soil post-fire are controlled by the amount and composition of fuel and the duration and temperature of the fire (Dyrness and Norum, 1983; Kasischke et al., 2008). Depending on burn severity, or the impact of the fire on the ecosystem, fires also control nutrient availability, water infiltration, soil pH (Certini, 2005), and OM stocks in soil (González-Pérez et al., 2004; Keeley, 2009). Moreover, fires can lead to the formation of pyrogenic carbon (PyC) from the incomplete combustion of biomass and soil organic matter (SOM) (Schmidt and Noack, 2000; Masiello, 2004; Preston and Schmidt, 2006). Pyrogenic carbon is a broad term for fire-altered materials that includes a continuum of materials such as soot, charcoal, lightly charred biomass, and biochar, or intentionally charred material for agricultural and carbon (C) sequestration purposes (Masiello, 2004; Bird et al., 2015; Lehmann and Joseph, 2015).

A growing body of literature now demonstrates that PyC is a major component of the global C cycle (Lehmann et al., 2008; Preston, 2009; Bird et al., 2015). PyC makes up 2.5–5% of global soil organic C (IPCC, 2013; Bird et al., 2015) and up to 30% of C in some soils (Skjemstad, 1996; Skjemstad et al., 1999), making it important not just for accounting of global soil C stocks but also for how the soil system plays an important role in regulation of global climate (Lehmann et al., 2008). In soil, PyC has an overall longer mean residence time (MRT, centuries to millennia) (Hammes et al., 2008; Lehmann et al., 2008), compared with non-pyrogenically altered OM (decades to centuries) (Torn et al., 1997; Schmidt et al., 2011). Current estimates of the MRT of PyC in the soil are considerably shorter than previously reported estimates (on the order of millennia), as several studies have demonstrated that some PyC is degraded on shorter (months to years) time scales in both laboratory (Nguyen et al., 2009; Whitman et al., 2014) and field studies (Soucémarianadin et al., 2015). Recent observations have indicated that current estimates of PyC residence times may be inaccurate due to failures in accurately quantifying lateral redistribution of PyC in the terrestrial ecosystem and its riverine transfer to the ocean (Rumpel et al., 2006; Jaffé et al., 2013; Masiello and Louchouarn, 2013).

## Effect of Fire and PyC on Soil Erosion

Elevated rates of post-fire soil erosion are typically observed after wildfires (Certini, 2005; Carroll et al., 2007; Shakesby, 2011). The extent to which fires lead to soil erosion and the nature of the eroded material vary depending on fire type (i.e., crown fire, ground fire), the environment where the fires occur, and post-fire climatic conditions (Certini, 2005; Shakesby, 2011). One of the main controls on the type of fire is the ecosystem type (Kozlowski and Ahlgren, 1974; Brown and Smith, 2000), which dictates the type and quantity of vegetation available for charring into PyC along with climatic variables responsible for controlling vegetation growth and fire conditions. During fires, typically only the top few (2–5) centimeters of soil are directly and significantly impacted by the high temperatures (DeBano, 2000). Charring intensity, or the integral of the duration and maximum temperature reached during combustion of organic matter (Pyle et al., 2015), at the soil surface controls the properties of the PyC formed during the fire, where PyC formed at higher temperatures (above ∼350°C) can be more persistent in soil (González-Pérez et al., 2004; Zimmerman, 2010). Generally, this PyC formed at higher temperatures (above ∼350°C) has a higher skeletal density and is more porous (Brewer et al., 2014), making it more susceptible to erosional transport than low temperature PyC.

Fire also changes the physical properties of soil with implications for lateral movement of water and PyC. Fires can lead to destabilization of topsoil, reducing aggregation and aggregate protected C, increased soil hydrophobicity, which can lead to increased erodibility of soil post-fires through both water and wind-driven erosion processes (Shakesby and Doerr, 2006; Johnson et al., 2007; Ravi et al., 2007; Al-Hamdan et al., 2012; Miller et al., 2012; Araya et al., 2017). Albalasmeh et al. (2013), for example, showed that low severity fires can have a lasting impact on soil aggregate stability. Moreover, low to moderate temperature, ground-level fires (soil temperatures reaching ∼175–250°C) can lead to the formation of a hydrophobic layer at or just below the soil surface, or increases in any pre-existing soil hydrophobicity, resulting in decreases in infiltration rates (DeBano, 2000; Shakesby and Doerr, 2006; Mataix-Solera et al., 2011). This decrease in infiltration and altered hydrologic flow paths though the soil matrix can lead to increases in overland flow (Hortonian flow, see **Figure 1**, Shakesby and Doerr, 2006). In combination with the loss of soil-stabilizing vegetation during fire, this increase in overland flow can drive increased erosion rates and sediment export in fire-affected landscapes (Shakesby et al., 1993).

# EROSION AND PyC PERSISTENCE IN SOIL

Over the last couple of decades, our understanding of how PyC becomes stabilized in, or is lost from, the soil system has advanced considerably. However, many of these calculations and measurements of PyC stabilization have not considered erosion. In the following sections, we discuss historical and modern ideas about PyC persistence within soil and the role of erosion as a loss and stabilization mechanism.

## Historical Perspective

Historically, PyC was thought to be a highly recalcitrant form of soil C that is inherently resistant to microbial decomposition. The presumed chemical recalcitrance of PyC was attributed to its chemical structure including large linkages of condensed aromatic structures (Skjemstad et al., 1999), as well as it forming chemical and physical associations with soil minerals (Lehmann et al., 2005; Brodowski et al., 2006). This idea of chemical recalcitrance prevailed for decades, even though there was evidence for the breakdown of PyC from the beginning of the twentieth century (Potter, 1908). This presumed inherent recalcitrance of PyC was even used to support arguments that PyC storage in soil might be part of the "missing C sink" because it seemed so environmentally stable (Lehmann, 2007). At the same time, the ability of PyC to persist in the soil longer than non-PyC OM, has also contributed to the widespread research

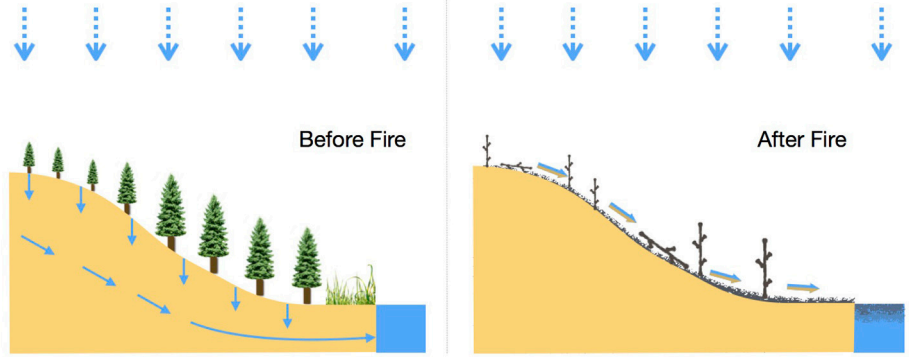


**FIGURE 1 |** On the hillslope scale, fires alter dominant hydrologic flow regimes in soil, reducing infiltration and subsurface flow of water, and increasing surface runoff.

on the potential of PyC to serve as an agricultural amendment (biochar) with the main aim of increasing soil C stocks and decreasing C turnover (i.e., improving a soil's potential to sequester atmospheric $CO_2$; Lehmann et al., 2008); however some other types of biochar can be utilized to improve soil productivity (Lehmann and Joseph, 2015). However, recent works showed PyC can become decomposed or lost from soil rather quickly, on the scale of months to years (Nguyen et al., 2010; Zimmerman, 2010; Zimmermann et al., 2012; Zimmerman and Gao, 2013).

There is now a major paradigm shift occurring in our understanding of PyC dynamics in the earth system. **Figure 2** shows how published estimates of PyC MRT have decreased over the last few decades. Some earlier studies reported MRT estimates over thousands of years, but around 2008, a gradual shift in viewpoints happened as evidence for rapid decomposition and mobilization became apparent (**Figure 2**). Some of the most recent research suggests that the rate of PyC decomposition is tightly controlled by environmental conditions and its persistence in soil is a property of the ecosystem (Schmidt et al., 2011).

## Stability and Turnover of PyC

PyC can become stabilized or lost from soil through similar processes that control the fate of bulk or non-pyrogenic carbon, including biotic and abiotic decomposition, leaching, and erosion (Rumpel et al., 2006; Major et al., 2010; Zimmerman, 2010). Current estimates of PyC MRT range from weeks to months to millennia (Bird et al., 2015). Lehmann et al. (2008) suggested that PyC MRT in soil could range between 700 and 9,000 years. However, other studies have argued that PyC has considerably shorter MRT in soil (**Table 1**). For example, Hammes et al. (2008) found a PyC turnover time of 239 years in a Russian steppe site, and similarly, Boot et al. (2015) found a similar MRT for PyC of 300 years. Overall, laboratory incubation derived estimates of loss of PyC are typically higher (1.5–20% PyC mass loss per year) than field studies (0.08–15% PyC mass loss per year), even though field studies include other forms of loss other than microbial decomposition (e.g., erosion and leaching, **Table 1**). Much of the variation in field and laboratory studies is due to the range of different processes that control PyC persistence in soil, and laboratory studies are commonly conducted under ideal decomposition conditions, which are more reflective of near maximum potential breakdown rates of PyC. Below, we present a discussion on the role of erosion in controlling the dynamics of PyC in the soil system.

## Erosion as a Driver of C Dynamics in Soil

Interest in the role of erosion on soil C and PyC dynamics and biogeochemical cycling of essential elements has increased over the last two decades. In particular, research has focused on the potential for erosion to constitute a net sink for atmospheric $CO_2$, on the order of 0.12–1.5 Gt C $y^{-1}$ (Stallard, 1998; Lal, 2003; Berhe et al., 2007; Battin et al., 2009; Regnier et al., 2013; Doetterl et al., 2016). In upland, eroding landform positions (shoulder positions), erosion leads to losses of SOM through direct removal of soil mass (Berhe et al., 2008; Harden et al., 2008; Berhe, 2012; Nadeu et al., 2012; Stacy et al., 2015; McCorkle et al., 2016). About 70–90% of the eroded topsoil material is redistributed downhill or downstream, and this material is not exported out of the source watersheds but instead is deposited in toeslope and footslope landform positions (Gregorich et al., 1998; Stallard, 1998; Lal, 2003). Erosion leads to stabilization of at least some of the eroded SOM in depositional landforms through new and reconfigured associations of the eroded SOM with soil minerals (Sharpley, 1985; Lal, 2003, 2004; Berhe, 2012; Berhe and Kleber, 2013). During the transport phase of erosion, eroded material is exposed to breakdown mechanisms and for non-pyrogenic C, over 20% of the OM transported from eroding landform positions is assumed to be lost via oxidative decomposition during or after transport (Jacinthe and Lal, 2001). Erosion is a particularly important flux for PyC in soil when it stays on surface layers (Rumpel et al., 2006) at least on the order of months, if not longer (Boot et al., 2015; Faria et al., 2015), because this leaves PyC vulnerable to weathering forces of wind and water. However, current research has focused on hillslope- and plot-scale erosion of PyC (Rumpel et al., 2006, 2009; Abney et al., 2017; Pyle et al., 2017), so its redistribution at the watershed and larger scales remains largely unknown.

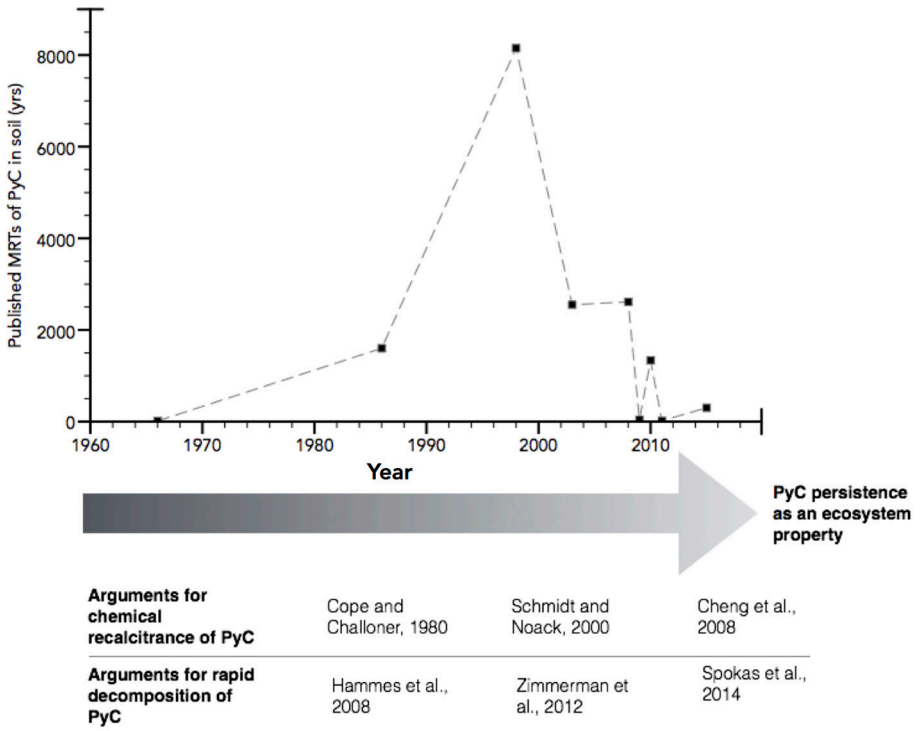


**FIGURE 2 |** This timeline of estimated MRTs of PyC and key papers illustrates the changing paradigm on controls of PyC persistence in the soil system. The estimate for char age from Cope and Chaloner (1980) was not included in the average of 300 million years, because it was not an estimate of turnover time, but it does reflect the view that PyC would reside in soil for very extended periods of time. Also, note that the x-axis is not numeric.

## Post-fire Erosion

Fire increases the susceptibility of soils, particularly surface soils, to erosion by changing soil physical and chemical properties (Certini, 2005). For example, the development of soil hydrophobicity post-fire can reduce water infiltration, increasing topsoil susceptibility to runoff (DeBano, 2000). The presence of PyC in litter and surface soil can also increase the rates of bulk erosion, as fire-affected biomass tends to have lower density, compared to uncharred biomass and litter, making it easier to transport by both water- (Rumpel et al., 2006) and wind-driven (Beyers et al., 2005; Shakesby, 2011) erosional processes. In many ecosystems, erosion preferentially transports carbonaceous topsoil material, compared to mineral constituents of soil, leading to C enrichment in eroded sediments compared to soil in source slopes (Avnimelech and McHenry, 1984; Stacy et al., 2015).

Similarly, Rumpel et al. (2006) found evidence for selective transport of PyC during interrill erosion due to its lower density and concentration on the soil surface. One study found that interrill sediment erosion was doubled in a burned watershed compared to a neighboring unburned watershed, along with increases in runoff velocity due to increased bare ground coverage (Pierson et al., 2008, 2013). The relative extent of interrill compared with rill erosion depends upon local landscape and precipitation conditions, where higher precipitation intensity and steeper slopes can drive increased rill formation (Moody et al., 2013). The relative role of rill and interrill erosion can control the mobility of PyC throughout a landscape, as rill erosion likely would not preferentially transport PyC and would result in transport of bulk soil material (Schiettecatte et al., 2008), while sheet or interrill erosion can preferentially transport smaller, lighter, and organic-rich material (Wang et al., 2010).

## Atmospheric and Aeolian Transport of PyC

The atmospheric component of the global PyC cycle has received considerably more research focus than soil PyC, largely due to the interest in air pollution associated with soot and other aerosols released to the atmosphere during fires (Seiler, 1980; Campbell et al., 2007), and their implications for global climate change and public health (Highwood and Kinnersley, 2006; Bond et al., 2013). Fossil fuel combustion and biomass burning produce the majority of atmospheric PyC, which has a relatively short residence time (up to months) in the atmosphere (Chapin et al., 2006; Preston and Schmidt, 2006), and an even shorter (<week) in the lower atmosphere (Parungo et al., 1994).

Dry and wet deposition of PyC from the atmosphere is a global process that transports 2–10 Tg PyC per year, to both land and ocean depositional settings spanning thousands of km (Parungo et al., 1994; Jurado et al., 2008; Bond et al., 2013). From the soil surface, soot and smaller PyC constituents can be rapidly transported post-fire (**Figure 3**), depending on local wind and precipitation conditions, such that dry climates are

**TABLE 1 |** Examples of decomposition rates measured in laboratory and field studies, as converted to percent mass loss of PyC per year.

| %PyC mass loss in a year | Type of experiment | Source of PyC | Method to measure PyC | Citation |
|---|---|---|---|---|
| **LABORATORY EXPERIMENTS** | | | | |
| 2 | Incubation, at tropical conditions | Mulga (*Acacia aneura*) | $^{13}$C direct polarization NMR spectroscopy, hydrogen pyrolysis | Zimmermann et al., 2012 |
| 10–20 | Incubation, temperature change from 4 to 60°C | Laboratory generated corn (*Zea mays* L.) char at 350°C | $^{13}$C direct polarization NMR spectroscopy | Nguyen et al., 2010 |
| 4–20 | | Corn char at 600°C | | |
| 2.3–15 | | Oak (*Quercus* spp.) char at 350°C | | |
| 1.5–14 | | Oak char at 600°C | | |
| 0.02–4.89 | Three simulations of PyC loss via decomposition ranging from 2 to 2,000 years | N/A | N/A | Foereid et al., 2011 |
| 0.38 | Laboratory incubation–O horizon | Laboratory generated char from ponderosa pine (*Pinus ponderosa*) | Chemo-thermal oxidation at 375°C | Hatten and Zabowski, 2009 |
| 0.24 | A1 horizon | | | |
| 0.08 | A2 horizon | | | |
| 0.7 | Laboratory incubation: average over 8.5 years | Ryegrass (*Lolium* spp.) | $^{14}$C labeled biochar | Kuzyakov et al., 2009 |
| 0.25 | Average PyC loss between years 5 and 8 | | | |
| **FIELD EXPERIMENTS** | | | | |
| 1 | Field chronosequence: first 30 years after production | Field burning of maize (*Zea mays* L.) | $^{13}$C CPMAS NMR spectroscopy, FTIR | Nguyen and Lehmann, 2009 |
| 3.2 | Field chronosequence: first 5 years after production | | Manual identification | |
| 1.1 | Field experiment in native savannah | Mango trees (*Mangifera indica* L.) | Mixing model from $\delta^{13}$C of PyC and field soil | Major et al., 2010 |
| 0.25 | Field experiment | Natural PyC in chernozem | BPCA | Hammes et al., 2008 |

*The range of reported loss rates for incubation experiments (1.5–20%) is considerably higher than field experiments (0.08–15%). Several of these reported loss rates are different between lengths of experiments, indicating non-linear decomposition and breakdown kinetics for PyC. The difference between field and laboratory experiments is largely due to laboratory experiments being more representative of optimal or maximal decomposition conditions. Moreover, several of the laboratory studies use laboratory generated PyC, this is critical to control and account for the variation in PyC found in the field and in the case of wildfires.*

more susceptible to post-fire wind erosion (Shakesby, 2011; Pereira et al., 2015). Few studies have focused on wind-driven erosion, atmospheric transport, and terrestrial deposition of PyC post-fire, due to both methodological difficulties and widespread assumptions that it is a very small flux or only a site-specific phenomenon (Wondzell and King, 2003; Shakesby, 2011). However, it is likely that smaller, low-density PyC, or PyC produced by higher temperature fires (Brewer et al., 2014), could be rapidly transported significant distances, particularly with the loss of vegetation and breakdown of soil structure post-fire (Beyers et al., 2005).

### Stabilization of Eroded PyC via Burial

The stabilization of PyC can occur through post-erosion burial of a fraction of the eroded PyC in depositional landform positions, similar to non-pyrogenic C (Berhe et al., 2007; Berhe and Kleber, 2013; Doetterl et al., 2016). PyC-rich material eroded from hillslopes can get stabilized in deep soil layers of downhill or downstream depositional landform positions with repeated erosion/deposition events, especially if it is buried at >1 m depths, as was observed in char-rich Paleosols in Nebraska (Chaopricha and Marín-Spiotta, 2014; Marín-Spiotta et al., 2014). This deep-soil stabilization can also be driven by aeolian-derived deposits burying an existing soil (Chaopricha and Marín-Spiotta, 2014; Marín-Spiotta et al., 2014), via anthropogenic burial, such as the Terra Preta soils of the Amazon (Glaser et al., 2000; Glaser, 2002), or via charring of roots at depth during high intensity fires (Kyuma et al., 1985). The burial of PyC reduces PyC exposure to microbes, air, and extracellular enzymes, which are major drivers of decomposition.

## SIGNIFICANCE OF EROSIONAL REDISTRIBUTION OF PyC IN THE TERRESTRIAL ECOSYSTEM

As of yet, the relative rates of PyC erosion, compared with bulk SOM erosion at the plot, hillslope, or even watershed scale remain relatively unexplored, so the amount of PyC transported via erosion processes is largely unknown. Accurate quantification of the rates of PyC loss through biological (decomposition) versus physical (erosion, leaching) processes is necessary for fully understanding its role in the soil C pool, including its potential

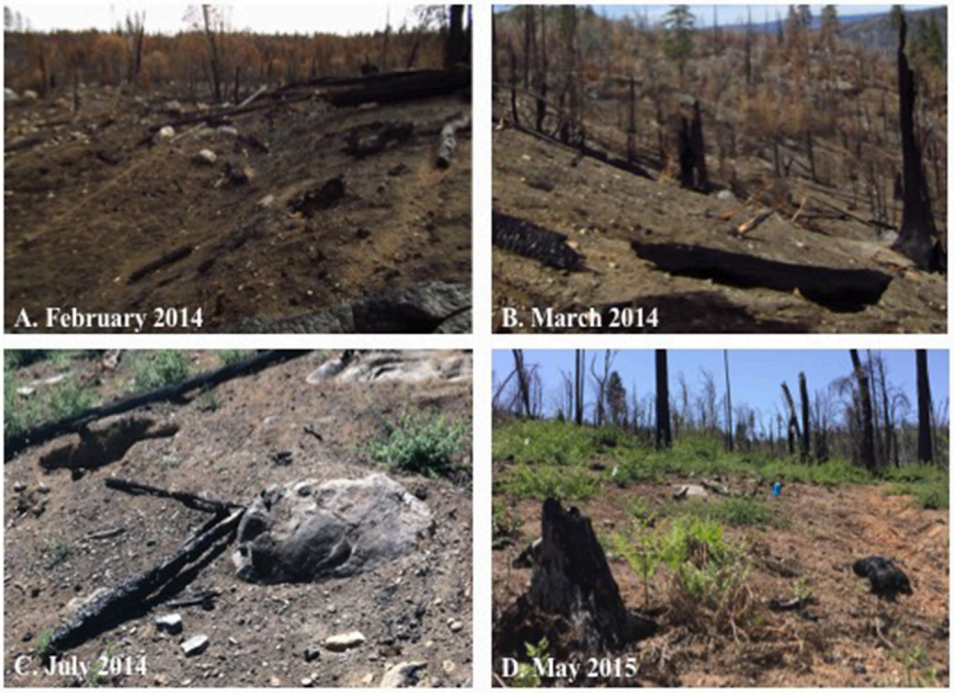


**FIGURE 3 |** Erosion in upland temperate forests is dependent upon precipitation and topography. This progression of photographs from the Rim Fire (2013, in Yosemite National Park and Stanislaus National Forest in California, USA) illustrates the significant loss of PyC post-fire in a high-severity burn area and post-fire vegetation regrowth (all photos, R. Abney). The Rim Fire began in August of 2013 and was contained in November of 2013, with the aid of snowfall. The picture in **(A)** (from February 2014, 3 month's post-fire) illustrates the significant PyC layer remaining after the first snowmelt. The picture in **(B)** from March 2014 is the remaining PyC after the first major rainfall post-fire. The soil color is considerably lighter (3–5/1 5YR dark gray compared with 2.5/1 5YR black), which is evidence of loss (erosion) of highly charred material (PyC). The pictures in **(C,D)** have considerably less PyC covering the soil surface and illustrate the beginnings of vegetation regrowth based on ocular assessment after the Rim Fire.

role as a C sink (Hammes et al., 2008). Due to recent research indicating that PyC is preferentially eroded (Rumpel et al., 2006, 2009), it is likely that it will be redistributed throughout the landscape differently than non-pyrogenic carbon, and this may have significant impacts on our understanding of its long-term persistence in soil, as is true for non-pyrogenic carbon (Berhe, 2012; Berhe et al., 2012).

Recent evidence suggests that PyC often interacts with the soil minerals and microbial community differently than some forms of non-pyrogenic C (Kuzyakov et al., 2009; Zimmerman, 2010; Zimmerman et al., 2011), which makes measuring the fluxes of PyC critical for quantifying global PyC stocks. Furthermore, understanding of the controls on the fluxes of PyC through soil is needed for generating more accurate and representative models of dynamics of the soil C pool and how the soil system controls global climate. Thus, improved understanding of PyC interactions in soil and its loss mechanisms are currently needed to elucidate the role of PyC in soil total C dynamics.

## Erosion and Soil PyC Dynamics

The role of erosion in controlling the fate of PyC is likely more important than for non-pyrogenic SOM, as fire can significantly increase the rate of soil erosion, and prior research has demonstrated that PyC is highly erodible (Rumpel et al., 2006; Yao et al., 2014). The increased rate of soil erosion post-fire results from a combination of environmental changes, including: loss of the protective litter layer, exposure of surface soil to erosive forces (precipitation, wind), increased hydrophobicity of the subsoil (DeBano et al., 1998; DeBano, 2000; Benavides-Solorio and MacDonald, 2001; MacDonald et al., 2001), and a reduction in water infiltration and water holding capacity of the surface soil (Robichaud, 1997; DeBano, 2000; Doerr and Thomas, 2000; Carroll et al., 2007). Furthermore, the time that elevated rates of soil erosion are sustained is at least partially controlled by the extent of vegetation recovery post-fire, but is typically around a year (Baker, 1988).

Erosion, in turn, can indirectly affect vegetation and soil water status. Both fire and erosion are controlled by climate to various extents (Imeson and Lavee, 1998; Neary et al., 1999; Riebe et al., 2001). Watershed size and topography (Liu et al., 2003; Iniguez et al., 2008), in addition to the amount, intensity, and temporal distribution of precipitation can influence the rate of bulk SOM and PyC loss from or redistribution within an eroding watershed (Nearing, 1998; Cain et al., 1999; Rumpel et al., 2009). These relationships have been documented by many erosion prediction models, such as the Universal Soil Loss Equation (Wischmeier and Smith, 1965, 1978) and the Water Erosion Prediction Project

(WEPP) model, which were originally developed in agricultural soils (Laflen et al., 1991).

Important inferences can be drawn on factors that control PyC erosion based on available data and by extrapolation of what we know about erosion of non-PyC or bulk C. Below we briefly discuss how specific variables (i.e., the amount and nature of PyC available for transport, climate, geomorphology of the landscape) control how strongly erosion can regulate soil PyC dynamics.

## The Erodible Nature of PyC

The amount and composition of PyC that is laterally distributed over the soil surface by erosion, at least in part, depends on the concentration, location, chemical composition, and physical size of the PyC. These variables are all products of complex interactions among the type and density of vegetation available to be combusted (i.e., fuel load), combustion conditions (e.g., temperature, duration, oxygen availability), and frequency of fire events (Schmidt and Noack, 2000; Masiello, 2004; Hockaday et al., 2006; Czimczik and Masiello, 2007; Knicker, 2007).

Transport of PyC is assumed to occur in erosion events immediately after fire when the land surface is covered by a layer of PyC, which can become quickly mobilized through the landscape via either wind- or water-driven erosion processes (Carroll et al., 2007; Pereira et al., 2015; Abney et al., 2017). The PyC on the soil surface is likely to be eroded before and more preferentially than mineral soil or mineral-associated PyC, except in the cases of landslides and other major mass wasting events. Additionally, the recently formed PyC would not have enough time to form stabilizing physical and chemical interactions with soil minerals prior to preferential transport, as these stabilizing interactions can take years to decades to form in natural settings (Faria et al., 2015). Over time, the PyC that is not transported by erosion is mobilized downward into the profile via dissolution, leaching, and biological processes that render it more susceptible to in-solution transport with flowing water (Güereña et al., 2015). However, the PyC that remains on the soil surface is exposed to wetting- and drying-cycles that are likely to render it more susceptible to leaching losses, although some research has indicated that the material left after leaching may be less easily decomposed (Naisse et al., 2015).

Among the most important physical and chemical properties of PyC that make it susceptible to erosion are its low density compared with soil minerals (Brewer et al., 2014), its hydrophobic properties when formed at lower ($< \sim 250^{\circ}C$) charring temperatures (Sander and Pignatello, 2005; Bodí et al., 2011), and its aromatic content and aromatic condensation (Preston and Schmidt, 2006). Generally, it is assumed that the low density ($<1\,Mg\ m^{-3}$) and hydrophobic properties of PyC allow for flotation and lateral transport of PyC with flowing water (Rumpel et al., 2006, 2009). The slow wetting and filling of the pores of PyC with water, however, should increase its density (Gray et al., 2014) and reduce its potential for flotation and transport with overland flow. Furthermore, the breakdown of PyC also depends on density of the PyC and on associations between PyC and non-pyrogenic SOM (Zimmermann et al., 2012; Pyle et al., 2017). The duration, intensity, and frequency of storm events also plays a significant role in controlling the wetting of PyC, as the hydrophobic properties of PyC can only delay wetting, not prevent it entirely (Bodí et al., 2011).

## Climate and Hydrology

The process of water-driven soil erosion occurs though detachment of a soil particle which is transported and deposited away from the source location. During rain-driven erosion, the impact of raindrops breaks down aggregates on the soil surface which leads to transport of soil away from the point of impact, and gravity leads to the downslope mobilization of detached particles across the soil surface (Kinnell, 2005). With all other erosion-driving factors held equal, the intensity of precipitation is the leading driver of erosion and runoff (Renard et al., 1997). Large storms are generally thought to drive the major erosion events within a landscape; however, intermediate storms can also mobilize significant amounts of material over the course of a year (Wischmeier, 1962). In addition to intense storms, rapid snowmelt and rain-on-snow events are important drivers of rapid runoff (Pierson et al., 2001). The loss or reduction of vegetation cover due to fires creates the opportunity for raindrops to reach the soil surface at high velocity, without being slowed down by aboveground vegetation and overlying litter layers. Hence, the same amount or intensity of rainfall can mobilize more PyC, and bulk C, from soil post-fire than it would under unburned conditions if there is loss of vegetation or litter layers (Inbar et al., 1998; Beyers et al., 2005; Cerdà and Doerr, 2005; Pierson et al., 2008, 2009, 2013). Generally, low intensity precipitation events drive preferential transport of light carbonaceous material (higher enrichment ratios, higher concentration of C) (Schiettecatte et al., 2008; Wang et al., 2010). However, during high intensity or longer duration rainfall events, a mixture of mineral material along with SOM, including pyrogenic carbon, is mobilized from the soil surface or even deeper soil horizons (large rainfall events lead to scouring of the surface or river banks or creation of deep rills and gullies), as was observed by Stacy et al. (2015) and McCorkle et al. (2016).

## Geomorphology of the Landscape

The geomorphology of a landscape can significantly impact the erosion of PyC. In particular, the steepness of a hillslope has a non-linear, direct effect on the amount of sediment transported by soil erosion, where increased gradient increases the mass of transported sediment (Montgomery and Brandon, 2002). Slope length and hillslope hydrology also likely play important roles on PyC transport, as they do in in non-fire impacted landscapes (Munro and Huang, 1997; Parsons et al., 2006; Istanbulluoglu et al., 2008), as moderate length slopes allow for the greatest transport of material, while shorter slopes are limited in space for runoff to build speed. Longer slopes have increased area for water to meet resistance and for particles to settle out, so the travel distance of particles is a function of their size.

Aspect of a hillslope can impact erosion due to its effects on plant growth, density, OM decomposition, with subsequent implications for fuel availability for fires and soil burning (Cerdà et al., 1995). The impacts of aspect on hillslope erosion can be compounded by delays in vegetation recovery, leading to longer-term enhanced erosion rates and continued loss of soil

nutrients, and weather-related events, which can cause different erosion rates on different aspects of the same hillslope (Cerdà et al., 1995; Pierson et al., 2008, 2009). Furthermore, the location within a landscape where PyC is formed or deposited can be critical for the long-term fate of the PyC. If PyC is produced on eroding landform positions (convex or linear positions such as summit, shoulder, or back/foot slope positions), then it is more likely to be transported laterally by wind or water erosion processes, or gravity driven diffusive mass transport, compared to PyC produced in depositional landform positions (concave or flat positions such as toeslopes, or alluvial and colluvial plains). However, if the PyC is either formed or deposited on depositional landform positions, then it is more likely to persist in the catchment longer and be stabilized in the depositional landform positions by forming physical and/or chemical associations with soil minerals, or to get buried by subsequent erosion/deposition events that bring sediment to the depositional position as has been found for non-pyrogenic carbon (Stallard, 1998; Berhe, 2012).

### Interactions

The three drivers of PyC erosion, fire, geomorphology, and climate, also interact with each other to control rates of PyC erosion (**Figure 4**). For example, different combinations of steepness of a hillslope, size of watershed, and intensity of precipitation may lead to differing rates of erosion (Pierson et al., 2001). Generally, climate describes the expected precipitation events, but local scale variations in weather, such as exceptionally large precipitation events, can drive the formation of rills or gullies and large mass wasting events. Furthermore, landscapes with very steep slopes, which could predispose a landscape to mass wasting events, could further enhance these large movement events. As another example, long-term climate patterns impact the type and amount of vegetation available as fuel for fire, which could further impact the quality and quantity of PyC left behind after fire. The amount and nature, such as density and water content, of available fuel play an import role in determining the intensity of fire, which controls the resulting PyC properties, such as aromatic content and aromatic condensation, as demonstrated by laboratory studies (Mimmo et al., 2014; Pyle et al., 2015; Wiedemeier et al., 2015). This more condensed PyC produced at higher temperatures is more susceptible to flotation and theoretically more susceptible to erosive forces (Brewer et al., 2014).

## Implications of Including Erosion as a PyC Flux Term

While the magnitude of PyC transported by soil erosion has not been fully determined, some estimate that this flux is on the order of 29–87 Tg PyC per year (Bird et al., 2015). Current evidence suggests that erosion is a significant driver of PyC redistribution in hillslopes (i.e., loss from soil profiles of eroding landform positions, that may or may not remain in the same catchment as input to the soil profiles of depositional landform positions; Rumpel et al., 2006, 2009; Abney et al., 2017). Environmental conditions post-fire and the nature of PyC lead to elevated rates of erosion and enrichment of PyC within the resulting eroded

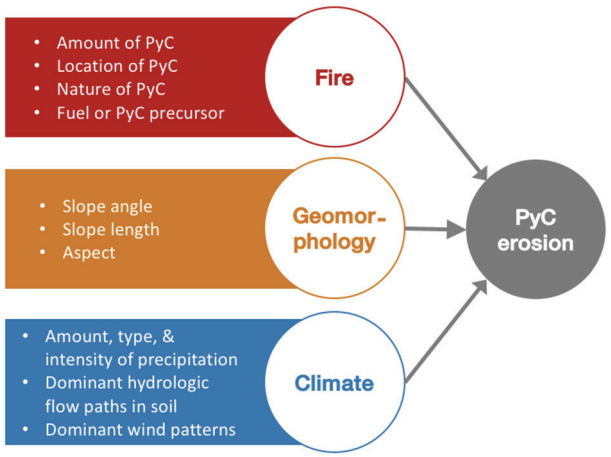


**FIGURE 4 |** Three main factors interact to control the erosion of PyC in any environment: landscape, climate, and hydrology, and the amount and nature of PyC produced from fire. These three factors interact with each other in both space and time to impact the fate of PyC.

sediments (Pierson et al., 2008; Rumpel et al., 2009). The large flux of PyC to oceans (Jaffé et al., 2013) is further indication that there is considerable transport of dissolved and particulate forms of PyC within the terrestrial and to the aquatic system. An approach that considers the geomorphologic and biogeochemical cycling changes associated with fires is needed to quantify stock and erosional fluxes of PyC in fire-affected dynamic landscapes and to determine *how* and *why* erosional distribution of PyC could affect our understanding of the dynamics of both bulk SOM and PyC in the terrestrial biosphere.

## Calculating Loss and MRT of PyC

One of the most common and simplest approaches to estimating PyC MRT is based on calculations of a loss rate from a given reservoir (i.e., soil) using simple one-pool box model approaches. Turnover time ($T$) is assumed to be equivalent to the inverse of the loss rate constant ($k$), with the assumption of steady state. Turnover time is imposed on a first-order kinetic model of PyC dynamics as:

$$T = 1/k \tag{1}$$

where,

$$dPyC/dt = I_{PyC} - k \times PyC \tag{2}$$

where $T$ is turnover time (years), $k$ is a loss rate constant (as a proportion of the PyC stock, $yr^{-1}$), $PyC$ is stock of PyC in a soil pool ($g/m^2$), $I_{PyC}$ ($g\ m^{-2}\ yr^{-1}$) is the rate of PyC input to the reservoir. This model assumes a single rate of loss of PyC that is solely comprised of decomposition, and a uniform input of PyC across the ecosystem. Below we argue for the role of erosion as a significant loss factor for PyC and demonstrate the error in MRT calculations when erosion is ignored using a specific case study.

## Estimating MRT of PyC in Dynamic Landscapes

Ignoring the contribution of erosion to soil PyC stocks can lead to errors in both the stock as well as estimated turnover time of PyC in dynamic landscapes. Many fires occur in areas that are prone to erosion, but even if an erosional loss term of PyC is included, the role of erosion as a gain term (in depositional landform positions) is not yet accounted for within soil PyC budget models, and rarely accounted for in field studies (Abney et al., 2017). Not accounting for this gain of PyC can lead to major errors within our budget models of PyC and C within eroding landscapes. We have considered three landform positions or types in the following model: (1) a landform where no sediment material is being transported to or from that area; (2) an eroding landform position (e.g., shoulder, backslope), where erosion represents a loss term for PyC; and (3) a depositional landform position (e.g., toeslope or plain), where deposition of PyC eroded from upslope positions leads to input of PyC. Following works of Stallard (1998) and Berhe et al. (2008) on erosional redistribution of bulk SOM, here, a model for first order C kinetics was modified to assess the potential effect of erosion on PyC dynamics. The first-order loss rate constant ($k$) in the first order model (Equation 2) was replaced with two separate constants for decomposition ($k_o$) and erosional redistribution ($k_e$,), where $k = k_o + k_e$ as:

$$\mathrm{dPyC/dt} = I - (k_0 + k_e) \times PyC \tag{3}$$

where $PyC$ = soil PyC stock (g $m^{-2}$); $I$ = soil pyrogenic carbon inputs (g $m^{-2}$ $yr^{-1}$); $k_o$ = first-order loss of PyC by abiotic or biological decomposition ($yr^{-1}$); and $k_e$ = first-order loss of PyC by erosion ($yr^{-1}$). This $k_e$ term describes the different trajectories of PyC at eroding or depositional landform positions and accounts for additions or losses of PyC via erosional processes. Additionally, in the depositional landform position, there is both a loss of PyC initially deposited that is a function of the stock of PyC in that landform position (Equation 4). There is also an increase in PyC stock in the depositional landform position due to the input from erosion, $k_e$ = first-order gain of PyC by erosion ($yr^{-1}$) which is a function of the PyC stock in the corresponding eroding landform position, $PyC_{ero}$ = eroding soil PyC stock (g $m^{-2}$):

$$\mathrm{dPyC/dt} = I - (k_0 \times PyC) + (k_e \times PyC_{er}) \tag{4}$$

For our model calculations, we used published results from Hammes et al. (2008) where they measured PyC stock in chernozem soils at a steppe preserve in Russia as a case study. The soils were sampled twice over about 100 years, first between 1895 and 1903, and then in 1997 and 2004. The authors then used the difference in PyC stock (measured using the BPCA marker technique) of the soil between the two time periods and radiocarbon measurements of SOM to derive MRT of PyC in soil using a one PyC pool, first-order decay (i.e., linear, donor-controlled) model (Hammes et al., 2008). Though, this study does not account for any leaching or erosion of PyC that could have occurred between the two sampling points. In our calculations, we assumed the soils had initial soil PyC stock of 2.5 kg PyC/$m^2$ (Hammes et al., 2008) and a relatively low decomposition constant ($k_o$) for PyC of 0.4%/year, which approximates a turnover time of 250 years (Hammes et al., 2008). Then, we considered erosion or deposition as loss or gain terms, as shown in Equations (3) and (4). We calculated the stock of PyC in the non-erosion (flat) position by assuming that $k = k_0$ and that $k_e = 0$. For the eroding position $k_e$ represents a loss term for PyC, while for the depositional position it represents a gain to the existing PyC stock. The depositional area has erosional inputs of PyC that maintain a higher PyC stock through the simulation. The eroding area has both erosion and decomposition acting together to remove PyC from the soil, so it has the lowest PyC stock at the end of the 150-year simulation (**Figure 5**).

This model scenario is an inherently simplified version of PyC dynamics within eroding hillslopes, and thus operates under several assumptions. This model assumes a single input of PyC, an initial even distribution and availability of PyC for erosional transport, and a landscape comprised of depositional and eroding landform positions. In real landscapes, landform positions can act as both eroding and depositional sites, such as flat locations that would serve as depositional sites can be susceptible to wind erosion (Pyle et al., 2017). However, depending on specific fire and environmental conditions, this model may still hold as a proximate estimation for the erosion

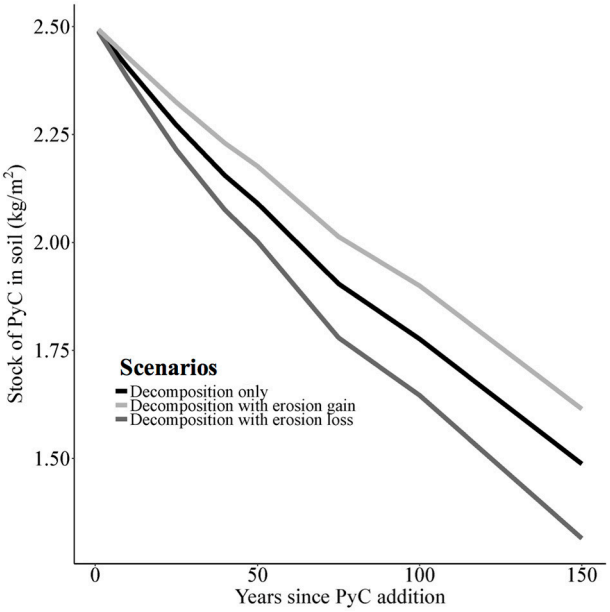


**FIGURE 5 |** The difference in PyC stock when erosion is considered as a loss (e.g., via transport out of a soil) vs. a gain (e.g., in depositional landform positions) in a model of PyC loss over 150 years can lead to around a 250 g difference in PyC stock per $m^2$ after 100 years. The assumed initial stock of PyC was 2.5 kg/$m^2$ (Hammes et al., 2008), and the base decomposition rate was derived from a 263-year turnover time ($k_0$ = 0.0038, from Equation 1). The rate of erosion was assumed to be 0.001 ($K_e$, from Equation 1), which equates to a 1,000-year turnover time. This model also assumes a single input of PyC into the soil. In reality, multiple fires would have occurred during the 150-year run of this model, suggesting that soil PyC stocks would not decline at this rate.

inputs of PyC into a depositional landform position, particularly as recent research has demonstrated the preferential erosion of PyC on even apparently flat landscapes (Pyle et al., 2017). This model assumes only a single fire event to input PyC, but in many environments, it is likely that there would be more than a single input of PyC over the duration of 150 years. This model also assumes a linear and constant rate of erosion, which is not likely to occur in natural ecosystem. However, this model estimation demonstrates the possible order of magnitude error that might be found in post-fire erodible landscapes, assuming similar initial stocks and losses via erosion and decomposition. We found that, for the specific conditions we considered, not accounting for erosional redistribution of PyC can lead to almost 300 g PyC $m^{-2}$ difference between the maximum gain of PyC stock from depositional of eroded material and minimum erosion loss scenarios over a 150-year simulation. Note that the model presented here is inherently simplistic by design, as it is aiming to demonstrate the role of soil erosion under three landform positions. In any given hillslope, the actual role of erosional redistribution depends on the nature of the landscape, rate of PyC input, and the environmental variables that control rate of PyC loss through decomposition, leaching, and/or erosion. For example, future models could be designed for specific environments to include additional fluxes of PyC that have yet to be well quantified, such as bioturbation, leaching, and subsequent fires, and likely control its stock and residence time in the soil.

The model presented above can also be used to determine the effect of erosion on mean residence times or persistence of PyC in soil. The more that erosion contributes to the $k$ term as a loss of PyC, the larger the overall $k$ term and the faster the turnover of PyC in a soil, since a portion of the PyC stock would be moved to downslope positions. Conversely, for depositional landform positions, the $k_e$ adds to the soil profile's PyC stock, and because $k_e$ would be negative in this case, it lowers the effective $k$ term in Equation (1), leading to longer turnover times for PyC in soil profiles of depositional landform positions.

On the local scale, explicitly considering erosion as a loss or gain term (depending on the landform positions considered) for PyC in dynamic landscapes leads to considerable differences in MRT at different geomorphic landform positions. Across even a single hillslope, soil properties and controls on decomposition vary considerably. We calculated turnover times for eroding and depositional landform positions, by assuming a decomposition rate [$k_0$ from Equation 3 of 0.04%/year and an erosion rate of 0.01%/year (1,000-year turnover time from erosion processes alone)]. This calculation also assumes that PyC that is eroded and left in place is similarly impacted by decomposition, which is not necessarily true based on preferential erosion of PyC (Rumpel et al., 2009). Under natural conditions, a considerable proportion of PyC eroded in the short term (up to 1 year) post-fire is likely mobilized further through the landscape on longer (10 + years) timescales (Abney et al., 2017).

In this simple model, the erosion rate ($k_e$) was positive for the eroding landform position (indicating erosional loss of PyC from eroding landform positions and making net loss of PyC faster) and negative for the depositional landform position (indicates an addition of PyC and decreasing the net loss of PyC). This erosion rate was further divided into five different fractions, such that 0% indicates no erosion, or no erosion accounted for, and 100% indicates 100% of the 0.01% erosion rate accounted for within the model. We found that if 100% of this theoretical erosion rate is accounted for, then the difference in calculated turnover time is ∼150 years (**Figure 6**). If 50% of the erosional loss of PyC from a soil is accounted for, then the difference between the maximum turnover time with erosion as a gain and the minimum turnover time with erosion as a loss is ∼70 years. If the erosion rate were higher (i.e., the theoretical 100% erosion was a higher background erosion rate), then this difference in turnover time would be even greater. This difference in erosion indicates that over the scale of a landscape, local topographical differences that determine whether PyC is eroded or deposited over time can play a major role in the fate of that PyC, depending on the relative rates of loss, deposition, and burial of PyC.

This model only applies to the fate PyC that remains on the surface soils, which is the fraction that is likely to experience erosion. The fraction of soil PyC that is found in deep soil layers or gets buried overtime is not likely to experience significant lateral redistribution with erosion, and hence is not included in this discussion. Also, the importance of the role of erosion as a gain or a loss term is also dependent on the relative role of erosion in each landscape (**Figure 6**), as different landscape geomorphologies can lead to drastically different erosional rates and processes (section Geomorphology of the

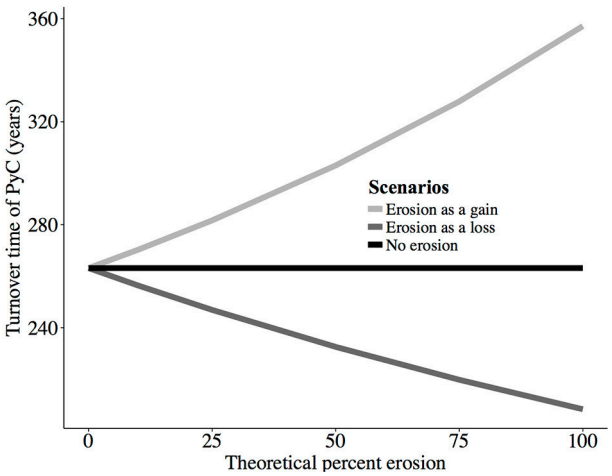


**FIGURE 6 |** The magnitude of difference in turnover time of PyC associated with discounting erosion as either an input (deposition of material) or loss (erosion of material) term can lead to an ∼150-year difference error in turnover time depending on the fractional amount of erosion occurring. The theoretical percent erosion is the percent of an erosion rate ($K_e$, from Equation 1) that is accounted for within this model from an assumed rate of erosion of 0.001 (1,000-year turnover time of PyC via erosion, a slow erosion rate). This erosion rate is added (deposition of material) or subtracted (erosion of material) from a base decomposition rate ($k_0$, from Equation 1) of 0.004, corresponding to a 250-year turnover time (Hammes et al., 2008). A theoretical percent erosion of 0% corresponds to no erosion contribution of input or output of PyC from a soil; whereas a theoretical percent erosion of 100% would lead to either an input (gain) of PyC into the soil or loss of PyC from the soil that would increase or decrease the turnover time of PyC by ∼70 years respectively.

Landscape). Furthermore, the intensity, type, and timing of post-fire precipitation play important roles in controlling the rate of PyC water-driven erosion (Hammes et al., 2008) and transport of other soil constituents (i.e., reactive minerals) that may influence the fate of PyC post-erosion and/or deposition.

## Explicitly Considering Erosion in Global PyC Budgets

The role of erosion in redistributing PyC can also impact global models of PyC cycling and storage (Bird et al., 2015). The major global stocks of PyC are $1.05 \times 10^{15}$ g PyC in the soil (Bird et al., 2015), $9.87 \times 10^{18}$ g PyC in the ocean (Ziolkowski and Druffel, 2010), and $1.79 \times 10^{22}$ g PyC in marine sediments (Masiello, 1998). The major fluxes of PyC are decomposition, which ranges from 0.25 to 20% loss per year depending on PyC properties and environment (**Table 1**), 1% loss per year from leaching and percolation (Major et al., 2010; Abiven et al., 2011), $7.4 \times 10^{12}$ g PyC per year transported to oceans by rivers (Dittmar et al., 2012; Jaffé et al., 2013), and 0.02% loss of ocean PyC to sediment per year (Masiello, 1998).

Current global and smaller-scale literature is not fully accounting for the erosion of PyC and transformations of PyC during and after erosion throughout the global ecosystem, even though the stocks are in approximate steady state (Bird et al., 2015). This indicates that while preferential loss of PyC via erosion may serve as a significant loss mechanism for PyC, it is also likely acting as a stabilization mechanism of PyC for the budget to remain roughly in balance. Furthermore, uncertainties also remain concerning the role of erosional transport in physical breakdown and decomposition of PyC during erosional transport. In the landform position model presented here, the rate of decomposition during erosional transport was assumed the same as non-pyrogenic carbon, although there is considerable evidence that this is not likely the case (Santos et al., 2012; Whitman et al., 2014). Since this assumption would likely prove invalid and PyC decomposition during erosion is considerably lower, this would have important implications for the long-term stabilization of PyC. Moreover, this model also assumes a steady state of erosion and even distribution and formation of PyC across the landscape, which is not representative of the heterogeneous nature of fire. Finally, even though erosion of PyC from slopes represents a loss process, it serves the opposite role when the PyC is buried in depositional landform positions. If we assume that erosional redistribution, and subsequent burial of eroded PyC in depositional soil profiles can effectively reduce its decomposition rate, then the process of soil erosion can potentially be a stabilization mechanism for PyC in dynamic landscapes (Berhe et al., 2007; Berhe and Kleber, 2013). Future research should investigate the long-term fate of PyC that is eroded and buried, and the magnitude that this can serve as a mechanism for increased soil C storage.

The models presented here do not necessarily represent natural variation in timing and magnitude of fire, erosion, and future climates that may alter the global PyC cycle, particularly as large erosion and fire events are strongly controlled by local climatic conditions (Westerling et al., 2006). The loss of PyC from the soil is likely more episodic and variable in nature than these scenarios account for, and therefore this loss may be different than predicted by constant rate functions used in this model. Also, these calculations do not account for the decomposition or loss of PyC from groundwater or through leaching.

In addition to the limited knowledge of the controls on breakdown of PyC in the soil system, it is widely agreed that the laboratory-based incubation studies are over-estimating the rate of PyC decomposition due to the disturbance of the soil and since decomposition conditions are considered to be more optimal in the laboratory compared with field conditions. Many of the laboratory based estimates are over 10% PyC loss per year (Nguyen et al., 2010; Foereid et al., 2011), which is inconsistent with calculated PyC MRT measurements that range from several hundred years to several millennia (Hammes et al., 2008; Lehmann et al., 2008; Singh et al., 2012; Bird et al., 2015). It is also possible that erosional deposition and burial of PyC is a more significant process for the long-term stabilization of PyC than previously considered. If erosion is playing a significant role in the stabilization of PyC and if decomposition rates of PyC are consistently over-estimated, this could have major implications for global models of PyC cycling and storage (Bird et al., 2015). Parameterizing global stocks and fluxes of PyC is critical, because PyC could be serving a major role that has so far not been accounted properly in global C budgets (Lehmann, 2007; Santín et al., 2015).

While current box models, such as in Bird et al. (2015), suggest that erosion is playing a role in redistributing PyC and a role in burying it for longer-term storage within the soil system, these models are a simplification of the global PyC cycle that do not include quantitative inputs such as type of erosion, climate data, and topography, which are critical for determining the effects of erosion on PyC turnover times and persistence. What can conclusively be drawn from the model scenarios presented here is that the role of erosion of PyC should not be ignored as a factor controlling its long-term fate within the soil and that further research is needed to quantitatively describe and realize the variability in these systems.

## Remaining Uncertainties in PyC Erosion and Recommendations for Future Research

The variation in the estimates of loss of PyC reflects both the spectrum of methodologies used to measure PyC and the lack of inclusion of erosion and other processes, such as leaching, as loss mechanisms. The dynamics of PyC within the soil system depends on prevalent environmental conditions, such as temperature, precipitation, land use, slope, aspect, and vegetation. Available data on the magnitude of loss of PyC from the soil by different processes is currently incomplete, and has a lot of uncertainty, making model parameterization very difficult (see **Table 1** for published magnitudes of fluxes of PyC). In particular, the rates of erosion and burial of PyC and the mechanisms and magnitude of the transport of PyC from land to water need further investigation (Bird et al., 2015; Santín et al.,

2016), particularly in ecosystems that are susceptible to erosion, such as upland temperate forests.

One of the major challenges in quantifying PyC fluxes within the environment is that no single analytical technique can measure the range of materials that make up PyC continuum, including soot, charcoal, and charred biomass (Masiello, 2004). Many different techniques (e.g., physical separation, nuclear magnetic resonance spectroscopy, mid-infrared spectroscopy, benzene polycarboxylic acid, mid-infrared spectroscopy, and partial least squares regression) are currently being used to measure PyC concentration and composition (Schmidt and Noack, 2000; Gustafsson et al., 2001; Masiello, 2004; Preston and Schmidt, 2006; Hammes et al., 2007; De La Rosa et al., 2008; Wiedemeier et al., 2013, 2015; Cotrufo et al., 2016), with varying degrees of accuracy for quantifying different types of compounds in the PyC continuum (Masiello, 2004; Hammes et al., 2007). Due to the variety of techniques currently used, and a lack of meaningful standardization methods for the different techniques, direct comparison of published results is extremely difficult. Many PyC-like, aromatic materials can be confounded with PyC in some of these techniques, further adding error to these analyses, along with some of them having varying degrees of sensitivity to aromatic condensation (Skjemstad et al., 1999). Hence, the data and arguments presented above are based on the most conservative results and least contradictory conclusions that we could draw from published literature.

In the simple decay model presented here (**Figure 5**), in the absence of new input, the soil's PyC stocks were declining considerably lower than the current PyC soil stock measurements would suggest. It is likely that the inferred or measured rates of PyC loss in soils are overestimating the effectiveness of microbial decomposition, especially for the studies generated from short-term laboratory experiments conducted under ideal climate and environmental conditions, especially since some research has indicated an initial priming effect with the addition of PyC (Zimmerman et al., 2011). In longer-term laboratory incubations and models, rates of PyC decomposition are considerably lower and are generally non-linear (Kuzyakov et al., 2009; Foereid et al., 2011), in contrast to the linear the model presented here. Future modeling efforts should focus on the temporal variability in inputs of PyC into the soil in addition to the role of erosion as both and input and loss process for PyC.

## CONCLUSIONS

Interactions of environmental perturbations such as fire and erosion can play significant roles in regulating PyC and SOM persistence in dynamic landscapes. The synthesis of published results and the model presented here illustrates how not accounting for integrated dynamic decomposition and geomorphological processes can lead to significant errors in our current understanding of PyC dynamics in the terrestrial ecosystem. Specifically, not accounting for post-fire erosion could lead to significant differences in projected stocks and turnover times of PyC within the soil, depending on specific ecosystem properties such as erosion and decomposition rates. These differences in stock and turnover time vary based on landform position, rates and drivers of erosion, among other factors.

Understanding the long-term fate of terrestrial OM and PyC is critical for generating accurate models and to better manage these ecosystems to maximize soil C storage. Considering climate change, understanding the controls on the PyC cycle may become ever more critical for managing soil C cycle. This is particularly relevant as the relative roles of fire and erosion as controlling forces of the soil PyC cycle may act in different ways under altered climatic regimes and across different ecosystems and regions. PyC is an important component of the global C cycle that is being assessed for its potential to account for the missing C sink and biochar addition to soil is being discussed as one of many approaches that can be used to mitigate climate change (Lehmann, 2007). It is critically important for future research to focus on more quantitative understanding of the production, stocks and major loss processes for PyC from the soil, including decomposition, erosion, leaching, and consumption in subsequent fires. However, currently, the uncertainties in comparing loss rates from different ecosystems and measurement techniques make global synthesis difficult, in addition to uncertainties in current stock estimates. Moreover, major gaps remain in our understanding of the mechanisms and magnitude of PyC loss from the soil system, and it is likely that erosional redistribution of PyC post-fire plays a major role in controlling the fate of PyC in the soil system.

## AUTHOR CONTRIBUTIONS

All authors listed have made a substantial, direct and intellectual contribution to the work, and approved it for publication.

## FUNDING

Funding for this work was provided from the National Science Foundation (CAREER EAR-1352627) award to AAB.

## ACKNOWLEDGMENTS

The authors gratefully acknowledge Caroline Masiello, Fernanda Santos, Stephen Hart, Marilyn Fogel, and Jonathan Sanderman for their helpful and detailed comments on earlier versions of this manuscript.

## REFERENCES

Abiven, S., Hengartner, P., Schneider, M. P. W., Singh, N., and Schmidt, M. W. I. (2011). Pyrogenic carbon soluble fraction is larger and more aromatic in aged charcoal than in fresh charcoal. *Soil Biol. Biochem.* 43, 1615–1617. doi: 10.1016/j.soilbio.2011.03.027

Abney, R., Sanderman, J., Johnson, D., Fogel, M., and Berhe, A. (2017). Post-wildfire erosion in mountainous terrain leads to rapid and major redistribution

of soil organic carbon. *Front. Earth Sci.* 5:99. doi: 10.3389/feart.2017.00099

Al-Hamdan, O. Z., Pierson, F. B., Nearing, M. A., Williams, C. J., Stone, J. J., Kormos, P. R., et al. (2012). Concentrated flow erodibility for physically based erosion models: temporal variability in disturbed and undisturbed rangelands. *Water Resour. Res.* 48:W07504. doi: 10.1029/2011WR011464

Albalasmeh, A. A., Berli, M., Shafer, D. S., and Ghezzehei, T. A. (2013). Degradation of moist soil aggregates by rapid temperature rise under low intensity fire. *Plant Soil* 362, 335–344. doi: 10.1007/s11104-012-1408-z

Andela, N., Morton, D. C., Giglio, L., Chen, Y., van der werf, G. R., Kasibhatla, P. S., et al. (2017). A human-driven decline in global burned area. *Science* 356, 1356–1362. doi: 10.1126/science.aal4108

Araya, S. N., Fogel, M. L., and Berhe, A. A. (2017). Thermal alteration of soil organic matter properties: a systematic study to infer response of Sierra Nevada climosequence soils to forest fires. *Soil* 3, 31–44. doi: 10.5194/soil-3-31-2017

Avnimelech, Y., and McHenry, J. (1984). Enrichment of transported sediments with organic carbon, nutrients, and clay. *Soil Sci. Soc. Am. J.* 48, 259–266. doi: 10.2136/sssaj1984.03615995004800020006x

Baker, V. R. (1988). "Flood erosion," in *Flood Geomorphology*, ed V. R. Baker (New York, NY: John Wiley & Sons), 81–95.

Battin, T., Luyssaert, S., Kaplan, L., Aufdenkampe, A., Richter, A., and Tranvik, L. (2009). The boundless carbon cycle. *Nat. Geosci.* 2, 598–600. doi: 10.1038/ngeo618

Benavides-Solorio, J., and MacDonald, L. H. (2001). Post-fire runoff and erosion from simulated rainfall on small plots, Colorado Front Range. *Hydrol. Process.* 15, 2931–2952. doi: 10.1002/hyp.383

Berhe, A. A. (2012). Decomposition of organic substrates at eroding vs. depositional landform positions. *Plant Soil* 350, 261–280. doi: 10.1007/s11104-011-0902-z

Berhe, A. A., Harden, J., Torn, M., Kleber, M., Burton, S., and Harte, J. (2012). Persistence of soil organic matter in eroding vs. depositional landform positions. *J. Geophys. Res. Biogeosci.* 117:G02019. doi: 10.1029/2011JG001790

Berhe, A. A., Harden, J. W., Torn, M. S., and Harte, J. (2008). Linking soil organic matter dynamics and erosion-induced terrestrial carbon sequestration at different landform positions. *J. Geophys. Res. Biogeosci.* 113:G04039. doi: 10.1029/2008JG000751

Berhe, A. A., Harte, J., Harden, J. W., and Torn, M. S. (2007). The Significance of erosion-induced terrestrial carbon sink. *Bioscience* 57, 337–346. doi: 10.1641/B570408

Berhe, A. A., and Kleber, M. (2013). Erosion, deposition, and the persistence of soil organic matter: mechanistic considerations and problems with terminology. *Earth Surf. Process. Landforms* 38, 908–912. doi: 10.1002/esp.3408

Beyers, J. L., Brown, J. K., Busse, M. D., DeBano, L. F., Elliot, W. J., Folliott, P. F., et al. (2005). *Wildland Fire in Ecosystems Effects of Fire on Soil and Water.* JFSP Synthesis Reports, United States Department of Agriculture.

Bird, M. I., Wynn, J. G., Saiz, G., Wurster, C. M., and McBeath, A. (2015). The pyrogenic carbon cycle. *Annu. Rev. Earth Planet. Sci.* 43, 273–298. doi: 10.1146/annurev-earth-060614-105038

Bodí, M. B., Mataix-Solera, J., Doerr, S. H., and Cerdà, A. (2011). The wettability of ash from burned vegetation and its relationship to Mediterranean plant species type, burn severity and total organic carbon content. *Geoderma* 160, 599–607. doi: 10.1016/j.geoderma.2010.11.009

Bond, T. C., Doherty, S. J., Fahey, D., Forster, P., Berntsen, T., Deangelo, B., et al. (2013). Bounding the role of black carbon in the climate system: a scientific assessment. *J. Geophys. Res. Atmos.* 118, 5380–5552. doi: 10.1002/jgrd.50171

Boot, C., Haddix, M., Paustian, K., and Cotrufo, M. (2015). Distribution of black carbon in ponderosa pine forest floor and soils following the High Park wildfire. *Biogeosciences* 12, 3029–3039. doi: 10.5194/bg-12-3029-2015

Brewer, C. E., Chuang, V. J., Masiello, C. A., Gonnermann, H., Gao, X., Dugan, B., et al. (2014). New approaches to measuring biochar density and porosity. *Biomass Bioener.* 66, 176–185. doi: 10.1016/j.biombioe.2014.03.059

Brodowski, S., John, B., Flessa, H., and Amelung, W. (2006). Aggregate-occluded black carbon in soil. *Eur. J. Soil Sci.* 57, 539–546. doi: 10.1111/j.1365-2389.2006.00807.x

Brown, J. K., and Smith, J. K. (2000). *Wildland Fire in Ecosystems: Effects of Fire on Flora.* General Technical Report. RMRS-GTR-42-vol. 2, US Department of Agriculture, Forest Service, Rocky Mountain Research Station, Ogden, UT.

Cain, M. L., Subler, S., Evans, J. P., and Fortin, M. J. (1999). Sampling spatial and temporal variation in soil nitrogen availability. *Oecologia* 118, 397–404. doi: 10.1007/s004420050741

Campbell, J., Donato, D., Azuma, D., and Law, B. (2007). Pyrogenic carbon emission from a large wildfire in oregon, United States. *J. Geophys. Res. Biogeosci.* 112:GO4014. doi: 10.1029/2007JG000451

Carroll, E. M., Miller, W. W., Johnson, D. W., Saito, L., Qualls, R. G., and Walker, R. F. (2007). Spatial analysis of a large magnitude erosion event following a Sierran Wildfire. *J. Environ. Qual.* 36, 1105–1105. doi: 10.2134/jeq2006.0466

Cerdà, A., and Doerr, S. H. (2005). Influence of vegetation recovery on soil hydrology and erodibility following fire: an 11-year investigation. *Int. J. Wildland Fire* 14, 423–437. doi: 10.1071/WF05044

Cerdà, A., Imeson, A., and Calvo, A. (1995). Fire and aspect induced differences on the erodibility and hydrology of soils at La Costera, Valencia, southeast Spain. *Catena* 24, 289–304. doi: 10.1016/0341-8162(95)00031-2

Certini, G. (2005). Effects of fire on properties of forest soils: a review. *Oecologia* 143, 1–10. doi: 10.1007/s00442-004-1788-8

Chaopricha, N. T., and Marín-Spiotta, E. (2014). Soil burial contributes to deep soil organic carbon storage. *Soil Biol. Biochem.* 69, 251–264. doi: 10.1016/j.soilbio.2013.11.011

Chapin, F., Woodwell, G., Randerson, J., Rastetter, E., Lovett, G., Baldocchi, D., et al. (2006). Reconciling carbon-cycle concepts, terminology, and methods. *Ecosystems* 9, 1041–1050. doi: 10.1007/s10021-005-0105-7

Cope, M., and Chaloner, W. (1980). Fossil charcoal as evidence of past atmospheric composition. *Nature* 283, 647–649. doi: 10.1038/283647a0

Cotrufo, M. F., Boot, C., Abiven, S., Foster, E. J., Haddix, M., Reisser, M., et al. (2016). Quantification of pyrogenic carbon in the environment: an integration of analytical approaches. *Org. Geochem.* 100, 42–50. doi: 10.1016/j.orggeochem.2016.07.007

Czimczik, C. I., and Masiello, C. A. (2007). Controls on black carbon storage in soils. *Glob. Biogeochem. Cycles* 21:GB3005. doi: 10.1029/2006GB002798

DeBano, L. F. (2000). The role of fire and soil heating on water repellency in wildland environments a review. *J. Hydrol.* 231, 195–206. doi: 10.1016/S0022-1694(00)00194-3

DeBano, L. F., Neary, D. G., and Ffolliott, P. F. (1998). *Fire's Effects on Ecosystems.* New York, NY: John Wiley and Sons.

De La Rosa, J. M., González-Pérez, J. A., González-Vázquez, R., Knicker, H., López-Capel, E., Manning, D., et al. (2008). Use of pyrolysis/GC–MS combined with thermal analysis to monitor C and N changes in soil organic matter from a Mediterranean fire affected forest. *Catena* 74, 296–303. doi: 10.1016/j.catena.2008.03.004

Dittmar, T., De Rezende, C. E., Manecki, M., Niggemann, J., Ovalle, A. R. C., Stubbins, A., et al. (2012). Continuous flux of dissolved black carbon from a vanished tropical forest biome. *Nat. Geosci.* 5, 618–622. doi: 10.1038/ngeo1541

Doerr, S. H., and Thomas, A. D. (2000). The role of soil moisture in controlling water repellency: new evidence from forest soils in Portugal. *J. Hydrol.* 231, 134–147. doi: 10.1016/S0022-1694(00)00190-6

Doetterl, S., Berhe, A. A., Nadeu, E., Wang, Z., Sommer, M., and Fiener, P. (2016). Erosion, deposition and soil carbon: a review of process-level controls, experimental tools and models to address C cycling in dynamic landscapes. *Earth Sci. Rev.* 154, 102–122. doi: 10.1016/j.earscirev.2015.12.005

Dyrness, C., and Norum, R. A. (1983). The effects of experimental fires on black spruce forest floors in interior Alaska. *Can. J. For. Res.* 13, 879–893. doi: 10.1139/x83-118

Faria, S., De La Rosa, J., Knicker, H., González-Pérez, J., and Keizer, J. (2015). Molecular characterization of wildfire impacts on organic matter in eroded sediments and topsoil in Mediterranean eucalypt stands. *Catena* 135, 29–37. doi: 10.1016/j.catena.2015.07.007

Foereid, B., Lehmann, J., and Major, J. (2011). Modeling black carbon degradation and movement in soil. *Plant Soil* 345, 223–236. doi: 10.1007/s11104-011-0773-3

Glaser, B. (2002). "Past anthropogenic influence on the present soil properties of anthropogenic dark earths (Terra Preta) in Amazonia (Brazil)," in *Amazonian Dark Earths: Explorations in Space and Time*, eds. B. Glaser and W. I. Woods (Berlin; Heidelberg: Springer-Verlag), 517–530.

Glaser, B., Balashov, E., Haumaier, L., Guggenberger, G., and Zech, W. (2000). Black carbon in density fractions of anthropogenic

soils of the Brazilian Amazon region. *Org. Geochem.* 31, 669–678. doi: 10.1016/S0146-6380(00)00044-9

González-Pérez, J. A., González-Vila, F. J., Almendros, G. and Knicker, H. (2004). The effect of fire on soil organic matter—a review. *Environ. Int.* 30, 855–870. doi: 10.1016/j.envint.2004.02.003

Gray, M., Johnson, M. G., Dragila, M. I., and Kleber, M. (2014). Water uptake in biochars: the roles of porosity and hydrophobicity. *Biomass Bioener.* 61, 196–205. doi: 10.1016/j.biombioe.2013.12.010

Gregorich, E., Greer, K., Anderson, D., and Liang, B. (1998). Carbon distribution and losses: erosion and deposition effects. *Soil Tillage Res.* 47, 291–302. doi: 10.1016/S0167-1987(98)00117-2

Güereña, D. T., Lehmann, J., Walter, T., Enders, A., Neufeldt, H., Odiwour, H., et al. (2015). Terrestrial pyrogenic carbon export to fluvial ecosystems: lessons learned from the White Nile watershed of East Africa. *Glob. Biogeochem. Cycles* 29, 1911–1928. doi: 10.1002/2015GB005095

Gustafsson, Ö., Bucheli, T. D., Kukulska, Z., Andersson, M., Largeau, C., Rouzaud, J. N., et al. (2001). Evaluation of a protocol for the quantification of black carbon in sediments. *Glob. Biogeochem. Cycles* 15, 881–890. doi: 10.1029/2000GB001380

Hammes, K., Schmidt, M. W. I., Smernik, R. J., Currie, L. A., Ball, W. P., Nguyen, T. H., et al. (2007). Comparison of quantification methods to measure fire-derived (black/elemental) carbon in soils and sediments using reference materials from soil, water, sediment and the atmosphere. *Glob. Biogeochem. Cycles* 21:GB3016. doi: 10.1029/2006GB002914

Hammes, K., Torn, M. S., Lapenas, A. G., and Schmidt, M. W. I. (2008). Centennial black carbon turnover observed in a Russian steppe soil. *Biogeosciences* 5, 1339–1350. doi: 10.5194/bg-5-1339-2008

Harden, J. W., Berhe, A. A., Torn, M., Harte, J., Liu, S., and Stallard, R. F. (2008). Soil erosion: data say C sink. *Science* 320, 178–179. doi: 10.1126/science.320.5873.178

Hatten, J. A., and Zabowski, D. (2009). Changes in soil organic matter pools and carbon mineralization as influenced by fire severity. *Soil Sci. Soc. Am. J.* 73, 262–273. doi: 10.2136/sssaj2007.0304

Highwood, E. J., and Kinnersley, R. P. (2006). When smoke gets in our eyes: the multiple impacts of atmospheric black carbon on climate, air quality and health. *Environ. Int.* 32, 560–566. doi: 10.1016/j.envint.2005.12.003

Hockaday, W. C., Grannas, A. M., Kim, S., and Hatcher, P. G. (2006). Direct molecular evidence for the degradation and mobility of black carbon in soils from ultrahigh-resolution mass spectral analysis of dissolved organic matter from a fire-impacted forest soil. *Org. Geochem.* 37, 501–510. doi: 10.1016/j.orggeochem.2005.11.003

Imeson, A., and Lavee, H. (1998). Soil erosion and climate change: the transect approach and the influence of scale. *Geomorphology* 23, 219–227. doi: 10.1016/S0169-555X(98)00005-1

Inbar, M., Tamir, M. I., and Wittenberg, L. (1998). Runoff and erosion processes after a forest fire in Mount Carmel, a Mediterranean area. *Geomorphology* 24, 17–33. doi: 10.1016/S0169-555X(97)00098-6

Iniguez, J., Swetnam, T., and Yool, S. (2008). Topography affected landscape fire history patterns in southern Arizona, USA. *For. Ecol. Manage.* 256, 295–303. doi: 10.1016/j.foreco.2008.04.023

IPCC (2013). "Summary for Policymakers," in *Climate Change 2013: The Physical Science Basis, Working Group I Contribution to the Fifth Assessment Report of the Intergovernmental Panel on Climate Change,* eds. T. F. Stocker, D. Qin, G.-K. Plattner, M. Tignor, S. K. Allen, J. Boschung, A. Nauels, Y. Xia, V. Bex, and P. M. Midgley (Cambridge, UK; New York, NY: Cambridge University Press).

Istanbulluoglu, E., Yetemen, O., Vivoni, E. R., Gutiérrez-Jurado, H. A., and Bras, R. L. (2008). Eco-geomorphic implications of hillslope aspect: inferences from analysis of landscape morphology in central New Mexico. *Geophys. Res. Lett.* 35:L14403. doi: 10.1029/2008GL034477

Jacinthe, P., and Lal, R. (2001). A mass balance approach to assess carbon dioxide evolution during erosional events. *Land Degr. Dev.* 12, 329–339. doi: 10.1002/ldr.454

Jaffé, R., Ding, Y., Niggemann, J., Vähätalo, A. V., Stubbins, A., Spencer, R. G., et al. (2013). Global charcoal mobilization from soils via dissolution and riverine transport to the oceans. *Science* 340, 345–347. doi: 10.1126/science.1231476

Johnson, D., Murphy, J., Walker, R., Glass, D., and Miller, W. (2007). Wildfire effects on forest carbon and nutrient budgets. *Ecol. Eng.* 31, 183–192. doi: 10.1016/j.ecoleng.2007.03.003

Jurado, E., Dachs, J., Duarte, C. M., and Simó, R. (2008). Atmospheric deposition of organic and black carbon to the global oceans. *Atmos. Environ.* 42, 7931–7939. doi: 10.1016/j.atmosenv.2008.07.029

Kasischke, E. S., Turetsky, M. R., Ottmar, R. D., French, N. H., Hoy, E. E., and Kane, E. S. (2008). Evaluation of the composite burn index for assessing fire severity in Alaskan black spruce forests. *Int. J. Wildland Fire* 17, 515–526. doi: 10.1071/WF08002

Keeley, J. E. (2009). Fire intensity, fire severity and burn severity: a brief review and suggested usage. *Int. J. Wildland Fire* 18, 116–126. doi: 10.1071/WF07049

Kinnell, P. (2005). Raindrop-impact-induced erosion processes and prediction: a review. *Hydrol. Process* 19, 2815–2844. doi: 10.1002/hyp.5788

Knicker, H. (2007). How does fire affect the nature and stability of soil organic nitrogen and carbon? A review. *Biogeochemistry* 85, 91–118. doi: 10.1007/s10533-007-9104-4

Kozlowski, T. T., and Ahlgren, C. E. (1974). *Fire and Ecosystems*. New York, NY: Academic Press.

Kuzyakov, Y., Subbotina, I., Chen, H., Bogomolova, I., and Xu, X. (2009). Black carbon decomposition and incorporation into soil microbial biomass estimated by C-14 labeling. *Soil Biol. Biochem.* 41, 210–219. doi: 10.1016/j.soilbio.2008.10.016

Kyuma, K., Tulaphitak, T., and Pairintra, C. (1985). Changes in soil fertility and tilth under shifting cultivation. *Soil Sci. Plant Nutr.* 31, 227–238. doi: 10.1080/00380768.1985.10557429

Laflen, J. M., Lane, L. J., Foster, G. R., and Usda, A. R. S. (1991). WEPP: a new generation of erosion prediction technology. *J. Soil Water Conserv.* 46, 34–38.

Lal, R. (2003). Soil erosion and the global carbon budget. *Environ. Int.* 29, 437–450. doi: 10.1016/S0160-4120(02)00192-7

Lal, R. (2004). Soil carbon sequestration impacts on global climate change and food security. *Science* 304, 1623–1627. doi: 10.1126/science.1097396

Lehmann, J. (2007). Bio-energy in the black. *Front. Ecol. Environ.* 5, 381–387. doi: 10.1890/1540-9295(2007)5[381:BITB]2.0.CO;2

Lehmann, J., and Joseph, S. (2015). *Biochar for Environmental Management: Science, Technology and Implementation*. Milton Park: Routledge.

Lehmann, J., Liang, B., Solomon, D., Lerotic, M., Luizão, F., Kinyangi, J., et al. (2005). Near-edge X-ray absorption fine structure (NEXAFS) spectroscopy for mapping nano-scale distribution of organic carbon forms in soil: application to black carbon particles. *Glob. Biogeochem. Cycles* 19, 1013–1025. doi: 10.1029/2004GB002435

Lehmann, J., Skjemstad, J., Sohi, S., Carter, J., Barson, M., Falloon, P., et al. (2008). Australian climate–carbon cycle feedback reduced by soil black carbon. *Nat. Geosci.* 1, 832–835. doi: 10.1038/ngeo358

Liu, S., Bliss, N., Sundquist, E., and Huntington, T. (2003). Modeling carbon dynamics in vegetation and soil under the impact of soil erosion and deposition. *Glob. Biogeochem. Cycles* 17:1074. doi: 10.1029/2002GB002010

MacDonald, L. H., Sampson, R. W., and Anderson, D. M. (2001). Runoff and road erosion at the plot and road segment scales, St John, US Virgin Islands. *Earth Surface Process. Landforms* 26, 251–272. doi: 10.1002/1096-9837(200103)26:3<251::AID-ESP173>3.0.CO;2-X

Major, J., Lehmann, J., Rondon, M., and Goodale, C. (2010). Fate of soil-applied black carbon: downward migration, leaching and soil respiration. *Glob. Chang. Biol.* 16, 1366–1379. doi: 10.1111/j.1365-2486.2009.02044.x

Marín-Spiotta, E., Chaopricha, N. T., Plante, A. F., Diefendorf, A. F., Muller, C. W., Grandy, S., et al. (2014). Long-term stabilization of deep soil carbon by fire and burial during early Holocene climate change. *Nat. Geosci.* 7, 428–432. doi: 10.1038/ngeo2169

Masiello, C. (2004). New directions in black carbon organic geochemistry. *Mar. Chem.* 92, 201–213. doi: 10.1016/j.marchem.2004.06.043

Masiello, C. A. (1998). Black carbon in deep-sea sediments. *Science* 280, 1911–1913. doi: 10.1126/science.280.5371.1911

Masiello, C. A., and Louchouarn, P. (2013). Fire in the Ocean. *Science* 340, 287–288. doi: 10.1126/science.1237688

Mataix-Solera, J., Cerda, A., Arcenegui, V., Jordan, A., and Zavala, L. M. (2011). Fire effects on soil aggregation: a review. *Earth Sci. Rev.* 109, 44–60. doi: 10.1016/j.earscirev.2011.08.002

McCorkle, E. P., Berhe, A. A., Hunsaker, C. T., Johnson, D. W., Macfarlane, K. J., Fogel, M. L., et al. (2016). Tracing the source of soil organic matter eroded from temperate forest catchments using carbon and nitrogen isotopes. *Chem. Geol.* 445, 172–184. doi: 10.1016/j.chemgeo.2016.04.025

Miller, M. E., Bowker, M. A., Reynolds, R. L., and Goldstein, H. L. (2012). Post-fire land treatments and wind erosion–lessons from the Milford Flat Fire, UT, USA. *Aeolian Res.* 7, 29–44. doi: 10.1016/j.aeolia.2012.04.001

Mimmo, T., Panzacchi, P., Baratieri, M., Davies, C., and Tonon, G. (2014). Effect of pyrolysis temperature on miscanthus (Miscanthus × giganteus) biochar physical, chemical and functional properties. *Biomass Bioener.* 62, 149–157. doi: 10.1016/j.biombioe.2014.01.004

Montgomery, D. R., and Brandon, M. T. (2002). Topographic controls on erosion rates in tectonically active mountain ranges. *Earth Planet. Sci. Lett.* 201, 481–489. doi: 10.1016/S0012-821X(02)00725-2

Moody, J. A., Shakesby, R., Robichaud, P., Cannon, S., and Martin, D. A. (2013). Current research issues related to post-wildfire runoff and erosion processes. *Earth Sci. Rev.* 122, 10–37. doi: 10.1016/j.earscirev.2013.03.004

Munro, D. S., and Huang, L. (1997). Rainfall, evaporation and runoff responses to hillslope aspect in the Shenchong Basin. *Catena* 29, 131–144. doi: 10.1016/S0341-8162(96)00051-3

Nadeu, E., Berhe, A. A., De Vente, J., and Boix-Fayos, C. (2012). Erosion, deposition and replacement of soil organic carbon in Mediterranean catchments: a geomorphological, isotopic and land use change approach. *Biogeosciences* 9, 1099–1111. doi: 10.5194/bg-9-1099-2012

Naisse, C., Girardin, C., Lefevre, R., Pozzi, A., Maas, R., Stark, A., et al. (2015). Effect of physical weathering on the carbon sequestration potential of biochars and hydrochars in soil. *Glob. Change Biol. Bioener.* 7, 488–496. doi: 10.1111/gcbb.12158

National Interagency Fire Center (2015). *National Report of Wildland Fires and Acres Burned by State.* Available online at: https://www.nifc.gov/fireInfo/fireInfo_statistics.html (Accessed June 5, 2015).

Nearing, M. (1998). Why soil erosion models over-predict small soil losses and under-predict large soil losses. *Catena* 32, 15–22. doi: 10.1016/S0341-8162(97)00052-0

Neary, D. G., Klopatek, C. C., DeBano, L. F., and Ffolliott, P. F. (1999). Fire effects on belowground sustainability: a review and synthesis. *For. Ecol. Manage.* 122, 51–71. doi: 10.1016/S0378-1127(99)00032-8

Nguyen, B. T., and Lehmann, J. (2009). Black carbon decomposition under varying water regimes. *Org. Geochem.* 40, 846–853. doi: 10.1016/j.orggeochem.2009.05.004

Nguyen, B. T., Lehmann, J., Hockaday, W. C., Joseph, S., and Masiello, C. A. (2010). Temperature sensitivity of black carbon decomposition and oxidation. *Environ. Sci. Technol.* 44, 3324–3331. doi: 10.1021/es903016y

Nguyen, B. T., Lehmann, J., Kinyangi, J., Smernik, R., Riha, S. J., and Engelhard, M. H. (2009). Long-term black carbon dynamics in cultivated soil. *Biogeochemistry* 92, 163–176. doi: 10.1007/s10533-008-9248-x

Parsons, A. J., Brazier, R. E., Wainwright, J., and Powell, D. M. (2006). Scale relationships in hillslope runoff and erosion. *Earth Surf. Process. Landforms* 31, 1384–1393. doi: 10.1002/esp.1345

Parungo, F., Nagamoto, C., Zhou, M.-Y., Hansen, A. D., and Harris, J. (1994). Aeolian transport of aerosol black carbon from China to the ocean. *Atmos. Environ.* 28, 3251–3260. doi: 10.1016/1352-2310(94)00164-G

Pereira, P., Cerdà, A., Úbeda, X., Mataix-Solera, J., Arcenegui, V., and Zavala, L. (2015). Modelling the impacts of wildfire on ash thickness in a short-term period. *Land Degr. Dev.* 26, 180–192. doi: 10.1002/ldr.2195

Pierson, F. B., Moffet, C. A., Williams, C. J., Hardegree, S. P., and Clark, P. E. (2009). Prescribed-fire effects on rill and interrill runoff and erosion in a mountainous sagebrush landscape. *Earth Surf. Process. Landforms* 34, 193–203. doi: 10.1002/esp.1703

Pierson, F. B., Robichaud, P. R., Moffet, C. A., Spaeth, K. E., Hardegree, S. P., Clark, P. E., et al. (2008). Fire effects on rangeland hydrology and erosion in a steep sagebrush-dominated landscape. *Hydrol. Process* 22, 2916–2929. doi: 10.1002/hyp.6904

Pierson, F. B., Slaughter, C. W., and Cram, Z. K. (2001). Long-term stream discharge and suspended-sediment database, Reynolds Creek experimental Watershed, Idaho, United States. *Water Resour. Res.* 37, 2857–2861. doi: 10.1029/2001WR000420

Pierson, F. B., Williams, C. J., Hardegree, S. P., Clark, P. E., Kormos, P. R., and Al-Hamdan, O. Z. (2013). Hydrologic and erosion responses of sagebrush steppe following juniper encroachment, wildfire, and tree cutting. *Rangeland Ecol. Manage.* 66, 274–289. doi: 10.2111/REM-D-12-00104.1

Potter, M. (1908). Bacteria as agents in the oxidation of amorphous carbon. *Proc. R. Soc. Lond. Ser. B Conf. Pap. Biol. Char.* 80, 239–259. doi: 10.1098/rspb.1908.0023

Preston, C. M. (2009). Biogeochemistry: fire and it's black legacy. *Nat. Geosci.* 2:674. doi: 10.1038/ngeo642

Preston, C., and Schmidt, M. (2006). Black (pyrogenic) carbon in boreal forests: a synthesis of current knowledge and uncertainties. *Biogeosci. Discuss.* 3, 211–271. doi: 10.5194/bgd-3-211-2006

Pyle, L. A., Hockaday, W. C., Boutton, T., Zygourakis, K., Kinney, T. J., and Masiello, C. A. (2015). Chemical and isotopic thresholds in charring: implications for the interpretation of charcoal mass and isotopic data. *Environ. Sci. Technol.* 49, 14057–14064. doi: 10.1021/acs.est.5b03087

Pyle, L. A., Magee, K. L., Gallagher, M. E., Hockaday, W. C., and Masiello, C. A. (2017). Short-term changes in physical and chemical properties of soil charcoal support enhanced landscape mobility. *J. Geophys. Res. Biogeosci.* 122, 3098–3107. doi: 10.1002/2017JG003938

Ravi, S., D'odorico, P., Zobeck, T. M., Over, T. M., and Collins, S. L. (2007). Feedbacks between fires and wind erosion in heterogeneous arid lands. *J. Geophys. Res. Biogeosci.* 112:G04007. doi: 10.1029/2007JG000474

Regnier, P., Friedlingstein, P., Ciais, P., Mackenzie, F. T., Gruber, N., Janssens, I. A., et al. (2013). Anthropogenic perturbation of the carbon fluxes from land to ocean. *Nat. Geosci.* 6, 597–607. doi: 10.1038/ngeo1830

Renard, K. G., Foster, G. R., Weesies, G., McCool, D., and Yoder, D. (1997). *Predicting Soil Erosion by Water: A Guide to Conservation Planning with the Revised Universal Soil Loss Equation (RUSLE).* Washington, DC: US Government Printing Office.

Riebe, C., Kirchner, J., Granger, D., and Finkel, R. (2001). Minimal climatic control on erosion rates in the Sierra Nevada, California. *Geology* 29, 447–450. doi: 10.1130/0091-7613(2001)029<0447:MCCOER>2.0.CO;2

Robichaud, P. R. (1997). *Spatially-Varied Erosion Potential from Harvested Hillslopes after Prescribed Fire in the Interior Northwest*. Ph.D. thesis, University of Idaho.

Rumpel, C., Ba, A., Darboux, F., Chaplot, V., and Planchon, O. (2009). Erosion budget and process selectivity of black carbon at meter scale. *Geoderma* 154, 131–137. doi: 10.1016/j.geoderma.2009.10.006

Rumpel, C., Chaplot, V., Planchon, O., Bernadou, J., Valentin, C., and Mariotti, A. (2006). Preferential erosion of black carbon on steep slopes with slash and burn agriculture. *CATENA* 65, 30–40. doi: 10.1016/j.catena.2005.09.005

Sander, M., and Pignatello, J. J. (2005). Characterization of charcoal sorption sites for aromatic compounds: insights drawn from single-solute and bi-solute competitive experiments. *Environ. Sci. Technol.* 39, 1606–1615. doi: 10.1021/es049135l

Santín, C., Doerr, S. H., Kane, E. S., Masiello, C. A., Ohlson, M., de la Rosa, M., et al. (2016). Towards a global assessment of pyrogenic carbon from vegetation fires. *Glob. Chang. Biol.* 22, 76–91. doi: 10.1111/gcb.12985

Santín, C., Doerr, S. H., Preston, C. M., and González-Rodríguez, G. (2015). Pyrogenic organic matter production from wildfires: a missing sink in the global carbon cycle. *Glob. Chang. Biol.* 21, 1621–1633. doi: 10.1111/gcb.12800

Santos, F., Torn, M. S., and Bird, J. A. (2012). Biological degradation of pyrogenic organic matter in temperate forest soils. *Soil Biol. Biochem.* 15, 115–124. doi: 10.1016/j.soilbio.2012.04.005

Schiettecatte, W., Gabriels, D., Cornelis, W., and Hofman, G. (2008). Enrichment of organic carbon in sediment transport by interrill and rill erosion processes. *Soil Sci. Soc. Am. J.* 72, 50–55. doi: 10.2136/sssaj2007.0201

Schmidt, M. W. I., and Noack, A. G. (2000). Black carbon in soils and sediments: analysis, distribution, implications, and current challenges. *Glob. Biogeochem. Cycles* 14, 777–793. doi: 10.1029/1999GB001208

Schmidt, M. W., Torn, M. S., Abiven, S., Dittmar, T., Guggenberger, G., Janssens, I. A., et al. (2011). Persistence of soil organic matter as an ecosystem property. *Nature* 478, 49–56. doi: 10.1038/nature10386

Seiler, W. (1980). Estimates of gross and net fluxes of carbon between the biosphere and the atmosphere from biomass burning. *Clim. Change* 2, 207–247. doi: 10.1007/BF00137988

Shakesby, R. (2011). Post-wildfire soil erosion in the Mediterranean: review and future research directions. *Earth Sci. Rev.* 105, 71–100. doi: 10.1016/j.earscirev.2011.01.001

Shakesby, R., Coelho, C., Ferreira, A., Terry, J., and Walsh, R. (1993). Wildfire impacts on soil-erosion and hydrology in wet Mediterranean forest, Portugal. *Int. J. Wildland Fire* 3, 95–110. doi: 10.1071/WF9930095

Shakesby, R., and Doerr, S. (2006). Wildfire as a hydrological and geomorphological agent. *Earth Sci. Rev.* 74, 269–307. doi: 10.1016/j.earscirev.2005.10.006

Sharpley, A. (1985). The selection erosion of plant nutrients in runoff. *Soil Sci. Soc. Am. J.* 49, 1527–1534. doi: 10.2136/sssaj1985.03615995004900060039x

Singh, N., Abiven, S., Torn, M. S., and Schmidt, M. (2012). Fire-derived organic carbon in soil turns over on a centennial scale. *Biogeosciences* 9, 2847–2857. doi: 10.5194/bg-9-2847-2012

Skjemstad, J. O. (1996). The chemistry and nature of protected carbon in soil. *Aust. J. Soil Res.* 34, 251–271. doi: 10.1071/SR9960251

Skjemstad, J., Taylor, J., and Smernik, R. (1999). Estimation of charcoal (char) in soils. *Commun. Soil Sci. Plant Anal.* 30, 2283–2298. doi: 10.1080/00103629909370372

Soucémarianadin, L. N., Quideau, S. A., Wasylishen, R. E., and Munson, A. D. (2015). Early-season fires in boreal black spruce forests produce pyrogenic carbon with low intrinsic recalcitrance. *Ecology* 96, 1575–1585. doi: 10.1890/14-1196.1

Stacy, E., Hart, S. C., Hunsaker, C. T., Johnson, D. W., and Berhe, A. A. (2015). Soil carbon and nitrogen erosion in forested catchments: implications for erosion-induced terrestrial carbon sequestration. *Biogeosci. Discuss.* 12, 2491–2532. doi: 10.5194/bgd-12-2491-2015

Stallard, R. F. (1998). Terrestrial sedimentation and the carbon cycle: coupling weathering and erosion to carbon burial. *Glob. Biogeochem. Cycles* 12, 231–257. doi: 10.1029/98GB00741

Torn, M., Trumbore, S., Chadwick, O., Vitousek, P., and Hendricks, D. (1997). Mineral control of soil organic carbon storage and turnover. *Nature* 389, 170–173. doi: 10.1038/38260

Wang, Z., Govers, G., Steegen, A., Clymans, W., Van Den Putte, A., Langhans, C., et al. (2010). Catchment-scale carbon redistribution and delivery by water erosion in an intensively cultivated area. *Geomorphology* 124, 65–74. doi: 10.1016/j.geomorph.2010.08.010

Westerling, A. L., Hidalgo, H. G., Cayan, D. R., and Swetnam, T. W. (2006). Warming and earlier spring increase western US forest wildfire activity. *Science* 313, 940–943. doi: 10.1126/science.1128834

Whitman, T. L., Zhu, Z., and Lehmann, J. (2014). Carbon mineralizability determines interactive effects on mineralization of pyrogenic organic matter and soil organic carbon. *Environ. Sci. Technol.* 48, 13727–13734. doi: 10.1021/es503331y

Wiedemeier, D. B., Abiven, S., Hockaday, W. C., Keiluweit, M., Kleber, M., Masiello, C. A., et al. (2015). Aromaticity and degree of aromatic condensation of char. *Org. Geochem.* 78, 135–143. doi: 10.1016/j.orggeochem.2014.10.002

Wiedemeier, D. B., Hilf, M. D., Smittenberg, R. H., Haberle, S. G., and Schmidt, M. W. (2013). Improved assessment of pyrogenic carbon quantity and quality in environmental samples by high-performance liquid chromatography. *J. Chromatogr. A* 1304, 246–250. doi: 10.1016/j.chroma.2013.06.012

Wischmeier, W. (1962). Storms and soil conservation. *J. Soil Water Conserv.* 17, 55–59.

Wischmeier, W. H., and Smith, D. D. (1965). "Predicting rainfall-erosion losses from cropland east of the Rocky Mountains-Guide for selection of practices for soil and water conservation," in *Agriculture Handbook No. 282* (Washington, DC: United States Department of Agriculture), 1–47.

Wischmeier, W. H., and Smith, D. D. (1978). "Predicting rainfall erosion losses," in *Agriculture Handbook No. 537* (Washington, DC: United States Department of Agriculture), 1–61.

Wondzell, S. M., and King, J. G. (2003). Postfire erosional processes in the Pacific Northwest and Rocky Mountain regions. *For. Ecol. Manage.* 178, 75–87. doi: 10.1016/S0378-1127(03)00054-9

Yao, J., Hockaday, W. C., Murray, D. B., and White, J. D. (2014). Changes in fire-derived soil black carbon storage in a subhumid woodland. *J. Geophys. Res. Biogeosci.* 119, 1807–1819. doi: 10.1002/2014JG002619

Zimmerman, A. (2010). Abiotic and microbial oxidation of laboratory-produced black carbon (biochar). *Environ. Sci. Technol.* 44, 1295–1301. doi: 10.1021/es903140c

Zimmerman, A. R., and Gao, B. (2013). "The stability of biochar in the environment," in *Biochar and Soil Biota*, eds N. Ladygina and F. Rineau (Boca Raton, FL: CRC press), 1–40.

Zimmerman, A. R., Gao, B., and Ahn, M.-Y. (2011). Positive and negative carbon mineralization priming effects among a variety of biochar-amended soils. *Soil Biol. Biochem.* 43, 1169–1179. doi: 10.1016/j.soilbio.2011.02.005

Zimmermann, M., Bird, M. I., Wurster, C., Saiz, G., Goodrick, I., Barta, J., et al. (2012). Rapid degradation of pyrogenic carbon. *Glob. Chang. Biol.* 18, 3306–3316. doi: 10.1111/j.1365-2486.2012.02796.x

Ziolkowski, L., and Druffel, E. (2010). Aged black carbon identified in marine dissolved organic carbon. *Geophys. Res. Lett.* 37:L16601. doi: 10.1029/2010GL043963

**Conflict of Interest Statement:** The authors declare that the research was conducted in the absence of any commercial or financial relationships that could be construed as a potential conflict of interest.

frontiers in Earth Science

ORIGINAL RESEARCH
published: 29 November 2017
doi: 10.3389/feart.2017.00099

# Post-wildfire Erosion in Mountainous Terrain Leads to Rapid and Major Redistribution of Soil Organic Carbon

*Rebecca B. Abney*[1,2*], *Jonathan Sanderman*[3,4], *Dale Johnson*[5], *Marilyn L. Fogel*[6] and *Asmeret Asefaw Berhe*[1]

[1] Environmental Systems, Life and Environmental Sciences, University of California, Merced, Merced, CA, United States, [2] School of Public and Environmental Affairs, Indiana University, Bloomington, IN, United States, [3] Woods Hole Research Center, Falmouth, MA, United States, [4] Commonwealth Scientific and Industrial Research Organisation, Hobart, TAS, Australia, [5] Department of Natural Resources and Environmental Science, University of Nevada, Reno, NV, United States, [6] Department of Earth Sciences, University of California, Riverside, Riverside, CA, United States

Catchments impacted by wildfire typically experience elevated rates of post-fire erosion and formation and deposition of pyrogenic carbon (PyC). To better understand the role of erosion in post-fire soil carbon dynamics, we determined distribution of soil organic carbon (SOC) in different chemical fractions before and after the Gondola fire in South Lake Tahoe, CA. We analyzed soil samples from eroding and depositional landform positions in control and burned plots pre- and post-wildfire (in 2002, 2003, and 10-years post-fire in 2013). We determined elemental concentrations, stable isotope compositions, and biochemical composition of organic matter (OM) using mid-infrared (MIR) spectroscopy for all of the samples. A subset of samples was analyzed by $^{13}C$ cross polarization magic angle spinning nuclear magnetic resonance spectroscopy (CPMAS $^{13}C$-NMR). We combined the MIR and CPMAS $^{13}C$-NMR data in the Soil Carbon Research Program (SCaRP) partial least squares regression model to predict distribution of soil carbon into three different fractions: (1) particulate, humic, and resistant OM fractions representing relatively fresh larger pieces of OM, (2) fine, decomposed OM, and (3) pyrogenic C, respectively. Samples from the post-fire eroding landform position showed no major difference in SOC fractions 1 year post-fire. The depositional samples, however, had increased concentrations of all SOC fractions, particularly the fraction that resembles PyC, 1 year post-fire (2002), which had a mean of 160 g/kg compared with burned hillslope soils, which had 84 g/kg. The increase in all SOC fractions in the post-fire depositional landform position 1 year post-fire indicates significant lateral mobilization of the eroded PyC. In addition, our NMR analyses revealed a post-fire increase in both the aryl and O-aryl carbon compounds in the soils from the depositional landform position, indicating increases in soil PyC concentrations post-fire. After 10 years, the C concentration from all three fractions declined in the depositional landform position to below pre-fire levels likely due to further erosion or elevated rates of decomposition. Thus, we found, at this site, that both fire and erosion exert significant influence on the distribution of PyC throughout a landscape and its long-term fate in the soil system.

**Keywords: erosion, pyrogenic carbon, soil organic carbon, stabilization, wildfire**

OPEN ACCESS

***Edited by:***
*Samuel Abiven,*
*University of Zurich, Switzerland*

***Reviewed by:***
*Caroline Margaret Preston,*
*Natural Resources Canada, Canada*
*Philippa Louise Ascough,*
*Scottish Universities Environmental Research Centre, United Kingdom*

***Correspondence:**
*Rebecca B. Abney*
*rebabney@iu.edu*

***Specialty section:***
*This article was submitted to Biogeoscience, a section of the journal Frontiers in Earth Science*

***Received:*** *16 September 2017*
***Accepted:*** *13 November 2017*
***Published:*** *29 November 2017*

***Citation:***
*Abney RB, Sanderman J, Johnson D, Fogel ML and Berhe AA (2017) Post-wildfire Erosion in Mountainous Terrain Leads to Rapid and Major Redistribution of Soil Organic Carbon. Front. Earth Sci. 5:99. doi: 10.3389/feart.2017.00099*

## INTRODUCTION

The soil system plays major role in the global terrestrial carbon (C) cycle, as it stores more C than the biosphere and atmosphere combined (Post and Kwon, 2000; Lal, 2003a; Scharlemann et al., 2014) in pools that cycle at a slower rate than the C in the atmosphere or biosphere (Lal, 2004). The ability of the soil system to store and cycle carbon, however, is modified by a range of physical perturbations that the soil system experiences, including fire and erosion (Lal, 2003b; Berhe et al., 2007; Bird et al., 2015; Santin et al., 2015).

Fire can have multiple direct and indirect effects on the biogeochemical cycling of C in the terrestrial ecosystem. For example, the release of nutrients from burned biomass can lead to a spike in initial productivity and subsequent regrowth in plant life post-fire (Johnson et al., 2004, 2007). The loss of vegetation that would otherwise stabilize soil in eroding landform positions, along with increased soil hydrophobicity after moderate severity fires leaves soil more directly exposed to weathering and erosion (DeBano, 2000; Shakesby et al., 2000; Larsen et al., 2009). Fires can also raise soil pH, alter cation exchange capacity, and change the soil organic matter (SOM) composition (Giovannini et al., 1988; DeBano, 1991; Certini, 2005; Liang et al., 2006; Araya et al., 2016).

Fire leads to the formation and deposition of pyrogenic carbon (PyC) on topsoil. Broadly, PyC is C that has been chemically altered by fire, and includes a spectrum of materials ranging from charred biomass to soot and ash (Masiello, 2004; Bird et al., 2015). Generally, PyC is considered to have a longer mean residence time than non-pyrogenic soil C, typically on the multi-centennial time scale (Hammes et al., 2008; Bird et al., 2015). However, in the past two decades, there has been growing evidence for PyC decomposing on shorter time scales, on the order of days to years (Cheng et al., 2006; Nguyen et al., 2009; Soucémarianadin et al., 2015). Furthermore, Bird et al. (2015) suggested a multi-pool model of PyC decomposition, where physical or chemical components of PyC are considerably more susceptible to decomposition than others. Ultimately, the breakdown of PyC and its loss from the soil system appear to be controlled by environmental conditions, particularly temperature and moisture, in addition to soil-specific conditions, such as landform position, aggregation, and depth, among others (Bird et al., 2015; Boot et al., 2015). Current estimates of PyC mean residence time in soil range from 250 to 300 years (Hammes et al., 2008), but the lack of data or predictive capability for the time scales and magnitude of PyC erosion post-fire potentially adds considerable uncertainty to these estimates (Bird et al., 2015).

Soil erosion laterally transports 1–5 Gt C per year (Stallard, 1998; Battin et al., 2009). The amount of material mobilized in a particular watershed is dependent on the intensity and duration of rainfall, groundcover, vegetation, slope gradient, and recent fire history (Renard et al., 1997; Pierson et al., 2009). Between 70 and 90% of the soil and associated carbon mobilized from eroding landscapes is deposited within the source or adjacent watersheds (Gregorich et al., 1998; Stallard, 1998). Local deposition of eroded material, along with dynamic replacement of eroded C by production of new photosynthate and stabilization of at least some of the eroded C in the depositional settings, leads to an erosion induced terrestrial sink for atmospheric $CO_2$ (Harden et al., 1999; Berhe et al., 2007).

Fire and erosion interact to modify a range of soil physical and chemical properties post-fire. The loss of vegetation after high severity fires is one of the main drivers of post-fire erosion, as vegetation plays a major role in stabilizing eroding soils (Shakesby et al., 1993; Larsen et al., 2009; Pierson et al., 2009). In extreme cases, this loss of vegetation can lead to debris and ash flows when intense rainfall events occur on recently burned hillslopes (Carroll et al., 2007). In addition to the loss of stabilizing vegetation, fire can produce a hydrophobic layer below the surface of the soil which can change the hydrologic flow along a hillslope (DeBano, 1991; Shakesby et al., 2000), reducing rate of water infiltration to soil and enhancing rates of runoff (DeBano, 1991; Shakesby et al., 2000; Pierson et al., 2013).

Post-fire erosion of topsoil rich in PyC can play an important role in controlling the stock and residence times of PyC in the soil system. So far, relatively few studies have focused specifically on the erosion of PyC. From the available data, it is becoming increasingly clear that PyC is highly susceptible to erosive forces, more so than non-pyrogenic C (Rumpel et al., 2006; Yao et al., 2014). After high severity wildfires, PyC has been documented to have enrichment ratios (concentration in eroded sediment divided by concentration in source soils) of up to 2.3 across the watershed scale (Rumpel et al., 2006). The observed high enrichment ratios of PyC are partly due to its relatively lower density compared with other SOM constituents, along with its concentration in the upper soil horizons and hydrophobicity (DeBano, 2000; Rumpel et al., 2006, 2015; Brewer et al., 2014). There is some evidence that erosion of PyC is controlled by different processes than non-pyrogenic C. Yao et al. (2014) found that the proportion of PyC compared with total C decreases with increasing soil erosion, while total C erosion increases with bulk soil erosion due to mobilization of deep and mineral-associated C. Erosional loss of PyC from sloping landform positions and depositional input of PyC into lower-lying depositional landform positions post-fire can significantly decrease or increase its mean residence time, as is observed with bulk C in soils that are not fire impacted (Berhe et al., 2007, 2012). Furthermore, the previous research on non-pyrogenic C has indicated that the burial of eroded C in lower lying depositional landform positions can lead to stabilization of through physical and chemical mechanisms (Berhe et al., 2007). It is likely that, in a similar manner, burial of eroded PyC can increase its mean residence time for up to millennia (Marin-Spiotta et al., 2014; Bird et al., 2015).

Vertical mobilization of PyC and other SOM within a soil profile occurs mainly due to leaching, bioturbation, and illuviation (Eckmeier et al., 2007; Rumpel et al., 2015). Leaching is primarily responsible for vertical transport of dissolved constituents, while bioturbation and illuviation, or the downwards transport of particles via water flow, can move particulate PyC and OM down the soil profile. In post-fire environments, the rate of vertical mobilization of PyC depends on the size and solubility of the PyC, the nature of the porous media, including soil texture, bulk density, and porosity, and the

rate of water flow through soil, which is driven by rainfall amount and intensity (Bird et al., 2015). Literature reported values for vertical mobilization of freshly applied PyC are typically on the order of mm per year (Major et al., 2010; Rumpel et al., 2015), although this may differ after natural wildfires and with aged char. The degradation of PyC, and release into the dissolved phase, creates a slow, centennial-scale loss of PyC from the soil. As PyC is exposed to environmental conditions, it degrades and becomes more soluble and can be mobilized at rates more than 40–55 times that from fresh char (Abiven et al., 2011).

The main objective of this study is to understand how PyC is mobilized laterally and vertically within soil profiles post-fire and to understand how mobilization of PyC impacts its long-term persistence in soil. To accomplish these objectives, we used a combination of spectroscopic techniques to determine how post-fire erosion changes distribution of C and soil organic carbon (SOC) fractions at eroding and depositional landform positions at the site of the Gondola Fire, South Lake Tahoe, California. Specifically, we determine: (a) how stocks of PyC and other SOC fractions in eroding and depositional landform positions change after fire; (b) how lateral distribution of material controls stocks of PyC and SOC fractions over short (1 year) and longer (10 year) timescales; and (c) the rates of vertical mobilization of PyC and C in other fractions down the soil profile post-fire.

# METHODS

## Site Description

The Gondola Fire burned over 270 ha on July 3, 2002, on the south shore of Lake Tahoe (38°57′ N; 119°55′ W, **Figure 1**), near Stateline, NV (Saito et al., 2007). The Gondola fire was characterized as a moderate severity burn, with partial consumption of the O horizon, and significant heat transfer down to 1 cm of mineral soil, where temperatures reached up to 200°C (Carroll et al., 2007). The loss of vegetation during the Gondola Fire lead to a loss of 20 Mg/ha of C and 257 kg/ha from the ecosystem (Johnson et al., 2007). Two weeks after the fire, on July 18, an intense precipitation event that deposited 15.2 mm of precipitation as rain and hail mobilized 380 Mg (metric tons) of material downslope, which was deposited in a downslope riparian area that borders the Edgewood Creek (**Figure 2**). The depositional area was about 0.8 ha in size and was densely vegetated with slopes of 0 to 5% (Carroll et al., 2007; Saito et al., 2007).

The study area is characterized by Mediterranean climate with cold and snowy winters and warm to hot summers. The site receives most of its 87 cm of mean annual precipitation as snow and has a mean annual temperature of 6.7°C. The study area is underlain by granitic parent material and is a part of the Cagwin-Rock Outcrop. Soils of the study area are classified as coarse, loamy sand, mixed Typic Cryopsamments (Carroll et al., 2007; Johnson et al., 2007). The dominant vegetation in the area includes white fir *(Abies concolor)*, Jeffery pine (*Pinus jeffreyi*), and Sugar pine (*Pinus lambertianna*) in the overstory; and Sierra chinquapin (*Castanopsis sempervirens*), currant (*Ribes* spp.), snowbrush (*Ceanothus velutinis*), and bitter brush (*Purshia tridentata*) in the understory (Saito et al., 2007).

## Sampling Design

This site had 16 previously established hillslope sampling plots (**Figure 1**), in which seven were burned during the fire, seven were unburned, and two were partially burned (Carroll et al., 2007). Directly below the burned hillslope, within the identified deposition area of eroded material from the hillslope plots, 17 sites were selected to represent the variability within the previously identified area where the eroded material from the ash flow was initially deposited (Carroll et al., 2007). These plots were sampled before the Gondola Fire, in late spring in 2002. The same plots were resampled 1-year post-fire, during the summer of 2003, and then 10-years post-fire in the summer of 2013, with the addition of 13 new sites in the depositional area. These additional sites were selected to better capture the variability in soil properties from this landform position, and since the previous C and N data from these sites were highly variable, likely resulting from the multitude of sources for material deposited

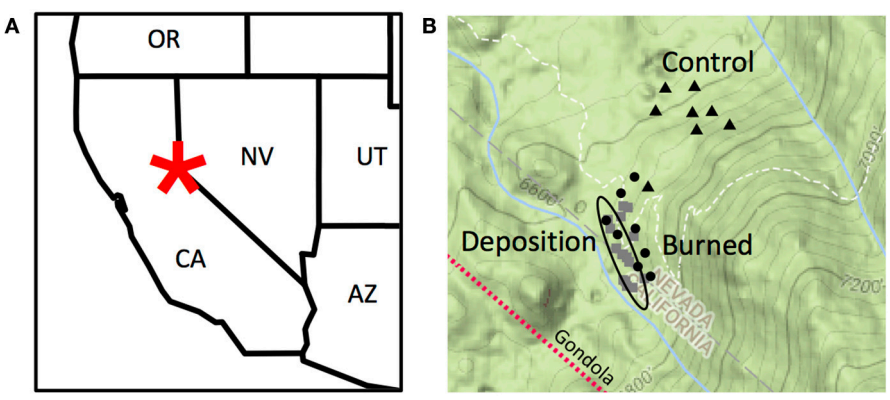


**FIGURE 1 |** The Gondola Fire occurred outside Stateline, Nevada, in the Van Sickle Bi-State Park **(A)**. Burned plots are indicated by circles; unburned, control plots are indicated by triangles; and selected depositional sites that were analyzed via nuclear magnetic resonance spectroscopy are indicated by squares and are encircled **(B)** in this topography map **(B)**. The topography map **(B)** is copyright Google Maps 2017.

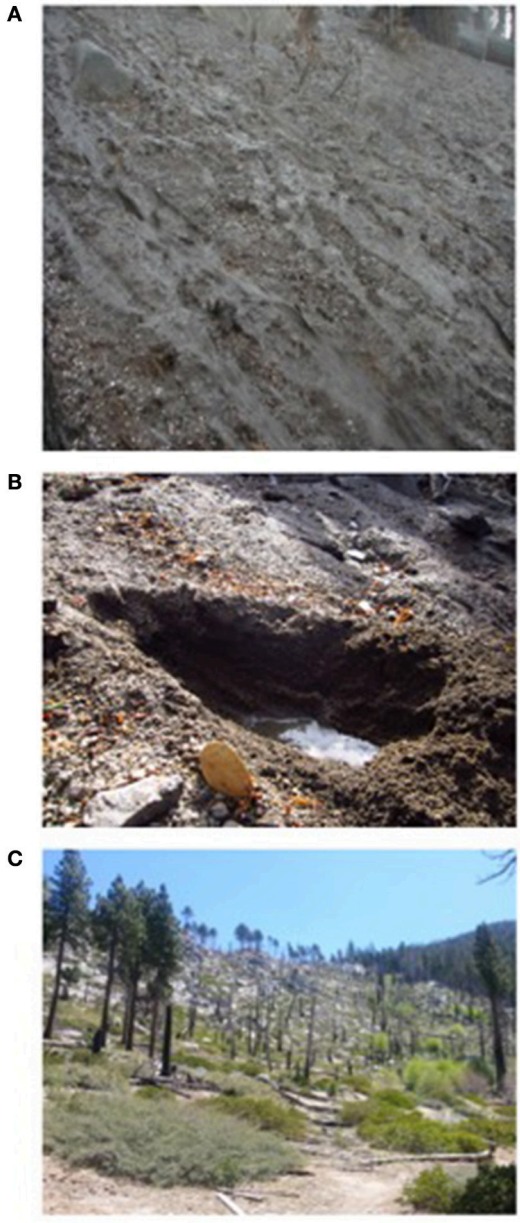


**FIGURE 2 |** A major ash flow occurred after the fire in 2002 (**A**, photo by J. Howard). The hydrophobic layer (**B**, photo R. Abney) created during the fire persists through the recent sampling (photo from November 2012, R. Abney). No canopy is left in portions of this moderate severity fire (**C**, May 2013, R. Abney).

in this location. In the eroding hillslope plots, soil samples were collected from five random locations within each plot by depths of 0–10, 10–30, 30–60, and 60–100 cm, which approximately corresponds to genetic horizons A11, A12, AC, and C (Johnson et al., 2007). In the depositional sites, soil was collected from the depth of 0–15 cm, to capture the mainly ash material that was initially deposited in that landform position, although the profile at this landform position extended deeper. The five replicates from the hillslope soils were composited and homogenized, and all samples were passed through a 2-mm sieve prior to further laboratory analysis. The 2002 and 2003 samples were previously analyzed for various soil and elemental properties, and section Basic Soil, Elemental, and Isotopic Analyses describes the analysis of samples collected in 2013, which duplicates the analyses conducted on the 2003 and 2003 samples, except for the addition of stable isotope analyses.

## Basic Soil, Elemental, and Isotopic Analyses

Air-dried, sieved soils were analyzed for pH in a 1:2 ratio of soil to both water and 0.01 M $CaCl_2$ solutions with a Fisher Scientific Basic Probe (AB15 meter, Waltham, MA). Gravimetric water content was measured via drying approximately 10 g subsets of field-moist soil in an oven at 105°C for 48 h. Bulk density was determined by the core method, where a 5 × 10 cm core was hammered into the soil, and dried at 105°C for 48 h.

Prior to C and N elemental and isotopic analysis, air-dried soils were ground for 3 min in a ball mill (8,000 M Spex Mill, SPEX Sample Prep, Metuchen, NJ) to a homogenous fine powder. Samples were tested for carbonates by reacting them with 1 M HCl. No effervescence was observed, so we concluded that these samples had no carbonates and hence the total organic carbon concentration in the soils is equal to total carbon concentration. For C, N, and stable isotopic analyses for $\delta^{13}C$ and $\delta^{15}N$, we weighed between 15 and 40 mg of ground soil into tin capsules. These samples were combusted in a Costech ECS 4010 CHNSO Environmental Analyzer (Valencia, CA) connected via a Conflo IV interface (Thermo Finnegan, San Jose, CA) to a Delta V Plus Isotope Ratio mass spectrometer (ThermoFisher Scientific, Waltham MA). All C and N concentration values are reported as oven-dry sample weight. The stable isotope values are reported using the δ notation, in units of per mil (‰). Samples were measured against peach leaf and acetanilide, with standard errors of ± 0.23 $\delta^{15}N$ and ± 0.09 $\delta^{13}C$ variation for peach leaf and ± 0.15 $\delta^{15}N$ and ± 0.07 $\delta^{13}C$ variation for acetanilide. Duplicate samples had standard errors of ± 0.20 $\delta^{15}N$ and ± 0.05 $\delta^{13}C$. The higher variation in standards compared with samples is likely due to them spanning numerous sample runs and due to variations in the size of the standards across different sample runs. Our results were calibrated relative to international standards (e.g., NBS-22, N-1, and N-2) and are referenced relative to atmospheric $N_2$ and Vienna Pee Dee Belemnite (VPDB).

## Spectroscopy

Bulk chemical characterization and determination of PyC concentrations in the samples were carried out by combining $^{13}C$-CPMAS-Nuclear Magnetic Resonance (NMR) and Mid-Infrared (MIR) Spectroscopy. The data derived from $^{13}C$ NMR and MIR along with partial least squares regression analysis (MIR/PLSR) was then used to determine the proportion of PyC in the soil samples. This NMR and MIR/PLSR technique reliably estimates the concentration of PyC across a range of soil types and concentrations of bulk C and PyC (Skjemstad et al., 2004; Janik et al., 2007; Baldock et al., 2013a) and is also the most cost

and time-effective technique for quantifying the amount of PyC in soil to date.

Mid-Infrared spectroscopy (MIR) analysis was conducted on all ground soils on a Thermo Nicolet 6700 spectrometer (ThermoFisher Scientific, Waltham, MA) using a Pike AutoDiff diffuse reflectance attachment (Pike Technologies, Madison, WI), as described in Sanderman et al. (2011). A KBr beam-splitter scanned the samples 60 times and produced absorbance spectra from wavenumbers 7,800–400 $cm^{-1}$. Spectra were background corrected against silicon carbide and then baseline corrected. Peak region assignments were adapted from Araya et al. (2017).

A subset of samples was analyzed via $^{13}$C-CPMAS NMR spectroscopy on a Bruker Avance system (200 MHz) equipped with a 4.7 T wide-bore magnet with a resonance frequency of 50.33 MHz. The Kennard-Stone algorithm was utilized to pick 20 samples for NMR analysis that incorporated the most variability in the MIR dataset (Kennard and Stone, 1969). This algorithm and principal components analysis demonstrated that most variability was in the deposition samples, and first axis accounted for 86% of the variance in the MIR data. The NMR analyses were conducted on only depositional landform position soils, as the eroding soils did not produce usable spectra, likely due to either the low C observability of these samples or paramagnetic interference. Principal component analysis of the MIR spectra confirmed that most of the variability in the soil chemical properties was in the depositional soil samples. Samples for NMR analysis were packed into a 7 mm zirconia rotor, and a standard cross polarization experiment was performed using a pulse of 3.2 μs, 195 W, 90°, a contact time of 1 ms and a recycle delay of 1 s (Sanderman et al., 2011; Baldock et al., 2013a).

Of the 20 samples selected for NMR, nine of them produced poor quality spectra and were demineralized with HF prior to re-analysis to increase C content of samples, decrease noise in the spectra, and remove interference from paramagnetic species in soil (Smernik and Oades, 2002). This method can alter SOM composition (Sanderman et al., 2017), but has been widely used to make spectra collection possible (Schmidt et al., 1997). To demineralize the samples, they were washed nine times with 45 mL of 2% HF over the course of a week, and then three times with DI water (Skjemstad, 1994; Sanderman et al., 2011). To determine C observability, glycine was used as an external reference (Smernik and Oades, 2000a,b), and from the NMR analysis, 18 usable spectra were produced, with C observability over 25%. Spectra were compared to a glycine standard for observability. For these NMR analyses, 10–20,000 scans were collected per sample, and the collected spectra were integrated into eight regions: 0–45 ppm (Alkyl), 45–60 ppm (N-Alkyl/Methoxyl), 60–95 ppm (O-Alkyl), 95–110 ppm (Di-O-Alkyl), 110–145 ppm (Aryl), 145–165 ppm (O-Aryl), 165–190 ppm (Amide/Carboxyl), and 190–215 ppm (Ketone).

For the samples from erosional sites, the Soil Carbon Research Program (SCaRP) MIR-PLSR model was used to predict three organic C fractions within the soil samples: resistant organic carbon (ROC, particles that are chemically similar to charcoal, or PyC), particulate organic carbon (POC, particles 50–2,000 μm excluding PyC), and humic organic carbon (HOC, particles <50 μm excluding PyC) (Baldock et al., 2014). This model has proven to be a reliable and time-effective method for predicting soil fractions and has been demonstrated a reasonable predictor across different land uses and vegetation types in and out of Australia (Baldock et al., 2013b; Ahmed et al., 2017; Jauss et al., 2017). The SCaRP model is based on 312 soils collected from agricultural soils across Australia, and it independently predicts organic carbon originating from three fractions without the need for mechanical processing of samples (Baldock et al., 2013a). Due to the independent predictions of the three fractions within this model, the sum of C in each fraction does not necessarily add up to 100%, and the error of the total C predictions averaged 108 ± 11% of the measured total C concentration.

However, due to a poor fit of the SCaRP model to the PyC fraction in the depositional soils, a separate NMR/MIR PLSR was created from the NMR and MIR data collected on these samples using the partitioning of OC into PyC and non-PyC components using the NMR data as described by Baldock et al. (2013a). This separate, 6-factor model built on square root of transformed PyC data ($n = 18$) explained 87% of the variance using leave-one-out cross validation with a relative root mean square error of 17%.

## Data Analysis

All data analyses and figure generation for this observational study were conducted in RStudio (version 1.0.316, rstudio.com). Separate linear mixed effects models were built to (1) assess the transport of organic carbon fractions and bulk carbon through the soil profile with time, and (2) to assess surficial transport of these fractions across the surface of the landscape (0–10 cm for eroding hillslope and 0–15 cm for depositional soil). The depth model (1) predicted SOC fraction using time, depth, and burning as fixed factors and plot number as a random factor. The surface transport model (2) predicted SOC fraction used time, landform position, and burning as fixed factors and plot as a random factor. Models were tested for significance ($p < 0.05$) by comparing null intercept-only models to models with fixed and random effects using the likelihood test. Differences between treatments were assessed using a Tukey Honest Significant Difference test and were also assumed significant at $p < 0.05$. For all other statistical comparisons without time as a factor, two-way ANOVAs were used with depth and burn or control as predictors. Means are presented with standard error with $n = 8$ for eroding hillslope samples and $n = 30$ for depositional samples.

# RESULTS

## Bulk Soil Properties and Elemental Concentrations

Soils from the eroding landform positions were generally acidic pre-fire across all sampling times. However, at depths below 30 cm in 10-year post-fire sampling period the soil pH values were in the neutral range (**Table 1**). The pH of the eroding soils, in both the burn and control plots, increased after the fires by up to 1.25 units. Bulk density showed <0.2 $g/cm^3$ change in the 1 year post-fire time point, with the values increasing in the burned plots and decreasing in control plots. Soils at the depositional landform

position had a pH range and bulk density values that were similar to the topsoil from the eroding position.

Soils from the eroding positions had <20 g/kg C, in which C concentrations showed a consistent, but statistically not significant ($p = 0.83$), decreasing trend with depth in both the burn and control plots in the control and burn plots (**Figure 3**). The soils generally had very low N concentrations (<0.01 g/kg). There was a marked decrease in concentration of both C and N in topsoil (0–10 cm) immediately post-fire, but the values reverted to pre-fire levels at the 10-year post-fire sampling period (**Figure 3**).

In contrast to the eroding soils, the total C concentrations in depositional soils ranged from 20 to 100 g/kg, and increased significantly between the pre-fire and post-fire time points ($p = 0.00$, **Figure 4**). The depositional soils did not significantly ($p = 0.38$) differ in N concentration than those from the eroding

**TABLE 1 |** Soil pH and bulk density for the eroding landform position.

| Location | Depth | Pre-fire | | | Post-fire | | Ten-years post-fire | | |
|---|---|---|---|---|---|---|---|---|---|
| | | pH in $H_2O$ | pH in $CaCl_2$ | Bulk density ($g/cm^3$) | pH in $H_2O$ | pH in $CaCl_2$ | pH in $H_2O$ | pH in $CaCl_2$ | Bulk density ($g/cm^3$) |
| Eroding (burned) | 0–10 cm | 5.82 (0.11) | 5.09 (0.11) | 1.24 (0.07) | 6.69 (0.11) | 5.98 (0.20) | 6.54 (0.13) | 5.57 (0.11) | 1.41 (0.05) |
| | 10–30 cm | 5.77 (0.10) | 4.98 (0.08) | - | 6.37 (0.23) | 5.74 (0.29) | 6.64 (0.10) | 5.68 (0.13) | - |
| | 30–60 cm | 6.08 (0.24) | 5.30 (0.28) | - | 6.35 (0.19) | 5.65 (0.22) | 6.77 (0.11) | 5.72 (0.12) | - |
| | 60–100 cm | 6.12 (0.17) | 5.39 (0.15) | - | 6.40 (0.09) | 5.61 (0.11) | 7.37 (n/a) | 6.15 (n/a) | - |
| Eroding (control) | 0–10 cm | 5.99 (0.18) | 5.33 (0.20) | 1.24 (0.05) | 6.09 (0.06) | 5.46 (0.05) | 6.79 (0.14) | 5.91 (0.18) | 1.13 (0.04) |
| | 10–30 cm | 5.85 (0.22) | 5.03 (0.23) | - | 5.87 (0.06) | 5.21 (0.06) | 6.77 (0.17) | 5.57 (0.17) | - |
| | 30–60 cm | 5.37 (0.14) | 4.88 (0.17) | - | 5.59 (0.11) | 4.98 (0.03) | 6.40 (0.21) | 5.23 (0.27) | - |
| | 60–100 cm | 5.86 (0.11) | 5.10 (0.16) | - | 5.97 (0.09) | 5.17 (0.08) | 6.65 (0.12) | 5.72 (0.24) | - |

*Standard error presented in parentheses (n = 7 control, and n = 8 burned).*

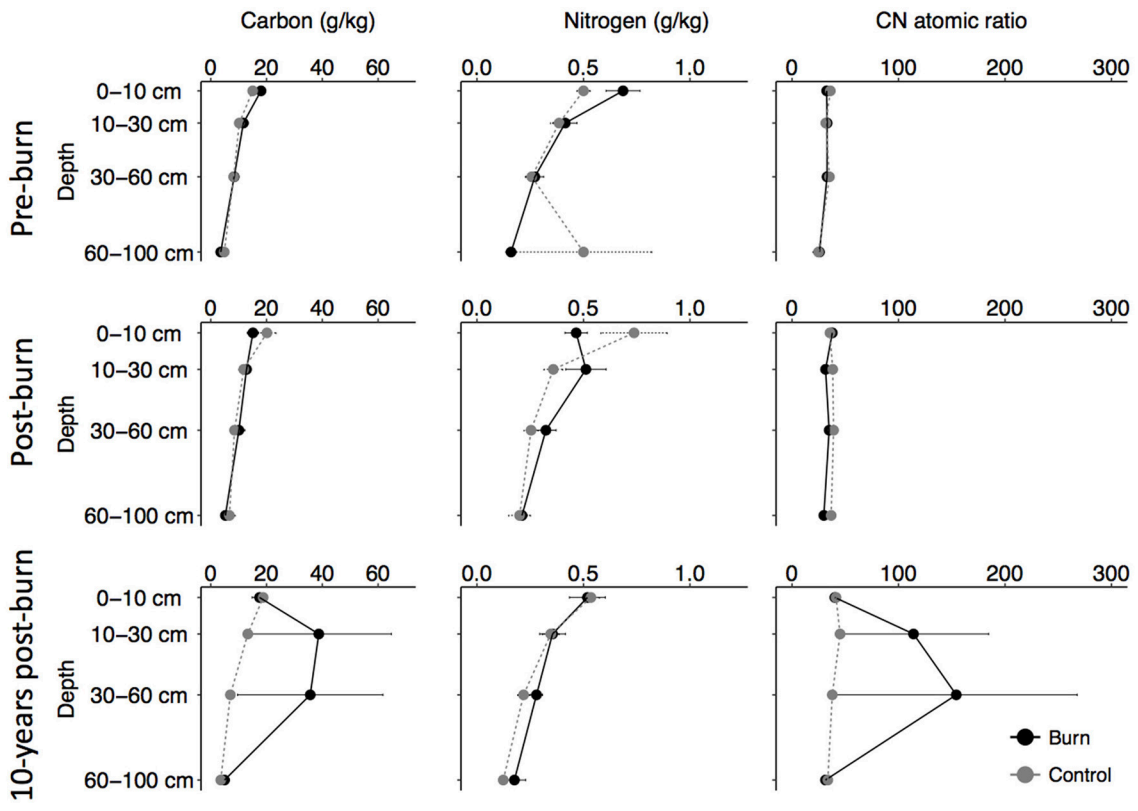


**FIGURE 3 |** Carbon (C), nitrogen (N), and the atomic C:N ratio in the eroding position before burn, 1 year post-fire, and 10-years post-fire. Error bars represent standard error.

positions, when accounting for the effects of depth and time. The mean total N during the 2013 sampling period was 0.005 g/kg and the mean total C was 18.7 g/kg (**Table 2**).

## SOC in Fractions and PyC

The concentrations of SOC fractions in the depositional landform position increased significantly between the pre-fire and 1-year post-fire sampling time points ($p = 0.00$, **Figure 5**). However, there was a significant decrease in the concentration of all three SOC fractions at the 10-year post-fire sampling point ($p = 0.00$) to below the pre-fire concentrations.

Linear mixed effects models indicated that the C concentration in the organic carbon fractions from the eroding soils (**Figure 6**) significantly depended on sampling time, depths, and burn condition (**Tables 3**, **4**). Concentrations of SOC fractions did not decline significantly with depth (PyC $p = 0.82$, POC $p = 0.94$, HOC $p = 0.60$), but the top horizon had higher concentrations of each of the SOC fractions than the deeper horizons. The eroding soil regressions also indicated that the 2013 sampling time had significantly higher concentrations ($p = 0.02$) of each of the SOC fractions than was non-significantly (PyC $p = 0.66$, POC $p = 0.36$, HOC $p = 0.18$), more concentrated in burn plots compared with control plots, and was significantly ($p = 0.02$) more concentrated in 2013 compared with the earlier sampling points.

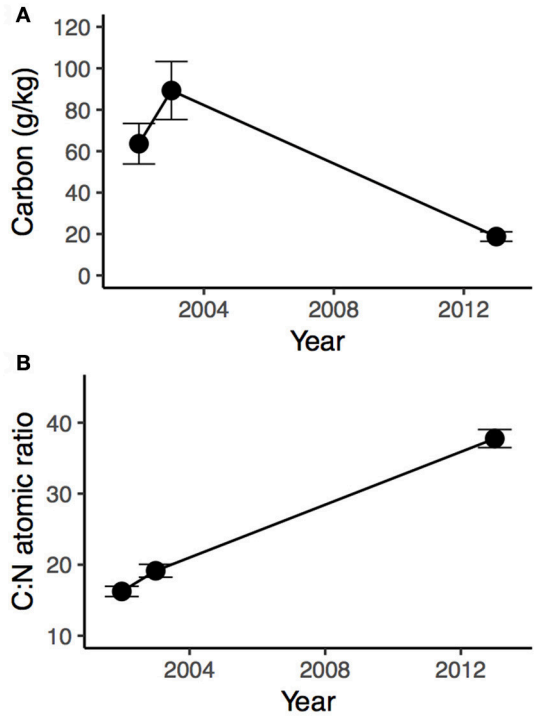


**FIGURE 4 |** Total C **(A)** and C:N ratio **(B)** for the depositional landform position for samples taken at 0–15 cm. Error bars represent standard error with $n = 30$.

The statistical model of the SOC fractions in the surface soil indicated that there was no statistical difference between the pre-burn and 1 year post-fire sampling times, but that the 10-year post-fire sampling had significantly lower SOC concentrations ($p = 0.00$), largely driven by the large decline in SOC fractions in the depositional landform positions. There were no significant differences in the burn and control plots on the eroding hillslope (PyC $p = 0.92$, POC $p = 0.79$, HOC $p = 0.834$). Across the three SOC fractions and accounting for sampling time and burn, the eroding plots had significantly lower concentrations of the SOC fractions than the depositional landform positions (HOC $p = 0.00$, POC $p = 0.00$), except for the PyC fraction ($p = 0.05$). However, the eroding landform position had significantly higher concentration of SOC fractions at the final sampling point than the depositional landform position.

In the eroding plots only model, the burned plots had non-significantly higher PyC concentrations than the unburned plots, and the 10-years post-fire sampling point had significantly higher concentrations of PyC compared with pre-burn ($p = 0.00$) and 1-year post-burn ($p = 0.02$) concentrations. Both the burned and unburned plots had significantly higher HOC concentrations in the 10-years post-fire sampling point compared with the pre- and post-fire sampling point ($p = 0.00$ and $p = 0.00$). The unburned plots had slightly, but non-significantly ($p = 0.64$), lower concentrations of HOC than the burned plots.

In each of the sites, the three SOC fractions in the surface soils were summed and the proportion of PyC to total C was calculated (**Figure 7**, **Tables 3**, **4**). There was no significant trend with ROC fraction with depth ($p = 0.11$) or between burn and control plot ($p = 0.44$), but PyC made up a significantly higher proportion of hillslope SOC compared with the depositional landform position ($p = 0.00$). The PyC fraction was also significantly lower in the 10-years post-fire time point compared with either of the first two time points ($p = 0.00$).

## Isotopic and Spectroscopic Composition of SOM

For the 10-year post fire eroding plots, $\delta^{13}C$ values were significantly more positive ($p = 0.02$) in the control vs. burned plots (**Figure 8**). The $\delta^{13}C$ of bulk SOM decreased with depth but the relationship was not statistically significant ($p = 0.72$). With increasing depth into the soil profiles of the eroding plots, the

**TABLE 2 |** Soil pH and bulk density for the depositional landform position, and summary elemental and stable isotope analyses for the depositional landform position soil collected in 2013.

| Depth | pH in $H_2O$ | pH in $CaCl_2$ | Bulk density (g/cm$^3$) | $\delta^{15}N$ | $\delta^{13}C$ | C:N atomic ratio | Nitrogen (g/kg) | Carbon (g/kg) |
|---|---|---|---|---|---|---|---|---|
| 0–15 cm | 6.85 (0.12) | 5.80 (0.14) | 1.22 (0.12) | 3.84 (0.18) | −25.73 (0.47) | 37.76 (1.27) | 0.005 (0.000) | 18.7 (2.2) |

*Standard error presented in parentheses (n = 30).*

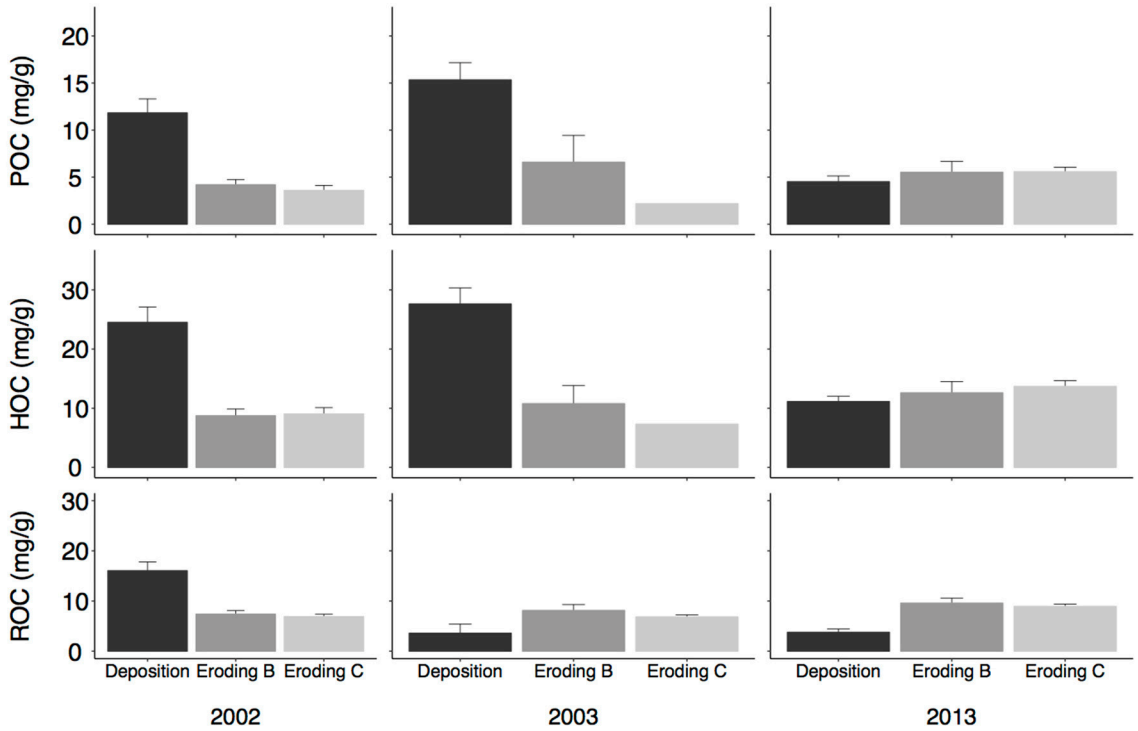


**FIGURE 5 |** Soil organic carbon fractions (particulate organic carbon, or POC; humic organic carbon, or HOC, and pyrogenic carbon, or ROC) from pre-fire (2002), 1-year post-fire (2003), and 10-years post-fire (2013) surface soils. Eroding surface soils were collected from 0 to 10 cm and depositional soils were collected from 0 to 15 cm. Error bars represent standard error with $n = 16$ for eroding sites and $n = 30$ for depositional sites. Eroding B refers to the burned eroding plots, and Eroding C refers to the control (unburned) eroding plots.

$\delta^{15}$N values were significantly more positive in the control plots compared with the burned plots ($p = 0.02$).

The MIR data indicate that both the control and 10-year post-fire plots showed an increase in peak heights in the –OH function group (3,700 $cm^{-1}$) with depth and a decrease in the −CH (2,940 $cm^{-1}$). The ester and phenol regions (1,159 and 995 $cm^{-1}$) also showed a decrease in peak heights with depth into the soil profile in both the pre- and post-fire spectra based on DRIFT spectra designations of Araya et al. (2017). The most important differences in the MIR spectra in the soils from the burned and control plots, for regions of interest to SOM composition, (**Figure 9**) were observed in the spectral regions representing asymmetric and symmetric C-H stretching vibrations in aliphatic compounds (2,924 and 2,850 $cm^{-1}$, respectively); C = C stretching vibrations of aromatic compounds (1,650 $cm^{-1}$); N-H bending vibrations and C = N stretching vibrations in amides (1,575 $cm^{-1}$); C-H bending (1,390, 1,405, and 1,470 $cm^{-1}$) in aliphatic groups; C-O stretching and asymmetric stretching vibrations in carboxylic and phenolic groups (1,270 $cm^{-1}$); and C-O symmetric vibrations in polysaccharides (1,080 and 1110 $cm^{-1}$). The peak heights in the aromatic and polysaccharide regions were highest in the top soil (0–10 cm) of all landform positions and burned and control soils, due to higher C concentrations there. We also observed increased peak highest in the aromatic region at 10–30 and 60–100 cm depths, and in the polysaccharide regions below 60 cm depths in the burned soils. All soil depths had increased peak heights in the amide region.

Comparing the pre-fire (2002) and post-fire (2003) NMR spectra of soil from the depositional position (**Table 5**, **Figure 10**) shows increased contribution of aryl and O-aryl groups (110–165 ppm), alkyl (0–45 ppm), and ketones (190–215 ppm); and reduced contribution of O- and N-substituted alkyls (45–110 ppm) and amide and carboxylic groups (165–190 ppm). The largest shift in distribution of C in the different organic functional groups was observed in the aryl region that saw an increase by 1.9% post-fire.

## DISCUSSION

Following the Gondola fire, erosion redistributed soil C and PyC laterally down the hillslope. Overall, we found an increase in all SOC fractions in the depositional landform position 1-year post-fire. By conservatively assuming the concentration of C and PyC in the transported sediment was equivalent to the concentration in post-fire control eroding plots, the initial mass movement of 380 Mg of material (Carroll et al., 2007) equates to the transport of 7.6 Mg C and 2.4 Mg PyC. When accounting for the 3.8 ha of source area, this is transport equates to 2.0 Mg C and 0.6 Mg PyC per ha. The post-fire transport contributed to the increase in the depositional soil C content from 63 to 89 g/kg C, but by itself, did not contribute all the increase in soil C. It is likely that erosion

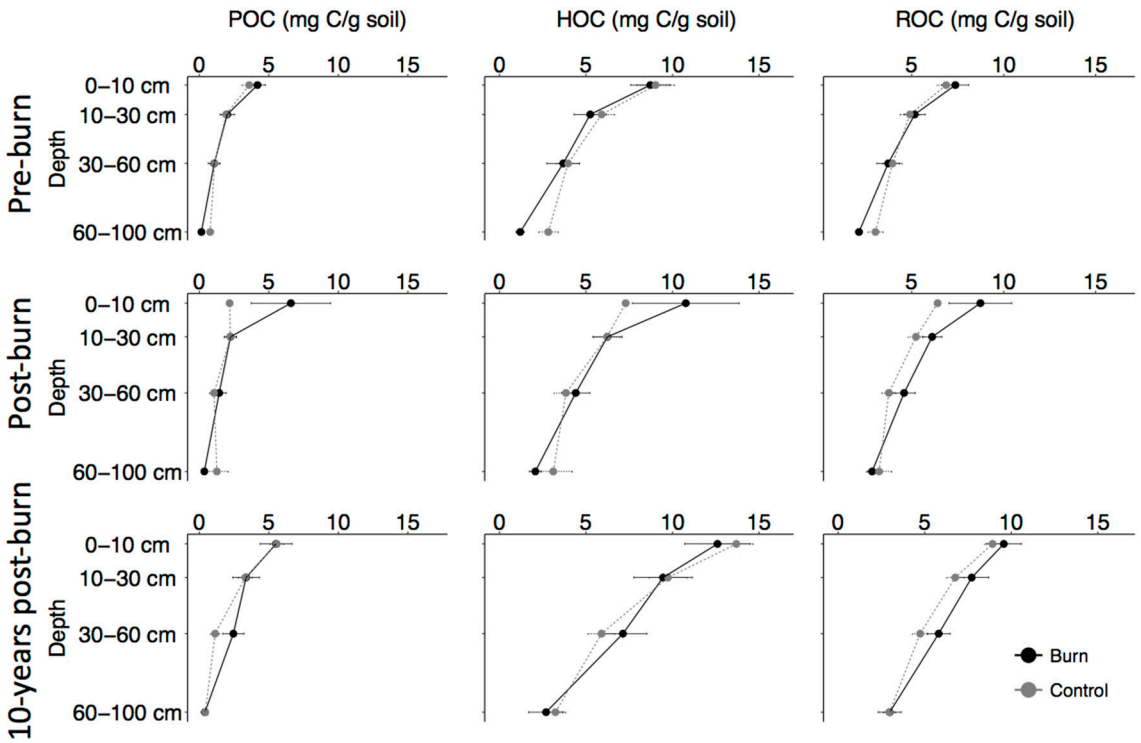


**FIGURE 6 |** Organic carbon fractions (particulate organic carbon, or POC; humic organic carbon, or HOC, and pyrogenic carbon, or ROC) for the eroding hillslope position from pre-fire, 1-year post-fire, and 10-years post-fire in burn and eroding plots. Error bars represent standard error with $n = 8$, and where they are not visible the error is very small.

events from the remainder of the post-fire year preferentially transported SOC and PyC to this depositional landform position (Rumpel et al., 2006; Stacy et al., 2015). However, by 10-years post-fire, the SOC fractions in the depositional landform position sites declined to below pre-fire levels. This decline suggests either burial by subsequently eroded material with lower SOC levels or the rapid decomposition of SOC in that landform position. In the long-term, there were no significant changes in the carbon concentration of the top soil of the eroding plots, even after the major erosion event post-fire.

## Transport and Loss of Different SOC Fractions Due to Post-fire Erosion

The slightly increased contribution of the PyC fraction in eroding hillslope plots that persisted even 10 years after the Gondola fire confirms the input of PyC from the fire (**Figures 5**, **6**, **10**). From our findings, the PyC continued to be lost from the eroding plots, presumably via ongoing erosion processes. Our data also show that PyC is a dynamic pool of SOC, as seen by the significant drop in the PyC fraction in the topsoil of the depositional landform position (**Figure 5**). These findings are consistent with previous work, where erosion was demonstrated to play a major role in lateral redistribution of PyC post-fire, with implications for persistence of PyC in dynamic landscapes (Rumpel et al., 2009, 2015).

All the SOC fractions in the depositional landform position increased in the 1-year post-fire sampling point and then decreased to below pre-fire concentrations at the 10-year sampling point. Based on our data, we conclude that this large initial increase is likely due to the mass-movement erosion event that deposited fire-altered material downhill after the fire. The subsequent loss of C in all the SOC fractions in the long-term suggests that this SOC material may not be stabilized if it remains on the surface of the depositional landform position. The depositional, riparian area characterized by higher concentrations of both C and N, as well as wetter soil water conditions, could support higher decomposition rates. In comparison, the well-drained coarse soils in the eroding landform positions were relatively C- and N-poor, but contained a higher proportion of the PyC as a fraction of total C (**Figure 7**). This finding is consistent with previous decomposition and other SOC studies that showed that rate of SOC loss through decomposition could be faster on the surface of OM rich and poorly drained depositional landform positions (Berhe, 2012, 2013). In addition to decomposition, SOC loss from the surface soil in the depositional landform position may become stabilized in the depositional landform positions particularly if it is buried by subsequently eroded material (Berhe et al., 2007; Doetterl et al., 2016).

The cycling and persistence of ROC or PyC, post-fire is controlled by numerous factors, including erosion and

**TABLE 3 |** Eroding hillslope and surface soil model parameter estimates.

| | Eroding hillslope model | | | | Surface soil model | | | |
|---|---|---|---|---|---|---|---|---|
| | **Parameter** | **Estimate** | **Std. error** | ***t*-value** | **Parameter** | **Estimate** | **Std. error** | ***t*-value** |
| PyC | Intercept | −210.75 | 49.17 | −4.28 | Intercept | 1634.39 | 295.22 | 5.53 |
| | Time | 0.10 | 0.02 | 4.46 | Time | −0.80 | 0.14 | −5.49 |
| | Depth: 10–30 cm | −2.16 | 0.33 | −6.52 | Eroding hillslope | −3.74 | 1.95 | −1.91 |
| | Depth: 30–60 cm | −3.73 | 0.33 | −11.26 | Control (unburned) | −0.25 | 2.82 | −0.09 |
| | Depth: 60–100 cm | −4.94 | 0.36 | −13.55 | | | | |
| | Control (unburned) | −0.92 | 0.69 | −1.32 | | | | |
| POC | Intercept | −96.99 | 67.76 | −1.43 | Intercept | 1101.91 | 272.39 | 4.04 |
| | Time | 0.05 | 0.03 | 1.51 | Time | −0.54 | 0.13 | −4.00 |
| | Depth: 10–30 cm | −2.44 | 0.46 | −5.30 | Eroding hillslope | −4.96 | 1.80 | −2.75 |
| | Depth: 30–60 cm | −3.57 | 0.46 | −7.74 | Control (unburned) | −0.66 | 2.60 | −0.25 |
| | Depth: 60–100 cm | −4.21 | 0.50 | −8.31 | | | | |
| | Control (unburned) | −0.59 | 0.65 | −0.90 | | | | |
| HOC | Intercept | −441.09 | 87.56 | −5.03 | Intercept | 1723.54 | 428.06 | 4.02 |
| | Time | 0.22 | 0.04 | 5.17 | Time | −0.84 | 0.21 | −3.97 |
| | Depth: 10–30 cm | −3.59 | 0.59 | −6.08 | Eroding hillslope | −10.07 | 2.83 | −3.55 |
| | Depth: 30–60 cm | −5.90 | 0.59 | −10.00 | Control (unburned) | 0.85 | 4.10 | 0.20 |
| | Depth: 60–100 cm | −7.72 | 0.64 | −11.89 | | | | |
| | Control (unburned) | −0.59 | 1.21 | −0.48 | | | | |
| PyC fraction | Intercept | 7.39 | 1.90 | 3.88 | Intercept | 24.20 | 2.59 | 9.31 |
| | Time | −0.00 | 0.00 | −3.68 | Time | −0.01 | 0.00 | −9.21 |
| | Depth: 10–30 cm | 0.04 | 0.01 | 3.14 | Eroding hillslope | 0.11 | 0.01 | 6.65 |
| | Depth: 30–60 cm | 0.08 | 0.01 | 6.40 | Control (unburned) | −0.02 | 0.02 | −0.93 |
| | Depth: 60–100 cm | 0.16 | 0.01 | 11.27 | | | | |
| | Control (unburned) | −0.03 | 0.02 | −1.58 | | | | |

decomposition conditions (Bird et al., 2015). The PyC fraction in eroding positions increased slightly over time from pre-fire to 10 years after the Gondola Fire. This increase is likely due to the redistribution of material or further inputs of charred material. The Sierra Nevada is a highly fire-prone region (Westerling et al., 2006), and it might be that numerous fires in the Sierras after the Gondola Fire deposited ash and smoke in the vicinity (Peterson et al., 2015). The lack of significant difference in the PyC and other SOC fractions in the eroding burn and control plots also suggests input of PyC from sources other than the Gondola Fire itself, or that much of the PyC formed on the eroding hillslope was lost in the initial erosion event (Carroll et al., 2007) or via rapid decomposition (Kuzyakov et al., 2009; Nguyen et al., 2009). Reported decomposition rates for PyC range from decadal to millennial time scales (Kuzyakov et al., 2009; Lehmann et al., 2009; Bird et al., 2015), and reflect the source material for the PyC and environmental conditions. Reported rates of PyC breakdown can be orders of magnitude higher from controlled laboratory studies compared with field studies, but they suggest that under some conditions, microbial decomposition is responsible for the relatively rapid breakdown of PyC (Bird et al., 2015).

In the depositional landform position, undocumented further erosion events may have resulted in the loss of SOC fractions on the longer-term scale. At this site, erosion in the depositional landform position likely served as only a small loss for soil PyC, due to the lower slope in this landform position, no evidence for rill formation, which would drive elevated erosion, and the long-term preservation of this site from development. The initial eroded material contained a considerable concentration of ash (Carroll et al., 2007), which is highly susceptible to both wind and water erosion (Pereira et al., 2015). The mobilization of 1.5 Mg C/ha and 0.7 Mg PyC/ha in the initial erosion event was significant, however, the 1-year post-fire concentration of PyC in the depositional landform position is double that of the hillslope plots, suggesting that after the initial erosion event, more pyrogenic material was eroded and deposited there.

Topsoil material in depositional landform positions can become buried by subsequently eroded material, such that it is possible that the eroded SOC fractions that were initially eroded were buried by subsequent deposition of eroded material without higher levels of PyC-SOC (Berhe et al., 2007). These later erosion events generally transport more mineral material than the earlier erosion events, since pyrogenic material is typically preferentially transported in early erosion events after a fire (Rumpel et al., 2006, 2009; Yao et al., 2014). If the relatively SOC-rich material that was originally deposited in the depositional landform position is buried with subsequent erosion, PyC and

associated other soil C is likely to be physically stabilized in the soil profile of the depositional position.

The more negative $\delta^{13}C$ in the surface soil of burned eroding sites at the 10-year post-fire sampling time point (**Figure 8**) suggests that there may have been preferential combustion of OM with more positive $\delta^{13}C$, such as cellulose and hemicellulose in plant fragments, leaving behind more isotopically light material, such as lignin (Benner et al., 1987; Preston et al., 2006; Preston and Trofymow, 2015). For the $\delta^{15}N$ values, which are more negative post-fire, this observation is opposite to previously published work that demonstrated that soil $\delta^{15}N$ values increase with increasing charring temperature and time (Saito et al., 2007; Pyle et al., 2015). Nitrogen in soils is complex, and without further chemical description, difficult to interpret.

**TABLE 4 |** Eroding hillslope and surface soil model comparisons with null model with maximum likelihood method.

| SOC fraction | $\chi^2$ | *df* | *p* | AIC | BIC |
|---|---|---|---|---|---|
| **HILLSLOPE MODEL** | | | | | |
| PyC | 149.33 | 5 | 0.00 | 629.8 | 654.4 |
| null model | | | | 769.2 | 778.4 |
| POC | 73.18 | 5 | 0.00 | 722.7 | 747.3 |
| null model | | | | 785.9 | 795.1 |
| HOC | 130.48 | 5 | 0.00 | 812.8 | 837.4 |
| null model | | | | 933.3 | 942.5 |
| PyC fraction | 110.87 | 6 | 0.00 | −408.9 | −381.2 |
| Null model | | | | −310.0 | −300.8 |
| **SURFACE SOIL MODEL** | | | | | |
| PyC | 34.30 | 3 | 0.00 | 1011.3 | 1029.0 |
| null model | | | | 1039.6 | 1048.5 |
| POC | 28.36 | 3 | 0.00 | 988.7 | 1006.4 |
| null model | | | | 1011.1 | 1020.0 |
| HOC | 32.50 | 3 | 0.00 | 1115.4 | 1133.0 |
| null model | | | | 1141.9 | 1150.7 |
| PyC fraction | 91.67 | 4 | 0.00 | −310.6 | −290.0 |
| | | | | −226.9 | −218.1 |

At the 10-years post-fire sampling point, the depositional landform position had relatively similar isotopic compositions to the eroding surface soil, $\delta^{15}N$ values of 2.44‰ (±0.30‰ standard error, s.e.) and 3.84‰ (±0.18‰ s.e.) and $\delta^{13}C$ values of −26.22‰ (±0.34‰ s.e.) and −25.73‰ (±0.47‰ s.e.) for the burned eroding hillslope and depositional landform positions, respectively (**Table 2** and **Figure 8**). This similarity is further evidence for the connection between surface soil and OM from the eroding positions and the soil within the depositional landform position. This long-term erosion may have led to the burial of earlier deposited material, which had much higher SOC concentration 1-year post-fire, such that what was sampled as top soil in the depositional landform position 10-years post-fire was mineral material that was more recently transported from the upslope eroding landform position.

It is likely that at least a fraction of the SOC fractions in the depositional landform position post-fire were lost via increased rates of decomposition (Berhe, 2012; Doetterl et al., 2012). The input of SOC and nutrients into the depositional landform position from the original mass flow event, along with the accumulation of water from precipitation and the nearby creek, could create ideal conditions for decomposition at this location compared with the eroding plots (Cheng et al., 2006; Johnson et al., 2007). The depositional landform position presents a range of conditions that can favor rapid loss of PyC that remains on the surface.

## Downwards Mobilization of SOC and SOM

Leaching can also mobilize SOC downward in a soil profile, as evidenced by the small, but not significant, increase in HOC and PyC fractions at depth in the eroding landform positions at the final time point (**Figure 6**), along with a decrease in $\delta^{13}C$ and $\delta^{15}N$ values throughout the burned eroding plots in the final sampling point (**Figure 8**). The HOC fraction may have also been more susceptible to leaching based on

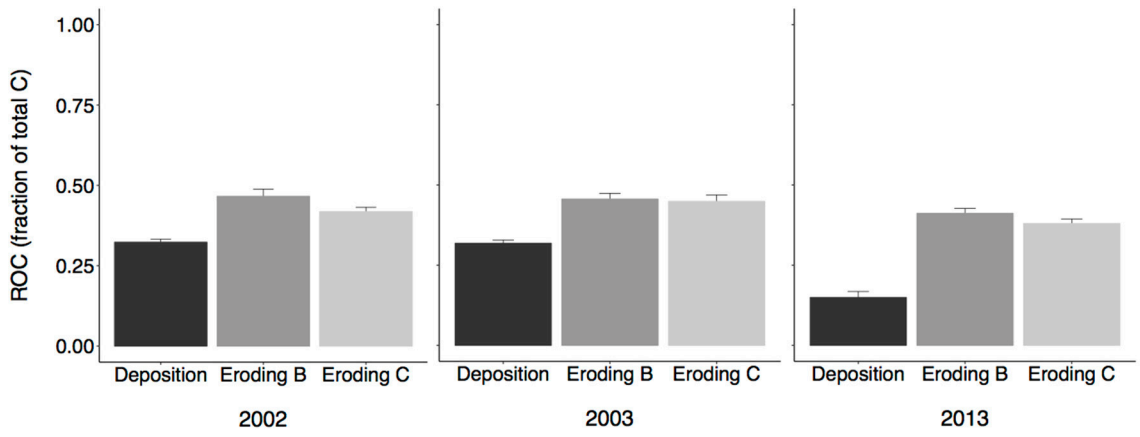


**FIGURE 7 |** Resistant organic carbon (ROC or PyC) as a fraction of total soil carbon in surface soils from burn and control plots. Eroding B refers to the burned eroding plots, and Eroding C refers to the control (unburned) eroding plots. Means are presented here for each sampling year with error bars representing standard error.

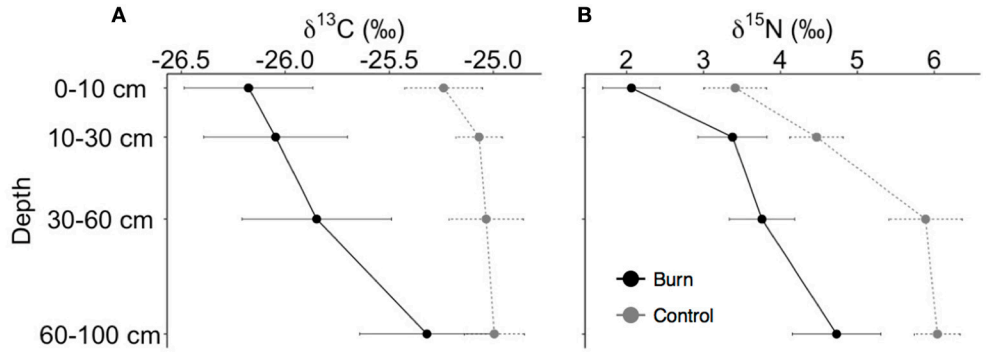


**FIGURE 8 |** Stable carbon **(A)** and nitrogen **(B)** isotopes for the eroding landform position 10 years post-fire. Error bars represent standard error.

its smaller size compared with POC. This HOC fraction may also serve as a more stable, deep soil C sink, as previous research has indicated that this smaller material is typically older than more particulate SOC constituents (Kleber et al., 2011).

The soils in the eroding positions of the Gondola fire site are coarse textured and porous, creating optimum conditions for vertical mobilization of bulk C, N, and PyC in dissolved and/or particulate form. The small shift in isotopic compositions of SOM suggests a shift in organic material and nutrients quality during post-fire recovery. The OM that is left behind may be more complex biomolecules, such as lignin that are more difficult to breakdown, or possibly more susceptible to leaching. Santos et al. (2016) previously showed that thermal alterations of topsoil can include leaching of dissolved PyC from soil, in particular after low and medium severity fire temperature regimes. It is possible though, in particular in soils with high clay content, the leaching process can be relatively slow. Major et al. (2010) found that in a year only 1% of their applied PyC was mobilized downward in the profile, and this change was not apparent in this study at the 1-year post-fire sampling point. The leaching of PyC also depends on the particle size (dissolved vs. particulate form) and vegetation type. Slow leaching of PyC downward may be altered by the quality of PyC material left after the initial mass movement event and the post-fire vegetation recovery (Major et al., 2010; Kindler et al., 2011; Güereña et al., 2015). Leaching may be occurring in the depositional landform position, but we did not sample at depth into this landform position, as no pre-fire comparison samples exist for the deep soils in the depositional landform position.

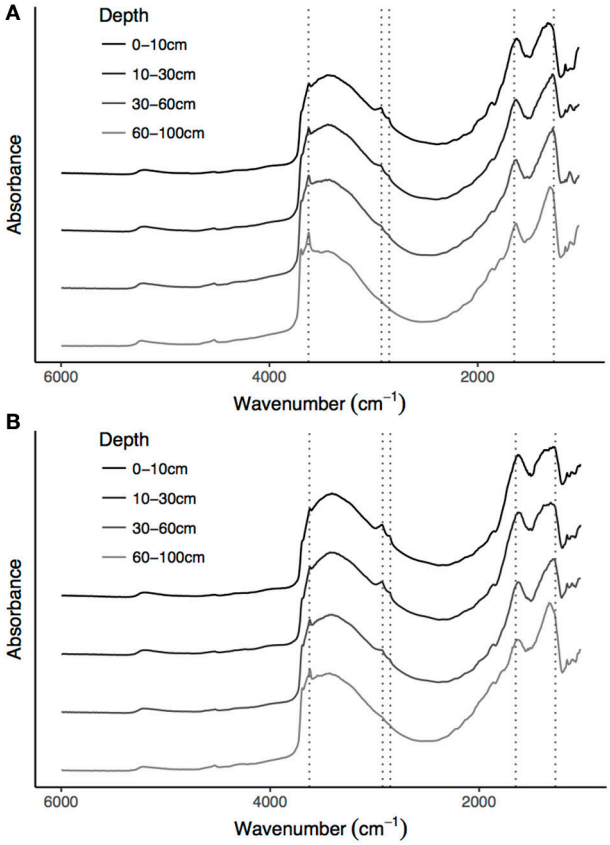


**FIGURE 9 |** Examples of MIR spectra of soil from a control **(A)** and burned **(B)** plot from the eroding position in the 10-year post-fire sampling time point. Shifts in peak intensities occurred at wavenumbers 1,270 $cm^{-1}$ (carboxylic and phenolic groups), 1,650 $cm^{-1}$ (aromatic compounds), 2,924 $cm^{-1}$ (asymmetric C-H stretching), 2,850 $cm^{-1}$ (symmetric C-H stretching), and 3,625 $cm^{-1}$ (O-H bonding).

## Implications of Post-fire Erosion for Long-Term Persistence of SOC and PyC

Lateral redistribution of topsoil by soil erosion after wildfires has important implications for the dynamics of both bulk SOC and specific fractions. In the Gondola fire site, large amounts of C in all the SOC fractions were mobilized by a large erosion event immediately post-fire. However, we also found that significant amount of C from all the SOC fractions was lost from the surface depositional zone in the long term. It is clear from this 10 year, three sampling period study that C in all the SOC fractions in the eroding plots was considerably altered in the 10-years post-fire.

**TABLE 5 |** NMR functional group assignments of the depositional samples from before (2002) and after (2003) the Gondola Fire.

| Sample number | Alkyl (0–45 ppm) | N-Alkyl/Methoxyl (45-60 ppm) | O-Alkyl (60–95 ppm) | Di-O-Alkyl (95–110 ppm) | Aryl (110–145 ppm) | O-Aryl (145–165 ppm) | Amide/Carboxyl (165–190 ppm) | Ketone (190–215 ppm) |
|---|---|---|---|---|---|---|---|---|
| **PRE-FIRE DEPOSITION** | | | | | | | | |
| 70† | 12.9 | 5.7 | 17.4 | 6.0 | 31.5 | 11.2 | 12.0 | 3.2 |
| 74 | 14.0 | 7.2 | 26.8 | 7.4 | 18.9 | 8.7 | 13.2 | 3.7 |
| 90* | 16.5 | 6.3 | 22.1 | 6.3 | 26.1 | 8.9 | 11.7 | 2.2 |
| 114* | 17.0 | 5.4 | 14.0 | 5.1 | 37.9 | 9.9 | 7.8 | 2.7 |
| 118* | 15.9 | 6.5 | 22.2 | 6.2 | 22.5 | 9.6 | 13.8 | 3.3 |
| 67* | 16.2 | 7.4 | 25.2 | 7.3 | 20.2 | 8.7 | 11.9 | 3.0 |
| 77 | 14.8 | 6.6 | 24.9 | 6.7 | 20.6 | 8.5 | 14.5 | 3.4 |
| 85*† | 18.9 | 7.5 | 25.6 | 6.9 | 18.7 | 7.0 | 12.9 | 2.5 |
| 99* | 13.5 | 6.3 | 16.1 | 5.3 | 32.8 | 12.1 | 10.6 | 3.3 |
| 109* | 14.1 | 6.4 | 21.0 | 7.7 | 23.5 | 11.6 | 11.6 | 4.1 |
| Mean | 15.4 (0.5) | 6.5 (0.2) | 21.5 (1.3) | 6.5 (0.2) | 25.3 (2.1) | 9.6 (0.5) | 12.0 (0.5) | 3.1 (0.1) |
| **POST-FIRE DEPOSITION** | | | | | | | | |
| 6† | 15.6 | 5.8 | 20.5 | 6.1 | 29.9 | 10.6 | 8.4 | 3.1 |
| 26 | 18.3 | 7.1 | 25.6 | 6.4 | 17.2 | 7.2 | 15.2 | 3.0 |
| 28 | 18.7 | 6.5 | 18.1 | 5.6 | 29.4 | 9.3 | 9.3 | 3.1 |
| 32 | 15.7 | 6.6 | 20.8 | 6.5 | 25.4 | 9.8 | 11.9 | 3.4 |
| 40 | 15.5 | 6.4 | 20.5 | 5.7 | 26.7 | 9.3 | 12.9 | 3.0 |
| 48*† | 13.3 | 5.7 | 14.8 | 5.5 | 34.8 | 12.5 | 10.2 | 3.3 |
| 52 | 15.8 | 6.9 | 25.6 | 7.2 | 17.5 | 8.2 | 14.8 | 3.8 |
| 64* | 14.0 | 4.6 | 13.5 | 5.7 | 37.1 | 13.1 | 8.7 | 3.3 |
| Mean | 15.9 (0.6) | 6.2 (0.2) | 19.9 (1.5) | 6.1 (0.2) | 27.2 (2.5) | 10.0 (0.7) | 11.4 (0.9) | 3.3 (0.1) |

*Samples analyzed with NMR were chosen using the Kennard-Stone algorithm to accurately include the variance within the dataset. Standard errors of mean functional group distributions are presented in parentheses. *indicates samples that were treated with HF prior to NMR analysis due to extremely poor signal acquisition. †indicates samples that have spectra plotted in **Figure 10**.*

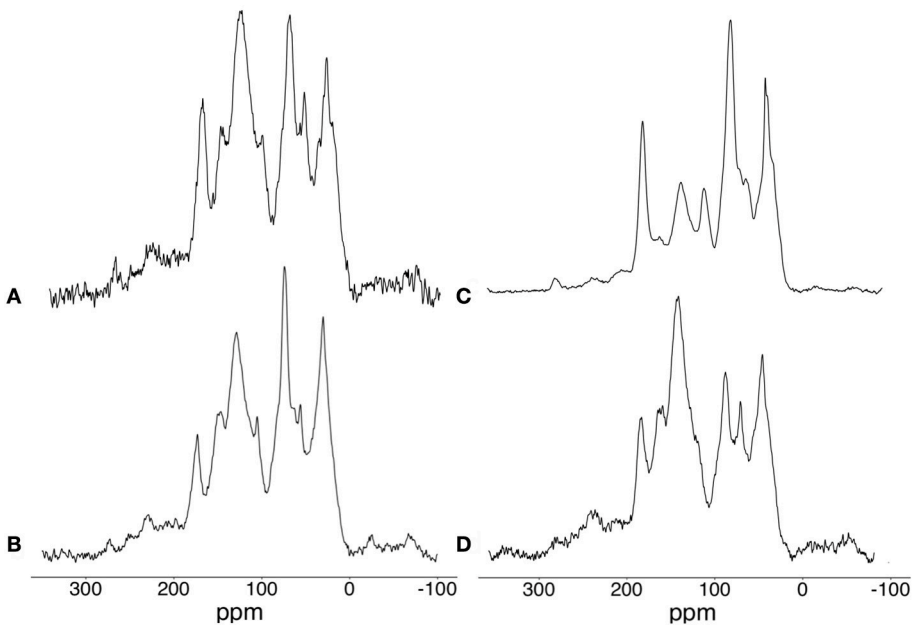


**FIGURE 10 |** Representative $^{13}C$ CPMAS NMR spectra of soil from pre-fire **(A)** and 10-year post-fire **(B)** samples from the depositional landform position that were not treated with HF, and pre-burn **(C)** and post-burn **(D)** samples that were treated with HF.

This change in C in the different SOC fractions in the depositional landform position suggests some elevated biological processing of SOM in the long-term post-fire. The increase in the PyC fraction that we observed could be due to either erosion of PyC from upslope or from deposition of PyC in the form of ash or soot from nearby wildfires, such as the Rim Fire (Peterson et al., 2015). Vertical mobilization of C in the different SOC fractions can lead to enhanced protection of both bulk C and PyC due to the decline in availability of oxygen and/or lower microbe biomass or active in deeper soil layers (Marin-Spiotta et al., 2014).

In contrast to the eroding landform positions, the depositional landform position lost significant proportions of C from all the SOC fractions over the 10 years likely due to combination of factors that includes ongoing transport and burial of top soil material from the eroding hillslope, leaching of C down the soil profile, and decomposition *in situ*. The long-term stability of SOC in depositional landform positions critically depends on the local decomposition conditions (Berhe, 2012) and erosion potential, as burial of SOC in depositional landform has also been demonstrated to be a stabilization mechanism for SOC and PyC (Berhe et al., 2007; Berhe and Kleber, 2013; Chaopricha and Marín-Spiotta, 2014).

While this study follows a single wildfire and its impacts on soil erosion, it highlights the roles that lateral and vertical redistribution of C post-fire can have implications for soil carbon dynamics. However, gaps remain in our understanding of the mechanisms through which erosional redistribution of PyC across fire-impacted landscapes can affect its stock and persistence in soil. So far, the relative rates of lateral and vertical transport of PyC, with erosion, leaching, and bioturbation, across differing landscapes remains largely unknown (Güereña et al., 2015; Rumpel et al., 2015). The erosion of PyC is also significant, because this loss from eroding hillslopes post-fire, as illustrated after the Gondola fire, can lead to differences in its apparent environmental persistence based upon topographic features of a landscape. If eroded PyC is buried, it may act as an even more persistent C sink. However, if eroded PyC is deposited into a landform position that has more favorable conditions for microbial breakdown, such as higher water content or higher nutrient availability, then the environmental persistence of PyC may be shorter. Considering that 1–5 Gt C is annually eroded (Stallard, 1998), and PyC makes up around 3% of total soil C (Bird et al., 2015), erosion is responsible for the lateral transport of 3–5 Mt PyC annually. Hence, PyC transport is an important variable for accurately determining its mean residence time in the terrestrial ecosystem and its implications for soil carbon dynamics overall.

## CONCLUSIONS

Our results show that erosion plays major roles in controlling stock, fluxes, and potentially stability and stabilization mechanisms of bulk C and PyC post-fire. After the Gondola fire, erosion changed the carbon sequestration trajectory of the system as over 1.5 Mg PyC/ha and 0.7 Mg C/ha of C in all SOC fractions was distributed away from the surface of the eroding landform positions, and deposited in the downhill riparian area. Ten years after the fire, soils at the depositional landform position had considerably lower concentrations of all SOC fractions, and retained proportionally lower concentrations of PyC than the eroding hillslope. We conclude that either the highly charred and SOC-rich material was buried in the depositional landform position with subsequent erosion events, or was more rapidly decomposed than in the eroding hillslope landform position.

The relatively low $\delta^{13}C$ and $\delta^{15}N$ values in the burned soils suggests persistence of SOM with isotopically lower values, such as those from lignin, while other material with higher isotopic values, i.e., cellulose, was consumed either during combustion or via post-fire microbial processing. Better understanding of the long-term fate of C in dynamic landscapes post-fire is critical for constraining of terrestrial carbon budgets in a changing world.

## AUTHOR CONTRIBUTIONS

AB conceived the study. RA, AB, and DJ designed the field sampling component of this research. DJ provided archived samples and data pertaining to them. JS contributed spectroscopic analyses of samples and statistical analysis of the spectral results. MF assisted with stable isotope analyses and interpretation. RA conducted majority of soil and statistical analyses, and was lead author of the manuscript. AB, DJ, JS, and MF contributed in writing of the manuscript and approve it for publication.

## FUNDING

Funding for this work was provided from Hellman Family Foundation Grant and a National Science Foundation award (CAREER EAR-1352627) to AB and from UC Merced School of Natural Science to MF.

## ACKNOWLEDGMENTS

We thank Emma McCorkle for her help in the field and lab, and Erin Carroll for help with archived data on the study site. We thank Bruce Hawke and Janine McGowan for performing FTIR and NMR spectroscopic analyses of soil samples at CSIRO in Adelaide, Australia, and David Araiza, Christina Bradley, Elizabeth Williams, and Bobby Nakamoto of the MF Stable Isotope lab at UC Merced for their assistance with the elemental and isotopic analyses. We also thank Stephen Hart for comments on earlier versions of this manuscript.

## REFERENCES


Abiven, S., Hengartner, P., Schneider, M. P. W., Singh, N., and Schmidt, M. W. I. (2011). Pyrogenic carbon soluble fraction is larger and more aromatic in aged charcoal than in fresh charcoal. *Soil Biol. Biochem.* 43, 1615–1617. doi: 10.1016/j.soilbio.2011.03.027

Ahmed, Z. U., Woodbury, P. B., Sanderman, J., Hawke, B., Jauss, V., Solomon, D., et al. (2017). Assessing soil carbon vulnerability in the Western USA by geospatial modeling of pyrogenic and particulate carbon stocks. *J. Geophys. Res. Biogeosci.* 122, 354–369. doi: 10.1002/2016JG003488

Araya, S., Meding, S., and Berhe, A. (2016). Thermal alteration of soil physico-chemical properties: a systematic study to infer response of Sierra Nevada climosequence soils to forest fires. *Soil* 2, 351–366. doi: 10.5194/soil-2-351-2016

Araya, S. N., Fogel, M. L., and Berhe, A. A. (2017). Thermal alteration of soil organic matter properties: a systematic study to infer response of Sierra Nevada climosequence soils to forest fires. *Soil* 3, 31–44. doi: 10.5194/soil-3-31-2017

Baldock, J., Hawke, B., Sanderman, J., and Macdonald, L. (2013a). Predicting contents of carbon and its component fractions in Australian soils from diffuse reflectance mid-infrared spectra. *Soil Res.* 51, 577–595. doi: 10.1071/SR13077

Baldock, J., MacDonald, L., and Sanderman, J. (2013b). Foreword to 'Soil carbon in Australia's agricultural lands'. *Soil Res.* 51, i–ii. doi: 10.1071/SRv51n8_FO

Baldock, J., Sanderman, J., Macdonald, L., Puccini, A., Hawke, B., Szarvas, S., et al. (2014). Quantifying the allocation of soil organic carbon to biologically significant fractions. *Soil Res.* 51, 561–576. doi: 10.1071/SR12374

Battin, T., Luyssaert, S., Kaplan, L., Aufdenkampe, A., Richter, A., and Tranvik, L. (2009). The boundless carbon cycle. *Nat. Geosci.* 2, 598–600. doi: 10.1038/ngeo618

Benner, R., Fogel, M. L., Sprague, E. K., and Hodson, R. E. (1987). Depletion of $^{13}C$ in lignin and its implications for stable carbon isotope studies. *Nature* 329, 708–710. doi: 10.1038/329708a0

Berhe, A. A. (2012). Decomposition of organic substrates at eroding vs. depositional landform positions. *Plant Soil* 350, 261–280. doi: 10.1007/s11104-011-0902-z

Berhe, A. A. (2013). Effect of litterbags on rate of organic substrate decomposition along soil depth and geomorphic gradients. *J. Soils Sediments* 13, 629–640. doi: 10.1007/s11368-012-0639-1

Berhe, A. A., Harden, J. W., Torn, M. S., Kleber, M., Burton, S. D., and Harte, J. (2012). Persistence of soil organic matter in eroding versus depositional landform positions. *J. Geophys. Res. Biogeosci.* 117:G02019. doi: 10.1029/2011JG001790

Berhe, A. A., Harte, J., Harden, J. W., and Torn, M. S. (2007). The significance of erosion-induced terrestrial carbon sink. *Bioscience* 57, 337–346. doi: 10.1641/B570408

Berhe, A. A., and Kleber, M. (2013). Erosion, deposition, and the persistence of soil organic matter: mechanistic considerations and problems with terminology. *Earth Surf. Process. Landforms* 38, 908–912. doi: 10.1002/esp.3408

Bird, M. I., Wynn, J. G., Saiz, G., Wurster, C. M., and McBeath, A. (2015). The pyrogenic carbon cycle. *Annu. Rev. Earth Planet. Sci.* 43, 273–298. doi: 10.1146/annurev-earth-060614-105038

Boot, C., Haddix, M., Paustian, K., and Cotrufo, M. (2015). Distribution of black carbon in ponderosa pine forest floor and soils following the High Park wildfire. *Biogeosciences* 12, 3029–3039. doi: 10.5194/bg-12-3029-2015

Brewer, C. E., Chuang, V. J., Masiello, C. A., Gonnermann, H., Gao, X., Dugan, B., et al. (2014). New approaches to measuring biochar density and porosity. *Biomass Bioenergy* 66, 176–185. doi: 10.1016/j.biombioe.2014.03.059

Carroll, E. M., Miller, W. W., Johnson, D. W., Saito, L., Qualls, R. G., and Walker, R. F. (2007). Spatial analysis of a large magnitude erosion event following a Sierran Wildfire. *J. Environ. Qual.* 36, 1105–1105. doi: 10.2134/jeq2006.0466

Certini, G. (2005). Effects of fire on properties of forest soils: a review. *Oecologia* 143, 1–10. doi: 10.1007/s00442-004-1788-8

Chaopricha, N. T., and Marín-Spiotta, E. (2014). Soil burial contributes to deep soil organic carbon storage. *Soil Biology Biochem.* 69, 251–264. doi: 10.1016/j.soilbio.2013.11.011

Cheng, C., Lehmann, J., Thies, J., Burton, S., and Engelhard, M. (2006). Oxidation of black carbon by biotic and abiotic processes. *Org. Geochem.* 37, 1477–1488. doi: 10.1016/j.orggeochem.2006.06.022

DeBano, L. (2000). The role of fire and soil heating on water repellency in wildland environments: a review. *J. Hydrol.* 231, 195–206. doi: 10.1016/S0022-1694(00)00194-3

DeBano, L. F. (1991). "The effect of fire on soil properties," in *Symposium on Management and Productivity of Westero-Montane Forest Soils*, eds A. E. Harvey and L. F. Neuenschwander (Ogden, UT: USDA Forest Service, Intermountain Research Station).

Doetterl, S., Berhe, A. A., Nadeu, E., Wang, Z., Sommer, M., and Fiener, P. (2016). Erosion, deposition and soil carbon: a review of process-level controls, experimental tools and models to address C cycling in dynamic landscapes. *Earth Sci. Rev.* 154, 102–122. doi: 10.1016/j.earscirev.2015.12.005

Doetterl, S., Six, J., Van Wesemael, B., and Van Oost, K. (2012). Carbon cycling in eroding landscapes: geomorphic controls on soil organic C pool composition and C stabilization. *Glob. Chang. Biol.* 18, 2218–2232. doi: 10.1111/j.1365-2486.2012.02680.x

Eckmeier, E., Gerlach, R., Skjemstad, J., Ehrmann, O., and Schmidt, M. (2007). Minor changes in soil organic carbon and charcoal concentrations detected in a temperate deciduous forest a year after an experimental slash-and-burn. *Biogeosciences* 4, 377–383. doi: 10.5194/bg-4-377-2007

Giovannini, G., Lucchesi, S., and Giachetti, M. (1988). Effect of heating on some physical and chemical parameters related to soil aggregation and erodibility. *Soil Sci.* 146, 255–262. doi: 10.1097/00010694-198810000-00006

Gregorich, E., Greer, K., Anderson, D., and Liang, B. (1998). Carbon distribution and losses: erosion and deposition effects. *Soil Tillage Res.* 47, 291–302. doi: 10.1016/S0167-1987(98)00117-2

Güereña, D. T., Lehmann, J., Walter, T., Enders, A., Neufeldt, H., Odiwour, H., et al. (2015). Terrestrial pyrogenic carbon export to fluvial ecosystems: lessons learned from the White Nile watershed of East Africa. *Glob. Biogeochem. Cycles* 29, 1911–1928. doi: 10.1002/2015GB005095

Hammes, K., Torn, M. S., Lapenas, A. G., and Schmidt, M. W. I. (2008). Centennial black carbon turnover observed in a Russian steppe soil. *Biogeosciences* 5, 1339–1350. doi: 10.5194/bg-5-1339-2008

Harden, J. W., Sharpe, J. M., Parton, W. J., Ojima, D. S., Fries, T. L., Huntington, T. G., et al. (1999). Dynamic replacement and loss of soil carbon on eroding cropland. *Glob. Biogeochem. Cycles* 13, 885–901. doi: 10.1029/1999GB900061

Janik, L. J., Skjemstad, J. O., Shepherd, K. D., and Spouncer, L. R. (2007). The prediction of soil carbon fractions using mid-infrared-partial least square analysis. *Aust. J. Soil Res.* 45, 73–81. doi: 10.1071/SR06083

Jauss, V., Sullivan, P. J., Sanderman, J., Smith, D. B., and Lehmann, J. (2017). Pyrogenic carbon distribution in mineral topsoils of the northeastern United States. *Geoderma* 296, 69–78. doi: 10.1016/j.geoderma.2017.02.022

Johnson, D., Murphy, J., Walker, R., Glass, D., and Miller, W. (2007). Wildfire effects on forest carbon and nutrient budgets. *Ecol. Eng.* 31, 183–192. doi: 10.1016/j.ecoleng.2007.03.003

Johnson, D., Susfalk, R., Caldwell, T., Murphy, J., Miller, W., and Walker, R. (2004). Fire effects on carbon and nitrogen budgets in forests. *Water Air Soil Pollut. Focus* 4, 263–275. doi: 10.1023/B:WAFO.0000028359.17442.d1

Kennard, R. W., and Stone, L. A. (1969). Computer aided design of experiments. *Technometrics* 11, 137–148. doi: 10.1080/00401706.1969.10490666

Kindler, R., Siemens, J., Kaiser, K., Walmsley, D. C., Bernhofer, C., Buchmann, N., et al. (2011). Dissolved carbon leaching from soil is a crucial component of the net ecosystem carbon balance. *Glob. Chang. Biol.* 17, 1167–1185. doi: 10.1111/j.1365-2486.2010.02282.x

Kleber, M., Nico, P. S., Plante, A., Filley, T., Kramer, M., Swanston, C., et al. (2011). Old and stable soil organic matter is not necessarily chemically recalcitrant: implications for modeling concepts and temperature sensitivity. *Glob. Chang. Biol.* 17, 1097–1107. doi: 10.1111/j.1365-2486.2010.02278.x

Kuzyakov, Y., Subbotina, I., and Chen, H. (2009). Black carbon decomposition and incorporation into soil microbial biomass estimated by C labeling. *Soil Biol. Biochem.* 41, 210–219. doi: 10.1016/j.soilbio.2008.10.016

Lal, R. (2003a). Global potential of soil carbon sequestration to mitigate the greenhouse effect. *CRC Crit. Rev. Plant Sci.* 22, 151–184. doi: 10.1080/713610854

Lal, R. (2003b). Soil erosion and the global carbon budget. *Environ. Int.* 29, 437–450. doi: 10.1016/S0160-4120(02)00192-7

Lal, R. (2004). Soil carbon sequestration impacts on global climate change and food security. *Science* 304, 1623–1627. doi: 10.1126/science.1097396

Larsen, I., Macdonald, L., Brown, E., Rough, D., Welsh, M., Pietraszek, J., et al. (2009). Causes of post-fire runoff and erosion: water repellency, cover, or soil sealing? *Soil Sci. Soc. Am. J.* 73, 1393. doi: 10.2136/sssaj2007.0432

Lehmann, J., Czimczik, C., Laird, D., and Sohi, S. (2009). "Stability of biochar in soil," in *Biochar for Environmental Management. Science and Technology*, eds J. Lehmann and S. Joseph (Sterling, VA: Earthscan), 183–205.

Liang, B., Lehmann, J., Solomon, D., Kinyangi, J., Grossman, J., O'Neill, B., et al. (2006). Black carbon increases cation exchange capacity in soils. *Soil Sci. Soc. Am. J.* 70, 1719–1730. doi: 10.2136/sssaj2005.0383

Major, J., Lehmann, J., Rondon, M., and Goodale, C. (2010). Fate of soil-applied black carbon: downward migration, leaching and soil respiration. *Glob. Chang. Biol.* 16, 1366–1379. doi: 10.1111/j.1365-2486.2009.02044.x

Marin-Spiotta, E., Chaopricha, N. T., Plante, A. F., Diefendorf, A. F., Mueller, C. W., Grandy, A. S., et al. (2014). Long-term stabilization of deep soil carbon by fire and burial during early holocene climate change. *Nat. Geosci.* **7**, 428–432. doi: 10.1038/ngeo2169

Masiello, C. (2004). New directions in black carbon organic geochemistry. *Mar. Chem.* 92, 201–213. doi: 10.1016/j.marchem.2004.06.043

Nguyen, B. T., Lehmann, J., Kinyangi, J., Smernik, R., Riha, S. J., and Engelhard, M. H. (2009). Long-term black carbon dynamics in cultivated soil. *Biogeochemistry* 92, 163–176. doi: 10.1007/s10533-008-9248-x

Pereira, P., Cerdà, A., Úbeda, X., Mataix-Solera, J., Arcenegui, V., and Zavala, L. (2015). Modelling the impacts of wildfire on ash thickness in a short-term period. *Land Degradat. Dev.* 26, 180–192. doi: 10.1002/ldr.2195

Peterson, D. A., Hyer, E. J., Campbell, J. R., Fromm, M. D., Hair, J. W., Butler, C. F., et al. (2015). The 2013 rim fire: implications for predicting extreme fire spread, pyroconvection, and smoke emissions. *Bull. Am. Meteorol. Soc.* 96, 229–247. doi: 10.1175/BAMS-D-14-00060.1

Pierson, F. B., Moffet, C. A., Williams, C. J., Hardegree, S. P., and Clark, P. E. (2009). Prescribed-fire effects on rill and interrill runoff and erosion in a mountainous sagebrush landscape. *Earth Surf. Process. Landforms* 34, 193–203. doi: 10.1002/esp.1703

Pierson, F. B., Williams, C. J., Hardegree, S. P., Clark, P. E., Kormos, P. R., and Al-Hamdan, O. Z. (2013). Hydrologic and erosion responses of sagebrush steppe following juniper encroachment, wildfire, and tree cutting. *Rangeland Ecol. Manag.* 66, 274–289. doi: 10.2111/REM-D-12-00104.1

Post, W. M., and Kwon, K. C. (2000). Soil carbon sequestration and land-use change: processes and potential. *Glob. Chang. Biol.* 6, 317–327. doi: 10.1046/j.1365-2486.2000.00308.x

Preston, C. M., Trofymow, J. A., and Flanagan, L. B. (2006). Decomposition, $\delta^{13}C$, and the "lignin paradox". *Can. J. Soil Sci.* 86, 235–245. doi: 10.4141/S05-090

Preston, C. M., and Trofymow, J. A. (2015). The chemistry of some foliar litters and their sequential proximate analysis fractions. *Biogeochemistry* 126, 197–209. doi: 10.1007/s10533-015-0152-x

Pyle, L. A., Hockaday, W. C., Boutton, T., Zygourakis, K., Kinney, T. J., and Masiello, C. A. (2015). Chemical and isotopic thresholds in charring: implications for the interpretation of charcoal mass and isotopic data. *Environ. Sci. Technol.* 49, 14057–14064. doi: 10.1021/acs.est.5b03087

Renard, K. G., Foster, G. R., Weesies, G., McCool, D., and Yoder, D. (1997). Predicting *Soil Erosion* by *Water: A Guide to Conservation Planning with the Revised Universal Soil Loss Equation (RUSLE)*. Washington, DC: US Government Printing Office.

Rumpel, C., Ba, A., Darboux, F., Chaplot, V., and Planchon, O. (2009). Erosion budget and process selectivity of black carbon at meter scale. *Geoderma* 154, 131–137. doi: 10.1016/j.geoderma.2009.10.006

Rumpel, C., Chaplot, V., Planchon, O., Bernadou, J., Valentin, C., and Mariotti, A. (2006). Preferential erosion of black carbon on steep slopes with slash and burn agriculture. *CATENA* 65, 30–40. doi: 10.1016/j.catena.2005.09.005

Rumpel, C., Leifeld, J., Santin, C., and Doerr, S. (2015). "Movement of biochar in the environment," in *Biochar for Environmental Management: Science, Technology and Implementation 2nd Edn.,* eds J. Lehmann and S. Joseph (New York, NY: Routledge), 283–298.

Saito, L., Miller, W. W., Johnson, D. W., Qualls, R., Provencher, L., Carroll, E., et al. (2007). Fire effects on stable isotopes in a sierran forested watershed. *J. Environ. Qual.* 36, 91–100. doi: 10.2134/jeq2006.0233

Sanderman, J., Baldock, J., Hawke, B., Macdonald, L., Massis-Puccini, A., and Szarvas, S. (2011). *National Soil Carbon Research Programme: Field and Laboratory Methodologies*. Urrbrae, SA: CSIRO.

Sanderman, J., Farrell, M., Macreadie, P. I., Hayes, M., McGowan, J., and Baldock, J. (2017). Is demineralization with dilute hydrofluoric acid a viable method for isolating mineral stabilized soil organic matter? *Geoderma* 304, 4–11. doi: 10.1016/j.geoderma.2017.03.002

Santin, C., Doerr, S. H., Preston, C. M., and Gonzalez-Rodriguez, G. (2015). Pyrogenic organic matter production from wildfires: a missing sink in the global carbon cycle. *Glob. Chang. Biol.* 21, 1621–1633. doi: 10.1111/gcb.12800

Santos, F., Russell, D., and Berhe, A. A. (2016). Thermal alteration of water extractable organic matter in climosequence soils from the Sierra Nevada, California. *J. Geophys. Res. Biogeosci.* 121, 2877–2885. doi: 10.1002/2016JG003597

Scharlemann, J. P., Tanner, E. V., Hiederer, R., and Kapos, V. (2014). Global soil carbon: understanding and managing the largest terrestrial carbon pool. *Carbon Manag.* 5, 81–91. doi: 10.4155/cmt.13.77

Schmidt, M. W. I., Knicker, H., Hatcher, P. G., and Kogel-Knabner, I. (1997). Improvement of $^{13}C$ and $^{15}N$ CPMAS NMR spectra of bulk soils, particle size fractions and organic material by treatment with 10% hydrofluoric acid. *Eur. J. Soil Sci.* 48, 319–328. doi: 10.1111/j.1365-2389.1997.tb00552.x

Shakesby, R., Coelho, C., Ferreira, A., Terry, J., and Walsh, R. (1993). Wildfire impacts on soil-erosion and hydrology in wet Mediterranean forest, Portugal. *Int. J. Wildland Fire* 3, 95–110. doi: 10.1071/WF9930095

Shakesby, R., Doerr, S., and Walsh, R. (2000). The erosional impact of soil hydrophobicity: current problems and future research directions. *J. Hydrol.* 231, 178–191. doi: 10.1016/S0022-1694(00)00193-1

Skjemstad, J. O. (1994). The removal of magnetic materials from surface soils. *Aust. J. Soil Res.* 32, 1215–1229. doi: 10.1071/SR9941215

Skjemstad, J. O., Spouncer, L. R., Cowie, B., and Swift, R. S. (2004). Calibration of the Rothamsted organic carbon turnover model (RothC ver. 26.3) using measurable soil organic carbon pools. *Aust. J. Soil Res.* 42, 79–88. doi: 10.1071/SR03013

Smernik, R. J., and Oades, J. M. (2000a). The use of spin counting for determining quantitation in solid state 13 C NMR spectra of natural organic matter: 1. Model systems and the effects of paramagnetic impurities. *Geoderma* 96, 101–129. doi: 10.1016/S0016-7061(00)00006-9

Smernik, R. J., and Oades, J. M. (2000b). The use of spin counting for determining quantitation in solid state 13C NMR spectra of natural organic matter. 2. HF-treated soil fractions. *Geoderma* 96, 159–171. doi: 10.1016/S0016-7061(00)00007-0

Smernik, R., and Oades, J. (2002). Paramagnetic effects on solid state carbon-13 nuclear magnetic resonance spectra of soil organic matter. J. Environ. *Qual.* 31, 414–420. doi: 10.2134/jeq2002.4140

Soucémarianadin, L. N., Quideau, S. A., Wasylishen, R. E., and Munson, A. D. (2015). Early-season fires in boreal black spruce forests produce pyrogenic carbon with low intrinsic recalcitrance. *Ecology* 96, 1575–1585. doi: 10.1890/14-1196.1

Stacy, E., Hart, S. C., Hunsaker, C. T., Johnson, D. W., and Berhe, A. A. (2015). Soil carbon and nitrogen erosion in forested catchments: implications for erosion-induced terrestrial carbon sequestration. *Biogeosci. Discuss.* 12, 2491–2532. doi: 10.5194/bgd-12-2491-2015

Stallard, R. (1998). Terrestrial sedimentation and the carbon cycle: coupling weathering and erosion to carbon burial. *Glob. Biogeochem. Cycles* 12, 231–257. doi: 10.1029/98GB00741

Westerling, A. L., Hidalgo, H. G., Cayan, D. R., and Swetnam, T. W. (2006). Warming and earlier spring increase western US forest wildfire activity. *Science* 313, 940–943. doi: 10.1126/science.1128834

Yao, J., Hockaday, W. C., Murray, D. B., and White, J. D. (2014). Changes in fire-derived soil black carbon storage in a subhumid woodland. *J. Geophys. Res. Biogeosci.* 119, 1807–1819. doi: 10.1002/2014JG002619

**Conflict of Interest Statement:** The authors declare that the research was conducted in the absence of any commercial or financial relationships that could be construed as a potential conflict of interest.

frontiers in Earth Science

ORIGINAL RESEARCH
published: 12 January 2018
doi: 10.3389/feart.2017.00115

# Preferential Production and Transport of Grass-Derived Pyrogenic Carbon in NE-Australian Savanna Ecosystems

*Gustavo Saiz[1*†], Iain Goodrick[1], Christopher Wurster[1,2], Paul N. Nelson[1], Jonathan Wynn[3] and Michael Bird[1,2]*

[1] Centre for Tropical Environmental and Sustainability Science, College of Science and Engineering, James Cook University, Cairns, QLD, Australia, [2] ARC Centre of Excellence for Australian Biodiversity and Heritage, James Cook University, Cairns, QLD, Australia, [3] School of Geosciences, University of South Florida, Tampa, FL, United States

Understanding the main factors driving fire regimes in grasslands and savannas is critical to better manage their biodiversity and functions. Moreover, improving our knowledge on pyrogenic carbon (PyC) dynamics, including formation, transport and deposition, is fundamental to better understand a significant slow-cycling component of the global carbon cycle, particularly as these ecosystems account for a substantial proportion of the area globally burnt. However, a thorough assessment of past fire regimes in grass-dominated ecosystems is problematic due to challenges in interpreting the charcoal record of sediments. It is therefore critical to adopt appropriate sampling and analytical methods to allow the acquisition of reliable data and information on savanna fire dynamics. This study uses hydrogen pyrolysis (HyPy) to quantify PyC abundance and stable isotope composition ($\delta^{13}C$) in recent sediments across 38 micro-catchments covering a wide range of mixed $C_3/C_4$ vegetation in north Queensland, Australia. We exploited the contrasting $\delta^{13}C$ values of grasses (i.e., $C_4$; $\delta^{13}C > -15‰$) and woody vegetation (i.e., $C_3$; $\delta^{13}C < -24‰$) to assess the preferential production and transport of grass-derived PyC in savanna ecosystems. Analyses were conducted on bulk and size-fractionated samples to determine the fractions into which PyC preferentially accumulates. Our data show that the $\delta^{13}C$ value of PyC in the sediments is decoupled from the $\delta^{13}C$ value of total organic carbon, which suggests that a significant component of PyC may be derived from incomplete grass combustion, even when the proportion of $C_4$ grass biomass in the catchment was relatively small. Furthermore, we conducted 16 experimental burns that indicate that there is a comminution of PyC produced in-situ to smaller particles, which facilitates the transport of this material, potentially affecting its preservation potential. Savanna fires preferentially burn the grass understory rather than large trees, leading to a bias toward the finer $C_4$-derived PyC in the sedimentary record. This in turn, provides further evidence for the preferential production and transport of $C_4$-derived PyC in mixed ecosystems where grass and woody vegetation coexist. Moreover, our isotopic approach provides independent validation of findings derived from conventional charcoal counting techniques concerning the appropriateness of adopting a relatively small particle size threshold (i.e., $\sim 50\,\mu m$) to reconstruct savanna fire regimes

OPEN ACCESS

***Edited by:***
*Cristina Santin, Swansea University, United Kingdom*

***Reviewed by:***
*Yamina Pressler, Colorado State University, United States*
*Stefan Doerr, Swansea University, United Kingdom*

****Correspondence:***
*Gustavo Saiz*
*g.saiz@imperial.ac.uk*

***†Present Address:***
*Gustavo Saiz, Department of Life Sciences, Imperial College London, Ascot, United Kingdom*

***Specialty section:***
*This article was submitted to Biogeoscience, a section of the journal Frontiers in Earth Science*

***Received:*** *03 July 2017*
***Accepted:*** *29 December 2017*
***Published:*** *12 January 2018*

***Citation:***
*Saiz G, Goodrick I, Wurster C, Nelson PN, Wynn J and Bird M (2018) Preferential Production and Transport of Grass-Derived Pyrogenic Carbon in NE-Australian Savanna Ecosystems. Front. Earth Sci. 5:115. doi: 10.3389/feart.2017.00115*

using sedimentary records. This work allows for a more nuanced understanding of the savanna isotope disequilibrium effect, which has significant implications for global $^{13}C$ isotopic disequilibria calculations and for the interpretation of $\delta^{13}C$ values of PyC preserved in sedimentary records.

**Keywords: carbon isotopes, savanna, biomass burning, black carbon, pyrogenic carbon, charcoal, hydrogen pyrolysis**

## INTRODUCTION

Fires are common in many ecosystems, but are particularly ubiquitous in seasonally dry savannas and grasslands, which comprise more than 80% of the area globally burnt (Giglio et al., 2013). However, a decreasing trend in global area being burnt has been reported over the past 18 years, which appears to be significant in grass-dominated ecosystems (Andela et al., 2017). Understanding past fire regimes and the main factors driving fire dynamics is important to better manage biodiversity and ecosystem functions (Conedera et al., 2009; Santín and Doerr, 2016). It is equally relevant to improve our knowledge of recent pyrogenic carbon (PyC) dynamics, including the provision of accurate information on PyC formation, transport and deposition, which is fundamental to better understand a significant slow-cycling component of the global carbon cycle (Bird et al., 2015).

Sediment charcoal records of small lakes have been extensively exploited to reconstruct fire histories across a range of ecosystems (Patterson et al., 1987; Millspaugh and Whitlock, 1995; Duffin et al., 2008; Leys et al., 2017). However, a disproportionate number of studies have focused on forested ecosystems despite the spatial significance and higher fire frequency of ecosystems where grasses either dominate (e.g., grasslands) or co-exist with woody vegetation (e.g., savannas) (Leys et al., 2015). The assessment of past fire regimes using charcoal peaks in the sedimentary record is particularly problematic in grass-dominated ecosystems due to the relatively high frequency of fire events, which makes very difficult to detect individual fire episodes (Leys et al., 2017). Other challenges associated with the interpretation of the charcoal record in sediments range from the lack of a standardized methodology for preparation, quantification and identification of samples, to resolution constraints inherent to the method used (i.e., the degree of temporal, spatial, and event resolution that sedimentary charcoal can offer) (Patterson et al., 1987; Conedera et al., 2009). It is therefore critical to adopt appropriate sampling and analytical methods to allow for the acquisition of reliable data and information on ecosystem fire dynamics (Conedera et al., 2009).

Research exploiting the sedimentary terrestrial record to reconstruct past fire regimes has typically investigated a number of physical characteristics of charcoal such as particle counts, size distribution, and morphotype analyses (Patterson et al., 1987; Clark, 1988; Duffin et al., 2008; Crawford and Belcher, 2014; Leys et al., 2015, 2017). For example, the size of source areas for micro- and macroscopic charcoal have been assessed through charcoal counts of different size classes in surface sediment samples collected across 17 savanna water bodies in Kruger National Park, South Africa (Duffin et al., 2008). This study showed that fire intensity, proximity, and area are unequally reflected in the charcoal record of tropical savannas, and concluded that the relevant source area for charcoal in lakes was between 0 and 5 km for pyrogenic particles $>50\,\mu m$. Other research has further confirmed that charcoal count in mixed fuel source landscapes is a function of local area burned (Leys et al., 2015), and subsequent work recommends the adoption of a small particle size thresholds (i.e., $60\,\mu m$) in ecosystems having a significant presence of grass biomass due to the relatively small size and easily comminuted nature of grass-derived PyC (Leys et al., 2017). The importance of discriminating between herbaceous and woody derived charcoal in sediment records is a research priority, since it could significantly improve the assessment of the temporal variability of fuel types in charcoal-based reconstructions of past fire regimes (Marlon et al., 2016).

The assessment of particle size distribution may also be significant in ecological studies investigating PyC dynamics as micro- and macroscopic charcoal may have different preservation potentials (Kuhlbusch et al., 1996; Thevenon et al., 2010; Mastrolonardo et al., 2017). Saiz et al. (2015a) conducted 16 experimental fires across a broad range of savannas in NE Australia, and showed that <10% of the total PyC produced by biomass burning in those ecosystems is emitted into the atmosphere as particles capable of moving far from the site of production, while a much larger proportion remains (initially) close to the site of production. PyC remaining on the ground may subsequently be re-mineralised by biotic and/or abiotic processes, be re-combusted in subsequent fire events, be exported in dissolved or particulate form, and/or accumulate in the soil or in the sedimentary record (Bird et al., 2015).

Previous work recommends the discrete analyses of contrasting particle sizes to gain deeper insights in charcoal taphonomy, especially if combined with independent validation of the pyrogenic origin of the particles (Thevenon et al., 2003; Conedera et al., 2009). In this context, the carbon isotope composition of PyC is amenable for use in fire reconstructions, particularly in savanna environments, as it represents one of the main tracers capable of providing a fingerprint of the type of vegetation being burnt (Bird et al., 2015). Indeed, the contrasting $\delta^{13}C$ values of tropical grasses, which primarily use the $C_4$ photosynthetic pathway ($\delta^{13}C > -15‰$), and woody vegetation, all having the $C_3$ photosynthetic pathway ($\delta^{13}C < -24‰$) allow for a discrete differentiation of the precursor biomass in studies assessing PyC in mixed $C_3/C_4$ ecosystems (Saiz et al., 2015a). There are however, potential complications limiting the interpretation of the isotopic signal, which includes isotopic fractionation effects associated with the production of

PyC during combustion. Saiz et al. (2015a) have demonstrated that savanna fires produce PyC that is relatively $^{13}C$ depleted (up to 7‰) with respect to the precursor biomass. This has been referred to as the savanna isotope disequilibrium effect (SIDE), which is a concept that explains the difference in $\delta^{13}C$ between the precursor vegetation and PyC compounds produced during the combustion of biomass. Other factors precluding a straightforward interpretation of isotopic results are the physical fractionation of PyC particles derived from $C_3$ vs. $C_4$ sources as a result of the preferential combustion of grass biomass, and potentially differing transport efficiencies of PyC (Bird and Gröcke, 1997; Saiz et al., 2015a).

While there has been some recent progress in our current understanding of PyC produced during tropical savanna fires (Saiz et al., 2015a), there remains limited information available on its dispersal pathways. Therefore, in the present study we use hydrogen pyrolysis (HyPy) and carbon isotopic analyses to investigate the relationship between ecosystem $\delta^{13}C$ and the $\delta^{13}C$ of PyC derived from burning of those ecosystems in recent sedimentary records across a broad range of tropical savannas in NE Australia. The HyPy methodology consistently isolates highly condensed (stable) carbon components (HyPyC or SPAC–see methods) that are pyrogenic in origin, from complex organic and sedimentary matrices (Wurster et al., 2012, 2013; Cotrufo et al., 2016). This material corresponds to the most recalcitrant component of the PyC spectrum, and can be used for the purposes of PyC quantification and isotope analyses. Despite being a relatively novel technique, there is already abundant literature demonstrating that HyPy satisfactorily isolates PyC in aromatic clusters (with a ring size $> 7$) from other organic carbon (OC) across a wide range of environmental matrices (e.g., Meredith et al., 2012; Wurster et al., 2012, 2013; Saiz et al., 2015a; Cotrufo et al., 2016). Meredith et al. (2012) observed a lower PyC abundance for grass char using HyPy than with other analytical methods (i.e., CTO-375 and NaClO), and inferred that the latter techniques reflected carbon trapped within silica phytoliths in the grass char, which also suggests that phytolith occluded carbon was effectively removed by HyPy. Therefore, even if the potential bias that phytoliths might exert on the $\delta^{13}C$ of HyPyC has not yet been specifically assessed, we believe that such influence may be limited.

Our first hypothesis (H1) proposes that the relative contribution of PyC to total organic carbon (TOC) in sediment samples is higher in grass-dominated ecosystems than in more wooded savannas as a result of both the higher incidence of fires (Furley et al., 2008), and the production of proportionally more recalcitrant PyC (HyPyC) per unit of total carbon exposed (TCE; this term includes all carbon from biomass, necromass, and ground litter). Saiz et al. (2015a) showed that the latter is the result of the incomplete combustion resultant from fast-moving fires characteristic of grass-dominated savannas. This does not mean that the combustion woody vegetation does not produce large amounts of PyC, quite the contrary. However, the difference lies in the fact that, while most of TCE in grass-dominated fires does get combusted, or at least thermally altered, most of the carbon stored in woodier ecosystems is commonly unaffected by fire (i.e., tree stems). Moreover, the sustained high temperatures of these fires may promote a more complete combustion of the fuels, and thus, the production of proportionally lower amounts of highly recalcitrant PyC (HyPyC) compared to grass-dominated savannas. We also hypothesize (H2) that fine material produced during the combustion of grass-derived biomass will be preferentially exported from the site of production and this will be reflected to some degree in its preferential accumulation in the sedimentary record. In addition to assessing the sedimentary record across a broad range of mixed $C_3/C_4$ ecosystems, we analyzed surface material collected immediately after experimental fires and compared results against neighboring locations left unburnt. The aim of this component of the study was to provide an estimate of the evolution of TOC and PyC abundance in different size fractions of material remaining on the ground following a fire to further test for differential transport efficiencies between PyC derived from grass and woody biomass sources.

The objectives of this study were therefore to: (i) assess the variation of PyC abundance in recently deposited sediments across a broad range of tropical savannas (Objective 1); (ii) evaluate the preferential combustion of grass biomass and factors affecting the isotopic composition of PyC (Objective 2); (iii) assess the potentially superior transport efficiency of grass-derived PyC (Objective 3); and (iv) use the isotopic approach to validate the establishment of a particle size threshold that is optimal for conducting fire research in tropical savannas (Objective 4). The latter having been advocated by previous research employing charcoal counting techniques to study past fire regimes in savanna environments (e.g., Duffin et al., 2008; Leys et al., 2017).

# MATERIALS AND METHODS

## Field Sampling Methodology

### Sediment Sampling

This study was conducted along a 500-km transect in Queensland (Australia) between May and September 2011. **Figure 1** shows the sampling location and the distribution of green perennial vegetation in northeast Australia, which represents a proxy for the relative proportion of woody vegetation (e.g., trees and shrubs) in total vegetation. The contrasting climate across the sampling locations had a strong influence on both the species and structural composition of the local ecosystems. As such, there was a noticeable trend to both higher total biomass and relative contribution of woody ($C_3$) vegetation to the total biomass as rainfall increases from SW to NE (**Figure 1**). The vegetation transect spanned humid savanna woodlands to comparatively dry Mitchell grasslands characterized by >95% $C_4$ grass biomass (Saiz et al., 2015a). Tree canopy cover ranged from <5% for a site established in a heavily dominated grassland ecosystem at the SW end of the transect (Mitchell grassland) to 50% for a woodland savanna occurring ∼80 km away from the coast at the NE end of the transect (Saiz et al., 2015a). The vegetation present at all studied sites comprised a grass layer beneath varying densities of *Eucalyptus* and *Acacia* species, which reached up to 25 m tall at the humid end of the transect (Torello-Raventos et al., 2013). The

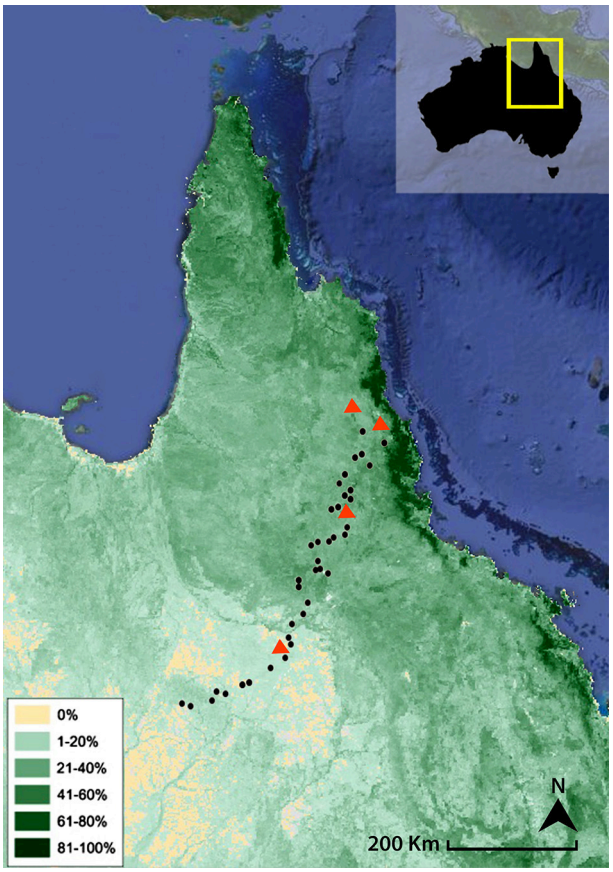


**FIGURE 1 |** Map showing the relative distribution (%) of green perennial vegetation in northeast Australia. Land cover data is derived from VegMachine® CSIRO (Karfs et al., 2004). Dots represent the farm dams on which superficial sediment was sampled, while triangles denote the locations of the experimental burns.

most abundant grass species were *Themeda australis, Imperata cylindrica* and *Heteropogon contortus*.

Surficial sediment was collected from 38 micro-catchments (farm dams) encompassing a wide variety of savanna ecosystems along the transect. Farm dams are purposely-built, small-scale water reservoirs established for agricultural purposes (e.g., cattle drinking and small-scale irrigation; Supplementary Figure 1), and are relatively common across NE Queensland. Sampled dams extended from relatively humid environments near the northeast coast (21°S–143°E; MAP = 1,650 mm) to the much drier inner regions (17°S–145°E; MAP = 435 mm) (**Figure 1**). Sampled dams were typically smaller than 100 m in diameter, with catchments generally extending <1 km. A wide climatic range was chosen to provide the experiment with the broadest possible range of woody vs. grass biomass proportions in order to enable the establishment of broad patterns in the abundance and isotopic composition of PyC from recent sedimentary records.

We used a purposely-made extensible collector to retrieve surficial sediment (top 5 mm) from submerged locations as far away as possible from the shore. The sediment sample collected at each dam was a composite of three sampling locations. Sampling distances typically ranged from 15 to 20 m from the shore. Sampling was restricted to dams showing little or no evidence of algal or macrophyte presence in order to minimize the potentially confounding influence of autochthonous vegetation in our results. However, it is clear that the influence of autochthonous vegetation on TOC cannot be entirely dismissed on the basis of their visual absence, thus we established a relationship between the stable carbon isotope composition of sediment samples and: (i) the proportion of vegetation remaining green throughout the year (perennial biomass photosynthetically active); (ii) the relative reduction in green vegetation between the wet and the dry seasons at each micro-basin, in order to identify samples exhibiting significant deviations from the general trend (**Figure 2**). These relationships were explored to provide additional confidence that any potential impact of algal and/or macrophyte carbon on the $\delta^{13}C$ values of TOC was minimal. As such, strong individual deviations from robust relationships could then be singled out as potentially having a strong influence of autochthonous vegetation, and thus be confidently excluded from further data interpretation.

## Sampling of Surface Material in Burned and Unburned Quadrats

We sampled surface (vacuumed) material at four sites along the transect to obtain information about ground OC dynamics as impacted by fire (**Figure 1**). The sampling procedure has been described in detail in Saiz et al. (2015a), and we only provide a brief description here. Four small-scale (1 $m^2$) burning experiments were carried out at each of the four sites selected ($n$ = 16). The experimental setup was designed to ensure capture of all particulates remaining on the ground immediately after the fire (burnt quadrats). Fires took place within a metallic structure fitted with leaning side panels that were lowered after the flames self-extinguished to minimize the lateral export of burnt material. After the unit had cooled, remaining stubble within the enclosed burn was cut at ground level and the quadrat was subsequently vacuumed with a DC 23 Motorhead vacuum cleaner (Dyson Appliances Ltd., NSW, Australia). This operation was systematically carried out by the same user across all burning experiments and over the same length of time to allow for inter-comparison of results. Vacuuming is unable to systematically retrieve the characteristically highly heterogeneous coarse woody debris, and it was therefore not included in this sampling. The vacuumed material was stored in separate labeled containers. Vacuuming may potentially disrupt the true distribution of size aggregates, which may be particularly significant in the case of very brittle, recently burnt grass biomass. However, we suggest that such experimental bias may be of relatively minor importance in this context if one considers that such fragile material gets rapidly comminuted in the environment by wind and rainfall anyway, and that the smallest fraction (<10 μm) represents on average less than 4% of the total mass vacuumed (data not shown).

Additionally, the same vacuum procedure was used on two adjacent 1 $m^2$ biomass quadrats (16 × 2; $n$ = 32) to determine TOC and PyC present on the soil surface prior to burning (a surrogate for the evolution of PyC abundance since a previous

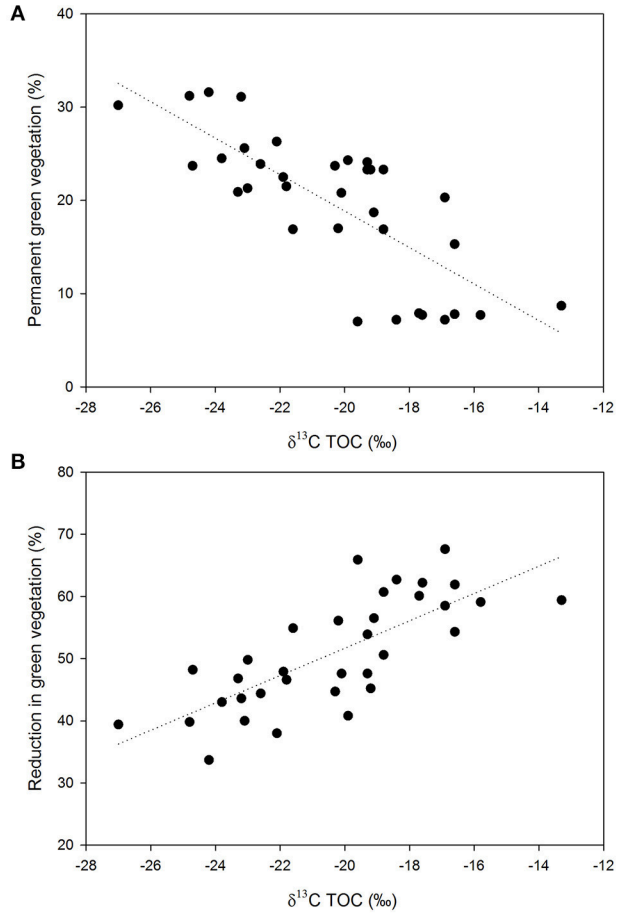


**FIGURE 2 | (A)** Relationship between the stable carbon isotope composition of sediment samples and the proportion of vegetation remaining green throughout the year (perennial biomass photosynthetically active) at each micro-basin; **(B)** Relationship between the stable carbon isotope composition of sediment samples and the relative reduction in green vegetation between the wet and the dry seasons. Regression coefficients ($r^2$) are 0.60 and 62 for **(A,B)** respectively; $p < 0.05$ in both regressions. Land cover data is derived from VegMachine® (Karfs et al., 2004), a software tool that summarizes decades of Landsat satellite imagery processed and compiled by the Remote Sensing Centre, Queensland Department of Science, Information Technology and Innovation (Australia).

fire at the site). The purpose was to broadly assess the evolution of surface C (both TOC and PyC) on locations unaffected by fire for longer than 2 years. We refer to these plots as "unburnt" to distinguish them from the burnt quadrats. Before vacuuming, all the aboveground biomass was harvested and separately quantified. This sampling procedure was carried out in duplicate at each burning location, thus resulting in a total of 8 × 1 $m^2$ vegetation quadrats sampled per studied site. This provides an estimate of initial TOC and PyC abundance before the fire, which could serve as reference to compare against burnt quadrats in order to obtain information about the carbon distribution dynamics of different size fractions (i.e., < 10, 10–125, and >125 μm). Upon collection, all samples were individually stored inside labeled plastic containers.

# Laboratory Methods

## Sample Preparation

On arrival at the laboratory, samples were dried at 60°C for 5 days before being weighed and sieved to 2 mm. Samples were subsequently size fractionated by wet sieving at 125 and 10 μm to conform with the definition of microcharcoal (10–125 μm) (Haberle, 2005). This procedure thereby also enables the discrete analysis of very fine <10 μm PyC, which is relevant as it is likely to be a major component of aerosol PyC (Andreae and Merlet, 2001). Bulk samples and the resultant fractions were then freeze-dried, weighed and finely milled prior to further analyses. Visually distinct coarse textured sediment samples were purposely tagged to help with the interpretation of their potentially distinct behaviors, as values of coarse textured samples may be strongly influenced by the inherently low physicochemical protection they offer against decomposition.

## Hydrogen Pyrolysis

The HyPy technique has been shown to perform satisfactorily in characterizing PyC abundance in a range of environmental matrices (Meredith et al., 2012). The method separates PyC in aromatic clusters having with a ring size >7 from other OC. This component is usually referred to as HyPyC or as stable polycyclic aromatic carbon (SPAC), and represents PyC that is likely to be resistant to environmental degradation. Therefore, HyPy effectively isolates a component that is distinct in isotopic composition from the TOC of the sample. In the present work, and for the sake of simplicity, we use the term PyC to generically refer to the most recalcitrant component of PyC isolated by HyPy, and equivalent to both HyPyC and SPAC.

HyPy has been described detailedly in a number of publications (e.g., Meredith et al., 2012; Wurster et al., 2012, 2013). In short, samples are loaded with a Molybdenum catalyst (∼10% of dry weight) by means of an aqueous/methanol solution of ammonium dioxydithiomolybdate [$(NH_4)_2MoO_2S_2$]. Dried, catalyst-loaded samples are then placed in a reactor to be pressurized at 150 bar $H_2$ under a sweep gas flow of 5 L $min^{-1}$, heated at 300°C $min^{-1}$ to 250°C, then stepped at 8°C $min^{-1}$ to a final hold T of 550°C for 2 min. There is a need to account for the mass loss of the loaded catalyst during HyPy. Therefore, the abundance of carbon in the sample after HyPy is determined relative to TOC (initial mass of carbon after treatment/the mass of carbon loaded) and reported as the relative contribution of PyC/TOC or PyC/Sample (% or mg $g^{-1}$ units).

## Carbon Abundance and Isotope Composition

The carbon abundance and stable isotopic composition ($\delta^{13}C$) of samples were determined using a Costech Elemental Analyzer (EA) fitted with a zero-blank auto-sampler coupled via a ConFloIV to a ThermoFinnigan DeltaV$^{PLUS}$ mass spectrometer using Continuous-Flow Isotope Ratio Mass Spectrometry (EA-IRMS). Analyses were conducted at James Cook University's Cairns Analytical Unit. Stable isotope results are reported as per mil (‰) deviations from the VPDB reference standard scale for $\delta^{13}C$ values. Precisions (S.D.) on internal standards for elemental carbon abundance and stable carbon

isotopic composition were better than ±0.08% and ±0.2‰ respectively.

## Statistical Methods

Data for any measured variable were tested for normal distribution by Kolmogorov-Smirnov tests, and where necessary data were log- transformed. Regression analyses were conducted for estimating the relationships among the variables of interest. All reported regressions were significant at $P < 0.05$ level. Specific regressions using bulk samples include all sites ($n = 38$) unless specifically stated. Analyses of covariance (ANCOVA) were performed to test for significant differences between regressions obtained between $\delta^{13}C$ values of bulk sediment samples and differences in $\delta^{13}C$ between the PyC component and the TOC pool for different size fractions. The ANCOVA test is shown in Supplementary Table 1. One-way ANOVA with Tukey HSD post hoc comparison was performed to test for significant differences in $\delta^{13}C$ values and comparable relative contributions of PyC to TOC between the different size fractions. All statistical analyses were carried out with SPSS 17.0 (SPSS Inc. Chicago, IL, USA).

# RESULTS

## Variation in $\delta^{13}C$ Values and Carbon Contents in Surface Sediments of Farm Dams

TOC concentrations ranged from 77.2 mg C $g^{-1}$ at the NE (higher precipitation) end of the transect to 2.1 mg C $g^{-1}$ observed in a very coarse-textured sample (**Figure 3A**). $\delta^{13}C$ values of TOC ranged from −13.3‰ in grass-dominated environments in the interior to −28.1‰ observed in closed-canopy woodlands occurring near the coast. There was a negative correlation between $\delta^{13}C$ of bulk sediments and TOC abundance (**Figure 3A**; $r^2$ 0.40; $p < 0.05$). Similarly, there was a negative correlation between $\delta^{13}C$ values of bulk sediments and PyC contents (**Figure 3B**; $r^2$ 0.37; $p < 0.05$). The absolute concentration of PyC showed a gradual decrease toward the drier southwestern end of the transect similar to the trend observed in TOC contents. However, the relative contribution of PyC to TOC was lower in the wetter more heavily wooded savannas, and showed a steady increase toward the drier, grass-dominated ecosystems to the SW (**Figure 3C**; $r^2$ 0.15; $p < 0.05$).

Samples with low TOC concentrations had a greater relative contribution of PyC (**Figure 4**). Very coarse-textured samples ($n = 5$) showed much greater relative contributions of PyC relative to their TOC concentration regardless of their $\delta^{13}C$ values (**Figure 3C**). This proportion reached a maximum of 39%, and was relatively uniform in samples with TOC contents greater than 25 mg C $g^{-1}$ (with values ranging from 2 to 10%; **Figure 4**; $r^2$ 0.74; $p < 0.05$).

**Figure 5** shows the differences in $\delta^{13}C$ values between TOC and PyC along the transect. The $\delta^{13}C$ value of PyC in the sediments is decoupled from the $\delta^{13}C$ value of TOC, suggesting that HyPy effectively isolates a component that is distinct in isotopic composition from TOC. Differences were greater (up to 7‰) in more heavily wooded savanna where the PyC component generally showed less negative $\delta^{13}C$ values compared to the TOC in the same sample. These variations were smaller, and occasionally reversed, both in grass-dominated ecosystems and in the very coarse textured samples (**Figure 5**). Small or negative differences in $\delta^{13}C$ values were associated with greater relative contributions of PyC to TOC (**Figure 6**).

The separate analysis of the different size fractions revealed large differences in $\delta^{13}C$ values between the TOC and PyC

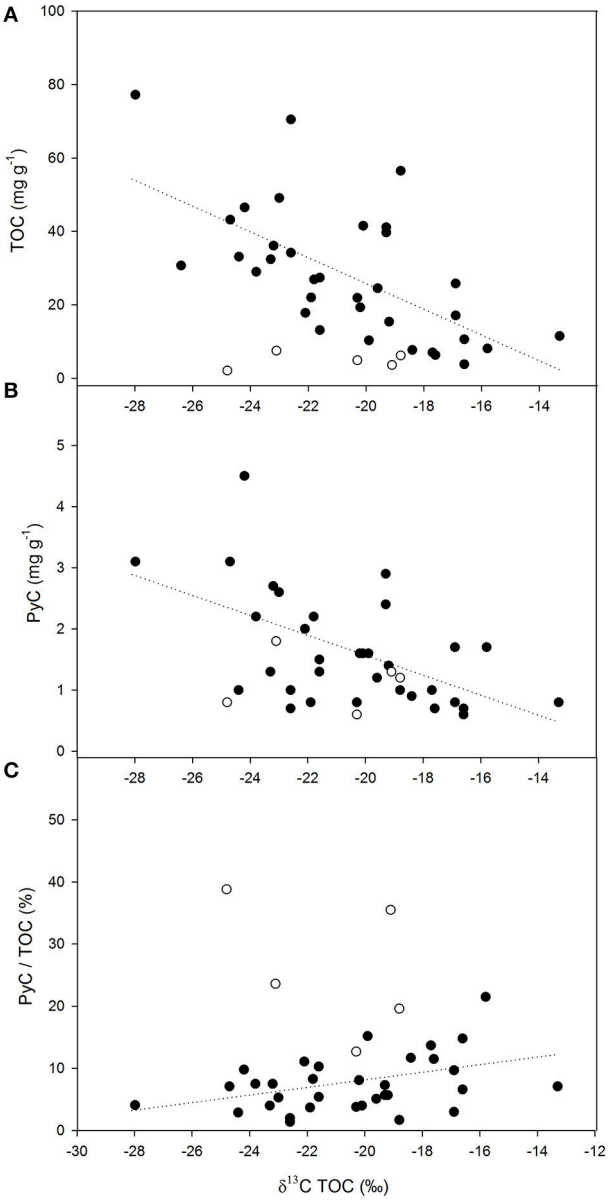


**FIGURE 3 |** Relationships between $\delta^{13}C$ values of bulk sediment samples and: **(A)** TOC content (mg $g^{-1}$), $r^2$ 0.40; $p < 0.05$; **(B)** PyC content (mg $g^{-1}$), $r^2$ 0.37; $p < 0.05$; and **(C)** the relative contribution of PyC to TOC (%), $r^2$ 0.15; $p < 0.05$. Total number of samples is 38. Open symbols correspond to samples with very coarse texture ($n = 5$). These were not included in the regressions.

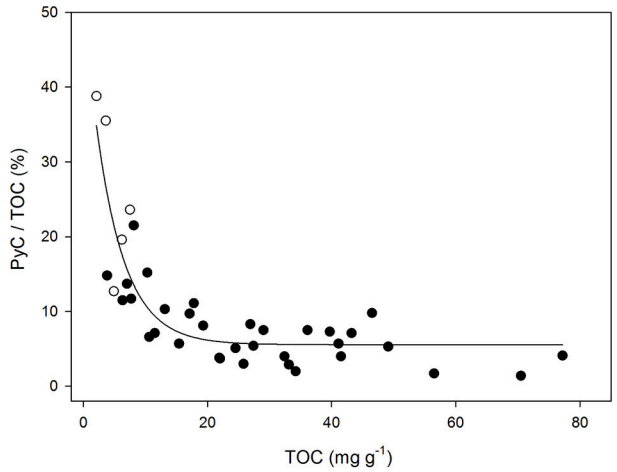


**FIGURE 4 |** Relationship between TOC content (mg $g^{-1}$) of bulk sediment samples and the relative contribution of PyC to TOC (%); $r^2$ 0.74; $p < 0.05$. Open symbols correspond to samples with very coarse texture ($n = 5$).

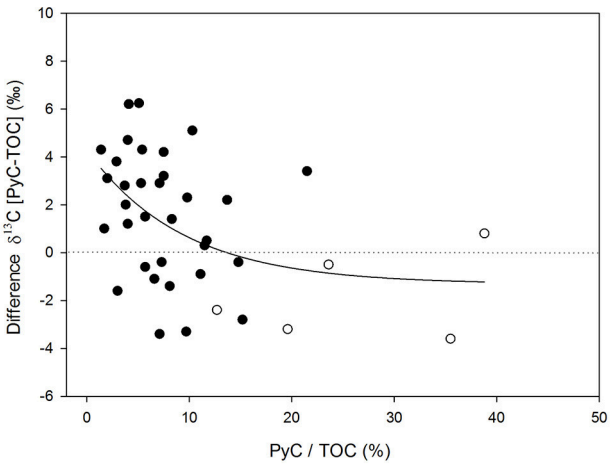


**FIGURE 6 |** Relationship between the relative contribution of PyC to TOC (%) and differences in $\delta^{13}C$ between the PyC component and the TOC pool; $r^2$ 0.19; $p < 0.05$. Open symbols correspond to samples with very coarse texture ($n = 5$).

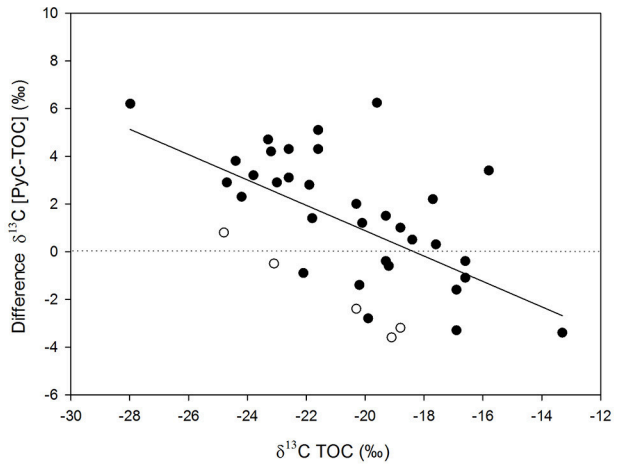


**FIGURE 5 |** Relationship between $\delta^{13}C$ values of bulk sediment samples and differences in $\delta^{13}C$ between the PyC component and the TOC pool; $r^2$ 0.34; $p < 0.05$. Open symbols correspond to samples with very coarse texture ($n = 5$).

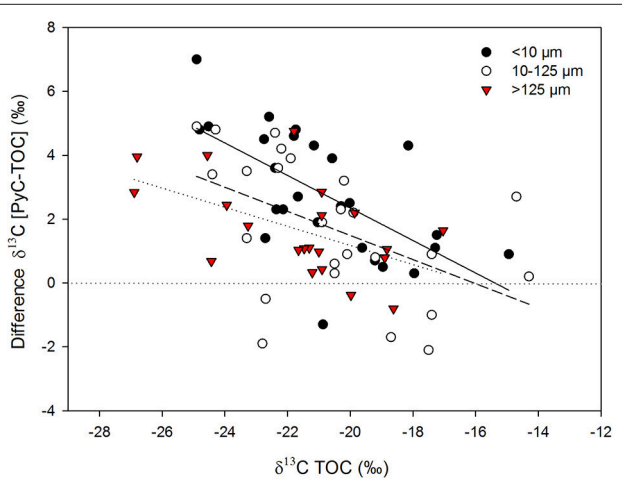


**FIGURE 7 |** Relationship between $\delta^{13}C$ values of bulk sediment samples and differences in $\delta^{13}C$ between the PyC component and the TOC pool for different size fractions; regression coefficients ($r^2$) are 0.41 for the fractions < 10 µm (solid line), 0.34 for the fractions between 10 and 125 µm (dashed line), and 0.29 for the fractions > 125 µm (dotted line); $p < 0.05$ for all regressions.

pools in samples from more heavily wooded (wetter) savannas, while variations between size fractions were minimal in grass-dominated environments (**Figure 7**). ANCOVA analyses showed that the regression obtained for the smallest fraction (<10 µm) was significantly different to those obtained for larger fractions (Supplementary Table 1). Particle size fractions >10 µm had similar differences in $\delta^{13}C$ values and comparable relative contributions of PyC to TOC ($P > 0.05$), while the finest fraction (< 10 µm) showed the largest differences in $\delta^{13}C$ values between TOC and PyC, and had the greatest relative contribution of PyC to TOC of the three size fractions considered (**Figure 8**). Differences in $\delta^{13}C$ values and comparable relative contributions of PyC to TOC were significant ($P < 0.05$) between the <10 and >125 µm fractions.

## Relative Contribution of Size Fractions to Surface Carbon Pools in Fire Experiments

**Table 1** shows the relative contribution to TOC and PyC from different size fractions in vacuumed material from burnt and unburnt plots. There was a trend to increasing relative contributions with increasing particle size, with the largest fractions (>125 µm) accounting for more than half of the total carbon in both the TOC and PyC pools. The smaller fractions showed a relative reduction in carbon contributions from burnt to unburnt plots, while the relative changes exhibited by the largest fraction were positive.

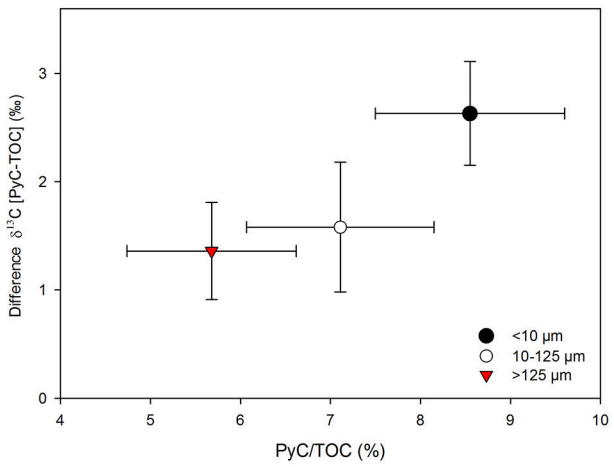


**FIGURE 8 |** Relationship between the relative contribution of PyC to TOC (%) and differences in $\delta^{13}C$ between the PyC component and the TOC pool for different size fractions ($n = 23$). Bars are standard errors of the means.

# DISCUSSION

## Variation in the Geographical Distribution of PyC in Surface Sediments (Objective 1)

This study focuses in particular on surficial sediments collected from farm dams in very small catchments. These locations were chosen as they collect erodible material that best reflects fresh organic matter (OM) inputs and PyC produced by recent fires within each micro-basin. The variation in carbon content and stable isotopic composition of bulk sediment samples corresponded well with the gradual shift in vegetation along the transect (**Figure 1**). **Figure 2** shows a consistent trend between the stable carbon isotope composition of sediment samples and two separate variables, each being a proxy for the proportions of $C_3$ and $C_4$ biomass in each micro-basin. The existence of these strong relationships provides additional confidence that the impact of algal and/or macrophyte carbon on the $\delta^{13}C$ values of TOC is minimal. Distinctly lower $\delta^{13}C$ values and higher TOC contents were observed in the more heavily wooded savannas occurring in the wetter northeastern end of the transect, in contrast to the higher $\delta^{13}C$ values and generally lower TOC abundances of grass-dominated environments (**Figure 3**). This trend may be attributed to differences in the input rates and turnover times of grass and woody-derived carbon (Bird et al., 2000, 2004; Saiz et al., 2015b).

Besides environmental and biotic factors, the specific characteristics of the soil have also been shown to exert a strong influence on the potential preservation of OM (Saiz et al., 2012), and thus, may also represent a key factor affecting the relationship between $\delta^{13}C$ and TOC in recent sediments. However, the degree of physical protection and chemical stabilization of OM that can be provided by the loose, recently eroded surface sediment, must be necessarily lower than that existing at deeper locations within the soil profile (Rumpel and Kögel-Knabner, 2011). We therefore suggest that the influence exerted by micro-basin soil characteristics on the relationship between $\delta^{13}C$ and sediment TOC is of limited relevance in the present work, but cannot be entirely dismissed. In this regard, the impact of soil characteristics was particularly noticeable in very coarse-textured samples, which showed consistently low $\delta^{13}C$ values of TOC values regardless of vegetation cover (**Figure 3A**).

While the relationship between $\delta^{13}C$ values and TOC abundance showed a close parallel to the relationship between $\delta^{13}C$ values and PyC content (**Figures 3A,B**), the relative contribution of PyC to TOC showed the opposite trend (**Figure 3C**). The contribution of PyC to TOC tended to be higher in grass-dominated savannas than in those dominated by woody vegetation, which supports our first hypothesis (H1) and the conclusion of Saiz et al. (2015a) that proportionally more recalcitrant PyC (HyPyC or SPAC) is produced per unit of TCE during combustion of grass-dominated savannas. The latter is the result of the incomplete combustion resultant from short-lived fires characteristic of these ecosystems. Moreover, work conducted along a precipitation gradient in West Africa reported higher contributions of resistant OC (inferred to be dominantly PyC) to the total soil organic carbon (SOC) pool in low rainfall open-canopy savannas, with this attributed to the frequent fire events characteristic of those ecosystems (Saiz et al., 2012). It is worth noting that other fire-prone land cover types (e.g., forests) typically have longer fire return intervals, and also much higher TCE to fire. However, besides soils, the largest proportion of carbon stored in forest ecosystems is in tree stems, Though wildfires may combust whole trees, usually only a fraction of the TCE gets significantly affected or combust during forest fires (Santín et al., 2015), with leaves, twigs, barks, down wood, and forest floor being the fuels most commonly affected.

Nonetheless, frequent fires in a given ecosystem may not necessarily be always associated with high PyC contents above- or belowground, as this material undergoes a series of transformations (e.g., mineralization, infiltration, lateral translocation, etc.; Bird et al., 2015; Reisser et al., 2016), which will ultimately define the relative contribution of PyC to the TOC pool at a final location of deposition. In this regard, the characteristics of the soil also play an important role in modulating such contributions. Soils with low OC contents have shown to make relatively larger PyC contributions to total SOC than soils with higher OC contents (Reisser et al., 2016). Very coarse-textured materials have characteristically low nutrient levels, as well as limited water retention capacities (Schimel et al., 1994; Silver et al., 2000; Saiz et al., 2012), and the associated low net primary productivity may have contributed to the low TOC contents observed in some samples in the present study (**Figures 3A**, **4**). Furthermore, the relatively high proportion of PyC in these sediments suggests the low degree of physicochemical protection that coarse-textured soils offer against OM decomposition, given that a significant proportion of the TOC corresponds to highly recalcitrant PyC material (i.e., HyPyC). Sediment samples containing over 20 mg $g^{-1}$ TOC showed relatively uniform PyC contributions to TOC (∼7%; **Figure 4**), broadly consistent with the global observations compiled by Reisser et al. (2016) for soil samples collected from the 0–30 cm depth interval.

**TABLE 1 |** Relative contribution (%) of different size fractions to both TOC and PyC in vacuumed material from recently burnt ($n = 16$) and unburnt ($n = 32$) vegetation quadrats.

| Size fraction (μm) | TOC | | | PyC | | |
|---|---|---|---|---|---|---|
| | Burnt | Unburnt | Relative change (%) | Burnt | Unburnt | Relative change (%) |
| <10 | 4.3 ± 5.7 | 1.4 ± 0.5 | −67 | 6.4 ± 8.9 | 2.5 ± 2.0 | −60 |
| 10–125 | 28.0 ± 10.5 | 15.8 ± 8.1 | −44 | 41.8 ± 14.9 | 23.8 ± 11.7 | −43 |
| >125 | 67.7 ± 10.9 | 82.8 ± 8.1 | 22 | 51.8 ± 14.4 | 73.6 ± 13.1 | 42 |

*Values are averages and standard deviations. The relative changes in carbon contributions between treatments are also shown for each size fraction to obtain information about their distribution dynamics. TOC and PyC were determined from the mass of the material collected for each of the fractions, and their carbon content measured before and after the HyPy treatment. Unburnt quadrats had not experienced fire for at least two years.*

Belowground OM inputs are directly subject to physicochemical protection offered by the soil matrix, but charcoal or PyC is overwhelmingly produced aboveground, and thus, is more prone to mineralization and/or transport from the site of production (Zimmermann et al., 2012; Bird et al., 2015). Rumpel et al. (2006) worked along the slopes of slash and burn agricultural land and noted that PyC from topsoil horizons was not primarily bound to mineral phases, which made it susceptible to translocation downslope. In the present study we made use of the relative changes in carbon contributions observed between burnt and unburnt treatments in 16 burning experiments to obtain information about the temporal evolution of TOC and PyC pools in three size fractions.

Earlier work by Saiz et al. (2015a) on the same experimental fires report an average PyC production of about 16% of all carbon being exposed, of which particles >125 μm represented more than 90% of the total mass. This particle size fraction has been shown to remain initially in the vicinity of the site of production (Clark, 1988; Saiz et al., 2015a), and was therefore classified as "proximal" PyC. Once produced, PyC remaining on the soil surface may subsequently (i) be re-combusted in future fires (Santín et al., 2013; Saiz et al., 2014) (ii) be re-mineralized by abiotic/biotic processes (Zimmerman, 2010; Zimmermann et al., 2012), (iii) accumulate in the SOC pool (Lehmann et al., 2008) and/or (iv) be re-mobilized by bioturbation, wind or water in either particulate (Rumpel et al., 2006; Major et al., 2010; Cotrufo et al., 2016) or dissolved form Dittmar et al. (2012). **Table 1** reveals that proximal PyC contained in small-size fractions on the soil surface is gradually lost after a fire, thereby increasing the relative contribution of the largest size fraction to the total carbon pool over time. Therefore, comparatively finer material, such as that derived from grass biomass, would get more easily transported from the site of production, which is in support of the differential transport efficiencies between grass and woody fuels we hypothesized in H2 [see also section Preferential Transport of Grass-Derived PyC (Objective 3)]. Particle comminution makes it easier for proximal PyC to be exported from the site of production, and temporarily accumulate in lower locations within the landscape (e.g., farm dams). Small airborne particles exported during fire (i.e., distal PyC; Saiz et al., 2015a) may also contribute to the loading of PyC particles at these locations, although the reach of distal PyC may also be realized at regional and even much larger spatial scales (Kuhlbusch et al., 1996; Bird et al., 2015). Indeed, Duffin et al. (2008) suggested that in tropical savannas more than half of relatively small charcoal size (<50 μm) is likely to be transported >15 km from the fire line.

## Preferential Combustion of Grass Biomass and Factors Affecting the Isotopic Composition of PyC (Objective 2)

Differences between the $\delta^{13}C$ values of TOC and its PyC component in surface sediments sampled across a wide range of tropical savannas indicate that the $\delta^{13}C$ value of PyC is partly decoupled from that of TOC and therefore of local biomass (**Figure 5**). This further supports previous conclusions that HyPy effectively isolates a distinct component of TOC (Wurster et al., 2012, 2013). While the carbon isotopic composition of PyC can provide very useful information of the type of vegetation being burnt in mixed $C_3/C_4$ ecosystems (Bird and Gröcke, 1997), there are several factors that need to be considered when interpreting these data. These include: (i) the physical fractionation of PyC particles derived from mixed $C_3/C_4$ vegetation due to preferential combustion of grasses in savannas (Furley et al., 2008; Saiz et al., 2015a), (ii) the savanna isotope disequilibrium effect (SIDE) that is the isotope fractionation accompanying the production of PyC during biomass combustion (Saiz et al., 2015a), (iii) the contrasting transport efficiencies, related to particle size differences, of particulate PyC derived from woody or grass sources (i.e., $C_3/C_4$ vegetation) (Clark, 1988; Duffin et al., 2008), and (iv) the specific characteristics of the topsoil where PyC is originally produced (Bird et al., 2000).

Analyses of the surficial sediment samples in this study indicate that the $\delta^{13}C$ value of PyC is up to 7‰ higher than that of TOC, with these differences being largest when the $\delta^{13}C$ values of TOC were low (i.e., characteristic of more wooded ecosystems; **Figure 5**). This suggests that a significant component of $C_4$-derived PyC is present at most locations, even when the proportion of $C_4$ biomass in the catchment is relatively small (**Figure 1**). Recent work employing carbon isotopic analyses in pools and fluxes of experimental fires conducted across mixed $C_3/C_4$ ecosystems shows that, compared to woody material, grass biomass is preferentially combusted (Saiz et al., 2015a), which would largely explain the presence of $C_4$-derived PyC in woodland ecosystems. However, this mechanism cannot explain the observation that $\delta^{13}C$ differences between TOC and PyC

were smaller and even reversed in grass-dominated ecosystems (**Figure 5**).

The trends discussed above show the combined influence of some of the factors mentioned earlier. Firstly, the SIDE is more marked in grass-dominated ecosystems. Saiz et al. (2015a) showed that while the $\delta^{13}C$ values of total PyC and HyPyC were generally lower by 1–3‰ compared to the original biomass across mixed $C_3/C_4$ savanna ecosystems, Mitchell grasslands—an ecosystem almost exclusively composed of $C_4$ vegetation—showed strong $^{13}C$ depletion (up to 7‰) in recently produced total PyC and HyPyC, resulting in comparatively larger SIDE values with the differences particularly pronounced in the fine size fractions. Secondly, the preferential export of fine particle size fractions during fire in grass-dominated ecosystems is likely to be dominated by low $\delta^{13}C$ components (e.g., methoxyl-groups, lignins, phytoliths, etc.) preserved in PyC (O'Malley et al., 1997; Krull et al., 2003; Keppler et al., 2004; Das et al., 2010). Therefore, the comparatively smaller $\delta^{13}C$ differences observed between TOC and PyC in grass-dominated ecosystems may also be influenced by the superior transport efficiency of small particulate PyC derived from grass vegetation (Clark, 1988; H2). This latter aspect will be dealt with in more detail in the following section. Thirdly, the characteristics of the topsoil upon which PyC is produced may potentially affect carbon isotopic dynamics by means of differential physicochemical protection (Krull et al., 2003; Sollins et al., 2009; Zimmermann et al., 2012). In this regard, analyses of sediment samples show that $\delta^{13}C$ values of PyC were consistently higher than those of TOC across a broad range of savanna sites occurring on coarse-textured soils (**Figure 5**).

The specific chemical, mineralogical, and textural properties of the topsoil may play a critical role on the preservation of OC (e.g., through the formation of aggregates, association with clay particles, etc.), and on its potential export (e.g., infiltration, erosion, etc.) (Brodowski et al., 2006; Knicker, 2011; Saiz et al., 2012; Singh et al., 2012). Hence, a limited physicochemical protection of OC would promote the preferential mineralization of labile compounds relative to more recalcitrant ones (e.g., PyC). In the present study the low degree of physicochemical protection offered to TOC in coarse-textured soils is revealed by the greater relative contributions of PyC to TOC observed in those samples, which are also associated with larger positive differences in $\delta^{13}C$ values between TOC and PyC (**Figure 6**).

Other potential fractionation processes occurring within the soil profile such as the microbial reprocessing of SOM or the differential stabilization of naturally heterogeneous SOM compounds (Bird et al., 1996; Ehleringer et al., 2000; Blagodatskaya et al., 2011; Rumpel and Kögel-Knabner, 2011) are of more limited significance in our work since we focus on very surficial sediments. Finally, differential mineralization patterns in PyC derived from different biomass sources (e.g., Saiz et al., 2015b) are not considered significant in this context given the very short timeframe since the PyC was produced.

## Preferential Transport of Grass-Derived PyC (Objective 3)

Savanna fires preferentially burn the grass understory and surface litter rather than over-story trees (Furley et al., 2008), which may lead to a bias toward generally smaller $C_4$-derived PyC. Several studies have demonstrated that charcoal in contrasting size fractions exhibit fundamentally different aerodynamic behaviors (Clark, 1988; Duffin et al., 2008). This behavior exerts a strong influence on their transport efficiencies whereby larger particles remain closer to their site of production than smaller particles. However, the preferential export of PyC is not only constrained to airborne particles produced during the fire. Indeed, PyC remaining close to the site of burning (proximal PyC) will undergo continuous transformations after production. **Table 1** demonstrates that both the abundance of TOC and PyC in small-size surface material decrease over time after fire, which increases the relative contribution of larger particles to the total carbon pools at the site of burning. Because the stable components of PyC accrue both in situ and distally, the SIDE caused by fire produces soil or sedimentary records in savanna environments that are relatively $^{13}C$-depleted with respect to the original biomass (Wynn and Bird, 2008; Saiz et al., 2015a). This has significant implications for the interpretation of $\delta^{13}C$ values of PyC preserved in the geological record, and for global $^{13}C$ isotopic disequilibria calculations needed in modeling studies that use variations in the $CO_2$ $^{13}C$ record to apportion sources and sinks of $CO_2$ (Randerson et al., 2005; Saiz et al., 2015a).

The finest—most comminuted—size fraction ($<10\,\mu m$) consistently showed the largest differences in $\delta^{13}C$ values between TOC and PyC along the transect (**Figure 7**), indicating that $C_4$-derived PyC is more disproportionately represented in the finest size fraction. Moreover, the observed differences in $\delta^{13}C$ values between size fractions decrease from the more wooded savannas to more grass-dominated savannas, with the resultant regressions being significantly different in the case of the smallest fraction (**Figure 7**, Supplementary Table 1). This can be explained by preferential transport of PyC generated from heterogeneous fuel sources. In savanna ecosystems, finer grass-derived PyC particles are preferentially exported from the site of initial production and accumulate in the sedimentary record, while the commonly larger PyC particles derived from the combustion of woody biomass ($C_3$) are more likely to remain closer to the site of burning (Saiz et al., 2015a). This differential particle transport efficiency will be more clearly reflected in the sedimentary record of more wooded savannas than in more grass-dominated savannas where the isotopic composition of the fuel source is much less heterogeneous. These results support our second hypothesis (H2) that proposed that fine material produced during the combustion of grass-derived biomass may be preferentially exported from the site of production, with this being reflected in the preferential accumulation of $C_4$ grass-derived PyC in the sedimentary record, even in cases where the proportion of $C_4$ grass biomass in the catchment was small.

While one of the main aims of this work is to infer a general pattern of PyC transportation across a broad gradient of tropical savannas, there are additional factors operating at a more local

scale that may play a significant role in the spatial dynamics of PyC particle deposition and accumulation. In this regard, both the climatic and physical characteristics of the landscape may exert a strong influence in the erosional patterns of PyC (Rumpel et al., 2006, 2015; Cotrufo et al., 2016). Furthermore, the specific characteristics of the soil where PyC is produced may also have a strong impact on its transport and mineralization dynamics (e.g., contrasting PyC preservation in swelling and cracking Vertisols vs. loose sandy soils; Supplementary Table 2), which could ultimately affect both the abundance and carbon isotopic composition of PyC in the sedimentary record.

## Charcoal Particle Size Thresholds for Fire Research in Tropical Savannas (Objective 4)

The particle size ranges adopted in this study were chosen to conform to standard dimensions adopted to classify micro- and macro-charcoal in palynological studies and in work assessing PyC production in tropical savannas (e.g., Blackford, 2000; Haberle, 2005; Saiz et al., 2015a). The significantly different behavior shown by the smallest particle size fraction ($<10\,\mu m$) in regards to: (i) the relative changes in carbon contributions between burnt and unburnt plots (**Table 1**), (ii) the differences in $\delta^{13}C$ values between TOC and PyC across the vegetation transect (**Figure 7**), and (iii) the relative contribution of PyC to TOC (**Figure 8**), demonstrate that PyC of this size exhibits a substantially different behavior compared to PyC in the coarser fractions. This supports findings from previous research concluding that contrasting particle sizes of charcoal have different aerodynamic behaviors (Clark, 1988; Duffin et al., 2008), and further support the hypothesis (H2) that coarser charcoal fragments derived from combustion of woody sources accumulate close to the site of production.

Our results agree well with the statement by Duffin et al. (2008) about the need to use just a few size classes of charcoal in the sedimentary record of savanna environments to obtain relevant information on fire proximity and relevant source areas of pyrogenic material. These authors advocate the use of a $50\,\mu m$ threshold for savannas as they identified a differential behavior of charcoal particles up to and beyond that fraction size. Such a threshold seems plausible in view of our own results, as the intermediate particle size range considered in the present study show mixed patterns between the smallest ($<10\,\mu m$) and largest ($>125\,\mu m$) fractions (**Figure 8**).

# CONCLUSIONS

We used HyPy to obtain robust estimates of PyC abundance and stable isotope composition in surface sediments in small dams across a broad range of mixed $C_3/C_4$ tropical vegetation. Our study shows that the contribution of highly recalcitrant PyC to TOC in grass-dominated savannas tends to be higher than in savannas where woody vegetation was more prominent. This is partly because fires characteristic of grass-dominated savannas significantly affect, if not all, most of the TCE. However, the short-lived nature of these fires may cause an incomplete combustion of the fuels, which results in the production of proportionately more recalcitrant PyC (HyPyC) per unit of TCE than that observed in woodier savannas (Saiz et al., 2015a).

This work also provides evidence for the preferential combustion of grass biomass and higher transport efficiency of $C_4$-derived PyC in mixed ecosystems where grass and woody vegetation coexist. In savanna ecosystems finer grass-derived PyC particles are preferentially exported and accumulated in sediments, while the commonly larger PyC particles derived from the combustion of woody biomass ($C_3$) are more likely to remain closer to the site of burning. We demonstrate that after a fire there is a comminution of PyC produced in-situ to smaller particles, which then facilitates transport away from the site of production and may also affect the preservation potential of this material. Our isotopic approach provides independent validation of findings by Duffin et al. (2008) concerning the appropriateness of adopting a relatively small particle size threshold (i.e., $\sim 50\,\mu m$) to reconstruct fire regimes using sedimentary records by conventional charcoal counting techniques.

While the isotopic composition of PyC contained in sediment records can greatly assist in reconstructing past fire regimes, this study suggests that there are several factors that need to be considered when interpreting these data. These include the physical fractionation and contrasting transport efficiencies of PyC particles derived from mixed $C_3/C_4$ sources, the savanna isotope disequilibrium effect accompanying the production of PyC during biomass combustion, and the specific characteristics of the topsoil where PyC is originally produced. Our work also allows for a more nuanced understanding of the savanna isotope disequilibrium effect, which has significant implications for global $^{13}C$ isotopic disequilibria calculations and for the interpretation of $\delta^{13}C$ values of PyC preserved in sedimentary records (Saiz et al., 2015a). While we have conducted this study in tropical savannas, we believe it is highly likely that the findings of this study can directly apply to savannas in temperate environments.

We suggest that the combined use of an isotopic approach and classical research methods exploiting the sedimentary record, including charcoal counting and the interpretations of charcoal morphotypes, appears to be particularly suitable for use in mixed fuel source fire regimes (Leys et al., 2015, 2017). This combined approach will allow for more accurate reconstructions of past fire regimes and promote a better understanding of PyC dynamics in tropical savannas. This research further demonstrates that the HyPy technique enables an accurate quantification of an essential component of terrestrial carbon, and that it is a very useful tool for promoting a better understanding of the dynamic role of biomass burning in the global carbon cycle.

# AUTHOR CONTRIBUTIONS

GS, IG, and MB designed the experiment. GS, IG, and CW carried out the fieldwork and conducted laboratory analyses. GS wrote the manuscript with contributions from all co-authors.

## FUNDING

This work was supported by Australia Research Council Grants DP1096586 and FF0883221.

## ACKNOWLEDGMENTS

We are indebted to the many generous individuals who granted us access to their farms. We gratefully acknowledge Queensland Parks and Wildlife staff, and particularly Rob Miller, for access to sites at Undara and Davies Creek. We also thank Sandra Lopez for her continuous support in this study. We are also thankful to the Australian Wildlife Conservancy Society for allowing access and permits to undertake research at the Brooklyn Sanctuary site.

## SUPPLEMENTARY MATERIAL

The Supplementary Material for this article can be found online at: https://www.frontiersin.org/articles/10.3389/feart.2017.00115/full#supplementary-material

## REFERENCES

Andela, N., Morton, D. C., Giglio, L., Chen, Y., van der Werf, G. R., Kasibhatla, P. S., et al. (2017). A human-driven decline in global burned area. *Science* 356, 1356–1362. doi: 10.1126/science.aal4108

Andreae, M. O., and Merlet, P. (2001). Emission of trace gases and aerosols from biomass burning. *Global Biogeochem. Cycles* 15, 955–966. doi: 10.1029/2000GB001382

Bird, M. I., Chivas, A. R., and Head, J. (1996). A latitudinal gradient in carbon turnover times in forest soils. *Nature* 381, 143–146. doi: 10.1038/381143a0

Bird, M. I., and Gröcke, D. R. (1997). Determination of the abundance and carbon isotope composition of elemental carbon in sediments. *Geochim. Cosmochim. Acta* 61, 3413–3423. doi: 10.1016/S0016-7037(97)00157-9

Bird, M. I., Veenendaal, E. M., and Lloyd, J. J. (2004). Soil carbon inventories and $\delta^{13}C$ along a moisture gradient in Botswana. *Global Change Biol.* 10, 342–349. doi: 10.1046/j.1365-2486.2003.00695.x

Bird, M. I., Veenendaal, E. M., Moyo, C., Lloyd, J., and Frost, P. (2000). Effect of fire and soil texture on soil carbon in a sub-humid savanna (Matopos, Zimbabwe). *Geoderma* 94, 71–90. doi: 10.1016/S0016-7061(99)00084-1

Bird, M., Wynn, J. G., Saiz, G., Wurster, C. M., and McBeath, A. (2015). The Pyrogenic Carbon Cycle. *Annu. Rev. Earth Planet. Sci.* 43, 273–298. doi: 10.1146/annurev-earth-060614-105038

Blackford, J. J. (2000). Charcoal fragments in surface samples following a fire and the implications for interpretation of subfossil charcoal data. *Palaeogeogr. Palaeoclimatol. Palaeoecol.* 164, 33–42. doi: 10.1016/S0031-0182(00)00173-5

Blagodatskaya, E., Yuyukina, T., Blagodatsky, S., and Kuzyakov, Y. (2011). Turnover of soil organic matter and of microbial biomass under $C_3$-$C_4$ vegetation change: consideration of $^{13}C$ fractionation and preferential substrate utilization. *Soil Biol. Biochem.* 43, 159–166. doi: 10.1016/j.soilbio.2010.09.028

Brodowski, S., John, B., Flessa, H., and Amelung, W. (2006). Aggregate-occluded black carbon in soil. *Eur. J. Soil Sci.* 57, 539–546. doi: 10.1111/j.1365-2389.2006.00807.x

Clark, J. S. (1988). Particle motion and the theory of charcoal analysis: source area, transport, deposition, and sampling. *Quat. Res.* 30, 67–80. doi: 10.1016/0033-5894(88)90088-9

Conedera, M., Tinner, W., Neff, C., Meurer, M., Dickens, A. F., and Krebs, P. (2009). Reconstructing past fire regimes: methods, applications, and relevance to fire management and conservation. *Quat. Sci. Rev.* 28, 555–576. doi: 10.1016/j.quascirev.2008.11.005

Cotrufo, M. F., Boot, C., Abiven, S., Foster, E. J., Haddix, M., Reisser, M., et al. (2016). Quantification of pyrogenic carbon in the environment: an integration of analytical approaches. *Org. Geochem.* 100, 42–50. doi: 10.1016/j.orggeochem.2016.07.007

Crawford, A. J., and C. M., Belcher (2014). Charcoal morphometry for paleoecological analysis: the effects of fuel type and transportation on morphological parameters. *Appl. Plant Sci.* 2:1400004. doi: 10.3732/apps.1400004

Das, O., Wang, Y., and Hsieh, Y.-P. (2010). Chemical and carbon isotopic characteristics of ash and smoke derived from burning of C 3 and C 4 grasses. *Org. Geochem.* 41, 263–269. doi: 10.1016/j.orggeochem.2009.11.001

Dittmar, T., De Rezende, C. E., Manecki, M., Niggemann, J., Ovalle, A. R. C., Stubbins, A., et al. (2012). Continuous flux of dissolved black carbon from a vanished tropical forest biome. *Nat. Geosci.* 5, 618–622. doi: 10.1038/ngeo1541

Duffin, K. I., Gillson, L., and Willis, K. J. (2008). Testing the sensitivity of charcoal as an indicator of fire events in savanna environments: quantitative predictions of fire proximity, area and intensity. *Holocene* 18, 279–291. doi: 10.1177/0959683607086766

Ehleringer, J. R., Buchmann, N., and Flanagan, L. B. (2000). Carbon isotope ratios in belowground carbon cycle processes. *Ecol. Appl.* 10, 412–422. doi: 10.1890/1051-0761(2000)010[0412:CIRIBC]2.0.CO;2

Furley, P. A., Rees, R. M., Ryan, C. M., and Saiz, G. (2008). Savanna burning and the assessment of long-term fire experiments with particular reference to Zimbabwe. *Prog. Phys.* 32, 611-634. doi: 10.1177/0309133308101383

Giglio, L., Randerson, J. T., and Werf, G. R. (2013). Analysis of daily, monthly, and annual burned area using the fourth-generation global fire emissions database (GFED4). *J. Geophys. Res. Biogeosci.* 118, 317–328. doi: 10.1002/jgrg.20042

Haberle, S. G. (2005). A 23,000-yr pollen record from Lake Euramoo, wet tropics of NE Queensland, Australia. *Quat. Res.* 64, 343–356. doi: 10.1016/j.yqres.2005.08.013

Karfs, R., Daly, C., Beutel, T., Peel, L., and Wallace J. F., (2004). "VegMachine–Delivering monitoring information to northern Australia's pastoral industry," in *Proceedings of the 12th Australasian Remote Sensing and Photogrammetry Conference*' (Deakin, ACT: Spatial Sciences Institute).

Keppler, F., Kalin, R. M., Harper, D. B., McRoberts, W. C., and Hamilton, J. (2004). Carbon isotope anomaly in the major plant C 1 pool and its global biogeochemical implications. *Biogeosciences* 1, 123–131. doi: 10.5194/bg-1-123-2004

Knicker, H. (2011). Pyrogenic organic matter in soil: its origin and occurrence, its chemistry and survival in soil environments. *Quat. Int.* 243, 251–263. doi: 10.1016/j.quaint.2011.02.037

Krull, E., Skjemstad, J., Graetz, D., Grice, K., Dunning, W., Cook, G., et al. (2003). C-13-depleted charcoal from C4 grasses and the role of occluded carbon in phytoliths. *Org. Geochem.* 34, 1337–1352. doi: 10.1016/S0146-6380(03)00100-1

Kuhlbusch, T., Andreae, M. O., Cachier, H., Goldammer, J. G., Lacaux, J. P., Shea, R., et al. (1996). Black carbon formation by savanna fires: measurements and implications for the global carbon cycle. *J. Geophys. Res. Atmos.* 101, 23651–23665. doi: 10.1029/95JD02199

Lehmann, J., Skjemstad, J., Sohi, S., Carter, J., Barson, M., Falloon, P., et al. (2008). Australian climate-carbon cycle feedback reduced by soil black carbon. *Nat. Geosci.* 1, 832–835. doi: 10.1038/ngeo358

Leys, B. A., Brewer, S. C., McConaghy, S., Mueller, J., and McLauchlan, K. K. (2015). Fire history reconstruction in grassland ecosystems: amount of charcoal reflects local area burned. *Environ. Res. Lett.* 10:114009. doi: 10.1088/1748-9326/10/11/114009

Leys, B. A., Commerford, J. L., and McLauchlan, K. K. (2017). Reconstructing grassland fire history using sedimentary charcoal: considering count, size and shape. *PLoS ONE* 12:e0176445. doi: 10.1371/journal.pone.0176445

Major, J., Lehmann, J., Rondon, M., and Goodale, C. (2010). Fate of soil-applied black carbon: downward migration, leaching and soil respiration. *Global Change Biol.* 16, 1366–1379. doi: 10.1111/j.1365-2486.2009.02044.x

Marlon, J. R., Kelly, R., Daniau, A.-L., Vannière, B., Power, M. J., Bartlein, P., et al. (2016). Reconstructions of biomass burning from sediment charcoal records to improve data-model comparisons. *Biogeosciences* 13, 3225–3244. doi: 10.5194/bg-13-3225-2016

Mastrolonardo, G., Hudspith, V. A., Francioso, O., Rumpel, C., Montecchio, D., Doerr, S. H., et al. (2017). Size fractionation as a tool for separating charcoal

of different fuel source and recalcitrance in the wildfire ash layer. *Sci. Total Environ.* 595, 461–471. doi: 10.1016/j.scitotenv.2017.03.295

Meredith, W., Ascough, P. L., Bird, M. I., Large, D. J., Snape, C. E., Sun, Y., et al. (2012). Assessment of hydropyrolysis as a method for the quantification of black carbon using standard reference materials. *Geochim. Cosmochim. Acta* 97, 131–147. doi: 10.1016/j.gca.2012.08.037

Millspaugh, S. H., and Whitlock, C. (1995). A 750-year fire history based on lake sediment records in central Yellowstone National Park, USA. *Holocene* 5, 283–292. doi: 10.1177/095968369500500303

O'Malley, V. P., Burke, R. A., and Schlotzhauer, W. S. (1997). Using GC–MS/Combustion/IRMS to determine the $^{13}C/^{12}C$ ratios of individual hydrocarbons produced from the combustion of biomass materials—application to biomass burning. *Org. Geochem.* 27, 567–581. doi: 10.1016/S0146-6380(97)00087-9

Patterson, W. A., Edwards, K. J., and Maguire, D. J. (1987). Microscopic charcoal as a fossil indicator of fire. *Quat. Sci. Rev.* 6, 3–23. doi: 10.1016/0277-3791(87)90012-6

Randerson, J. T., Van der Werf, G. R., Collatz, G. J., Giglio, L., Still, C. J., Kasibhatla, P., et al. (2005). Fire emissions from $C_3$ and $C_4$ vegetation and their influence on interannual variability of atmospheric $CO_2$ and $^{13}CO_2$. *Global Biogeochem. Cycles* 19, GB2019. doi: 10.1029/2004GB002366

Reisser, M., Purves, R., Schmidt, M. W., and Abiven, S. (2016). Pyrogenic Carbon in soils: a literature-based inventory and a global estimation of its content in soil organic carbon and stocks. *Front. Earth Sci.* 4:80. doi: 10.3389/feart.2016.00080

Rumpel, C., Alexis, M., Chabbi, A., Chaplot, V., Rasse, D. P., Valentin, C., et al. (2006). Black carbon contribution to soil organic matter composition in tropical sloping land under slash and burn agriculture. *Geoderma* 130, 35–46. doi: 10.1016/j.geoderma.2005.01.007

Rumpel, C., and Kögel-Knabner, I. (2011). Deep soil organic matter—a key but poorly understood component of terrestrial C cycle. *Plant Soil* 338, 143–158. doi: 10.1007/s11104-010-0391-5

Rumpel, C., Leifeld, J., Santin, C., and Doerr, S. (2015). "Movement of biochar in the environment," in *Biochar for Environmental Management: Science, Technology and Implementation*, eds J. Lehmann and S. Joseph (Abingdon: Routledge), 283–300.

Saiz, G., Bird, M. I., Domingues, T., Schrodt, F., Schwarz, M., Feldpausch, T. R., et al. (2012). Variation in soil carbon stocks and their determinants across a precipitation gradient in West Africa. *Global Change Biol.* 18, 1670–1683. doi: 10.1111/j.1365-2486.2012.02657.x

Saiz, G., Wynn, J. G., Wurster, C. M., Goodrick, I., Nelson, P. N., and Bird, M. I. (2015a). Pyrogenic carbon from tropical savanna burning: production and stable isotope composition. *Biogeosciences* 12, 1849–1863. doi: 10.5194/bg-12-1849-2015

Saiz, G., Bird, M., Wurster, C., Quesada, C. A., Ascough, P., Domingues, T., et al. (2015b). The influence of $C_3$ and $C_4$ vegetation on soil organic matter dynamics in contrasting semi-natural tropical ecosystems. *Biogeosciences* 12, 5041–5059. doi: 10.5194/bg-12-5041-2015

Saiz, G., Goodrick, I., Wurster, C. M., Zimmermann, M., Nelson, P. N., and Bird, M. I. (2014). Charcoal re-combustion efficiency in tropical savannas. *Geoderma* 219, 40–45. doi: 10.1016/j.geoderma.2013.12.019

Santín, C., and Doerr, S. H. (2016). Fire effects on soils: the human dimension. *Philos. Trans. R. Soc. Lond. B Biol. Sci.* 371:20150171. doi: 10.1098/rstb.2015.0171

Santín, C., Doerr, S. H., Preston, C., and Bryant, R. (2013). Consumption of residual pyrogenic carbon by wildfire. *Int. J. Wildland Fire* 22, 1072–1077. doi: 10.1071/WF12190

Santín, C., Doerr, S. H., Preston, C., and González-Rodríguez, G. (2015). Pyrogenic organic matter production from wildfires: a missing sink in the global carbon cycle. *Glob. Chang. Biol.* 21, 1621–1633. doi: 10.1111/gcb.12800

Schimel, D. D., Braswell, B. H., Holland, E. E., McKeown, R., Ojima, D. S., Painter, T. H., et al. (1994). Climatic, Edaphic, and Biotic controls over storage and turnover of carbon in soils. *Global Biogeochem. Cycles* 8, 279–293. doi: 10.1029/94GB00993

Silver, W., Neff, J., McGroddy, M., Veldkamp, E., Keller, M., and Cosme, R. (2000). Effects of soil texture on belowground carbon and nutrient storage in a lowland Amazonian forest ecosystem. *Ecosystems* 3, 193–209. doi: 10.1007/s100210000019

Singh, N., Abiven, S., Torn, M. S., and Schmidt, M. W. I. (2012). Fire-derived organic carbon in soil turns over on a centennial scale. *Biogeosciences* 9, 2847–2857. doi: 10.5194/bg-9-2847-2012

Sollins, P., Kramer, M. G., Swanston, C., Lajtha, K., Filley, T., Aufdenkampe, A. K., et al. (2009). Sequential density fractionation across soils of contrasting mineralogy: evidence for both microbial-and mineral-controlled soil organic matter stabilization. *Biogeochemistry* 96, 209–231. doi: 10.1007/s10533-009-9359-z

Thevenon, F., Williamson, D., Bard, E., Anselmetti, F. S., Beaufort, L., and Cachier, H. (2010). Combining charcoal and elemental black carbon analysis in sedimentary archives: implications for past fire regimes, the pyrogenic carbon cycle, and the human–climate interactions. *Glob. Planet. Change* 72, 381–389. doi: 10.1016/j.gloplacha.2010.01.014

Thevenon, F., Williamson, D., Vincens, A., Taieb, M., Merdaci, O., Decobert, M., et al. (2003). A late-Holocene charcoal record from Lake Masoko, SW Tanzania: climatic and anthropologic implications. *Holocene* 13, 785–792. doi: 10.1191/0959683603hl665rr

Torello-Raventos, M., Feldpausch, T. R., Veenendaal, E., Schrodt, F., Saiz, G., Domingues, T. F., et al. (2013). On the delineation of tropical vegetation types with an emphasis on forest/savanna transitions. *Plant Ecol. Divers.* 6, 101–137. doi: 10.1080/17550874.2012.762812

Wurster, C. M. C., Lloyd, J. J., Goodrick, I. I., Saiz, G. G., and Bird, M. I. M. (2012). Quantifying the abundance and stable isotope composition of pyrogenic carbon using hydrogen pyrolysis. *Rapid Commun. Mass Spectrom.* 26, 2690–2696. doi: 10.1002/rcm.6397

Wurster, C. M., Saiz, G., Schneider, M. P., Schmidt, M. W., and Bird, M. I. (2013). Quantifying pyrogenic carbon from thermosequences of wood and grass using hydrogen pyrolysis. *Org. Geochem.* 62, 28–32. doi: 10.1016/j.orggeochem.2013.06.009

Wynn, J. G., and Bird, M. I. (2008). Environmental controls on the stable carbon isotopic composition of soil organic carbon: implications for modelling the distribution of $C_3$ and $C_4$ plants, Australia. *Tellus B* 60, 604–621. doi: 10.1111/j.1600-0889.2008.00361.x

Zimmerman, A. R. (2010). Abiotic and microbial oxidation of laboratory-produced black carbon (biochar). *Environ. Sci. Technol.* 44, 1295–1301. doi: 10.1021/es903140c

Zimmermann, M., Bird, M. I., Wurster, C., Saiz, G., Goodrick, I., Barta, J., et al. (2012). Rapid degradation of pyrogenic carbon. *Global Change Biol.* 18, 3306–3316. doi: 10.1111/j.1365-2486.2012.02796.x

**Conflict of Interest Statement:** The authors declare that the research was conducted in the absence of any commercial or financial relationships that could be construed as a potential conflict of interest.

The reviewer SD, and handling Editor declared their shared affiliation.

frontiers in Earth Science

ORIGINAL RESEARCH
published: 26 September 2017
doi: 10.3389/feart.2017.00075

# A New Perspective on the Apparent Solubility of Dissolved Black Carbon

*Sasha Wagner†, Yan Ding and Rudolf Jaffé**

*Department of Chemistry and Biochemistry, Southeast Environmental Research Center, Florida International University, North Miami, FL, United States*

Black carbon (BC), pyrogenic organic matter generated from the incomplete combustion of biomass, is ubiquitous in the environment. The molecular structures which comprise the BC pool of compounds are defined by their condensed aromatic core structures polysubstituted with O-containing functionalities (e.g., carboxyl groups). Despite the apparent hydrophobicity of BC molecules, a considerable portion of BC is translocated from terrestrial to aquatic systems in the form of dissolved BC (DBC). However, the specific biogeochemical mechanisms which control the transfer of BC from the land to the water remain elusive. In the current study, the apparent solubility of DBC was inferred from octanol-water partition coefficients ($K_{ow}$) modeled for proposed DBC structures with varying degrees of polycondensation and polar functionality. Modeled $K_{ow}$ values indicated that DBC molecules with small aromatic ring systems and high degrees of hydrophilic functionality may be truly solubilized in the aqueous phase. However, large and highly condensed DBC structures yielded high $K_{ow}$ values, which suggested that a considerable portion of the DBC pool which has been quantified in aquatic environments is not truly dissolved. We hypothesized that other DOM components may act as mediators in the solubilization of condensed aromatic molecules and serve to increase the solubility of DBC via hydrophobic, intermolecular associations. This hypothesis was tested through controlled leaching experiments to determine whether the mobilization of DBC from particulate soils and chars became enhanced in the presence of DOM. However, we observed that characteristics inherent to each sample type had a greater influence than added DOM on the apparent solubility of DBC. In addition, the direct comparison of molecular marker (benzenepolycarboxylic acids) and ultrahigh resolution mass spectral data (FT-ICR/MS) on leachates obtained from the same set of soils and char did not show a clear overlap in DBC quantification or characterization between the two analytical methods. Correlations between FT-ICR/MS results and BPCA were not significant possibly due to differences in the methodological windows and/or small sample size. Our results were unable to provide evidence in support of proposed hydrophobic interactions between DOM and DBC, suggesting that other physical/chemical mechanisms play important roles in the dissolution of BC.

**Keywords: Dissolved Black Carbon, octanol-water partition coefficient, $K_{ow}$, soil, charcoal, benzenepolycarboxylic acid method, apparent solubility, condensed aromatics**

OPEN ACCESS

***Edited by:***
*Cristina Santin, Swansea University, United Kingdom*

***Reviewed by:***
*William C. Hockaday, Baylor University, United States*
*Philippa Louise Ascough, Scottish Universities Environmental Research Centre, United Kingdom*

****Correspondence:***
*Rudolf Jaffé*
*jaffer@fiu.edu*

***†Present Address:***
*Sasha Wagner, Marine Sciences Department, Skidaway Institute of Oceanography, University of Georgia, Savannah, GA, United States*

***Specialty section:***
*This article was submitted to Biogeoscience, a section of the journal Frontiers in Earth Science*

***Received:*** *31 May 2017*
***Accepted:*** *12 September 2017*
***Published:*** *26 September 2017*

***Citation:***
*Wagner S, Ding Y and Jaffé R (2017) A New Perspective on the Apparent Solubility of Dissolved Black Carbon. Front. Earth Sci. 5:75. doi: 10.3389/feart.2017.00075*

## INTRODUCTION

Black carbon (BC) is generated from the incomplete combustion of biomass and fossil fuel (Goldberg, 1985). The chemical composition of BC is heterogeneous (Masiello, 2004), ranging from mildly thermally altered biomolecules (Myers-Pigg et al., 2015) to condensed aromatic structures produced during high temperature combustion (Schneider et al., 2010). It is estimated that global production of BC from biomass burning is up to 383 Tg per year and most of the BC produced through fire is deposited on the landscape (Santín et al., 2015). The stability of BC which is incorporated into soils is highly variable, with residence times ranging from days to millennia (Bird et al., 2015). The ubiquity of fire and the refractory nature of condensed aromatics have resulted in the accumulation of BC in soils, where it comprises ∼14% of global soil C stores (Reisser et al., 2016). Despite the observed refractory nature of soil BC (Kuzyakov et al., 2014), the apparent solubilization and subsequent transport via rivers as DBC has been identified as a major loss process of BC from terrestrial environments (Dittmar et al., 2012; Jaffé et al., 2013; Stubbins et al., 2015). As such, it was estimated that DBC accounts for ∼10% of the total DOC flux exported annually by global rivers to the oceans (Jaffé et al., 2013). It seems clear that fluvial transfer of DBC to the ocean represents a key component of global C cycles (Santín et al., 2015). However, very little is known regarding the geochemical mechanisms which control the release of soil BC to inland waters as DBC.

Although, recent wildfire activity does not seem to have a significant effect on in-stream DBC (Ding et al., 2013; Güereña et al., 2015; Wagner et al., 2015a), this material is continually exported from fire-impacted watersheds for decades after a burn event (Dittmar et al., 2012). This suggests that the aging of BC in soils may be a prerequisite to its dissolution and export to aquatic systems as DBC. Soil BC structures undergo surface oxidation with increasing soil residence time (Cheng et al., 2006; Zimmerman, 2010), and it is thought that this type of oxidation enhances the mobilization of DBC from aged charcoal (Abiven et al., 2011). Although, the oxidation of BC has been shown to result in the formation of O-containing functional groups on condensed aromatic structures (Cheng et al., 2006; Zimmerman, 2010), it is unknown whether such diagenetic processing increases the polarity of BC molecules above a threshold where DBC molecules are truly solubilized in water.

This study refers to specifically BC and DBC as the polycondensed aromatics isolated from soils, chars, and natural waters and then oxidized to yield benzenepolycarboxylic acid (BPCA) products (Dittmar, 2008). The BPCA method, which chemically converts condensed aromatics to individual benzene rings substituted with three, four, five, and six carboxylic acid groups (B3CA, B4CA, B5CA, and B6CA, respectively), has been identified as a robust approach for measuring and characterizing BC in environmental matrices (Roth et al., 2012). To generate B6CA, the parent DBC structure must contain 5 or more non-linear fused aromatic rings (Ziolkowski et al., 2011), which equates to a structure containing a minimum of 20 carbon atoms. Since DBC collected from surface waters yields considerable amounts of B6CA (e.g., Ding et al., 2013; Wagner et al., 2015a), it can be inferred that larger DBC structures (>5 fused aromatic rings) are readily mobilized to the dissolved phase in natural systems. However, the stabilization of such large DBC molecules in the water column is not well understood as the hydrophobic, condensed aromatic core structures of these pyrogenic compounds would suggest they are largely insoluble in water.

The aqueous solubility of molecular structures can be inferred from the octanol-water partition coefficient ($K_{ow}$), which is experimentally defined as the ratio of a compound's concentration in octanol to its concentration in pure water (Schwarzenbach et al., 2003 and references therein). For compounds that cannot be isolated or do not have commercially-available standards, such as the molecules which comprise the DBC pool, $K_{ow}$ is estimated using computational calculations based upon the atom/fragment contribution method which breaks down the proposed chemical structure into its fragment components and functional groups (Meylan and Howard, 1995). The $K_{ow}$ is also a proxy for the DOC-water partition coefficient (Karickhoff, 1981; Seth et al., 1999; Schwarzenbach et al., 2003), where compounds with high $K_{ow}$ values have greater affinities for organic matter (OM), including DOC in aqueous solution. The apparent solubilities of polyaromatic hydrocarbons (PAHs), which feature a condensed aromatic structure similar to DBC, are enhanced by DOM (Perminova et al., 1999; Durjava et al., 2007). Therefore, DOM may assist in the solubilization and stabilization of DBC molecules in the water column.

Since DOM is operationally-defined as organic matter which passes through a filter (pore size = 0.7 μm in the current study), the term "DBC" should include all physical forms of BC associated with the operationally-defined DOM pool (e.g., truly dissolved molecules, colloids, micelles, nanoparticles, etc.). Humic substances are proposed to exist as supramolecular assemblies of relatively small, heterogeneous molecules, which likely includes DBC, stabilized by weak hydrophobic interactions such as van der Waals forces, H-bonding, cation bridging, etc. (Piccolo, 2001; Simpson et al., 2002). In addition, DBC has been reported to preferentially associate with high molecular weight, humic-type DOM (Wagner and Jaffé, 2015), further supporting a potential DBC-DOM hydrophobic partitioning mechanism. The aromatic content of natural organic matter seems to play a key role in the binding of condensed aromatic compounds (Perminova et al., 1999), which suggests that conjugated aromatic π-systems may strengthen DBC-DOM relationships via specific electron donor-acceptor interactions (Keiluweit and Kleber, 2009). As such, we hypothesized that the apparent solubility of DBC (i.e., the amount of solubilized DBC, as defined by BC which passes through a 0.7 μm filter) may be facilitated or enhanced via macromolecular associations with components of natural DOM. In the current study, we have taken a three-pronged approach by combining computer modeling techniques, controlled leaching experiments, and ultrahigh resolution FT-ICR/MS analysis to test the effects of added DOM on the dissolution of DBC from soils and chars and to investigate the discrepancy between DBC molecular structure and its apparent solubility.

# MATERIALS AND METHODS

## Selection of Dissolved Black Carbon Molecular Formulae

The DBC molecules selected to be modeled in this study were chosen from existing literature reports. DOM from charcoal leachates had been previously characterized using Fourier transform ion cyclotron resonance mass spectrometry (FT-ICR/MS; Hockaday et al., 2007), an ultrahigh resolution analytical technique which allows for the assignment of individual molecular formulae to mass spectral peaks (Kujawinski, 2002; Sleighter and Hatcher, 2007; Dittmar and Paeng, 2009). Details regarding instrumental conditions and assignment of molecular formulas have been previously described by Hockaday et al. (2006, 2007). From the list of assigned molecular formulae identified for the charcoal leachate samples (**Table 1**; Hockaday et al., 2006), limitations for normalized double bond equivalents (DBE/C $\geq$ 0.7; Hockaday et al., 2006) and the aromaticity index (AI $\geq$ 0.67; Koch and Dittmar, 2006) were applied to specifically select molecular formulae with condensed aromatic ring structures. DBC molecular formulae which fit the following criteria were chosen for further consideration: (a) DBE/C $\geq$ 0.7, (b) AI $\geq$ 0.67, and (c) carbon number > 20 (strongly indicative of pyrogenic origin; Wagner et al., 2015b). Using this approach, a total of 32 formula combinations in the form of $C_mH_nO_{x1\sim x2}$ (where m, n, and x designate numbers of C, H, and O atoms, respectively) were selected to represent a range of DBC compounds (Table S1). From the list of 32 formulas, 12 molecular formulae, which covered the entire mass range, were chosen for the modeling of $K_{ow}$ DBC values. The 12 selected DBC molecular formulae are summarized in **Table 1**. Since the $K_{ow}$ of a DBC molecular structure was expected to be inversely correlated with the number of O-containing functionalities it contained, formulas with the smallest number of O atoms ($C_mH_nO_{x1}$) were chosen to represent the upper range of $K_{ow}$ values and molecular formulas with the largest number of O atoms ($C_mH_nO_{x2}$) were chosen to represent the lower range of $K_{ow}$ values for DBC formulae sharing the same number of C and H atoms (**Table 1** and Table S1).

**TABLE 1 |** Empirical DBC molecular formulae selected for $K_{ow}$ modeling.

| Formula | #C (m) | #H (n) | #O (×1) | #O (×2) | DBE/C | AI (min) | AI (max) |
|---|---|---|---|---|---|---|---|
| $C_{20}H_{12}O_{5\sim5}$ | 20 | 12 | 5 | 5 | 0.75 | 0.67 | 0.67 |
| $C_{21}H_{12}O_{5\sim6}$ | 21 | 12 | 5 | 6 | 0.76 | 0.67 | 0.69 |
| $C_{22}H_{12}O_{4\sim7}$ | 22 | 12 | 4 | 7 | 0.77 | 0.67 | 0.72 |
| $C_{23}H_{14}O_{5\sim5}$ | 23 | 14 | 5 | 5 | 0.74 | 0.67 | 0.67 |
| $C_{24}H_{14}O_{3\sim6}$ | 24 | 14 | 3 | 6 | 0.75 | 0.67 | 0.71 |
| $C_{26}H_{16}O_{4\sim5}$ | 26 | 16 | 4 | 5 | 0.73 | 0.67 | 0.68 |
| $C_{26}H_{14}O_{4\sim8}$ | 26 | 14 | 4 | 8 | 0.77 | 0.67 | 0.73 |
| $C_{28}H_{18}O_{4\sim4}$ | 28 | 18 | 4 | 4 | 0.71 | 0.67 | 0.67 |
| $C_{28}H_{14}O_{4\sim10}$ | 28 | 14 | 4 | 10 | 0.79 | 0.67 | 0.75 |
| $C_{30}H_{18}O_{5\sim6}$ | 30 | 18 | 5 | 6 | 0.73 | 0.67 | 0.68 |
| $C_{30}H_{14}O_{5\sim12}$ | 30 | 14 | 5 | 12 | 0.8 | 0.67 | 0.76 |
| $C_{32}H_{14}O_{6\sim14}$ | 32 | 14 | 6 | 14 | 0.81 | 0.67 | 0.77 |

*The formulae were originally identified in soil charcoal DOM by Hockaday et al. (2006).*

## Assembling Proposed Dissolved Black Carbon Molecular Structures

All possible arrangements for polyaromatic core structures containing 5–8 fused rings were drawn using Chem3D (Version Pro 12; CambridgeSoft Corporation). A selection of some of the proposed core structures and calculated H/C ratios are shown in Table S2. While the number of possible arrangements for small core structures (e.g., 5-ring systems) was limited, the number of possible arrangements for large core structures (e.g., 8-ring systems) was more extensive and it would have been prohibitively difficult to assess them all. Thus, core structures which exhibited the highest and lowest H/C ratios (the most linear and most condensed ring arrangements, respectively) were selected to model a range of possible $K_{ow}$ values for proposed DBC structures with large aromatic ring systems. Although, condensed aromatic molecules with unsatisfied valences (radicals) can exist as part of DBC, radical-containing DBC structures were not considered for $K_{ow}$ modeling.

DBC structures were assembled by first choosing an aromatic core structure from **Table 1**, then using the remaining numbers of C, H, and O atoms for the assignment of O-containing functional groups (e.g., −OH, −CHO, −COOH). Any remaining C and H atoms after O-assignments were incorporated into the structure as aliphatic side chains (e.g., $-CH_3$, $-CH_2-$). The effect of O-containing functional groups on increasing the $K_{ow}$ of a condensed aromatic structure is in the order of −OH < −CHO < −COOH (Meylan and Howard, 1995). To estimate the highest $K_{ow}$ values for $C_mH_nO_{x1}$ formulae, O-functionalities were added primarily as carboxyl groups. To estimate the lowest $K_{ow}$ values for $C_mH_nO_{x2}$ formulae, O-functionalities were added primarily as hydroxyl groups. This approach allowed for the assessment of the widest possible range of modeled $K_{ow}$ values for each DBC formula pair. Structural planarity enhances the partitioning of hydrophobic organic compounds to humic substances (Gauthier et al., 1987; Chin et al., 1997; Uhle et al., 1999). Since we hypothesize DBC molecules to participate in such hydrophobic interactions with DOM, we sought to maximize the structural planarity of proposed DBC structures in the current study. To minimize steric hindrance, which compromises the molecular planarity of DBC molecules, adjacent positioning of functional groups was avoided. Proposed DBC structures which exhibited the lowest molecular energy and the highest planarity were ultimately selected for $K_{ow}$ modeling. The determination of proposed molecular structures for an exemplary pair of DBC formulae is detailed in the Supporting Information (Tables S2, S3; Figure S3).

## Modeling $K_{ow}$ for Proposed Dissolved Black Carbon Molecular Structures

The atom/fragment contribution method (Meylan and Howard, 1995) was used to estimate the $K_{ow}$ of proposed DBC molecular structures. The modeling of $K_{ow}$ values for DBC structures

was performed using the EPI Suite™-Estimation Program Interface program developed by the Environmental Protection Agency (EPA; USA; https://www.epa.gov/tsca-screening-tools/epi-suitetm-estimation-program-interface), which operates based upon the atom/fragment contribution method. Briefly, DBC molecular structures were disassembled into "fundamental fragments" consisting of isolated C atoms, H atoms, O atoms, and functional groups. The coefficient values of individual fragments were summed and correction factors were applied to obtain the $K_{ow}$ value for DBC structures.

## Collection and Characterization of Soil and Char Samples

Soil and char samples were obtained from diverse sources and locations to comprise a suite of naturally-occurring organic matter samples and reference materials which were expected to yield a gradient of OC content, BC content, and physical characteristics. Soils were collected from the natural environment in areas having a known history of biomass burning. Peat soil was obtained from the Florida Coastal Everglades (SRS2S; Florida, USA) in an area which undergoes prescribed burning and potentially receives additional pyrogenic inputs from burned sugarcane fields located upstream through canal inputs. Surface soil was collected from a historic charcoal blast furnace site (PA2S; Pennsylvania, USA) which known to contain high amounts of BC (Cheng et al., 2008). Surface soil collected from a forested area which burned during the High Park wildfire in June of 2012 (PNAS; Colorado, USA) represented a soil with relatively fresh pyrogenic inputs. Topsoil was collected from the Hubbard Brook Experimental Forest (HBRS; New Hampshire, USA) from an area which experienced a large wildfire during the 1920s and was therefore used as reference of soil containing aged charcoal. Char samples representing diverse biomass sources and charring conditions were also obtained. Charcoal standards generated from rice straw (RICEC) and chestnut wood (WOODC) were obtained from the University of Zurich (Switzerland). Formation conditions and characterization of these two chars are described in detail by Hammes et al. (2006). Wildfire-derived char was directly removed from a severely burned pine tree from the area of the High Park wildfire (PNAC; Colorado, USA). Although, PNAC was exposed to some degree of natural weathering and sunlight prior to collection, it had experienced no direct soil interaction. Pieces of charcoal were collected from the crater left by an uprooted tree (∼8 cm from ground surface) at the site of the 1920s wildfire in the Hubbard Brook Experimental Forest (HBRC; New Hampshire, USA). Since this area of the Hubbard Brook forest has experienced no direct wildfires since the 1920s, HBRC represented an aged char sample. Field-collected soils and chars were stored frozen at −20°C and charcoal standards were stored in the dark at room temperature until further processing. Frozen samples were subsequently thawed and air dried. Coarse particulates were removed by hand and samples were ground using a mortar and pestle and passed through a sieve (30 mesh; 600 μm pore size). Homogenized samples were then dried overnight at 60°C and stored in a desiccator until further use. The OC content of soils and chars was measured via elemental analysis-isotope ratio mass spectrometry using a NA 1,500 Elemental analyzer and a Delta Plus IRMS with a Conflo 2 Dilution interface. Mineral content was determined using the loss on ignition method as described by Hammes et al. (2006). Briefly, samples were dried at 105°C for 24 h, then ignited at 500°C for 4 h. The mineral content was calculated as the proportion of the mass remaining after ignition to the total mass of the sample prior to ignition.

## Leaching Experiment and Analysis of Soil and Char Leachates

Dry soils and chars (0.4 g OC) were directly weighed into pre-combusted glass Erlenmeyer flasks and leached with three different aqueous phases (150 mL): deionized water (pH = 7), Pony Lake fulvic acid solution (PLFA; 5 mg-C $L^{-1}$; pH = 6), and Suwannee River humic acid solution (SRHA; 5 mg-C $L^{-1}$; pH = 6). PLFA and SRHA DOM standards were purchased from the International Humic Substances Society (IHSS; www.ihss.humicsubstances.org). Leachates were obtained in triplicate. Individual flasks containing deionized water, PLFA solution, and SRHA solution were included as controls for each leaching setup. Soil/Char suspensions and controls were capped and agitated on a shaker table (160 rpm) in the dark at 25°C for 72 h. The samples were subsequently filtered through pre-combusted 0.7 μm GF/F filters and rinsed with 110 mL deionized water, which brought final sample volumes to 260 mL. Filtered leachates and control solutions were stored at 4°C until further analysis.

DOC was measured using a Shimadzu TOC-V-CSH analyzer (Shimadzu Corporation, Tokyo, Japan). Ionic strength and pH were obtained with Accumet conductivity and pH probes (Fisher Scientific). Filtrates were acidified to pH 2 with concentrated HCl and DOM was isolated by solid phase extraction using the method outlined by Dittmar et al. (2008). Briefly, the Varian Bond Elut PPL cartridge (1 g) was first conditioned with Optima-grade MeOH and equilibrated with pH 2 MilliQ water. The acidified filtrate was then passed through the cartridge by gravity and the sorbent was subsequently rinsed with pH 2 MilliQ water to remove excess salts and subsequently dried under a stream of $N_2$. The DOM was then eluted with MeOH and stored in the dark at −20°C until DBC quantification.

## Black Carbon Quantification and Characterization via the Benzenepolycarboxylic Acid (BPCA) Method

BC was quantified and characterized in all samples using the BPCA method (Dittmar, 2008; Ding et al., 2013; Wiedemeier et al., 2016). For leachate samples, where DOM was isolated via solid phase extraction, aliquots of the DOM-containing MeOH elute were transferred to 2 mL glass ampules and the MeOH evaporated under a stream of $N_2$ gas. Concentrated nitric acid (0.5 mL) was subsequently added to each ampule, which were then flame-sealed and heated to 160°C for 6 h in a programmable oven to oxidize the condensed aromatic DOM to BPCAs. After oxidation, the ampules were heated to 50°C in a sand bath and the $HNO_3$ was evaporated under a stream of $N_2$ gas.

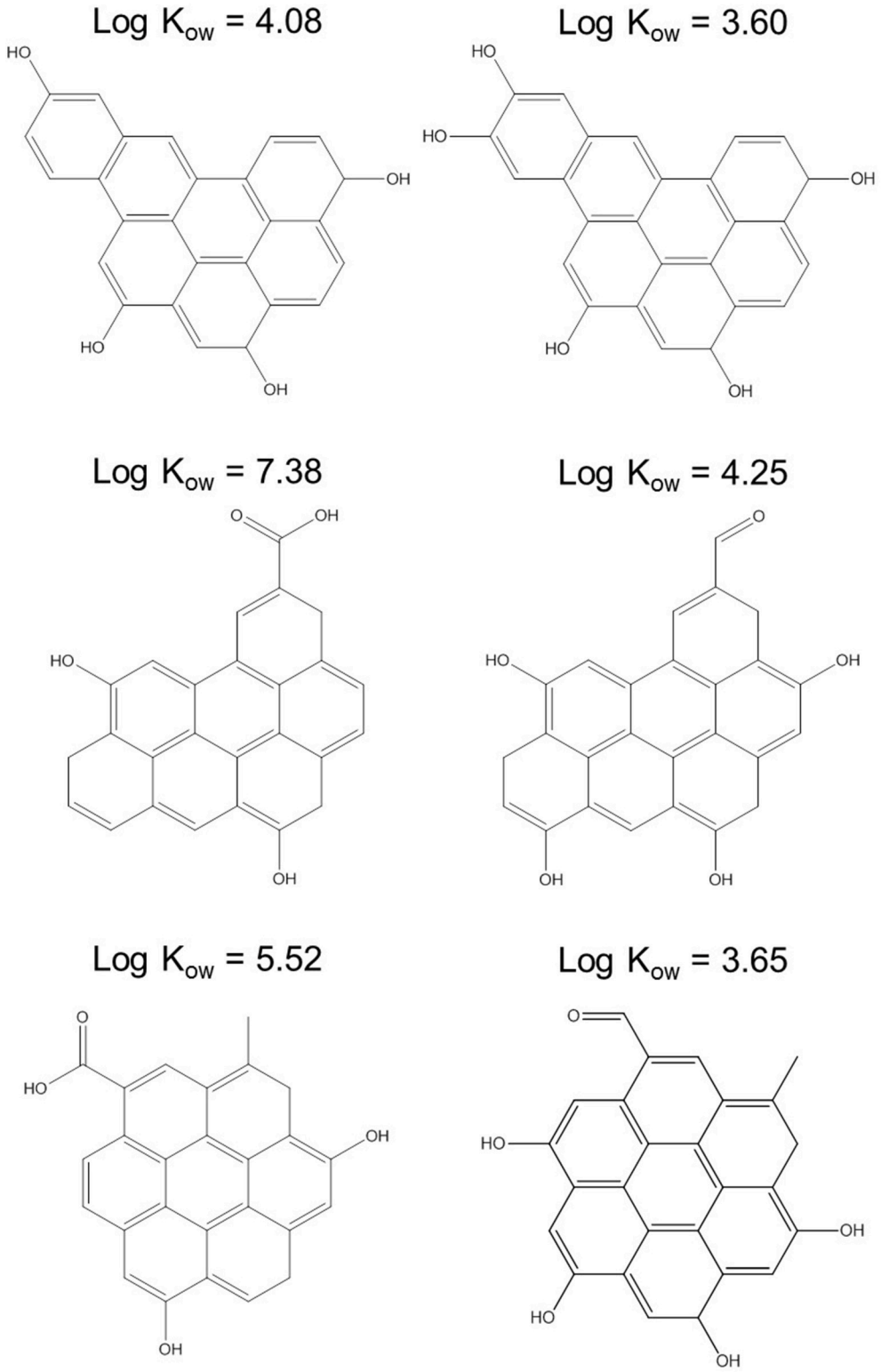


**FIGURE 1 |** A selection of proposed DBC molecular structures and modeled log $K_{ow}$ values.

The residue containing BPCAs was dissolved in the mobile phase for analysis. High pressure liquid chromatography (HPLC) separation of BPCAs was performed using a Sunfire C18 reversed phase column (3.5 μm, 2.1 × 150 mm; Waters Corporation). A gradient elution method was employed with mobile phase A (4 mM tetrabutylammonium bromide, 50 mM sodium acetate, 10% MeOH) and mobile phase B (100% MeOH) as described in detail by Dittmar (2008). BPCA oxidation and analysis for each sample was carried out in triplicate (CV < 5%).

Procedures for measuring DBC were scaled up to accommodate the oxidation of larger amounts of organic material for the determination of BC in the particulate soil and char samples. Additional clean-up steps were also required for the BC analysis of solid samples in order to remove metals and other interfering compounds prior to BPCA analysis (Schneider et al., 2010, 2011). The particulate BPCA procedure has been described in detail by Wiedemeier et al. (2016). Briefly, dry sample (∼2 mg) was directly transferred to 20 mL glass ampules. Concentrated $HNO_3$ (2 mL) was added and ampules were immediately flame-sealed and oxidized under the conditions described above. After oxidation, contents of each ampule were filtered through a pre-rinsed filter (0.7 μm GF/F), passed over a cation exchange resin (Dowex 50 WX8 400) and the eluent freeze-dried. The BPCA-containing residue was then re-dissolved in a 1:1 solution of Milli-Q water and MeOH and passed through a C18 solid phase extraction cartridge (Supelco). The eluent was collected, freeze-dried and re-dissolved for a final time in the mobile phase for HPLC analysis as described above. BPCA determinations for soils and chars were carried out in triplicate.

## Fourier Transform Ion Cyclotron Resonance Mass Spectral (FT-ICR/MS) Analysis of Water-Leached Soils and Chars

Methanol DOM extracts for water-leached soils and chars were diluted to DOC concentrations of ∼20 mg-C $L^{-1}$ in MeOH and Milli-Q water (1:1 v/v) and passed through a Teflon filter (0.2 μm) prior to electrospray ionization. Mass spectral analyses were carried out at the University of Oldenburg (Germany) on a Bruker Solarix 15 Tesla FT-ICR/MS instrument in negative ion mode, with 500 scans collected per sample. A reference mass list was used to calibrate each spectrum. The data were filtered to remove peaks that only appeared in one sample and those with low signal/noise ratio (<3). Formulas containing C, H, O, N, S, and P were assigned to mass spectral peaks, then filtered to remove unlikely DOM molecular combinations as described by Koch et al. (2007). The modified aromaticity index ($AI_{mod} \geq 0.67$) outlined by Koch and Dittmar (2006) was used to unambiguously categorize formulae with condensed aromatic structures, here referred to as DBC.

# RESULTS

## Modeled $K_{ow}$ Values for Proposed Dissolved Black Carbon Structures

In total, 90 molecular structures were derived from DBC formulae (**Table 1**) to constrain upper ($C_mH_nO_{x1}$; $n = 42$) and lower ($C_mH_nO_{x2}$; $n = 48$) ranges in $K_{ow}$ for compounds with five to eight fused aromatic rings. Exemplary molecular structures and modeled log $K_{ow}$ values for a selection of DBC formulae used in this exercise are shown in **Figure 1**. The modeled DBC structures in the current study are similar to those previously derived from molecular formulas assigned to FT-ICR mass spectral peaks (Kramer et al., 2004; Dittmar and Koch, 2006). The number of C+H-O atoms was calculated for each of the selected DBC molecular formulae in **Table 1** (C+H-O ranged from 27 to 44) and regressed against the log $K_{ow}$ values determined using the atom-fragment contribution method for O-depleted ($C_mH_nO_{x1}$) and O-enriched ($C_mH_nO_{x2}$) molecular structures. Linear correlations and associated regression equations between log $K_{ow}$ and number of C+H-O atoms are shown in **Figure 2**. Log $K_{ow}$ values estimated for O-depleted DBC formulae ranged from 3.51 to 8.04 and averaged 5.74 ± 1.26. Log $K_{ow}$ values estimated for O-enriched DBC formulae ranged from 1.48 to 6.67 and averaged 3.97 ± 1.35.

## Analysis of Particulate Soils, Particulate Chars, and Leachate Samples

The amount of DOC in each leachate solution (from deionized water, SRHA, and PLFA treatments) was corrected for the contribution of DOC from PLFA and SRHA (0.50 ± 0.05 and 0.47 ± 0.07 mg-C, respectively) and normalized to the amount of OC in the particulate sample. Leachate DOC ranged from 0.98 to 22.0 mg g-$OC^{-1}$ with a median DOC yield of 3.74 mg g-$OC^{-1}$. The amount of DBC in each leachate solution was also corrected for the contribution of DBC from PLFA and SRHA (quantified via the BPCA method in our lab as contributing 0.011 ± 0.003 and 0.043 ± 0.005 mg-C, respectively)

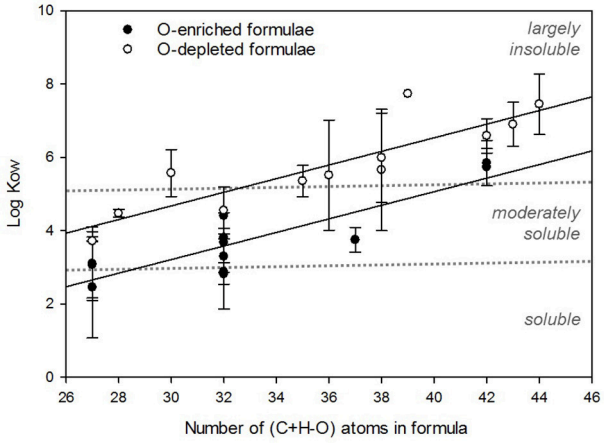


**FIGURE 2 |** Linear correlations between the log $K_{ow}$ and C+H–O number for 90 proposed DBC structures. Data points were binned according to their C+H–O number. O-depleted formulae ($C_mH_nO_{x1}$) were used to calculate the high log $K_{ow}$ regression (y = 0.186x – 0.907; $R^2 = 0.77$) and O-enriched formulae (all $C_mH_nO_{x2}$) were used to calculate the low log $K_{ow}$ regression (y = 0.185x – 2.350; $R^2 = 0.76$). Each point represents the binned mean and error bars represent 1 SD.

and normalized to the amount of OC in the particulate sample. Leachate DBC ranged from 0.04 to 2.58 mg g-$OC^{-1}$ with a median DBC yield of 0.26 mg g-$OC^{-1}$. Deionized water blanks contained negligible amounts of DOC and DBC. The pH of leachate solutions ranged from 4.3 to 8.4 and conductivity spanned a range of 6–417 μs $cm^{-1}$. A complete list of data for the leachate solutions is listed in **Table 2**. Error associated with experimental replicates (median and average CV across all experimental conditions were 22 and 32%, respectively) was greater than the error associated with analytical replicates (CV $< 5\%$). Therefore, analytical error was assumed to be negligible when calculating net DBC values. Standard deviations listed in **Table 2** are instead representative of the larger error associated with experimental replicates. A detailed description on error propagation in the current study can be found in the Supporting Information.

The OC content of the soils and chars ranged from 7.6 to 65.8 g $kg^{-1}$ with a median of 59.1 g $kg^{-1}$. Mineral content, calculated as the mass of material remaining after loss on ignition, ranged from 36 to 837 g $kg^{-1}$ with a median value of 193 g $kg^{-1}$. The BC content of the particulate samples spanned a range of 28–357 g kg-$OC^{-1}$ with a median value of 272 g kg-$OC^{-1}$. A complete list of data for particulate soil and char samples is listed in **Table 3**.

## Fourier Transform Ion Cyclotron Resonance Mass Spectral (FT-ICR/MS) Assessment of Water-Leached Soils and Chars

Ultra high resolution mass spectral analysis yielded more than 5,000 mass peaks per leachate sample. On average, water-leached soils and chars yielded 6,999 ± 1,271 mass peaks, to which an average of 4,874 ± 1,049 molecular formulas were assigned. The number of assigned molecular formulas which represented condensed aromatic structures (DBC; $AI_{mod} \geq 0.67$) containing only C, H, and O atoms ranged from 339 to 787. Mean-weighted average values for molecular weight (m/z) and number of C atoms per formula (#C) ranged from 283 to 355 and from 15.8 to 18.9, respectively. The linear regression between C+H-O and log $K_{ow}$ established in **Figure 2** and described in section Modeled $K_{ow}$ Values for Proposed Dissolved Black Carbon Structures was used to estimate log $K_{ow}$ values for DBC formulas identified in the soil and char leachates. Most DBC formulas had an estimated log $K_{ow}$ value $< 3$ (323 ± 45). Fewer DBC formulas had an estimated log $K_{ow}$ between 3 and 5 (212 ± 77). A small number of DBC formulas had estimated log $K_{ow}$ values $> 5$ (32 ± 28). Results of FT-ICR/MS analysis for individual leachate samples are listed in **Table 4**.

**TABLE 2 |** Experimental data for the DOM leached from soils and chars with deionized water, PLFA, and SRHA.

| Sample | Treatment | DOC (g kg-$OC^{-1}$) | DBC (g kg-$OC^{-1}$) | pH | Conductivity (us $cm^{-1}$) |
|---|---|---|---|---|---|
| SRS2 Soil | Water | 2.44 ± 0.06 | 0.18 ± 0.09 | 8.33 ± 0.06 | 131 ± 1 |
| SRS2 Soil | PLFA | 2.26 ± 0.17 | 0.17 ± 0.04 | 8.30 ± 0.05 | 132 ± 2 |
| SRS2 Soil | SRHA | 1.92 ± 0.17 | 0.13 ± 0.02 | 8.36 ± 0.03 | 134 ± 2 |
| PA2 Soil | Water | 1.22 ± 0.09 | 0.22 ± 0.08 | 6.12 ± 0.04 | 6 ± 0 |
| PA2 Soil | PLFA | 0.98 ± 0.15 | 0.27 ± 0.07 | 5.90 ± 0.11 | 7 ± 1 |
| PA2 Soil | SRHA | 0.98 ± 0.20 | 0.26 ± 0.11 | 5.88 ± 0.09 | 6 ± 0 |
| PNA Soil | Water | 5.44 ± 0.06 | 0.67 ± 0.08 | 8.08 ± 0.04 | 89 ± 1 |
| PNA Soil | PLFA | 6.41 ± 2.58 | 0.68 ± 0.09 | 8.06 ± 0.05 | 88 ± 1 |
| PNA Soil | SRHA | 4.45 ± 0.31 | 0.65 ± 0.09 | 8.08 ± 0.06 | 87 ± 4 |
| HBR Soil | Water | 7.87 ± 0.18 | 0.24 ± 0.09 | 4.33 ± 0.02 | 21 ± 0 |
| HBR Soil | PLFA | 7.08 ± 0.53 | 0.24 ± 0.04 | 4.37 ± 0.06 | 22 ± 1 |
| HBR Soil | SRHA | 7.50 ± 0.23 | 0.25 ± 0.05 | 4.30 ± 0.03 | 23 ± 0 |
| RICE Char | Water | 21.97 ± 1.87 | 2.15 ± 0.12 | 8.11 ± 0.01 | 397 ± 2 |
| RICE Char | PLFA | 21.54 ± 0.70 | 2.06 ± 0.08 | 8.09 ± 0.04 | 402 ± 9 |
| RICE Char | SRHA | 21.97 ± 0.24 | 1.81 ± 0.31 | 8.02 ± 0.05 | 417 ± 9 |
| WOOD Char | Water | 3.49 ± 0.22 | 0.04 ± 0.00 | 8.01 ± 0.03 | 92 ± 4 |
| WOOD Char | PLFA | 2.86 ± 0.57 | 0.07 ± 0.01 | 8.07 ± 0.08 | 90 ± 5 |
| WOOD Char | SRHA | 2.86 ± 0.18 | −0.02 ± 0.03 | 5.87 ± 1.86 | 37 ± 47 |
| PNA Char | Water | 2.57 ± 0.04 | 0.26 ± 0.18 | 7.49 ± 0.13 | 49 ± 0 |
| PNA Char | PLFA | 2.22 ± 0.17 | 0.29 ± 0.14 | 7.51 ± 0.08 | 48 ± 1 |
| PNA Char | SRHA | 2.24 ± 0.24 | 0.31 ± 0.15 | 7.57 ± 0.08 | 46 ± 1 |
| HBR Char | Water | 4.18 ± 0.18 | 0.27 ± 0.03 | 4.79 ± 0.27 | 12 ± 1 |
| HBR Char | PLFA | 3.99 ± 0.13 | 0.24 ± 0.07 | 4.35 ± 0.01 | 17 ± 0 |
| HBR Char | SRHA | 4.24 ± 0.20 | 0.22 ± 0.07 | 4.34 ± 0.01 | 17 ± 0 |

*DOC and DBC values have been corrected for the inherent amount of DOC and DBC in PLFA or SRHA and are normalized by the mass of OC in the source soil or char. Conductivity and pH measurements were taken after the leachates were rinsed and diluted. All measurements were obtained in triplicate (mean ± 1 SD).*

**TABLE 3 |** Characterization of soil and char samples.

| Sample | Description | Sample ID | OC (g $kg^{-1}$) | Mineral Content (g $kg^{-1}$) | BC (g kg-$OC^{-1}$) |
|---|---|---|---|---|---|
| SRS2 Soil | Everglades peat soil | SRS2S | 509 | 345 ± 14 | 28 ± 8 |
| PA2 Soil | Soil from historic charcoal furnace site | PA2S | 570 | 342 ± 4 | 357 ± 12 |
| PNA Soil | Alpine forest soil from area of recent wildfire | PNAS | 76 | 837 ± 20 | 288 ± 120 |
| HBR Soil | Temperate forest soil from area of historic wildfire | HBRS | 494 | 113 ± 6 | 37 ± 2 |
| RICE Char | Generated from rice straw (Hammes et al., 2006) | RICEC | 632 | 193 ± 2 | 271 ± 4 |
| WOOD Char | Generated from chestnut wood (Hammes et al., 2006) | WOODC | 658 | ND | 274 ± 5 |
| PNA Char | Charred pine tree burned in recent wildfire | PNAC | 620 | 46 ± 3 | 259 ± 5 |
| HBR Char | Derived from historic wildfire (wood type unknown) | HBRC | 613 | 36 ± 13 | 295 ± 19 |

*Mineral content was estimated by loss on ignition. ND denotes values below the detection limit.*

**TABLE 4 |** FT-ICR mass spectral data for soils and chars leached with deionized water.

| Sample | # mass peaks | # assigned formulas | # DBC formulas | m/z (w.a.) | #C (w.a.) | C+H-O (w.a.) | log $K_{ow}$ (w.a.) | # formulas log $K_{ow}$ <3 | # formulas log $K_{ow}$ 3–5 | # formulas log $K_{ow}$ >5 |
|---|---|---|---|---|---|---|---|---|---|---|
| SRS2 Soil | 7,907 | 6,021 | 467 | 301 | 15.8 | 18.1 | 1.72 | 310 | 149 | 8 |
| PA2 Soil | 8,517 | 5,942 | 787 | 355 | 18.9 | 21.3 | 2.33 | 380 | 326 | 78 |
| PNA Soil | 8,292 | 6,037 | 607 | 307 | 16.2 | 18.5 | 1.81 | 342 | 234 | 29 |
| HBR Soil | 6,180 | 4,169 | 563 | 330 | 16.6 | 17.9 | 1.70 | 341 | 212 | 8 |
| RICE Char | 6,069 | 4,126 | 575 | 299 | 16.3 | 20.1 | 2.10 | 285 | 227 | 61 |
| WOOD Char | 5,883 | 3,758 | 504 | 300 | 14.9 | 15.7 | 1.28 | 317 | 164 | 21 |
| PNA Char | 5,272 | 3,676 | 339 | 283 | 14.6 | 16.6 | 1.46 | 243 | 93 | 1 |
| HBR Char | 7,872 | 5,262 | 728 | 348 | 17.9 | 19.8 | 2.04 | 371 | 298 | 56 |

*Mean-weighted average (w.a.) values and the number of formulas with log $K_{ow}$ values <3, 3–5, and >5 are calculated from DBC formulae containing only C, H, and O.*

# DISCUSSION

## Expected Solubility of Proposed Dissolved Black Carbon Structures Based Upon Modeled $K_{ow}$ Values

The hydrophobic character and aqueous solubility of DBC cannot be experimentally determined since standard compounds which accurately represent the DBC pool do not exist. Instead, we gained insight into the solubility properties of DBC molecular structures from modeled $K_{ow}$ coefficients (typically expressed as log $K_{ow}$) which were estimated using the atom/fragment contribution method (Meylan and Howard, 1995). As expected, DBC molecular structures with more O-containing functional groups exhibited, on average, significantly lower log $K_{ow}$ values ($p < 0.05$), which suggests that more oxidized DBC molecules would have enhanced solubility in water. Significant, positive correlations were found between log $K_{ow}$ and the number of C+H–O atoms ($p < 0.001$; **Figure 2**). The contribution of aromatic C fragments (e.g., = CH−) to a molecular structure increases its log $K_{ow}$, whereas the addition of O-containing functional groups (e.g., −OH, −COOH) decreases its log $K_{ow}$ (Meylan and Howard, 1995; Schwarzenbach et al., 2003), therefore the positive relationship between C+H-O and log $K_{ow}$ was expected. Log $K_{ow}$ was also significantly positively correlated with the number of C+H atoms ($p < 0.001$; Figure S1) the number of fused aromatic rings in the DBC core structure ($p < 0.001$; Figure S2). Condensed aromatic structures with log $K_{ow}$ values < 3 are quite soluble in water, with concentrations >1 mg $L^{-1}$ (Tobiszewski and Namiesnik, 2012). Considering this conventional threshold for solubility assessment, it seems that some DBC structures may exist in a truly dissolved form (**Figure 2**). However, only 14% of the 90 proposed DBC structure are considered dissolved (log $K_{ow}$ < 3), the rest fell within moderately soluble (3 < log $K_{ow}$ < 5, 40%) and largely insoluble (log $K_{ow}$ > 5, 46%) ranges. The majority of modeled log $K_{ow}$ values derived from proposed DBC structures are above 3, indicating that many of the condensed aromatic structures which we have selected to represent the DBC pool have solubility limitations in water.

The log $K_{ow}$ is inversely related to the aqueous solubility of hydrophobic organic compounds (Schwarzenbach et al., 2003 and references therein), such as polyaromatic hydrocarbons (PAHs), which share similar condensed aromatic structures as molecules within the DBC pool. Since PAHs are environmental pollutants, they have been well-characterized with regards to their solubility in water. PAHs containing 20 or more C atoms with log $K_{ow}$ values > 5 are largely insoluble in water (corresponding to a concentration of ∼0.001 mg-C $L^{-1}$ at 25°C; Tobiszewski and Namiesnik, 2012). From the apparent insolubility of large PAHs, we would expect DBC concentrations to be equally low in natural waters due to the structural similarities between DBC molecules and PAHs. DBC concentrations in natural waters often exceed 1 mg-C $L^{-1}$ (Jaffé et al., 2013) and are enriched in B6CA (Ding et al., 2013, 2014; Wagner et al., 2015a). Taken together, the data yielded from BPCAs suggest that large (>20 C atoms) DBC molecules exist

and are somehow stabilized within the water column. However, this observation is at odds with $K_{ow}$ modeling of DBC molecular structures derived from assigned molecular formulae (**Figure 2**).

## Composition of Dissolved Black Carbon Leached from Soils and Chars

We carried out a controlled leaching experiment to investigate the discrepancy between the expected solubility of DBC (based upon above-described $K_{ow}$ estimations from FT-ICR/MS formula assignments) and the quantity/quality of DBC measured in aquatic systems using the BPCA method. The composition of DBC, described by the relative abundance of individual BPCA molecular markers, in leachates extracted from soils and chars with deionized water was quite variable (**Figure 3A**). The relative abundance of BPCAs has been used as a proxy for BC condensed aromaticity, and greater proportions of B5CA and B6CA are indicative of more highly condensed aromatic BC (Schneider et al., 2010; Abiven et al., 2011). Molecular markers B5CA and B6CA were abundant in all leachate samples, comprising ∼20–50% of total BPCAs (**Figure 3A**). DBC leached from the soils was generally more enriched in B5CA and B6CA compared to DBC leached from the fresh chars, with the exception of PNAS. PNAS is a soil sample that received fresh charcoal inputs from a recent wildfire. Therefore, it was not surprising to find that the BPCA composition of PNAS resembled that of the fresh char leachates (WOODC, RICEC, PNAC; **Figure 3A**). HBRC, an aged char, leached greater proportions of B5CA and B6CA compared to the freshly-produced chars (**Figure 3A**). Similar findings have been previously reported in the literature (Abiven et al., 2011). Soil samples which have received historic inputs of BC (SRS2S, PA2S, HBRS) leached DBC with BPCA compositions similar to that of aged char. Over time, BC is presumably degraded and oxidized via biotic and abiotic processes (Cheng et al., 2006; Zimmerman, 2010) and it is proposed that the increase in polar functionality enhances the dissolution of larger DBC structures (those which generate greater proportions of B5CA and B6CA upon oxidation) from aged charcoal (Abiven et al., 2011). However, the modeling of log $K_{ow}$ values for proposed DBC structures indicated that such oxidation processes do not sufficiently increase molecular polarity for the true solubilization of highly condensed DBC compounds in water. Therefore, other physico-chemical processes were considered to explain this phenomenon.

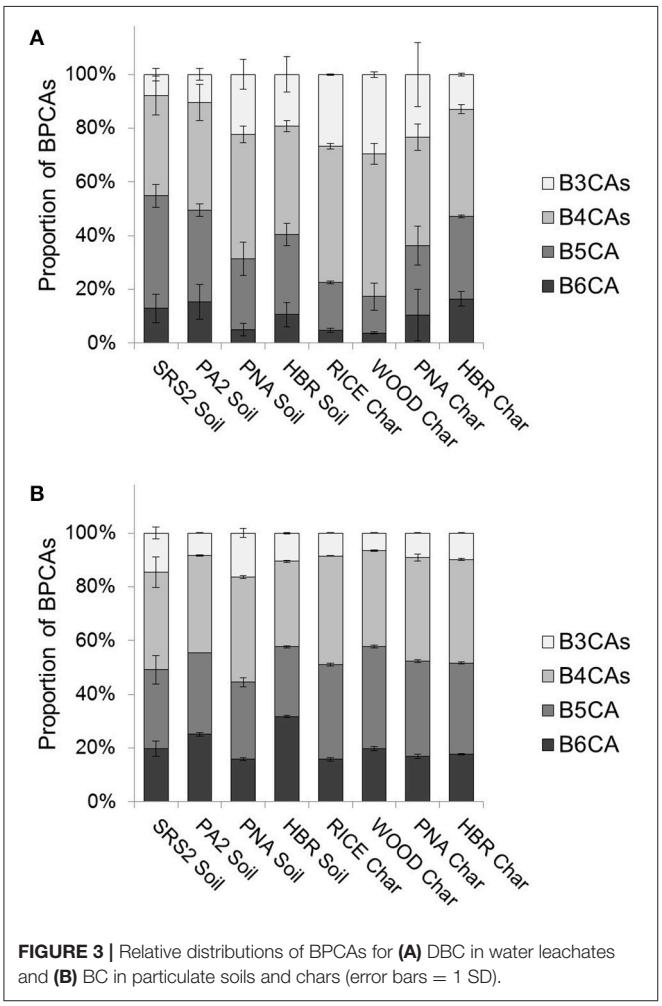


**FIGURE 3 |** Relative distributions of BPCAs for **(A)** DBC in water leachates and **(B)** BC in particulate soils and chars (error bars = 1 SD).

## Effects of Dissolved Organic Matter on the Apparent Solubility of Dissolved Black Carbon

The DOM pool is operationally-defined by what passes through a filter (0.7 μm pore size in the current study), and therefore represents both truly dissolved compounds and macromolecular DOM structures (e.g., microparticulates, colloids, micelles, and molecular assemblies; Azam and Malfatti, 2007). In light of supramolecular theory, where humic substances are considered to be aggregates of smaller heterogeneous compounds held together by weak intermolecular forces (Piccolo, 2001; Simpson et al., 2002; Sutton and Sposito, 2005), it is hypothesized that the stabilization of DBC may result from hydrophobic interactions between condensed aromatic structures and other DOM components. Hydrophobic DOM aggregates in water as a result of entropy-driven associations to minimize contact with highly polar water molecules (Kleber and Johnson, 2010). Therefore, molecular interactions between highly condensed DBC compounds and DOM are likely to be more energetically-favorable than interactions between highly condensed DBC compounds and water. Supramolecular interactions have been shown to occur between high molecular weight PAHs and humic substances (Perminova et al., 1999) which enhances the apparent solubility of PAHs in solution (Chin et al., 1997; Mitra and Dickhut, 1999; Durjava et al., 2007). Considering the shared structural features between DBC and PAHs, DOM may facilitate the translocation of BC to surface waters via similar mechanisms. The proposed interactive relationship between DBC and other components of DOM is further supported by the global correlation observed between DBC and DOC in rivers (Jaffé et al., 2013).

The log $K_{ow}$ has been used as a proxy for the partitioning of PAHs between the aqueous phase and natural organic matter (Karickhoff, 1981; Kopinke et al., 2002; Schwarzenbach et al., 2003). Therefore, highly polycondensed aromatic DBC compounds with modeled log $K_{ow}$ values > 5 should have similarly high affinities for DOC. As such, we expected the leaching experiment to show enhanced solubilization of DBC from soils and chars in the presence of DOM compared with leaching with just deionized water alone. Commercially-available DOM standards, PLFA and SRHA, were selected to test the apparent solubility of DBC from soils and chars because they represent two distinct sources of natural DOM which exhibit different molecular characteristics. PLFA is sourced from an Antarctic lake, and contains DOM which is of predominantly autochthonous/microbial origin. SRHA is sourced from a blackwater river fed by peat swamps, and contains DOM of primarily terrigenous origin. We chose PLFA and SRHA for our controlled leaching experiments to determine whether the apparent solubility of DBC was at all affected by the molecular composition of the added DOM. The molecular structure of PLFA is primarily aliphatic with limited regions of aromatic functionality (Thorn et al., 1989), however, condensed aromatics have been shown to strongly interaction with fulvic acids in solution (Lu et al., 2013). As such, the apparent solubility of DBC was expected to increase when soils and chars were leached in the presence of PLFA. Since SRHA exhibits greater degrees of aromaticity than PLFA (Thorn et al., 1989), the apparent solubility of DBC was expected to be the greatest when soils and chars were leached in the presence of SRHA due to favorable interactions between the aromatic π-systems of fused ring structures and humic acids (Keiluweit and Kleber, 2009). The experimental data for soils and chars leached with water, PLFA, and SRHA are detailed in **Table 2**. Although enhanced mobilization of DBC was expected in the presence of PLFA and SRHA, this effect was not observed. The results of a two-way ANOVA showed that the effect of added DOM was not significant ($p = 0.17$), but the effect of sample type was significant ($p < 0.001$) for the net amount of DBC leached from soils and chars (**Figure 4**). This finding suggested that other factors, such as the characteristics of the soils and chars themselves, had a greater influence over the translocation of DBC to the dissolved phase than the proposed hydrophobic interactions with added DOM.

Supramolecular associations among organic matter components are complex and the specific mechanisms driving their relationships are not well-understood (Sutton and Sposito, 2005). Under the described experimental conditions, added humic and fulvic acid DOM did not have a significant effect on the net amount of DBC leached from soils and char (**Figure 4**; **Table 2**). The Supporting Information contains a detailed description of how errors were propagated for DBC values in **Figure 4**. There are several possible reasons for this observation: First, a considerable amount of DOC was generated from the soil and char samples themselves (2–20 mg-C $L^{-1}$; **Table 2**), and DBC may have been stabilized via thermodynamically favorable associations with existing soil DOM components. Interactions between BC and specific soil constituents have been demonstrated on the microscopic scale

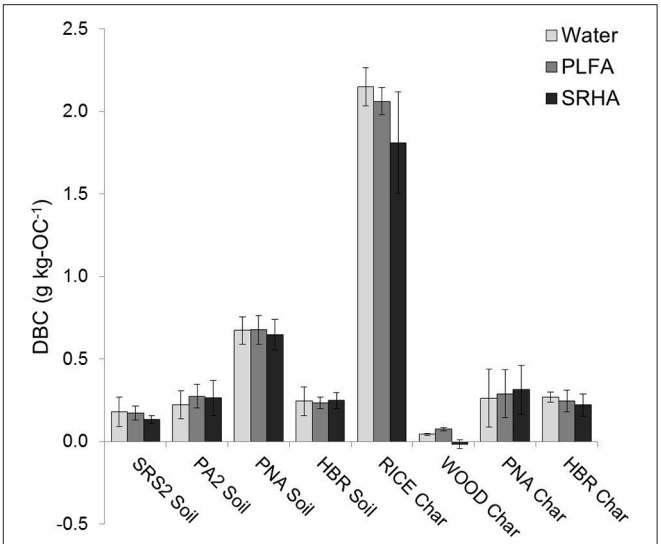


**FIGURE 4 |** Net DBC leached from soils and chars with water, PLFA, and SRHA (error bars = 1 SD).

(Lehmann et al., 2008; Kuo et al., 2013) and these existing associations could have minimized the potential effects of added DOM on DBC dissolution. Second, the concentrations of DOC generated directly from the soils and chars exceeded the concentrations of added PLFA and SRHA. DOC contributions from PLFA and SRHA were between 5 and 50% of final leachate DOC concentrations. Therefore, it is conceivable that the concentration of added DOM (5 mg-C $L^{-1}$) was too low to have a significant effect on the solubility of DBC. Third, in-lab experimental conditions are likely not an accurate reflection of leaching processes which occur in the natural environment. Batch experiments, in which the native aggregation of organic material and mineral components is destroyed and dry particulates are resuspended in solution, do not necessarily mimic the typical environmental conditions under which DOM is mobilized to surface waters (Kaiser et al., 2015). Finally, hydrophobic interactions may play more of a secondary role in the apparent solubility of DBC. Hydrophobic π-bond interactions are indeed the dominant interactive forces which mediate interactions for aromatic compounds lacking ionizable functional groups (e.g., PAHs; Keiluweit and Kleber, 2009). However, DBC structures are highly polysubstituted with polar, O-containing functionalities (Kramer et al., 2004; Wagner et al., 2015b), which may govern the interactions of these condensed aromatics with organic matter components by participating in other types of intermolecular forces, such as H-bonding, cation bridging, and chelation. If this is the case, then π-bond interactions would play more of an assistive role in the favorable interaction of DBC components to environmental sorbents (Keiluweit and Kleber, 2009). Chelation has been shown to distinctly affect DOM components differently based on their molecular character (Yamashita and Jaffé, 2008). Therefore, chelation processes could be an equally important driver of DBC molecular associations. The involvement of metals in the formation of inner-sphere complexes between

polar substituents, such as carboxylic groups, in DBC and between DBC and DOM, may indeed play a considerable, yet undetermined, role in DBC mobilization.

## Comparing the Quantity and Quality of Dissolved Black Carbon Leached from Different Soils and Chars

This study was unable to provide experimental evidence to support the hypothesis that hydrophobic interactions with added DOM enhances the apparent dissolution of DBC. However, the significant variation in net amount DBC leached from a suite of soils and chars (**Figure 4**) suggested that physico-chemical factors other than associations between DBC and added DOM may drive the translocation of BC from soils and chars to the dissolved phase. HBRC leached more DBC than WOODC and PNAC which provides further support for the enhanced solubility of condensed aromatics in aged charcoal, relative to fresh charcoal, due to the increased degree of BC oxidation (Abiven et al., 2011). The RICEC sample leached, by far, the most DBC of all samples in the current study (**Figure 4**). Interestingly, the mineral content of RICEC was also high, ∼5 times greater than the mineral content of the wood chars (**Table 3**). Aromatic compounds, including BC, have been shown to preferentially interact with and sorb to mineral surfaces in soils (Brodowski et al., 2005; Kothawala et al., 2012) which suggests that mineral content may be an important control in the mobilization of DBC. However, no significant correlation was observed between mineral content of source soils and chars and net amount of DBC leached ($R^2 = 0.03$; $p = 0.66$; $n = 24$). Alternatively, charcoal generated from herbaceous-type biomass, such as RICEC, exhibits greater carboxyl functionality compared to wood-derived charcoal (Knicker et al., 1996), which may have contributed to the enhanced dissolution of DBC from RICEC.

The BC content of soil and char samples in this study varied considerably (**Table 3**), likely owing to diverse sources of biomass, combustion conditions, and compositions of the pyrogenic material (Masiello, 2004). Solid samples which were more enriched in BC did not necessarily yield greater amounts of DBC, as a significant correlation between BC content and net DBC leached was not observed ($R^2 = 0.04$; $p = 0.65$; $n = 24$). This finding suggests that measured amounts of BC in soils may not be indicative of expected DBC concentrations in soil pore water or inland waters which drain the local landscape. Since the leaching experiments were not buffered, the water-soluble components of soils and chars controlled the pH and ionic strength of their respective leachates (**Table 2**). Solution pH and ionic strength affect the conformation and macromolecular interactions of DOM (Kalbitz et al., 2000). However, leachate pH values were not found to be significantly correlated with amounts of leached DBC ($R^2 = 0.08$; $p = 0.17$; $n = 24$). Although, a significant linear correlation between conductivity and net amount of DBC released was observed ($R^2 = 0.80$; $p < 0.005$; $n = 24$), this relationship was diminished when the high conductivity values for RICEC were removed from the correlation ($R^2 = 0.00$; $p = 0.87$; $n = 21$). Similarly, a significant linear correlation between DBC and DOC was observed for all samples ($R^2 = 0.90$; $p < 0.001$; $n = 24$). However, this relationship was driven by the high amounts of DBC and DOC leached from RICEC, and the significance was diminished when RICEC was removed from the correlation ($R^2 = 0.00$; $p = 0.94$; $n = 21$). While potential effects of ionic strength and pH on the mobilization of DBC are indeed possible, the results presented here were inconclusive based upon the small set of samples in the current study.

To assess how the BPCA composition of mobilized DBC may be related its source, BC was characterized in the particulate soil and char samples (**Figure 3B**). The quality of BC across the entire sample set was generally similar, with B5CA and B6CA comprising ∼50% of total BPCAs. The degree of aromatic condensation for BC produced during wildfires is diverse, owing primarily to different biomass sources and combustion conditions (McBeath et al., 2013; Schneider et al., 2013). Therefore, the use of BPCA ratios as the sole proxy for DBC source is speculative since we still have a very poor understanding of the biogeochemical factors which influence BPCA composition during BC formation, mobilization, and degradation in the environment. However, we observed that leached DBC was consistently depleted in B5CA and B6CA relative to BC in their respective source soils and chars (**Figure 3**). This discrepancy suggests that the soluble portion of BC is indeed more enriched in DBC with smaller condensed aromatic ring systems than its particulate source. Results from the modeling of log $K_{ow}$ for DBC structures, which predicts the enhanced solubility of condensed aromatic compounds with <5 fused rings, is in agreement with the observed preferential dissolution of less condensed DBC. However, BPCA compositions indicate that DBC leached from soils and chars also contained highly condensed aromatic structures (**Figure 3A**).

## Contrasting the Quantification of DBC with Mass Spectral Data for Water-Leached Soils and Chars

To further probe the observed disconnect between DBC molecular markers and mass spectral composition, we applied the relationship between C+H-O and log $K_{ow}$ (section Expected Solubility of Proposed Dissolved Black Carbon Structures Based upon Modeled $K_{ow}$ Values ) to estimate log $K_{ow}$ values for DBC formulas identified by FT-ICR/MS in the current suite of soil and char leachates. Log $K_{ow}$ values were estimated by averaging the log $K_{ow}$ values obtained from both the O-depleted and O-enriched regression equations (**Figure 2**). A summary of the mass spectral data, including weighted-average values for C+H-O and estimated log $K_{ow}$, for water-leached soils and chars is listed in **Table 4**. The number of condensed aromatic molecular formulae varied among the sample set, with PA2S yielding the highest number of DBC peaks (787; **Table 4**). To visualize the mass spectral composition of DBC identified in PA2S, the condensed aromatic formulae were displayed in Van Krevelen space, where molecular formulas are plotted according to their H/C and O/C ratios (**Figure 5**). Modeled log $K_{ow}$ values for DBC formulae generally increase with decreasing O/C ratio, which is in agreement with the hypothesis that the apparent solubility of DBC is enhanced by oxidation of condensed aromatic structures

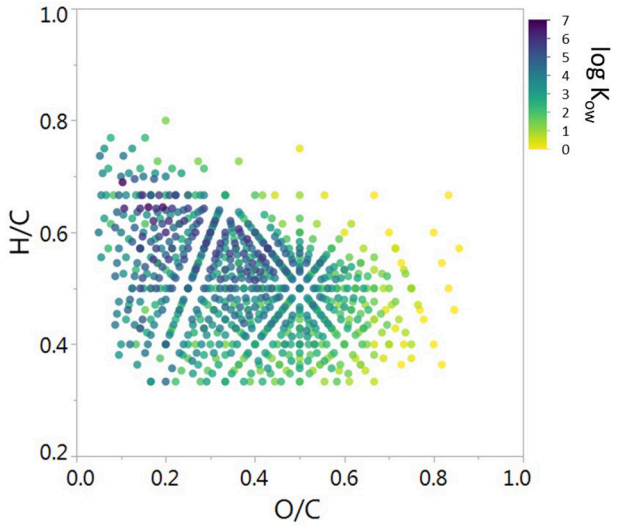


**FIGURE 5 |** Van Krevelen diagram of assigned DBC molecular formulae in the water leachate of PA2 Soil. Points are colored according to the estimated $K_{ow}$ calculated from C+H-O regressions.

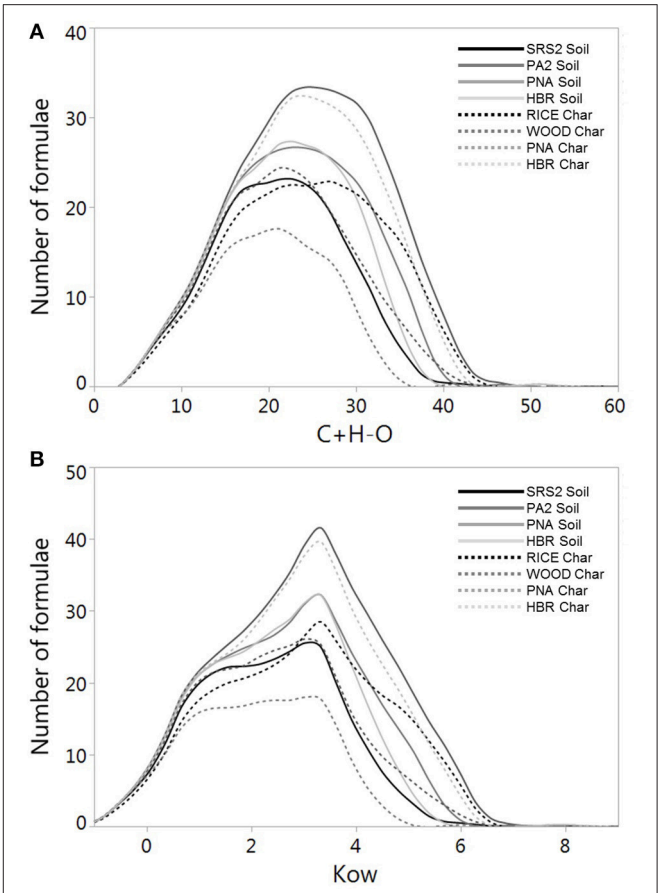


**FIGURE 6 |** Line plots showing the distribution of **(A)** C+H-O and **(B)** log $K_{ow}$ for DBC formulae identified in soil and char leachates.

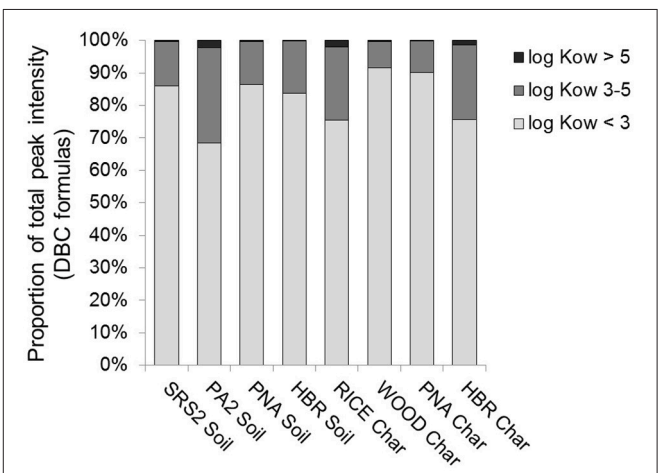


**FIGURE 7 |** Relative abundance of DBC formula-assigned peaks, as determined from FT-ICR/MS analysis, categorized according to log $K_{ow}$, for soil and char leachates.

($K_{ow}$ et al., 2011). The Van Kevelen distribution also indicates that a large portion of DBC molecular formulae are quite soluble in water (log $K_{ow}$ < 3; **Figure 5**). Line plots showing the distribution of C+H-O and estimated log $K_{ow}$ for all soil and charcoal leachates are shown in **Figure 6**. Samples HBRC and PA2S, both of which contain aged charcoal, yielded the largest number of assigned DBC formulae with greater log $K_{ow}$ values (**Figure 6B**). Interestingly, RICEC also yielded a relatively large number of high log $K_{ow}$ DBC formulae. The DBC molecular character of RICEC contradicts what we would expect to observe for fresh charcoal leachates, such as WOODC and PNAC, which yielded lower numbers of identified DBC formulae occupying a lower range of log $K_{ow}$ (**Figure 6B**).

Ultrahigh resolution mass spectrometry is a semi-quantitative method where molecular formulae associated with peaks of higher relative intensity are considered to be more abundant within the sample (Kujawinski et al., 2002). The relative abundance of DBC formula-assigned peaks, categorized according to log $K_{ow}$, for each soil and char leachate is shown in **Figure 7**. DBC formulae with estimated log $K_{ow}$ values > 5 are not only the most underrepresented with regards to number of assigned molecular formulas, but they are also the least abundant in terms of mass spectral peak intensity. In comparison, DBC formulae with estimated log $K_{ow}$ values < 3 comprised roughly 80% of mass spectral peak intensity. Taken together with the abundance of B5CA and B6CA generated from DBC in soil and char leachates (**Figure 3A**), it seems that the molecular composition of DBC derived from FT-ICR/MS underrepresents this highly condensed aromatic molecular component of the DBC pool. Although, it should be noted that the list of formulas used for $K_{ow}$ modeling (**Table 1**) and to draw subsequent relationships between log $K_{ow}$ and C+H-O (**Figure 2**) included formulas with higher masses and number of carbon atoms >20. Therefore, the low range of log $K_{ow}$ values for the soil and charcoal leachates is likely, in part, driven by the abundance of DBC formulae with low numbers of carbon. Correlations

between FT-ICR/MS results (total DBC peak intensity, percent DBC peak intensity with log $K_{ow}$ > 5, 3–5, or < 3) and BPCA results (ratios of [B5CA+B6CA]:[B3CA+B4CA] and DBC:DOC) were not significant ($p > 0.1$). We also did not find any significant correlation between DBC concentration and the total number of DBC formulas, or between DBC concentration and the number of DBC formulas in each log $K_{ow}$ class (log $K_{ow}$ < 3, 3–5, and > 5) for the water leachate samples ($R^2 = 0.09$–0.18; $p > 0.3$; $n = 24$). As discussed previously, this is most likely due to the RICE Char sample, which produced significantly more DBC than any other soil or char, thus preventing any meaningful correlations between DBC quantity and quality as described by modeled $K_{ow}$ or mass spectral analysis.

The apparent discrepancy between FT-ICR/MS and BPCA data with regards to DBC quantification and characterization could arise for several reasons. The BPCA method relies on the chromatographic separation and quantification of molecular markers formed from the chemical oxidation of condensed aromatic structures (Dittmar, 2008). Whereas, FT-ICR/MS relies on the soft (non-destructive) ionization of polar, organic molecules comprising the bulk DOM pool, of which DBC is only a part. Although, FT-ICR/MS is semi-quantitative, it is well understood that ionization efficiencies are not equal among different compound classes. Therefore, the mass spectral signal of highly condensed DBC compounds could have been suppressed by more easily ionizable compounds within the bulk DOM pool. Recent research has demonstrated that, based upon FT-ICR/MS analysis and fragmentation of deep sea DOM, a significant degree of structural diversity is contained within assigned molecular formulas (Zark et al., 2017). Although, the exact number of isomers represented by each molecular formula is unknown, Zark et al. (2017) estimate that the number of unique compounds in DOM is at least one order of magnitude greater than the total number of molecular formulas assigned via FT-ICR/MS. Since it is not unreasonable to assume the degree of molecular diversity in soil and charcoal leachates is similar to that of deep sea DOM, we would expect each DBC formula, especially those assigned to higher mass-to-charge ratios, to represent a large number of structural isomers. Therefore, although the expected solubility of individual condensed aromatic structures may be low (based upon calculated $K_{ow}$), actual bulk concentrations of DBC may be much higher if summed up over all possible isomers associated with each assigned DBC formula. The current study did not exhaustively consider every possible DBC structure. Therefore, we may have underestimated the true solubility of the bulk DBC pool, which may explain, in part, discrepancies between BPCA and mass spectral results. It is also possible that the observed discrepancy results from the overestimation of DBC content via the BPCA method. Previous studies have shown BPCAs to be primarily derived from charred material (Dittmar, 2008; Roth et al., 2012), especially for pyrogenic organic matter formed at high temperatures (Schneider et al., 2010). However, a recent study points to a potentially non-pyrogenic source for some BPCAs (Kappenberg et al., 2016). Since our DBC concentrations are derived from an accumulated total of all BPCAs (including B3CAs and B4CAs, which have been shown to be produced in small quantities from non-pyrogenic organic matter; Kappenberg et al., 2016), the overestimation of DBC is possible. However, since B5CA and B6CA (presumed to be exclusively pyrogenic; Kappenberg et al., 2016), give the most weight in converting BPCA amounts to DBC concentrations (Dittmar, 2008) the slight overestimation of DBC would not significantly change the results or interpretation of the current study. The BPCA and FT-ICR/MS methodologies for detecting DBC across the combustion continuum are fairly well-understood, but not definitively constrained (Masiello, 2004). Although, we assume some portion of their analytical windows to overlap, the observed disconnect between BPCA and FT-ICR/MS data for the soil and char leachates is not unexpected, especially for such a small number of compositionally-varied samples.

## Summary and Implications

Identifying the chemical and environmental factors which control the translocation of DBC from the particulate to the dissolved phase and the subsequent stabilization of DBC within the water column is still a largely open question within the pyrogenic carbon research community. The $K_{ow}$ modeling data presented herein suggested that proposed DBC molecular structures presented a large range of solubility, depending on size and degree of condensation, as well as on the degree of oxidation (O-content). However, while 14% of the 90 proposed DBC molecular structures yielded log $K_{ow}$ values indicative of good aqueous solubility, the fraction of the DBC which exhibited limited solubility was still significant (40% has moderate solubility and 46% are considered insoluble). Therefore, we hypothesized that DBC must partition to an intermediate phase, such as DOM, in order to increase apparent solubility of condensed aromatic structures in order to be stabilized in the aqueous phase. However, the results of the current study were unable to provide experimental support for the enhanced mobilization of DBC in the presence of added DOM alone.

The apparent solubility of DBC, which consists of a pool of compounds of diverse molecular size, degree of oxidation, and condensed aromaticity, is likely controlled, in part, by simple aqueous solubility for low log $K_{ow}$ compounds, particularly for less polycondensed and more polar DBC structures. However, controls on the mobilization of larger, highly polycondensed DBC structures are less clear. Stabilization of BC in the dissolved phase may instead be driven by the formation of supramolecular assemblies or micelles, or by association with colloidal fractions and/or microparticulates. While DBC-DOM hydrophobic interactions might play a role in the mobilization process, the formation of molecular assemblies between DBC and DOM components via weak molecular forces and/or interactions with metals may also be important processes to consider. This study highlights the analytical and experimental challenges in unraveling the environmental dynamics of DBC, suggesting that the translocation of soil BC and char to DBC in aquatic systems is controlled by complex biogeochemical processes, whose environmental drivers continue to remain elusive.

## AUTHOR CONTRIBUTIONS

YD performed the $K_{ow}$ modeling portion of this study. SW carried out all leaching experiments, performed black carbon and mass spectral analyses. SW drafted the manuscript with significant inputs from YD and RJ, who contributed to the writing and data interpretation.

## ACKNOWLEDGMENTS

This work was supported by the National Science Foundation through the Florida Coastal Long Term Ecological Research program (Grant No. DEB-1237517) and the George Barley endowment. The authors thank Dr. Thorsten Dittmar for his insightful feedback on the manuscript and assistance in working up FT-ICR mass spectral data. K. Klaproth is thanked for helping with sample FT-ICR/MS analysis. YD thanks FIU for a DOI Fellowship. The authors thank John Harris for performing the %OC determinations, and Drs. J. Lehmann and J. Campbell for kindly providing the PA2 Soil and HBR Soil sampler, respectively. Support for field logistics for the collection of the PNA samples by Dr. F. Rosario-Ortiz is appreciated. This is Contribution Number 844 from the Southeast Environmental Research Center.

## SUPPLEMENTARY MATERIAL

The Supplementary Material for this article can be found online at: http://journal.frontiersin.org/article/10.3389/feart.2017.00075/full#supplementary-material

## REFERENCES

Abiven, S., Hengartner, P., Schneider, M. P. W., Singh, N., and Schmidt, M. W. I. (2011). Pyrogenic carbon soluble fraction is larger and more aromatic in aged charcoal than in fresh charcoal. *Soil Biol. Biochem.* 43, 1615–1617. doi: 10.1016/j.soilbio.2011.03.027

Azam, F., and Malfatti, F. (2007). Microbial structuring of marine ecosystems. *Nat. Rev. Microbiol.* 5, 782–791. doi: 10.1038/nrmicro1747

Bird, M. I., Wynn, J. G., Saiz, G., Wurster, C. M., and McBeath, A. (2015). The pyrogenic carbon cycle. *Annu. Rev. Earth Planet. Sci.* 43, 273–298. doi: 10.1146/annurev-earth-060614-105038

Brodowski, S., Rodionov, A., Haumaier, L., Glaser, B., and Amelung, W. (2005). Revised black carbon assessment using benzene polycarboxylic acids. *Org. Geochem.* 36, 1299–1310. doi: 10.1016/j.orggeochem.2005.03.011

Cheng, C.-H., Lehmann, J., Thies, J. E., and Burton, S. D. (2008). Stability of black carbon in soils across a climatic gradient. *J. Geophys. Res.* 113:G02027. doi: 10.1029/2007JG000642

Cheng, C.-H., Lehmann, J., Thies, J. E., Burton, S. D., and Engelhard, M. H. (2006). Oxidation of black carbon by biotic and abiotic processes. *Org. Geochem.* 37, 1477–1488. doi: 10.1016/j.orggeochem.2006.06.022

Chin, Y.-P., Aiken, G. R., and Danielsen, K. M. (1997). Binding of pyrene to aquatic and commercial humic substances: the role of molecular weight and aromaticity. *Environ. Sci. Technol.* 31, 1630–1635. doi: 10.1021/es960404k

Ding, Y., Cawley, K. M., da Cunha, C. N., and Jaffe, R. (2014). Environmental dynamics of dissolved black carbon in wetlands. *Biogeochemistry* 119, 259–273. doi: 10.1007/s10533-014-9964-3

Ding, Y., Yamashita, Y., Dodds, W. K., and Jaffé, R. (2013). Dissolved black carbon in grassland streams: is there an effect of recent fire history? *Chemosphere* 90, 2557–2562. doi: 10.1016/j.chemosphere.2012.10.098

Dittmar, T. (2008). The molecular level determination of black carbon in marine dissolved organic matter. *Org. Geochem.* 39, 396–407. doi: 10.1016/j.orggeochem.2008.01.015

Dittmar, T., de Rezende, C. E., Manecki, M., Niggemann, J., Ovalle, A. R. C., Stubbins, A., et al. (2012). Continuous flux of dissolved organic carbon from a vanished tropical forest biome. *Nat. Geosci.* 5, 618–622. doi: 10.1038/ngeo1541

Dittmar, T., Koch, B., Hertkorn, N., and Kattner, G. (2008). A simple and efficient method for the solid-phase extraction of dissolved organic matter (SPE-DOM) from seawater. *Limnol. Oceanogr. Methods* 6, 230–235. doi: 10.4319/lom.2008.6.230

Dittmar, T., and Koch, B. P. (2006). Thermogenic organic matter dissolved in the abyssal ocean. *Mar. Chem.* 102, 208–217. doi: 10.1016/j.marchem.2006.04.003

Dittmar, T., and Paeng, J. (2009). A heat-induced molecular signature in marine dissolved organic matter. *Nat. Geosci.* 2, 175–179. doi: 10.1038/ngeo440

Durjava, M. K., ter Laak, T. L., Hermens, J. L. M., and Struijs, J. (2007). Distribution of PAHs and PCBs to dissolved organic matter: high distribution coefficients with consequences for environmental fate modeling. *Chemosphere* 67, 990–997. doi: 10.1016/j.chemosphere.2006.10.059

Gauthier, T. D., Seitz, W. R., and Grant, C. L. (1987). Effects of structural and compositional variations of dissolved humic materials on pyrene $K_{oc}$ values. *Environ. Sci. Technol.* 21, 243–248. doi: 10.1021/es00157a003

Goldberg, E. (1985). *Black Carbon in the Environment*. New York, NY: John Wiley and Sons.

Güereña, D. T., Lehmann, J., Walter, T., Enders, A., Neufeldt, H., Odiwour, H., et al. (2015). Terrestrial pyrogenic carbon export to fluvial ecosystems: lessons learned from the White Nile watershed of East Africa. *Glob. Biogeochem. Cycles* 29, 1911–1928. doi: 10.1002/2015GB005095

Hammes, K., Smernik, R. J., Skjemstad, J. O., Herzog, A., Vogt, U. F., and Schmidt, M. W. I. (2006). Synthesis and characterisation of laboratory-charred grass straw (*Oryza sativa*) and chestnut wood (*Castanea sativa*) as reference materials for black carbon quantification. *Org. Geochem.* 37, 1629–1633. doi: 10.1016/j.orggeochem.2006.07.003

Hockaday, W. C., Grannas, A. M., Kim, S., and Hatcher, P. G. (2006). Direct molecular evidence for the degradation and mobility of black carbon in soils from ultrahigh-resolution mass spectral analysis of dissolved organic matter from a fire-impacted forest soil. *Org. Geochem.* 37, 501–510. doi: 10.1016/j.orggeochem.2005.11.003

Hockaday, W. C., Grannas, A. M., Kim, S., and Hatcher, P. G. (2007). The transformation and mobility of charcoal in a fire-impacted watershed. *Geochim. Cosmochim. Acta* 71, 3432–3445. doi: 10.1016/j.gca.2007.02.023

Jaffé, R., Ding, Y., Niggeman, J., Vähätalo, A. V., Stubbins, A., Spencer, R. G. M., et al. (2013). Global charcoal mobilization via dissolution and riverine transport to the oceans. *Science* 340, 345–347. doi: 10.1126/science.1231476

Kaiser, M., Kleber, M., and Berhe, A. A. (2015). How air-drying and rewetting modify soil organic matter characteristics: an assessment to improve data interpretation and inference. *Soil Biol. Biochem.* 80, 324–340. doi: 10.1016/j.soilbio.2014.10.018

Kalbitz, K., Solinger, S., Park, J.-H., Michalzik, B., and Matzner, E. (2000). Controls on the dynamics of dissolved organic matter in soils: a review. *Soil Sci.* 165, 277–304. doi: 10.1097/00010694-200004000-00001

Kappenberg, A., Blasing, M., Lehndorff, E., and Amelung, W. (2016). Black carbon assessment using benzenepolycarboxylic acids: limitations for organic-rich matrices. *Org. Geochem.* 94, 47–51. doi: 10.1016/j.orggeochem.2016.01.009

Karickhoff, S. W. (1981). Semi-empirical estimation of sorption of hydrophobic pollutants on natural sediments and soils. *Chemosphere* 10, 833–846. doi: 10.1016/0045-6535(81)90083-7

Keiluweit, M., and Kleber, M. (2009). Molecular-level interactions in soils and sediments: the role of aromatic π-systems. *Environ. Sci. Technol.* 43, 3421–3429. doi: 10.1021/es8033044

Kleber, M., and Johnson, M. G. (2010). Advances in understanding the molecular structure of soil organic matter: implications for interactions in the environment. *Adv. Agron.* 107, 77–142. doi: 10.1016/S0065-2113(10)06003-7

Knicker, H., Almendros, G., González-Vila, F. J., Martin, F., and Lüdemann, H. D. (1996). $^{13}$C- and $^{15}$N-NMR spectroscopic examination of the transformation of

organic nitrogen in plant biomass during thermal treatment. *Soil Biol. Biochem.* 28, 1053–1060. doi: 10.1016/0038-0717(96)00078-8

Koch, B. P., and Dittmar, T. (2006). From mass to structure: an aromaticity index for high resolution mass data of natural organic matter. *Rapid Commun. Mass Spectrom.* 20, 926–932. doi: 10.1002/rcm.2386

Koch, B. P., Dittmar, T., Witt, M., and Kattner, G. (2007). Fundamentals of molecular formula assignment to ultrahigh resolution mass data of natural organic matter. *Anal. Chem.* 79, 1758–1763.

Kopinke, F.-D., Georgi, A., Mackenzie, K., and Kumke, M. U. (2002). "Sorption and chemical reactions of polycyclic aromatic hydrocarbons with dissolved refractory organic substances and related model polymers," in *Refractory Organic Substances in the Environment*, eds F. H. Frimmel, G. Abbt-Braun, K. G. Heumann, B. Hock, H.-D. Lüdemann, and M. Spiteller (Weinheim: Wiley), 475–515.

Kothawala, D. N., Roehm, C., Blodau, C., and Moore, T. R. (2012). Selective adsorption of dissolved organic matter to mineral soils. *Geoderma* 189–190, 334–342. doi: 10.1016/j.geoderma.2012.07.001

Kramer, R. W., Kujawinski, E. B., and Hatcher, P. G. (2004). Identification of black carbon derived structures in a volcanic ash soil humic acid by Fourier transform ion cyclotron resonance mass spectrometry. *Environ. Sci. Technol.* 38, 3387–3395. doi: 10.1021/es030124m

Kujawinski, E. B. (2002). Electrospray ionization Fourier transform ion cyclotron resonance mass spectrometry (ESI FT-ICR MS): characterization of complex environmental mixtures. *Environ. Forensics* 3, 207–216. doi: 10.1080/713848382

Kujawinski, E. B., Freitas, M. A., Zang, X., Hatcher, P. G., Green-Church, K. B., and Jones, B. (2002). The application of electrospray ionization mass spectrometry (ESI MS) to the structural characterization of natural organic matter. *Org. Geochem.* 33, 171–180. doi: 10.1016/S0146-6380(01)00149-8

Kuo, D. T. F., Vander Sande, J. B., and Gschwend, P. M. (2013). Characterization of black carbon in geosorbents at the nanometer scale by STEM–EDX elemental mapping. *Org. Geochem.* 56, 81–93. doi: 10.1016/j.orggeochem.2012.12.012

Kuzyakov, Y., Bogomolova, I., and Glaser, B. (2014). Biochar stability in soil: decomposition during eight years and transformation as assessed by compound-specific $^{14}$C analysis. *Soil Biol. Biochem.* 70, 229–236. doi: 10.1016/j.soilbio.2013.12.021

Lehmann, J., Solomon, D., Kinyangi, J., Dathe, L., Wirick, S., and Jacobsen, C. (2008). Spatial complexity of soil organic matter forms at nanometer scales. *Nat. Geosci.* 1, 238–242. doi: 10.1038/ngeo155

Lu, R., Sheng, G.-P., Liang, Y., Li, W.-H., Tong, Z.-H., Chen, W., et al. (2013). Characterizing the interactions between polycyclic aromatic hydrocarbons and fulvic acids in water. *Environ. Sci. Pollut. Res.* 20, 2220–2225. doi: 10.1007/s11356-012-1087-6

Masiello, C. A. (2004). New directions in black carbon organic geochemistry. *Mar. Chem.* 92, 201–213. doi: 10.1016/j.marchem.2004.06.043

McBeath, A. V., Smernik, R. J., and Krull, E. S. (2013). A demonstration of the high variability of chars produced from wood in bushfires. *Org. Geochem.* 55, 38–44. doi: 10.1016/j.orggeochem.2012.11.006

Meylan, W. M., and Howard, P. H. (1995). Atom/Fragment contribution method for estimating octanol-water partition coefficients. *J. Pharm. Sci.* 84, 84–92. doi: 10.1002/jps.2600840120

Mitra, S., and Dickhut, R. M. (1999). Three-phase modeling of polycyclic aromatic hydrocarbon association with pore-water-dissolved organic carbon. *Environ. Toxicol. Chem.* 18, 1144–1148. doi: 10.1002/etc.5620180611

Myers-Pigg, A. N., Louchouarn, P., Amon, R. M. W., Prokushkin, A., Pierce, K., and Rubtsov, A. (2015). Labile pyrogenic dissolved organic carbon in major Siberian Arctic rivers: implications for wildfire-stream metabolic linkages. *Geophys. Res. Lett.* 42, 377–385. doi: 10.1002/2014GL062762

Perminova, I. V., Grechishcheva, N. Y., and Petrosyan, V. S. (1999). Relationships between structure and binding affinity of humic substances for polycyclic aromatic hydrocarbons: relevance of molecular descriptors. *Environ. Sci. Technol.* 33, 3781–3787. doi: 10.1021/es990056x

Piccolo, A. (2001). The supramolecular structure of humic substances: a novel understanding of humus chemistry and implications in soil science. *Adv. Agron.* 75, 57–134. doi: 10.1016/S0065-2113(02)75003-7

Reisser, M., Purves, R. S., Schmidt, M. W. I., and Abiven, S. (2016). Pyrogenic carbon in soils: a literature-based inventory and a global estimation of its content in soil organic carbon and stocks. *Front. Earth Sci.* 4:80. doi: 10.3389/feart.2016.00080

Roth, P. J., Lehndorff, E., Brodowski, S., Bornemann, L., Sánchez-García, L., Gustafsson, Ö., et al. (2012). Differentiation of charcoal, soot and diagenetic carbon in soil: method comparison and perspectives. *Org. Geochem.* 46, 66–75. doi: 10.1016/j.orggeochem.2012.01.012

Santín, C., Doerr, S. H., Kane, E. S., Masiello, C. A., Ohlson, M., de la Rosa, J. M., et al. (2015). Towards a global assessment of pyrogenic carbon from vegetation fires. *Global Change Biol.* 22, 76–91. doi: 10.1111/gcb.12985

Schneider, M. P. W., Hilf, M., Vogt, U. F., and Schmidt, M. W. I. (2010). The benzene polycarboxylic acid (BPCA) pattern of wood pyrolyzed between 200°C and 1000°C. *Org. Geochem.* 41, 1082–1088. doi: 10.1016/j.orggeochem.2010.07.001

Schneider, M. P. W., Pyle, L. A., Clark, K. L., Hockaday, W. C., Masiello, C. A., and Schmidt, M. W. I. (2013). Toward a "molecular thermometer" to estimate the charring temperature of wildland charcoals derived from different biomass sources. *Environ. Sci. Technol.* 47, 11490–11495. doi: 10.1021/es401430f

Schneider, M. P. W., Smittenberg, R. H., Dittmar, T., and Schmidt, M. W. I. (2011). Comparison of gas with liquid chromatography for the determination of benzenepolycarboxylic acids as molecular tracers of black carbon. *Org. Geochem.* 42, 275–282. doi: 10.1016/j.orggeochem.2011.01.003

Schwarzenbach, R. P., Gschwend, P. M., and Imboden, D. M. (2003). *Environmental Organic Chemistry: Second Edition*. Hoboken: John Wiley and Sons, Inc.

Seth, R., MacKay, D., and Muncke, J. (1999). Estimating organic carbon partition coefficient and its variability for hydrophobic chemicals. *Environ. Sci. Technol.* 33, 2390–2394. doi: 10.1021/es980893j

Simpson, A. J., Kingery, W. L., Hayes, M. H. B., Spraul, M., Humpfer, E., Dvortsak, P., et al. (2002). Molecular structures and associations of humic substances in the terrestrial environment. *Naturwissenschaften* 89, 84–88. doi: 10.1007/s00114-001-0293-8

Sleighter, R. L., and Hatcher, P. G. (2007). The application of electrospray ionization coupled to ultrahigh resolution mass spectrometry for the molecular characterization of natural organic matter. *J. Mass Spectrom.* 42, 559–574. doi: 10.1002/jms.1221

Stubbins, A., Spencer, R. G. M., Mann, P. J., Holmes, R. M., McClelland, J. W., Niggemann, J., et al. (2015). Utilizing colored dissolved organic matter to derive dissolved black carbon export by arctic rivers. *Front. Earth Sci.* 3:63. doi: 10.3389/feart.2015.00063

Sutton, R., and Sposito, G. (2005). Molecular structure in soil humic substances: the new view. *Environ. Sci. Technol.* 39, 9009–9015. doi: 10.1021/es050778q

Thorn, K. A., Folan, D. W., and MacCarthy, P. (1989). *Characterization of the International Humic Substances Society Standard and Reference Fulvic and Humic Acids by Solution State Carbon-13 ($^{13}$C) and Hydrogen-1 ($^{1}$H) Nuclear Magnetic Resonance Spectrometry, U.S. Geological Survey, Water-Resources Investigations Report 89-4196*, Denver, CO, 93.

Tobiszewski, M., and Namiesnik, J. (2012). PAH diagnostic ratios for the identification of pollution emission sources. *Environ. Pollut.* 162, 110–119. doi: 10.1016/j.envpol.2011.10.025

Uhle, M. E., Chin, Y.-P., Aiken, G. R., and McKnight, D. M. (1999). Binding of polychlorinated biphenyls to aquatic humic substances: the role of substrate and sorbate properties on partitioning. *Environ. Sci. Technol.* 33, 2715–2718. doi: 10.1021/es9808447

Wagner, S., Cawley, K. M., Rosario-Ortiz, F., and Jaffé, R. (2015a). In-stream sources and links between particulate and dissolved black carbon following a wildfire. *Biogeochemistry* 124, 145–161. doi: 10.1007/s10533-015-0088-1

Wagner, S., Dittmar, T., and Jaffé, R. (2015b). Molecular characterization of dissolved black nitrogen via electrospray ionization Fourier transform ion cyclotron resonance mass spectrometry. *Org. Geochem.* 79, 21–30. doi: 10.1016/j.orggeochem.2014.12.002

Wagner, S., and Jaffé, R. (2015). Effect of photodegradation on molecular size distribution and quality of dissolved black carbon. *Org. Geochem.* 86, 1–4. doi: 10.1016/j.orggeochem.2015.05.005

Wiedemeier, D. B., Lang, S. Q., Gierga, M., Abiven, S., Bernasconi, S. M., and Früh-Green, G. L. (2016). Characterization, quantification and compound-specific isotopic analysis of pyrogenic carbon using benzene polycarboxylic acids (BPCA). *J. Vis. Exp.* 111:E53922. doi: 10.3791/53922

Yamashita, Y., and Jaffé R. (2008). Characterizing the interactions between trace metals and dissolved organic matter using excitation-emission matrix and parallel factor analysis. *Environ. Sci. Technol.* 42, 7374–7379. doi: 10.1021/es801357h

Zark, M., Christoffers, J., and Dittmar, T. (2017). Molecular properties of deep-sea dissolved organic matter are predictable by the central limit theorem: evidence from tandem FT-ICR-MS. *Mar. Chem.* 191, 9–15. doi: 10.1016/j.marchem.2017.02.005

Zimmerman, A. R. (2010). Abiotic and microbial oxidation of laboratory-produced black carbon (biochar). *Environ. Sci. Technol.* 44, 1295–1301. doi: 10.1021/es903140c

Ziolkowski, L. A., Chamberlin, A. R., Greaves, J., and Druffel, E. R. M. (2011). Quantification of black carbon in marine systems using the benzene polycarboxylic acid method: a mechanistic and yield study. *Limnol. Oceanogr. Methods* 9, 140–149. doi: 10.4319/lom.2011.9.140

**Conflict of Interest Statement:** The authors declare that the research was conducted in the absence of any commercial or financial relationships that could be construed as a potential conflict of interest.

frontiers in Earth Science

ORIGINAL RESEARCH
published: 27 February 2017
doi: 10.3389/feart.2017.00011

# Dissolved Black Carbon in the Headwaters-to-Ocean Continuum of Paraíba Do Sul River, Brazil

*Jomar S. J. Marques[1,2]*, Thorsten Dittmar[2], Jutta Niggemann[2], Marcelo G. Almeida[1], Gonzalo V. Gomez-Saez[2] and Carlos E. Rezende[1]*

*[1] Research Group for Biogeochemistry of Aquatic Ecosystems, Laboratório de Ciências Ambientais, Centro de Biociências e Biotecnologia Universidade Estadual do Norte Fluminense, Campos dos Goytacazes, Brazil, [2] Research Group for Marine Geochemistry (ICBM—MPI Bridging Group), Institute for Chemistry and Biology of the Marine Environment, Carl von Ossietzky University, Oldenburg, Germany*

Rivers annually carry 25–28 Tg carbon in the form of pyrogenic dissolved organic matter (dissolved black carbon, DBC) into the ocean, which is equivalent to about 10% of the entire riverine land-ocean flux of dissolved organic carbon (DOC). The objective of this study was to identify the main processes behind the release and turnover of DBC on a riverine catchment scale. As a model system, we chose the headwater-to-ocean continuum of Paraíba do Sul River (Brazil), the only river system with long-term DBC flux data available. The catchment was originally covered by Atlantic rain forest (mainly C3 plants) which was almost completely destroyed over the past centuries by slash-and-burn. As a result, large amounts of wood-derived charcoal reside in the soils. Today, fire-managed pasture and sugar cane (both dominated by C4 plants) cover most of the catchment area. Water samples were collected along the river, at the main tributaries, and also along the salinity gradient in the estuary and up to 35 km offshore during three different seasons. DBC was determined on a molecular level as benzenepolycarboxylic acids (BPCAs). Stable carbon isotopes ($\delta^{13}C$) were determined in solid phase extractable DOC (SPE-DOC) to distinguish C4 and C3 sources. Our results clearly show a relationship between hydrology and DBC concentrations in the river, with highest DBC concentrations and fluxes in the wet season (flux of 770 moles $s^{-1}$ in 2013 and 59 moles $s^{-1}$ in 2014) and lowest in the dry season (flux of 27 moles $s^{-1}$). This relationship indicates that DBC is mainly mobilized from the upper soil horizons during heavy rainfalls. The relationship between DBC concentrations and $\delta^{13}C$-SPE-DOC indicated that most of DBC in the river system originated from C3 plants, i.e., from the historic burning event of the Atlantic rain forest. A conservative mixing model could largely reproduce the observed DBC fluxes within the catchment and the land to ocean continuum. Comparably slight deviations from conservative mixing were accompanied by changes in the molecular composition of DBC (i.e., the ratio of benzenepenta- to benzenehexacarboxylic acid) that are indicative for photodegradation of DBC.

**Keywords: headwaters-to-ocean, black carbon, dissolved black carbon, dissolved organic carbon, Paraíba do Sul River**

OPEN ACCESS

***Edited by:***
*Samuel Abiven,*
*University of Zurich, Switzerland*

***Reviewed by:***
*Philippa Louise Ascough,*
*Scottish Universities Environmental Research Centre, UK*
*Alysha Coppola,*
*University of Zurich, Switzerland*

****Correspondence:***
*Jomar S. J. Marques*
*jomar.uenf@gmail.com*

***Specialty section:***
*This article was submitted to Biogeoscience, a section of the journal Frontiers in Earth Science*

***Received:*** *12 November 2016*
***Accepted:*** *31 January 2017*
***Published:*** *27 February 2017*

***Citation:***
*Marques JSJ, Dittmar T, Niggemann J, Almeida MG, Gomez-Saez GV and Rezende CE (2017) Dissolved Black Carbon in the Headwaters-to-Ocean Continuum of Paraíba Do Sul River, Brazil. Front. Earth Sci. 5:11. doi: 10.3389/feart.2017.00011*

## INTRODUCTION

Forest fires produce airborne combustion products and charred residues on and in the ground (Preston and Schmidt, 2006). Charred materials include a wide range of compounds, from dehydrated sugars formed at low charring temperature to highly-condensed graphite-like material produced at high temperatures, and secondary condensation products like soot (Santín et al., 2016). Also fuel characteristics are important, charcoal from woody and soft plant tissues often have different levels of condensation and oxygen content (Forbes et al., 2006; Schneider et al., 2010; Ding et al., 2014). The entire continuum of charred material is considered pyrogenic organic matter, of which the most condensed fraction is commonly referred to as black carbon (BC; Forbes et al., 2006).

Black carbon, which is largely derived from high-temperature woody chars, has received large attention in the literature, because it is more resistant to further biological and chemical degradation than the biomolecular precursors (Forbes et al., 2006). As a consequence, BC is ubiquitous in soils, sediments, and aquatic environments (Forbes et al., 2006; Jaffé et al., 2013). Important removal mechanisms of BC from soils are solubilization and subsequent transport in the dissolved phase (Dittmar et al., 2012a) and lateral transport of BC particles in the landscape (Major et al., 2010). During degradation in soils, oxygen atoms can be introduced into condensed aromatic structures of charcoal (Abiven et al., 2011). The resulting carboxylated molecular subunits partially dissolve in water and migrate through the soil as dissolved BC (DBC; Cheng and Lehmann, 2009). There is a significant time lag between wildfire induced BC production, incorporation into soils, and the actual release of DBC to aquatic systems (Dittmar et al., 2012a; Ding et al., 2014). Microbial reworking of charcoal may be required to enhance the translocation of soil BC to DBC (Ding et al., 2014). This translocation process can explain the presence of DBC in dissolved organic matter (DOM) in rivers, estuaries, and the ocean (Kim et al., 2004; Mannino and Harvey, 2004; Ziolkowski and Druffel, 2010). Global export of DBC from land to ocean amounts to ∼27 Tg carbon year$^{-1}$, which is equivalent to 10% of the entire riverine dissolved organic carbon (DOC) flux (Jaffé et al., 2013). DBC is distributed throughout the ocean and may impact biogeochemical processes on a global scale (Ziolkowski and Druffel, 2010). Even in the most remote basins of the deep ocean, ∼2% of DOM contains a heat-induced molecular signature (Dittmar and Koch, 2006; Dittmar and Paeng, 2009).

Very little is known on how DBC behaves in aquatic environments. While there is evidence that DBC is very stable in the deep ocean having conservative, salt-like properties (Dittmar and Paeng, 2009; Ziolkowski and Druffel, 2010), it is very susceptible to UV radiation in sunlit waters (Stubbins et al., 2012). Once exposed to sunlight, most of DBC is lost from seawater (Stubbins et al., 2012) and river water (Riedel et al., 2016). It is unclear what proportion of DBC that is introduced from soils and groundwater into the rivers eventually survives riverine transport from the headwaters to the estuaries and from there into the open ocean. The objective of this study was to fill this gap of knowledge for one of the best studied rivers in this context. Paraíba do Sul River (PSR) in Brazil is the only river system for which long-term DBC flux data are available (Dittmar et al., 2012a). In this river, DBC annual export exceeds by far present BC production rates, and charcoal still residing in the soils after historic forest fires is the most likely source of DBC in the river today. PSR drains an area formerly covered entirely by Brazilian Atlantic Forest. Its original area comprised 1.3 million km$^2$, but nowadays, only 12–15% of its original extension remains as secondary forest distributed as isolated, disconnected patches (Ribeiro et al., 2009; Fundação SOS Mata Atlântica Instituto Nacional de Pesquisas Espaciais, 2011; Lira et al., 2012). Deforestation occurred mainly between 1850 and 1970 via slash-and-burn (Warren, 1995). Today, 74% of the watershed is covered by fire-managed grassland and, in the area close to the coastal region, fire-managed sugar cane plantations. DBC concentration in PSR fluctuates with seasons, with highest concentrations during wet seasons and lowest ones during dry seasons, excluding direct deposition as a significant source (Dittmar et al., 2012a).

In this study we tested the hypothesis that due to limited light penetration and bio-recalcitrant properties, DBC is funneled unmodified within the PSR from the headwaters to the estuary and into the open ocean. We focused on the polycyclic aromatic fraction of DBC that can be quantified in natural waters with help of molecular proxies, i.e., benzenepolycarboxylic acids that are released from DBC during nitric acid oxidation (Hammes et al., 2007; Dittmar, 2008). We tested for conservative behavior of DBC in the headwaters-to-ocean continuum in three sampling campaigns, two in the rainy and one in the dry season.

Furthermore, we searched for chemical evidence that DBC in PSR is indeed mainly released from charcoal produced in historic forest fires and not primarily derived from today's fire management practice, as deduced previously from budget calculations (Dittmar et al., 2012a). We took advantage of the fact that the historic Atlantic forest vegetation was composed mainly of C3 plants, while today's pastures and sugar cane plantations are dominated by plants with the C4 photosynthetic pathway. Both types of plants carry a distinct carbon isotopic signature ($\delta^{13}$C) in their organic tissue. We determined $\delta^{13}$C on bulk SPE-DOM along the headwater-to-ocean continuum, which provided us with information about the main sources of DOM, of which DBC is a significant fraction.

## MATERIALS AND METHODS

### Study Area

The PSR watershed occupies an area of 57,300 km$^2$ in the states of São Paulo, Minas Gerais and Rio de Janeiro, located between 20°26′ and 23°28′S latitude and 41°00′ and 46°30′W longitude (Ovalle et al., 2013). The headwaters of the PSR are formed by the confluence of the Paraitinga and Paraibuna Rivers. The total length of the river channel is ∼1150 km. The PSR basin can be divided into three macro-sectors (**Figure 1A**): (1) An upper basin sector with an area of 7,300 km$^2$, where the river descends from an altitude of around 1800 to 600 m through narrow and embedded valleys carved out of crystalline rocks; (2) A middle

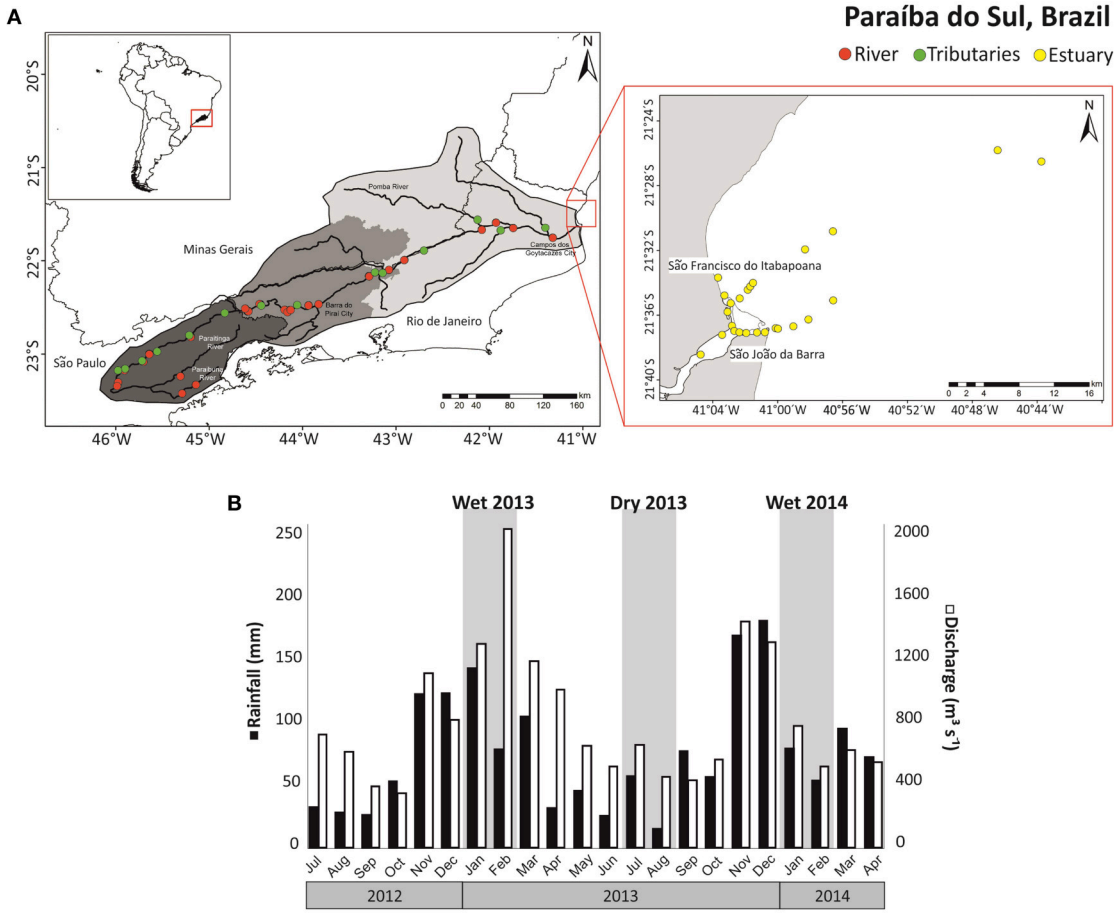


**FIGURE 1 | (A)** Map showing the Paraíba do Sul (Brazil) basin and the sampling locations in the river (red), tributaries (green), and estuary (yellow); **(B)** discharge of PSR (white) and rainfall at Campos (black) during the times series of 2012-2014, highlighting (gray) the seasons when sampling was performed (wet 2013, 2014, and dry 2013).

basin sector with an area of 27,500 km$^2$ and average elevation of 510 m, this sector is most influenced by industry, meanly for steel, chemicals, food, and paper; (3) A lower basin sector with an area of 22,500 km$^2$ that is mainly occupied by coastal plain with numerous riverine meanders and islands.

The area within the PSR watershed is highly urbanized and industrialized, with about 5 million inhabitants. The PSR is used for supplying drinking water to over 14 million people. Close to Barra do Piraí city, ~160 m$^3$ s$^{-1}$ of water is diverted from PSR for water supply to Rio de Janeiro city. There is a strong seasonality in water discharge in PSR. The high and low water periods range from December to February and from June to August, respectively. Major industrial areas are concentrated in the middle and upper sector basin and in the sub-basins of the Pomba and Paraibuna Rivers (Ovalle et al., 2013). In the lower basin sector, extensive farming prevails, especially sugar cane production. In addition, 47 different reservoirs and hydroelectric dams with varying sizes influence the hydrology of the river system throughout the basin (Ovalle et al., 2013). The Paraíba do Sul estuary is located at the coastal plain formed by the PSR delta in the North of Rio de Janeiro state, near São João da Barra city (Souza et al., 2010).

## Sampling

Samples from rivers, estuary, and adjacent ocean (**Figure 1A**) were collected during the wet seasons in January 2013 and February 2014. Average fluvial discharge in the lower reaches of PSR (Campos dos Goytacazes) was 1875 m$^3$ s$^{-1}$ in January 2013 and 719 m$^3$ s$^{-1}$ in February 2014. Sampling in the dry season was done in July and August of 2013, with an average discharge of 478 m$^3$ s$^{-1}$. The discharge value was estimated using river velocity and cross-sectional area measurements (General Oceanic model 2030 current meter). Surface water samples (3 L) were collected in acid rinsed bottles at 24 sites along the main channel of the PSR (**Figure 1A**, red symbols) and 14 sites at the PSR tributaries (**Figure 1A**, green symbols). In the estuary and adjacent ocean up to 35 km offshore, 24 samples were collected along the salinity gradient in the wet season of 2013, and 21 sites during the other campaigns (**Figure 1A**, yellow symbols). The PSR and tributaries were sampled from bridges while the estuary and ocean were

sampled from a trawler. All samples were retrieved from the water surface with acid-rinsed buckets. We collected superficial soil samples in the forest and pasture sites (three samples at each site) to constrain the end-members used in the two-source isotopic model as C3 plants (forest site) and C4 plants (pasture site).

## Sample Processing

Immediately after sampling, samples were filtered through pre-combusted GF/F filters (Whatman, nominal pore size 0.7 μm). After filtration, samples were acidified with HCl (32%, analytical grade) to pH 2 and DOM was isolated from the water samples via solid-phase extraction (SPE; Dittmar et al., 2008). In brief, filtered and acidified samples were passed by gravity through solid-phase cartridges (1 g PPL, Agilent). The cartridges were desalted with 0.01 mol $L^{-1}$ HCl, dried with a stream of $N_2$, and DOM was eluted with 8 mL of methanol (HPLC grade). The DOC extraction efficiency was determined for each sample by evaporating an aliquot of the methanol extract to dryness, re-dissolving it in ultrapure water at pH 2, and relating the DOC concentration of this solution to that of the original sample. On average among all samples ($n = 177$), 45% (SE ± 13%) of DOC was recovered by the SPE. Extraction efficiency did not systematically vary along the river and along the salinity gradient. Soil samples were freeze-dried and the fraction >2.0 mm removed by sieving.

## Dissolved Organic Carbon and Stable Carbon Isotope Determination

The concentration of DOC in filtered samples was determined by the high-temperature catalytic oxidation method on an automated TOC analyzer (Shimadzu TOC 5000), using five calibration solutions spanning the concentration range of the samples. All DOC data reported are the mean of three replicate injections, for which the coefficient of variance was <5%. Procedural blanks, including the filtration step, were obtained using ultrapure water. These blank samples did not contain any detectable amounts of DOC. The detection limit for DOC was 5 μM, and the analytical accuracy (relative to the reference material) and precision (replicate injections) were within ± 1 μM. The deep sea reference material provided by D. Hansell (University of Miami, USA) was repeatedly analyzed in each run to control accuracy.

The stable carbon isotope composition of SPE-DOM was determined following an established protocol (Seidel et al., 2015). In brief, an aliquot of 800–1600 μL of SPE-DOM extract, corresponding to ∼20 μg of SPE-DOC, was dried under $N_2$ flux. Then, it was re-dissolved in 50 μL of methanol, transferred into Sn combustion capsules (Elemental) and dried in an oven at 60°C for 24 h. Soil samples were weighed (10 mg) in Sn combustion capsules (Elemental). The isotopic composition was analyzed on an elemental analyzer (Flash 2000) coupled to an isotope-ratio mass spectrometer Delta V Advantage (Thermo Scientific, Germany). Stable carbon isotope ratio is expressed as $\delta^{13}C$ (%) relative to the Pee Dee Belemnite (PDB) standard reference.

## Dissolved Black Carbon

The benzenepolycarboxylic acids (BPCAs) method (Dittmar, 2008) was used to quantify the condensed polyaromatic fraction of DBC. This method is the most sensitive and unequivocal method for the determination of BC in fluvial and marine DOM (Dittmar et al., 2012b). Moreover, the proportions of the different detectable BPCAs are indicative of the extent of condensation and size of the polycyclic aromatics. For example, char produced at 1000°C is typically highly condensed and BPCAs released by nitric acid oxidation are basically composed of benzenehexacarboxylic acid. Charcoal produced at 200°C is characterized by a low number of condensed aromatic rings, and BPCAs are less carboxylated compared to high-temperature chars (Schneider et al., 2010). For BPCA analysis, 300–500 μL of the methanol extracts, corresponding to 1–10 μmol of SPE-DOC, were transferred into 2 mL glass ampoules, evaporated to dryness in an oven at 60°C and dissolved in 0.5 mL of concentrated $HNO_3$ (65%). The ampoules were flame sealed, placed in a stainless-steel pressure bomb and kept for 9 h at 170°C in a furnace. After the ampoules had cooled, the $HNO_3$ was evaporated to dryness in a speed vacuum centrifuge (60°C, Christ RV2-18). Samples were dissolved in 100 μL of phosphate buffer at pH 7.2 ($Na_2HPO_4$ and $NaH_2PO_4$, each 0.5 mM) and analyzed on an ultrahigh performance liquid chromatography system (Waters Acquity UPLC), equipped with a photodiode array light-absorbance detector. BPCAs were identified in accordance to retention time and absorbance spectra (220–380 mm). Quantification was performed using the absorbance signal at 240 mm and an external calibration. The injection volume was 1 μl. BPCA concentrations were converted into DBC concentrations after the equation of Dittmar (2008), with the slight modification outlined in Stubbins et al. (2015), where the most robustly quantified B6CA and B5CA are used for estimating DBC. For the equations we refer to Stubbins et al. (2015).

## Two Source Isotopic Model

To estimate the contribution of $C_4$ plant derived organic matter to PSR and tributaries DOM, we used a linear two-source mixing model (Martinelli et al., 2002):

$$C4(\%) = \frac{\delta^{13}C_{sample} - \delta^{13}C_{C3\ soil}}{\delta^{13}C_{C4\ soil} - \delta^{13}C_{C3\ soil}} \text{ X } 100 \quad (1)$$

where $\delta^{13}C_{sample}$ is the isotopic composition of SPE-DOM in a given sample, $\delta^{13}C_{C3soil}$ (−29.4 ± 0.4%) is the isotopic composition of the forest soil and $\delta^{13}C_{C4soil}$ (−14.9 ± 0.3%) is the isotopic composition of the pasture soil. An underlying assumption of our calculations is that there are only two main sources of SPE-DOM. Other sources, like sewage or autochthonous production by algae reduce the accuracy of our calculations. Also isotope fractionation during DOM decomposition is not considered in our model.

## Hydrological and Conservative Mixing Models

Daily water discharge data are available for the lower reach of PSR, at the city of Campos dos Goytacazes. We used

electric conductivity as a tracer to backwards calculate the water discharge of the tributaries and at each sampling point of PSR. Electrical conductivity was determined *in situ* with a WTW portable probe calibrated directly before each measurement. Under the reasonable assumption that electrical conductivity behaves conservatively during mixing, the relative proportion of water discharge of a tributary and the mainstream before and after the effluent was calculated, based on the principles of mass conservation:

$$Q_{after} = Q_{before} + Q_{tributary} \quad (2)$$

$$\sigma_{after} \cdot Q_{after} = \sigma_{before} \cdot Q_{before} + \sigma_{tributary} \cdot Q_{tributary} \quad (3)$$

Q is the water discharge after the tributary ($Q_{after}$), before the tributary ($Q_{before}$), and of the tributary ($Q_{tributary}$); and σ is the electrical conductivity at the respective position. For example, the water discharge in Campos dos Goytacazes ($Q_{after}$) was 1875 $m^3\ s^{-1}$ in January 2013 and $\sigma_{after}$ at that site was 65 $\mu S\ cm^{-1}$. From the electrical conductivity of the next upstream tributary ($\sigma_{tributary}$; 73 $\mu S\ cm^{-1}$) and the river sample before the tributary ($\sigma_{before}$; 59 $\mu S\ cm^{-1}$), we calculated a water discharge of 803 $m^3\ s^{-1}$ from the tributary and 1071 $m^3\ s^{-1}$ from the PSR upstream the tributary. Loss of water (e.g., through evaporation) and unknown sources of water (e.g., groundwater inputs) are sources of errors in this model.

As a second step we calculated the respective fluxes of DBC ($F_{DBC}$) as water discharge multiplied by DBC concentration ($c_{DBC}$) at each site.

$$F_{DBC} = Q \cdot c_{DBC} \quad (4)$$

DBC fluxes were then compared to the theoretical DBC fluxes for ideal conservative behavior at each site. Deviations of the measured fluxes from these conservative fluxes indicate additional source and sink terms along the river. Conservative fluxes were calculated on the assumption that DBC behaves like electrical conductivity in the conservative case. Consequently, the theoretical, conservative DBC flux at a given station is the DBC flux of the uppermost station in PSR, plus the additive flux of each tributary upstream of a given station:

$$F_{DBC,\ conservative} = F_{DBC,\ uppermost\ station} + \Sigma F_{DBC,\ all\ tributaries\ upstream} \quad (5)$$

The theoretical, conservative DBC concentration ($c_{DBC,\ conservative}$) at each station is:

$$c_{DBC,\ conservative} = F_{DBC,\ conservative}/Q \quad (6)$$

Similar calculations were done for the estuary. The proportion of freshwater ($\%_{fresh}$) and seawater ($\%_{sea}$) in each estuarine sample was calculated from electrical conductivity. We considered the samples taken in PSR in Campos dos Goytaczes (freshwater) and the outermost marine station (seawater) as endmembers for these calculations. Based on the principles of mass conservation:

$$c_{DBC,\ conservative} = {}_{fresh(\%)} \cdot c_{DBC,\ fresh} + {}_{sea(\%)} \cdot c_{DBC,\ sea} \quad (7)$$

$c_{DBC,fresh}$ and $c_{DBC,sea}$ are the DBC concentrations of the endmembers.

In the conservative case, the freshwater flux of DBC throughout the entire estuary is equal to the DBC flux in the lowermost riverine station:

$$F_{DBC,\ conservative} = F_{fresh} \quad (8)$$

The real flux of freshwater-derived DBC in the estuary is approximated from the deviations of DBC concentration from conservative mixing:

$$F_{DBC} = c_{DBC}/c_{DBC,\ conservative} \cdot F_{fresh} \quad (9)$$

## RESULTS

DOC and DBC concentrations were highly variable between sites and seasons in the main stem of the river, the tributaries, and the estuary. The DOC concentration in the PSR system ranged between 168 and 894 $\mu mol\ L^{-1}$ in riverine samples, 72–529 $\mu mol\ L^{-1}$ in estuarine samples and 143–1381 $\mu mol\ L^{-1}$ in tributaries (**Figure 2A**, Tables S1–S3). Riverine and estuarine DOC concentrations were distinctly higher during the wet season of 2013, while during the dry season of 2013 and the wet season of 2014 DOC concentrations were lower (Student's *t*-test, $p < 0.01$, **Figure 2A**, Tables S1–S3). In contrast, DOC concentrations in the tributaries were not significantly different between both wet seasons, but differed between wet and dry seasons (Student's *t*-test, $p < 0.05$, **Figure 2A**, Tables S1–S3). DOC concentrations in the estuary decreased with distance offshore. In all the sampling periods, DOC concentrations slightly deviated from conservative mixing in the river and estuary (**Figure 2A**), but the resulting DBC fluxes were not significantly different from those calculated from the conservative mixing model. The stable carbon isotopic composition ($\delta^{13}C$) of SPE-DOM ranged between −29.0 and −23.5% in the main stem of PSR, and from −28.0 to −21.3% in the tributaries. In the estuary, $\delta^{13}C$ increased from a minimum of −25.7% inshore to −20.0% in the marine endmember offshore (**Figure 2B**, Tables S1–S3). Riverine and estuarine $\delta^{13}C$ were more depleted (more negative $\delta^{13}C$ values) in the wet season of 2013 (Student's *t*-test, $p < 0.05$, **Figure 2B**), followed by the wet season of 2014 and finally of dry season of 2013 (Student's *t*-test, $p < 0.05$, **Figure 2B**). The $\delta^{13}C$ of forest soil sample was $-29.4 \pm 0.4\%$ whilst it was $-14.9 \pm 0.3\%$ for the pasture soil sample.

DBC concentrations in PSR ranged between 5 and 35 $\mu mol\ L^{-1}$, with significantly higher values during the wet season of 2013 compared to the other sampling campaigns (Student's *t*-test, $p < 0.01$, **Figure 2C**, Table S1). DBC concentrations in the tributaries ranged from 3 to 26 $\mu mol\ L^{-1}$, and were similar in both wet seasons, but distinctly different between wet and dry seasons (Student's *t*-test, $p < 0.01$, **Figure 2C**, Table S2). Estuarine DBC concentrations ranged from 0.3 to 17 $\mu mol\ L^{-1}$, strongly decreasing from in- to offshore; they were similar in both wet seasons, and distinctly different between wet and dry seasons (Student's *t*-test, $p < 0.01$, **Figure 2C**, Table S3). The concentration ratio of benzenehexa- to benzenepentacarboxylic acids (B6CA/B5CA) in PSR ranged between 0.27 and 0.36, in the

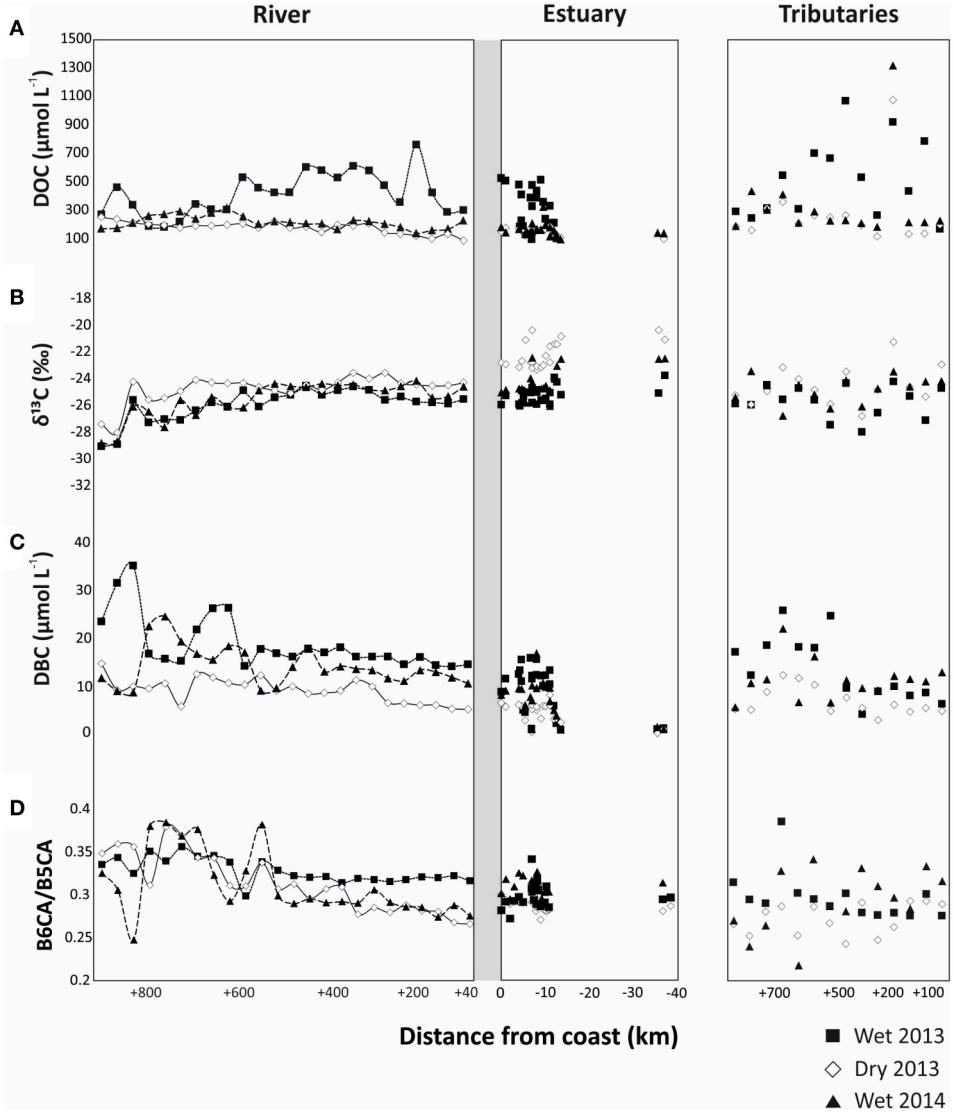


**FIGURE 2 | Spatial distributions of (A)** DOC concentrations, **(B)** $\delta^{13}C$ of SPE-DOC, **(C)** DBC concentrations, and **(D)** B6CA/B5CA ratio in the river, estuary and tributaries of Paraíba do Sul during the different sampling seasons.

tributaries between 0.22 and 0.34 and in the estuary between 0.27 and 0.34 (**Figure 2D**, Tables S1–S3), with a decreasing trend from in- to offshore.

# DISCUSSION

## The Source of DBC

The PSR catchment area was once covered by Atlantic forest. Due to almost complete destruction via the slash-and-burn practice until the mid-1970's large amounts of charcoal had been deposited in the soils of the catchment. DBC is slowly released when charcoal ages in soils (Ding et al., 2013). Simultaneous microbial oxidation of soil organic matter and charcoal likely results in a strong relationship between DOC and DBC concentrations in the rivers draining the area (Ding et al., 2013). Consistent with this concept, statistically significant correlations between DBC and DOC concentrations were observed for PSR, tributaries, and estuary (**Figure 3**). Similar relationships were previously found in intertidal systems (Dittmar et al., 2012b), intermittent grassland streams (Ding et al., 2013), and fluvial systems (Dittmar et al., 2012a; Jaffé et al., 2013; Stubbins et al., 2015). In our study, the slope of the resulting regressions indicated that the DOC pool in the river contained 12.2% of DBC, followed by the estuary with 11.8% and the tributaries with 10.5%, which is close to the previously reported global riverine average (Jaffé et al., 2013).

It was proposed that DBC in PSR is largely derived from historic charcoal deposits in the soils, and only to a minor degree from today's fire-management practice (Dittmar et al., 2012a). The historic forest vegetation was composed mainly of C3 plants,

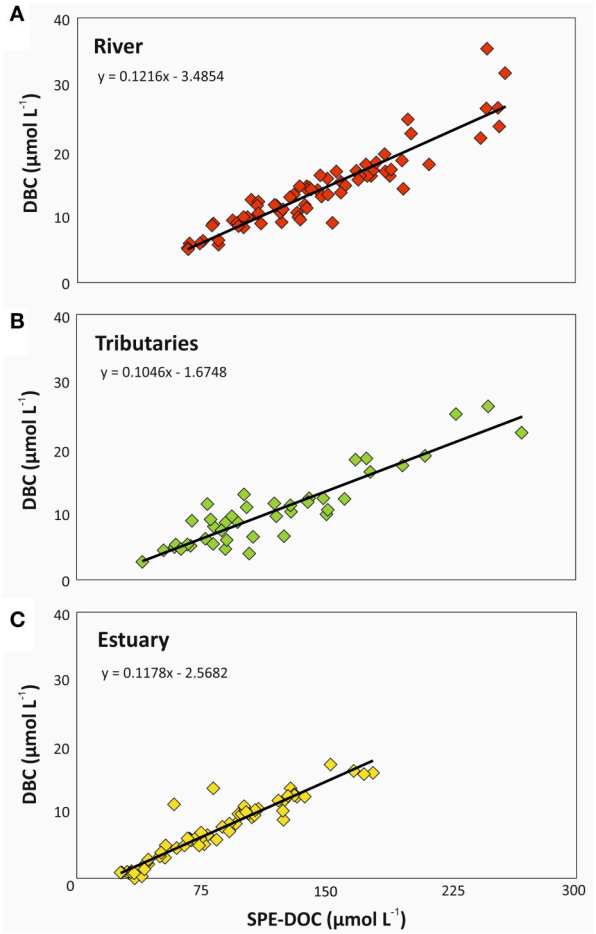


**FIGURE 3 | Geometric mean regression between SPE-DOC and DBC concentrations in (A)** Paraíba do Sul river, **(B)** tributaries, and **(C)** estuary.

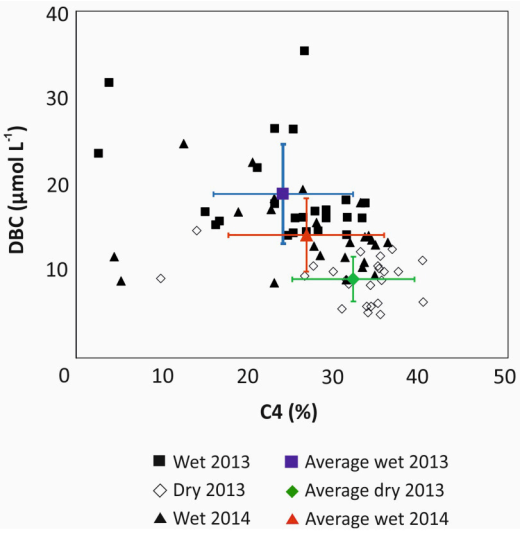


**FIGURE 4 | Relationship between the estimated percentage of C4-derived carbon in SPE-DOC (derived from $\delta^{13}C$) and DBC concentrations in Paraíba do Sul river and tributaries.**

while today's pastures and sugar cane plantations are dominated by C4 plants. DBC concentrations in the river system inversely correlated with the percentage of DOC that was derived from C4 plants (**Figure 4**; Figure S1). The higher the contribution of C3 plants the higher was the concentration of DBC in the river. The relationship between all samples presented a strong negative correlation ($r_s = -0.605$, $p < 0.001$, $n = 114$) indicating that historical fire events from Atlantic Forest represented a more important source of DBC to the river water today than recent burning activities.

The source of DOC shifted between the seasons and was consistent with DBC concentrations. During the rainy season, DBC concentrations were high, and the DOC was largely derived from historic carbon sources (C3) with more depleted $\delta^{13}C$ values. In the dry season, DBC concentration was lower and the contribution of today's vegetation (C4) was higher, with $\delta^{13}C$ values more enriched. The identification of C3 or C4 plants with carbon isotopic composition was possible due the marked differences in $\delta^{13}C$ values between each kind of plants. C3 plants have $\delta^{13}C$ values depleted close to −31%, while C4 plants have $\delta^{13}C$ values less depleted close to −14% (Kruche et al., 2002). This observation is probably a reflection of water flow paths. During the rainy season, upper soil horizons, where most (historic) charcoal deposits are flushed. Deeper groundwater that fuels the river during base flow seems to be less influenced by soil-derived DOM. In accordance, in the Amazon Forest, the upper soil horizons (upper 60 cm) contain higher amounts of BC and char than deeper horizons (Glaser et al., 2001). The char in soil in the Amazon had an apparent radiocarbon age of 1775 ± 325 years (Glaser et al., 2001), indicating a long residence time of char in tropical soils. In addition, enhanced *in-situ* production by algae during the dry season caused by deeper light penetration should be taken into account. Algae are potentially another source of isotopically heavy and DBC-poor DOC to the river. Nevertheless, the historic C3 vegetation is apparently the predominant source of bulk DOC and associated DBC to the river system.

## Processing of DBC in the River-to-Ocean Continuum

In the headwaters-to-ocean continuum of PSR, the DBC concentrations varied over one order of magnitude. Within the main river, the DBC concentrations matched those reported earlier for PSR in Campos dos Goytacazes (Dittmar et al., 2012a), and are within the range of global rivers (Jaffé et al., 2013) and coastal wetlands (Dittmar et al., 2012b; Ding et al., 2014). The much lower concentrations offshore are consistent with the low DBC concentrations reported for the sea surface in the Gulf of Mexico (Dittmar, 2008) and the Southern Indian Ocean (Dittmar and Paeng, 2009).

To identify potential sources and sinks along the PSR and estuary we compare the observed trends with those expected from conservative mixing, i.e., a scenario in which DBC has salt-like characteristics in the headwater-to-ocean continuum. In all sampling campaigns a cumulative net-removal of DBC was

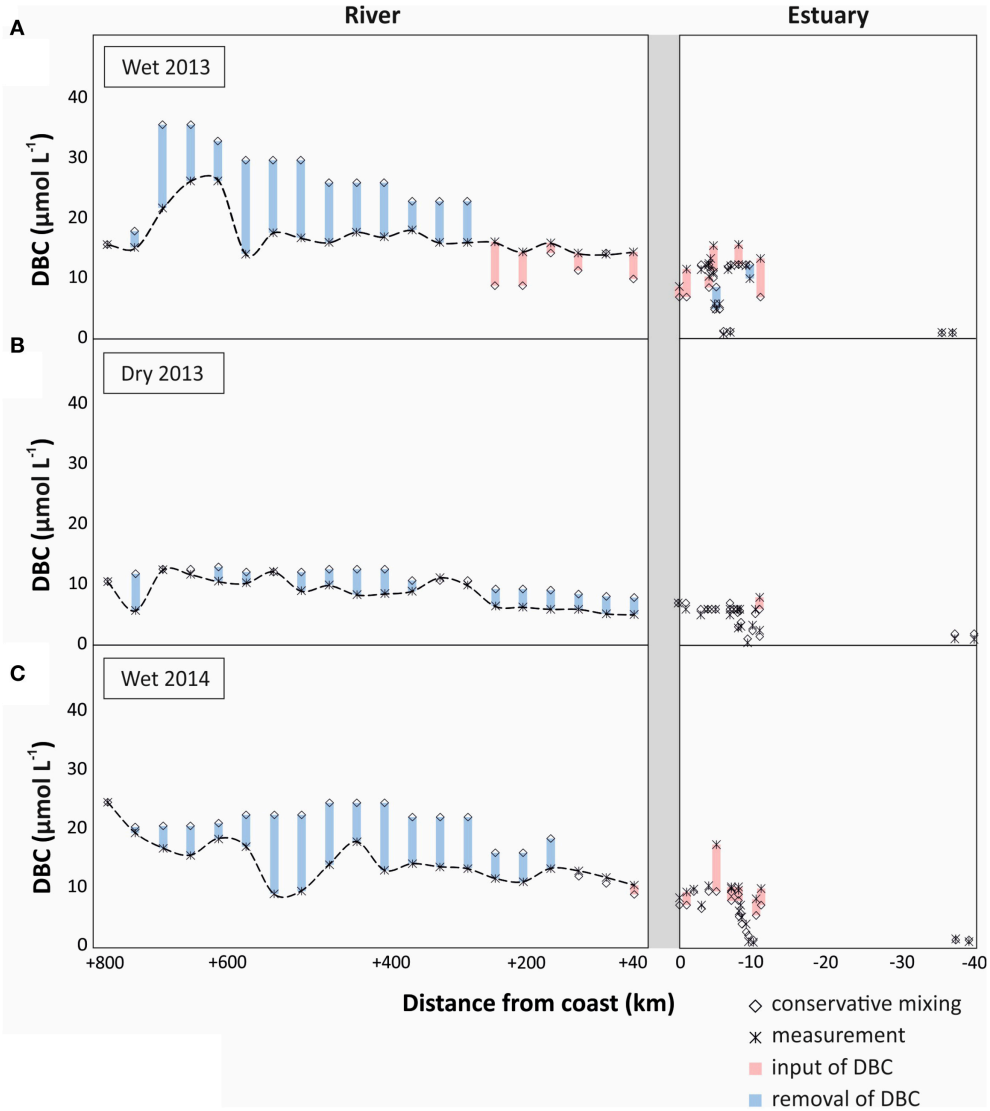


**FIGURE 5 | DBC concentration along the headwaters-to-ocean continuum of Paraíba do Sul (measured concentration and conservative mixing model), indicating potential inputs of DBC (in red; real measurement > conservative mixing model value) and potential sinks of DBC (in blue; conservative mixing model value > real measurement). (A)** wet season 2013, **(B)** dry season 2013, and **(C)** wet season 2014.

observed from the headwaters down to the lower reaches of the riverine system (300 km inland, **Figure 5**). This apparent non-conservative behavior of DBC was restricted to few sites and the introduced deviation propagated downstream. An apparent net-removal of DBC persisted all the way to the estuary in the dry season of 2013, but was counteracted or even outbalanced by inputs of DBC in the lower reaches of the river during the wet seasons. In the estuary, a net-input was observed in both rainy seasons; in the dry season, DBC mixed conservatively in the estuary and inner shelf. Overall, the slight deviations of DBC concentration from the conservative mixing model had comparatively little effect on DBC fluxes in the rivers system that were dominated by the large discharge of few tributaries in the lower reaches of PSR (**Figure 6**).

In principle, two explanations can be put forward for a non-conservative behavior of DBC in the river-to-ocean continuum. First, unknown sources of water with different DBC to conductivity ratios than the sampled tributaries introduce errors in our mass balance calculations. Deep groundwater is generally poor in DBC (Dittmar et al., 2012a; Stubbins et al., 2015). With increased rainfall, the hydrological pathway also incorporates active soil layers that are rich in organic compounds and charcoal (Guggenberger et al., 2008; Stubbins et al., 2015). At base flow during the dry season, deep groundwater is the main source of water to PSR and the DBC concentrations are consequently lower than during the rainy season when upper soil horizons are flushed (Dittmar et al., 2012a). Lateral input of groundwater into the tributaries is indirectly considered in our

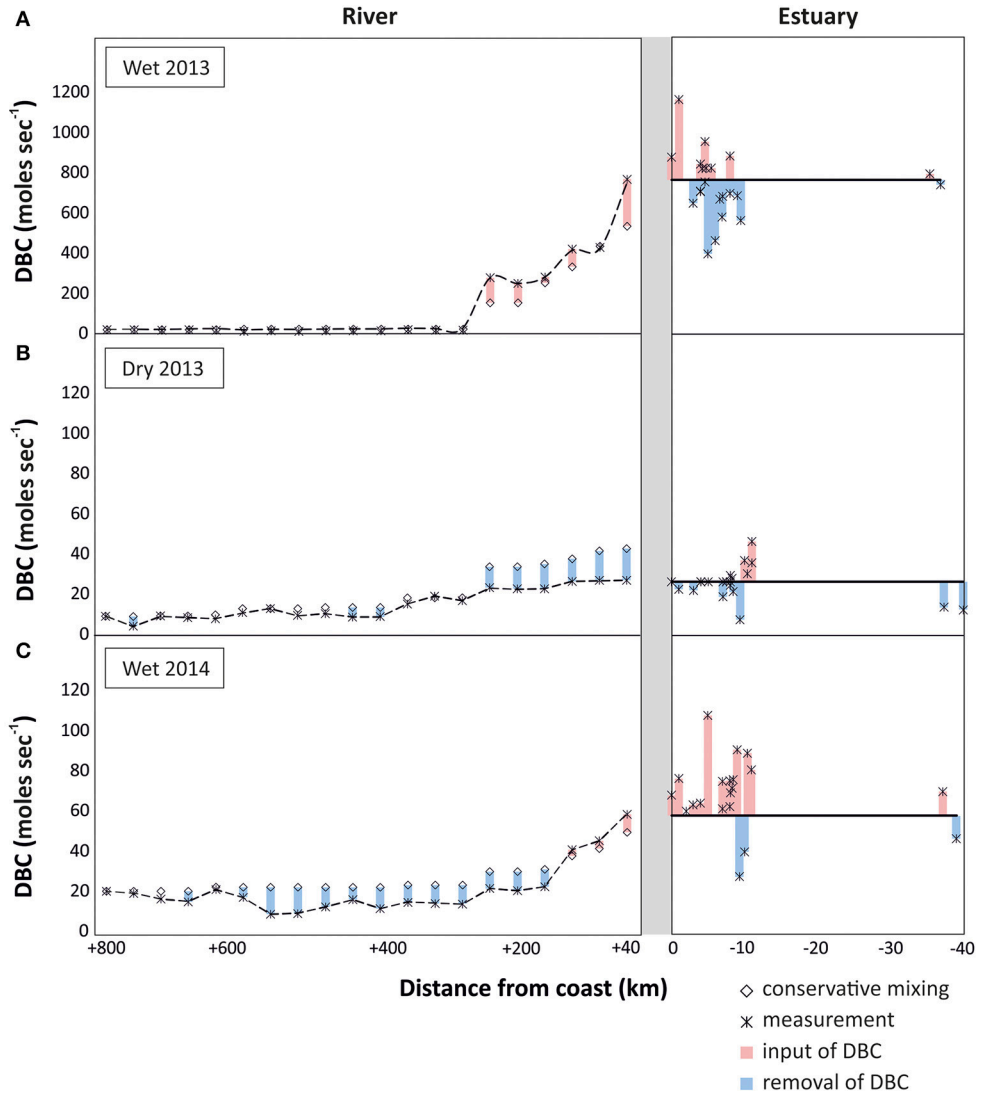


**FIGURE 6 | Flux of DBC (moles $s^{-1}$) in the headwaters-to-ocean continuum of Paraíba do Sul system, indicating potential inputs of DBC (in red; real measurement > conservative mixing model value) and potential sinks of DBC (in blue; conservative mixing model value > real measurement), for the different sampled seasons: (A)** wet season 2013, **(B)** dry season 2013, and **(C)** wet season 2014. Note different scales for DBC fluxes.

mass balance model, but direct inputs of groundwater into the main stem not. Depending on the source of groundwater, these undetected inputs may cause net-inputs from upper soil horizons (rainy seasons) or an apparent net-removal due to dilution with deep groundwater (dry season). Because we observed an overall consistent pattern of net-removal of DBC during wet and dry seasons we consider methodological artifacts as an unlikely reason for the observed net-removal. About 23–40% of DBC was lost along the transect from river to estuary during the various seasons.

DBC consists of condensed organic compounds, and is thus sensible to photooxidation (Stubbins et al., 2008; Spencer et al., 2009). This could be an important sink for DBC in the riverine system, and explain the observed net-removal. One way to assess whether photooxidation indeed occurred is provided by changes of the B6CA/B5CA ratio. Benzenehexacarboxylic acid (B6CA) is indicative of highly condensed aromatics, whereas benzenepolycarboxylic acids with a lower number of carboxylic substitutes are indicative of molecules with a lower number of condensed rings in their core structure (Schneider et al., 2010). Thus, the B6CA/B5CA ratio was proposed as a measure for the degree of condensation of DBC (Stubbins et al., 2012). Highly condensed structures are preferentially degraded by irradiation, and 28 days of exposure to sunlight of North Atlantic Deep Water caused a decrease of B6CA/B5CA from 0.32 to 0.23 (Stubbins et al., 2012). Similarly in our study, apparent loss of DBC was associated with a decrease of B6CA/B5CA (**Figure 2D**). In the dry season of 2013 and the wet season of 2014, the B6CA/B5CA

ratio decreased from 0.38 to 0.27 along the river, which is a clear indication for photodegradation. In the wet season of 2013, the change in B6CA/B5CA was not as pronounced, as there was a net-input of DBC in the lower reaches of the river. In the lower reaches of PSR and next to the estuary, there are extensive fire-managed sugar cane plantations located in direct vicinity of the estuary. These areas of sugar cane plantations have been managed since 1538 (Oscar, 1985). It is plausible that lateral inputs from these areas especially during the rainy season caused the observed net-inputs in the corresponding areas. DBC from upper soil horizons has not been exposed to sunlight yet, which is consistent with the relatively high B6CA/B5CA in the respective area and season. Furthermore, during the wet season of 2013, the load of suspended particles in the river was almost one order of magnitude higher than during the other campaigns at station Campos dos Goytacazes (120 mg $L^{-1}$, compared to 15 mg $L^{-1}$, unpublished data). Particles shade the water and reduce photodegradation. In addition, DBC may desorb from the particles thereby contributing to the apparent net-input of DBC in the lower reaches of the river during the rainy season of 2013.

In the rainy seasons, DBC concentrations were higher than during the dry season. In conjunction with the higher water discharge, DBC fluxes were even more enhanced during the rainy seasons (**Figure 6**). This cumulative effect of higher DBC concentration and higher water discharge was most pronounced during the wet season of 2013. During this campaign water discharge was more than one order of magnitude higher at the lowest reaches of PSR compared to the other sampling campaigns, resulting in correspondingly high fluxes of DBC from the river to the ocean. The flux of DBC fluctuated in the estuary, but there was no indication for net-removal of DBC. Fluctuations are likely due to spatial heterogeneity of DBC concentration and local inputs from resuspended sediments, tidal creeks and groundwater discharge. Overall, it appears that a large fraction of the DBC survived transport through the estuary and onto the inner shelf, and possibly over larger scales in the ocean.

## CONCLUSIONS

This study presents the first data about the DBC spatial and seasonal behavior in a tropical basin. As model system, we chose the Paraíba do Sul system (Brazil), the only river system for which long-term DBC flux data exist. Our study indicates that hydrology plays an important role in DBC dissolution and migration, with highest DBC concentrations in the wet season and lowest in the dry season. This relationship suggests that DBC is mainly mobilized from the upper soil horizons during heavy rainfalls. Therefore, lateral transport to the ocean seems to be an important removal mechanism for BC in soils. A direct relationship between DOC and DBC concentrations was observed, indicating fire-altered carbon as an intrinsic component of the DOC pool. The similarities in the mechanisms of DOC and DBC stabilization and loss, suggested that DOC may contribute to the mobilization of soil BC to the aquatic systems. In addition, a statistically significant relationship between DBC and $\delta^{13}$C-SPE-DOC is consistent with previous literature suggestion (Dittmar et al., 2012a), that DBC in the PSR system is derived from aged charcoal, produced during the Atlantic forest destruction and historically accumulated in soils. Future studies should be directed toward compound-specific carbon isotope analysis on BPCAs to unambiguously confirm the source and age of DBC.

A simple mixing model could largely reproduce the observed DBC fluxes within the catchment and the headwaters-to-ocean continuum. Photooxidation likely removed some DBC along the course of the river-to-ocean-continuum. High water discharge and increased DBC concentrations had a cumulative effect on DBC flux during the rainy seasons. We found no evidence for net DBC removal in the estuary or inner shelf, thus large-scale transport in the ocean is likely. Anticipated temperature increase and changes in the water cycle may result in an increase of fire frequency. As global climate change effects promote extreme dry and wet seasons, the DBC export may increase proportionally and alter the size of the refractory DOM pool in the deep ocean.

## AUTHOR CONTRIBUTIONS

All authors contributed to the design of the study. JM and MA analyzed samples for stable carbon isotopic composition. JM and JN analyzed samples for dissolved black carbon. TD, CR, and JM conducted modeling studies. All authors contributed to data interpretation and writing of the manuscript. JM and GG built the figures.

## FUNDING

INCT-TMCOcean on the Continent-Ocean Materials Transfer (CNPq: 573.601/08-9). CR received financial support from CNPq (506.750/2013-2) and FAPERJ (E-26/111.616/2011 and E-26/201.188/2014). The Science without Border (CNPq CSF 400.963/2012-4) provided financial support for JM 1 year in a sandwich program at the University of Oldenburg; MA 1 year of Post Doctor position in Environmental Sciences Laboratory (UENF) and TD 3 months as a Visiting Professor at Universidade Estadual do Norte Fluminense.

## ACKNOWLEDGMENTS

The authors are grateful to the *Laboratório de Ciências Ambientais* of the *Centro de Biociências e Biotecnologia* at the *Universidade Estadual do Norte Fluminense* and the University of Oldenburg Research Group for Marine Geochemistry (ICBM—MPI Bridging Group), Institute for Chemistry and Biology of the Marine Environment (ICBM) for the use of its facilities. We thank Thiago Rangel, Diogo Quitete for sampling assistance and Ina Ulber and Matthias Friebe for assistance in the lab.

## SUPPLEMENTARY MATERIAL

The Supplementary Material for this article can be found online at: http://journal.frontiersin.org/article/10.3389/feart.2017.00011/full#supplementary-material

## REFERENCES


Abiven, S., Hengartner, P., Schneider, M. P. W., Singh, N., and Schmidt, M. W. I. (2011). Pyrogenic carbon soluble fraction is larger and more aromatic in aged charcoal than in fresh charcoal. *Soil Biol. Biochem.* 43, 1615–1617. doi: 10.1016/j.soilbio.2011.03.027

Cheng, C. H., and Lehmann, J. (2009). Ageing of black carbon along a temperature gradient. *Chemosphere* 75, 1021–1027. doi: 10.1016/j.chemosphere.2009.01.045

Ding, Y., Cawlley, K. M., Cunha, C. N., and Jaffé, R. (2014). Environmental dynamics of dissolved black carbon in wetlands. *Biogeochemistry* 119, 259–273. doi: 10.1007/s10533-014-9964-3

Ding, Y., Yamashita, Y., Dodds, W. K., and Jaffé, R. (2013). Dissolved black carbon in grassland streams: is there an effect of recent fire history? *Chemosphere* 90, 2557–2562. doi: 10.1016/j.chemosphere.2012.10.098

Dittmar, T. (2008). The molecular level determination of black carbon in marine dissolved organic matter. *Organ. Geochem.* 39, 396–407. doi: 10.1016/j.orggeochem.2008.01.015

Dittmar, T., and Koch, B. P. (2006). Thermogenic organic matter dissolved in the abyssal ocean. *Mar. Chem.* 102, 208–217. doi: 10.1016/j.marchem.2006.04.003

Dittmar, T., Koch, B., Hertkorn, N., and Kattner, G. (2008). A simple and efficient method for the solid-phase extraction of dissolved organic matter (SPE-DOM) from seawater. *Limnol. Oceanogr. Methods* 6, 230–235. doi: 10.4319/lom.2008.6.230

Dittmar, T., and Paeng, J. (2009). A heat-induced molecular signature in marine dissolved organic matter. *Nat. Geosci.* 2, 175–179. doi: 10.1038/ngeo440

Dittmar, T., Paeng, J., Gihring, T. M., Suryaputra, I. G. N. A., and Huettel, M. (2012b). Discharge of dissolved black carbon from a fire-affected intertidal system. *Limnol. Oceanogr.* 57, 1171–1181. doi: 10.4319/lo.2012.57.4.1171

Dittmar, T., Rezende, C. E., Manecki, M., Niggemann, J., Ovalle, A. R. C., Stubbis, A., et al. (2012a). Continuous flux of dissolved black carbon from a vanished tropical forest biome. *Nat. Geosci.* 5, 618–622. doi: 10.1038/ngeo1541

Forbes, M. S., Raison, R. J., and Skjemstad, J. O. (2006). Formation, transformation and transport of black carbon (charcoal) in terrestrial and aquatic ecosystems. *Sci. Total Environ.* 370, 190–206. doi: 10.1016/j.scitotenv.2006.06.007

Fundação SOS Mata Atlântica and Instituto Nacional de Pesquisas Espaciais (2011). *Atlas dos Remansecentes Florestais da Mata Atlântica*, *Período 2008–2010.*

Glaser, B., Haumaier, L., and Guggenberger, G., Zech, W. (2001). The 'Terra Preta' phenomenon: a model for sustainable agriculture in the humid tropics. *Naturwissenschaffen* 88, 37–41. doi: 10.1007/s001140000193

Guggenberger, G., Rodionov, A., Shibistova, O., Grabe, M., Kasansky, O., Fuchs, H., et al. (2008). Storage and mobility of black carbon in permafrost soils of the forest tundra ecotone in Northern Siberia. *Glob. Change Biol.* 14, 1397–1381. doi: 10.1111/j.1365-2486.2008.01568.x

Hammes, K., Schmidt, M. W. I., Smernik, R. J., Currie, L. A., Ball, W. P., Nguyen, T. H., et al. (2007). Comparison of quantification methods to measure fire-derived (black/elemental) carbon in soils and sediments using reference materials from soil, water, sediment and the atmosphere. *Glob. Biogeochem. Cycles* 21:GB3016. doi: 10.1029/2006GB002914

Jaffé, R., Ding, Y., Niggemann, J., Vähätalo, A. V., Stubbins, A., Spencer, R. G. M., et al. (2013). Global charcoal mobilization from soils via dissolution and riverine transport to the oceans. *Science* 340, 345–347. doi: 10.1126/science.1231476

Kim, S., Kaplan, L. A., Benner, R., and Hatcher, P. G. (2004). Hydrogen-deficient molecules in natural riverine water sample – evidence for existence of black carbon in DOM. *Mar. Chem.* 92, 225–234. doi: 10.1016/j.marchem.2004.06.042

Kruche, A. V., Martinelli, L. A., Victoria, R. L., Bernades, M. C., Camargo, P. B., Ballester, M. V., et al. (2002). Compositional of particulate and dissolved organic matter in a disturbed watershed of southeast Brazil (Piracicaba River basin). *Water Res.* 36, 2743–2752. doi: 10.1016/S0043-1354(01)00495-X

Lira, P. K., Tambosi, L. R., Ewers, R. M., and Metzger, J. P. (2012). Land-use and land-cover change in Atlantic Forest landscapes. *Forest Ecol. Manage.* 15, 80–89. doi: 10.1016/j.foreco.2012.05.008

Major, J., Lehmann, J., Rondon, M., and Goodale, C. (2010). Fate of soil-applied black carbon: downward migration, leaching and soil respiration. *Glob. Change Biol.* 16, 1366–1379. doi: 10.1111/j.1365-2486.2009.02044.x

Mannino, A., and Harvey, H. R. (2004). Black carbon in estuarine and coastal ocean dissolved organic matter. *Limnol. Oceanogr.* 49, 735–740. doi: 10.4319/lo.2004.49.3.0735

Martinelli, L. A., Camargo, P. B., Lara, L. B. L. S., Victoria, R. L., and Artaxo, P. (2002). Stable carbon and nitrogen isotopic composition of bulk aerosol particles in a C4 landscape of southeast Brazil. *Atmos. Environ.* 36, 2427–2432. doi: 10.1016/S1352-2310(01)00454-X

Oscar, J. (1985). *Escravidão and Engenhos*: *Campos, São João da Barra, Macaé, e São Fidélis*. Rio de Janeiro: Rio de Janeiro Achiame.

Ovalle, A. R. C., Silva, C. F., Rezende, C. E., Gatts, C. E. N., Suzuki, M. S., and Figueiredo, R. O. (2013). Long-term trends in hydrochemistry in the Paraíba do Sul River, southeastern Brazil. *J. Hydrol.* 481, 191–203. doi: 10.1016/j.jhydrol.2012.12.036

Preston, C. M., and Schmidt, M. W. I. (2006). Black (pyrogenic) carbon in boreal forests: a synthesis of current knowledge and uncertainties. *Biogeosciences* 3, 211–271. doi: 10.5194/bg-3-397-2006

Ribeiro, M. C., Metzger, J. P., Martensen, A. C., Ponzoni, F. J., and Hirota, M. M. (2009). The Brazilian Atlantic Forest: how much is left, and how the remaining forest distributed? *Implications for conservation. Biol. Conserv.* 142, 1141–1153. doi: 10.1016/j.biocon.2009.02.021

Riedel, T., Zark, M., Vähätalo, A. V., Niggemann, J., Spencer, R. G. M., Hernes, P. J., et al. (2016). Molecular signatures of biogeochemical transformations in dissolved organic matter from ten World Rivers. *Front. Earth Sci.* 4:85. doi: 10.3389/feart.2016.00085

Santín, C., Doerr, S. H., Kane, E. S., Masiello, C. A., Ohlson, M., Rosa, J. M., et al. (2016). Towards a global assessment of pyrogenic carbon from vegetation fires. *Glob. Change Biol.* 22, 76–91. doi: 10.1111/gcb.12985

Schneider, M. P. W., Hilf, M., Vogt, U. F., and Schmidt, M. W. I. (2010). The benzene polycarboxylic acid (BPCA) pattern of wood pyrolyzed between 200 C° and 1000 C°. *Organ. Geochem.* 41, 1082–1088. doi: 10.1016/j.orggeochem.2010.07.001

Seidel, M., Yager, P. L., Ward, N. D., Carpenter, E. J., Gomes, H. R., Kruske, A. L., et al. (2015). Molecular-level changes of dissolved organic matter along the Amazon River-to-ocean continuum. *Mar. Chem.* 177, 218–231. doi: 10.1016/j.marchem.2015.06.019

Souza, T. A., Godoy, J. M., Godoy, M. L, Moreira, I., Carvalho, Z. L., Salomão, M. S., et al. (2010). Use of multitracers of the study of water mixing in the Paraíba do Sul River estuary. *J. Environ. Radioact.* 101, 564–570. doi: 10.1016/j.jenvrad.2009.11.001

Spencer, R. G. M., Stubbins, A., Hernes, P. J., Baker, A., Mopper, K., Aufdenkampe, A. K., et al. (2009). Photochemical degradation of dissolved organic matter and dissolved lignin phenols from the Congo River. *J. Geophys. Res.* 114:G03010. doi: 10.1029/2009jg000968

Stubbins, A., Hubbard, V., Uher, G., Law, C. S., Upstill-Goddard, R. C., et al. (2008). Relating carbon monoxide photoproduction to dissolved organic matter functionality. *Environ. Sci. Technol.* 42, 3271–3276. doi: 10.1021/es703014q

Stubbins, A., Niggemann, J., and Dittmar, T. (2012). Photo-lability of deep ocean dissolved black carbon. *Biogeosciences* 9, 1661–1670. doi: 10.5194/bg-9-1661-2012

Stubbins, A., Spencer, R. G. M., Mann, P. J., Holmes, R. M., McClelland, J. W., Niggemann, J., et al. (2015). Utilizing colored dissolved organic matter to derive dissolved black carbon export

by Artic Rivers. *Front. Earth Sci.* 3:63. doi: 10.3389/feart.2015.00063

Warren, D. (1995). *With Broadax and Firebrand. The Destruction of the Brazilian Atlantic forest*. California: University of California Press.

Ziolkowski, L. A., and Druffel, E. R. M. (2010). Aged black carbon identified in marine dissolved organic carbon. *Geophys. Res. Lett.* 37:L16601. doi: 10.1029/2010GL043963

**Conflict of Interest Statement:** The authors declare that the research was conducted in the absence of any commercial or financial relationships that could be construed as a potential conflict of interest.

The reviewer AC and handling Editor declared their shared affiliation, and the handling Editor states that the process nevertheless met the standards of a fair and objective review.

frontiers in Earth Science

ORIGINAL RESEARCH
published: 16 May 2017
doi: 10.3389/feart.2017.00034

# Distribution and Sources of Dissolved Black Carbon in Surface Waters of the Chukchi Sea, Bering Sea, and the North Pacific Ocean

*Motohiro Nakane*[1], *Taku Ajioka*[2†] *and Youhei Yamashita*[1,2*]

[1] Division of Earth System Science, Graduate School of Environmental Science, Hokkaido University, Sapporo, Japan,
[2] Faculty of Environmental Earth Science, Hokkaido University, Sapporo, Japan

OPEN ACCESS

**Edited by:**
Cristina Santin,
Swansea University, UK

**Reviewed by:**
Matthew William Jones,
University of Exeter, UK
Philippa Louise Ascough,
Scottish Universities Environmental Research Centre, UK

***Correspondence:**
Youhei Yamashita
yamashiy@ees.hokudai.ac.jp

**†Present Address:**
Taku Ajioka,
Geological Survey of Japan, National Institute of Advanced Industrial Science and Technology AIST, Tsukuba, Japan

**Specialty section:**
This article was submitted to Biogeoscience, a section of the journal Frontiers in Earth Science

**Received:** 09 March 2017
**Accepted:** 27 April 2017
**Published:** 16 May 2017

**Citation:**
Nakane M, Ajioka T and Yamashita Y (2017) Distribution and Sources of Dissolved Black Carbon in Surface Waters of the Chukchi Sea, Bering Sea, and the North Pacific Ocean. Front. Earth Sci. 5:34. doi: 10.3389/feart.2017.00034

Pyrogenic carbon, also called black carbon (BC), is an important component in the global carbon cycle. BC produced by biomass burning or fossil fuel combustion is transported to oceans by the atmosphere or rivers. However, environmental dynamics (i.e., major sources and sinks) of BC in marine environments have not been well-documented. In this study, dissolved BC (DBC) collected from surface waters of the Chukchi Sea, the Bering Sea, and the subarctic and subtropical North Pacific were analyzed using the benzene polycarboxylic acid (BPCA) method. The DBC concentration and the ratio of B5CA and B6CA to all BPCAs (an index of the DBC condensation degree) ranged from 4.8 to 15.5 $\mu$g-C $L^{-1}$ and from 0.20 to 0.43, respectively, in surface waters of the Chukchi/Bering Seas and the North Pacific Ocean. The concentration and condensation degree of DBC in the Chukchi/Bering Seas were higher and more variable than those in the subarctic and subtropical North Pacific, which implies that the major factors controlling DBC distribution were different in these marine provinces. In the Chukchi/Bering Seas, the DBC concentration was negatively correlated to salinity but positively correlated to chromophoric dissolved organic matter (CDOM) quantity and total dissolved lignin phenol concentration estimated by CDOM parameters. These correlations indicated that the possible major source of DBC in the Chukchi/Bering Seas was Arctic rivers. However, in the North Pacific, where riverine inputs are negligible for most sampling sites, DBC was possibly derived from the atmosphere. Although spectral slopes of CDOM at 275–295 nm (an index of the photodegradation degree of CDOM) differed widely between the subarctic and subtropical North Pacific, the concentration and condensation degrees of DBC were similar between the subarctic and subtropical North Pacific, which suggests that photodegradation was not the only major factor controlling DBC distribution. Therefore, DBC distributions of the North Pacific Ocean were considered to be mainly controlled by atmospheric deposition of BC and subsequent losses by photodegradation and adsorption onto sinking particles. This study implies that the main influence on DBC distribution in the open ocean and the coastal ocean are atmospheric deposition and fluvial inputs, respectively.

**Keywords: pyrogenic carbon, dissolved black carbon, surface waters, Chukchi Sea, Bering Sea, North Pacific**

## INTRODUCTION

Pyrogenic carbon (PyC), including soot, char, black carbon, and biochar, is produced by incomplete combustion of organic matter by biomass burning or fossil fuel combustion (Masiello, 2004). The physical and chemical characteristics of PyC vary widely and depend on formation temperature (Hedges et al., 2000; Masiello, 2004). Less aromatic PyC (e.g., char) produced at lower temperature is considered to be biologically degradable (Bruun et al., 2008); however, PyC produced at higher temperature forms more condensed polyaromatic compounds (e.g., soot and elemental carbon) and is considered to be stable in reduced carbon pools for at least thousands of years (e.g., Masiello and Druffel, 1998). Although the values are largely variable and depend on quantification methods, PyC content has been determined to be <1–60% (Preston and Schmidt, 2006) and generally 5–15% (Hockaday et al., 2007) of soil organic carbon and 2–50% of sedimentary organic carbon (Kuhlbusch, 1998). Recently, Reisser et al. (2016) generated a soil PyC database and found that global PyC represents 13.7% of the SOC on average and can even be up to 60%. Therefore, PyC has been considered an important potentially slow-cycling refractory component of the global carbon cycle, although the magnitude of key pools and fluxes in the global cycle of PyC remain poorly constrained (Kuhlbusch, 1998; Bird et al., 2015; Santín et al., 2016).

Recent studies have revealed occurrences of PyC in the dissolved organic matter (DOM) fraction, and such dissolved PyC has often been defined as dissolved black carbon (DBC) in aquatic environments (e.g., Dittmar, 2008; Jaffé et al., 2013). Fourier transform ion cyclotron resonance mass spectrometry (FT-ICR-MS) identified condensed aromatic ring structures in the DOM from soil pore water (Hockaday et al., 2006) and riverine water (Kim et al., 2004), indicating that a part of PyC in soils becomes water soluble during degradation and that the soluble fraction of PyC (DBC) in soil pore waters is exported to rivers (Hockaday et al., 2006, 2007).

To determine factors controlling riverine DBC concentrations and fluxes, spatial and temporal distributions of riverine DBC have been clarified from watersheds to global scales using benzene polycarboxylic acid (BPCA) methods. The method quantifies BPCAs produced through the oxidation of polyaromatic compounds in PyC (Dittmar, 2008). Dittmar et al. (2012a) determined the seasonal/annual variation of riverine DBC from 1997 to 2008 in tropical Atlantic forest watersheds that were extensively burned from the 1850s to 1973. They found that DBC continues to be mobilized from a watershed every year in rainy seasons, although widespread forest burning ceased more than 20 years ago. From the highest DBC concentrations in the wet season to the lowest in the dry season for the same river, Marques et al. (2017) indicated the important role of hydrology in DBC dissolution and migration. A strong linear correlation between DBC concentration and dissolved organic carbon (DOC) concentration has generally been found in rivers regardless of differences in watershed size or type or climatic provinces (Dittmar et al., 2012a,b; Ding et al., 2013, 2014, 2015; Wagner et al., 2015). It has recently been estimated that DBC contributes to the ∼10% of DOC in global rivers (Jaffé et al., 2013; Stubbins et al., 2015). The riverine DBC is finally transported to oceans (Mannino and Harvey, 2004; Masiello and Louchouarn, 2013; Huang et al., 2016), and the global flux was estimated to be 26.5 ± 1.8 million tons, which is of the same order of magnitude as the estimated range of the annual production of PyC from vegetation fires (Jaffé et al., 2013).

In marine environments, Dittmar and Koch (2006) used FT-ICR-MS and identified polyaromatic compounds with hydrophilic functional groups as DBC from DOM collected from the Southern Ocean. Using the BPCA method, the percentage of DBC in bulk marine DOM has been estimated to be 2.0–2.6% (Dittmar, 2008; Dittmar and Paeng, 2009; Coppola and Druffel, 2016), which is comparable to most chromatographically identifiable compounds (i.e., amino acids and neutral sugars) in marine DOM (Benner, 2002). Additionally, the apparent $^{14}C$ age of DBC was estimated to be 5,000–23,000 years (Ziolkowski and Druffel, 2010; Coppola and Druffel, 2016). These findings imply that DBC is likely a major fraction of refractory DOM in marine environments and is possibly important as a long-term carbon reservoir of the global carbon cycle.

Riverine and groundwater input (Dittmar et al., 2012a; Jaffé et al., 2013; Huang et al., 2016), atmospheric deposition (Jurado et al., 2008), and hydrothermal fluids (Dittmar and Koch, 2006; Dittmar and Paeng, 2009) have been proposed as possible sources of DBC in marine environments, whereas photodegradation (Stubbins et al., 2012) and adsorption onto sinking particles (Coppola et al., 2014) have been considered as potential sinks. However, because spatial and temporal distributions of DBC have scarcely been reported in marine environments (Dittmar and Paeng, 2009), the environmental dynamics (i.e., major sources and sinks) of marine DBC have not been well-documented, even in possible ranges of DBC concentration. Such knowledge is essential to evaluate not only the global PyC cycle but also the global carbon cycle. Therefore, distribution patterns of DBC in surface waters of the marginal seas (the Chukchi/Bering Seas) and the open ocean (the North Pacific Ocean) were determined in this study using the BPCA method to evaluate the range of DBC concentration and its controlling factors in the surface ocean. The major sources and possible loss processes are discussed from the geographical patterns of DBC, chromophoric DOM (CDOM, the UV, and visible light-absorbing constituent in DOM), and salinity.

## MATERIALS AND METHODS

### Sampling

Sampling locations with observed salinities are shown in **Figure 1**. Samplings of the Chukchi/Bering Seas and the subarctic North Pacific Ocean were carried out during two cruises in July 2013 by the T/S *Oshoro-Maru* (C255) and in July–August 2014 by the R/V *Hakuhou Maru* (KH-14-3). Samplings of the subtropical North Pacific Ocean were carried out at 10 sites in July 2016 during the R/V *Shinsei Maru* cruise (KS-16-9). Surface water samples ($n = 38$) were collected using a towed fish metal-free sampling system (1–3 m below the surface, Tsumune et al., 2005; Nishioka et al., 2011) or an underway pumping system (∼5 m

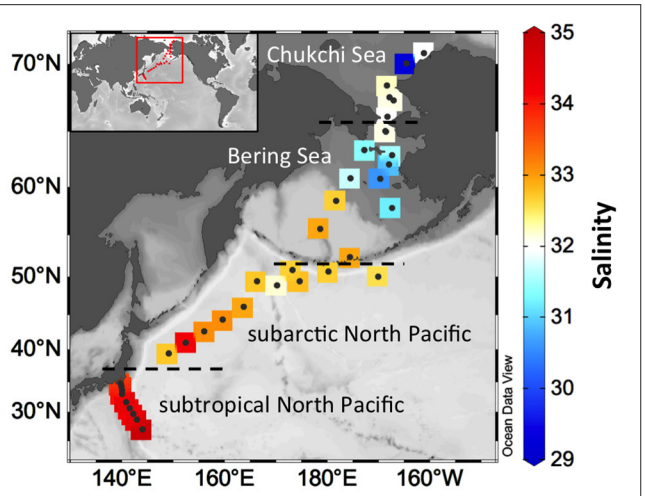


**FIGURE 1 | Map of the study area showing sampling sites with observed salinity.**

below the surface). Some samples ($n$ = 4 at 70.7°N/161.3°W, 70.1°N/164.6°W, 67.7°N/167.9°W, and 50.1°N/170.1°W) were collected at 5–10 m using a conductivity-temperature-depth (CTD) system equipped with Niskin bottles. A deep seawater sample was also collected at 2,000 m at the subarctic western North Pacific Ocean in March 2015 during the R/V *Hakuhou Maru* KH-15-1 cruise. The deep seawater DOM sample was used to examine the BPCA method under nitric oxidation conditions as mentioned below.

Approximately 6–9 L of seawater was collected for DBC analysis. Seawater samples were filtered using a pre-combusted (450°C, 3–5 h) Whatman GF/F filter (0.7 μm of nominal pore size), and the filtrate was then poured into a 9-L acid-washed polycarbonate bottle. The polycarbonate bottle was covered with a black plastic bag to avoid photodegradation of DBC during sampling. Immediately after sampling, the filtrate pH was adjusted to 2 by HCl and the acidified filtrate was immediately subjected to solid phase extraction, as discussed in Section Solid Phase Extraction.

Samples for DOM optical analysis were filtered using a pre-combusted GF/F filter (KH-14-3 and KS-16-9 cruises) or an acid-washed 0.22-μm filter (C255 cruise). The filtered seawater was poured into a pre-combusted glass vial with a Teflon-lined cap after triple rinsing and then stored frozen (−20°C) in the dark until analysis.

Temperature was determined with CTD sensors during all the cruises. Salinity was also determined with a CTD sensor during the KS-16-9 cruise but was determined with a salinometer (AUTOSAL8400B, Guildline Instruments, Smiths Falls, ON, Canada) during the KH-14-3 and C255 cruises.

## Solid Phase Extraction

A pre-concentration of DBC by solid phase extraction (SPE) was performed aboard a ship using the method of Dittmar (2008) with some modifications. The 6–9 L of acidified seawater was passed through an SPE cartridge (1 g, Bond Elut PPL, Agilent Technologies) pre-conditioned by two column volumes of methanol. After the passage of acidified seawater, the cartridge was rinsed by two-column volumes of 0.01 M HCl, wrapped with aluminum foil, placed inside a plastic bag, and then stored frozen (−20°C) in the dark. In a laboratory on land, the frozen SPE cartridge was thawed and then dried under an $N_2$ stream. Two-column volumes of methanol were passed through the cartridge to elute the organic compounds, including DBC adsorbed on the cartridge resins. The eluate was poured into a glass vial with a Teflon-lined cap pre-cleaned by methanol and then stored frozen (−20°C) in the dark until DBC analysis by the BPCA method, as discussed in the following two sections.

## Nitric Oxidation for the Benzene Polycarboxylic Acid (BPCA) Method

The BPCA method, a method for determining the molecular pyrogenic carbon, was originally employed for the quantification of PyC in soils (Glaser et al., 1998), but has been modified for a DBC analysis by Dittmar (2008). Polyaromatic compounds in PyC are oxidized to BPCAs by nitric acid, and the produced BPCAs are separated and can be quantified by using a high-performance liquid chromatograph coupled with a photodiode-array detector (HPLC-DAD), a gas chromatograph (GC) coupled with a flame ionization detector, or a GC coupled with mass spectrometer (e.g., Dittmar, 2008; Ziolkowski et al., 2011). BPCAs were not produced from non-thermogenic organic matter (Dittmar, 2008; Ding et al., 2013). In addition, the condensation degree, which may help to evaluate the source/processing of PyC, can also be obtained from the BPCA method (Glaser et al., 1998).

DBC analysis by the BPCA method was performed using the method of Dittmar (2008) and Ding et al. (2013). The eluate (3 ml) was transferred into a 2-ml glass ampoule over drying under an $N_2$ stream at room temperature; then, the ampoule was flame-sealed after the addition of 0.5 ml of concentrated $HNO_3$. The sealed ampoule was kept in an oven at 170°C for 6 h. After the oxidation, $HNO_3$ was evaporated under an $N_2$ stream at 50°C, and samples in the ampoules were re-dissolved in 0.2 ml of mobile phase A (see details in the following section) for high-performance liquid chromatography (HPLC) analysis.

Different conditions have been reported for nitric oxidation for the BPCA method, e.g., 160°C for 6 h (Ding et al., 2013) or 170°C for 8 or 9 h (Glaser et al., 1998; Dittmar, 2008), and 180°C for 8 h (Ziolkowski et al., 2011). To compare the oxidation efficiencies under different conditions, the Suwannee River Humic Acid Standard II (SRHA, 2S101H) and the deep seawater DOM sample collected in this study were analyzed with various oxidation conditions of 160, 170, and 180°C for up to 10 h (**Figure 2**). The C-recovery of SRHA ranged from 3.9 to 5.3% (**Figure 2A**). Under oxidation at 160°C, there were no differences in C-recovery among the oxidation times (4.8–5.1%). The C-recoveries of oxidation times of 4–8 h (5.2–5.3%) were higher than those of 2 and 10 h (4.8%) at 170°C. The C-recovery under 180°C oxidation decreased with increasing oxidation time from 5.3% (2 h) to 3.9% (10 h). The oxidation at 170°C for 4–8 h showed the highest C-recovery of SRHA in

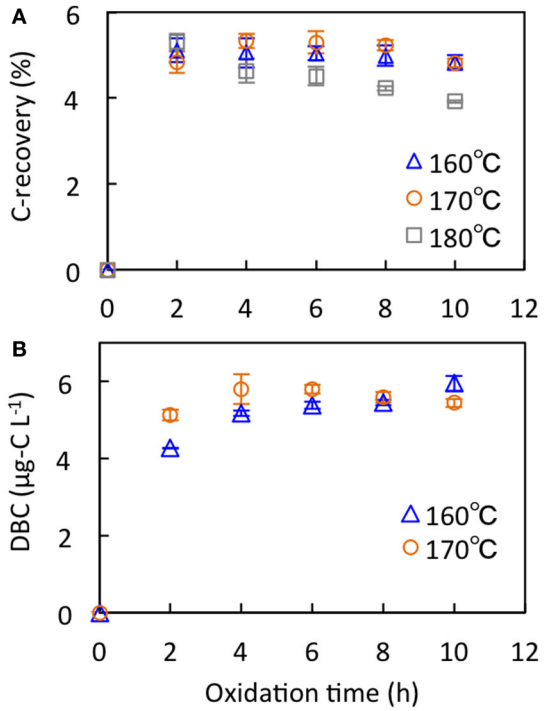


**FIGURE 2 | BPCA carbon-based recoveries (C-recovery, %) of Suwannee River Humic Acid Standard II (SRHA) (A)** and DBC concentration of deep seawater **(B)** after nitric oxidation under various temperatures and oxidation times.

this study and showed slightly higher C-recovery compared with the highest value observed at 160°C for 6 h reported by Ding et al. (2013). The DBC concentration of deep seawater ranged from 4.2 to 6.0 μg-C $L^{-1}$ (**Figure 2B**). Under oxidation at 160°C, the DBC concentration increased with increasing oxidation time from 4.2 μg-C $L^{-1}$ (2 h) to 6.0 μg-C $L^{-1}$ (10 h), and the DBC concentration under 170°C oxidation for 4–6 h (5.7–5.8 μg-C $L^{-1}$) was higher than that for other times (5.1–5.6 μg-C $L^{-1}$). From these two experimental results, the oxidation at 170°C for 6 h was used as the condition of nitric oxidation for the BPCA method. Note that the C-recovery and DBC concentration at 170°C for 6 h were reproducible within ±5% for triplicate runs.

## High Performance Liquid Chromatography to Quantify BPCAs

BPCAs were analyzed using an Agilent 1260 Infinity HPLC system equipped with a photodiode array detector (DAD; Dittmar, 2008). Briefly, samples/standards were eluted at a flow rate of 0.18 ml $min^{-1}$ following gradients from 94% mobile phase A (4 mM tetrabutylammonium bromide, 50 mM sodium acetate, and 10% MeOH) to 80% mobile phase B (MeOH) over 100 min with a $C_{18}$ column (3.5 μm, 2.1 × 150 mm, Waters Sunfire). A column oven of the HPLC system was set to 16°C. The quantification of the BPCAs was carried out with absorbance at 235 nm using the calibration curve of the BPCA standards mixture. The standards mixture of the BPCAs was prepared with commercially available BPCAs (1,2,3-B3CA; 1,2,4-B3CA; 1,3,5-B3CA; 1,2,4,5-B4CA; B5CA; B6CA). Two commercially non-available BPCAs (1,2,3,4-B4CA and 1,2,3,5-B4CA) were identified by retention time and absorbance spectrum (220–380 nm; Dittmar, 2008). The quantification of these two BPCAs was performed using the calibration curve of 1,2,4,5-B4CA.

The DBC concentration was estimated from BPCA concentrations using an equation proposed by Dittmar (2008). The contribution (ratio) of B5CA and B6CA to total BPCAs was calculated as an index for condensation degree of DBC. The analytical error of the methods determined using triplicate seawater samples was <4% in terms of the DBC concentration.

## Analysis of DOM Optical Properties

The absorbance spectrum between 200 and 800 nm was measured using a spectrophotometer (UV-1800, Shimadzu) with a 5-cm quartz windowed cell using the method of Yamashita et al. (2013). Briefly, water samples were thawed and allowed to stand prior to analysis until they reached room temperature (~23°C). Absorbance spectra of a blank (Milli-Q) and samples were obtained against air, and a blank spectrum was subtracted from each sample spectrum. The sample spectra were then baseline corrected by subtracting average values ranging from 590 to 600 nm from the entire spectrum (Yamashita and Tanoue, 2009). Absorbance was converted to the absorption coefficient $a(\lambda)$ ($m^{-1}$) and then fitted to an exponential function as follows (Green and Blough, 1994):

$$a(\lambda) = a(\lambda i)e^{-S(\lambda-\lambda i)},$$

where $a(\lambda)$ and $a(\lambda i)$ are the absorption coefficients at wavelength $\lambda$ and reference wavelength $\lambda i$, respectively. $S$ is the spectral slope parameter. In this study, the absorption coefficient at 254 nm ($a_{254}$) was reported as a quantitative parameter of CDOM. The $S$ obtained between 275 and 295 nm ($S_{275-295}$) was calculated using the method of Helms et al. (2008). $S_{275-295}$ has been used as a proxy for the molecular weight of the DOM (e.g., Helms et al., 2008), a tracer for terrigenous DOM in coastal environments (Fichot et al., 2013; Fichot and Benner, 2014), and an index for the degree of photodegradation (e.g., Helms et al., 2008; Yamashita et al., 2013). In this study, the value of $S_{275-295}$ was used as indexes for the contribution of terrigenous DOM and the degree of photodegradation in the Chukchi/Bering Seas and the North Pacific Ocean. A smaller value of $S_{275-295}$ indicated a greater contribution of terrigenous DOM or a lower degree of photodegradation and *vice versa* (Fichot et al., 2013; Yamashita et al., 2013). Notably, the DBC determined by the BPCA method is one of the constituents of CDOM. However, although CDOM is a mixture of terrigenous organic matter such as lignin (e.g., Fichot et al., 2016), autochthonous humic-like materials (e.g., Yamashita and Tanoue, 2009), proteins (e.g., Yamashita and Tanoue, 2009), and so on, in addition to DBC, the contribution of DBC to CDOM remains poorly constrained. Thus, $a_{254}$ and $S_{275-295}$ were used for indexes of bulk CDOM rather than DBC in this study.

Total dissolved lignin phenol concentration ($TDLP_9$, nM), a proxy for terrigenous DOM (Meyers-Schulte and Hedges, 1986; Opsahl and Benner, 1997; Fichot and Benner, 2012), was estimated using absorption coefficients and the equation proposed by Fichot et al. (2016). Note that the estimated $TDLP_9$ concentrations for samples in the open ocean most likely included some uncertainties because the equation was established with samples obtained from coastal environments while the autochthonous components possibly occupy major fractions of CDOM in the open ocean.

# RESULTS

## Oceanographic Characteristics of the Study Area

Temperature and salinity of surface waters observed in the Bering Sea showed relatively wide ranges, from 3.8 to 10.7°C (Supplemental Figure 1) and from 30.6 to 33.0 (**Figure 1**), respectively. The Bering Sea has a deep basin in the south and a shallow continental shelf in the northeast. The observed salinities in the shelf were lower than those in the basin. Levels of terrigenous CDOM are high in the shelf compared with the outer shelf (D'Sa et al., 2014). Temperature and salinity in the Chukchi Sea were lower than in the Bering Sea and ranged from −0.09 to 4.6°C and from 29.3 to 32.2, respectively. In the Bering-Chukchi shelf, several water masses, e.g., the Alaskan Coastal Water, the Bering Shelf Water, and the Anadyr Water, flow from the Bering Sea to the Chukchi Sea through the Bering Strait (Shimada et al., 2001; Grebmeier et al., 2006). The Alaskan Coastal Water, characterized by low salinity (Grebmeier et al., 2006), can be affected by riverine terrigenous DOM (Shin and Tanaka, 2004; Tanaka et al., 2016).

Sampling sites located between 39 and 51°N can be defined as within the subarctic North Pacific. In surface waters of the subarctic North Pacific, temperature and salinity were variable and ranged from 10.1 to 22.7°C and from 32.2 to 34.2, respectively. Sampling sites in this province were mainly located in the Western Subarctic Gyre (WSG), an area surrounded by the East Kamchatka, the Oyashio, and the Kuroshio currents. Some sites were located near the Aleutian Islands and are considered affected by the Alaskan Stream (Onishi and Ohtani, 1999).

In the subtropical region of the North Pacific (south of 35°N in this study), the temperature and salinity of surface waters ranged from 25.0 to 29.0°C and from 33.6 to 34.9, respectively. Sampling sites in this province were located at the western edge of the North Pacific Subtropical Gyre (NPSG); the sites covered the inside of the NPSG, the Kuroshio, and the outside of the NPSG. The Kuroshio water is characterized as warmer and more saline compared with the coastal water located at the outside of the NPSG (Kawabe and Yoneno, 1987). As shown in Supplemental Figure 2, five, two, and three sampling sites in the subtropical North Pacific were located at the inside of the NPSG, the Kuroshio, and the outside of the NPSG, respectively.

## Spatial Distribution of DOM Optical Properties in Surface Waters

In the marginal seas, the levels of CDOM, expressed as $a_{254}$, were generally high in the Chukchi Sea (1.9–2.2 $m^{-1}$) compared with the Bering Sea (1.4–2.7 $m^{-1}$), although the highest level was observed at a site in the Bering Sea (**Figures 3A,B**). In the Bering Sea, levels of CDOM in the shelf were higher than those in the basin. The lowest level of CDOM was evident in surface waters of the subtropical North Pacific (0.8–1.5 $m^{-1}$); CDOM in surface waters of the subarctic North Pacific (1.1–1.7 $m^{-1}$) was in the middle range. Overall, the distribution pattern of CDOM levels in surface waters was similar to that of colored dissolved and detrital material (CDM) observed by ocean color imagery (Siegel et al., 2005) and that of humic-like fluorophores determined by excitation emission matrices combined with parallel factor analysis (Yamashita et al., 2017).

In analogy with the distribution pattern of $a_{254}$, the $TDLP_9$ concentration estimated from absorption coefficients was highest in the Chukchi Sea (2.4–3.1 nM), except for two samples obtained from the Bering Sea (3.0 and 4.1 nM), whereas the lowest values were observed in the subtropical North Pacific (1.1–1.8 nM; **Figures 3C,D**). Among the middle ranges of the $TDLP_9$ concentration, that of the Bering Sea (without two outliers, 1.7–2.1 nM) tended to be higher than that of the subarctic North Pacific (1.3–2.2 nM). Although the $TDLP_9$ concentration observed in the Chukchi Sea was within the range previously observed in the same region, the range of $TDLP_9$ observed in this study was extremely narrow compared with the range observed in various coastal environments (1–500 nM; Fichot et al., 2016).

$S_{275-295}$ was the lowest in the Chukchi Sea (0.025–0.027 $nm^{-1}$; **Figures 3E,F**). In the Bering Sea and the subarctic North Pacific, $S_{275-295}$ had middle values and ranged from 0.026 to 0.035 $nm^{-1}$ and from 0.029 to 0.040 $nm^{-1}$, respectively. In the subtropical North Pacific, $S_{275-295}$ had the highest value with greatest variability (0.031–0.055 $nm^{-1}$). Overall, the $S_{275-295}$ values observed in the Chukchi/Bering Seas were similar to previous observations in the same region (Dainard and Guéguen, 2013; D'Sa et al., 2014; Tanaka et al., 2016) but were higher than those in other Arctic margins, including the Eurasian Arctic Ocean, the Beaufort Sea, and the Gulf of Ob (Fichot et al., 2013). $S_{275-295}$ values observed in the subarctic and subtropical North Pacific were roughly the same as previously reported values in the western North Pacific (Yamashita et al., 2013).

## Spatial Distribution of DBC Concentration and Composition in Surface Waters

**Figures 4A,B** show spatial distributions and box and whisker plots of DBC concentration in surface waters of the Chukchi Sea, the Bering Sea, and the subarctic and subtropical North Pacific. Overall, DBC concentrations ranged from 4.8 to 15.5 μg-C $L^{-1}$ and were largely different among marine provinces. The DBC concentrations in the Chukchi Sea (7.9–12.1 μg-C $L^{-1}$) and the Bering Sea (4.8–15.5 μg-C $L^{-1}$) were higher than those in the subarctic and subtropical North Pacific (5.3–8.6 and 4.9–7.9 μg-C $L^{-1}$, respectively). In this study, the highest DBC concentrations were found at two sites in the shelf of the Bering

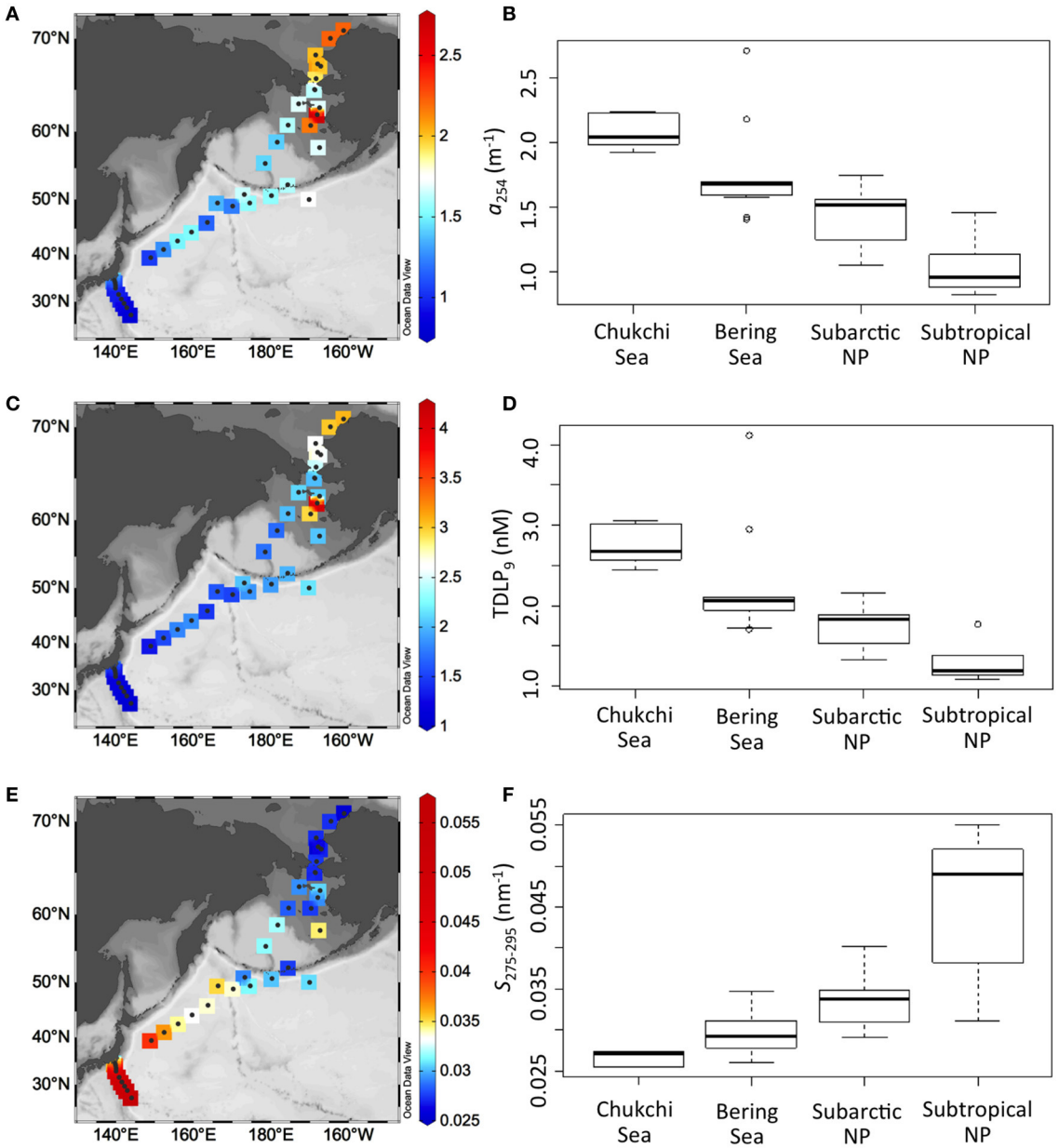


**FIGURE 3 | Spatial distributions of $a_{254}$ (A)**, $TDLP_9$ **(C)**, and $S_{275-295}$ **(E)**, and box and whisker plots of $a_{254}$ **(B)**, $TDLP_9$ **(D)**, and $S_{275-295}$ **(F)** in surface waters of the Chukchi/Bering Seas, subarctic, and subtropical North Pacific (NP). In box and whisker plots, the central bold line represents the median of the dataset. The upper and lower ends of the box represent the first and third quartiles of the dataset, respectively. The upper and lower whiskers represent the dataset maximum and minimum, respectively. The open circle represents the outlier (more than 2 standard deviations).

Sea. Because the DBC concentrations in the shelf were generally higher than those in the basin of the Bering Sea, the variability in the DBC concentration was greatest for the Bering Sea. DBC concentrations in the subarctic and subtropical North Pacific were within a narrow range and were similar to those in the basin of the Bering Sea.

Spatial distributions and box and whisker plots of the ratio of B5CA and B6CA to all BPCAs in surface waters of the Chukchi Sea, the Bering Sea, and the subarctic and subtropical North Pacific are shown in **Figures 4C,D**. During nitric oxidation, highly substituted BPCAs (i.e., B6CA and B5CA) are formed from aromatic rings surrounded by many aromatic rings, whereas poorly substituted BPCAs (i.e., B3CA) are formed from aromatic rings surrounded by a few aromatic rings (Ziolkowski et al., 2011). Therefore, the ratio of B5CA and B6CA to all BPCAs can be used as an index for condensation degree of DBC. Overall, the ratio of B5CA and B6CA to all BPCAs ranged from 0.20 to 0.43 and showed systematic differences among marine provinces

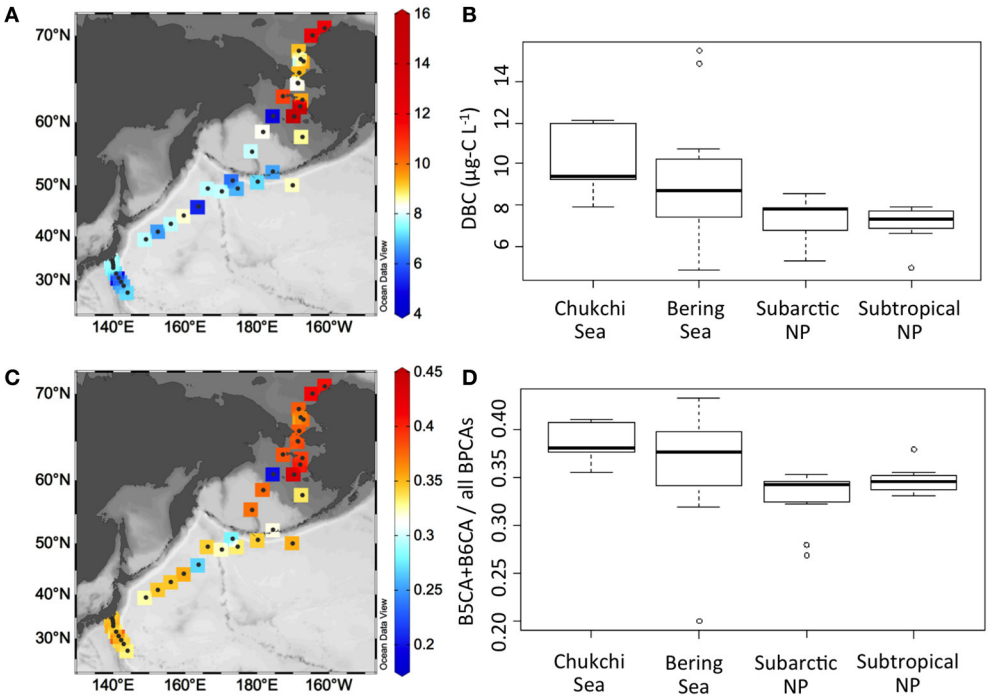


**FIGURE 4 | Spatial distributions of DBC concentration (A)** and condensation degree (ratio of B5CA and B6CA to all BPCAs) of DBC **(C)**, and box and whisker plots of DBC concentration **(B)** and condensation degree of DBC **(D)** in surface waters of the Chukchi/Bering Seas, the subarctic and the subtropical North Pacific (NP). In box and whisker plots, the central bold line represents the median of the dataset. The upper and lower ends of the box represent the first and third quartiles of the dataset, respectively. The upper and lower whiskers represent the dataset maximum and minimum, respectively. The open circle represents the outlier (more than 2 standard deviations).

(**Figures 4C,D**). The ratio was high in the Chukchi Sea (0.36–0.41) and Bering Sea (0.20–0.43) compared with the subarctic and subtropical North Pacific (0.27–0.35 and 0.33–0.38, respectively). In analogy with DBC concentration, the ratio in the Bering Sea was highly variable because of large differences between the shelf and the basin regions. The variability of the ratio in the subarctic and subtropical North Pacific was smaller than in the Chukchi/Bering Seas.

# DISCUSSION

## Characteristics of DBC in Surface Waters of the Chukchi Sea, Bering Sea, and North Pacific Ocean

DBC concentrations observed in this study were higher in the Chukchi/Bering Seas compared with the North Pacific Ocean (**Figures 4A,B**). The range of salinity (**Figure 1**), $TDLP_9$ (**Figures 3C,D**), and $S_{275-295}$ (**Figures 3E,F**) indicated that the study area at the Chukchi/Bering Seas received some riverine inputs. Previous studies reported DBC concentrations in riverine and marine DOM using the BPCA method with the same conversion method from BPCA to DBC concentration. Overall, the range of DBC concentration in marine environments observed in this study is one to three orders of magnitude lower than those observed in terrestrial aquatic environments (e.g., Jaffé et al., 2013; Stubbins et al., 2015), which indicates that DBC in surface waters of coastal as well as oceanic environments is possibly derived from terrestrial environments by riverine inputs and/or atmospheric deposition, as previously reported (Dittmar, 2008; Dittmar and Paeng, 2009). The DBC concentrations in the Chukchi/Bering Seas (4.8–15.5 μg-C $L^{-1}$) were similar to a value reported for the open Gulf of Mexico (14.4 μg-C $L^{-1}$; Dittmar, 2008), and the DBC concentration in the North Pacific Ocean (4.9–8.6 μg-C $L^{-1}$) was slightly lower than those observed in the Southern Ocean (7.2–9.6 μg-C $L^{-1}$; Dittmar and Paeng, 2009) and in the North Atlantic Deep Water (12.5 ± 1.9 μg-C $L^{-1}$; Stubbins et al., 2012).

The condensation degree of DBC was higher in marginal seas, i.e., the Chukchi/Bering Seas, compared with the open ocean, i.e., the subarctic and subtropical North Pacific (**Figures 4C,D**). Higher condensation degrees of DBC in coastal environments compared with the open ocean have also been reported (Dittmar, 2008; Dittmar and Paeng, 2009; Ziolkowski and Druffel, 2010). Interestingly, higher DBC concentration was generally accompanied by higher condensation degree of DBC, and *vice versa* throughout the study area (**Figure 4**). However, concentration and condensation degree of DBC were more variable in the Chukchi/Bering Seas compared with the North Pacific Ocean. Such a difference in variability possibly reflects different environmental dynamics (source and/or sink) of DBC between marginal seas and the open ocean.

## Factors Controlling DBC Distributions in Surface Waters of the Chukchi/Bering Seas

DBC concentration was negatively correlated with salinity but was positively correlated with $a_{254}$ and $TDLP_9$ in the surface waters of the Chukchi/Bering Seas (**Figure 5**). It has been recently reported that $a_{254}$ is strongly correlated with DBC concentration in Arctic rivers (Stubbins et al., 2015). $TDLP_9$ has been used as a proxy of terrigenous DOM (Meyers-Schulte and Hedges, 1986; Opsahl and Benner, 1997; Fichot and Benner, 2012). Therefore, relationships between DBC and salinity, $a_{254}$, and $TDLP_9$ indicate that a major source of DBC in surface waters of the Chukchi/Bering Seas is riverine input. Rivers carry a large amount of DBC to global oceans, including the Arctic region (Jaffé et al., 2013; Stubbins et al., 2015). The correlation coefficient between DBC and salinity was lower than between DBC and $a_{254}$ as well as $TDLP_9$ (**Figure 5**). The DOC concentration was not correlated to salinity in the Chukchi/Bering Seas because of the complex mixing of water masses, including sea-ice melt water, which can be characterized by low DOC concentration (Shin and Tanaka, 2004; Mathis et al., 2005; Tanaka et al., 2016). Therefore, it can be expected that the contribution of DBC in the sea-ice melt water disturbs the relationship between DBC and salinity in surface waters.

The plots were highly scattered between DBC concentration and $S_{275-295}$(**Figure 5D**). Fichot and Benner (2012) noted that CDOM quality expressed as $S_{275-295}$ is photochemically altered in surface waters of salinities >30, regardless of origin. Several water masses, e.g., Alaskan Coastal Water (salinity < 31.8), Anadyr Water (salinity > 32.5), Bering Shelf Water (31.8–32.5 of salinity), have been known to distribute in the Chukchi/Bering Seas as marine end-members (Grebmeier et al., 2006). Therefore, scattered plots between DBC concentration and $S_{275-295}$ suggest the various degrees of photochemical degradation of DBC as well as CDOM among water masses of marine end-members.

The DBC concentration of the Yukon River in summer was 430 $\mu$g-C $L^{-1}$ (Stubbins et al., 2015). This value is higher than the intercept (69.7 $\pm$ 19.3 $\mu$g-C $L^{-1}$) of the linear regression between DBC concentration and salinity (**Figure 5A**). DBC concentrations in the glacier-fed and glacier-influenced rivers have been lower than those in rivers draining Alaskan boreal forest (Ding et al., 2015). Therefore, a part of the large difference in DBC concentration between the Yukon River (Stubbins et al., 2015) and the intercept (**Figure 5A**) is possibly a result of variable DBC concentrations among Arctic rivers, although sea-ice melt water should also contribute to the differences discussed above.

## Factors Controlling DBC Distributions in Surface Waters of the North Pacific Ocean

DBC in surface waters of the North Pacific Ocean was characterized as having relatively low concentration and condensation (**Figure 4**). Because condensation degree of DBC becomes lower with photodegradation (Stubbins et al., 2010, 2012; Ward et al., 2014; Wagner and Jaffé, 2015; Fu et al., 2016), the relatively low concentration and condensation degree of DBC found in the North Pacific Ocean may result from extensive photodegradation. A large difference in $S_{275-295}$ was evident between the subarctic and subtropical North Pacific (**Figures 3E,F**). Because $S_{275-295}$ becomes larger with photodegradation of CDOM in the open ocean (Helms et al., 2008; Yamashita et al., 2013), the difference in $S_{275-295}$ suggests that the degree of photodegradation of CDOM (including DBC) was largely different between the subarctic and subtropical North Pacific. However, the DBC concentration and condensation degree were similar between the subarctic and subtropical North Pacific (**Figure 4**), which implies that photodegradation is not the sole major factor determining concentration and condensation degree of DBC in surface waters of the North Pacific Ocean. The other factor shaping the concentration and condensation degree of DBC in surface waters is adsorption onto sinking particles. Coppola et al. (2014) suggested that the transfer of hydrophobic, highly aromatic/condensed BC from DOC to particles is one of the important loss processes of DBC. The annual average flux of sinking particles from surface waters (at 60 and 100 m) to beneath the subarctic western North Pacific was similar or slightly higher than that in the subtropical western North Pacific (Honda et al., 2016). Thus, the similar ranges of the DBC concentration and condensation degree between the subarctic and subtropical North Pacific implies that the adsorption onto sinking particles is one of the processes shaping the DBC distribution in surface waters of the open ocean.

Atmospheric PyC (i.e., soot), produced during combustion at high temperature, such as fossil fuel combustion, can be characterized by a high condensation degree, and its oxidation products (BPCAs) are rich in B6CA and B5CA (Ziolkowski and Druffel, 2010; Roth et al., 2012). Therefore, we considered that the condensation degree of DBC derived from atmospheric deposition of PyC would be high. However, Ding et al. (2015) have recently reported that water soluble organic carbon extracted from atmospheric dust was rich in B3CA and B4CA and suggested that riverine DBC, which was rich in B3CA and B4CA, was the result of soot deposited onto the watersheds. Additionally, Khan et al. (2016) observed BPCA composition in recent freshwaters and ancient brines of perennially ice-covered, closed-basin Antarctic lakes and noted that the condensation degree of DBC derived from PyC of fossil fuel combustion was lower than that derived from wildfires. It has been well-recognized that soot particles in the atmosphere are rendered hydrophilic with chemical and photochemical aging (e.g., Petters et al., 2006; Weitkamp et al., 2007; Han et al., 2012). Thus, DBC with a low condensation degree is possibly derived from aged soot.

Salinity and $S_{275-295}$ ($a_{254}$ and $TDLP_9$) in surface waters of the North Pacific Ocean were higher (lower) than those of the Chukchi/Bering Seas (**Figures 1**, **3**), which implies that riverine inputs are minor in the North Pacific Ocean compared with those in the Chukchi/Bering Seas. Although the air-sea gas exchange fluxes of polycyclic aromatic hydrocarbons (PAHs) are high in the Arctic region, the PyC concentrations in aerosol particles and dry deposition of particle-bound PAHs in the North Pacific Ocean were greater than those in the Chukchi/Bering Seas (Hadley et al., 2007; Ma et al., 2013; Taketani et al., 2016). Low condensation degrees of DBC observed in surface waters of the subarctic and subtropical

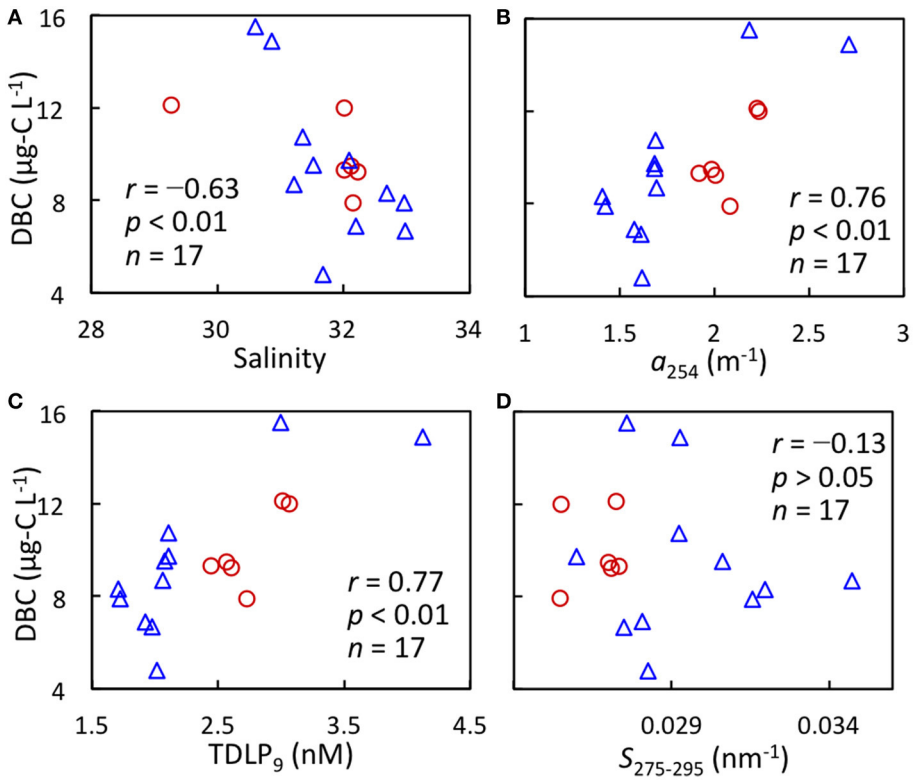


**FIGURE 5 | Relationships between DBC concentration and salinity (A)**, $a_{254}$ **(B)**, estimated $TDLP_9$ **(C)**, and $S_{275-295}$ **(D)** in surface waters of the Chukchi Sea (red circle) and Bering Sea (blue triangle).

North Pacific thus imply that atmospheric deposition of BC and subsequent dissolution is an important source of DBC in these provinces.

Distributional patterns of DBC concentration and condensation in the subtropical North Pacific support this conclusion. The sampling sites located at the outside of the NPSG may exhibit greater influence of riverine water compared with the sites located at the Kuroshio and the inside of the NPSG (Supplemental Figure 2). If major sources of DBC were riverine inputs in the subtropical North Pacific, there would be large gradients of DBC concentration and condensation from the outside to the inside of the NPSG. However, gradients of DBC concentration and condensation were not evident from the outside to the inside of the NPSG, although salinities in the outside of the NPSG were lower than those in the Kuroshio Current and the inside of the NPSG (**Figure 6**). These spatial distributions indicate that atmospheric deposition rather than riverine input is an important source of DBC in the surface waters of the North Pacific Ocean.

In summary, the relatively low concentration and condensation degree of DBC in the surface waters of the North Pacific Ocean are mainly because of atmospheric deposition of BC, with substantial effects of photodegradation and adsorption onto sinking particles.

## CONCLUSIONS AND REMARKS

DBC in the ocean is one of the important PyC pools on the Earth's surface. However, because ranges in DBC concentration and factors controlling DBC distribution have scarcely been reported, the environmental dynamics of marine DBC have not been well-documented. This study provides important insights about the environmental dynamics of DBC in surface waters of marginal seas and the open ocean.

The riverine input of DBC as a major source affects the distribution of DBC in the surface waters of the Chukchi/Bering Seas, in addition to possible contributions of DBC from sea-ice melt water, photodegradation of DBC in marine end-members, and variable DBC concentration among Arctic rivers.

The atmospheric deposition of BC and subsequent losses by photodegradation and adsorption onto sinking particles are the major factors shaping the relatively low concentration and condensation degree of DBC in the surface waters of the North Pacific Ocean.

This study indicates that the major sources of DBC in the open ocean and coastal ocean are atmospheric deposition and fluvial inputs, respectively. For the major loss processes of DBC in surface waters, photodegradation and adsorption onto sinking particles are considered. However, since atmospheric deposition, photodegradation, and adsorption onto sinking particles affect DBC distribution, all of which lower the condensation degree

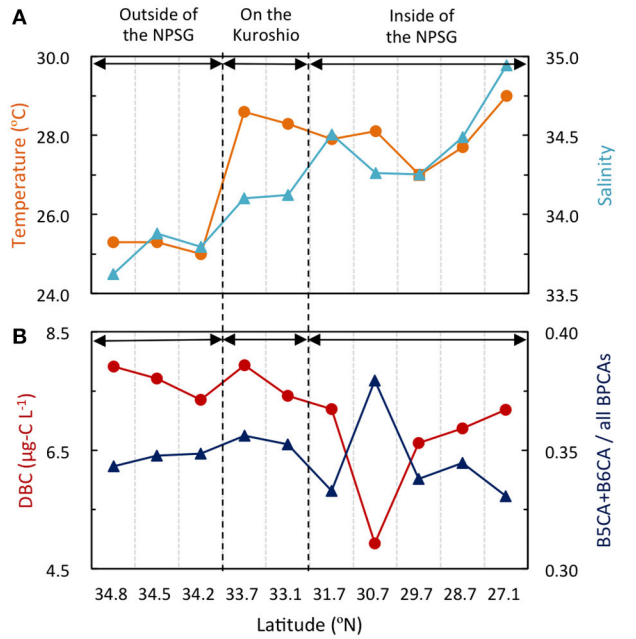


**FIGURE 6 | Distributions of salinity and temperature (A)** and concentration and condensation degree (ratio of B5CA and B6CA to all BPCAs) of DBC **(B)** in surface waters of the subtropical North Pacific. The outside of the North Pacific Subtropical Gyre (NPSG) is close to Japan.

of DBC, the possible contributions of these processes could not be separated by the DBC proxy applied in this study (i.e., the ratio of B5CA and B6CA to total BPCAs). A new compositional proxy of DBC is needed to separately evaluate the effect of atmospheric deposition, photodegradation, and adsorption onto sinking particles. The evaluation of the DBC concentration in sea-ice melt water, various riverine waters, including glacier-fed and glacier-influenced water, and marine end-members are also necessary to clarify the factors shaping DBC distribution in the Arctic Ocean, including the Chukchi/Bering Seas.

## AUTHOR CONTRIBUTIONS

MN and YY contributed to the design of the study. YY collected samples, performed SPE, and analyzed CDOM. MN performed BPCA analyses and data analyses with the help of TA and YY. MN wrote the initial draft of the manuscript, and all authors contributed to its revision.

## ACKNOWLEDGMENTS

We are grateful to H. Ogawa, J. Nishioka, T. Hirawake, and the captains and crews of the R/V *Hakuho Maru*, the R/V *Shinsei Maru*, and the T/S *Oshoro-Maru* for their assistance with sample collection. We also thank the reviewers and guest editor, Dr. Santín, for their helpful and constructive comments and suggestions, which have improved the quality of this manuscript. This study was financially supported by the Grants-in-Aid (No. 16H0293006 and 24121003) from Japan Society for the Promotion of Science (JSPS) to YY.

## SUPPLEMENTARY MATERIAL

The Supplementary Material for this article can be found online at: http://journal.frontiersin.org/article/10.3389/feart.2017.00034/full#supplementary-material

## REFERENCES

Benner, R. (2002). "Chemical composition and reactivity," in *Biogeochemistry of Marine Dissolved Organic Matter*, eds D. A. Hansell and C. A. Carlson (San Diego, CA: Academic Press), 59–90.

Bird, M. I., Wynn, J. G., Saiz, G., Wurster, C. M., and McBeath, A. (2015). The pyrogenic carbon cycle. *Annu. Rev. Earth Planet. Sci.* 43, 273–298. doi: 10.1146/annurev-earth-060614-105038

Bruun, S., Jensen, E. S., and Jensen, L. S. (2008). Microbial mineralization and assimilation of black carbon: dependency on degree of thermal alteration. *Organ. Geochem.* 39, 839–845. doi: 10.1016/j.orggeochem.2008.04.020

Coppola, A. I., and Druffel, E. R. M. (2016). Cycling of black carbon in the ocean. *Geophys. Res. Lett.* 43, 4477–4482. doi: 10.1002/2016GL068574

Coppola, A. I., Ziolkowski, L. A., Masiello, C. A., and Druffel, E. R. M. (2014). Aged black carbon in marine sediments and sinking particles. *Geophys. Res. Lett.* 41, 2427–2433. doi: 10.1002/2013GL059068

Dainard, P. G., and Guéguen, C. (2013). Distribution of PARAFAC modeled CDOM components in the North Pacific Ocean, Bering, Chukchi and Beaufort seas. *Mar. Chem.* 157, 216–223. doi: 10.1016/j.marchem.2013.10.007

Ding, Y., Cawley, K. M., Da Cunha, C. N., and Jaffé, R. (2014). Environmental dynamics of dissolved black carbon in wetlands. *Biogeochemistry* 119, 259–273. doi: 10.1007/s10533-014-9964-3

Ding, Y., Yamashita, Y., Dodds, W. K., and Jaffé, R. (2013). Dissolved black carbon in grassland streams: is there an effect of recent fire history? *Chemosphere* 90, 2557–2562. doi: 10.1016/j.chemosphere.2012.10.098

Ding, Y., Yamashita, Y., Jones, J., and Jaffé, R. (2015). Dissolved black carbon in boreal forest and glacial rivers of central Alaska: assessment of biomass burning versus anthropogenic sources. *Biogeochemistry* 123, 15–25. doi: 10.1007/s10533-014-0050-7

Dittmar, T. (2008). The molecular level determination of black carbon in marine dissolved organic matter. *Organ. Geochem.* 39, 396–407. doi: 10.1016/j.orggeochem.2008.01.015

Dittmar, T., De Rezende, C. E., Manecki, M., Niggemann, J., Ovalle, A. R. C., Stubbins, A., et al. (2012a). Continuous flux of dissolved black carbon from a vanished tropical forest biome. *Nat. Geosci.* 5, 618–622. doi: 10.1038/ngeo1541

Dittmar, T., and Koch, B. P. (2006). Thermogenic organic matter dissolved in the abyssal ocean. *Mar. Chem.* 102, 208–217. doi: 10.1016/j.marchem.2006.04.003

Dittmar, T., and Paeng, J. (2009). A heat-induced molecular signature in marine dissolved organic matter. *Nat. Geosci.* 2, 175–179. doi: 10.1038/ngeo440

Dittmar, T., Paeng, J., Gihring, T. M., Suryaputra, I. G. N. A., and Huettel, M. (2012b). Discharge of dissolved black carbon from a fire-affected intertidal system. *Limnol. Oceanogr.* 57:1171. doi: 10.4319/lo.2012.57.4.1171

D'Sa, E. J., Goes, J. I., Gomes, H., and Mouw, C. (2014). Absorption and fluorescence properties of chromophoric dissolved organic matter of the eastern Bering Sea in the summer with special reference to the influence of a cold pool. *Biogeosciences* 11, 3225–3244. doi: 10.5194/bg-11-3225-2014

Fichot, C. G., and Benner, R. (2012). The spectral slope coefficient of chromophoric dissolved organic matter (S275-295) as a tracer of terrigenous dissolved organic carbon in river-influenced ocean margins. *Limnol. Oceanogr.* 57, 1453–1466. doi: 10.4319/lo.2012.57.5.1453

Fichot, C. G., and Benner, R. (2014). The fate of terrigenous dissolved organic carbon in a river-influenced ocean margin. *Global Biogeochem. Cycles* 28, 300–318. doi: 10.1002/2013GB004670

Fichot, C. G., Benner, R., Kaiser, K., Shen, Y., Amon, R. M., Ogawa, H., et al. (2016). Predicting dissolved lignin phenol concentrations in the coastal ocean from chromophoric dissolved organic matter (CDOM) absorption coefficients. *Front. Mar. Sci.* 3:7. doi: 10.3389/fmars.2016.00007

Fichot, C. G., Kaiser, K., Hooker, S. B., Amon, R. M., Babin, M., Bélanger, S., et al. (2013). Pan-Arctic distributions of continental runoff in the Arctic Ocean. *Sci. Rep.* 3:1053. doi: 10.1038/srep01053

Fu, H., Liu, H., Mao, J., Chu, W., Li, Q., Alvarez, P. J. J., et al. (2016). Photochemistry of dissolved black carbon released from biochar: reactive oxygen species generation and phototransformation. *Environ. Sci. Technol.* 50, 1218–1226. doi: 10.1021/acs.est.5b04314

Glaser, B., Haumaier, L., Guggenberger, G., and Zech, W. (1998). Black carbon in soils: the use of benzenecarboxylic acids as specific markers. *Organ. Geochem.* 29, 811–819. doi: 10.1016/S0146-6380(98)00194-6

Grebmeier, J. M., Cooper, L. W., Feder, H. M., and Sirenko, B. I. (2006). Ecosystem dynamics of the Pacific-influenced northern Bering and Chukchi Seas in the Amerasian Arctic. *Prog. Oceanogr.* 71, 331–361. doi: 10.1016/j.pocean.2006.10.001

Green, S. A., and Blough, N. V. (1994). Optical absorption and fluorescence properties of chromophoric dissolved organic matter in natural waters. *Limnol. Oceanogr.* 39, 1903–1916. doi: 10.4319/lo.1994.39.8.1903

Hadley, O. L., Ramanathan, V., Carmichael, G. R., Tang, Y., Corrigan, C. E., Roberts, G. C., et al. (2007). Trans-Pacific transport of black carbon and fine aerosols (D< 2.5 μm) into North America. *J. Geophys. Res. Atmos.* 112:D05309. doi: 10.1029/2006JD007632

Han, C., Liu, Y., Ma, J., and He, H. (2012). Key role of organic carbon in the sunlight-enhanced atmospheric aging of soot by O2. *Proc. Natl. Acad. Sci. U.S.A.* 109, 21250–21255. doi: 10.1073/pnas.1212690110

Hedges, J. I., Eglinton, G., Hatcher, P. G., Kirchman, D. L., Arnosti, C., Derenne, S., et al. (2000). The molecularly-uncharacterized component of nonliving organic matter in natural environments. *Organ. Geochem.* 31, 945–958. doi: 10.1016/S0146-6380(00)00096-6

Helms, J. R., Stubbins, A., Ritchie, J. D., Minor, E. C., Kieber, D. J., and Mopper, K. (2008). Absorption spectral slopes and slope ratios as indicators of molecular weight, source, and photobleaching of chromophoric dissolved organic matter. *Limnol. Oceanogr.* 53, 955–969. doi: 10.4319/lo.2008.53.3.0955

Hockaday, W. C., Grannas, A. M., Kim, S., and Hatcher, P. G. (2006). Direct molecular evidence for the degradation and mobility of black carbon in soils from ultrahigh-resolution mass spectral analysis of dissolved organic matter from a fire-impacted forest soil. *Organ. Geochem.* 37, 501–510. doi: 10.1016/j.orggeochem.2005.11.003

Hockaday, W. C., Grannas, A. M., Kim, S., and Hatcher, P. G. (2007). The transformation and mobility of charcoal in a fire-impacted watershed. *Geochim. Cosmochim. Acta* 71, 3432–3445. doi: 10.1016/j.gca.2007.02.023

Honda, M. C., Kawakami, H., Matsumoto, K., Wakita, M., Fujiki, T., Mino, Y., et al. (2016). Comparison of sinking particles in the upper 200 m between subarctic station K2 and subtropical station S1 based on drifting sediment trap experiments. *J. Oceanogr.* 72, 373–386. doi: 10.1007/s10872-015-0280-x

Huang, G., Chen, Y., Tian, C., Tang, J., Zhang, H., Luo, Y. M., et al. (2016). Spatial distributions and seasonal variations of dissolved black carbon in the Bohai Sea, China. *J. Coast. Res.* 74, 214–227. doi: 10.2112/SI74-019.1

Jaffé, R., Ding, Y., Niggemann, J., Vähätalo, A. V., Stubbins, A., Spencer, R. G. M., et al. (2013). Global charcoal mobilization from soils via dissolution and riverine transport to the oceans. *Science* 340, 345–347. doi: 10.1126/science.1231476

Jurado, E., Dachs, J., Duarte, C. M., and Simo, R. (2008). Atmospheric deposition of organic and black carbon to the global oceans. *Atmos. Environ.* 42, 7931–7939. doi: 10.1016/j.atmosenv.2008.07.029

Kawabe, M., and Yoneno, M. (1987). Water and flow variations in Sagami Bay under the influence of the Kuroshio path. *J. Oceanogr. Soc. Japan* 43, 283–294. doi: 10.1007/BF02108696

Khan, A. L., Jaffé, R., Ding, Y., and McKnight, D. M. (2016). Dissolved black carbon in Antarctic lakes: chemical signatures of past and present sources. *Geophys. Res. Lett.* 43, 5750–5757. doi: 10.1002/2016GL068609

Kim, S., Kaplan, L. A., Benner, R., and Hatcher, P. G. (2004). Hydrogen-deficient molecules in natural riverine water samples—evidence for the existence of black carbon in DOM. *Mar. Chem.* 92, 225–234. doi: 10.1016/j.marchem.2004.06.042

Kuhlbusch, T. A. (1998). Black carbon and the carbon cycle. *Science* 280, 1903–1904. doi: 10.1126/science.280.5371.1903

Ma, Y., Xie, Z., Yang, H., Möller, A., Halsall, C., Cai, M., et al. (2013). Deposition of polycyclic aromatic hydrocarbons in the North Pacific and the Arctic. *J. Geophys. Res. Atmos.* 118, 5822–5829. doi: 10.1002/jgrd.50473

Mannino, A., and Harvey, H. R. (2004). Black carbon in estuarine and coastal ocean dissolved organic matter. *Limnol. Oceanogr.* 49, 735–740. doi: 10.4319/lo.2004.49.3.0735

Marques, J. S. J., Dittmar, T., Niggemann, J., Almeida, M. G., Gomez-Saez, G. V., and Rezende, C. E. (2017). Dissolved black carbon in the headwaters-to-ocean continuum of Paraíba Do Sul River, Brazil. *Front. Earth Sci.* 5:11. doi: 10.3389/feart.2017.00011

Masiello, C. A. (2004). New directions in black carbon organic geochemistry. *Mar. Chem.* 92, 201–213. doi: 10.1016/j.marchem.2004.06.043

Masiello, C. A., and Druffel, E. R. M. (1998). Black carbon in deep-sea sediments. *Science* 280, 1911–1913. doi: 10.1126/science.280.5371.1911

Masiello, C. A., and Louchouarn, P. (2013). Fire in the ocean. *Science* 340, 287–288. doi: 10.1126/science.1237688

Mathis, J. T., Hansell, D. A., and Bates, N. R. (2005). Strong hydrographic controls on spatial and seasonal variability of dissolved organic carbon in the Chukchi Sea. *Deep Sea Res. Part II Top. Stud. Oceanogr.* 52, 3245–3258. doi: 10.1016/j.dsr2.2005.10.002

Meyers-Schulte, K. J., and Hedges, J. I. (1986). Molecular evidence for a terrestrial component of organic matter dissolved in ocean water. *Nature* 321, 61–63. doi: 10.1038/321061a0

Nishioka, J., Ono, T., Saito, H., Sakaoka, K., and Yoshimura, T. (2011). Oceanic iron supply mechanisms which support the spring diatom bloom in the Oyashio region, western subarctic Pacific. *J. Geophys. Res. Oceans* 116:C02021. doi: 10.1029/2010JC006321

Onishi, H., and Ohtani, K. (1999). On seasonal and year to year variation in flow of the Alaskan Stream in the central North Pacific. *J. Oceanogr.* 55, 597–608. doi: 10.1023/A:1007840802296

Opsahl, S., and Benner, R. (1997). Distribution and cycling of terrigenous dissolved organic matter in the ocean. *Nature* 386, 480–482. doi: 10.1038/386480a0

Petters, M. D., Prenni, A. J., Kreidenweis, S. M., DeMott, P. J., Matsunaga, A., Lim, Y. B., et al. (2006). Chemical aging and the hydrophobic-to-hydrophilic conversion of carbonaceous aerosol. *Geophys. Res. Lett.* 33:L24806. doi: 10.1029/2006GL027249

Preston, C. M., and Schmidt, M. W. I. (2006). Black (pyrogenic) carbon in boreal forests: a synthesis of current knowledge and uncertainties. *Biogeosciences* 3, 397–420. doi: 10.5194/bg-3-397-2006

Reisser, M., Purves, R. S., Schmidt, M. W. I., and Abiven, S. (2016). Pyrogenic carbon in soils: a literature-based inventory and a global estimation of its content in soil organic carbon and stocks. *Front. Earth Sci.* 4:80. doi: 10.3389/feart.2016.00080

Roth, P. J., Lehndorff, E., Brodowski, S., Bornemann, L., Sanchez-García, L., Gustafsson, Ö., et al. (2012). Differentiation of charcoal, soot and diagenetic carbon in soil: method comparison and perspectives. *Organ. Geochem.* 46, 66–75. doi: 10.1016/j.orggeochem.2012.01.012

Santín, C., Doerr, S. H., Kane, E. S., Masiello, C. A., Ohlson, M., Rosa, J. M., et al. (2016). Towards a global assessment of pyrogenic carbon from vegetation fires. *Glob. Chang. Biol.* 22, 76–91. doi: 10.1111/gcb.12985

Shimada, K., Carmack, E. C., Hatakeyama, K., and Takizawa, T. (2001). Varieties of shallow temperature maximum waters in the western Canadian Basin of the Arctic Ocean. *Geophys. Res. Lett.* 28, 3441–3444. doi: 10.1029/2001GL013168

Shin, K. H., and Tanaka, N. (2004). Distribution of dissolved organic matter in the eastern Bering Sea, Chukchi Sea (Barrow Canyon) and Beaufort Sea. *Geophys. Res. Lett.* 31:L24304. doi: 10.1029/2004gl021039

Siegel, D. A., Maritorena, S., Nelson, N. B., and Behrenfeld, M. J. (2005). Independence and interdependencies among global ocean color properties: Reassessing the bio-optical assumption. *J. Geophys. Res. Oceans* 110:C07011. doi: 10.1029/2004JC002527

Stubbins, A., Niggemann, J., and Dittmar, T. (2012). Photo-lability of deep ocean dissolved black carbon. *Biogeosciences* 9, 1661–1670. doi: 10.5194/bg-9-1661-2012

Stubbins, A., Spencer, R. G. M., Chen, H., Hatcher, P. G., Mopper, K., Hernes, P. J., et al. (2010). Illuminated darkness: molecular signatures of Congo River dissolved organic matter and its photochemical alteration as revealed by ultrahigh precision mass spectrometry. *Limnol. Oceanogr.* 55, 1467–1477. doi: 10.4319/lo.2010.55.4.1467

Stubbins, A., Spencer, R. G. M., Mann, P. J., Holmes, R. M., McClelland, J. W., Niggemann, J., et al. (2015). Utilizing colored dissolved organic matter to derive dissolved black carbon export by arctic rivers. *Front. Earth Sci.* 3:63. doi: 10.3389/feart.2015.00063

Taketani, F., Miyakawa, T., Takashima, H., Komazaki, Y., Pan, X., Kanaya, Y., et al. (2016). Shipborne observations of atmospheric black carbon aerosol particles over the Arctic Ocean, Bering Sea, and North Pacific Ocean during September 2014. *J. Geophys. Res. Atmos.* 121, 1914–1921. doi: 10.1002/2015JD023648

Tanaka, K., Takesue, N., Nishioka, J., Kondo, Y., Ooki, A., Kuma, K., et al. (2016). The conservative behavior of dissolved organic carbon in surface waters of the southern Chukchi Sea, Arctic Ocean, during early summer. *Sci. Rep.* 6:34123. doi: 10.1038/srep34123

Tsumune, D., Nishioka, J., Shimamoto, A., Takeda, S., and Tsuda, A. (2005). Physical behavior of the SEEDS iron-fertilized patch by sulphur hexafluoride tracer release. *Prog. Oceanogr.* 64, 111–127. doi: 10.1016/j.pocean.2005.02.018

Wagner, S., Cawley, K. M., Rosario-Ortiz, F. L., and Jaffé, R. (2015). In-stream sources and links between particulate and dissolved black carbon following a wildfire. *Biogeochemistry* 124, 145–161. doi: 10.1007/s10533-015-0088-1

Wagner, S., and Jaffé, R. (2015). Effect of photodegradation on molecular size distribution and quality of dissolved black carbon. *Organ. Geochem.* 86, 1–4. doi: 10.1016/j.orggeochem.2015.05.005

Ward, C. P., Sleighter, R. L., Hatcher, P. G., and Cory, R. M. (2014). Insights into the complete and partial photooxidation of black carbon in surface waters. *Environ. Sci. Process. Impacts* 16, 721–731. doi: 10.1039/C3EM00597F

Weitkamp, E. A., Sage, A. M., Pierce, J. R., Donahue, N. M., and Robinson, A. L. (2007). Organic aerosol formation from photochemical oxidation of diesel exhaust in a smog chamber. *Environ. Sci. Technol.* 41, 6969–6975. doi: 10.1021/es070193r

Yamashita, Y., Hashihama, F., Saito, H., Fukuda, H., and Ogawa, H. (2017). Factors controlling the geographical distribution of fluorescent dissolved organic matter in the surface waters of the Pacific Ocean. *Limnol. Oceanogr.* doi: 10.1002/lno.10570. [Epub ahead of print].

Yamashita, Y., Nosaka, Y., Suzuki, K., Ogawa, H., Takahashi, K., and Saito, H. (2013). Photobleaching as a factor controlling spectral characteristics of chromophoric dissolved organic matter in open ocean. *Biogeosciences* 10, 7207–7217. doi: 10.5194/bg-10-7207-2013

Yamashita, Y., and Tanoue, E. (2009). Basin scale distribution of chromophoric dissolved organic matter in the Pacific Ocean. *Limnol. Oceanogr.* 54, 598–609. doi: 10.4319/lo.2009.54.2.0598

Ziolkowski, L. A., Chamberlin, A. R., Greaves, J., and Druffel, E. R. M. (2011). Quantification of black carbon in marine systems using the benzene polycarboxylic acid method: a mechanistic and yield study. *Limnol. Oceanogr. Methods* 9, 140–149. doi: 10.4319/lom.2011.9.140

Ziolkowski, L. A., and Druffel, E. R. M. (2010). Aged black carbon identified in marine dissolved organic carbon. *Geophys. Res. Lett.* 37:L16601. doi: 10.1029/2010GL043963

**Conflict of Interest Statement:** The authors declare that the research was conducted in the absence of any commercial or financial relationships that could be construed as a potential conflict of interest.

# Advantages of publishing in Frontiers

**OPEN ACCESS**
Articles are free to read for greatest visibility and readership

**FAST PUBLICATION**
Around 90 days from submission to decision

**HIGH QUALITY PEER-REVIEW**
Rigorous, collaborative, and constructive peer-review

**TRANSPARENT PEER-REVIEW**
Editors and reviewers acknowledged by name on published articles

**Frontiers**
Avenue du Tribunal-Fédéral 34
1005 Lausanne | Switzerland

**Visit us:** www.frontiersin.org
**Contact us:** info@frontiersin.org | +41 21 510 17 00

**REPRODUCIBILITY OF RESEARCH**
Support open data and methods to enhance research reproducibility

**DIGITAL PUBLISHING**
Articles designed for optimal readership across devices

**FOLLOW US**
@frontiersin

**IMPACT METRICS**
Advanced article metrics track visibility across digital media

**EXTENSIVE PROMOTION**
Marketing and promotion of impactful research

**LOOP RESEARCH NETWORK**
Our network increases your article's readership